13 August 2010 | $10

Science



Scaling Up Alternative Energy

AAAS



Next-gen GWAS. NOW.

It's a content revolution.

Up to 50% more coverage of common and rare variants than all other arrays. Maximum power for any population.

The Omni family of microarrays can propel your studies into true next-gen GWAS. With a clearly defined product path to the future. Immediate utility. Future flexibility.

Get on the path to next-gen GWAS.

Now is the time. Get started at
www.illumina.com/GWAS

illumina®

ARE YOU ON TRACK?

Investment guidance for higher education professionals

Unsure of how to get and keep your retirement on track?
We're ready to help. Together, we can:

- **Analyze your portfolio.** We'll help you bring your total financial picture—both workplace and personal savings—into focus.
- **Review your plan.** We can help you prepare for up and down markets.
- **Choose investments.** We'll help you choose low-cost investments, from bonds and annuities to no-load mutual funds.

SET UP YOUR COMPLIMENTARY ONE-ON-ONE CONSULTATION TODAY.

800.823.0172
FIDELITY.COM/RESERVE

Turn here℠

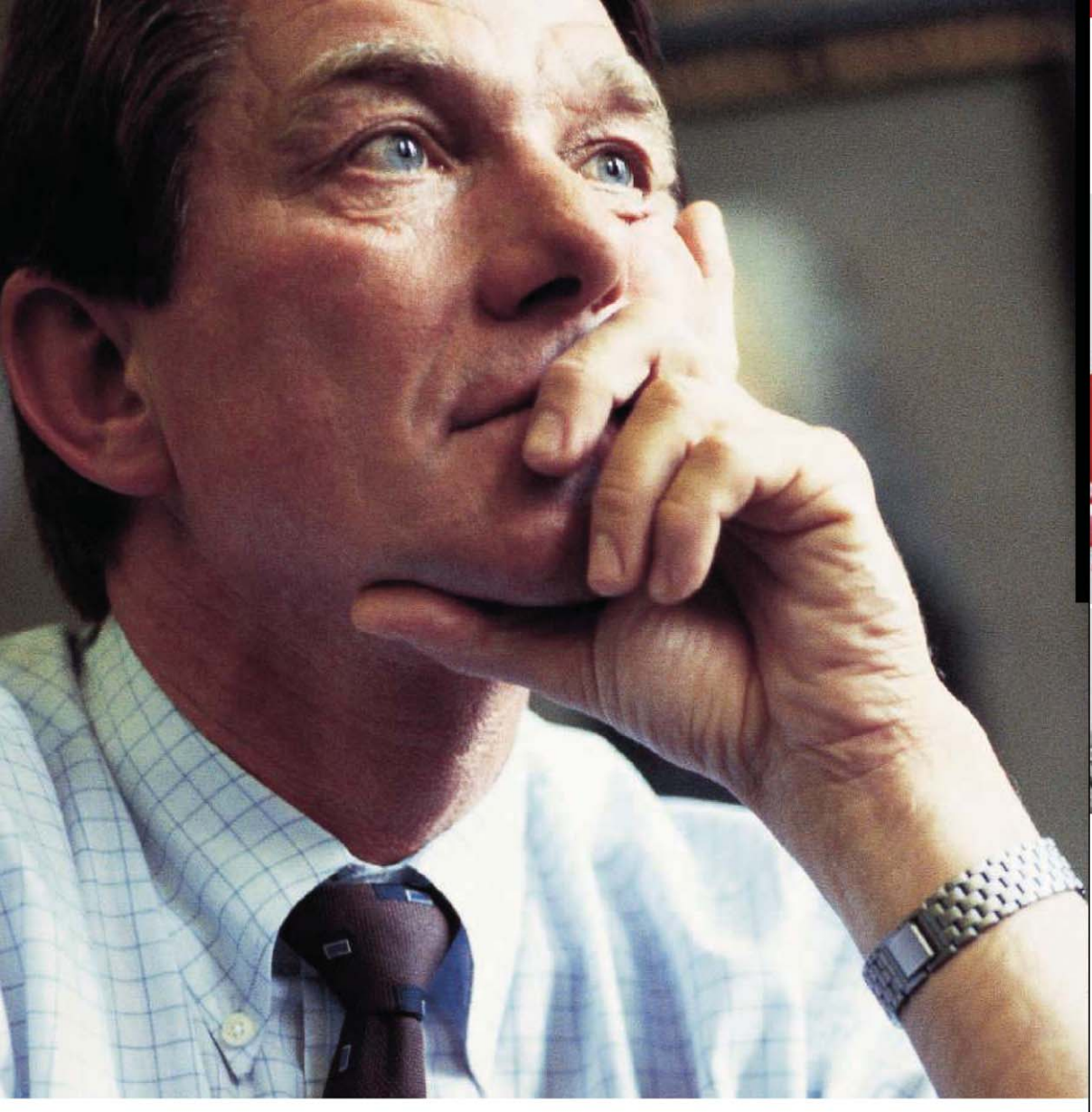
Fidelity INVESTMENTS

Before investing, consider the funds' investment objectives, risks, charges, and expenses. Contact Fidelity for a prospectus or, if available, a summary prospectus containing this information. Read it carefully.

Investing involves risk, including the risk of loss.

Products or services mentioned above may not be applicable, depending on your particular financial situation. Restrictions may apply. Please contact Fidelity for additional information.

Fidelity Brokerage Services LLC, Member NYSE, SIPC. © 2010 FMR LLC. All rights reserved. 553769.2







Dedication to Science
How is the light wavelength of knowledge calculated? Leica Microsystems has mapped its corporate values.
For more information, visit our website.

Professor Tanke, why is curiosity a building block of life?

Hans Tanke, a researcher and pioneer of digital fluorescence microscopy, is driven by passionate curiosity. He is Head of the Department of Molecular Cell Biology at Leiden University Medical Center, Netherlands, where he gives young scientists creative freedom: this enables them to develop the ethically responsible dedication with which he himself keeps tracking down the building blocks of life.

www.leica-microsystems.com

Living up to Life

Leica
MICROSYSTEMS

SPECIAL SECTION

Scaling Up Alternative Energy

INTRODUCTION

779 Getting Better to Get Bigger

NEWS

780 Do We Have the Energy for the Next Transition?

782 Sending African Sunlight to Europe, Special Delivery

784 Is There a Road Ahead for Cellulosic Ethanol?

786 Energy's Tricky Tradeoffs

788 Out of Site
Other Siting Problems

PERSPECTIVES

790 Feedstocks for Lignocellulosic Biofuels
C. Somerville et al.

793 Challenges in Scaling Up Biofuels Infrastructure
T. L. Richard

796 An Outlook on Microalgal Biofuels
R. H. Wijffels and M. J. Barbosa

REVIEW

799 Generating the Option of a Two-Stage Nuclear Renaissance
R. W. Grimes and W. J. Nuttall

>> Editorial p. 727; Policy Forum p. 762; Perspective p. 773; Science *Podcast*



page 734

EDITORIAL

727 Beyond Petroleum?
Donald Kennedy
>> Scaling Up Alternative Energy section p. 779

NEWS OF THE WEEK

734 A Lot of Oil on the Loose, Not So Much to Be Found

735 An Audacious Decision in Crisis Gets Cautious Praise

736 Yellow Fever Mosquito Shows Up in Northern Europe

737 From Science's Online Daily News Site

738 Lucy's Toolkit? Old Bones May Show Earliest Evidence of Tool Use

738 Russia's Forest Fires Ignite Concerns About Chornobyl's Legacy

739 From the *Science* Policy Blog

NEWS FOCUS

740 Tracing Evolution's Recent Fingerprints

743 Anthropologist Brings Worlds Together

746 Climate Scientists Shine Light on Cave Ice

LETTERS

748 Science Education: Neglected
R. Calfee and R. Bruning

Science Education: Narrative Nonfiction
J. Miller

Science Education: Poetry
A. J. Stewart

Science Education: Learn by Listening
P. S. Kessler

Response
P. Webb

Science Education: Flouting Formality
M. Stewart

Science Education: Mixed Messages
H. A. Scarbro

750 CORRECTIONS AND CLARIFICATIONS

BOOKS *ET AL.*

759 The Cybernetic Brain
A. Pickering, reviewed by T. H. Abraham

760 Skin
J. Moscoso et al., *curators;*
The Book of Human Skin
M. Lovric

POLICY FORUM

762 Nuclear Waste: Knowledge Waste?
E. A. Rosa et al.
>> Scaling Up Alternative Energy section p. 779;
Science *Podcast*

PERSPECTIVES

765 Structure and Dynamics of Ecological Networks
J. Bascompte
>> Report p. 853

766 The Proteome in Balance
D. Hutt and W. E. Balch
>> Research Article p. 805

767 β-Catenin Balances Immunity
I. Mellman and B. E. Clausen
>> Report p. 849

CONTENTS continued >>



COVER

A large-scale algae growing system. Oil extraction from algae is one approach being actively explored to replace petroleum as an energy source. A special section beginning on page 779 highlights worldwide research efforts aimed at scaling up this and other carbon-neutral processes to generate cleaner power.

Photo: Ashley Cooper/Visuals Unlimited, Inc.

DEPARTMENTS

723 This Week in *Science*
729 Editors' Choice
732 *Science* Staff
733 Random Samples
862 New Products
863 *Science* Careers

Free up your time



Automated sample and assay technologies by QIAGEN

Automated solutions from sample to result:

- **The widest choice of sample processing protocols**
- **Low-, medium-, and high-throughput automation**
- **Leading solutions for molecular diagnostics**
- **Plug-and-play automated sample preparation**
- **Quantitative, real-time PCR detection**
- **Automated analysis of DNA fragments and RNA**
- **High-resolution sequence-based DNA detection and quantification**
- **HPV testing**

Making improvements in life possible — www.qiagen.com

QIAGEN®

AUTOProf0110S1WW

Sample & Assay Technologies

Qs & AAAs



www.sciencedigital.org/subscribe

For just US$99, you can join AAAS TODAY and start receiving *Science* Digital Edition immediately!

Qs & AAAs



www.sciencedigital.org/subscribe

For just US$99, you can join AAAS TODAY and start receiving *Science* Digital Edition immediately!

769 Sedimentary Basins Feeling the Heat from Below
R. D. Müller
>> Report p. 827

770 A Boost for HIV Vaccine Design
D. R. Burton and R. A. Weiss
>> Research Article p. 811; Report p. 856

773 Concentrating on Solar Electricity and Fuels
M. Roeb and H. Müller-Steinhagen
>> Scaling Up Alternative Energy section p. 779

774 The Carbon Dioxide Exchange
P. B. Reich
>> Reports pp. 834 and 838

776 Retrospective: Stephen Schneider (1945–2010)
P. R. Ehrlich

BREVIA

804 The Kamil Crater in Egypt
L. Folco et al.
An unusually well-preserved 45-meter-diameter crater provides ground truth for small-scale meteorite impacts on Earth.

RESEARCH ARTICLES

805 Peripheral Protein Quality Control Removes Unfolded CFTR from the Plasma Membrane
T. Okiyoneda et al.
Cells clear misfolded and damaged proteins from the cell surface, sometimes frustrating attempts to treat protein-folding diseases.
>> Perspective p. 766

811 Structural Basis for Broad and Potent Neutralization of HIV-1 by Antibody VRC01
T. Zhou et al.
A human antibody achieves broad neutralization by binding the viral site of recognition for the primary host receptor, CD4.
>> Perspective p. 770; Report p. 856

REPORTS

817 Gamma-Ray Emission Concurrent with the Nova in the Symbiotic Binary V407 Cygni
The Fermi-LAT Collaboration
Satellite observations probe high-energy particle acceleration from a white dwarf star orbiting a red giant.

821 Quantum Oscillations and Hall Anomaly of Surface States in the Topological Insulator Bi_2Te_3
D.-X. Qu et al.
Quantum oscillations are used to detect the surface current of a topological insulator, yielding high carrier mobilities.

824 In-Plane Resistivity Anisotropy in an Underdoped Iron Arsenide Superconductor
J.-H. Chu et al.
Electronic ordering coincides with a lattice structural transition in an exotic superconductor.

827 Small-Scale Mantle Convection Produces Stratigraphic Sequences in Sedimentary Basins
K. D. Petersen et al.
Sedimentary stratigraphic sequences may result from sea-level changes that were induced by small-scale mantle convection.
>> Perspective p. 769

830 Three-Dimensional, Flexible Nanoscale Field-Effect Transistors as Localized Bioprobes
B. Tian et al.
Kinked nanowire transistors can measure intracellular electric potentials.

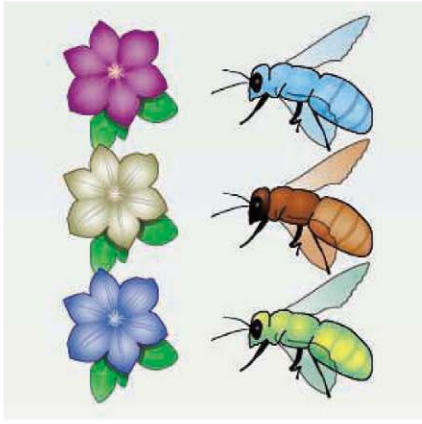
834 Terrestrial Gross Carbon Dioxide Uptake: Global Distribution and Covariation with Climate
C. Beer et al.
A combination of data and models provides an estimate of how much photosynthesis by all the world's plants occurs each year.

838 Global Convergence in the Temperature Sensitivity of Respiration at Ecosystem Level
M. D. Mahecha et al.
The long-standing discrepancy between modeled and empirical measures of ecosystem temperature sensitivity is resolved.
>> Perspective p. 774

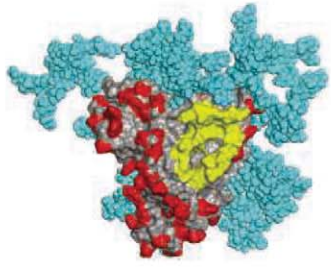
841 Association of Trypanolytic ApoL1 Variants with Kidney Disease in African Americans
G. Genovese et al.
Genetic variants associated with kidney disease in African Americans may confer protection against trypanosomes.

845 An Allosteric Self-Splicing Ribozyme Triggered by a Bacterial Second Messenger
E. R. Lee et al.
A metabolite-sensing riboswitch regulates the splicing of a "selfish" group I self-splicing ribozyme.

849 Activation of β-Catenin in Dendritic Cells Regulates Immunity Versus Tolerance in the Intestine
S. Manicassamy et al.
Gut-specific signaling pathways regulate immune cell–mediated tolerance in the intestine.
>> Perspective p. 767



pages 765 & 853

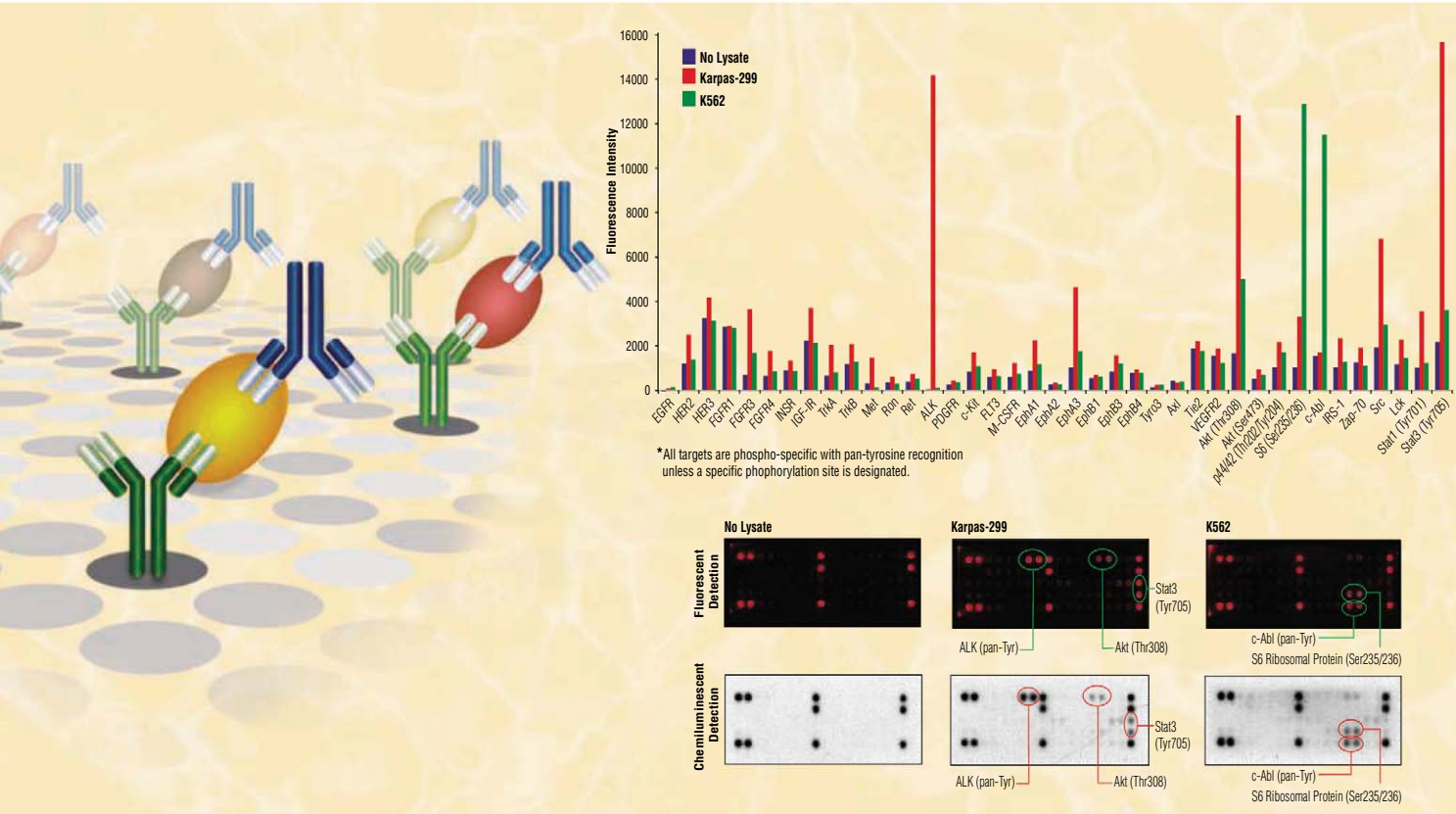


pages 770, 811, & 856

853 Stability of Ecological Communities and the Architecture of Mutualistic and Trophic Networks
E. Thébault and C. Fontaine
Ecological network architecture differs between models of trophic (herbivore) and mutualistic (pollination) communities.
>> Perspective p. 765

856 Rational Design of Envelope Identifies Broadly Neutralizing Human Monoclonal Antibodies to HIV-1
X. Wu et al.
A human antibody achieves broad neutralization by binding the viral site of recognition for the primary host receptor, CD4.
>> Perspective p. 770; Research Article p. 811

CONTENTS continued >>



New PathScan® RTK Signaling

Antibody Array Kits

...from Cell Signaling Technology®

New PathScan® RTK Signaling Antibody Array Kits are slide-based antibody arrays founded on the sandwich immunoassay principle.

- Arrays are produced and optimized in-house, incorporating the highest quality antibodies and ensuring results you can trust.
- Arrays allow the analysis of phosphorylation levels of 39 proteins per assay, saving valuable time and reagents.
- Arrays are designed to detect receptor tyrosine kinases (RTKs) and key downstream signaling molecules, allowing the most comprehensive readout of signaling events.
- Technical support is provided by the same scientists who developed and produce the product, which translates into a thorough, fast and accurate response.
- Chemiluminescent detection kit offers convenient and easy detection without specialized instrumentation.
- Fluorescent detection kit offers a broad linear range for the most accurate quantification.

Unparalleled product quality, validation and technical support.

Above: Analysis of Karpas-299 and K562 cells using the PathScan® RTK Signaling Antibody Array Kits reveals various phosphorylated RTKs and signaling nodes. The fluorescent readout and corresponding quantification were obtained using PathScan® RTK Signaling Antibody Array Kit (Fluorescent Readout) #7949 (middle and upper panels). The chemiluminescent readout was obtained using PathScan® RTK Signaling Antibody Array Kit (Chemiluminescent Readout) #7982 (lower panel).

Visit us at AACR Booth #1211

Meet our product scientists who will answer questions and provide in-depth insight into some of our most innovative products and services.

Featuring PathScan® RTK Signaling Antibody Array Kits

Monday, April 19th, 9 a.m. - 5 p.m.

for more information visit...

www.cellsignal.com

China www.cst-c.com.cn | **Europe** www.cellsignal.eu | **Japan** www.cstj.co.jp

Cell Signaling TECHNOLOGY®

U.S.: 978-867-2300 | **E-mail:** info@cellsignal.com

SCIENCEONLINE

SCIENCEXPRESS
www.sciencexpress.org

Dendritic Discrimination of Temporal Input Sequences in Cortical Neurons
T. Branco et al.

Dendrites of neurons are sensitive to the sequence of synaptic activation and can implement cortical computation.
10.1126/science.1189664

Survivin Reads Phosphorylated Histone H3 Threonine 3 to Activate the Mitotic Kinase Aurora B
A. E. Kelly et al.
10.1126/science.1189505

Histone H3 Thr-3 Phosphorylation by Haspin Positions Aurora B at Centromeres in Mitosis
F. Wang et al.

A critical regulator of cell division is recruited to chromosomes through the specific phosphorylation of a chromatin protein.
10.1126/science.1189435

Detection of a Trailing (L5) Neptune Trojan
S. S. Sheppard and C. A. Trujillo

An asteroid follows the orbit of the planet Neptune in a region of gravitational stability.
10.1126/science.1189666

Pulsar Discovery by Global Volunteer Computing
B. Knispel et al.

Einstein@home, a distributed computing project, discovered a rare, isolated pulsar with a low magnetic field.
10.1126/science.1195253

SCIENCENOW
www.sciencenow.org
Highlights From Our Daily News Coverage

Busy Brains Make for Deeper Sleep

Bursts of brain activity keep heavy sleepers from waking.

A Cheap, Fast Way to Write Nanoscale Patterns

New technique could speed development of electronics.

Turning Scar Tissue Into a Beating Heart

Reprogramming common cells could help repair damage from heart attacks.

SCIENCESIGNALING
www.sciencesignaling.org
The Signal Transduction Knowledge Environment

RESEARCH ARTICLE: The PI3K Isoforms p110α and p110δ Are Essential for Pre–B Cell Receptor Signaling and B Cell Development
F. Ramadani et al.

PERSPECTIVE: B Cell Receptor Signaling—Picky About PI3Ks
J. J. Limon and D. A. Fruman
Different isoforms of phosphatidylinositol 3-kinase have distinct roles in B cell receptor signaling.

PERSPECTIVE: Trafficking, Acidification, and Growth Factor Signaling
C. Niehrs and M. Boutros
Activation of Wnt and Notch pathways requires endocytosis of receptor complexes to an acidified vesicular compartment.

NETWATCH: GenBank, Gene Expression Omnibus (GEO), and Worldwide Protein Data Bank (wwPDB)
Deposit sequence, microarray, and structural data into public data banks; in Technical Information.

SCIENCECAREERS
www.sciencecareers.org/career_magazine
Free Career Resources for Scientists

Scientist's Work Bridges Math and Cancer
S. Webb
Franziska Michor's research skills involve equations and computers, but her goal is clinical: to eliminate cancer.

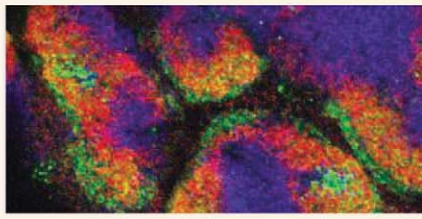
Improving Science Through Animal Welfare
E. Pain
First trained as a biology and geology teacher, Portuguese researcher Nuno Henrique Franco looks to improve science by improving animal welfare.

SCIENCETRANSLATIONAL MEDICINE
www.sciencetranslationalmedicine.org
Integrating Medicine and Science

COMMENTARY: Pharmacy Benefit Managers, Pharmacies, and Pharmacogenomic Testing—Prescription for Progress?
E. J. Topol
As prescription drug costs rise, some companies are moving to promote pharmacogenomics-based testing to inform therapeutic choices.

RESEARCH ARTICLE: Bacteria-Induced Gap Junctions in Tumors Favor Antigen Cross-Presentation and Antitumor Immunity
F. Saccheri et al.

PERSPECTIVE: Coupled for Cross-Presentation in Tumor Immunotherapy
B. Pang and J. Neefjes
Bacterial infection–induced gap junctions in melanoma cells shuttle tumor antigens to immune cells and spur a successful antitumor immune response.



SCIENCESIGNALING
Developing B cells.

RESEARCH ARTICLE: Fatty Acid Oxidation and Malonyl-CoA Decarboxylase in the Vascular Remodeling of Pulmonary Hypertension
G. Sutendra et al.

The overgrowth of vascular cells that causes pulmonary hypertension can be prevented by inhibiting a metabolic shift toward glycolysis.

SCIENCEPODCAST
www.sciencemag.org/multimedia/podcast
Free Weekly Show

Download the 13 August *Science* Podcast for a special show all about energy, including fossil-fuel use, nuclear waste disposal, biofuel crops, and more.

>> Scaling Up Alternative Energy section p. 779 and www.sciencemag.org/special/energy/

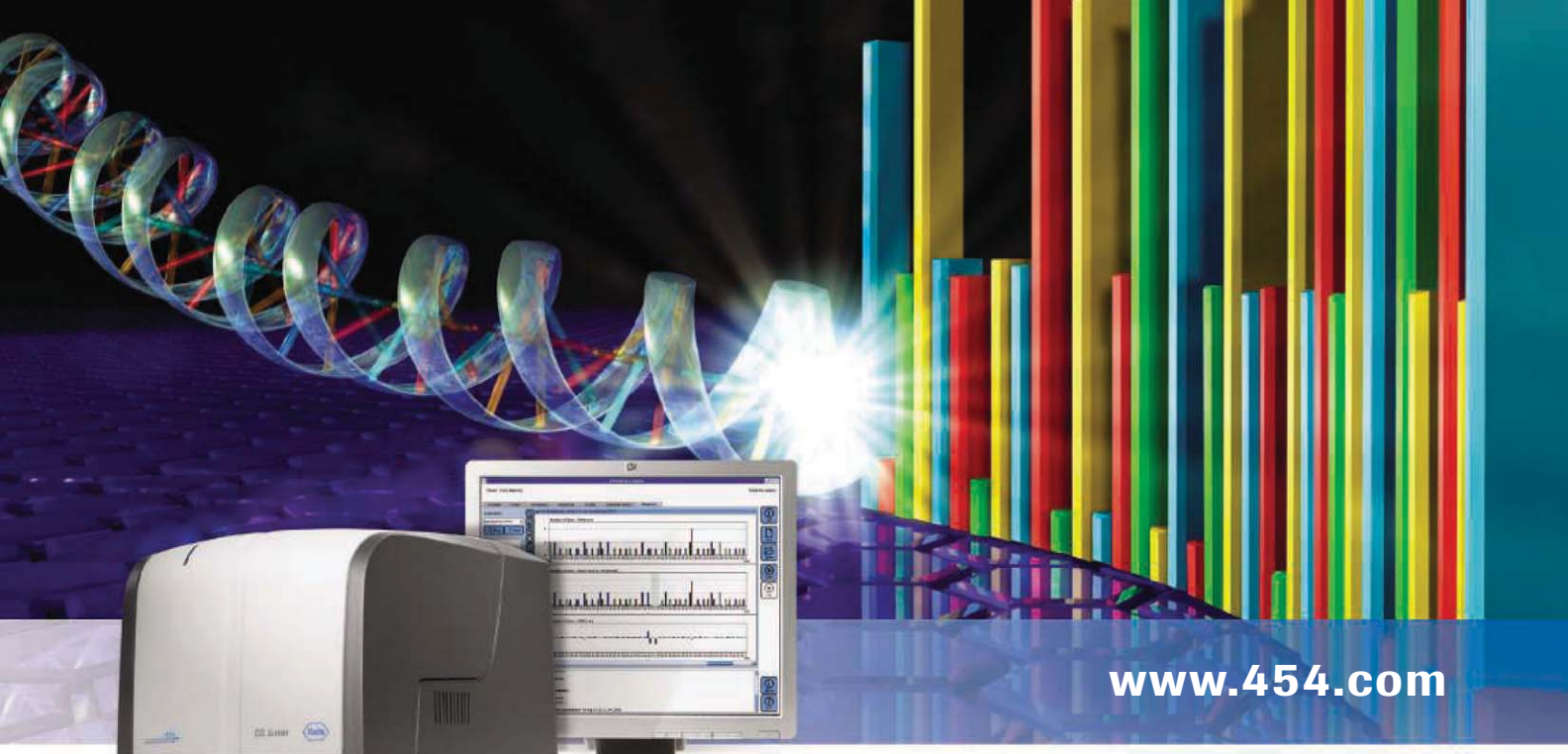
SCIENCEINSIDER
news.sciencemag.org/scienceinsider
Science Policy News and Analysis

SCIENCE (ISSN 0036-8075) is published weekly on Friday, except the last week in December, by the American Association for the Advancement of Science, 1200 New York Avenue, NW, Washington, DC 20005. Periodicals Mail postage (publication No. 484460) paid at Washington, DC, and additional mailing offices. Copyright © 2010 by the American Association for the Advancement of Science. The title SCIENCE is a registered trademark of the AAAS. Domestic individual membership and subscription (51 issues): $146 ($74 allocated to subscription). Domestic institutional subscription (51 issues): $910; Foreign postage extra: Mexico, Caribbean (surface mail) $55; other countries (air assist delivery) $85. First class, airmail, student, and emeritus rates on request. Canadian rates with GST available upon request, GST #1254 88122. Publications Mail Agreement Number 1069624. **Printed in the U.S.A.**

Change of address: Allow 4 weeks, giving old and new addresses and 8-digit account number. **Postmaster:** Send change of address to AAAS, P.O. Box 96178, Washington, DC 20090–6178. **Single-copy sales:** $10.00 current issue, $15.00 back issue prepaid includes surface postage; bulk rates on request. **Authorization to photocopy** material for internal or personal use under circumstances not falling within the fair use provisions of the Copyright Act is granted by AAAS to libraries and other users registered with the Copyright Clearance Center (CCC) Transactional Reporting Service, provided that $20.00 per article is paid directly to CCC, 222 Rosewood Drive, Danvers, MA 01923. The identification code for *Science* is 0036-8075. *Science* is indexed in the *Reader's Guide to Periodical Literature* and in several specialized indexes.

AAAS
ADVANCING SCIENCE, SERVING SOCIETY

CREDIT: FABIEN GARCON/LABORATORY OF LYMPHOCYTE SIGNALLING AND DEVELOPMENT/BABRAHAM INSTITUTE, CAMBRIDGE, UK



GS Junior Sequencing System

A *NEW* Scale of Sequencing –

Amplicon Sequencing on Your Benchtop

Amplicon Assay	Samples per Run
HIV Drug Targets (*e.g.*, 16 amplicons covering 5 regions at 1500X [Protease, RT, Integrase, Envelope V3, gp41 heptad repeats])	**8**
Gene Sequencing (*e.g.*, CFTR, 34 amplicons covering 27 exons at 50X)	**48**
HLA Sequencing (*e.g.*, high-resolution genotyping at 7 loci)	**16**
VDJ Sequencing (*e.g.*, for vaccine response or minimal residue detection for known clonality)	**8**

Figure 1: Get the right depth and coverage for your amplicon project. You can customize your experimental design to maximize data throughput for optimal sample coverage per sequencing run. Examples of various applications and optimum sample number per run are shown for the GS Junior System.

Bring the power of 454 pyrosequencing to your amplicon projects. Now available, the new small-footprint **GS Junior System** generates 70,000 reads per run, and delivers the performance and long reads (up to 500 base pairs) of the GS FLX Titanium chemistry to your benchtop.

- **Detect SNPs, insertions, and deletions.**
- **Discover rare somatic mutations in complex samples based on ultra-deep sequencing of amplicons.**
- **Sequence and analyze collections of human exons for identifications of rare alleles.**
- **Find viral quasispecies present within infected populations.**
- **Identify rare alleles associated with diseases.**

For complete information on the GS Junior System and all of the Roche sequencing solutions, visit ***www.454.com*** or contact your local Roche representative today.

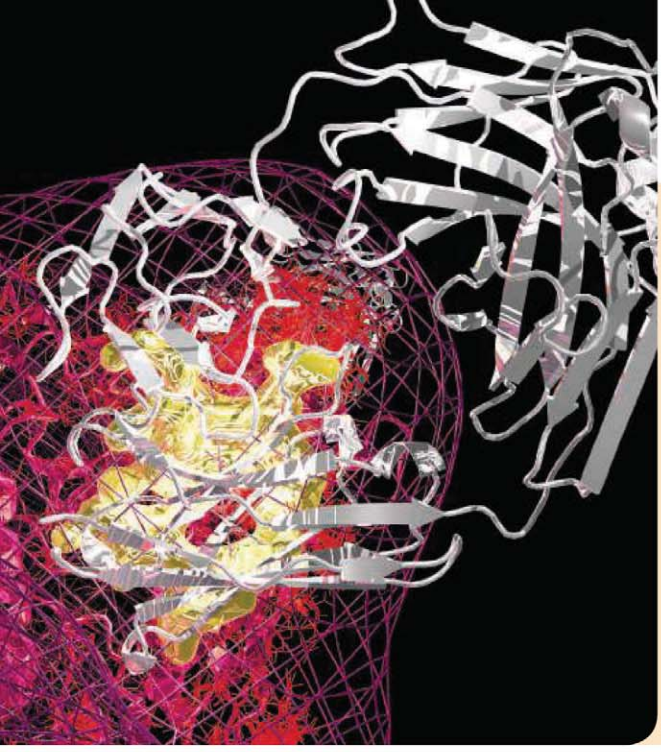
For life science research only.
Not for use in diagnostic procedures.

454 SEQUENCING

454, 454 SEQUENCING, GS JUNIOR, and GS FLX are trademarks of Roche.
© 2010 Roche Diagnostics. All rights reserved.

Roche Diagnostics Corporation
Roche Applied Science
Indianapolis, Indiana

Roche



CREDITS (TOP TO BOTTOM): NIH/NIAID/VRC/SBS; CHU *ET AL.*

<< Designer Anti-HIV

Developing a protective HIV vaccine remains a top global health priority. One strategy to identify potential vaccine candidates is to isolate broadly neutralizing antibodies from infected individuals and then attempt to elicit the same antibody response through vaccination (see the Perspective by **Burton and Weiss**). **Wu *et al.*** (p. 856, published online 8 July) now report the identification of three broadly neutralizing antibodies, isolated from an HIV-1–infected individual, that exhibited great breadth and potency of neutralization and were specific for the co-receptor CD4-binding site of the glycoprotein 120 (gp120), part of the viral Env spike. **Zhou *et al.*** (p. 811, published online 8 July) analyzed the crystal structure for one of these antibodies, VRC01, in complex with an HIV-1 gp120. VRC01 focuses its binding onto a conformationally invariant domain that is the site of initial CD4 attachment, which allows the antibody to overcome the glycan and conformational masking that diminishes the neutralization potency of most CD4-binding-site antibodies. The epitopes recognized by these antibodies suggest potential immunogens that can inform vaccine design.

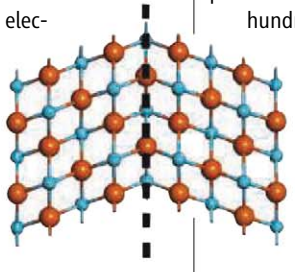
Peripheral Quality Control

Protein misfolding diseases often lead to the retention and degradation of important proteins within the endoplasmic reticulum (ER). Strategies to reduce the stringency of ER quality control that allow the proteins to carry on through the secretory pathway to reach their destination at the cell surface have shown some promise. **Okiyoneda *et al.*** (p. 805, published online 1 July; see the Perspective by **Hutt and Balch**) wanted to understand how, even if a protein reaches its destination, it may still be subjected to a second level of quality control and be cleared from the plasma membrane. Using functional small-interfering RNA screens in cells expressing the common cystic fibrosis mutation F508CFTR, the authors identified a pair of chaperones that promoted clearance of defective proteins from the plasma membrane. This peripheral quality-control step will also need to be overcome to increase the effectiveness of strategies to overcome protein misfolding disorders.

A Nova Source of Gamma Rays

Novae are thermonuclear explosions that occur at the surface of a white dwarf when material is pulled onto it from a companion star in a binary system. They are different from supernovae because the explosion does not completely destroy the white dwarf. Novae have not been widely considered as high-energy gamma-ray sources. Using the Fermi Large Area Telescope, **Abdo *et al.*** (p. 817) now report the detection of a nova explosion in gamma rays. The observations provide evidence for the acceleration to relativistic energies of particles in the shock wave following the explosion.

De-Twinning a Superconductor



Insight into the mechanism of electrical transport in a solid can often be gained by measuring its resistivity along different spatial directions. However, iron-based superconductors form numerous twin boundaries where two different orientations of a crystal meet, and so the measured resistivity along any in-plane direction will be averaged over these orientations. **Chu *et al.*** (p. 824) were able to "de-twin" the compound $Ba(Fe_{1-x}Co_x)_2As_2$, enabling unambiguous measurements of its normal-state resistivity along the in-plane lattice axes. Differences were observed in the resistivity values along the two axes, which suggests that the breaking of the symmetry of the lattice and electron subsystems occur simultaneously.

Changes in the Rocks

Changing sea level or major tectonic events, such as continental collisions, shift stratigraphic sequences by changing the depositional environment where certain rock types form. For example, a deep marine environment where limestone formation is favored may shift relatively quickly to a near-shore environment favoring sandstone formation because the relative sea level has dropped several meters. **Petersen *et al.*** (p. 827; see the Perspective by **Müller**), however, suggest that small-scale convection in the mantle may also induce appreciable changes in the sequence of sedimentary deposits. Using a modeling approach, they found that this is possible on a small scale (that is, just a few hundreds of kilometers) over variable time scales. Thus, while the co-occurrence of sedimentary deposit sequences at regional and global scales can allow sedimentary rocks to serve as markers of marine environments, it should be kept in mind that local changes in surface movements may also manifest themselves in the rock record.

Nanoprobes of Cell Potential

Direct electrical measurements of cell potentials usually face design compromises. Microelectrodes probe within the cytosol of cells but have a minimum size (hundreds of nanometers in width) for obtaining useful signals. Nanoscale field effect transistors (FETs) can have an active probe size of only tens of nanometers but generally allow only the outer cell potential to be measured. **Tian *et al.*** (p. 830) fabricated nanowires in which kinks could be introduced to create a sharp probe tip pointing away from the fabrication substrate. Coating the tip with a phospholipid bilayer allowed the probe to be inserted through the membranes of beating cardiac cells, where it could be used to follow temporal changes in cell potential.

Continued on page 725

SIGMA-ALDRICH®

SIGMA® Life Science Where bio begins™

Bioperspective.

Exposing new perspectives on the role of epigenetics in biology.

With more than 15,000 epigenetic target-specific products, including antibodies, shRNA, siRNA and small molecules, Sigma® Life Science is committed to providing you with one of the most comprehensive suites of products and innovative technologies on the market for the study of DNA methylation, chromatin modification and RNA regulation.

wherebiobegins.com/bioregulation



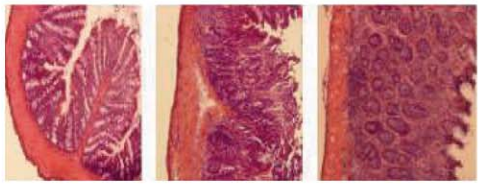
bioregulation

Sigma and Sigma-Aldrich are registered trademarks of Sigma-Aldrich and its affiliate Sigma-Aldrich Biotechnology, L.P.

Continued from page 723

Carbon Cycle and Climate Change

As climate change accelerates, it is important to know the likely impact of climate change on the carbon cycle (see the Perspective by **Reich**). Gross primary production (GPP) is a measure of the amount of CO_2 removed from the atmosphere every year to fuel photosynthesis. **Beer *et al.*** (p. 834, published online 5 July) used a combination of observation and calculation to estimate that the total GPP by terrestrial plants is around 122 billion tons per year; in comparison, burning fossil fuels emits about 7 billion tons annually. Thirty-two percent of this uptake occurs in tropical forests, and precipitation controls carbon uptake in more than 40% of vegetated land. The temperature sensitivity (Q10) of ecosystem respiratory processes is a key determinant of the interaction between climate and the carbon cycle. **Mahecha *et al.*** (p. 838, published online 5 July) now show that the Q10 of ecosystem respiration is invariant with respect to mean annual temperature, independent of the analyzed ecosystem type, with a global mean value for Q10 of 1.6. This level of temperature sensitivity suggests a less-pronounced climate sensitivity of the carbon cycle than assumed by recent climate models.



CREDIT: MANICASSAMY *ET AL.*

A Gut Feeling

Special immune controls are necessary in the gut to prevent the immune system from reacting to the commensal microbiota and to food antigens. Dendritic cells (DCs) are important for maintaining gut tolerance because they help to keep T cells in an unresponsive state. However, in other environments, DCs activate T cells. What signals determine whether DCs induce T cell tolerance or activation? **Manicassamy *et al.*** (p. 849; see the Perspective by **Mellman and Clausen**) found that β-catenin–dependent signaling is required for maintaining DC-mediated gut tolerance in mice. Wnt ligands were expressed in the gut, and β-catenin signaling was activated in DCs in the small and large intestines but not in the spleen. When β-catenin was specifically deleted from DCs in mice, the frequency of regulatory T cells and anti-inflammatory cytokines was reduced, whereas the frequency of pro-inflammatory T helper 1 and T helper 17 cells and their associated cytokines was increased. Mice lacking β-catenin in dendritic cells also exhibited enhanced susceptibility in a mouse model of colitis.

Out of Africa

Kidney disease is more common in African Americans than in Americans of European descent, and genetics is likely to be a major contributing factor. **Genovese *et al.*** (p. 841, published online 15 July) now show that African Americans who carry specific sequence variants in a gene on chromosome 22 encoding apolipoprotein L-1 (APOL1) have an increased risk of developing hypertension-attributed end-stage kidney disease or focal segmental glomerulosclerosis. These variants are absent from European chromosomes. Among the functions ascribed to APOL1 is the ability to lyse and kill trypanosomes. Intriguingly, APOL1 derived from the risk alleles, but not the "wild-type" allele, killed *Trypanosoma brucei rhodesiense*, which causes African sleeping sickness.

Riboswitch Revealed

Short regulatory regions—riboswitches—are found in the messenger RNAs of many bacteria, plants, and fungi. They bind to small-molecule metabolites and, through switching between alternate RNA secondary structures, regulate the expression of the linked RNA. **Lee *et al.*** (p. 845) have identified a c-di-GMP (cyclic di-guanosyl-5′-monophosphate)–binding riboswitch in the bacterium *Clostridium difficile* that regulates the splicing of a group I self-splicing ribozyme. Binding of c-di-GMP to the riboswitch favors a conformation of the ribozyme that promotes splicing in the presence of guanosine triphosphate (as is typical for this class of ribozymes). Concomitantly, splicing promotes the formation of a ribosome binding site, thereby stimulating protein production from the downstream pathogenesis-related gene. This regulatory region may thus constitute a two-input gene-control system that reads the concentration of both GTP and c-di-GMP. Thus, not all group I self-splicing ribozymes represent selfish genetic elements.

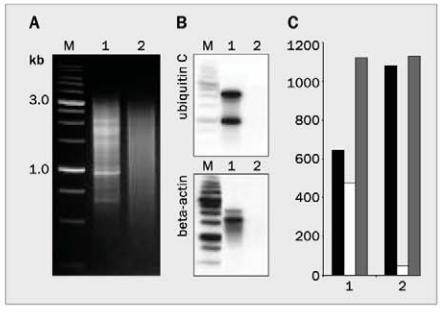


Reduce high-copy number transcripts before any sequencing choices

Evrogen normalization service is a highly efficient and well-established way to equalize transcript abundance in cDNA populations.

New service options are tailored specifically for preparation of normalized cDNA for further next generation sequencing using

- Roche / 454
- Illumina / Solexa
- AB I / SOLiD approaches



Typical cDNA normalization result.
(A) Agarose gel electrophoresis of cDNA samples;
(B) Virtual Northern blot analysis of abundant transcripts in these cDNA samples;
(C) Sequencing of randomly picked clones: black columns - unique, white columns - non-unique, grey columns - all sequences. 1 - non-normalized cDNA; 2 - normalized cDNA. M - 1 kb DNA size markers.

Evrogen JSC, Moscow, Russia
Tel: +7(495) 988 40 84
Fax: +7(495) 988 40 85
E-mail: evrogen@evrogen.com
Web site: www.evrogen.com

evrogen

Premier Scientific Partner

华大基因 BGI

BGI (previously known as Beijing Genomics Institute) was founded in Beijing in 1999 for the Human Genome Project. Our headquarters was relocated to Shenzhen, China in 2007. BGI has become the largest genomic organization in the world with a focus in research and application in personalized healthcare, agriculture, conservation and bio-energy fields. We ascribe to the highest standards in genomics solutions for sample preparation, sequencing experimental design and customized bioinformatics analysis for our research collaborators and project partners.

Scientific Milestones (2001 to Jun 2010)

- ***167*** Scientific publications
- ***29*** ***Science & Nature*** publication groups



Front Cover Publications

Genomics Solutions

1 ***de novo***
- Human
- Plant & Animal
- Resequencing

2 **RNA Sequencing**
- Transcriptome
- RNA-Seq
- small RNA

3 **Disease studies**
(Monogenic & Complex)
- Exome
- Target region
- Metagenomics
- Whole genome

4 **Others**
- Microbes
- Plasmids
- Epigenomics

Bioinformatics Centre

- Data analysis methods and computational tools development in a wide range of applications including ***de novo*** sequencing; RNA sequencing; exome sequencing; individual/large-scale re-sequencing; epigenomics; and metagenomics
- Eliminates data analysis bottlenecks and quickly translates sequencing data into powerful scientific discoveries
- ***9*** Publications on Bioinformatics tools: Short Oligonucleotide Alignment Program（SOAP, SOAP2, SOAPsnp, SOAPdenovo）
 >10,000 users

Sequencing & Computing Platforms

- The largest sequencing capacity in the world by 137 Illumina HiSeq 2000 and 27 Applied Biosystems SOLiD 4 System
- Reliable, high quality sequencing results with the industry-leading turnaround time
- High-performance supercomputing centers with a total peak performance up to 102 T flops, 20 TB memory and 10 PB storage



We provide stable and efficient resources to store, process and analyze massive bioinformatics data.

Locations:

China (Mainland)
BGI-Shenzhen
Main building, Bei Shan Industrial Zone
Yantian District, Shenzhen, 518083
China
Tel: +86-755-25273395

Asia (Hong Kong)
BGI-HongKong Co.,Limited
21/F., Far East Consortium Building
121 Des Voeux Road Central
Hong Kong
Tel: +852-69363890

North America (Boston)
BGI Americas Corporation
One Broadway, 14th Floor
Cambridge, MA 02142
Tel: +1-617-401-2656

Europe (Copenhagen)
BGI Europe A/S
Bülowsvej 15
DK-1870 Frederiksberg C
Tel: +45-70-26-08-06

Email: tech@genomics.cn Web: www.genomics.cn



Donald Kennedy is Editor Emeritus of *Science*.

Beyond Petroleum?

REMEMBER SOME YEARS BACK, WHEN BRITISH PETROLEUM CLAIMED THAT ITS INITIALS STOOD FOR "Beyond Petroleum?" Its competitors were furious at the suggestion that it was leading the push toward renewable energy. Now that BP is responsible for an oil spill that is ruining beaches, livelihoods, and wildlife, these same competitors are telling U.S. senators that "We would not have drilled the well that way." Believe that or not, "Beyond Petroleum" could be the right slogan for the policy changes needed to end the U.S. national addiction to oil. That outcome will require a mix of solutions involving the Congress, the American public, businesses, the Administration, and environmental organizations—all driven by passionate conviction about the need for change.

This isn't exactly new. In 1977, President Carter referred to dealing with the energy crisis by ending the country's dependence on oil as "the moral equivalent of war." Despite an epidemic of gasoline lines in 1978 and 1979, the "moral equivalent" imperative failed, leaving the United States in the middle of another oil crisis quite different from the one that Carter faced. The contemporary challenge is not that there isn't enough oil; there is far too much of it. Oil has produced environmental devastation on Gulf shores, more of the same in Amazonian forests, emissions from transportation systems that endanger public health, and supplies managed by nation-states that threaten global security. The abuses that result from an overdependence on oil amount to a national crisis, and its resolution will depend on cooperative actions taken by government, industry, and the public.



The government needs to take action at the administrative level: through subsidies for investment in renewable energy, research grants for solar and wind applications, the green jobs needed to do that work, and policy support for vehicle electrification. Those actions require no new statutes; neither does the needed regulation of existing coal-fired power plants by the Environmental Protection Agency. But legislative hopes died when the Senate majority leader killed hopes for a climate-energy bill. Eventually, dealing with those together will be necessary to reduce carbon intensity by changing the energy mix. Businesses and environmental organizations such as the Sierra Club should work with government to resolve struggles over large-scale renewable energy projects on public lands. Large solar-thermal units or wind farms require space; so do the transmission lines needed to connect wind or solar sources with the power grid. These climate-worthy projects may affect areas that even their proponents treasure for other uses: recreation, wildlife conservation, or the protection of endangered species. Resolution will involve government agencies (the Departments of Energy and the Interior) that may have different interests in the outcome.

And because oil dependence is so tightly linked to the transportation sector, reducing oil dependence requires increasing vehicle efficiency using current technologies: lowering weight and improving engines and aerodynamics. Biofuels don't really mitigate carbon emissions and have brought new problems to the food sector. But burning biomass to produce electricity, if carbon costs are carefully considered, could encourage vehicle electrification. For electric charging, tax structures that take account of carbon emissions will be needed, and road-use taxes comparable to those now paid only by the gasoline tax will probably be assessed as well. Finally, there is a pressing need for incentives to drive investments in public transportation as well as in "smart" community designs that shorten the trip between home and job.

Coal and oil—the real "Axis of Evil" in the United States today—present a major challenge in the context of climate change. The nation has taken strong actions to reduce coal-fired power, yet it faces an electric power marketplace dominated by coal that may discourage vehicle electrification. And the current Gulf situation raises the ante on getting Beyond Petroleum. When BP first said that, they didn't really mean it … but we should!

– Donald Kennedy

10.1126/science.1194561

CREDIT: (RIGHT) PHOTOS.COM

A New Perspective.

A Legendary Journal.



At the Journal of Biological Chemistry, we've broadened our scope to welcome the very best papers in all areas of molecular and cellular biology. Partner with us as we forge new paths to discovery.

Submit to the Journal of Biological Chemistry.

You'll be in great company.

www.jbc.org

EDITED BY GILBERT CHIN AND JAKE YESTON



EVOLUTION

A Hop, Skip, and a Jump

Marsupial mammals bear their young much earlier than placental mammals and then nurture them in a maternal pouch. They split from the placental line more than 100 million years ago, and the evolutionary relationships among the Australasian (left) and South American (right) species have been debated. Nilsson *et al.* have performed genome-wide scans for retroposon integrations in the opossum and kangaroo genomes. A subset of the resulting loci was validated in 20 species from the seven marsupial orders, yielding 53 phylogenetically informative retroposon markers that root modern marsupials and demonstrate a clear separation between the South American and Australasian denizens. Furthermore, they support the view that the marsupial fauna of Australia was populated by a single Gondwanan migration event originating from what is today South America. — LMZ



PLoS Biol. **8**, e1000436 (2010).

IMMUNOLOGY

Too Much Recognition

Multiple sclerosis is an autoimmune disease of the central nervous system; normally tolerant T cells attack the myelin sheaths that surround nerve fibers. Although some viruses have been fingered as environmental triggers of the disease, how they would cause multiple sclerosis has not been established. Ji *et al.* show that $CD8^+$ T cells that express two antigen receptors with distinct specificities can drive the development of a virus-induced, multiple sclerosis–like condition [experimental autoimmune encephalitis (EAE)] in mice. The authors used mice whose $CD8^+$ T cells expressed a transgenic antigen receptor that specifically recognized myelin basic protein. These mice did not spontaneously develop autoimmunity, but infection with vaccinia virus that had been engineered to express recombinant myelin basic protein did trigger the onset of EAE. Surprisingly, viral expression of myelin basic protein was not required because mice infected with wild-type vaccinia virus also developed EAE, and the authors found that EAE only developed in mice whose T cells were of dual specificity. That is, the engagement of the endogenous T cell receptors by virus leads to T cell activation, but because these T cells can also recognize myelin basic protein, they then promote EAE development. Similar results were seen when mice were infected with adenovirus, indicating that viral infections generally could promote the development of multiple sclerosis in some of the infected individuals. — KLM

Nat. Immunol. **11**, 628 (2010).

CLIMATE SCIENCE

Antarctica's Adolescence

Antarctica, particularly East Antarctica, harbors much of the world's ice. Thus, accurate knowledge of its sensitivity to melting from global warming is critical for assessing likely sea-level rise in the years ahead. To this end, two recent studies examine the region's dynamics during past glacial cycles and the period when it first grew. Lilly *et al.* use cosmogenic isotopes, which accumulate in exposed bedrock, to show that the height of the East Antarctic ice sheet fluctuated by only about 100 m through at least the last glacial cycle; the best model fit to the data includes a slow decline in height over longer times. Thus, the East Antarctic ice sheet has had a stable height during past glaciations. In exploring its stability during warmer times, Peters *et al.* show that an incised coastal valley in Egypt records a sudden and rapid change (within 2 million years) in sea level of about 40 m, at the time when global records imply that major ice sheets first grew in Antarctica, about 35 million years ago. Several smaller fluctuations in sea level (of about 10 m) are also recorded. The rapid changes correlate with estimated fluctuations in atmospheric CO_2 levels and occurred when levels dropped below about 750 ppm. — BH



Geology **38**, p. 703; 723 (2010).

PHYSICS

An Orderly Transition

Classical phase transitions, such as boiling or freezing, are usually driven by heat exchange, which introduces the order or disorder necessary for rearrangement. In contrast, quantum phase transitions occur at zero temperature as a result of quantum (rather than thermal) fluctuations and are controlled by parameters such as pressure or chemical composition. Most quantum phase transitions have been observed in compounds with carefully tuned chemical compositions, which are inevitably subject to disorder. Jaramillo *et al.* now induce such a

Continued on page 731

CREDITS: (TOP LEFT TO RIGHT) ISTOCKPHOTO.COM, JOSÉ LUIS BARTHELD; (BOTTOM) DON BLANKENSHIP/UTIG



Need to assess the novelty of substances?
SciFinder is the answer.

It includes CAS REGISTRY,SM the most comprehensive substance information available, integrated with relevant journal articles and patents.

Give your research team the highest quality and most timely scientific information resource.

Make SciFinder an essential part of your research process.

For more information about SciFinder, visit www.cas.org or e-mail help@cas.org.

an essential

SciFinder®—Part of the process.™

CAS | SciFinder®

www.cas.org

CAS is a division of the American Chemical Society

Continued from page 729

transition in elemental chromium, which presents an unusually clean system. Chromium is antiferromagnetic at ambient pressure with a transition (Néel) temperature T_N close to room temperature; as the authors increase the pressure, T_N decreases and eventually disappears at a quantum critical point close to 10 GPa. Along the way, the antiferromagnetic phase changes character from mean-field–like to quantum critical. This change is reflected in the value of a critical exponent for resistivity, which approaches 0.25 at very low temperatures, easily distinguishable from the mean-field value of 0.5. Comparison with a related nonstoichiometric system indicates that pressure and chemical doping lead to distinct phase transitions. — JS

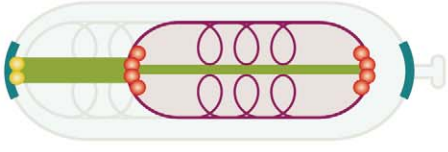
Proc. Natl. Acad. Sci. U.S.A. **107**, 13631 (2010).

CELL BIOLOGY

Splitting Image

Occasionally, complex cellular structures previously thought to be devised by eukaryotes turn out to have functional counterparts in prokaryotes. In eukaryotes, mitosis is an intricate process regulated by many different proteins. It requires the assembly of a filamentous structure composed of microtubule polymers known as the mitotic spindle, which is used to segregate homologous chromosomes into daughter cells during cell division. Many bacteria use simpler approaches known as DNA partitioning systems to segregate their chromosomes.

Using super-resolution microscopy, Ptacin *et al.* have captured images of a mitotic spindle-like structure in the bacterium *Caulobacter crescentus*. Fluorescent labeling revealed that the ATPase ParA formed a narrow linear structure (green) stretching from pole to pole during segregation of the newly replicated DNA (purple) in *C. crescentus*. Additionally, electron micrographs of purified ParA confirmed that the protein could



CREDIT: ADAPTED FROM PTACIN *ET AL.*, *NAT. CELL BIOL.* **12**, 791 (2010)

form linear polymers in vitro. The authors also identified another component of the partitioning system, TipN (yellow), which binds to ParA and is required for its function. Previous analogies have been made between bacterial chromosome segregation and eukaryotic mitosis; these findings narrow the gap between these two domains of life. — HP

Nat. Cell Biol. **12**, 791 (2010).

CHEMISTRY

A Peek at Polymerization

The properties of plastics depend intimately on the dynamics of the polymerization reactions used to produce them. Because the reactions are often quite rapid, though, they can prove hard to track. Christianson *et al.* have adapted a nuclear magnetic resonance (NMR) spectrometer in order to monitor polymerization reactions on a millisecond time scale. Using a stopped-flow approach more common in optical spectroscopy, they set up the probe to acquire data just after pneumatically driven mixing of a catalyst solution stream with a stream of reactive monomer. With this system in hand, they examined the room-temperature polymerization of 1-hexene by a borane-activated zirconium catalyst. They were able to observe initiation and chain propagation steps directly, and also monitor buildup of a transiently deactivated form of the catalyst, resulting from borane binding to a zirconium hydride ligand after chain elimination from the metal center. The results bolster previous mechanistic hypotheses surrounding this catalyst's behavior and highlight the utility of stopped-flow NMR. — JSY

J. Am. Chem. Soc. **132**, 10.1021/ja105107y (2010).

PSYCHOLOGY

Mindless Reading

Having gotten this far, do you remember what you read just a minute ago? Or did your eyes scan the previous five or six sentences without any of that information having been absorbed? And if you did zone out, were you aware of having done so? Reichle *et al.* have studied precisely this kind of behavior by developing a protocol for interrogating subjects who were reading *Sense and Sensibility*. One theoretical framework posits that a meta-processor oversees cognitive components that support reading (including oculomotor systems and lexical lookup) and also a default or task-decoupled network that mediates mind wandering. The authors found that people were less likely to fixate for longer durations and that their eye movements were more sensitive to parameters such as word length and frequency when they were reading attentively. On the other hand, when people were reading mindlessly, their awareness of having become decoupled from the text surfaced only after a few minutes. — GJC

Psychol. Sci. **21**, 10.1177/0956797610378686 (2010).

Visit us at ACS in Boston, August 22-26, Booth #1211

ReichertSPR

Surface Plasmon Resonance Technology in a Modular System



- Label-free molecular interaction analysis in real-time
- Measure kinetics, affinity/equilibrium, thermodynamics, concentration
- Component-based
- Low operating costs
- Low maintenance
- Manual or fully automated
- High quality performance

Reichert™ TECHNOLOGIES Life Sciences

Talk to an SPR representative:
Tel: +1 716-686-4500
Toll free USA: 1-888-849-8955
lifesciences@reichert.com
www.ReichertSPR.com

Innovative precision instruments for over a century

www.sciencemag.org

Science

1200 New York Avenue, NW
Washington, DC 20005
Editorial: 202-326-6550, FAX 202-289-7562
News: 202-326-6581, FAX 202-371-9227
Bateman House, 82-88 Hills Road
Cambridge, UK CB2 1LQ
+44 (0) 1223 326500, FAX +44 (0) 1223 326501

Subscription Services For change of address, missing issues, new orders and renewals, and payment questions: 866-434-AAAS (2227) or 202-326-6417, FAX 202-842-1065. Mailing addresses: AAAS, P.O. Box 96178, Washington, DC 20090-6178 or AAAS Member Services, 1200 New York Avenue, NW, Washington, DC 20005

Institutional Site Licenses please call 202-326-6755 for any questions or information

Reprints: Author Inquiries 800-635-7181
Commercial Inquiries 803-359-4578

Permissions 202-326-7074, FAX 202-682-0816

Member Benefits AAAS/Barnes&Noble.com bookstore www.aaas.org/bn; AAAS Online Store www.apisource.com/aaas/ code MKB6; AAAS Travels: Betchart Expeditions 800-252-4910; Apple Store www.apple.com/eppstore/aaas; Bank of America MasterCard 1-800-833-6262 priority code FAA3YU; Cold Spring Harbor Laboratory Press Publications www.cshlpress.com/affiliates/aaas.htm; GEICO Auto Insurance www.geico.com/landingpage/go51.htm?logo=17624; Hertz 800-654-2200 CDP#343457; Office Depot https://bsd.officedepot.com/portalLogin.do; Seabury & Smith Life Insurance 800-424-9883; Subaru VIP Program 202-326-6417; VIP Moving Services www.vipmayflower.com/domestic/index.html; Other Benefits: AAAS Member Services 202-326-6417 or www.aaasmember.org.

science_editors@aaas.org	(for general editorial queries)
science_letters@aaas.org	(for queries about letters)
science_reviews@aaas.org	(for returning manuscript reviews)
science_bookrevs@aaas.org	(for book review queries)

Published by the American Association for the Advancement of Science (AAAS), *Science* serves its readers as a forum for the presentation and discussion of important issues related to the advancement of science, including the presentation of minority or conflicting points of view, rather than by publishing only material on which a consensus has been reached. Accordingly, all articles published in *Science*—including editorials, news and comment, and book reviews—are signed and reflect the individual views of the authors and not official points of view adopted by AAAS or the institutions with which the authors are affiliated.

AAAS was founded in 1848 and incorporated in 1874. Its mission is to advance science, engineering, and innovation throughout the world for the benefit of all people. The goals of the association are to: enhance communication among scientists, engineers, and the public; promote and defend the integrity of science and its use; strengthen support for the science and technology enterprise; provide a voice for science on societal issues; promote the responsible use of science in public policy; strengthen and diversify the science and technology workforce; foster education in science and technology for everyone; increase public engagement with science and technology; and advance international cooperation in science.

Information for Authors
See pages 352 and 353 of the 15 January 2010 issue or access www.sciencemag.org/about/authors

EDITOR-IN-CHIEF **Bruce Alberts**
EXECUTIVE EDITOR **Monica M. Bradford**
NEWS EDITOR **Colin Norman**
MANAGING EDITOR, RESEARCH JOURNALS **Katrina L. Kelner**
DEPUTY EDITORS **R. Brooks Hanson, Barbara R. Jasny, Andrew M. Sugden**

Editorial senior editors/commentary Lisa D. Chong, Brad Wible; **senior editors** Gilbert J. Chin, Pamela J. Hines, Paula A. Kiberstis (Boston), Marc S. Lavine (Toronto), Beverly A. Purnell, L. Bryan Ray, Guy Riddihough, H. Jesse Smith, Phillip D. Szuromi (Tennessee), Valda Vinson, Jake S. Yeston; **associate editors** Kristen L. Mueller, Jelena Stajic, Nicholas S. Wigginton, Laura M. Zahn; **research associate** Alexis Wynne Mogul; **book review editor** Sherman J. Suter; **associate letters editor** Jennifer Sills; **editorial manager** Cara Tate; **senior copy editors** Jeffrey E. Cook, Cynthia Howe, Harry Jach, Lauren Kmec, Barbara P. Ordway, Trista Wagoner; **copy editor** Chris Filiatreau; **editorial coordinators** Carolyn Kyle, Beverly Shields; **publications assistants** Ramatoulaye Diop, Joi S. Granger, Emily Guise, Jeffrey Hearn, Michael Hicks, Lisa Johnson, Scott Miller, Jerry Richardson, Jennifer A. Seibert, Brian White, Anita Wynn; **editorial assistants** Emily C. Horton, Patricia M. Moore, Miriam Weinberg; **executive assistant** Alison Crawford; **administrative support** Maryrose Madrid; **editorial fellow** Melissa R. McCartney

Editorial director, web and new media Stewart Wills; **senior web editor** Tara S. Marathe; **web editor** Robert Frederick; **web development manager** Martyn Green; **web developer** Andrew Whitesell; **intern** Sophia Cai

News deputy news editors Robert Coontz, David Grimm, Eliot Marshall, Jeffrey Mervis, Leslie Roberts; **contributing editors** Elizabeth Culotta, Polly Shulman; **news writers** Yudhijit Bhattacharjee, Adrian Cho, Jennifer Couzin, Jocelyn Kaiser, Richard A. Kerr, Eli Kintisch, Greg Miller, Elizabeth Pennisi, Lauren Schenkman, Robert F. Service (Pacific NW), Erik Stokstad (Online); **web developer** Daniel Berger; **intern** Kristen Minogue; **contributing correspondents** Jon Cohen (San Diego, CA), Daniel Ferber, Ann Gibbons, Sam Kean, Robert Koenig, Andrew Lawler, Mitch Leslie, Charles C. Mann, Virginia Morell, Gary Taubes; **copy editors** Linda B. Felaco, Melvin Gatling, Melissa Raimondi; **administrative support** Scherraine Mack; **bureaus** San Diego, CA: 760-942-3252, FAX 760-942-4979; Pacific Northwest: 503-963-1940

Production director James Landry; **senior manager** Wendy K. Shank; **assistant manager** Rebecca Doshi; **senior specialists** Steve Forrester, Chris Redwood, Anthony Rosen; **Preflight director** David M. Tompkins; **manager** Marcus Spiegler; **specialist** Jason Hillman

Art director Yael Fitzpatrick; **associate art director** Laura Creveling; **senior illustrators** Chris Bickel, Katharine Sutliff; **illustrator** Yana Hammond; **senior art associates** Holly Bishop, Preston Huey, Nayomi Kevitiyagala; **art associates** Kay Engman, Matthew Twombly; **photo editor** Leslie Blizard

***Science* International**

Europe (science@science-int.co.uk) **editorial: international managing editor** Andrew M. Sugden; **senior editor/commentary** Julia Fahrenkamp-Uppenbrink; **senior editors** Caroline Ash, Stella M. Hurtley, Ian S. Osborne, Peter Stern; **associate editor** Maria Cruz; **locum editor** Helen Pickersgill; **editorial support** Rachel Roberts, Alice Whaley; **administrative support** John Cannell, Janet Clements, Louise Hartwell; **news: europe news editor** John Travis; **deputy news editor** Daniel Clery; **contributing correspondents** Michael Balter (Paris), John Bohannon (Vienna), Martin Enserink (Amsterdam and Paris), Gretchen Vogel (Berlin); **intern** Sarah Reed

Latin America contributing correspondent Antonio Regalado

Asia Japan Office: Asca Corporation, Tomoko Furusawa, Rustic Bldg. 7F, 77 Tenjin-cho, Shinjuku-ku, Tokyo 162-0808, Japan; +81 3 6802 4616, FAX +81 3 6802 4615, inquiry@sciencemag.jp; **asia news editor** Richard Stone (Beijing: rstone@aaas.org); **contributing correspondents** Dennis Normile [Japan: +81 (0) 3 3391 0630, FAX +81 (0) 3 5936 3531; dnormile@gol.com]; Hao Xin [China: cindyhao@gmail.com]; Pallava Bagla [South Asia: +91 (0) 11 2271 2896; pbagla@vsnl.com]

EXECUTIVE PUBLISHER **Alan I. Leshner**
PUBLISHER **Beth Rosner**

Fulfillment Systems and Operations (membership@aaas.org); **director** Waylon Butler; **customer service supervisor** Pat Butler; **specialists** Latoya Casteel, LaVonda Crawford, Vicki Linton, April Marshall; **data entry supervisor** Cynthia Johnson; **specialists** Shirlene Hall, Tarrika Hill, William Jones

Business Operations and Administration director Deborah Rivera-Wienhold; **business systems and financial analysis director** Randy Yi; **manager, business analysis** Eric Knott; **manager, business operations** Jessica Tierney; **financial analysts** Priti Pamnani, Celeste Troxler; **rights and permissions: administrator** Emilie David; **associate** Elizabeth Sandler; **marketing director** Ian King; **marketing managers** Allison Pritchard, Alison Chandler, Julianne Wielga; **marketing associates** Aimee Aponte, Mary Ellen Crowley, Wendy Wise; **senior marketing executive** Jennifer Reeves; **director, site licensing** Tom Ryan; **director, corporate relations** Eileen Bernadette Moran; **publisher relations, eresources specialist** Kiki Forsythe; **senior publisher relations specialist** Catherine Holland; **publisher relations, east coast** Phillip Smith; **publisher relations, west coast** Philip Tsolakidis; **fulfillment supervisor** Iquo Edim; **fulfillment coordinator** Carrie MacDonald; **marketing manager** Christina Schlecht; **marketing associate** Laura Tutino; **electronic media: manager** Lizabeth Harman; **project manager** Trista Snyder; **assistant manager** Lisa Stanford; **senior production specialists** Ryan Atkins, Christopher Coleman, **computer specialist** Walter Jones, Kai Zhang; **production specialists** Angela Forest, Nichele Johnston, Kimberly Oster; **director, web and new media** Will Collins

advertising director, worldwide ad sales Bill Moran
commercial editor Sean Sanders: 202-326-6430
assistant commercial editor Tianna Hicklin 202-326-6463
project director, outreach Brianna Blaser

Product (science_advertising@aaas.org); **midwest** Rick Bongiovanni: 330-405-7080, FAX 330-405-7081; **east coast/e. canada** Laurie Faraday: 508-747-9395, FAX 617-507-8189; **west coast/w. canada** Lynne Stickrod: 415-931-9782, FAX 415-520-6940; **uk/europe/asia** Roger Goncalves: TEL/FAX +41 43 243 1358; **japan** ASCA Corporation, Nanako Ide +81 (0) 3 6802 4616, FAX +81 (0) 3 6802 4615; ads@sciencemag.jp; **senior traffic associate** Deiandra Simms

worldwide associate director of *Science* Careers Tracy Holmes: +44 (0) 1223 326525, FAX +44 (0) 1223 326532

Classified (advertise@sciencecareers.org); **u.s.: midwest/west coast/south central/canada** Tina Burks: 202-326-6577; **east coast/industry** Elizabeth Early: 202-326-6578; **advertising operations manager** Kate Panganiban **sales coordinators** Rohan Edmonson, Shirley Young; **europe/row sales:** Susanne Kharraz, Dan Pennington, Alex Palmer; **sales assistant** Lisa Patterson; **japan** ASCA Corporation, Jie Chin +81 (0) 3 6802 4616, FAX +81 (0) 3 6802 4615; careerads@sciencemag.jp; **advertising support manager** Karen Foote: 202-326-6740; **advertising production operations manager** Deborah Tompkins; **senior production specialist/graphic designer** Amy Hardcastle; **production specialist** Yuse Lajiminmuhip; **senior traffic associate** Christine Hall

AAAS Board of Directors retiring president, chair Peter C. Agre; **president** Alice Huang; **president-elect** Nina Fedoroff; **treasurer** David E. Shaw; **chief executive officer** Alan I. Leshner; **board** Linda P. B. Katehi, Nancy Knowlton, Stephen Mayo, Cherry A. Murray, Julia M. Phillips, Sue V. Rosser, David D. Sabatini, Thomas A. Woolsey

AAAS
ADVANCING SCIENCE, SERVING SOCIETY

SENIOR EDITORIAL BOARD

John I. Brauman, *Chair, Stanford Univ.*
Richard Losick, *Harvard Univ.*
Linda Partridge, *Univ. College London*
Michael S. Turner, *University of Chicago*

BOARD OF REVIEWING EDITORS

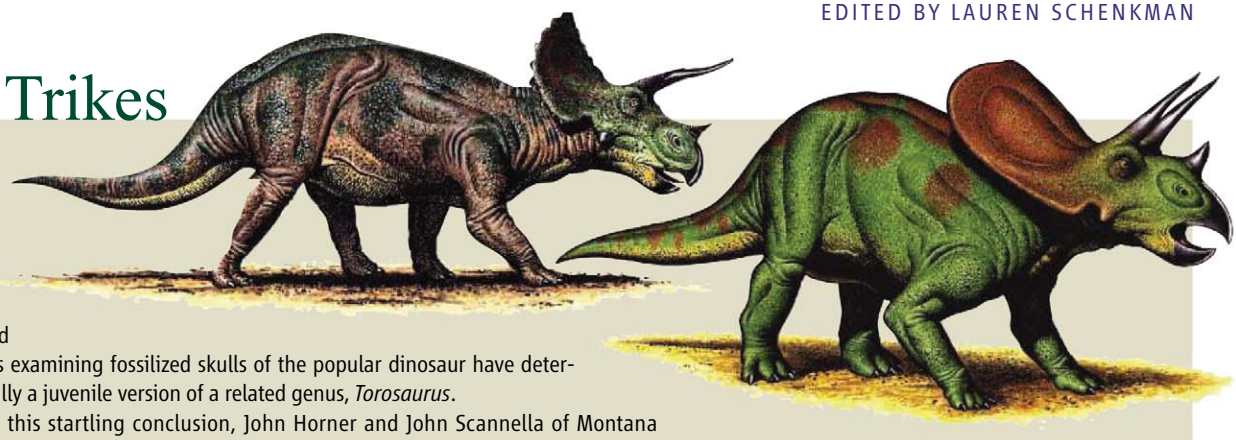
Adriano Aguzzi, *Univ. Hospital Zürich*
Takuzo Aida, *Univ. of Tokyo.*
Sonia Altizer, *Univ. of Georgia*
David Altshuler, *Broad Institute*
Arturo Alvarez-Buylla, *Univ. of California, San Francisco*
Richard Amasino, *Univ. of Wisconsin, Madison*
Angelika Amon, *MIT*
Kathryn Anderson, *Memorial Sloan-Kettering Cancer Center*
Siv G. E. Andersson, *Uppsala Univ.*
Peter Andolfatto, *Princeton Univ.*
Meinrat O. Andreae, *Max Planck Inst., Mainz*
John A. Bargh, *Yale Univ.*
Ben Barres, *Stanford Medical School*
Marisa Bartolomei, *Univ. of Penn. School of Med.*
Jordi Bascompte, *Estación Biológica de Doñana, CSIC*
Facundo Batista, *London Research Inst.*
Ray H. Baughman, *Univ. of Texas, Dallas*
Yasmine Belkaid, *NIAID, NIH*
Stephen J. Benkovic, *Penn State Univ.*
Gregory C. Beroza, *Stanford Univ.*
Ton Bisseling, *Wageningen Univ.*
Mina Bissell, *Lawrence Berkeley National Lab*
Peer Bork, *EMBL*
Robert W. Boyd, *Univ. of Rochester*
Paul M. Brakefield, *Leiden Univ.*
Christian Büchel, *Universitätsklinikum Hamburg-Eppendorf*
Joseph A. Burns, *Cornell Univ.*
William P. Butz, *Population Reference Bureau*
Mats Carlsson, *Univ. of Oslo*
Mildred Cho, *Stanford Univ.*
David Clapham, *Children's Hospital, Boston*
David Clary, *Oxford University*
J. M. Claverie, *CNRS, Marseille*
Jonathan D. Cohen, *Princeton Univ.*
Andrew Cossins, *Univ. of Liverpool*
Robert H. Crabtree, *Yale Univ.*
Wolfgang Cramer, *Potsdam Inst. for Climate Impact Research*
F. Fleming Crim, *Univ. of Wisconsin*
Jeff L. Dangl, *Univ. of North Carolina*
Stanislas Dehaene, *Collège de France*
Edward DeLong, *MIT*
Emmanouil T. Dermitzakis, *Univ. of Geneva Medical School*
Robert Desimone, *MIT*
Claude Desplan, *New York Univ.*
Dennis Discher, *Univ. of Pennsylvania*
Scott C. Doney, *Woods Hole Oceanographic Inst.*
Jennifer A. Doudna, *Univ. of California, Berkeley*
Julian Downward, *Cancer Research UK*
Bruce Dunn, *Univ. of California, Los Angeles*
Christopher Dye, *WHO*
Michael B. Elowitz, *Calif. Inst. of Technology*
Gerhard Ertl, *Fritz-Haber-Institut, Berlin*
Mark Estelle, *Indiana Univ.*
Barry Everitt, *Univ. of Cambridge*
Paul G. Falkowski, *Rutgers Univ.*
Ernst Fehr, *Univ. of Zurich*
Tom Fenchel, *Univ. of Copenhagen*
Alain Fischer, *INSERM*
Wulfram Gerstner, *EPFL Lausanne*
Charles Godfray, *Univ. of Oxford*
Diane Griffin, *Johns Hopkins Bloomberg School of Public Health*
Christian Haass, *Ludwig Maximilians Univ.*
Steven Hahn, *Fred Hutchinson Cancer Research Center*
Gregory J. Hannon, *Cold Spring Harbor Lab.*
Niels Hansen, *Technical Univ. of Denmark*
Dennis L. Hartmann, *Univ. of Washington*
Chris Hawkesworth, *Univ. of St Andrews*
Martin Heimann, *Max Planck Inst., Jena*
James A. Hendler, *Rensselaer Polytechnic Inst.*
Janet G. Hering, *Swiss Fed. Inst. of Aquatic Science & Technology*
Ray Hilborn, *Univ. of Washington*
Michael E. Himmel, *National Renewable Energy Lab.*
Kei Hirose, *Tokyo Inst. of Technology*
Ove Hoegh-Guldberg, *Univ. of Queensland*
Lora Hooper, *UT Southwestern Medical Ctr at Dallas*
Ronald R. Hoy, *Cornell Univ.*
Jeffrey A. Hubbell, *EPFL Lausanne*
Steven Jacobsen, *Univ. of California, Los Angeles*
Peter Jonas, *Universität Freiburg*
Barbara B. Kahn, *Harvard Medical School*
Daniel Kahne, *Harvard Univ.*
Bernhard Keimer, *Max Planck Inst., Stuttgart*
Robert Kingston, *Harvard Medical School*
Hanna Kokko, *Univ. of Helsinki*
Alberto R. Kornblihtt, *Univ. of Buenos Aires*
Leonid Kruglyak, *Princeton Univ.*
Lee Kump, *Penn State Univ.*
Mitchell A. Lazar, *Univ. of Pennsylvania*
David Lazer, *Harvard Univ.*
Virginia Lee, *Univ. of Pennsylvania*
Julian Lewis, *Cancer Research UK*
Olle Lindvall, *Univ. Hospital, Lund*
Marcia C. Linn, *Univ. of California, Berkeley*
John Lis, *Cornell Univ.*
Richard Losick, *Harvard Univ.*
Ke Lu, *Chinese Acad. of Sciences*
Laura Machesky, *CRUK Beatson Inst. for Cancer Research*
Andrew P. MacKenzie, *Univ. of St Andrews*
Anne Magurran, *Univ. of St Andrews*
Oscar Marin, *CSIC & Univ. Miguel Hernández*
Charles Marshall, *Univ. of California, Berkeley*
Martin M. Matzuk, *Baylor College of Medicine*
Grahma Medley, *Univ. of Warwick*
Virginia Miller, *Washington Univ.*
Yasushi Miyashita, *Univ. of Tokyo*
Richard Morris, *Univ. of Edinburgh*
Edvard Moser, *Norwegian Univ. of Science and Technology*
Sean Munro, *MRC Lab. of Molecular Biology*
Naoto Nagaosa, *Univ. of Tokyo*
James Nelson, *Stanford Univ. School of Med.*
Timothy W. Nilsen, *Case Western Reserve Univ.*
Pär Nordlund, *Karolinska Inst.*
Helga Nowotny, *European Research Advisory Board*
Stuart H. Orkin, *Dana-Farber Cancer Inst.*
Christine Ortiz, *MIT*
Elinor Ostrom, *Indiana Univ.*
Andrew Oswald, *Univ. of Warwick*
Jonathan T. Overpeck, *Univ. of Arizona*
P. David Pearson, *Univ. of California, Berkeley*
John Pendry, *Imperial College*
Reginald M. Penner, *Univ. of California, Irvine*
John H. J. Petrini, *Memorial Sloan-Kettering Cancer Center*
Simon Phillpot, *Univ. of Florida*
Philippe Poulin, *CNRS*
Colin Renfrew, *Univ. of Cambridge*
Trevor Robbins, *Univ. of Cambridge*
Barbara A. Romanowicz, *Univ. of California, Berkeley*
Jens Rostrup-Nielsen, *Haldor Topsoe*
Edward M. Rubin, *Lawrence Berkeley National Lab*
Shimon Sakaguchi, *Kyoto Univ.*
Michael J. Sanderson, *Univ. of Arizona*
Jürgen Sandkühler, *Medical Univ. of Vienna*
Randy Seeley, *Univ. of Cincinnati*
Christine Seidman, *Harvard Medical School*
David Sibley, *Washington Univ*
Joseph Silk, *Univ. of Oxford*
Montgomery Slatkin, *Univ. of California, Berkeley*
Davor Solter, *Inst. of Medical Biology, Singapore*
Allan C. Spradling, *Carnegie Institution of Washington*
Jonathan Sprent, *Garvan Inst. of Medical Research*
Elsbeth Stern, *ETH Zürich*
Yoshiko Takahashi, *Nara Inst. of Science and Technology*
Jurg Tschopp, *Univ. of Lausanne*
Herbert Virgin, *Washington Univ.*
Bert Vogelstein, *Johns Hopkins Univ.*
Bruce D. Walker, *Harvard Medical School*
Christopher A. Walsh, *Harvard Medical School*
David A. Wardle, *Swedish Univ. of Agric Sciences*
Colin Watts, *Univ. of Dundee*
Detlef Weigel, *Max Planck Inst., Tübingen*
Jonathan Weissman, *Univ. of California, San Francisco*
Sue Wessler, *Univ. of Georgia*
Ian A. Wilson, *The Scripps Res. Inst.*
Timothy D. Wilson, *Univ. of Virginia*
Xiaoliang Sunney Xie, *Harvard Univ.*
John R. Yates III, *The Scripps Res. Inst.*
Jan Zaanen, *Leiden Univ.*
Mayana Zatz, *University of Sao Paolo*
Huda Zoghbi, *Baylor College of Medicine*
Maria Zuber, *MIT*

BOOK REVIEW BOARD

John Aldrich, *Duke Univ.*
David Bloom, *Harvard Univ.*
Angela Creager, *Princeton Univ.*
Richard Shweder, *Univ. of Chicago*
Ed Wasserman, *DuPont*
Lewis Wolpert, *Univ. College London*

EDITED BY LAUREN SCHENKMAN

Tricky Trikes



Dinosaur buffs, you may want to sit down for this: *Triceratops* was not quite the critter you have come to know and love. Paleontologists examining fossilized skulls of the popular dinosaur have determined that it's actually a juvenile version of a related genus, *Torosaurus*.

Before reaching this startling conclusion, John Horner and John Scannella of Montana State University, Bozeman, spent 10 years studying every *Triceratops* (above left) and *Torosaurus* (above right) fossil ever unearthed. By microscopically examining signs of growth in the skulls and bones, the pair determined approximately how old each of the more than 50 animals was at the time of its death. The *Triceratops* fossils, it turned out, were all from either babies or juveniles, whereas the torosaurs were all either young adults or fully mature.

When laid out from youngest to oldest, the skulls showed a gradual but striking evolution: *Triceratops*'s thick horns thinned, lengthened, and changed orientation slightly as it grew older. Its signature jagged neck frill, meanwhile, smoothed out into the round frill typical of torosaurs, the team reported in the July *Journal of Vertebrate Paleontology.*

The morphing was possible because the dinosaur's skull, horns, and frill never fully develop into hard bone but instead stay relatively plastic, Horner says. Analysis of the more mature animals showed that their skulls were continuing to change.

Horner has good news for *Triceratops* fans: Despite the discovery, the beloved name isn't going anywhere. Because paleontologists named the genus *Triceratops* first, he says, "*Torosaurus* is the name that is being delisted."

THEY SAID IT

"Ooh my / I ain't nothing but a tour guide, / Using science like an x-ray to see into your mind / … Yeah welcome to the future, baby, / A time when science is even illuminating / The roots of human behavior."

—Canadian "lit-hop" artist Baba Brinkman, from his album *The Rap Guide to Human Nature*, released this month. A follow-up to *The Rap Guide to Evolution*, the new album is an "introduction to evolutionary psychology and the science of human behaviour," he writes on his blog. In one song, for instance, Brinkman raps a nature-video-style analysis of the human behavior he observes at a night club.

'Ick' Factor

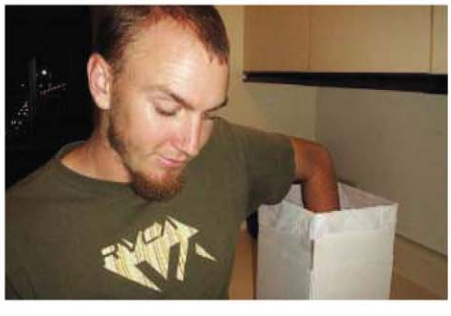
If you've ever found yourself wrist deep in peeled grapes at a Halloween party, then a new study's results won't surprise you: Researchers have found that touch and disgust can—quite literally—go hand in hand.

Scientists consider disgust a universal emotion and think it probably evolved to help people avoid pathogens. Gagging at the smell of rotten eggs, for example, discourages hungry humans from eating spoiled food that could make them sick.

Psychologist Debra Lieberman and colleagues at the University of Miami in Florida wondered whether the often-overlooked sense of touch could elicit that icky feeling. So the team brought the classic Halloween game into the lab: They asked 50 students to touch and rate the yuckiness of wet and dry pieces of rope and dough that were hidden out of sight in boxes. The students consistently ranked the wet items as more disgusting and found the wet dough to be the grossest of all.

That's natural enough, says Lieberman, because soft, moist things have a more "biological consistency"—that is, they're more reminiscent of the wet environments in which pathogens like to live.

The study, published online 20 July in *Cognition & Emotion*, is the first of its kind and "makes a lot of sense," says Daniel Fessler, an evolutionary anthropologist at the University of California, Los Angeles. But he notes that testing a more cross-cultural selection of disgustees would strengthen the results. "We live in a society of soap and Purell," he says. "College-age Americans are probably the most disgust-sensitive population in the world."



Citizen Scientist



University of Southern California (USC) neuroscientist Roberta Diaz Brinton was among 13 people honored at the White House last week with the 2010 Presidential Citizens Medal, the nation's second highest civilian honor. Brinton, who studies how aging and neurodegenerative disease affect the neural mechanisms of cognition, was recognized for her contributions to science and technology education.

"When I was a graduate student in neuropharmacology, I was one of the only females and the only student from a working-class background, and I was determined somehow to change that," Brinton says. After meeting a group of promising high school students whose classroom was a trailer in the back lot of a school in East Los Angeles, Brinton founded the USC STAR Program, which she has directed for the past 19 years. The program teaches elementary through high school students and their teachers about science and provides hands-on research opportunities in labs at USC.

CREDITS (TOP TO BOTTOM): © ROBERT WALTERS; STEVEN HELLER/USC; DEBRA LIEBERMAN



Tropical mosquitoes in the Netherlands 736



Evidence of early tool use 738



GULF OIL SPILL

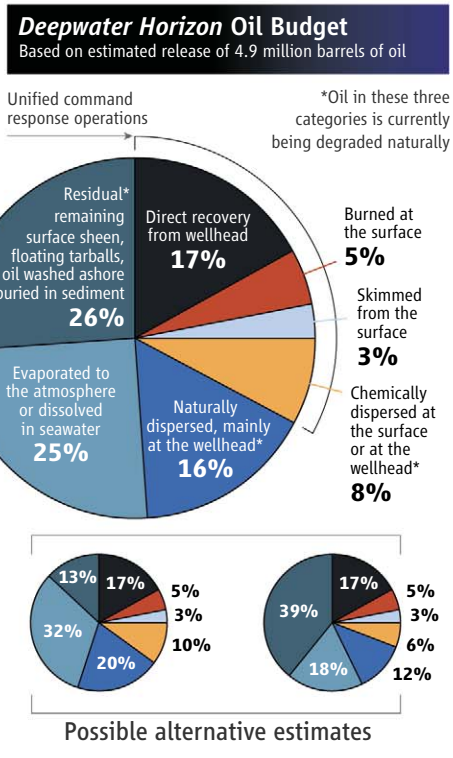
A Lot of Oil on the Loose, Not So Much to Be Found

Now that the gusher that spewed oil for 85 days into the Gulf of Mexico has stopped, scientists are wondering where it all went. A federal report released last week should have begun to answer that question. Instead, political spin and media hype transformed the scientists' message even before it was released. According to one CNN reporter, the interagency report led by the Department of the Interior and the National Oceanic and Atmospheric Administration (NOAA) said that of the 4.9 million barrels of oil spilled, "75% has been cleaned up by Man or Mother Nature."

Nothing in the report supports that interpretation. But there are multiple ways to read the report's iconic pie chart while remaining grounded in fact. One is that responders have—with herculean effort—intercepted 25% of the oil, leaving 75% to have its way with the environment. Under this interpretation, "raising the flag and declaring victory is premature," says biogeochemist Samantha Joye of the University of Georgia, Athens.

Another take on the report finds that three-quarters of the oil is gone from the gulf or is dispersed in the water in its most easily degraded form. This remaining oil "is degrading quickly right now," says marine geochemist Edward Overton of Louisiana State University, Baton Rouge.

Overton and other optimists note that today official maps from NOAA no longer show any surface oil in the gulf. And the "massive" deep oil plumes of media fame now appear to have been faint shadows of their public images. Resolving the inevitable uncertainties and filling in the gaps of such an early report will no doubt take many months.



Fuzzy budget. A federal report divvies up the oil (*top*) but allows for uncertainties (*bottom*).

The report's most certain conclusion was that responders managed to collect or remove about 25% of the oil released from the damaged well. Seventeen percent was collected at the wellhead in an unprecedented technological feat. About 5% was burned at the surface, an exceptionally large proportion for a U.S. spill, experts say. But skimmers captured only 3% of the total, despite the high-profile effort. Such meager results are to be expected in the open ocean, says William Lehr of NOAA's emergency response division in Seattle, Washington, who worked on the report. Less than 0.1% had been recovered from beaches and marshes.

That leaves 75% of the spill that remained in the environment, but just how it entered it—as oily scum on the surface, as more readily degraded microscopic droplets at depth, or as vapors into the atmosphere—is far less certain. That's because these flows were calculated, not measured. Despite the seeming precision of the pie chart, "there's a large degree of uncertainty," says Lehr. Uncertainties crop up, for example, in calculations of "natural dispersion" involving the physics of oil and gas jetting into seawater from the wellhead. These calculations yield an estimate of how much oil ends up dispersing as droplets smaller than 100 micrometers in diameter. That's the size range that can drift away in a horizontal plume the way dust can float in the air.

Add up all the uncertainties and they can be considerable. There are uncertainties in calculating the natural and chemical dispersion that produces deep plumes as well as dissolution in seawater or evaporation from the surface. Then there is the ±10% uncertainty in the total volume of the spill. All told, the "residual oil"—what could not be measured or estimated but is left to float as tarballs or be washed ashore—could be as high as 39% of the total or as low as 13%, by a simple accounting from charts in the report's supplement.

Perhaps the most muddled calculation involves the fraction of oil that went into the dreaded subsurface plumes. The media "created an image of an underwater river of oil," says Steven Murawski, NOAA's chief scientist for fisheries in Silver Spring, Maryland, who is overseeing spill science for NOAA. "In a glass, [plume water] looks like clear seawater." He says that measurements of oil reveal a principal plume confined to depths of 1000 meters to 1300 meters that in spots

CREDITS (TOP TO BOTTOM): AFP/GETTY IMAGES; ADAPTED FROM NOAA/DOI



Human evolution in action

740



Climate history in ice caves

746

contained 1 to 2 parts per million of oil (1 or 2 milliliters in a cubic meter of seawater). Most parts of the plume, however, had lower concentrations; farther than 10 kilometers from the wellhead, concentrations were in the parts-per-billion range.

If something like 20% of the oil—15,000 barrels a day—dispersed into the deep sea, as the report has it, precious little of it has been showing up in plume observations. That raises the issue of biodegradation and how quickly microbes might be consuming the oil. The report states that according to early signs, the oil "is biodegrading quickly." It provides no documentation for that claim, while hearsay about observations awaiting publication and public release is mixed. "The message I've heard is that everywhere we look, oil is degrading extremely rapidly," says Overton. Joye, who has generated some of the relevant data, is more cautious. "Sure it's getting degraded, but we don't know how fast," she says.

Ultimately, determining the rates of oil degradation, evaporation, and dilution in the gulf rather than this report's parsing of the oil's immediate fate will show where the oil went. Such analysis should determine whether, as Lehr puts it, "Mother Nature is almost always the best removal mechanism."

–RICHARD A. KERR

GULF OIL SPILL

An Audacious Decision in Crisis Gets Cautious Praise

How BP came to spray 1.1 million gallons of chemical dispersants a mile beneath the ocean surface is a story of scientists turning to desperate measures during desperate times. And the government's decision to let BP do so, among the most gutsy calls of the entire *Deepwater Horizon* saga, was a classic case of pitting the devil you know against the devil you don't.

Roughly a week after the magnitude of the gusher became clear in late April, former Exxon-Mobil scientist Gerard Canevari suggested that BP might try spraying chemicals called dispersants right at the billowing wellhead. Dispersants are usually used in small quantities on the surface of the ocean to break up slicks. Canevari's idea would mean releasing giant amounts of the fairly nasty chemicals in the cold and high-pressure world of the ocean floor, something that had never been tried. "At first we were going, 'Yeah, right,'" recalls Charlie Henry, a top scientist on Gulf of Mexico issues for the National Oceanic and Atmospheric Administration (NOAA). "It was out of the norm"—a massive proposed undersea experiment.

But, he says, the unprecedented nature of the problem meant nothing was off the table. While outlining the pros and cons on white boards in NOAA's New Orleans office, says Henry, the basic tradeoff seemed clear. Every drop of oil that made it to the surface was a potential threat to coastal ecosystems, fish, and marine mammals. Dispersants, which are mostly detergents, break up globs of crude into microscopic droplets that are more readily devoured by microbes. So keeping as much oil as possible below the surface would give microbes a leg up in eating the oil. And injecting dispersants into the hot, vigorously mixing oil of the busted riser would presumably mean they would work especially effectively. Smaller quantities would then presumably be needed at the ocean surface.

Some drawbacks emerged during a conference call with 25 industry and academic scientists arranged by NOAA in early May: The risks to undersea marine life—eggs, larvae, fish, coral, and other bottom dwellers—were largely unknown. One possibility was particularly frightening: Giving microbes a feast of hydrocarbons might massively increase their numbers, starving the water column of oxygen and creating dead zones.

So government scientists proposed a three-tiered plan to try the undersea injection as safely as possible. First, teams across the country began adapting existing undersea models of oil plumes to predict how they might move, referencing data on nearby sea life from the Department of the Interior. Second, they required that BP conduct aggressive monitoring, including ocean surface-to-floor water sampling, toxicity tests using zooplankton, and tests with fluorometers, which would continuously track the oil droplets. And if the dispersant injection created unexpected effects during tests, an "adaptive management" plan would enable the feds to halt the procedure immediately.

The Environmental Protection Agency (EPA) and the Coast Guard agreed to the procedure on 15 May. "I don't think I've had to make a harder decision," EPA Administrator Lisa Jackson told reporters at the time. BP deployed a specially built tube with tiny ▶





Desperate measures. Spraying chemical dispersants at the undersea wellhead seems to have spared coastal ecosystems, but at what cost?

CREDITS: REUTERS (INSET); AFP/GETTY IMAGES

holes that was clamped in place to release the chemical right at the spurting pipe.

On 27 May, the first real vetting of the new approach came at a meeting of scientists culled largely from academia and the nonprofit sector, hastily organized by NOAA. The outsiders were asked "to second-guess us," says Henry. Chemist Jeffrey Short of Washington, D.C.–based Oceana recalls feeling skeptical on his way to Louisiana State University (LSU). "You don't want me down there; you know what I think about dispersants," he told Nancy Kinner of the University of New Hampshire, the organizer.

But the fluorometry data presented at LSU showed that the dispersant was working and had broken up the big globs into droplets between 1 and 10 micrometers—and the microbial feast wasn't starving the system of oxygen. So after 2 days of intense debate, Short and the rest of the group gave their approval in a report. "I was struck by the fact that all 50 were in agreement that continuing the subsurface injection was the best option in a bad situation," recalls toxicologist Ronald Tjeerdema of the University of California, Davis.

Since then, researchers have by and large stuck with that opinion. NOAA estimates that roughly 409,000 barrels of oil have been dispersed underwater by the technique. Toxicity tests have suggested an acute risk of dispersant-oil mixtures no greater than that of oil alone. Daniels says some of the dispersed oil has risen toward the surface, while some has formed a loose band, or plume, between 1000 and 1300 meters in depth. No negative impacts on deep-sea life have yet been recorded, although NOAA Administrator Jane Lubchenco says one of the worst case scenarios involving longer exposures due to dispersed oil—big losses of spawning bluefin tuna populations—may not be detectable for years. That's led some scientists to suggest that letting the oil rise to the surface would have been a better move, as it could be more easily collected.

Jacqueline Savitz, an environmental scientist with Oceana, says because of the unknown risks of dispersants, it was "a lose-lose" decision—and despite optimistic projections (p. 734), all the benefits and costs may not be known for decades. **–ELI KINTISCH**

With reporting by Erik Stokstad.

INFECTIOUS DISEASES

Yellow Fever Mosquito Shows Up in Northern Europe

AMSTERDAM—In the latest display of mosquitoes' predilection for modern travel, entomologists have found a small colony of the tropical species *Aedes aegypti*—also known as the yellow fever mosquito—in the Netherlands. The insects were found on and near two facilities of a company that imports used tires and presumably originated in the hot southern part of the United States. *Ae. aegypti* is an important vector not just of yellow fever but also of two other viral diseases, dengue and chikungunya.



The mosquitoes, found by a team led by Ernst-Jan Scholte of the Dutch government's Center for Vector Monitoring, don't pose a direct public health threat and are unlikely to survive the winter, says Scholte. Still, scientists are amazed, because the insects were last seen in Europe more than 50 years ago. "You're kidding. … Really?" entomologist Paul Reiter of the Pasteur Institute in Paris says when told about the find. "Wow."

Ae. aegypti originated in Africa but has colonized tropical and subtropical areas around the world. It's notorious as the vector of the dengue virus, which can cause severe malaise and fever, unbearable joint pains, and a fatal syndrome called dengue hemorrhagic fever. *Ae. aegypti* once roamed southern Europe as well but probably disappeared after World War II, says Reiter, perhaps in response to DDT spraying. Although the Dutch climate may be inhospitable for the species, a similar transplantation to southern Europe could trigger a recolonization, says Francis Schaffner, a French mosquito-control expert at the University of Zürich in Switzerland.

The team found the mosquitoes during a routine surveillance program aimed at keeping out another species, the Asian tiger mosquito, or *Ae. albopictus*, which can transmit dengue and chikungunya as well. That mosquito has relentlessly colonized new territory over the past 2 decades, becoming a highly annoying fixture in many Mediterranean countries, from where it is now pushing northward (*Science*, 16 May 2008, p. 864). The "tiger" is known to hitch a ride in secondhand tires, shipped around the world in containers. In the Netherlands, tiger mosquitoes have also been found in greenhouses that import lucky bamboo, a popular plant from Asia.



Foreign trade. Spraying started at a Dutch tire yard on 30 July to wipe out three exotic mosquito species, including *Aedes aegypti* (*inset*).

But *Ae. aegypti* was not known to be such a frequent stowaway. When Scholte's team first caught the intruder in one of their traps, they misidentified it as a tiger mosquito, which they also found in the same area. When a genetic test unmasked it as *Ae. aegypti*, "I couldn't believe it, a tropical mosquito flying around in Holland," says Scholte. The team believes the most likely origin for both species is a tire shipment from Miami—where both occur—that arrived in late May.

Both last summer and this year, the team also found a third foreign species, *Ae. atropalpus*, or the American rock pool mosquito, near the tire importer. That species inhabits the northern United States and southeastern Canada and probably would have little trouble establishing itself this far north in Europe, says Scholte. But *Ae. atropalpus* is not believed to be an important disease vector.

The Dutch government—which ceased mosquito-control operations decades ago—has hired Schaffner and another French expert to help get rid of all three species, using a two-pronged attack involving deltamethrin for adults and biological control for larvae. Schaffner believes it's possible to nip the incursion of all three species in the bud. But countries that monitor for new invasions less rigorously may not be so lucky, says Scholte. "It's the shape of things to come," says Reiter. "Everything can be imported everywhere." **–MARTIN ENSERINK**

CREDITS: WIKIPEDIA (INSET); FRANCIS SCHAFFNER

ScienceNOW

From *Science's* Online Daily News Site



WHY MONGOOSE MOMS SYNCHRONIZE BIRTHS

Four times a year, a female mongoose gives birth to her pups on the exact same night as more than half of the other females in her group. The small carnivores aren't planning a massive birthday celebration. Rather, they're trying to ensure the survival of their pups. Researchers report in *Biology Letters* that mongoose litters born a day or two earlier than others were 30% more likely to be killed by adult female mongooses. These females don't want competition for their own offspring, so they kill the pups while their mothers are out foraging. But if the litters are born together, all of the moms are out foraging at the same time—so there's no one left behind to kill the babies. Similar scenarios in ancient human societies may explain why women often sync up their menstrual cycles if they spend a lot of time together. http://bit.ly/moms-sync



Turning Scar Tissue Into a Beating Heart

After a heart attack, the heart forms scar tissue dominated by fibroblasts, heart muscle cells that provide structural support. This leaves it with fewer cardiomyocytes, the muscle cells that beat—and thus less pumping capacity. But now a team has used a technique called cellular reprogramming to transform one cell into the other.

Developmental biologist Deepak Srivastava and cardiovascular researcher Masaki Ieda of the Gladstone Institute of Cardiovascular Disease in San Francisco, California, and their colleagues identified a trio of genes that together helped fibroblast cells take on characteristics of cardiomyocytes (pictured). The team inserted extra copies of the genes into lab-grown cardiac fibroblasts. After growing for a month, the reprogrammed cells began to contract, like beating heart cells, the researchers report in *Cell*.

Ideally, Srivastava says, researchers will find small molecules that can replace the three-gene cocktail. Such molecules could be applied directly to an injured heart and turn fibroblasts into cardiomyocytes. http://bit.ly/heart-cells

Busy Brains, Deeper Sleep

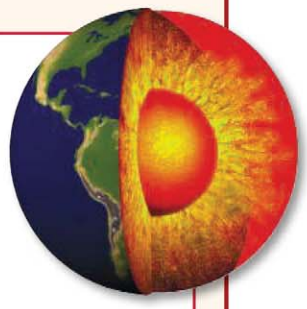
Sound sleepers share a surprising secret: a bustling brain.

Researchers long thought that people who can sleep through anything spend more time in the deeper stages of sleep. But Harvard Medical School sleep researcher Jeffrey Ellenbogen focused on something else: sleep spindles. These brief bursts of brain activity emanate from the thalamus, a brain region that regulates sleep and also processes and relays sensory information to the cerebral cortex.

To show the connection, Ellenbogen and colleagues played sounds like flushing toilets, loud conversations, ringing phones, and car traffic to 12 sleepers, gradually raising the volume of each sound until each sleeper stirred. When the team matched the sleepers' spindle production—which ranged from three to six spindles per minute and remained consistent for each sleeper across the nights—to the loudness required to rouse them, they found that sleepers with higher spindle rates were harder to wake up. The spindles seem to indicate when the thalamus is blocking noise from reaching the cortex and disrupting sleep, the team reports in *Current Biology*.

Researchers say the discovery could lead to spindle-enhancing techniques that offer lighter sleepers a chance at dead-to-the-world rest. http://bit.ly/deep-sleep

Earth's Moving, Melting Core



Earth's inner core acts in ways that befuddle scientists. But a new model might finally explain what's going on.

Researchers speculate that the inner core, a solid ball of mostly iron 1200 kilometers across, absorbs and hardens molten iron from the liquid outer core. This should make the liquid at the boundary lighter; instead, it's denser. The model also doesn't explain why seismic waves from earthquakes travel faster on the eastern side of the inner core than on the western side.

A new model published in *Nature* now gives the most plausible answer so far to these riddles, say experts. Lead author Thierry Alboussière, a geophysicist at the Laboratoire de Géophysique Interne et Tectonophysique in Grenoble, France, suggests that the inner core crystallizes in the west and melts in the east. The solid iron "moves" eastward at a pace of roughly 1.5 centimeters per year, melting when it reaches the eastern edge.

The model would explain why the liquid layer at the boundary between the inner and outer cores is denser than the rest of the outer core: It's fluid that has just melted out of the dense inner core. The lopsided melting would also account for the difference in seismic wave speeds. http://bit.ly/core-melt

Read the full postings, comments, and more at **news.sciencemag.org/sciencenow**.

CREDITS (TOP TO BOTTOM): ANDY YOUNG; THINKSTOCK; M. IEDA *ET AL.*, *CELL*, **142** (6 AUGUST 2010) ©ELSEVIER INC.

PALEOANTHROPOLOGY

Lucy's Toolkit? Old Bones May Show Earliest Evidence of Tool Use

Two nondescript scraps of animal bone that most fossil hunters would have left on the ground are being offered as the earliest known evidence for the first technological revolution in human evolution. A rib and a shaft of a thighbone bear "unambiguous evidence" of stone-tool marks made 3.4 million years ago by a member of the human family who used sharp stones to cut the meat off the bone and pound the bone open for marrow, according to a paper published this week in *Nature*. "This find will definitely force us to revise our textbooks on human evolution, since it pushes the evidence for tool use and meat eating in our family back by nearly a million years," says Ethiopian paleoanthropologist Zeresenay Alemseged of the California Academy of Sciences in San Francisco. Alemseged directs the Dikika Research Project, which found the bones last year in the Afar Depression of Ethiopia.

The age of the marks pegs them as the handiwork of *Australopithecus afarensis*, a species made famous by the 3.2-million-year-old partial skeleton nicknamed Lucy, says Alemseged. That suggests that our ancestors were already using sharp stones to cut meat when their brains and bodies were barely bigger than a chimpanzee's. The earliest known stone tools don't appear until 800,000 years later—also in Ethiopia—so some researchers say it will take more than two bones found on the surface to convince them that the marks were made by hominins instead of animals. Others, however, think the marked bones offer a glimpse of the earliest stage of tool use. "This is really a very exciting find," says archaeologist David Braun of the University of Cape Town in South Africa, who is not a co-author. "This find emphasizes that tool use and carnivory have very deep roots in human ancestry."

The butchered bones were found at Dikika, just 222 meters from the spot where Alemseged discovered the remarkably complete skeleton of Selam, a 3.3-million-year-old child of the species *A. afarensis* (*Science*, 22 September 2006, p. 1716). In January 2009, Alemseged and other members of an international team of researchers were using a new method to collect every scrap of bone from large mammals at Dikika so they could reconstruct the ancient environment there. Archaeologist Shannon McPherron of the Max Planck Institute for Evolutionary Anthropology in Leipzig, Germany, says he picked up an unimpressive rib from a cow-size ungulate and saw two "obvious, V-shaped cut marks." A few moments later, he found a thighbone shaft from a goat-sized antelope, with many cut marks on it. "In this case, they were incredibly obvious cut marks. But they were so old, we wanted to play it cautious," says McPherron.

Back in camp, the researchers examined the bones under a microscope and concluded that the marks were made when a hominin cut flesh from the bones and pounded the bones open for marrow. Later, paleoanthropologist Curtis Marean of Arizona State University in Tempe examined the bones and concluded that the marks were made by stone rather than by carnivore teeth. Other members of the team used secondary electron imaging and energy-dispersive x-ray spectrometry to show that the marks were created before the bones fossilized. They also found a tiny piece of rock embedded in a cut mark, per-



ENVIRONMENT

Russia's Forest Fires Ignite Concerns About Chornobyl's Legacy

Hot zone. Fires ripping through Russia's forests (*left*) sparked fears of a blaze among Chornobyl's radiation-contaminated tress.

CREDIT: AP IMAGES

In the midst of an unprecedented heat wave this summer, Russia has been scrambling to respond to a devastating epidemic of forest fires, some of which have threatened nuclear research and weapon facilities. Officials in Moscow last week warned of a further nightmarish scenario: Fires could spread to neighboring Ukraine, to its forests contaminated by the 1986 Chornobyl nuclear accident, sending radioactive smoke high into the air and downwind.

As *Science* went to press, this had not happened, but several forestry experts in Ukraine and abroad say a catastrophic fire will eventually break out in the forests of the Chornobyl Exclusion Zone, which covers 260,000 hectares—unless Ukrainian officials take action to reduce the growing risks of a conflagration. The Chornobyl forest "is ready to burn, now," says Chadwick Oliver, director of the Yale Global Institute of Sustainable Forestry. And a really big fire, he says, "can volatilize organic matter and move particles hundreds of kilometers."

Because the forest is contaminated, no one is managing it, thinning out trees, or harvesting those that are dying. It is even illegal to take lumber out of the Exclusion Zone; if trees are cut, they just stay in piles on the ground. On one recent visit to Chornobyl, Sergiy Zibtsev of Ukraine's National University of Life and Environmental Sciences in Kiev says he discovered "a really dangerous situation": a huge area, inaccessible by road, filled with downed, dead trees.

Although even the most ferocious fire in the exclusion zone would release only a tiny fraction of the radiation from the reactor accident, firefighters would face the clearest danger, mainly from the risk of inhaling particles of plutonium left behind by the nuclear reactor accident. "I worry about them, very much," says Zibtsev, who has met the region's firefighters during his frequent trips to Chornobyl. Villages or cities downwind would not have to be evacuated, according to a computer



Butchered? Fossil bones found in Ethiopia may show traces of early carving and pounding for marrow.

haps left during the butchering.

Radiometric dating of the sediments at Dikika shows that the marked bones date to almost 3.4 million years ago—a time when the only known hominin in east Africa was *A. afarensis*. This means the animals could have been butchered by Lucy's species. But Lucy had a brain and body barely larger than a chimp's, suggesting that our ancestors began using sharp stones to carve meat long before they had developed big brains or specialized hands, once thought to be prerequisites for tool use.

To butcher an ungulate as large as a cow, the researchers say, *A. afarensis* must have ventured into dangerous terrain to compete with other carnivorous scavengers, such as hyenas. That possibility should make researchers take a fresh look at scraps of animal bone from 3.7 million years ago, when *A. afarensis* arose, to 2.6 million years ago, when the first tools appear at Gona, Ethiopia. Others, though, say researchers have already scoured *A. afarensis* fossil sites for stone tools and cut marks and come up empty-handed. To push back tool use so early, they want to see more bones—and stronger evidence that the marks were not made by animals. "Extraordinary claims demand extraordinary evidence," says paleoanthropologist Tim White of the University of California, Berkeley.

–ANN GIBBONS

CREDIT: DIKIKA RESEARCH PROJECT

simulation of a "worst-case" conflagration carried out by forest specialist Aaron Hohl of Humboldt State University in California. But such a fire might cause mass panic and force many farmers to discard contaminated crops.

Hohl presented his preliminary results, which are currently going through peer review, at a conference last October in Kiev. Organizers of the conference, including Zibtsev, Oliver, and Johann Goldammer of the Global Fire Monitoring Center at the University of Freiburg in Germany, had hoped the gathering would win the attention of Ukrainian officials and persuade them to put more money—Oliver says $20 million a year would be adequate—into preventing, detecting, and fighting fires near Chornobyl.

But top Ukrainian officials failed to attend—and since the country held elections in February, many key positions responsible for the exclusion zone have remained vacant. Zibtsev and others are still trying to lobby government officials, "but it's very difficult due to this political situation." Other problems in Ukraine seem more urgent than a decaying forest, he says: "Until it burns, they will not do something, I think."

Goldammer sees the Chornobyl zone as an example of a wider problem. Many forests in areas of past or potential military conflict, he says, cannot be easily managed, and thus are vulnerable to fires, because they harbor land mines, bombs, or other unexploded ordnance. Last October's Kiev conference, in fact, included presentations on explosive contamination of forests across a broad swath of southeastern Europe and Asia, from Croatia to Armenia. One Turkish delegate reported that when fires break out along his country's heavily mined borders with Syria or Iraq, "what we do is, we do nothing." This hands-off attitude could lead to cross-border fires and international conflict, he said.

In a statement released after the conference, participants called for new international efforts to prevent and fight fires in contaminated areas. The recommendations were vague and have had little impact so far, but Goldammer insisted that the Kiev meeting was "an important first step." Never before, he said, had forest managers shared so much information about dangers that were long considered military secrets. Russia's fires may help bring those dangers to wider attention.

–DAN CHARLES

Dan Charles is a writer based in Washington, D.C.

ScienceInsider

From the *Science* Policy Blog



The U.S. Department of Energy has revised its **plans to sequester carbon emissions** from existing coal plants. FutureGen 2.0 would retrofit a plant that burns coal the old-fashioned way, by pulverizing it into fine powder, rather than by gasifying the coal before it's burned. The decision cedes to China the lead in developing more sophisticated coal technologies, but experts say that the project will give key insights on retrofitting hundreds of aging U.S. coal plants. http://bit.ly/FutureGen2

A U.S. judge has overturned a decision last year by the U.S. Fish and Wildlife Service to remove the **northern Rocky Mountain gray wolf** from the list of endangered species in Montana and Idaho but leave it in place in Wyoming. Conservationists applauded the decision, but state wildlife officials in Montana and Idaho say that the wolves' rebounding population should allow for some hunting under proper management. http://bit.ly/graywolves

Scott Doney, a marine geochemist at the Woods Hole Oceanographic Institution, has been nominated to be the chief scientist at the National Oceanic and Atmospheric Administration. And **Cora Marrett**, a sociologist and acting director of the National Science Foundation, has been chosen to be the agency's permanent deputy director. http://bit.ly/doneynamed, http://bit.ly/marrettnamed

Federal scientists want to close some Alaskan fisheries beginning in January to **protect the Steller sea lions** in the Aleutian Islands. While conservationists say the measures don't go far enough, industrial fishers are already objecting to the suggestion. http://bit.ly/aleutiansealions

A bill before the U.S. Senate would **ban invasive research** on the estimated 1000 "research" chimpanzees in the country that live in laboratories. Scientists say the measure, similar to one pending for the past year in the House of Representatives, would impose "extreme and unreasonable" restrictions. http://bit.ly/GreatApeBill

For more science policy news, visit **news.sciencemag.org/scienceinsider**.





Thriving in thin air. DNA studies (*top*) show that most highland Tibetans carry a mutation that helps them survive at high altitude.

Tracing Evolution's Recent Fingerprints

The once-stalled hunt for the genes that helped humans adapt to new climates, diseases, and diets is exposing how evolution works

FOR RASMUS NIELSEN, IT WAS A REVELATORY moment. He was analyzing the frequency of different mutations in the genomes of Tibetans living at high altitude, searching for adaptations that allow them to thrive in thin air. His team's analysis had generated a graph in which most of the mutations were clustered together. But two stood apart, indicating they existed in almost all Tibetan highlanders but not in their close relatives, the Han Chinese. The high frequency of the mutations showed that this was a radical example of rapid evolution, with strong natural selection acting on a single gene. "I have done many scans of selection before, but I've never seen such a clear result," says Nielsen, a population geneticist at the University of California, Berkeley.

Then, when Nielsen Googled the gene to find out its function, he got even more excited: Both mutations were in the *EPAS1* gene that regulates oxygen sensing in humans. One of the mutations was so advantageous that it had spread to 90% of all Tibetans in just 4000 years, Nielsen and his colleagues at BGI in Shenzhen, China, reported in the 2 July issue of *Science* (p. 75). But fewer than 10% of the Han Chinese sampled (who live at sea level) carried this version of *EPAS1*. Thus the team had discovered the most rapid and strongest example of selection known in modern humans.

It was the most radical of a flurry of recent discoveries of human genes that evolution has strongly favored, a process called positive selection. Four years ago, researchers thought that they would find hundreds of examples in which an advantageous mutation spread rapidly in a particular population. That prediction, based on the first scans of human genome sequence data, did not pan out, and by last year, some researchers were ready to give up. They now realize, however, that plenty of positive selection exists, but it is subtler and harder to trace than originally anticipated. Using new statistical methods, they have found many less dramatic mutations that, for example, also help highland Tibetans survive at high altitude. Others allow Yupik Eskimos to stay warm efficiently, Europeans to thrive on cereal grains, and, perhaps, East Asians avoid alcoholism.

A growing number of researchers now think it is rare for a particular mutation to spread rapidly to most people within a population, as was the case with the *EPAS1* gene. Instead, natural selection often acts in more complex ways, leaving a much more subtle trail in the genome, population geneticist Jonathan Pritchard of the University of Chicago wrote in *Current Biology* in February. Several genes may work together to boost an advantageous trait. Or different versions of the same gene may rise in frequency at the same time to produce the same beneficial result, such as boosting height or altering skin color. Such polygenic selection doesn't leave the classic genomic signature of a "hard" selective sweep, like the one Nielsen saw in his Tibetan data, and is thus tougher to detect. "There have been a bunch of papers that show very consistently selection across a lot of our genome, but of a type that doesn't leave these massive footprints," says Gilean McVean, a population geneticist at the University of Oxford in the United Kingdom.

Although natural selection's trail in the human genome is less obvious than researchers had hoped, they are now crafting new methods to follow it. New data sets, including the complete genomes of 1000 individuals from diverse populations, will be online by December. And researchers are testing new ways to detect selection acting on many gene variants at once or on particular adaptive traits. "We're moving beyond the paradigm of whether selection acted on one newly arisen gene to more complicated models that think about selection on multiple pathways," says population geneticist Joshua Akey of the University of Washington, Seattle.

Seeking selection

Many researchers have argued that most of the obvious differences between humans today are the result of recent positive selection rather than mutations that accumulated randomly over time. All living humans are remarkably similar genetically because we all descended from a small founder population that arose in Africa about 200,000 years ago. As these modern humans moved around

CREDITS (LEFT TO RIGHT): CHENG ZHU, BGI

and, eventually, out of Africa in the past 80,000 years or so, they evolved genetic differences that helped them adapt to new climates, digest novel foods, and fight off new illnesses and parasites.

Sometimes, dramatic new mutations produced those differences. Other times, selection acted on standing variation: variants that existed but had been rare in a founding population. When the variants suddenly became advantageous in a new environment, they became more common.

But identifying the underlying gene variants that make a willowy Maasai warrior different from a compact Yupik Eskimo, for example, was "frustratingly slow" until recently, says Akey. Researchers had to guess which gene might be involved in an adaptive trait and study it within families. This method produced a few well-known successes, such as the discovery of mutations in genes that protect Africans from malaria or allow adults in dairy-farming groups to digest the sugar lactose in milk.

With the sequencing of the complete human genome for the first time a decade ago, researchers were able to get a better handle on how selection has shaped the genome. Several large-scale projects used different methods to identify millions of single-nucleotide polymorphisms (SNPs) from across the genomes of people in different populations in Europe, Asia, and Africa. By comparing SNPs at the same sites in individuals from different populations, researchers could detect those where positive selection had driven a mutation to high frequencies in a population.

Some of the first scans of the genome-wide databases produced tantalizing results. In 2006, Robert Moyzis of the University of California, Irvine, and colleagues identified 1800 such genes representing 7% of the genome. Two months later, Pritchard and his colleagues scanned a SNP catalog called the HapMap and also found "widespread signals of recent positive selection": high frequencies of alleles in some groups that were rare in others from Europe, Asia, or Africa. But neither group identified precise locations of the newly evolved mutations.

As more researchers mined these data sets and added DNA from new populations, they dug out nuggets of positive selection in genes that seem to reflect adaptations to different environments or diets. Europeans have particular versions of the *SLC24A5* gene—one of a half-dozen different genes now known to affect the color of skin, hair, or eyes. East Asians have variants of the *EDAR* gene that cause thicker hair and, possibly, changes in eyes, skin, and sweat glands, likely adaptations to a humid climate. Asians with high-starch diets have more copies of the gene for salivary amylase, which digests starch in the mouth.

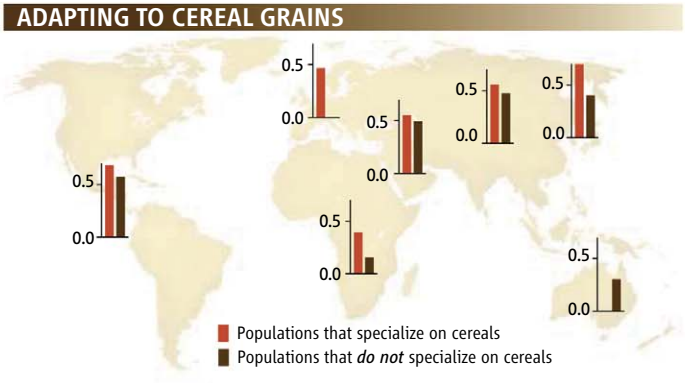
Interestingly, few of the mutations under strong selection were associated with dramatic stories of human triumph over dire circumstances, such as the bubonic plague. "Selection is not as sexy as you think," says evolutionary geneticist Pardis Sabeti of Harvard University. "It's not just about mass famines and the plague. It's also about women who drank milk, gained a little more weight, and had seven kids to their neighbor's six. That's enough to have a huge effect over time."

In the past 4 years, these discoveries of selection for relatively mundane adaptations set off an intense competition to find more. Researchers were scanning data sets at a "frenetic pace," Akey wrote last year in a review in *Genome Research*. He counted more than 21 genome-wide scans that identified 2465 genes in 722 regions of the genome thought to have undergone positive selection. The identification of so many regions of the genome under positive selection prompted some researchers to conclude that evolution had accelerated as humans spread around the globe and adapted to new challenges.

But by the middle of 2009, enthusiasm began to wane. Researchers had scrutinized only a few of those 2465 in detail, netting only a handful of obvious mutations under selection, partly because it is so difficult to test function in the lab, says Akey. They were also unable to confirm that many of the genes discovered really were under strong selection. Out of 21 scans, 722 regions were identified by two or more studies, but only 129 regions were found by four or more studies, Akey wrote. "Sometimes, when people have gone fishing with the same pole and the same bait in the same lake, they have found completely different fish," says Akey.

Those researchers who did find interesting targets couldn't always rule out that demographics—the size and movements of populations—had produced signals that mimicked selection. For example, did certain populations share high frequencies of the same rare allele because it was under strong selection there, or just because the populations were recently descended from the same small group of ancestors? "I think people had naïve expectations about how easy it would be to detect positive selection in the genome," says Nielsen.

Finally, few teams have been able to prove that a particular allele actually affects the function of a trait under selection. In many cases, researchers couldn't even name the gene involved because the regions detected contain many genes or do not code for proteins. "In only a handful has there been much progress in identifying the causal mutations and extracting these biological insights about their function," Sabeti wrote in the 12 February issue of *Science* (p. 883). Says McVean: "That's why the whole field—the program of trying to find selective sweeps—kind of ground to a halt."



Cereal genes. Populations whose main food is cereal grains have higher frequencies of a *PRLP2* gene variant than do people who have other diets.

Soft sweeps

Yet McVean and others were convinced that positive selection had shaped much of the genome but lay beneath the radar of methods used to detect it. Those methods are particularly crude when it comes to detecting subtle signs of positive selection, such as when selection acts on several genes at once or on standing variation. "It's very likely that many traits that are different between populations are coded by different alleles; any one may not be so strong," says population geneticist Pleuni Pennings of Ludwig Maximilian University of Munich in Germany.

Consequently, earlier this year Pritchard and his colleagues proposed an alternative to strong selection on single new mutations. In *Current Biology*, they argued that selection on more than one gene at once could allow a new trait—such as increased height—to sweep more rapidly through a group.

Detecting such polygenic selection is one of the new frontiers. Mark Stoneking of the Max Planck Institute for Evolutionary

SOURCE: A. HANCOCK *ET AL.*, *PNAS* **107** (MAY 2010)





Milky way. This Datog woman from Tanzania (*left*) and Turkana man from Kenya are pastoralists who can digest milk as adults.

CREDITS (LEFT TO RIGHT): SARAH TISHKOFF; JIBRIL HIRBO

Anthropology in Leipzig, Germany, and his colleagues have identified what they think is parallel selection of three variants of the gene for TRPV6 that aids in the digestion of milk.

When Stoneking's team looked at the full sequences of this gene and others in 24 African Americans and 23 individuals of European descent, they found many variants of the genes in African Americans but just three types in Europeans. This distribution suggested that the three variants originated in Africa but were swept to high frequency in the ancestors of Europeans after they migrated out of Africa and became dairy farmers, Stoneking reported in *PLoS ONE* in 2008. They also showed in patch-clamp studies of intestinal cells that TRPV6 regulates the uptake of dietary calcium and, thus, may have co-evolved with lactose tolerance.

Another tactic for finding selection acting on several genes at once is to look at phenotypes—or physical traits—in humans who live in extreme environments. Although the *EPAS1* allele found in 90% of Tibetan highlanders was a dramatic case, it is just one of more than three dozen gene variants under positive selection that work together to help Tibetans survive at 4200 meters, according to work this year by three international teams. Their success in finding so much positive selection in one population "suggests if we want to find unique genes under selection, we should look in other extreme environments," says geneticist Lynn Jorde of the University of Utah in Salt Lake City, leader of one team.

A new way to spot subtle selection acting on more than one gene at once is to compare populations that have faced similar evolutionary challenges. For example, human geneticist Anna Di Rienzo of the University of Chicago and her graduate student Angela Hancock have looked at frequencies of SNPs in groups, such as the Chukchee and the Naukan Yup'ik of Siberia, that have adapted to life in polar regions, or that ate more cereal grains after the transition to agriculture, such as the French, Tuscans, Palestinians, and Druze. They gathered environmental and dietary data for 61 populations cataloged in various databases, including the Human Genome Diversity Project. Then they compared frequencies of alleles in all the populations sorted according to the environment in which they lived (dry, humid, polar, or temperate); mode of subsistence (agriculture, foraging, horticulture, or pastoralism); and diet (cereals; fats, meat, and milk; or roots and tubers).

They identified the alleles that varied the most consistently in frequency across all populations (low in some; high in others). People who lived in similar habitats or ate similar foods had similar frequencies of the same alleles, they reported online 5 May in the *Proceedings of the National Academy of Sciences*. For example, more individuals in polar regions had the same alleles in genes associated with energy metabolism, and more people who foraged for roots and tubers had alleles that were rare in groups with other diets. Specifically, more Europeans and Middle Easterners have a variant of the *PRLP2* gene, which encodes a protein important for breaking down fats in plant foods, which may reflect their ancestors' adaptation to agriculture. "This method has the power to detect advantageous alleles that escape other methods," says Di Rienzo.

While several teams are developing new methods to identify polygenic soft sweeps, others are working to pinpoint more precisely the DNA under positive selection. Sabeti and her team reported in their 12 February *Science* paper that they have increased the resolution of SNP data by 100-fold by combining five different statistical methods to detect patterns of selection in the genome. By analyzing the same regions of DNA with different methods, Sabeti's team was able to home in on 64 regions containing just a single gene, which narrows the search for a SNP that may boost an adaptive trait.

Many groups are also ramping up efforts to do functional studies of the gene variants they have identified. Some labs are seeing if a gene variant is expressed in different tissues or at different times in development. Others are collaborating with labs that create mice with or without specific gene variants to see how they develop. And some are using microarrays to see how different gene variants affect gene regulation.

Finally, many researchers are looking forward to the complete genomes of 1000 individuals in the 1000 Genomes Project. This project includes more diverse populations from Africa, which have not been sampled as well as Asians and Europeans. The data will be available by the end of the year. Others are searching for recent evolution in large, multigenerational data sets to spot changes in the age of first reproduction and menopause, or total blood cholesterol, for example, in different generations and populations, Stephen Stearns of Yale University wrote online 3 August in *Nature Reviews Genetics*.

As researchers look forward to scanning these new data sets, they say that the key question is no longer how much positive selection is in the genome. "I want to move beyond simple laundry lists of candidate gene regions to understand what are the real stories that went on," says Stoneking. "What did our ancestors have to adapt to as they spread round the world?" **–ANN GIBBONS**



CREDIT: MICHAEL BALTER

Engaged anthropologist. Polly Wiessner with her pet cockatoo and gifts from friends in the Kalahari and Papua New Guinea.

PROFILE: PAULINE WIESSNER

Anthropologist Brings Worlds Together

Polly Wiessner unites past and present, science and advocacy in her studies of traditional peoples in Africa and Papua New Guinea

SALT LAKE CITY—Late one night around 2003, University of Utah anthropologist Pauline Wiessner was awakened by a telephone call from some Kalahari Bushmen she had studied in Namibia. The Bushmen, also known as San, had managed to get hold of a satellite phone belonging to a safari company. They told her that they had just called the famous musician Yo-Yo Ma about an offer he had made when he toured the Kalahari a decade earlier: Ma had apparently agreed to buy shoes for their soccer team. Now the Bushmen wanted to draw outlines of their feet, send them to Wiessner in Salt Lake City, and have her buy the shoes and send the bill to Ma.

Wiessner didn't worry that helping her research subjects, former hunter-gatherers now coping with the modern world, would compromise her scientific objectivity. She simply agreed, realizing that the Bushmen were using borrowed modern technology to expand their traditional social networks across the globe. And, as she had put it in a recent talk, such social networks had probably been key to the evolutionary success of our hunter-gatherer ancestors, allowing them to travel great distances and eventually "move out of Africa and colonize much of the planet."

As it happened, the Bushmen, lacking postal services, had no way to get the drawings to her, and the shoes were never purchased. But Wiessner, 62, known as Polly, sees no conflict in her dual role as both observer and participant in traditional societies. For nearly 4 decades, she has been carrying out anthropological fieldwork that links science with advocacy and ties the present to the past. Her research on exchange networks in Africa's Kalahari Desert and in Papua New Guinea (P.N.G.) has provided anthropologists with some of their best models for the cultural evolution of prehistoric societies. It forms "the basis of a lot of people's thinking about how we became human," says anthropologist Alison Brooks of George Washington University in Washington, D.C. Adds archaeologist Clive Gamble of Royal Holloway, University of London: "Take away Polly's insights, and our view of the social world of our Paleolithic ancestors would contract back to the scale of the cave." Along the way, Wiessner has helped the traditional peoples she works with navigate the modern world. She is regarded as a leading practitioner of "engaged anthropology," in which researchers collaborate with the people they study. Although she now lives in Salt Lake City (with a pet cockatoo that drinks from her coffee cup in the morning and her margarita glass in the evening), she still works closely with African Bushmen and P.N.G.

tribesmen and is considered a friend to both cultures. "Polly wanted to continue working with the people here," says Akii Tumu, director of the Enga Tradition and Transition Center in Wabag, a cultural center that Wiessner helped to create and fund. Tumu, who has collaborated on Wiessner's research for 25 years, says this makes her "outstandingly different from all other foreign people." Wiessner's ability to bridge the many worlds in which she works makes her one of anthropology's "great souls," says anthropologist Sarah Blaffer Hrdy, professor emeritus at the University of California (UC), Davis. "She is the old-fashioned kind of anthropologist, … a scholar who studies human nature in all its diversity."

Long nights in the Kalahari

Wiessner, who has spent years living among poor people in traditional societies, was born in Vermont into a comfortable existence, the daughter of a famed mountain climber. She began climbing and skiing early on, fostering her love of the outdoors. And she says her experiences at a strict Canadian boarding school prepared her for the hardships of fieldwork.

But she was a troublemaker at school and unable to get into a good college at first. So she went to the now-defunct Bennett College in Millbrook, New York, which Wiessner says catered to wealthy young women who wanted to marry well. Wiessner thrived and soon transferred to Sarah Lawrence College. While at Sarah Lawrence, she volunteered for a summer dig at a prehistoric site in France. There she met Lewis Binford, a founder of the scientifically oriented New Archaeology movement, and later worked on his analyses of Paleolithic stone tools.

After graduating, Wiessner was introduced to the new field of ethnoarchaeology, the study of modern people to see how the archaeological record was created. She hooked up with John Yellen, now archaeology program director at the National Science Foundation, and helped him draw maps of Bushmen camps in Botswana, recording the spatial patterns of discarded animal bones.

These early experiences taught Wiessner that the present and the past were inextricably linked, a theme that would come to dominate her research career. As a graduate student at the University of Michigan, she started out studying the stylistic differences among Late Stone Age stone tools called microliths in Botswana. But after 2 weeks in the field, Wiessner says, "I realized this was probably the most boring project in the world. I was looking at variation in microliths when I should be looking at living people and the social processes that generate stylistic variation."

Wiessner set about recording the stylistic variations among artifacts such as projectile points and beadwork that were produced by different groups of Bushmen, who in the 1970s still lived mostly by hunting and gathering. She traveled all over Botswana, usually alone. "She is a really tough cookie," says Yellen.

Then months of heavy rains hit her field area. The rain knocked the nuts out of trees, triggered the growth of tall grasses that choked off more edible plants, and dispersed the large antelopes that the Bushmen relied upon. "The people went through a period of extreme hunger," recalls Wiessner. But the episode was a "turning point" in her research. The Bushmen were often too hungry to talk about style. So Wiessner, who by now had some competency speaking Ju/'hoansi, the Bushman language there, spent her time sitting around the camps and writing down what people were saying and doing.

She observed that the men and women were busy making objects, such as arrowheads, knives, beads, and clothing, and talking about loved ones far away and how much they missed them. Meanwhile, young men went off to areas up to 200 kilometers distant to see who was there and how well they were doing. Then, when the people were on the brink of starvation, they set off with their objects—which Wiessner soon realized were gifts—to visit other Bushmen camps. Thus Wiessner deciphered the gift-giving exchange that the Bushmen called *hxaro*, which ties Kalahari peoples together in far-flung social networks.

Between 1973 and 1975, Wiessner stayed in Botswana, tracking the *hxaro* networks. She found that adults had an average of about 16 stable partners in Bushmen camps near and far, some with more closely related people such as first cousins but many with more distantly related kin. Her study formed the basis of her 1977 Ph.D. thesis, which is still widely cited for its potential insights into how prehistoric hunter-gatherers survived rapidly changing climates and environments. "The central question … was how hunter-gatherers with no money in the bank, no grain in the larder, and no animals on the hoof deal with risk when the environment fails," Wiessner says. Her findings had an immediate impact on anthropology, says Hrdy: "Polly showed not only how central such sharing and exchange systems were but also how strategic and innovative humans must have been in establishing and maintaining them."

After the rains had subsided, Wiessner continued her work on style and found that the styles conveyed information about the social identities of various Bushmen groups. Archaeologists immediately leaped on her work for its potential applications in understanding stylistic variation in past cultures. "She saw the functions of style more clearly than anyone," says archaeologist Iain Davidson of the University of New England in Armidale, Australia.



Well connected. The late Chu!o n!a, shown here in the 1970s, had 25 Bushmen gift-exchange partners across the Kalahari Desert.

CREDIT: POLLY WIESSNER

The engaged anthropologist

In 1981, Wiessner landed a job as a research associate at the Max Planck Institute for Human Ethology in Andechs, Germany, and in 1985, still on the Max Planck payroll, she moved to Enga province in the highlands of P.N.G., where her then-husband had been hired as a health administrator. Although she hadn't planned to do research in P.N.G., Wiessner took advantage of her new circumstances to launch the next phase of her career:

a 10-year oral-history project, with P.N.G. colleagues and the elders of 110 Enga tribes, that covered seven generations of Enga history. Once again, Wiessner was engaged in a project that used past and present to inform each other. Wiessner and Tumu cross-correlated the oral histories among tribes going back hundreds of years. They were able to trace the cultural evolution of Enga exchange networks and social hierarchies as the people transitioned from hunting and gathering and subsistence agriculture to a society with agricultural surpluses. This shift was triggered about 350 years ago by the introduction of the sweet potato, which grows more easily in poor highland soils than taro, the previous staple crop. Surplus production fostered increased competition, the emergence of ceremonial exchange networks linking tens of thousands of people, and the rise of leaders who managed large amounts of wealth, including pigs, which thrived on sweet potatoes and could be given as gifts or exchanged.

The book that she and Tumu published in 1998, titled *Historical Vines*, is "one of the best case studies of cultural evolution in the literature," says ecologist Peter Richerson of UC Davis.

In 1995, when its director retired, the Max Planck institute closed its doors. Wiessner returned to the Kalahari, this time to Namibia, where social and political changes had forced the Bushmen into towns with few jobs and little means of livelihood. Wiessner teamed up with the late anthropologist and filmmaker John Marshall (anthropology.si.edu/johnmarshall) to both study and try to do something about the changes in land use and conservation policies that threatened the Bushmen's survival. One result was the 2002 classic documentary film series *A Kalahari Family*, for which Wiessner, Brooks, and Yellen served as advisers. Since Marshall's death in 2005, Wiessner has continued to advocate for the Bushmen.

"Polly made the well-being of the [Bushmen] her priority as they made the transition from nomadic hunter-gatherers to sedentary rural workers and herders," says anthropologist Nancy Howell of the University of Toronto in Canada. Wiessner has been "extremely generous with her time and money," adds anthropologist Robert Hitchcock of Michigan State University in East Lansing. For example, she helped the Bushmen build protective structures for their waterholes so they wouldn't be overrun by elephants. She also provided "connections to funding sources, technical assistance, and recommendations to the [Bushmen] themselves and to the nongovernmental organizations, government agencies, and international organizations working with them," Hitchcock says.

In 1998, Wiessner returned to live in the United States for the first time in nearly 30 years, taking first a temporary and then a permanent position at the University of Utah. She continued to make regular visits to both Namibia and P.N.G. In Enga province, she turned her attention to one of the deadly consequences of social hierarchy: warfare. Tribal wars had plagued the region for hundreds of years, but when she first came to P.N.G., Wiessner says, these wars were serious yet still largely contained. "In 1985, I would take my lunch, go up on a hillside, and watch. The wars were fought with bows and arrows and … to reestablish power balances, not to wipe anyone out." After two or three deaths, Wiessner says, "they would call an end to the fight and pigs would be exchanged." That all changed when M-16s came to Enga and fell into the hands of what Wiessner calls "young Rambos" who were poor and had nothing to lose. Once guns arrived, up to 200 people could die in a war, "and you wouldn't want to go near them."





Reparations. A Papua New Guinea clan avoids war over a recent murder with payment of cash and nearly 200 pigs.

CREDITS: POLLY WIESSNER

Wiessner began collecting data on the wars and shared it with tribal leaders and local magistrates eager to stop the escalating violence. When the Enga Tradition and Transition Center—which serves as a museum, meeting place, and repository for Enga's cultural history—opened its doors last September, it was immediately pressed into service as a safe, neutral place where community leaders could come together. Tumu says Wiessner was the "driving force" behind the center. She personally funded half the $1.25 million price tag by selling land she owned in Vermont. (The Enga provincial government paid the other half.)

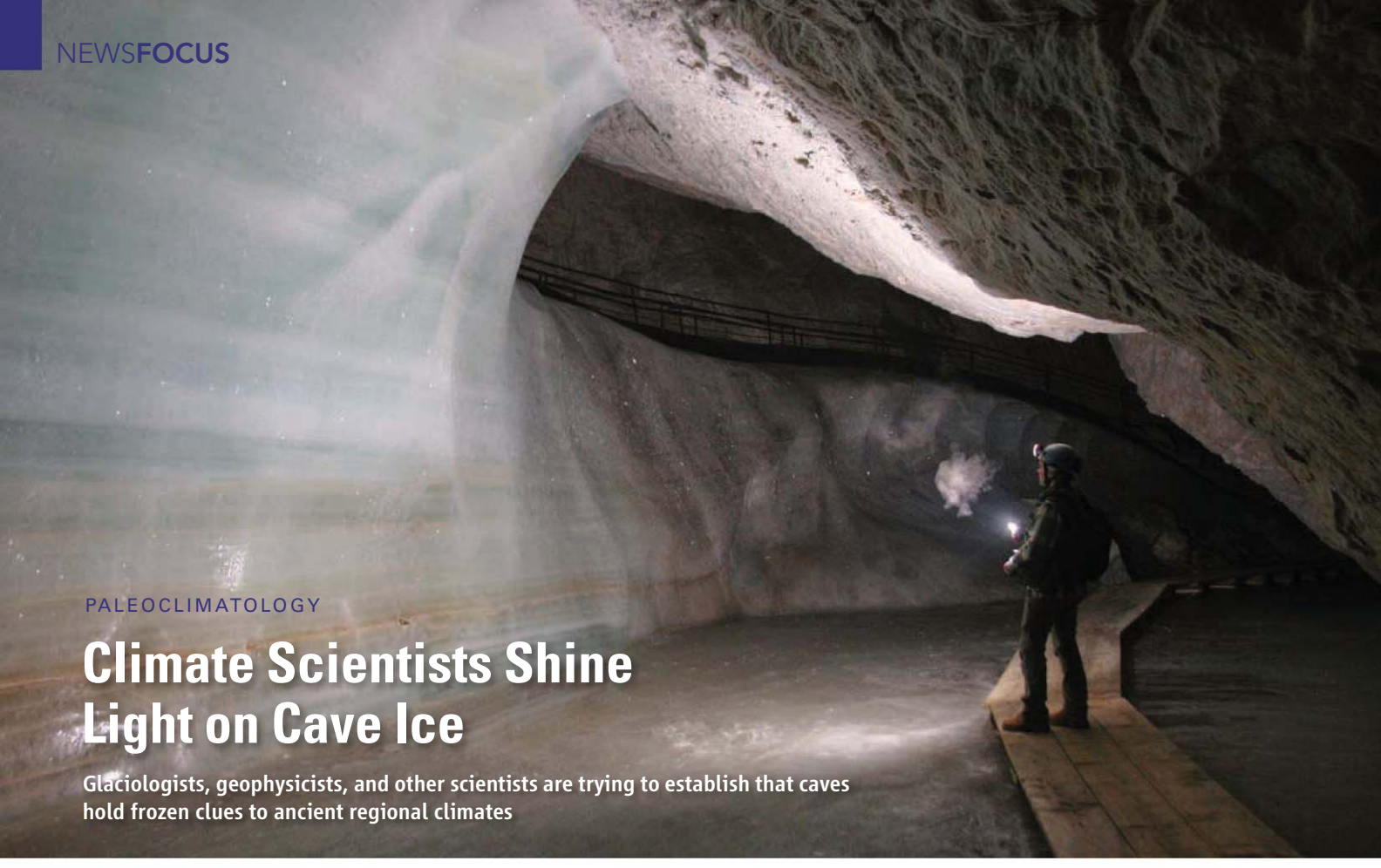
The latest data collected by Wiessner's collaborators from Enga court records indicate that the total number of deaths from warfare has fallen over the past 4 years, accompanied by "a real change in attitude about how to deal with conflict," she says.

Not all anthropologists embrace Wiessner's highly engaged style; the field continues to debate just what the relationship between an anthropologist and his or her "subjects" should be. But Wiessner's approach, some researchers say, fits a recent trend in anthropology. Setha Low, an anthropologist at City University of New York, says that over the past 20 years or so the field has been undergoing a transition from a more detached to a more engaged attitude toward the peoples it studies. Low, who is coediting a special supplement of *Current Anthropology* on engaged anthropology scheduled for this fall, adds that "anthropology originally started out very engaged." Thus early-20th-century researchers like Franz Boas and Margaret Mead were outspoken critics of racism and colonialism. But by the 1950s, a sharp increase in the number of anthropologists based in the universities—where scientific objectivity was prized—and the rise of McCarthyism, which targeted many anthropologists considered activist and left-leaning, took a big toll on engaged anthropology. The field is now reverting to its engaged roots, Low says.

And Wiessner is confident that active collaborations with her subjects aids rather than hinders her research. "All the research I've done has been as part of a team. Many people feel this is something different than science. But if you are returning something to the people you work with, and working on their problems, you find out more and you go deeper."

For many of her colleagues, Wiessner is the ideal of what an anthropologist should be. "She pioneered a new kind of collaborative research, where you don't just use informants but you involve them in your research," says Brooks. "She fulfills the dream of being a universal anthropologist, the kind we rarely see these days."

–MICHAEL BALTER



PALEOCLIMATOLOGY

Climate Scientists Shine Light on Cave Ice

Glaciologists, geophysicists, and other scientists are trying to establish that caves hold frozen clues to ancient regional climates

EISRIESENWELT, AUSTRIA—Tracing his glove along a chalky layer in a house-size block of ice that lines this cave in the Austrian Alps, Michael Behm can feel all that is left of an ancient warm spell. The ice, likely formed over the decades or centuries as calcium-enriched rainwater trickled deep into the cave and froze, must have once warmed enough on top to melt and release a few years' worth of the mineral, the Vienna University of Technology geophysicist explains.

Behm is one of a small but growing number of researchers who are investigating whether persistent ice that drapes the inside of some caves can reveal what the climate outside was once like. At a recent workshop in Austria,* which included visits to several nearby ice caves, about 50 such scientists discussed this formidable challenge and reported tantalizing progress. One team, for example, has been using ice within a Romanian cave to reconstruct a 1000-year climate history of the local region.

By dating layers of cave ice that form from ponds of trapped rainwater and then analyzing the isotopes and other substances that make up those layers, these scientists aim to chart past changes in temperature, rainfall, and other climate indicators such as carbon dioxide levels. It's a strategy paleoclimatologists have long pursued with ice cores taken from glaciers and polar caps, or with layers of lake sediment, but cave ice has proven much more difficult to study and interpret. Every cave is unique in how water trickles in and freezes, and researchers have to go to great lengths to establish whether the ice layers they see represent annual, seasonal, or other time scales of deposition. "Cave ice is a complicated business," says Greenland ice core specialist Sigfús Johnsen of the University of Copenhagen.

But it's one worth pursuing, say Behm and others at the Austrian workshop, as polar ice cores don't offer insight into the climate histories of temperate regions, where most people live. "There's an urgent need to look for ice archives outside the polar region," says environmental scientist Dietmar Wagenbach of the University of Heidelberg in Germany, who attended the workshop.

Mountain glaciers aren't the easy answer either, because they are less representative of the climate near settled areas. Glaciers require massive snowfall and long-lasting cold to form, but ice can form in caves and trap climate information even in regions that don't normally frost over. A cave with small temperature differences at its entrances can develop strong internal winds, as air moves to equalize the cave's internal temperature. If the wind gets fast enough, as in a constriction, it can also get cold enough to freeze standing or dripping water. Long before electric refrigerators, ancient Persians used the same principle to make ice.

The study of tree rings, lake sediments, and other so-called climate proxies has provided some history of the climate in temperate regions, but paleoclimatologists are still eager for other sources of data to help them predict how future changes in climate might alter these locations. And ice is a paleoclimatologist's best friend because it can retain many different clues to the past climate. In polar regions, recently fallen snow slowly becomes compressed into a layer of ice whose ratios of hydrogen and oxygen isotopes reflect the atmospheric temperature at the time of condensation. Such ice can also trap grains of pollen and dust and air bubbles that reveal concentrations of gases such as carbon dioxide that are important to reconstructing past climates.

Climate studies of ice cores from glaciers and polar caps took off in the 1960s, and some of those cores may record climate histories going back a million years. Similar studies of cave ice, however, have lagged far behind. Speleology, the scientific study of

CREDIT: NENAD BUZJAK

*4th International Workshop on Ice Caves, 5–11 June 2010.

Illuminating. Some cave ice dates back thousands of years.

caves, dates back to the 19th century, but most such work has concentrated on the geology of the caverns, or the unusual flora and fauna found within them. Emil Racoviţă of Cluj University in Romania, a pioneering cave biologist, may have been among the first to recognize the record-keeping potential of cave ice. In a 1927 report on his exploration of the Scărişoara cave in Romania, he notes that such ice must have formed under different climatic conditions and that it would be good to "decipher the passionate enigmas of the history of the ice." Decades later, Racoviţă's assistant Mihai Serban followed up on this idea, reporting in an Italian journal that he could measure certain isotopes in cave ice from Scărişoara, although the data didn't provide climate clues.

The idea of doing paleoclimatology on cave ice attracted serious international attention about 11 years ago, when a pair of Canadian cavers—one a cave operator in Alberta and the other a geography master's student at the University of Calgary—published a study that identified different mechanisms of cave-ice formation. They reported in the journal *Boreas* that by looking in the right places in caves and taking into account how the ice formed, they could extract paleoclimatic information from isotopes in the cave ice.

The idea gained more momentum from the first workshop on ice caves, held in 2004. But even now, few scientific papers have been published on the topic, as a variety of technical difficulties have stymied researchers. Small rocks in the ice have halted efforts to extract long ice cores. And Wagenbach's student Barbara May notes that cave ice is actually too warm for drills designed for extracting ice cores from glaciers; melted and refrozen ice jammed her drill until she added a lubricant, which she fears could interfere with many analyses, including those of air bubbles, isotopes, and particles in the ice.

Teasing climate clues from cave ice isn't as simple as extracting a clean core, however. The most commonly drilled cave ice mimics the tidy horizontal layers seen in sedimentary rock. A single layer, however, could represent either a year's worth of rain that trickled into the cave or just a few months when a river poured in a torrent of water. Each process would preserve different clues to climate, so researchers need to determine how water has historically entered a cave. The size of the ice crystals, whether the ice froze from the bottom up or from the top down, whether it partly melted or eroded after solidifying—these and other nuances can affect measurements and require careful interpretation, Behm says.

That complexity is one reason cave-ice studies have progressed so slowly. Another is that the topic is just a sideline for most researchers. Behm, for example, uses ground-penetrating radar (GPR) to study Earth's crust. He only recently began trying the technology on ice caves. "Cave ice is such a perfect insulator that the signal-to-noise ratio is very high for GPR," he says.

In studies of four Austrian caves, Behm has found layers in the ice that reflect his radar signal. He suspects that they may be accumulations of calcite from periods when ice melted and released its dissolved minerals, a possible sign of outside climate changes. In June 2007, May drilled a 7-meter ice core from one of the caves, but so far her isotope studies haven't nailed down firm dates along its length.

Others have had better luck. At the 2006 ice caves workshop, a Danish-Slovakian team reported extracting a 14-meter core that they dated at about 1250 years based on carbon-dating of a bat found in nearby ice. Sharp changes in the accumulation of ice from year to year make the core hard to interpret, but it does show signatures of some climate oscillations found in other records.

At this year's workshop, geology Ph.D. student Aurel Perşoiu of the University of South Florida in Tampa described even more promising work with ice from the same Scărişoara cave Racoviţă studied. Using a 6.5-meter ice core drilled from the cave, Perşoiu and colleagues are making an ambitious attempt to reconstruct the past 2000 years of the region's climate history. By carbon-dating organic remains such as leaves and insects in the ice, the team has related core depth to age in the top half of the core. And they've used that ice to reconstruct temperature variations within the region. The trends appear to match other regional climate proxies such as lake sediments, pollen, and stalagmites, Perşoiu says. A paper describing their methods is under review at the *Journal of Geophysical Research*. "We are being helped by paleoclimatologists," Perşoiu says. "They are pushing us toward more mainstream journals."



Cool science. Before extracting cores that might reveal past climate information, researchers use radar to measure the thickness of the ice.



Frozen past. A close look at the isotopes in ice can reveal climate information.

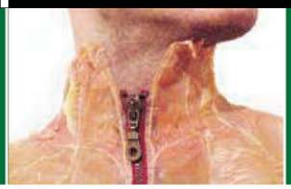
Some researchers at the Austrian workshop compared the debate over the usefulness of cave ice to a similar one that took place decades ago over stalagmites, towers of limestone that build up in active caves. At first, paleoclimatologists derided the idea that stalagmites could hold valuable data, but now studies of "speleothems" have become standard practice (*Science*, 27 July 2007, p. 448).

To spread the word about cave ice to a broader audience, glaciologist Stephan Gruber of the University of Zürich in Switzerland is now overseeing a special issue of *The Cryosphere* devoted to research presented at the workshop. Improving communication with scientists in related fields will be vital; one workshop attendee wore a baseball cap with "Glaciologist" printed on the front to remind cave experts to cut the jargon. (Cave scientists favor logos featuring bats, their unofficial mascot.) Yet with results from Scărişoara's ice in the pipeline and a book project to translate the backlog of European cave-ice articles into English in the works, Perşoiu is optimistic about the field's future. Cave-ice research, he predicts, "is about to reach a climax." **–LUCAS LAURSEN**

Lucas Laursen is a writer based in Madrid.

CREDITS (TOP TO BOTTOM): GERNOT WEYSS; ANDREAS NEUMANN

Boundary organ 760



Ecological network news 765

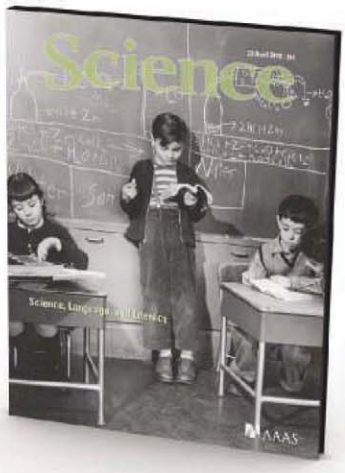


LETTERS

edited by Jennifer Sills

Science Education: Neglected

WE WERE PLEASED TO READ THE EDITORIAL BY B. ALBERTS, "PRIORITIZING SCIENCE EDUCATION" (special section on Science, Language, and Literacy, 23 April, p. 405). Having worked throughout our careers on methods for improving both science and literacy instruction, we heartily agree with the viewpoint that science and literacy instruction should be integrated.



Our deep concern, however, is with the significant barriers to integrating science and literacy instruction that presently exist, especially at the elementary level. Classroom practices in most elementary schools, which under No Child Left Behind emphasize reading and basic math, currently leave virtually no time for science instruction. In addition, many elementary teachers are poorly prepared and uneasy about teaching science. Until these barriers are removed, the possibility for greatly expanding the time spent on science in the elementary grades and for creating a synergy between science and literacy instruction is low.

As long as federal policy continues to focus on basic reading and math in the elementary grades, with standardized tests as the cudgel, science and most other disciplines seem certain to remain neglected. The evidence reviewed in the special section shows that, given adequate professional development and administrative support, elementary teachers can succeed in combining literacy and science to good advantage—but only after targeted outcomes and curriculum priorities are changed to establish a more balanced program for all children.

ROBERT CALFEE[1]* AND ROGER BRUNING[2]

[1]School of Education, Stanford University, Stanford, CA 94305–3096, USA. [2]Department of Educational Psychology, University of Nebraska, Lincoln, NE 68588–0384, USA.
*To whom correspondence should be addressed. E-mail: robert.calfee@ucr.edu

Science Education: Narrative Nonfiction

IN HIS EDITORIAL "PRIORITIZING SCIENCE education" (special section on Science, Language, and Literacy, 23 April, p. 405), B. Alberts distinguishes two forms of text: factual (or informational) text and fictional (or narrative) text. However, a third genre of text exists: narrative nonfiction. In narrative nonfiction, the writer conveys information and emotion through characters, scene, and a story unfolding in time (*1*).

Scientists such as E. O. Wilson, Stephen J. Gould, and Lewis Thomas as well as science writers such as Natalie Angier, Dava Sobel, and James Gleick have used narrative nonfiction to engage and inform the public about a wide range of topics in science. These stories motivate the reader to want to understand the science behind the plot.

E. O. Wilson proposes that science can be taught effectively through story (*2*). He states that the human brain functions by constructing narrative and that complicated, essential science can be communicated to a broad audience when presented as a story. The narrative can focus either on a historical period with scientists as the protagonists or on events that result from scientific phenomena.

Narrative nonfiction in science writing and curriculum offers a powerful approach to educating students and the general public about the wonders of the natural world.

JACQUELINE MILLER

Education Development Center, Inc., Newton, MA 02458, USA. E-mail: jsmiller@edc.org

References

1. L. Ureneck, presentation at "The Power of the Narrative: Timeless Art in an Urgent Age," Boston University, Boston, MA, 23 to 24 April 2010.
2. E. O. Wilson, *Am. Educ.* **26**, 8 (2002).

Science Education: Poetry

IN HIS EDITORIAL "PRIORITIZING SCIENCE education" (special section on Science, Language, and Literacy, 23 April, p. 405), B. Alberts suggests forging a connection between literacy and science teaching. Poetry is one means to do so.

Similes and metaphors are used extensively both in science and in poetry. The vocabulary of science is replete with words constructed to convey powerful scientific ideas unambiguously. Such vocabulary can be an obstacle, undermining the ability of a teacher to convey to students the fundamental, important ideas of science. Science teachers can use metaphors and similes to help these students learn. Similarly, a challenge of poetry is to cast words in a structure that captures the essence of a thing and invokes new thoughts and powerful feelings. The ideas of science and technology are powerful forces in today's societies, certainly worthy of conveying to a wide audience, using all available tools.

Such ideas are at the foundation of recent educational efforts to formally link poetry and science at the middle school level, through the Science, Art, Writing (SAW) program (*1*). These ideas also underpin efforts to encourage scientists to incorporate poetry into the way they think about, and

CREDIT: AAAS

Qs & AAAs



www.sciencedigital.org/subscribe

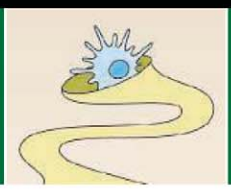
For just US$99, you can join AAAS TODAY and start receiving *Science* Digital Edition immediately!

Qs & AAAs

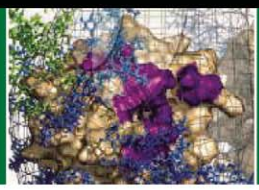


www.sciencedigital.org/subscribe

For just US$99, you can join AAAS TODAY and start receiving *Science* Digital Edition immediately!



DC dual roles
767



HIV antibodies
770

communicate, important ideas uncovered by their studies (*2*), and efforts to encourage science teachers to incorporate poetry into their science courses (*3*). To initiate a module on cellular respiration, for example, a teacher can have students read and discuss "Anorexia" in Jennifer Gresham's *Diary of a Cell* (*4*). Furthermore, poets with strong scientific perspectives and backgrounds are increasingly finding ways to push the ideas and language of science out into the public domain (*4*–*6*), to the benefit of science.

ARTHUR J. STEWART
Science Education Programs, Oak Ridge Associated Universities, Oak Ridge, TN 37831–0117, USA. E-mail: arthur.stewart@orau.org

References
1. A. Osbourn, *PLoS Biol*. **6**, e211 (2008).
2. A. J. Stewart, *Bull. Ecol. Soc. Am*. **80**, 133 (1995).
3. A. J. Stewart, *Amer. Biol. Teacher* **67**, 133 (2005).
4. J. Gresham, *Diary of a Cell* (Steel Toe Books, Bowling Green, KY, 2005).
5. S. Lindsay, *Twigs and Knucklebones* (Copper Canyon Press, Townsend, WA, 2008).
6. A. H. Deming, *Genius Loci* (Penguin Books, New York, 2005).

Science Education: Learn by Listening

WHILE READING P. WEBB'S PERSPECTIVE, "Science education and literacy: Imperatives for the developed and developing world" (special section on Science, Language, and Literacy, 23 April, p. 448), I was struck by the commonalities between second-language acquisition and scientific literacy. However, one aspect of the discussion was missing: Webb clearly identifies the roles of reading, writing, and talking, but he gives listening short shrift.

There is a great body of evidence supporting the idea that listening is essential for the acquisition of language. The foremost proponent of this idea is Stephen Krashen (*1*). Krashen's language-acquisition theories indicate that with a sufficient amount of comprehensible input (material that is meaningful and at a level appropriate to the listener's skills), the acquisition of language becomes a self-reinforcing process. Any language acquisition—whether it be a second language or the language of science—requires rich, varied, and authentic comprehensible input. This content is different from explicitly studying the rules of a language. As Webb notes, the exposure to science is made comprehensible when students are able to discuss the content in their native languages. Listening to scientific discourse is as essential a component of education as the other features so clearly delineated by Webb.

PETER S. KESSLER
School of Medicine, University of Washington, Seattle, WA 98104, USA. E-mail: psk@u.washington.edu

Reference
1. S. Krashen, *Principles and Practices in Second Language Acquisition* (Pergamon, Oxford, 1992).

Response

KESSLER IS CORRECT THAT THERE SEEM TO BE commonalities between second-language acquisition and the development of scientific literacy, and that listening to science is as essential a component of education as the other features delineated in my Perspective. The scientific literacy strategy that underpinned the studies undertaken in South Africa (*1*) included several exercises that tested listening skills. For example, teachers read students a story and then asked them comprehension questions. In another activity, teachers gave oral instructions to students to complete a diagram (*1*). The overall findings of the study suggest that, as Kessler succinctly points out, when students have genuine and engaging learning experiences, together with the opportunities for hearing scientific discourse, these processes are self-reinforcing and lead to acquisition of scientific literacy. Moreover, they appear to have a positive effect on both the native language and the second language used as the medium of instruction (English).

PAUL WEBB
Nelson Mandela Metropolitan University, Port Elizabeth, 6001, South Africa. E-mail: paul.webb@nmmu.ac.za

Reference
1. P. Webb, *Int. J. Environ. Sci. Educ.* **4**, 313 (2009).

Science Education: Flouting Formality

IN HER PERSPECTIVE "ACADEMIC LANGUAGE and the challenge of reading for learning about science" (23 April, special section on Science, Language, and Literacy, p. 450), C. E. Snow's observation that today's students are struggling with academic language did not surprise me. The nonfiction texts, including textbooks, that 21st-century students read are farther removed from academic texts than ever before. Most recent award-winning nonfiction trade books read like stories. The writing style is lively and engaging and often incorporates a variety of narrative elements. The design, format, and art in these books all work with the text to enrich the presentation.

Today, most schools teach writing using the Six Plus One Writing Traits, which guides students in crafting prose that is interesting, easy to understand, and enjoyable to read. Six Plus One emphasizes the use of strong, active verbs and colorful phrases to grab the reader's attention. Students are encouraged to use a conversational tone and to let their voice, or personality, infiltrate their writing. These traits are diametrically opposed to the standard conventions of academic writing, which features complex sentence structure, a distanced, authoritative tone, and judicious use of passive verbs.

When I first started reading academic texts in the 1980s, comprehending them was a challenge. The terse writing was thick with unfamiliar vocabulary and unfamiliar concepts, but the style was not all that different from the language in my high school science textbooks or the language I was expected to use when writing papers for English class.

Today's young people have a very different experience when they encounter academic texts. For them, navigating academic writing is like translating a foreign language. Not only do they have to confront the high-level vocabulary and sophisticated concepts, they must deal with language constructions and conventions that are completely new to them.

Snow recommends that educators spend more time helping students learn to process academic writing. But I worry that middle

Letters to the Editor

Letters (~300 words) discuss material published in *Science* in the previous 3 months or issues of general interest. They can be submitted through the Web (www.submit2science.org) or by regular mail (1200 New York Ave., NW, Washington, DC 20005, USA). Letters are not acknowledged upon receipt, nor are authors generally consulted before publication. Whether published in full or in part, letters are subject to editing for clarity and space.

school and high school students faced with the arduous task of deciphering academic text may become so frustrated that they lose their interest in science. Maybe it would be better if, instead, academic writing evolved to reflect the way 21st-century learners approach the world. Put another way, if academic writing were to become less formal and less terse, would the communication of scientific ideas suffer? I'm inclined to think that what matters is the writing process and the critical thinking it requires—not the language conventions used by the author.

MELISSA STEWART
Acton, MA 01720, USA. E-mail: hbeeprod@msn.com

Science Education: Mixed Messages

IN THE PERSPECTIVE "ACADEMIC LANGUAGE and the challenge of reading for learning about science" (23 April, special section on Science, Language, and Literacy, p. 450), C. E. Snow writes that nominalizations make academic language concise (such as the noun "application" in place of the phrase "how we apply").

Whether nominalizations are preferable is a matter of some dispute. The CBE Manual (*1*) says, "The frequent use of nouns formed from verbs and3 ending in 'ion' produces unnecessarily long sentences and dull, static prose." The APA Manual (*2*) urges us to use active verbs and to avoid wordiness. Williams (*3*) shows that rewriting nominalizations as active verbs clears up obscure sentences. Research supports the style manuals by showing that participants remember a denominalized report better than a nominalized version (*4*).

Advocates of nominalization cite the work of the linguist M. A. K. Halliday (*5*), who concluded that scientific language had advanced by nominalizing verbs and that such nominalizations better express scientific ideas. Books written by those subscribing to this theory [e.g., (*6*)] advise students to use nominalizations and passive verbs.

We need the right answer to this contradiction. Understanding science can be difficult, but we should not make it harder than it needs to be.

HAROLD A. SCARBRO
Scarbro Educational Consulting, Inc., 5057 Cedar Lawn Way, Las Vegas, NV 89130, USA. E-mail: harold@scarbro.com

References

1. Council of Biology Editors Style Manual Committee, *Scientific Style and Format: The CBE Manual for Authors, Editors, and Publishers* (Cambridge Univ. Press, Cambridge, 2002).
2. American Psychological Association, *Publication Manual of the American Psychological Association* (American Psychological Association, Washington, DC, 2001).
3. J. M. Williams, *Style: Ten Lessons in Clarity and Grace* (Pearson Education, New York, 2005).
4. J. H. Spyridakis, C. S. Isakson, *Annu. Conf. Soc. Tech. Commun.* **43**, 251 (1996).
5. M. A. K. Halliday, J. Webster, *The Language of Science* (Continuum, London, 2004).
6. A. Gillett, A. Hammond, M. Martala-Lockett, *Successful Academic Writing* (Pearson, Harlow, UK, 2009).

CORRECTIONS AND CLARIFICATIONS

SPORE Essay: "MIT OpenCourseWare: Unlocking knowledge, empowering minds" by C. d'Oliveira *et al.* (30 July, p. 525). The authors' roles in OpenCourseWare were described incorrectly: Kate James is senior manager, User Experience for OCW. Cecilia d'Oliveira is executive director of OCW. The Web site for the Highlights of Calculus course is http://ocw.mit.edu/high-school/courses/highlights-of-calculus/.

Letters: "Immigration law jeopardizes university collaboration" by J. A. de la Peña *et al.* (30 July, p. 511). The programs listed in Note 1 (and alluded to in the photograph caption) have been put on hold, not canceled.

MPC-200
Multi-manipulator system

Versatile:	User friendly interface controls up to two manipulators with one controller. Select components to tailor a system to fit your needs.
Expandable:	Daisy chain a second controller and operate up to four manipulators with one input device.
Stable:	Stepper motors and cross-rolled bearings guarantee reliable, drift-free stability.
Doubly Quiet:	Linear stepper-motor drive reduces electrical noise. Thermostatically-controlled cooling fans barely whisper.

Make the right move!



SUTTER INSTRUMENT
PHONE: 415.883.0128 | FAX: 415.883.0572
EMAIL: INFO@SUTTER.COM | WWW.SUTTER.COM

Call for Papers

Science Signaling



Science Signaling, from the publisher of ***Science***, AAAS, features top-notch, peer-reviewed, original research weekly. Submit your manuscripts in the following areas of cellular regulation:

- Biochemistry
- Bioinformatics
- Cell Biology
- Development
- Immunology
- Microbiology
- Molecular Biology
- Neuroscience
- Pharmacology
- Physiology and Medicine
- Systems Biology

Science Signaling is indexed in CrossRef and MEDLINE

Subscribing to ***Science Signaling*** ensures that you and your lab have the latest cell signaling resources. For more information visit **www.ScienceSignaling.org**

Submit your research at:
www.sciencesignaling.org/about/help/research.dtl

Science Signaling
AAAS


AAAS + U = Δ



Since 1848, AAAS has served as a prominent voice to advance science and as a valuable resource for scientists, educators, and policy makers. For the past 100 years, part of this mission has included publishing the journal *Science*, one of the world's premier peer-reviewed research journals. Working together to disseminate the most compelling discoveries across all scientific disciplines, AAAS and *Science* continue to fulfill their mission of advancing science for the benefit of all.

In addition to supporting *Science*, individual memberships are a driving force behind critical AAAS programs and activities designed to strengthen the global scientific enterprise. By becoming a AAAS member, you not only make a significant impact by allowing AAAS to continue its mission of advancing science and serving society, but you also gain powerful resources to develop your own career.

As a member, you'll receive 51 issues of the journal *Science* delivered weekly as well as online access to: groundbreaking research before it's published; the *Science* online archives dating back to 1880; and the current table of contents. In addition to all the benefits provided by the journal *Science*, AAAS has partnered on behalf of its members to provide substantial discounts with numerous organizations, including: Apple, VISA, GEICO, Barnes & Noble, and more.

If you're interested in becoming a AAAS member and changing the face of science, please visit **aaas.org**. Join us. Together we can make a difference.

AAAS + U = Δ

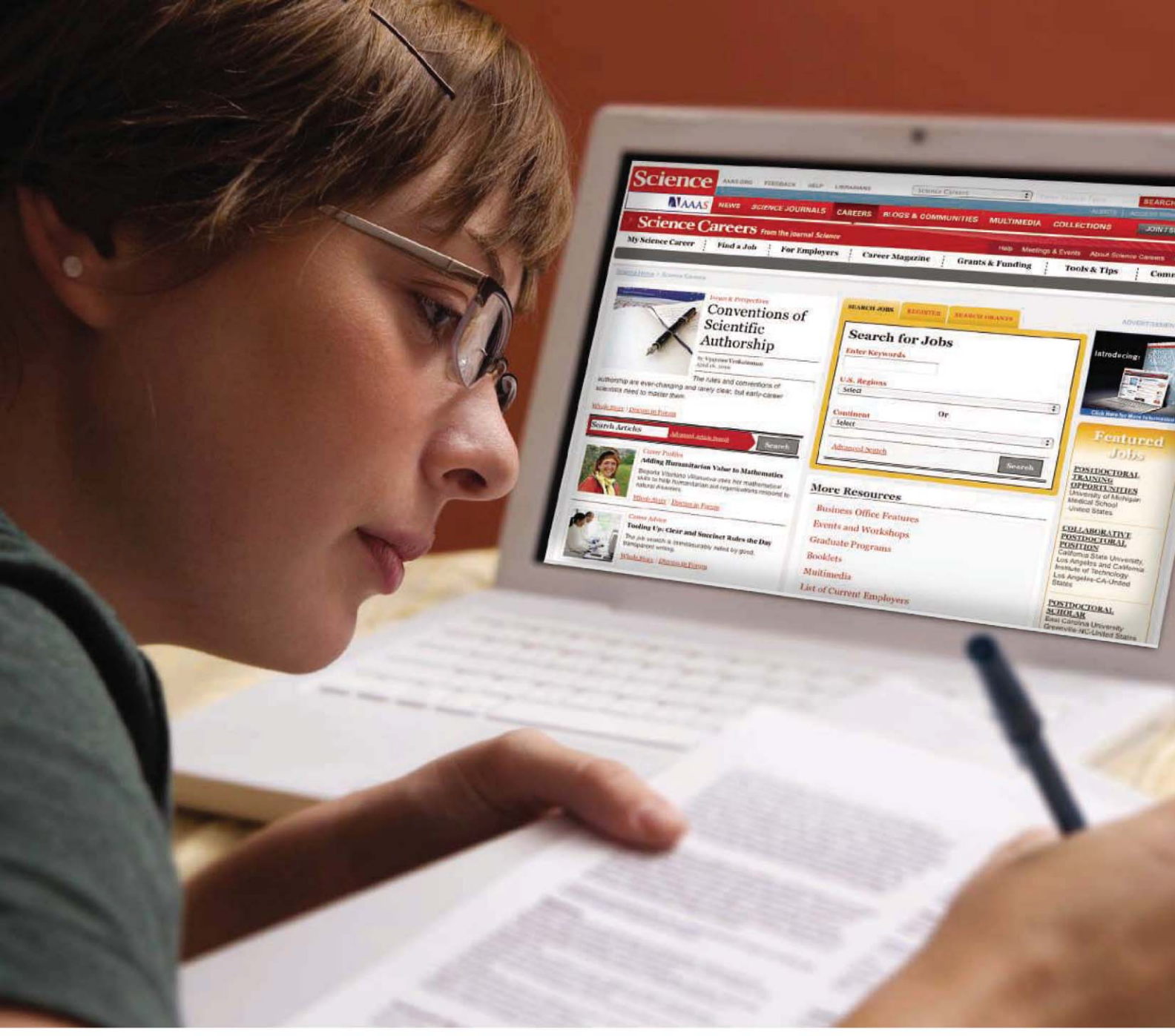


AAAS is here – bringing scientific expertise to policy making.

Good science policy is the result of politicians understanding science and scientists understanding policy. Toward this end, AAAS manages the Science & Technology Policy Fellowships program, which embeds scientists and engineers in the federal government for up to two years. From Congress to the State Department, each class of Fellows contributes to the policy-making process while getting hands-on experience at the intersection of science and policy. As a AAAS member your dues support these efforts. If you're not yet a AAAS member, join us. Together we can make a difference.

To learn more, visit aaas.org/plusyou/fellows

AAAS + U = Δ



AAAS is here – helping scientists achieve career success.

Every month, over 400,000 students and scientists visit ScienceCareers.org in search of the information, advice, and opportunities they need to take the next step in their careers.

A complete career resource, free to the public, *Science* Careers offers a suite of tools and services developed specifically for scientists. With hundreds of career development articles, a grants and scholarships database, webinars and downloadable booklets filled with practical advice, a community forum providing real-time answers to career questions, and thousands of job listings in academia, government, and industry, *Science* Careers has helped countless individuals prepare themselves for successful careers.

As a AAAS member, your dues help AAAS make this service freely available to the scientific community. If you're not a member, join us. Together we can make a difference.

To learn more, visit aaas.org/plusyou/sciencecareers

AAAS + U = Δ



AAAS is here – promoting universal science literacy.

In 1985, AAAS founded Project 2061 with the goal of helping all Americans become literate in science, mathematics, and technology. With its landmark publications *Science for All Americans* and *Benchmarks for Science Literacy*, Project 2061 set out recommendations for what all students should know and be able to do in science, mathematics, and technology by the time they graduate from high school. Today, many of the state standards in the United States have drawn their content from Project 2061.

Every day Project 2061 staff use their expertise as teachers, researchers, and scientists to evaluate textbooks and assessments, create conceptual strand maps for educators, produce groundbreaking research and innovative books, CD-ROMs, and professional development workshops for educators, all in the service of achieving our goal of universal science literacy.

As a AAAS member, your dues help support Project 2061 as it works to improve science education. If you are not yet a AAAS member, join us. Together we can make a difference.

To learn more, visit aaas.org/plusyou/project2061

AAAS + U = Δ



AAAS is here – bringing educational infrastructure to the developing world.

AAAS is helping the Rwandan government rebuild its educational infrastructure as a way to help drive economic growth and development. By providing materials such as the Project 2061 *Atlas of Science Literacy*, lesson plans from Science NetLinks, and access to *Science* digital libraries, AAAS is helping the people of Rwanda work toward a future built around science and technology. As a AAAS member your dues support these efforts. If you're not yet a AAAS member, join us. Together we can make a difference.

To learn more, visit aaas.org/plusyou/rwanda

AAAS + U = Δ



AAAS is here – preparing minority students for careers in science.

Part of AAAS's mission is to strengthen and diversify the scientific work force. To help achieve this goal AAAS partners with NSF to present the Historically Black Colleges and Universities Undergraduate Program, a conference where students from HBCUs get experience presenting their research, networking with peers, meeting with representatives from graduate schools, and learning about career opportunities. As a AAAS member your dues support these efforts. If you're not yet a AAAS member, join us. Together we can make a difference.

To learn more, visit aaas.org/plusyou/hbcuup

AAAS + U = Δ



AAAS is here – connecting government to the scientific community.

As a part of its efforts to introduce fully open government, the White House is reaching out to the scientific community for a conversation around America's national scientific and technological priorities.

To enable the White House's dialogue with scientists, AAAS launched Expert Labs, under the direction of blogger and tech guru Anil Dash. Expert Labs is building online tools that allow government agencies to ask questions of the scientific community and then sort and rank the answers they receive.

On April 12, 2010, AAAS asked scientists everywhere to submit their ideas to the Obama administration and at the same time launched the first of Expert Labs tools, Think Tank, to help policy makers collect the subsequent responses. The result was thousands of responses to the White House's request, many of which are already under consideration by the Office of Science and Technology Policy.

As a AAAS member, your dues support our efforts to help government base policy on direct feedback from the scientific community. If you are not already a member, join us. Together we can make a difference.

To learn more, visit aaas.org/plusyou/expertlabs

AAAS + U = Δ

HISTORY OF SCIENCE

Performance, Not Control

Tara H. Abraham

Standard histories and critiques have given us an image of cybernetics as a dry, foreboding, militarist science of command and control. The word cybernetics itself derives from the Greek word *kybernetes* ("governor" or "steersman"), and until now the paradigmatic case for the science of steersmanship has been the U.S. context, where cybernetics emerged in the wake of the Second World War. While the American case has received much attention from historians, the same cannot be said of British cybernetics. By focusing on the developments in Britain, Andrew Pickering's *The Cybernetic Brain: Sketches of Another Future* opens wide new vistas for exploring cybernetic practice and its legacy. For Pickering (a sociologist of science at the University of Exeter), cybernetics was primarily a science of the brain. As a protean science with connections to psychiatry, theater, music, politics, and counterculture, it was a lot more glamorous and fun than previous accounts of the field would have us believe.

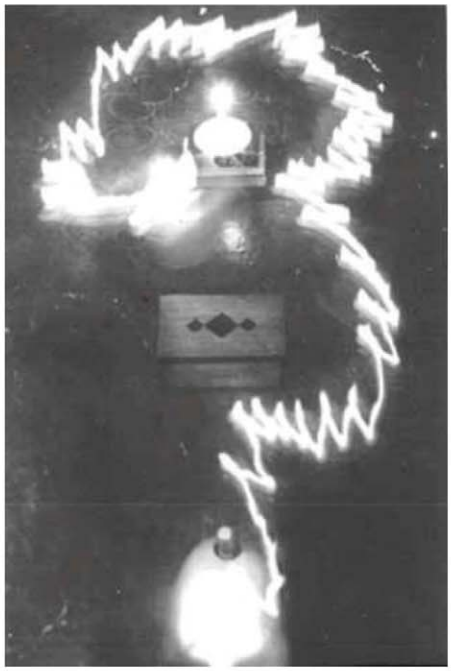
The Cybernetic Brain focuses on the colorful, lively, and sometimes strange world of British cybernetics from the late 1940s to the present. Pickering has selected a cast of four central players: "first generation" British cyberneticians W. Ross Ashby (1903–72) and W. Grey Walter (1910–77) and the second generation's Stafford Beer (1926–2002) and Gordon Pask (1928–96). Anthropologist Gregory Bateson (1904–1980) and psychiatrist R. D. Laing (1927–1989), who each developed a "cybernetic psychiatry" during the 1950s and 1960s, have the largest supporting roles. The brain itself is a central character in the story Pickering tells. Unlike many cognitive scientists, these cyberneticians did not view the brain as a system of representation but as a performative organ, and its main role as a performer was adaptation.

For example, Walter and Ashby, both trained in traditional brain sciences, built electromechanical models of the brain that were adaptive. Walter's robot tortoises were able to move and exhibit complex behavior through their detection of environmental changes in light and movement. By studying the behavior of such devices, Walter argued, one could learn something about how the human brain functions. The actual behavior of the machine was beyond prediction. Further, the behavior was performative: the machine actually had to "run" in order for one to discover what it was capable of doing. Like Walter, Ashby understood the brain to be adaptive, but in a different sense: the key, in his view, was finding and maintaining equilibrium rather than a "spatial engagement" with the environment. Ashby's homeostat connected adaptation fundamentally to learning: the machine engaged with its environment, but depending on what it encountered, it would review its circuitry until a configuration was found that placed it in dynamic equilibrium with its surroundings.

The Cybernetic Brain
Sketches of Another Future

by Andrew Pickering
University of Chicago Press, Chicago, 2010. 536 pp. $55, £35.50. ISBN 9780226667898.

Directly influenced by Ashby, Beer was concerned with what he called "exceedingly complex" systems, such as the economy, the company, and the brain. For Beer, these sorts of systems were the "province of cybernetics"—they were neither completely knowable nor predictable. He saw the factory as a biological organism, one that should be equipped with an adaptive brain to allow it to survive in the face of market fluctuations and changing circumstances.



A tortoise performance. Grey Walter's "Elsie" maneuvers around a stool and approaches the light (1950).

CREDIT: GREY WALTER/COURTESY BURDEN NEUROLOGICAL INSTITUTE, UNIVERSITY OF BRISTOL

Pask entered the world of cybernetics through the world of the arts—particularly theater and music. Pask's Musicolour machine used the sound generated by a musical performance to control a light show. What made this process open-ended and "cybernetic" was that the parameters of the circuitry were not constant: the rules about which sound frequencies corresponded to particular light colors varied continuously. The human performer and the machine would be in a constant reciprocal process of learning—neither in control of the performance.

According to Pickering, what drove the performative practice of these cyberneticians was an entirely distinct understanding of what the world is like. Traditional, noncybernetic sciences (what Pickering calls the "modern" sciences) are infused with a dualism in which people are distinct from things and scientists emphasize prediction and calculation. Cyberneticians rejected both aspects of modernity: people and things are not so different after all, and rather than cause-and-effect prediction, reality evolves temporally—it emerges. Thus, Pickering argues his principals were presenting a distinct cybernetic ontology—a different way of understanding what kinds of objects populate the natural world and how these engage with one another. For Pickering, this adaptive, performative cybernetic ontology can be likened to an ontological theatre, and this is at the root of what is so fascinating about work in cybernetics.

In a similar vein, the book displaces knowledge as the key to understanding what science is all about. Rather, the key is practice. Alluding to his ground-breaking *The Mangle of Practice* (*1*), Pickering argues that scientific practice is characterized by a nondualism: an intertwining of people and things in a temporally emergent process called "mangling"—a dance of agency between scientists and the natural world. What does this have to do with British cybernetics? This "performative engagement" that defines scientific practice also was what defined British cybernetics: the sensitive, responsive systems built by Ashby, Walter, Beer, and Pask modeled the performative aspects of the brain.

The Cybernetic Brain presents cybernetics as a true science of the sixties. That is partly due to the field's incompatibility with the modern sciences: socially, it was marginal, did not have a clear-cut institutional home, and thrived socially via formal and infor-

The reviewer is at the Department of History, University of Guelph, Guelph, Ontario N1G 2W1, Canada. E-mail: taabraha@uoguelph.ca

mal gatherings. Pickering finds this unstable social basis crucial to how cybernetics was disseminated. Because it bordered on amateurism, it had a stronger cultural resonance and popularity. Not only did cybernetic practices spill over into all sorts of disciplines and fields, such as management, politics, and the arts, there was also a strong affinity between cybernetics and Eastern philosophy and spirituality. For instance, the cybernetic psychiatry of Bateson and Laing stood in stark contrast to the mainstream psychiatry of the 1950s and 1960s—it was deemed "antipsychiatry" for its stance against the violent interventions that dominated mainstream practice (such as shock therapy and lobotomy). Both Bateson and Laing were deeply critical of traditional psychiatry and its hierarchical structures, and their version was more informed by Eastern philosophy and religion, which also happened to be hallmarks of the countercultural movements that defined the decade.

Why should we care about cybernetics? Pickering sees something vitally important in British cybernetics, and this explains the book's subtitle. Put simply, cybernetic practice can be seen as a model for future practice. We are increasingly confronted with problems that require different solutions—the "exceedingly complex systems" that modern sciences cannot tackle. There are systems that surprise us, that fall outside of the framework of calculability and prediction. The aspect of cybernetics that is most important and compelling for Pickering is its assumption of an ontology of unknowability. The term captures, for Pickering, what was novel and important about what the British cyberneticians were doing. This unknowability and awesome complexity is not cause for despair—in fact there are ways that scientists can be constructive and creative in tackling such systems—and Pickering's cyberneticians show us how. The author sees cybernetic science as fundamentally democratic: it forces us to have respect for the other, and it displaces the anthropomorphic stance we have on nature as a result of the dominance of modern sciences. Following political scientist James Scott's list (*2*) of "high modernist" projects that "aim at the rational reconstruction of large swathes of the material and social worlds," Pickering discusses the "dark side" of modernity. Here he includes projects that have had very disastrous consequences, such as the reform of agriculture with its effects on world famine and the effects of industrialization on global warming. It is in combating such projects—and the modernist attitude that fuels them—that Pickering sees the greatest merit in cybernetic ontology. It suggests that there is a way we might act differently. There is enormous value in adopting this different ontological stance, in which the world is not ours for the taking.

References

1. A. Pickering, *The Mangle of Practice: Time, Agency, and Science* (Univ. Chicago Press, Chicago, 1995).
2. J. Scott, *Seeing Like a State: How Certain Schemes to Improve the Human Condition Have Failed* (Yale Univ. Press, New Haven, CT, 1998).

10.1126/science.1192274

EXHIBITIONS

Skin Overlooked

> … when I was a young man just setting out on my career in skin.

George Nuku asked his cousin to carve him. It took 18 hours, and by the time his relative had finished George was blind from the swelling and inflammation. He wondered what he'd done. He couldn't see his new self until four days later. In traditional Maori culture, Ta Moko begins as a rite of passage at 15 years old. The intention, according to George, is to inscribe the person's soul on the outside. To achieve a full Ta Moko with ridges of scarification, George will need to be carved five times. But at the age of 46, his skin is thin, and the process time consuming. Plus, he doesn't have much time: he is fully occupied in traveling around the world promoting Maori culture.

George is a live exhibit (and consequently often not present) at the Wellcome Trust's current exhibition, *Skin*. The show is accompanied by a variety of events, from discussions about tattoos, the use and utility of cosmetics, and the theme of elasticity to a full frontal symposium on nudity and all its embarrassments. There is a series of tours of the exhibit given by the curators, contributing artists, and Michelle Lovric, the author of *The Book of Human Skin* (from which I have taken the quotations that act as subheadings here).

• • •

> Perhaps this is why I have always loved the skin: because it is both the story and the storyteller.

The exhibition comprehensively illustrates Lovric's book. Skin is the main character in her comic, gothic horror story: a black 'n' white, good 'n' evil story. The distinctive skins of the five voices of the book are constantly on display, even depicted by different typefaces on the paper skins of the book. As his own erupts in crops of maggoty pimples, the garrulous Minguillo Fasan pursues an obsessive desire to torment his beautiful and pusillanimous sister, Marcella, almost, but not quite, to the point of death. In balancing the evil characters, the other crazed lunatic, Sor Loreta, is determined to toy with her own life and masochistically destroys her skin in her madly competitive desire to appear holier than thou. And then there is the all-too-necessary resectioning of skin that the sympathetic young surgeon Dr. Santo Aldobrandini has to practice, not to mention the bruises, wounds, diseases, and other evidence of grotesque abuse witnessed by the noble servant Gianni delle Boccole. Nevertheless, the appalling Minguillo Fasan apparently has some redeeming characteristics: his love of his Venetian palazzo and of his books. As the story peels apart, this passion for books is revealed to be yet another grotesque compulsion, but one that rather satisfyingly supplies his nemesis. The author artfully implies this is not a nice book, and as she pulls us in, horrified and intrigued, we, the readers, become complicit in Fasan's crimes. Indeed, it's a truly nasty book.

• • •

> … we were dextrous tailors of human skin.
> … stitching together the cleaved and shattered flesh in neat, swift seams.

The exhibition and Lovric's novel each make it plain that skin is the principal component of our identity, both hiding and betraying our inner selves. Although skin is tough, renewable stuff, every breach of our wrapping leaves its mark: we minutely examine every spot and wrinkle, cut or bruise on our own

Skin

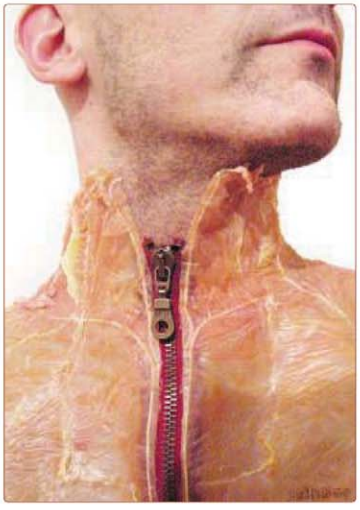
Javier Moscoso, Lucy Shanahan, and Nike Fakiner, Curators
Wellcome Collection, London. Through 26 September 2010.
www.wellcomecollection.org

The Book of Human Skin

by Michelle Lovric
Bloomsbury, London, 2010. 510 pp. Paper, £12.99.
ISBN 9781408805886.

dermis for the story it tells. Indeed, the scarring resulting from wounding, allergy, infection, or inherited disorders can leave profound marks on the inner person as well as the outer.

Some resort to artificial means to correct imperfections, using surgery to smooth away any signs of age distressing to the identity, ignoring that surgery cannot stop the rot within. Still, however much we might scorn the nip and tuck industry, its practice brings skills that, although honed on the wealthy and vain, can be employed with inestimable value to the less fortunate. For example, to aid children whose faces need reconstruction after the devastation of noma, cleft palate, burns, or leishmaniasis.



SkinBag jacket.

Reconstructive surgery means moving flesh around radically, which can create new problems. Skin behaves rather like cloth, and as it is cut and restitched it forms folds and tucks elsewhere over the body's contours. Rhian Solomon is a textile artist who teamed up with surgeon and fellow artist Brian Morgan to explore the pattern-making techniques of the Russian surgeon Alexander Limberg (1894–1974). Limberg wrote a treatise on geometrical surgery; he proposed that surgeons should practice their technique by folding paper patterns to see how resectioned skin falls into place. Solomon has applied her dress-making skills to observe how Limberg's geometry translates into a nose or a breast or covers a gap after excision of a tumor. She's hoping to obtain funding to develop novel patterns for skin reconstruction.

To satisfy mere vanity though, you could try SkinBag, a Parisian haute couture company that can provide you with an alternative skin to wear just for the day. Olivier Goulet manufactures apparel from latex to resemble skin of various colors. An array of jackets and overalls are hanging in the exhibition for the visitor to try on, although their texture is too repellent and the odor too offensive to be tempting.

• • •

> … I wanted to know the intimate details of flaying. Skin does not fall off of its own accord!

To the 17th-century anatomist, skin was an inconvenient barrier that obscured the interesting machinery beneath. There's a form of illustration, known as écorché (flayed), in which the body is sometimes depicted as removing and carefully putting aside its skin, almost as if it anticipated a museum curator would find the shed tissue 300 years later. In this tradition of revealing the body beneath the skin, exquisite wax models were made for medical education. Anna Morandi Manzolini (1714–1774) became an exceptional practitioner of ceroplasty and stepped into her departed husband's shoes as professor of anatomy at the University of Bologna. *Skin* has several wax models on display. Lying curled up on a silken bed is the piteous body of a boy smothered with encrustations of skin fungus. A row of amputated hands shows the wear and tear a laboring life brings. A replica of a fatal exfoliating disorder is contained in a glass bottle as if infectious, and, lastly, a collapsing head shows how even wax models age. To offer a counterpoint to the literal wax artworks, Tamsin van Essen has provided a selection of ceramic apothecary jars that bear abstract wounds as if the pots have caught syphilis or developed acne.

• • •

> … so many things going on between his thoughts and his skin.

As curator Javier Moscoso points out, the boundary the skin represents is a thin one, as is the boundary between appropriate and inappropriate. Topologically, the skin, or at least the epithelium, is endless. A tableau of orifices, ears, noses, and perinea attempts to demonstrate where the outside ends and the inside begins. Here we have a wax vagina. It is held open not by the owner's own fingers—as to do so the hands would have had to have been attached to the arms upside-down. Perhaps these intruding fingers represent the onlooker's own? And thus, helplessly, we become complicit voyeurs. Despite the assistance, there's not much to see within, so for whose edification was this model's virtue on display?

Medical examination requires inspection of the skin, and all the lewd possibilities this brings are summed up in *The Examination* by Jules-Abel Faivre (circa 1898), in which an elderly doctor has one ear planted firmly on a girl's breast. She looks directly out, discomforting us with her gaze.

There are few other breasts on view, with the exception of those depicted on samples of tattooed human skin. These came from 19th-century France and comprise large and crudely made sketches of naked women, which may have been removed from the bodies of prostitutes who were tattooed as a sign of their occupation. How and why were these collected?

• • •

> Some people see skin simply as a texture, that holds in place all the important organs, as a sack holds a squirming haul of fish. Few know what a strong lens reveals of that sack …

The curators dipped into the Wellcome Collection's film vault and found some interesting relics among the educational footage. A 1960 German film of skin sweating is almost beautiful. It zooms onto the ridges of a fingerprint, and gradually spits and spots of liquid shine on the crests, dry, and become replaced as regularly as the pulse of blood beneath. Similarly mesmerizing, until realization strikes, is the film *Sybille II* by Wim Delvoye (1999).

Unexpected beauty also comes from still artworks like Gemma Anderson's portrait of Melissa Smith that transforms disease and disfiguration. Smith has the genetic condition epidermolysis bullosa, which causes the skin to blister and erode painfully, leaving scarred and encrusted skin that has to be constantly tended to. Anderson's copperplate engravings transform the lesions into jewels and make a landscape appropriate for the women's common passion for the decadent novel *Against Nature* by Joris-Karl Huysmans (1848–1907).

• • •

> … all the rooms of my imagination were lined with soft human skin.

Like Lovric's book, *Skin* shocks and disgusts. Nonetheless, the curators had an overarching goal of showing how important the skin is as an organ and how much it is taken for granted. Moscoso described his criteria for the exhibition: the use of books, the importance of hands, avoidance of full frontal female nudity, no skin physiology, and almost no discussion of color (even the backdrop drapes of fake skin were pale). The curators did not want to encourage puerile gawping, but half of us have (had) breasts. I don't know whether we'd be better off being more formally educated about skin or meditating yet further on the boundaries skin represents. The exhibition didn't fail in provoking thought, and Lovric's book didn't fail in simply provoking.

–Caroline Ash

10.1126/science.1195197

CREDIT: WWW.SKINBAG.NET

NUCLEAR WASTE

Nuclear Waste: Knowledge Waste?

A stalled nuclear waste program, and possible increase in wastes, beg for social science input into acceptable solutions.

Eugene A. Rosa,[1,2]* Seth P. Tuler,[3] Baruch Fischhoff,[4] Thomas Webler,[3] Sharon M. Friedman,[5] Richard E. Sclove,[6] Kristin Shrader-Frechette,[7] Mary R. English,[8] Roger E. Kasperson,[9] Robert L. Goble,[9] Thomas M. Leschine,[10] William Freudenburg,[11] Caron Chess,[12] Charles Perrow,[13] Kai Erikson,[13] James F. Short[1]

Nuclear power is re-emerging as a major part of the energy portfolios of a wide variety of nations. With over 50 reactors being built around the world today and over 100 more planned to come online in the next decade, many observers are proclaiming a "nuclear renaissance" (*1*). The success of a nuclear revival is dependent upon addressing a well-known set of challenges, for example, plant safety (even in the light of improved reactor designs), costs and liabilities, terrorism at plants and in transport, weapons proliferation, and the successful siting of the plants themselves (*2*, *3*).

Particularly challenging is the disposal of high-level nuclear wastes (HLW). More than a quarter-million tons of commercial HLW is in need of disposal worldwide (*1*). Wastes accumulate at all stages of the fuel and weapons development cycle: mining, enrichment, fabrication, and reactor operation. The most dangerous of these wastes accumulate at the "back end" of the fuel cycle, particularly in the form of spent fuel, which, despite reprocessing technologies, may remain highly radioactive for a million years (*4*). Although disposal of HLW remains one of the most challenging scientific and social problems facing all nuclear nations, recent events in the United States, home of 60,000 tons of HLW, make this a particularly important time to highlight often-overlooked social science expertise needed to develop strategies for publicly acceptable solutions to the problem.

More Waste for a Stalled Waste Program

There is disagreement about short-term and mid-term approaches for disposing of HLW, which include hardened on-site or regional storage, but the global scientific and policy consensus for long-term disposal is through deep geological sequestration (*5*). In the United States, where a successful waste-disposal program has eluded 10 presidential administrations, the 1982 Nuclear Waste Policy Act, amended by Congress in 1987, designated a single deep geologic repository at Yucca Mountain, Nevada. Authorized to store 77,000 metric tons of spent fuel, this site was projected to begin accepting wastes by 31 January 1998. However, surprises arising from technical analyses of the site, such as the discovery that water flows more rapidly at the site than expected (*6*), increasing the chances of human exposure (*7*), led to this deadline being missed. Strong, persistent opposition among Nevada residents and others also contributed to delays, with the site not yet having accepted any waste (*8*, *9*). The Obama Administration withdrew funding for Yucca Mountain in its 2010 budget and directed the Department of Energy (DOE), the federal agency responsible for building a repository, to withdraw its licensing application to the Nuclear Regulatory Commission (NRC). These actions are currently the subject of multiple lawsuits and NRC review (*10*). If successfully upheld, they will effectively stop the Yucca Mountain project, despite its being the only congressionally authorized site for a repository.

The problem could worsen. The nuclear industry has taken advantage of a new one-step licensing process for commercial nuclear plants, submitting 22 applications to the NRC for 33 new reactors (*1*, *11*). Each new reactor could generate about 25 metric tons of HLW per year (*1*). President Obama confirmed the Administration's nuclear commitment by pledging $8.3 billion in federal loan guarantees for two new nuclear plants in Georgia (*12*) and by seeking to increase the total amount to $54.5 billion by next year (*13*).

Facing a stalled national waste program on one hand, and a possible increase in the volume of wastes on the other, the president directed the secretary of energy to appoint a Blue Ribbon Commission on America's Nuclear Future, which "should include recognized representatives and experts from a range of disciplines and with a wide range of perspectives" (*14*). The 15-member commission formed in January 2010 is charged with conducting "a comprehensive review of policies for managing the back end of the nuclear fuel cycle," including civilian and defense used nuclear fuel and nuclear waste (*14*). The White House further recognized that "Such a solution must be based upon sound science and capable of securing broad support, including support from those who live in areas that might be affected by the solution" (*15*).

Physical Constraints, Social Acceptability

Unfortunately, the scientists and officials seeking to craft an acceptable waste-management strategy are starting from the weak position created by the legacy of past actions. For example, the mishandling of wastes from military weapons facilities (*16*, *17*) generated considerable controversy and loss of social trust and confidence in the integrity of the siting and facility development program. Trust is a key factor in risk perceptions (*9*, *18*). The DOE is especially mistrusted (*19*) and has been unable to address this mistrust (*20*).

The key issue here is not only to get the science right but also to get the "right" science (*21*). Getting the right science means answering the right questions. Given the history of nuclear waste management, in the United States and elsewhere, those questions must focus on the conditions for social and political acceptability, within the constraints identified by physical science and engineering. Some communities will be asked to host the processing, storage, and disposal of used nuclear fuel and HLW. Others will be asked to allow the transport of these materials. All Americans will pay for the infrastructure. Although scientific and technical analyses are essential, they will not, and arguably should not, carry the day unless they address, both substantively and procedurally, the issues that concern the public.

Fortunately, there is a sizable social science literature that has systematically investigated the questions of public acceptability, making basic tenets of public concerns quite clear (*8*, *22*). People do not like projects that pose highly uncertain risks, unless they see great compensating benefits and have deep trust in the institutions managing them (*8*, *9*). Many studies have shown that these condi-

[1]Washington State University, Pullman, WA 99164, USA. [2]Woods Institute for the Environment, Stanford University, Stanford, CA 94305, USA. [3]Social and Environmental Research Institute, Greenfield, MA 01301, USA. [4]Carnegie Mellon University, Pittsburgh, PA 15213, USA. [5]Lehigh University, Bethlehem, PA 18015, USA. [6]The Loka Institute, Amherst, MA 01002, USA. [7]University of Notre Dame, Notre Dame, IN 46556, USA. [8]University of Tennessee, Knoxville, TN 37996, USA. [9]Clark University, Worcester, MA 01610, USA. [10]University of Washington, Seattle, WA 98105, USA. [11]University of California, Santa Barbara, CA 93106, USA. [12]Rutgers University, New Brunswick, NJ 08901, USA. [13]Yale University, New Haven, CT 06520, USA.

*Author for correspondence. E-mail: rosa@wsu.edu

tions for public acceptance are lacking with HLW (*8*, *9*, *18*, *23*). Citizens have expressed great concern about siting a repository in their vicinity, even while supporting nuclear power in the abstract (*8*, *18*).

Many studies have demonstrated the importance of engaging impacted publics at the beginning of policy planning and projects, to get the right questions to frame analyses, ensure that expectations for inclusive and fair processes are met, and ensure legitimacy of decisions (*24*–*26*). A variety of frameworks, such as the staged approach (*27*), have been developed for "analytic-deliberative" (*21*) processes to ensure a technically competent and publicly engaged solution. These frameworks emphasize "continuous, adaptive learning in both technical and societal areas," continuous public engagement, and transparent use of public inputs (*27*). Case studies show the benefits of public involvement, for example, the cleanup of an Ohio nuclear weapons facility (*28*) and the siting of a facility in New Mexico for storage of defense-generated transuranic wastes (*23*).

Moreover, public engagement and transparent deliberations are "communication acts" that build social trust and legitimacy, whatever their content. The social science needed to create such communications is well understood (*21*, *27*, *29*, *30*) and essential for strategies that rest on the principal of voluntary consent and the public's right to know (*31*, *32*).

However, despite decades of social science, guidance to promote adaptive learning, social trust, and legitimacy has not been followed in addressing waste and other challenges to nuclear power (*26*). For example, how state structures of democracy and the role of technical elites in policy formation and implementation may influence whether and how scientific evidence is used. Institutional cultures typically frame challenges as technical problems rather than societal challenges. To the extent that the social side is recognized, it has often been viewed as an obstacle to overcome, not an element of the democratic process; planners and officials can be fearful that public involvement may shift an unengaged or uninformed public toward more controversy or opposition, thus reducing their control. Those institutions may not trust the public to make the "right" decisions. Agency guidance is often very general, leaving planners vulnerable to missteps when dealing with contingencies of specific situations and averse to trying new approaches.

Rebuilding Trust

The Blue Ribbon Commission, the DOE, and other responsible agencies should make the rebuilding of social trust and credibility central to their operations and their proposed strategies for waste management, then draw on the social sciences needed to fulfill these commitments. This means making the public and the social sciences serving the public a driving priority (*33*). The science that can inform an adaptive learning process that involves the public in a way that improves decisions and enhances trust and credibility is remarkably inexpensive, compared with the stakes riding on their efforts.

The commission is particularly well positioned to begin the process of overcoming the problematic legacy that it inherited. It has taken steps toward transparency by fulfilling the requirements of the Federal Advisory Committee Act. However, there is little scientific reason to expect such a pro forma approach—where the emphasis is on meeting formal requirements, not the needs of the public—to succeed where its predecessors have failed. Rather, it runs the risk of exacerbating indifference, mistrust, and resistance (*24*). The alternative is to treat the public in a respectful, evidence-based way throughout the deliberations. Social science can provide effective guidance in the selection of representative publics, in the development of effective deliberation techniques, and in the integration of technical and lay knowledge. The commission, consistent with its charge and charter, should include expertise on its subcommittees to inform recommendations addressing social trust and credibility, perhaps even creating a subcommittee devoted specifically to procedural issues of a proposed waste-management strategy. The strategy adopted by the commission will affect not only how its recommendations are judged but also how the public should be involved in subsequent policy and siting decisions. Addressing relevant social issues does not guarantee success, but ignoring them increases the chances of repeating past failures.

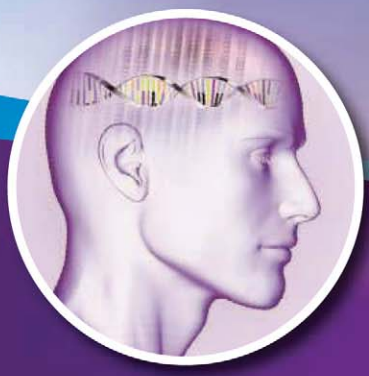
References

1. World Nuclear Association, www.world-nuclear.org/info/inf104.html.
2. M. V. Ramana, *Annu. Rev. Environ. Resour.* **34**, 127 (2009).
3. J. M. Deutsch *et al.*, Update of the MIT 2003 Future of Nuclear Power (Massachusetts Institute of Technology, Cambridge, MA, 2009); http://web.mit.edu/nuclearpower/pdf/nuclearpower-update2009.pdf.
4. National Research Council, *Technical Bases for Yucca Mountain Standards Waste* (National Academy Press, Washington, DC, 1995).
5. C. McCombie, T. Isaacs, *Daedalus* **139**(1), 32 (2009).
6. A. L. Flint, L. E. Flint, E. M. Kwicklis, G. S. Bodvarsson, J. M. Fabryka-Martin, *Rev. Geophys.* **39**, 447 (2001).
7. A. MacFarlane, R. C. Ewing, Eds., *Uncertainty Underground: Yucca Mountain and the Nation's High-Level Nuclear Waste* (MIT Press, Cambridge, MA, 2006).
8. R. E. Dunlap, M. E. Kraft, E. A. Rosa, Eds., *Public Reactions to Nuclear Waste: Citizens' Views of Repository Siting* (Duke Univ. Press, Durham, NC, 1993).
9. J. Flynn *et al.*, *One Hundred Centuries of Solitude* (Westview Press, Boulder, CO, 1995).
10. S. Tetreault, *Las Vegas Review-Journal*, 9 July 2010; www.lvrj.com/news/doe-appeals-on-yucca-decision-98143189.html?ref=189.
11. U.S. Nuclear Regulatory Commission, Expected New Nuclear Power Plant Applications; www.nrc.gov/reactors/new-reactors/new-licensing-files/expected-new-rx-applications.pdf.
12. Remarks by the President on Energy, Lanham, Maryland, 16 February 2010; http://www.whitehouse.gov/the-press-office/remarks-president-energy-lanham-Maryland.
13. White House Fact Sheet, Federal Budget, Fiscal Year 2011, Department of Energy; www.whitehouse.gov/omb/factsheet_department_energy.
14. Office of the Press Secretary, Presidential Memorandum: Blue Ribbon Commission on America's Nuclear Future (29 January 2010); www.whitehouse.gov/the-press-office/presidential-memorandum-blue-ribbon-commission-americas-nuclear-future.
15. U.S. Office of Management and Budget, *Terminations, Reductions, and Savings: Budget of the U.S. Government, Fiscal Year 2010* (OMB, Washington DC, 2009) p. 68; www.gpoaccess.gov/usbudget/fy10/browse.html
16. P. Slovic, J. H. Flynn, M. Layman, *Science* **254**, 1603 (1991).
17. J. Flynn, W. Burns, C. K. Mertz, P. Slovic, *Risk Anal.* **12**, 417 (2006).
18. S. C. Whitfield, E. A. Rosa, A. Dan, T. Dietz, *Risk Anal.* **29**, 425 (2009).
19. D. Metlay, in *Social Trust and the Management of Risk,* G. Cvetkovich and R. Löfstedt, Eds. (Earthscan, London, 1999), pp. 100–116.
20. Secretary of Energy Advisory Board (SEAB), *Earning Public Trust and Confidence: Requisites for Managing Radioactive Waste* (SEAB, Washington, DC, 1993).
21. National Research Council, *Understanding Risk: Informing Decisions in a Democratic Society*, P. C. Stern and H. V. Fineberg, Eds. (National Academy Press, Washington, DC, 1996).
22. B. Fischhoff, in *Oxford Textbook of Public Health*, R. Detels, R. Beaglehole, M. A. Lansang, M. Gulliford, Eds. (Oxford Univ. Press, Oxford, 2009), pp. 940–952.
23. H. Jenkins-Smith *et al.*, *Nuclear Reactions: A Synthesis of Survey Research Findings on Public Perceptions of Nuclear Materials Management Programs* (Institute for Public Policy, University of New Mexico, Albuquerque, 1999).
24. K. Shrader-Frechette, *Public Aff. Q.* **4**, 363 (1993).
25. K. McComas *et al.*, *J. Appl. Soc. Psychol.* **37**, 905 (2007).
26. National Research Council, *Public Participation in Environmental Assessment and Decision Making*, T. Dietz and P. C. Stern, Eds. (National Academies Press, Washington, DC, 2008).
27. National Research Council, *One Step at a Time: The Staged Development of Geological Repositories for High-Level Radioactive Waste* (National Academies Press, Washington, DC, 2003).
28. W. Lee, *Determining Our Environments: The Role of Department of Energy Citizen Advisory Boards* (Westview Press, Boulder, CO, 2002).
29. T. Webler, S. Tuler, in *Governance Reform Under Real-World Conditions: Citizens, Stakeholders, and Voice*, S. Odugbemi and T. Jacobson, Eds. (World Bank, Washington, DC, 2008), pp. 125–160.
30. Food and Drug Administration (FDA) Risk Communication Advisory Committee, FDA's Strategic Plan for Risk Communication (FDA, Washington, DC, 2009); www.fda.gov/downloads/AboutFDA/.../Reports/UCM183683.pdf.
31. A. MacFarlane, in *Uncertainty Underground: Yucca Mountain and the Nation's High-Level Nuclear Waste*, A. MacFarlane and R. C. Ewing, Eds. (MIT Press, Cambridge, MA, 2006), pp. 393–410.
32. H. Kunreuther, D. Easterling, *J. Policy Anal. Manage.* **15**, 601 (1996).
33. B. Geman, K. Howell, *Sci. Am.* Online, 7 May 2009; www.scientificamerican.com/article.cfm?id=doe-cuts-yucca.

10.1126/science.1193205

EXPLORING GENETIC DIVERSITY

Mapping the Genetic Landscape Through Next Generation Sequencing



August 31, 2010

12 noon ET, 9 am PT, 4 pm GMT

Characterizing the genetic diversity in a population comes with many challenges, one of which is the shear number of samples needed for analysis in order to provide a clear reading of underlying genetic variation. An effective way to solve this problem is through the use of multiplex polymerase chain reaction (PCR) run with barcoding, which offers the possibility of sequencing hundreds of unique samples per run using next generation sequencing technology. This process, known as amplicon resequencing, allows for each PCR amplicon to be sequenced individually, enabling both the identification of rare variants and the assignment of haplotypes.

This webinar will provide an overview of amplicon resequencing–based approaches, from the point of view of investigating the complexity and diversity seen in immune system genes. Experts will discuss topics such as site-specific recombination reactions and cellular dysfunction, as well as how to utilize cutting-edge technology to discover pathways and specific patterns which impact such factors as the inability of the body to mount an immune response and somatic recombination in antibody production.

DURING THIS WEBINAR, PANELISTS WILL:

- talk about best practices for setting up amplicon resequencing projects
- discuss the application of resequencing technologies to study immunologic and other forms of genetic diversity
- share their recent data and expert advice
- answer questions from the live, online audience in the field

PARTICIPATING EXPERTS

Michael W. Smith, Ph.D.
SAIC-Frederick
Frederick, MD

Francois Vigneault, Ph.D.
Harvard Medical School
Boston, MA

Henry A. Erlich, Ph.D.
Children's Hospital Oakland
Research Institute
Oakland, CA

REGISTER NOW!

Sign Up At:
www.sciencemag.org/webinar



Science
AAAS

Brought to you by the AAAS/*Science* Business Office

Webinar sponsored by Roche and 454 Sequencing

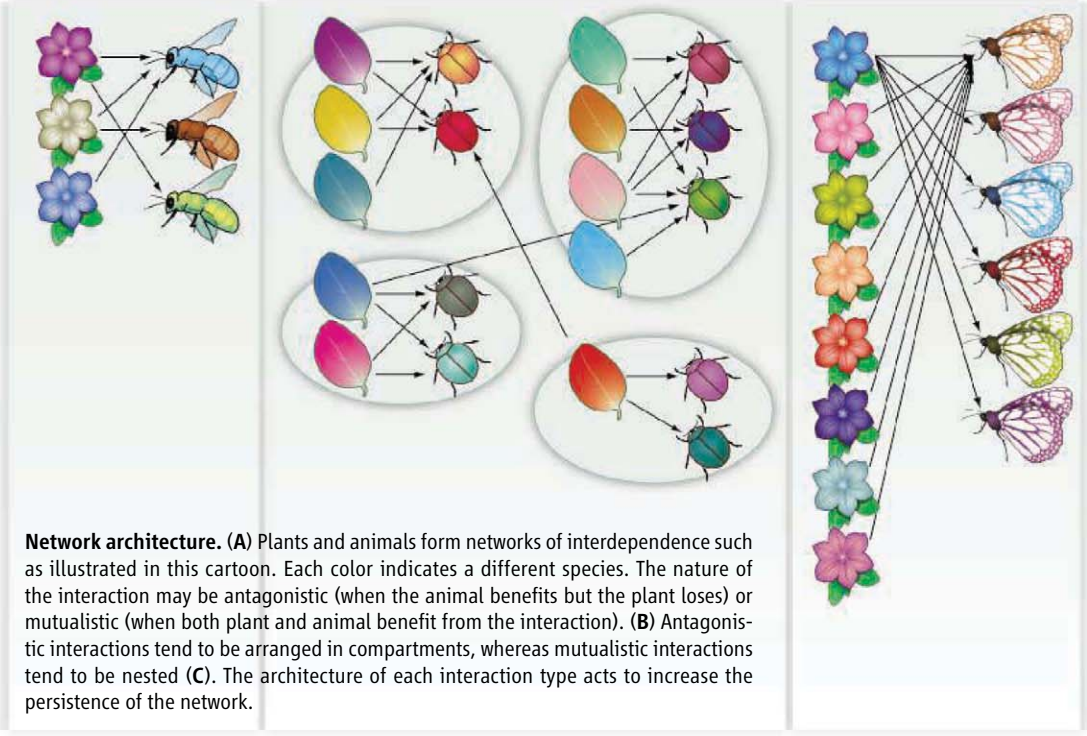
ECOLOGY

Structure and Dynamics of Ecological Networks

Understanding the architecture of species relationships may help predict how ecosystems respond to change.

Jordi Bascompte

Ecologists have a long tradition of studying how species interact. Almost all of this work, however, has focused on networks involved in a single type of interaction. For instance, ecologists have studied either "antagonistic" interactions, such as those in who-eats-who food webs, or, more recently, mutually beneficial interactions, such as those between flowering plants and their insect pollinators. Very few studies have embraced both (*1*–*3*), leaving a key question: To what degree do different kinds of interactions lead to ecological networks with different structures? The answer is crucial to understanding the suite of ecological, evolutionary, and coevolutionary processes that shape these networks and how they may respond to future changes. On page 853 of this issue, Thébault and Fontaine (*4*) take an important step forward by comparing the structure and dynamics of antagonistic and mutualistic networks.



Network architecture. (**A**) Plants and animals form networks of interdependence such as illustrated in this cartoon. Each color indicates a different species. The nature of the interaction may be antagonistic (when the animal benefits but the plant loses) or mutualistic (when both plant and animal benefit from the interaction). (**B**) Antagonistic interactions tend to be arranged in compartments, whereas mutualistic interactions tend to be nested (**C**). The architecture of each interaction type acts to increase the persistence of the network.

To understand community dynamics, ecologists must address two main issues. First, they must describe the architecture or structure of ecological networks. Second, they must illuminate how the architecture influences species extinction or persistence. The first task rests on countless hours of careful field work and imaginative statistical analyses. The second relies on analyzing mathematical models that encapsulate network dynamics. Thébault and Fontaine beautifully relate both structure and dynamics in a single, integrative study. To put their contribution in the best perspective, it helps to step back and consider some classic and more recent results of community ecology.

Integrative Ecology Group, Estación Biológica de Doñana, Consejo Superior de Investigaciones Científicas, Américo Vespucio s/n, E-41092 Sevilla, Spain. E-mail: bascompte@ebd.csic.es

Early research uncovered universal properties in the architecture of food webs, regardless of differences in species composition and network size (*5*). Parallel to this structural work, an influential paper by May illustrated that—contrary to intuition—the more complex a randomly built food web, the less stable it is (*6*). The main point of May's paper—and the reason that it continues to be influential almost four decades later—is not that complex ecological networks have to be unstable. Instead, the point is that real networks must have some contrasting, nonrandom structures that allow them to persist despite their complexity. One example of such a nonrandom pattern is "compartmentalization," or the tendency of a complex network to become organized in "compartments" characterized by a group of species interacting more strongly among themselves than with other species in the food web. A rich body of work has expanded this research (*7*) by documenting the numerous ways that the organization of food webs enables them to persist. However, this effort has focused almost exclusively on antagonistic interactions.

More recently, ecologists have turned their attention to mutualistic networks, bringing a quantitative framework to the study of coevolution in species-rich communities (*8*, *9*). This work has helped to dispel the frequently assumed view that coevolution has to lead to either highly specific, one-on-one species interactions or to diffuse assemblages that are intractable to analysis. Instead, this new generation of network studies has shown that mutualistic interactions have a "nested" architecture (*9*). In nested networks, more specialist species interact only with specific subsets of those species interacting with the more generalist species. This architecture—which researchers have compared to a set of nested Russian Matryoshka dolls—has been found to increase network robustness (*10*) and to maximize the number of coexisting species supported by these networks (*11*).

Still, the question remained: To what extent are these two types of ecological networks (antagonistic and mutualistic) arranged in different manners? To find out, Thébault and Fontaine simultaneously analyzed a large data set of both plant-pollinator and plant-

CREDIT: ADAPTED BY P. HUEY/*SCIENCE*

herbivore networks (*4*). They found that the mutualistic, plant-pollinator networks tend to be organized in a nested pattern; in contrast, the antagonistic, plant-herbivore networks tend to be organized in compartments (see the figure). Thébault and Fontaine next used a dynamical model to illustrate that, as species interact, mutualistic networks tend to become more nested than they were at the beginning. Antagonistic networks, in contrast, become more compartmentalized. Finally, the authors report that these contrasting architectures are the very ones that also increase the persistence of species in each network type.

These findings present a convincing case that the empirically observed architecture of an ecological network has clear implications for how it may respond to change. There are, however, important issues that remain to be explored. One is the mechanism leading to these contrasting network architectures. One could think that because each structure maximizes the persistence of its respective network type, increasing persistence is the driving force.

This may be the case, but—as with many other interpretations in biology—a correlation does not imply causality. Some researchers, for example, have argued that the "arms race" created by the tendency of herbivores to attack less-defended plants, and the subsequent tendency of plants to counteract such attacks, can by itself lead to networks with a compartmentalized structure (*8*). Here, each compartment would represent a close group of plants and insects participating in their own arms race toward specific adaptations. This mechanism, however, is not incompatible with others, and network structure probably reflects a combination of different processes (*12*).

The ultimate approach to disentangling the role of different mechanisms would be to create an experimental setting in which investigators can manipulate network structure while keeping other variables constant. This would pave the road toward exploring how the functional traits of species, and the many services provided by ecosystems, relate to ecological network structure. We might then be in a position to assess how the web of life, and the services it supports, will respond to global change.

References and Notes

1. T. M. Lewinsohn *et al*., *Oikos* **113**, 174 (2006).
2. M. A. Fortuna *et al*., *J. Anim. Ecol.* **79**, 811 (2010).
3. L. N. Joppa *et al*., *Ecol. Lett.* **12**, 961 (2009).
4. E. Thébault, C. Fontaine, *Science* **329**, 853 (2010).
5. J. E. Cohen, *Food Webs and Niche Space* (Princeton Univ. Press, Princeton, NJ, 1978).
6. R. M. May, *Nature* **238**, 413 (1972).
7. M. Pascual, J. A. Dunne, *Ecological Networks: Linking Structure to Dynamics in Food Webs* (Oxford Univ. Press, Oxford, 2006).
8. J. N. Thompson, *The Geographic Mosaic of Coevolution* (Univ. of Chicago Press, Chicago, 2005).
9. J. Bascompte, P. Jordano, C. J. Melián, J. M. Olesen, *Proc. Natl. Acad. Sci. U.S.A.* **100**, 9383 (2003).
10. J. Memmott, N. M. Waser, M. V. Price, *Proc. Biol. Sci.* **271**, 2605 (2004).
11. U. Bastolla *et al*., *Nature* **458**, 1018 (2009).
12. D. P. Vázquez, N. P. Chacoff, L. Cagnolo, *Ecology* **90**, 2039 (2009).

13. I thank D. B. Stouffer for comments on a previous draft. Funding was provided by the European Heads of Research Councils, the European Science Foundation, and the European Commission Sixth Framework Programme through a EURYI (European Young Investigator) Award.

10.1126/science.1194255

CELL BIOLOGY

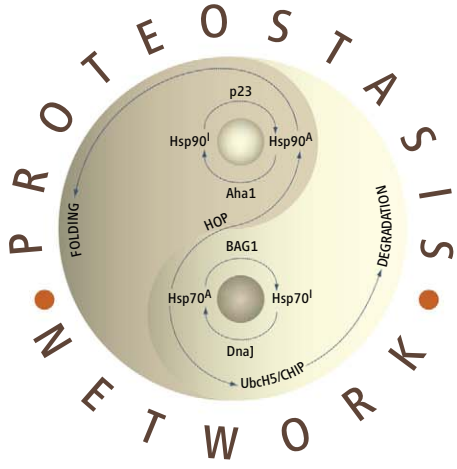
The Proteome in Balance

Cells monitor and maintain protein homeostasis by coordinating protein folding and degradation processes in multiple cellular locations.

Darren Hutt[1] and William E. Balch[1,2]

Inherited mutations and polymorphisms that alter the sequence of a polypeptide can affect its folding and stability, triggering disease at birth and during aging. A central cellular mechanism for generating and maintaining normal protein folds is the protein homeostasis or proteostasis network (referred to as the PN) (*1*). These processes sustain functional proteins as well as direct their removal from the cell during protein turnover or in response to misfolding. This "yin-yang" balance is critical for normal cellular, tissue, and organismal physiology. On page 805 in this issue, Okiyoneda *et al*. (*2*) show that the PN operates globally, constantly surveying protein folds, from co-translational insertion of proteins into the endoplasmic reticulum (ER) to removal of unstable proteins at the plasma membrane.

Okiyoneda *et al*. analyzed a mutant form of the cystic fibrosis transmembrane conductance regulator (CFTR) protein, an ion channel that transports chloride ions across mammalian epithelial cell membranes. The most prominent disease-causing mutation in cystic fibrosis is deletion of phenylalanine at position 508 (ΔF508) found in a cytosolic-oriented domain. This mutation causes an energetic destabilization that alters protein folding, targeting the mutant for removal (*3*). Whereas much work has focused on components of the PN that dictate folding and stability in the ER (*4*), Okiyoneda *et al*. have identified factors that regulate the stability of CFTR in the plasma membrane, the so-called peripheral quality control.



The yin and yang of proteostasis. Schematic representation of the balance between the folding (yang) and degradation (yin) branches of the cellular proteostasis network (PN) that globally manage protein folding in the cell in health and disease. Hsp70 and Hsp90 cycle between active (A) and inactive (I) forms by the regulatory co-chaperones shown. Hsp70/90 organizing protein (HOP) transfers proteins as shown. Prolonged binding of proteins to Hsp70 results in the recruitment of ubiquitin-conjugating (UbcH5) and ubiquitin-ligating (CHIP) enzymes that lead to degradative pathways. The balance between yin and yang pathways in human health and disease is regulated by the PN.

CREDIT: N. KEVITIYAGALA/*SCIENCE*

At physiological temperature (37°C), ΔF508 is rapidly degraded in the ER (*3*). This mutant can be delivered to the plasma membrane at a lower temperature (26°C), but a return to physiological temperature then triggers its degradation. Okiyoneda *et al*. took advantage of this temperature-sensitive local-

[1]Department of Cell Biology, Scripps Research Institute, La Jolla, CA 92037, USA. [2]Department of Chemical Physiology, Skaggs Institute for Chemical Biology, and Institute for Childhood and Neglected Diseases, Scripps Research Institute, La Jolla, CA 92037, USA. E-mail: webalch@scripps.edu

ization and identified a cytosolic ubiquitin-conjugating enzyme (UbcH5c) and ubiquitin ligase (CHIP) as key PN factors that direct plasma membrane–localized ΔF508 to the lysosome compartment of the cell for degradation. In addition, they elucidated critical roles for several proteins in stabilizing ΔF508 in the plasma membrane at low temperature: cytosolic heat shock proteins 70 and 90 (Hsp70 and Hsp90), the Hsp40 family of folding chaperones, and BCL2-associated anthanogene-1 (BAG1). Although UbcH5, CHIP, and Hsp70/90 proteins facilitate folding, export, and/or degradation of ΔF508 at the ER membrane during nascent protein synthesis (*4*, *5*), it was not anticipated that they would play similar roles at the plasma membrane. The findings support the principle that the PN dictates the fate of proteins throughout their functional life cycle.

The observations of Okiyoneda *et al*. have far-reaching implications for basic research and therapeutic approaches to human disease. The yin-yang nature of PN function is largely centered on core Hsp70 and Hsp90 chaperone systems (*6*) found in the cytosol and their homologs in the lumen of the ER (*7*). The balance between the degradative (yin) and folding (yang) pathways is tightly linked to the Hsp70/90 adenosine triphosphatase (ATPase) cycles (see the figure). These cycles are controlled by ATP-loading and ATPase-activating co-chaperones. In the case of cytosolic Hsp70, BAG acts as a nucleotide exchange factor, whereas Hsp40 proteins (DnaJ) serve as ATPase activators (*8*). Cytosolic Hsp90 ATPase activity is controlled by Aha1 and p23 and by many ancillary co-chaperones (*9*). The composition of these PN components varies considerably between different cell types (*7*, *10*). Moreover, folding is tightly linked to the folding energy landscape, a pathway of partially folded intermediates that a nascent protein must navigate to achieve its native state (*11*). Combining these observations, recent modeling (*7*, *12*) suggests that the rates of folding and misfolding as well as thermodynamic stability collectively influence the success or failure of the protein fold along the landscape in a process heavily managed by the yin and yang components of the proteostasis machinery (*1*, *7*, *12*).

The idea that ER- and plasma membrane–localized proteins are subject to the same surveillance system raises the specter that protein stability and function is continuously sensitive to the local cellular PN. Moreover, because the pathways dictated by the degradative side of the PN differ between the various compartments in which a protein can reside (e.g., chaperone-mediated translocation to the proteasome from the ER as opposed to delivery to the lysosome from the plasma membrane via vesicle transport), these results suggest that vesicular trafficking does not make the choice of protein life or death. Rather, it is a standard provided by the prevailing PN (*7*) that decides protein fate in health and disease. Thus, the network has the potential to provide global management to overcome loss- and/or gain-of-function mutations associated with numerous protein misfolding diseases. This conclusion is consistent with the fact that the standard can be varied between cell types and even within a given cell to meet folding demands in response to a broad range of signaling pathways, including the unfolded protein response, heat shock response, oxidative stress response, diet restriction, inflammatory signaling, and insulin growth factor 1 receptor signaling (*1*), all of which help protect the cell from environmental insults (*13*) and during aging (*14*, *15*).

The underlying operating principles of the PN highlighted by Okiyoneda *et al*. suggest that although various chemical, biochemical, and physiological approaches could solve the folding and trafficking defects in one cellular locale, we must ultimately address the folding and function problem for the cell as a whole through the malleable proteostasis network. Diverse human diseases, including cystic fibrosis, Alzheimer's disease, type II diabetes, cancer, and bacterial and viral pathologies (*16*), would benefit from better tools to control the PN therapeutically to restore human health. That is, we need to learn to use the biology of the yin and yang pathways to rebalance the biology that becomes unbalanced in human disease.

References

1. W. E. Balch, R. I. Morimoto, A. Dillin, J. W. Kelly, *Science* **319**, 916 (2008).
2. T. Okiyoneda *et al*., *Science* **329**, 805 (2010); published online 1 July 2010 (10.1126/science.1191542).
3. J. R. Riordan, *Annu. Rev. Biochem.* **77**, 701 (2008).
4. E. L. Turnbull, M. F. Rosser, D. M. Cyr, *BMC Biochem.* **8**, (suppl. 1), S11 (2007).
5. X. Wang *et al*., *Cell* **127**, 803 (2006).
6. S. A. Broadley, F. U. Hartl, *FEBS Lett.* **583**, 2647 (2009).
7. E. T. Powers, R. I. Morimoto, A. Dillin, J. W. Kelly, W. E. Balch, *Annu. Rev. Biochem.* **78**, 959 (2009).
8. M. J. Vos, J. Hageman, S. Carra, H. H. Kampinga, *Biochemistry* **47**, 7001 (2008).
9. S. K. Wandinger, K. Richter, J. Buchner, *J. Biol. Chem.* **283**, 18473 (2008).
10. D. M. Hutt, E. T. Powers, W. E. Balch, *FEBS Lett.* **583**, 2639 (2009).
11. F. U. Hartl, M. Hayer-Hartl, *Nat. Struct. Mol. Biol.* **16**, 574 (2009).
12. R. L. Wiseman, E. T. Powers, J. N. Buxbaum, J. W. Kelly, W. E. Balch, *Cell* **131**, 809 (2007).
13. R. I. Morimoto, *Genes Dev.* **22**, 1427 (2008).
14. S. H. Panowski, A. Dillin, *Trends Endocrinol. Metab.* **20**, 259 (2009).
15. R. I. Morimoto, A. M. Cuervo, *J. Gerontol. A* **64A**, 167 (2009).
16. R. Geller, M. Vignuzzi, R. Andino, J. Frydman, *Genes Dev.* **21**, 195 (2007).

10.1126/science.1194160

IMMUNOLOGY

β-Catenin Balances Immunity

Ira Mellman[1] and Björn E. Clausen[2]

Dendritic cells can limit responses to self antigens by activating the Wnt signaling pathway.

The human immune system ensures protective responses against pathogen-associated antigens while ignoring the individual's own proteins, carbohydrates, nucleic acids, and lipids. This balance of tolerance to "self" against immunity to "non-self" is crucial because its failure can lead to autoimmune and inflammatory disorders when tolerance is insufficient, or to unresolved chronic infections and possibly cancer when tolerance is too robust. On page 849 in this issue, Manicassamy *et al*. (*1*) demonstrate that β-catenin signaling, well known for its role in development, is key to balancing tolerance and immunity through the control of dendritic cell (DC) function.

Tolerance depends on two incompletely understood processes. "Central tolerance" largely operates perinatally in the thymus and eliminates T cells that detect self antigens (*2*). Deletion of such autoreactive T cells occurs when self proteins are expressed by antigen-presenting cells (e.g., thymic epithelial cells) under conditions that lead to T cell death rather than activation and proliferation. "Peripheral tolerance" is required throughout adulthood to eliminate autoreactive T cells not deleted by central tolerance (*3*). Peripheral tolerance also prevents immune responses to nonpathogenic organisms and environmental antigens that enter the airway or are ingested, as well as

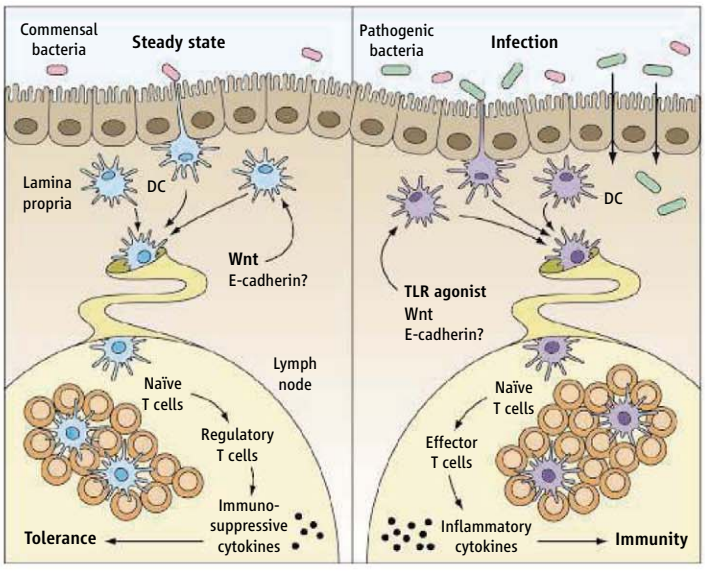
[1]Genentech, Inc., South San Francisco, CA 94080, USA. [2]Department of Immunology, Erasmus MC, University Medical Center, 3015 GE Rotterdam, Netherlands. E-mail: mellman.ira@gene.com; b.clausen@erasmusmc.nl

antigens associated with commensal bacteria that colonize the digestive tract.

DCs serve dual and seemingly opposite functions in generating and maintaining peripheral tolerance (*3*, *4*) and in initiating immunity, both by presenting foreign antigens to naïve T cells. In the absence of overt infection or inflammation, DCs in peripheral or lymphoid tissues are at "steady state" and are tolerogenic (see the figure). However, the exact nature of these tolerogenic DCs has not been clear. One early idea was that they are "immature," unable to produce the costimulatory molecules and cytokines needed to induce T cell immunity. However, immature DCs do not easily migrate from the periphery to draining lymph nodes, nor do they present antigen or interact effectively with T cells, characteristics of mature DCs (*5*). Production of regulatory T (T_{reg}) cells, purveyors of tolerance, requires DCs and DC-derived cytokines, further complicating the simple view that resting, immature DCs are tolerogenic (*3*). Even at the steady state, lymph nodes harbor DCs that express costimulatory molecules, indicating that some form of DC maturation occurs in the absence of infection (*6*, *7*).

DCs exist as multiple subsets, suggesting that one or more could be specialized for inducing tolerance. At least in the murine gut, a distinct DC population (expressing the markers CD103 and CD11b) from the mucosal lining performs this function (*8*). Yet it is unknown whether these cells require activation of a signaling pathway to enable tolerance induction.

Activation of a tolerogenic state in any DC population may indeed require an endogenous agonist or signaling pathway distinct from pathogen-derived products that induce immunogenic responses. One such pathway was first suggested by the finding that disruption of homophilic interaction between E-cadherin proteins at the surface of DCs causes their maturation. This occurs in part through inhibition of the cytoplasmic enzyme glycogen synthase kinase–3β (GSK3β) and activation of the β-catenin signaling pathway (which ultimately controls gene expression by the transcription factors T cell factor/lymphoid enhancer factor) (*9*). Although these mature DCs exhibited the expected increased expression of costimulatory molecules, they failed to produce immunogenic cytokines, instead inducing T_{reg} cell differentiation and tolerance to artificial and pathogenic antigens in mice. Thus, mature tolerogenic DCs can be generated by a signaling pathway that can be activated in the absence of microbial agonists.



Tolerance in the intestine. (Left) Under steady-state conditions, Wnt molecules (released by DCs, stromal cells, or mucosal cells) can activate multiple DC populations through the β-catenin signaling pathway (E-cadherin may also trigger this pathway). DCs migrate to lymph nodes where they promote the production of regulatory T cells and cytokines that lead to tolerance of self antigens. **(Right)** During infection, pathogenic organisms release agonists (TLR ligands) that overrule Wnt molecules (and perhaps E-cadherin) and trigger conventional DC maturation, leading to the generation of effector T cells and inflammatory immune responses.

Manicassamy *et al*. have not only put this idea to the test, but also revealed an attractive potential mechanism whereby tolerogenic DCs are generated by endogenous factors. By comparing the phenotypes of DCs from wild-type mice and from mice with DCs engineered to lack the gene encoding β-catenin, the authors found that intestinal lamina propria–derived DCs required activation of the β-catenin signaling pathway to secrete immunosuppressive cytokines essential for T_{reg} cell production. This was true not only for the CD103 and CD11b-positive DC population previously implicated in T_{reg} cell generation (*8*), but also for other gut DC populations. In DCs lacking β-catenin, production of immunosuppressive cytokines was decreased, as was their ability to stimulate the differentiation of naïve T cells into T_{reg} cells in vitro. Instead, inflammatory T cells (such as T helper 17 cells) were more efficiently produced. Importantly, mice lacking β-catenin were more susceptible to dextran sulfate sodium–induced colitis, as would be expected if T_{reg} cell production were reduced. Manicassamy *et al*. confirmed that key elements of the Wnt signaling pathway are expressed by gut DCs and macrophages, including several Wnt ligands and their receptors (Frizzled). Wnt-Frizzled interaction activates the canonical β-catenin signaling pathway in numerous developmental processes.

The results lead to an attractive model whereby the production of Wnts by DCs, macrophages, or other cells in the intestine results in constitutive activation of β-catenin signaling in DCs. This then facilitates their capacity to induce tolerance by favoring T_{reg} cell production over effector T cells (see the figure). Although loss of E-cadherin interactions concomitant with tissue emigration may also contribute to these events, Wnt-dependent signaling would enable activation of the canonical β-catenin signaling pathway even in DC populations that do not express E-cadherin (*8*).

A major attraction of this scheme is that it would be expected to operate at the steady state, with Wnts produced to a threshold concentration (by DC, mucosal, or stromal cells) that triggers the tolerogenic phenotype. However, this is not likely to be the entire story. Deletion of β-catenin from DCs reduced, but did not completely eliminate, their ability to generate T_{reg} cells, indicating that other mechanisms also contribute to tolerance induction. It may be that dependence on β-catenin for tolerogenic signaling is tissue or organ specific although overexpressing an active β-catenin allele may always enhance tolerance. T_{reg} cells themselves may also rely on β-catenin signaling for survival (*10*).

What remains unknown are the actual signaling pathways involved in producing the tolerogenic phenotype. Wnt signaling leads to inhibition of GSK3β (the kinase that phosphorylates β-catenin), which leads to the proteasomal destruction of β-catenin (*11*). Pharmacologic inhibition of GSK3β also results in DC maturation and acquisition of a tolerogenic potential (*9*). Not only might other downstream targets of GSK3β contribute to the phenotype, but also other signaling pathways that inactivate GSK3β could supply Wnt-independent mechanisms that promote tolerance. A variety of pathways can modulate GSK3β activity in DCs; ironically, this includes activation of Toll-like receptors (TLRs), which respond to pathogenic antigens (*12*, *13*). Thus, agonists that stimulate

CREDIT: A. BRUCE

the production of immunogenic DCs may simultaneously activate genes controlled by GSK3β or its targets. Such a mechanism could reflect feedback control mechanisms that attenuate T cell activation by DCs. Alternatively, the GSK3β or the β-catenin pathway could control aspects of DC function required for both immunogenic and tolerogenic T cell activation.

References

1. S. Manicassamy *et al.*, *Science* **329**, 849 (2010).
2. T. K. Starr, S. C. Jameson, K. A. Hogquist, *Annu. Rev. Immunol.* **21**, 139 (2003).
3. R. M. Steinman, D. Hawiger, M. C. Nussenzweig, *Annu. Rev. Immunol.* **21**, 685 (2003).
4. H. C. Probst, J. Lagnel, G. Kollias, M. van den Broek, *Immunity* **18**, 713 (2003).
5. E. S. Trombetta, I. Mellman, *Annu. Rev. Immunol.* **23**, 975 (2005).
6. S. Henri *et al.*, *J. Immunol.* **167**, 741 (2001).
7. P. Stoitzner, C. H. Tripp, P. Douillard, S. Saeland, N. Romani, *J. Invest. Dermatol.* **125**, 116 (2005).
8. K. R. Siddiqui, S. Laffont, F. Powrie, *Immunity* **32**, 557 (2010).
9. A. Jiang *et al.*, *Immunity* **27**, 610 (2007).
10. Y. Ding, S. Shen, A. C. Lino, M. A. Curotto de Lafaille, J. J. Lafaille, *Nat. Med.* **14**, 162 (2008).
11. W. J. Nelson, R. Nusse, *Science* **303**, 1483 (2004).
12. M. Martin, K. Rehani, R. S. Jope, S. M. Michalek, *Nat. Immunol.* **6**, 777 (2005).
13. H. R. Turnquist *et al.*, *Blood* **115**, 4758 (2010).

10.1126/science.1194185

GEOPHYSICS

Sedimentary Basins Feeling the Heat from Below

A major change may be taking place in underlying theories to explain sea level change over time scales of 2 to 20 million years.

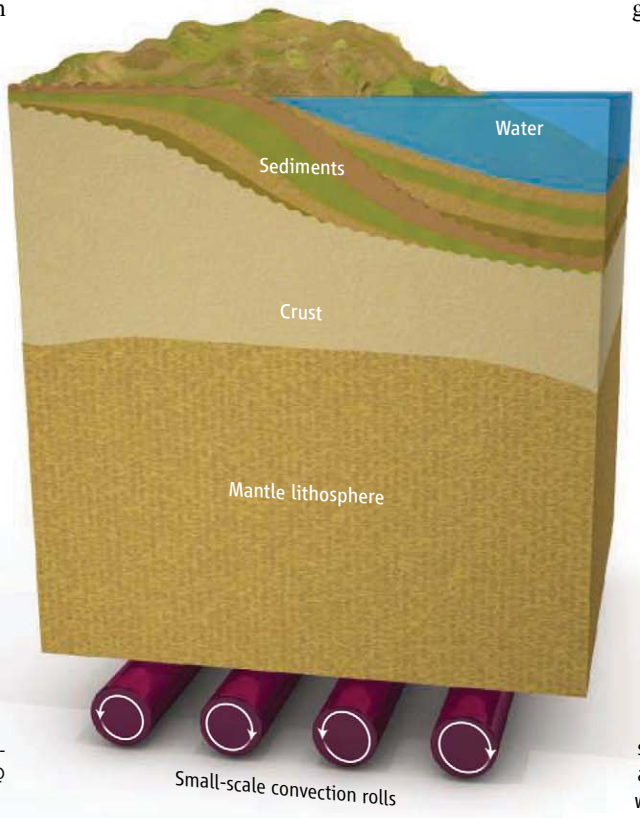
R. Dietmar Müller

Sea-level changes through Earth's history have profoundly affected the surface environment, resulting in alternating advances and retreats of the sea, called transgressions and regressions. An understanding of the mechanisms behind these major shifts in coastlines, and the associated patterns of sediment deposition and erosion over different time scales, is central to unraveling Earth's tectonic and climate history. On page 827 of this issue, Petersen *et al.* (*1*) report results from geodynamic modeling that give a potentially radical shift in concept, namely that oscillations in sedimentary sequences over time periods from 2 to 20 million years may be driven by regional patterns of small-scale convection in the mantle.

The changes we may expect over the next few generations in sea-level rise due to melting ice-sheets are tiny compared with the vast sea-level fluctuations that have occurred over geological time, as documented by marine sedimentary sequences covering large parts of the continents. In a pioneering effort in the 1970s, Vail and colleagues (*2*) collated industry seismic and well data to propose a global sea-level curve, which was later refined by Haq *et al.* (*3*). These curves provide a global reference frame to understand advances and retreats of the sea globally over geological time scales.

School of Geosciences, University of Sydney, Sydney, 2006 Australia. E-mail: dietmar.muller@usyd.edu.au

It is accepted that long-term sea-level change over tens and hundreds of millions of years is primarily caused by fluctuations of the volume of the ocean basins, driven by the time dependence of mid-ocean ridge creation and destruction (*4*). The higher frequency changes in sea level, over tens to hundreds of thousands of years, are due to changes in ice volume, and thus the volume of water in the ocean basins, at least during times when continental ice sheets existed on Earth (*5*).



CREDIT: ADAPTED BY P. HUEY/*SCIENCE*

However, published global sea-level curves are plagued by the problem that sea-level oscillations at so-called intermediate time periods, from 2 to 20 million years, have defied explanation. Transgressions and regressions at these time periods are ubiquitous in the geological record, both during ice ages and during ice-free periods. Therefore, these oscillations cannot be ascribed entirely to ice volume changes, and tectonic cycles in the ocean basins are too slow to produce them. In addition, the global correlation of stratigraphic sequences involved has been questioned, mainly because much of the data on which global sea-level charts are based are not publicly available, and the dating precision of sedimentary sequences is not sufficient to demonstrate global correlation (*6*).

Petersen *et al.* argue that intermediate-period sea-level change expressed in sedimentary basin sequences may not be global but may be due to regional effects caused by small-scale upwellings and downwellings below the base of the lithosphere. Using a model sedimentary basin and a geodynamic simulation, they show that this mechanism can generate sedimentary sequences akin

Simmering sediment. Sublithospheric small-scale convection underneath sedimentary basins may be responsible for cycles of regional tectonic subsidence/uplift and oscillating coastlines over time periods of 2 to 20 million years. In turn, these transgressions and regressions of the sea give rise to alternating successions of shallow and deeper water sediments in sedimentary basins.

to those observed (see the figure). The idea that small-scale convection should occur beneath sedimentary basins is not far-fetched. The mechanism was originally proposed by Richter (*7*) and later invoked to explain the flattening of old ocean floor (*8*), volcanism along passive margins (*9*), and volcanic activity along some hotspot chains (*10*).

The model of Petersen *et al*. implies that globally correlative sea-level fluctuations, with global causal mechanisms, occur only at very long time scales (more than 10 to 20 million years) and at geologically short time scales (less than 1 to 2 million years). The fluctuations at intermediate periods may be regional in origin. Other tectonic mechanisms proposed previously, such as intraplate stress changes (*11*), resulting in flexure of the lithosphere, can produce individual events of regional sea-level change but are less likely to produce oscillations. Unraveling global from regional causes of sea-level change over intermediate time periods has wide-ranging implications for understanding how mantle convection and plate tectonic processes ultimately affect the evolution of Earth's surface. Understanding these processes is also essential for exploration of deep Earth resources in sedimentary basins.

What is required now is to find a way of using geological observations to determine the extent of the contribution of small-scale convection to intermediate-period sea-level change. The detailed history of small-scale convection underneath sedimentary basins will likely remain unknown. The solution therefore lies in proving or disproving the global correlation of intermediate period sea-level fluctuations, as expressed by the geometry and age of boundaries between sedimentary sequences. The issue is beginning to be addressed by the Integrated Ocean Drilling Program (IODP), with two transects drilled in 2009 off the coasts of New Jersey (*12*) and the South Island of New Zealand (*13*). These transects will provide data for estimating regional sea level based on two-dimensional (2D) sequence stratigraphic backstripping (*14*) in geographically disparate regions. A compilation of key observations in a public, shared community database, including seismic data, well data, stratigraphic and structural field observations, and absolute ages of sequence boundaries would also go a long way in helping resolve the origin of intermediate-period sea-level changes. This effort, which may be regarded as the stratigraphic equivalent of initiatives such as EarthScope (www.earthscope.org) or OneGeology (www.onegeology.org), will require collaboration between industry, government organizations, and academia to devise a data infrastructure that is simple enough to be adopted and extensively used by the community, yet allows for extensive automatic data mining similar to the efforts in other fields, such as genomics or astrophysics. Only this way will it be possible to demonstrate or refute the global correlation of intermediate period sequences and obtain better understanding of vertical motions of Earth's surface over geological time.

The potential 3D effect of small-scale convection on basin evolution raises intriguing questions, considering that the model of Petersen *et al*. is 2D. How common is small-scale convection underneath sedimentary basins? What are the geodynamic niche environments that initiate and sustain the process? In three dimensions, small-scale sublithospheric convection is thought to be arranged into convective rolls (*10*), resulting in differential subsidence and uplift. This effect should be detectable in large sedimentary basins, and a combination of 3D geodynamic models and 3D stratigraphic data should be able to unravel the orientation and scale of such rolls, which are presumably oriented orthogonal to the direction of absolute plate motion. The message from this thought-provoking paper is that a collaboration between stratigraphers, basin analysts, and geodynamicists may hold the key for unraveling the sea-level history of planet Earth.

References

1. K. D. Petersen *et al*., *Science* **329**, 827 (2010).
2. P. R. Vail, R. M. Mitchum, S. Thompson III, in *Seismic Stratigraphy and Global Changes in Sea Level,* C. Payton, Ed. (Am. Assoc. Petro. Geol. Memoir, 1978), vol. 26, pp. 83–97.
3. B. U. Haq, J. Hardenbol, P. R. Vail, *Science* **235**, 1156 (1987).
4. R. D. Müller, M. Sdrolias, C. Gaina, B. Steinberger, C. Heine, *Science* **319**, 1357 (2008).
5. K. G. Miller *et al*., *Science* **310**, 1293 (2005).
6. A. D. Miall, *Geology* **20**, 787 (1992).
7. F. M. Richter, *J. Geophys. Res.* **78**, 8735 (1973).
8. B. Parsons, D. McKenzie, *J. Geophys. Res.* **83**, (B9), 4485 (1978).
9. R. R. Boutilier, C. E. Keen, *J. Geophys. Res.* **104**, (B4), 7389 (1999).
10. M. D. Ballmer, J. van Huenen, G. Ito, P. J. Tackley, T. A. Bianco, *Geophys. Res. Lett.* **34**, L23310 (2007).
11. S. Cloetingh, *Geology* **14**, 617 (1986).
12. Expedition 313 Scientists, *IODP Prel. Rept.* 313; http://publications.iodp.org/preliminary_report/313/index.html (2010).
13. Expedition 317 Scientists, *IODP Prel. Rept.* 317; http://publications.iodp.org/preliminary_report/317/317pr_2.htm (2010).
14. M. A. Kominz, S. F. Pekar, *Geol. Soc. Am. Bull.* **113**, 291 (2001).

10.1126/science.1194560

AIDS/HIV

A Boost for HIV Vaccine Design

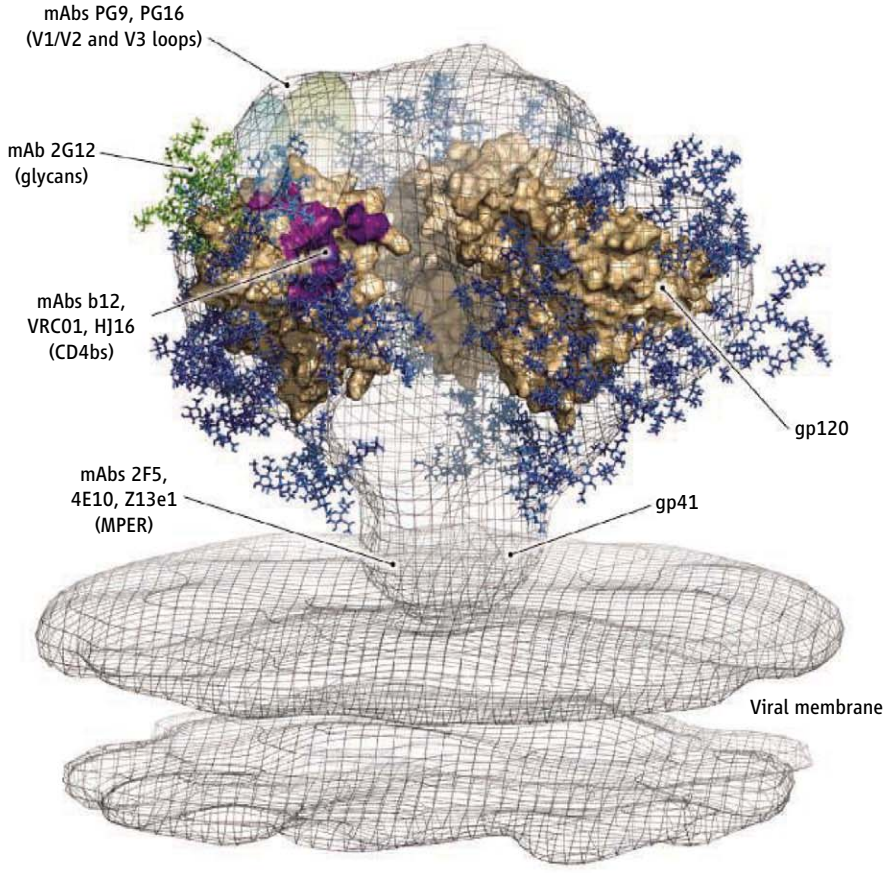
Dennis R. Burton[1,2] and Robin A. Weiss[3]

Antibodies that potently neutralize almost all HIV isolates could aid the rational design of a vaccine.

A major roadblock to the development of an effective vaccine against the human immunodeficiency virus (HIV-1) is the lack of an immunogen that elicits broadly protective antibodies (*1*). Passive transfer studies in animal models have associated protection with neutralizing antibodies and, encouragingly, serum studies show that a subset of HIV-infected individuals produces potent broadly neutralizing antibodies (*2*). Understanding the viral targets of such antibodies and how they achieve potent and broad neutralization has become a key endeavor in HIV vaccine research. On page 856 of this issue, Wu *et al*. (*3*) describe the isolation of particularly potent monoclonal broadly neutralizing antibodies using a novel selection strategy, and on page 811, Zhou *et al*. (*4*) solve the crystal structure of the most effective of these antibodies in complex with its target gp120, a viral envelope glycoprotein. These studies further invigorate the currently active field of discovering broadly neutralizing antibodies against HIV (*2*, *5*–*7*) and provide valuable molecular information for rational vaccine design.

The isolation of monoclonal broadly neutralizing antibodies from HIV-infected donors has so far proven immensely difficult. Following their initial characterization in the 1990s, only a few were available by early 2009. Part of the difficulty is that in HIV infection, a vast number of antibodies are produced to the viral glycoproteins (gp120 and gp41) that do not bind to the native trimeric spike formed by these pro-

[1]Department of Immunology and Microbial Science and IAVI Neutralizing Antibody Center, The Scripps Research Institute, La Jolla, CA 92037, USA. [2]Ragon Institute of Massachusetts General Hospital, Massachusetts Institute of Technology, and Harvard, Boston, MA 02114, USA. [3]Division of Infection and Immunity, University College London, London W1T 4JF, UK. E-mail: burton@scripps.edu; r.weiss@ucl.ac.uk



Neutralizing HIV antibodies. Broadly neutralizing monoclonal antibodies (mAbs) target epitopes on the viral envelope spike at the surface of HIV-1. The spike is a heterotrimer containing the viral glycoproteins $(gp120)_3$ $(gp41)_3$. This model is generated by combining cryoelectron tomographic (*13*), crystallographic (*14*), and computational analyses. It shows the gp120 core structure (tan) fitted in the electron density map (gray) of the spike. The membrane proximal external region (MPER) and viral membrane are shown. The V1/V2 and V3 protein loops are represented as ovals (light green and light blue) at the top of the spike. Glycans (green and blue) are indicated. The model is derived from (*5*) with permission from Wolters Kluwer Health–Lippincott Williams and Wilkins; from (*6*) with permission from Elsevier; and from (*13*) with permission from Macmillan Publishers Ltd./Nature Publishing Group.

teins (see the figure) and, hence, do not efficiently neutralize the virus. These antibodies generate considerable "noise" and present "needle-in-a-haystack" problems in screens based on recombinant gp120 and gp41 as selecting agents to capture immune cells (memory B cells) that produce antibodies of interest.

Walker *et al*. (*8*) circumvented this problem by selecting a donor with a high broadly neutralizing antibody response and then identified two antibodies (PG9 and PG16) with exceptional neutralizing breadth and potency through a large-scale direct functional screen of the individual's B cells. Corti *et al*. (*9*) used multiple viral envelopes in parallel capture assays to favor cross-reactive antibodies, and identified the broadly neutralizing antibody HJ16. Wu *et al*. used a donor with extraordinarily broad and potent serum neutralization directed mainly to the site in gp120 that binds to CD4 (CD4bs) (*10*), the receptor used by HIV to dock onto cells. Using an engineered gp120 that did not bind the great majority of nonneutralizing antibodies to gp120, but preferentially bound the broadly neutralizing antibody to the CD4bs (b12), Wu *et al*. selected B cells that produced potent neutralizing antibodies against the CD4bs of gp120. One of these antibodies, VRC01, neutralizes ~90% of nearly 200 viruses of different HIV clades tested. The outstanding potency and breadth of VRC01, together with the findings of other recent studies (*8*, *11*), show that one of the fears of this field—that potency increases only at the cost of reduced breadth of viral strains that can be neutralized—is unfounded. Another concern was that b12 might be a unique broadly neutralizing antibody to the CD4bs, and the CD4bs thus an almost intractable vaccine target. The description of several broadly neutralizing antibodies to the CD4bs from different HIV-infected individuals (*3*, *9*) lays this concern to rest and promotes interest in designing immunogens to elicit antibodies to CD4bs.

Zhou *et al*. describe the high-resolution crystal structure of the antigen-binding fragment (Fab) of VRC01 in complex with a core gp120 molecule. The antibody shows some similarities to and differences from the CD4 receptor in recognizing the CD4bs on gp120. The antibody targets amino acid residues in the outer domain of gp120, whereas the CD4 receptor also targets a region known as the bridging sheet. This difference in recognition appears to render VRC01 a more potent neutralizer than a CD4-antibody hybrid molecule (an "immunoadhesin"), suggesting that the antibody has evolved the most favored angle of approach to the CD4bs and/or requires the least conformational perturbation to bind to its critical contact residues.

The challenge now is to translate understanding of potent broadly neutralizing antibodies such as VRC01 and PG9/PG16 into the design of immunogens that elicit these types of antibody when incorporated in an HIV vaccine. Attempts using the early, less potent broadly neutralizing antibodies have so far been unsuccessful but have stimulated the development of promising concepts such as "scaffolds," in which viral epitopes that are targets for neutralization are presented in the context of proteins that lack some of the molecular trickery that HIV envelope proteins have evolved to evade antibody responses. The structure of the VRC01-gp120 complex provides detailed atomic-level data of a neutralizing epitope centered on the CD4bs and merits a massive effort in immunogen design.

Both arms of the adaptive immune response—cell-mediated immunity and humoral immunity mediated through antibodies—are likely to be important in developing a vaccine that will provide broad and long-lasting immunity to the diversity of HIV strains to which humans may be exposed. Cell-mediated immunity is important in controlling viral infection. Indeed, individuals with impaired cell-mediated immunity are prey to opportunistic viral infections such as herpes simplex virus, cytomegalovirus, and oncogenic viruses. But neutralizing antibodies are a good correlate of protection for successful antiviral vaccines such as yellow fever, smallpox, and measles (*12*). To prevent HIV from taking hold in the first place, humoral immunity in the form of broadly neutralizing antibodies in the blood and at mucosal surfaces

CREDIT: C. CORBACI AND W. SCHIEF



TOP-QUALITY LIFE SCIENCE RESEARCH CONFERENCES PRICELESS NETWORKING

KEYSTONE SYMPOSIA 40th MEETING SEASON

OCTOBER 2010

Immunological Mechanisms of Vaccination (S1)★, Seattle, Washington, USA

JANUARY 2011

TGF-β in Immune Responses: From Bench to Bedside (A2), Snowbird, Utah, USA

Functional Consequences of Structural Variation in the Genome (A1), Steamboat Springs, Colorado, USA

Frontiers of NMR in Biology (A3), Big Sky, Montana, USA

NK and NKT Cell Biology: Specificity and Redundancy (A4), Breckenridge, Colorado, USA

Adult Neurogenesis (A5), Taos, New Mexico, USA

Histone Code: Fact or Fiction? (A6), Midway, Utah, USA

Type 2 Diabetes, Insulin Resistance and Metabolic Dysfunction (J1), joint with **Obesity (J2)**, Keystone, Colorado, USA

Tuberculosis: Immunology, Cell Biology and Novel Vaccination Strategies (J3)★ joint with

Mycobacteria: Physiology, Metabolism and Pathogenesis – Back to the Basics (J4)★, Vancouver, British Columbia, Canada

Plant Abiotic Stress Tolerance Mechanisms, Water and Global Agriculture (A7), Keystone, Colorado, USA

Epithelial Plasticity and Epithelial to Mesenchymal Transition (A8), Vancouver, British Columbia, Canada

Transmembrane Signaling by GPCRs and Channels (B1), Taos, New Mexico, USA

Extracellular Matrix and Cardiovascular Remodeling (B2), Tahoe City, California, USA

The Evolution of Protein Phosphorylation (F1), Keystone, Colorado, USA

Stem Cells in Development, Tissue Homeostasis and Disease (B3), Santa Fe, New Mexico, USA

Genomic Instability and DNA Repair (B4), Keystone, Colorado, USA

FEBRUARY 2011

Lung Development and Repair (B5), Santa Fe, New Mexico, USA

Immunologic Memory, Persisting Microbes and Chronic Disease (B6), Banff, Alberta, Canada

Antibodies as Drugs (B7), Keystone, Colorado, USA

MicroRNAs and Non-Coding RNAs and Cancer (J5) joint with **MicroRNAs and Human Disease (J6)**, Banff, Alberta, Canada

Dendritic Cells and the Initiation of Adaptive Immunity (J7) joint with **Cancer Control by Tumor Suppressors and Immune Effectors (J8)**, Santa Fe, New Mexico, USA

Inositide Signaling in Pharmacology and Disease (X1) joint with **PI 3-Kinase Signaling Pathways (X2)**, Keystone, Colorado, USA

Genetics, Immunology and Repair in Multiple Sclerosis (B8), Taos, New Mexico, USA

FEBRUARY 2011 (continued)

Neurodegenerative Diseases: The Molecular and Cellular Basis for Neurodegeneration (F2), Taos, New Mexico, USA

Mechanisms of Cardiac Growth, Death and Regeneration (X3) joint with **Molecular Cardiology: Disease Mechanisms and Experimental Therapeutics (X4)**, Keystone, Colorado, USA

Mucosal Biology: A Fine Balance Between Tolerance and Autoimmunity (X5)★ joint with

Immunity in the Respiratory Tract: Challenges of the Lung Environment (X6), Vancouver, British Columbia, Canada

Evolutionary Developmental Biology (C1), Tahoe City, California, USA

DNA Replication and Recombination (C2), Keystone, Colorado, USA

MARCH 2011

Biofuels (C3), Singapore, Singapore

Stem Cells, Cancer and Metastasis (C4), Keystone, Colorado, USA

New Frontiers at the Interface of Immunity and Glycobiology (C5), Lake Louise, Alberta, Canada

AAA and Related ATP-Driven Protein Machines (C6), Tahoe City, California, USA

Mechanism and Biology of Silencing (C7), Monterey, California, USA

HIV Evolution, Genomics and Pathogenesis (X7)★ joint with **Protection from HIV: Targeted Intervention Strategies (X8)**★, Whistler, British Columbia, Canada

Microbial Communities as Drivers of Ecosystem Complexity (C8), Breckenridge, Colorado, USA

Autophagy (D1), Whistler, British Columbia, Canada

Hematopoiesis (D2), Big Sky, Montana, USA

Environmental Epigenomics and Disease Susceptibility (D3), Asheville, North Carolina, USA

APRIL 2011

Metabolic Responses to Extreme Conditions (D4), Big Sky, Montana, USA

Immunoregulatory Networks (D5), Breckenridge, Colorado, USA

Drugs from Bugs: The Anti-Inflammatory Drugs of Tomorrow (Z1) joint with **Evolving Approaches to Early-Stage Drug Discovery (Z2)**, Snowbird, Utah, USA

B Cells: New Insights into Normal versus Dysregulated Function (D6), Whistler, British Columbia, Canada

MAY 2011

Omics Meets Cell Biology (E1), Alpbach, Austria

Lipid Biology and Lipotoxicity (E2), Killarney, County Kerry, Ireland

Pathogenesis of Influenza: Virus-Host Interactions (E3), Hong Kong, China

JUNE 2011

Changing Landscape of the Cancer Genome (F3), Boston, Massachusetts, USA

Abstract and scholarship deadlines precede meetings by four months. Please check www.keystonesymposia.org/2011meetings for details.
★*Global Health Travel Award application deadlines for the six designated Global Health conferences precede meeting dates by five months.*

KEYSTONE SYMPOSIA™
on Molecular and Cellular Biology
Accelerating Life Science Discovery

www.keystonesymposia.org • 1.800.253.0685 • 1.970.262.1230

are likely to be a key component of protection. Developments such as those reported by Wu *et al*. and by Zhou *et al*. will help identify immunogens that can elicit broadly neutralizing antibodies and thereby become an essential part of an AIDS vaccine.

References

1. H. W. Virgin, B. D. Walker, *Nature* **464**, 224 (2010).
2. J. R. Mascola, D. C. Montefiori, *Annu. Rev. Immunol.* **28**, 413 (2010).
3. X. Wu *et al*., *Science* **329**, 856 (2010); published online 8 July 2010 (10.1126/science.1187659).
4. T. Zhou *et al., Science* **329**, 811 (2010); published online 8 July 2010 (10.1126/science.1192819).
5. W. R. Schief, Y. E. Ban, L. Stamatatos, *Curr. Opin. HIV AIDS* **4**, 431 (2009).
6. L. M. Walker, D. R. Burton, *Curr. Opin. Immunol.* **22**, 358 (2010).
7. J. A. Hoxie, *Annu. Rev. Med.* **61**, 135 (2010).
8. L. M. Walker *et al*., *Science* **326**, 285 (2009).
9. D. Corti *et al*., *PLoS ONE* **5**, e8805 (2010).
10. Y. Li *et al*., *Nat. Med.* **13**, 1032 (2007).
11. W. W. Koh *et al*., *J. Biol. Chem.* **285**, 19116 (2010).
12. I. J. Amanna, I. Messaoudi, M. K. Slifka, *Hum. Vaccin.* **4**, 316 (2008).
13. J. Liu, A. Bartesaghi, M. J. Borgnia, G. Sapiro, S. Subramaniam, *Nature* **455**, 109 (2008).
14. T. Zhou *et al*., *Nature* **445**, 732 (2007).

10.1126/science.1194693

ENGINEERING

Concentrating on Solar Electricity and Fuels

Thermal energy from mirror arrays that focus solar radiation not only generates electricity but also could be used to synthesize fuels from water and carbon dioxide.

Martin Roeb and Hans Müller-Steinhagen

Intermittent sources of renewable energy, such as solar and wind power, pose a "storage problem." They must generate more energy than the immediate demand, so that stored energy can be used when the resource is unavailable. Aside from pumped hydropower, large-scale storage of electricity is still technically and economically challenging. For solar energy, concentrating solar power (CSP) plants in regions in the sunbelt of Earth offer ways to store this energy on a large scale, either thermally or as chemical fuels.

These systems use a variety of mirror designs to focus solar radiation onto a relatively small absorber area and generate heat at temperatures ranging from 200°C to 1000°C, for example, the central receiver system shown in the figure (*1*). This heat can be converted into electricity with conventional steam cycles, and some of it can be stored. The Andasol CSP plants in southern Spain already have a storage capacity for 7 to 8 hours of its full-load electricity generation (*2*). Molten salt is used to store heat, but new materials, such as special concretes or high-temperature phase-change materials, are in an advanced stage of development. Furthermore, CSP plants can be operated in hybrid mode with fossil fuels or biomass and hence may have a capability for power generation near 100%.

Industry projections suggest that CSP-generated electricity will cost the same as that from coal-, gas-, and oil-fired power plants within less than 15 years for "mid-load" electricity at the middle ranges of cost and demand (*3*). The first commercial CSP plants erected in the California Mohave Desert more than 20 years ago still operate at a design capacity of 345 megawatts (MW). By the end of this year, 850 MW of solar-thermal capacity will be installed in Spain alone, and groundbreaking for the construction of 2500 GW of CSP plants will have occurred in the United States. In total, project pipelines could represent 7000 MW of generating capacity worldwide.

Although the potential for energy generation by CSP is vast, it is geographically maldistributed relative to the main electricity consumers (*4*). Detailed studies have identified the economic and environmental benefits of a high-voltage direct-current electricity link between the MENA countries (Middle East and North Africa) and Europe (*5*). The DESERTEC Industrial Initiative aims to provide 15% of the European and most of the local electricity demand from renewable sources in the MENA countries by 2050 (*6*). CSP plants will make the main contribution, but other renewable resources, such as wind and photovoltaics, are also included. The electricity imported through DESERTEC will complement and stabilize the fluctuating local renewable energy production in Europe.

However, the potential of concentrating solar power systems is not limited to electricity generation. The heat provided by CSP systems can be used in industrial processes, for seawater desalination, or for driving chemical reactions that produce fuels for the transportation sector. A challenging goal will be to use only water and CO_2 as the feedstocks for synthesis gas. The direct splitting of water and CO_2 requires operating temperatures above 2000°C, and present research activities focus on alternative thermochemical cycles that lower the required temperature (*7*). A promising representative of these thermochemical cycles is the two-step water or CO_2 splitting cycle that uses materials containing metal ions that can be oxidized and reduced. The reactor developed within the HYDROSOL project (*8*) uses a thin-walled ceramic monolith that has honeycomb channels coated with the active redox materials and is designed to



Mirror site. Photograph of PS-10 solar tower plant near Seville, Spain (courtesy of Abengoa Solar). Solar energy is concentrated with mirrors to generate heat for electricity generation and chemical synthesis.

Institute of Technical Thermodynamics, Deutsches Zentrum für Luft-und Raumfahrt, Linder Hoehe, Koeln, 51147 Germany. E-mail: Martin.Roeb@dlr.de; Hans.Mueller-Steinhagen@dlr.de

absorb solar radiation. When steam or CO_2 are passed through the reactor, the coating material splits the molecules by adsorbing and incorporating oxygen to form a higher oxide. The effluent gas stream then consists of pure H_2 or CO. The temperature in the reactor is then increased, for example, by focusing more mirrors onto the aperture of this reactor. The feed gas stream is cut off, which releases the trapped oxygen and regenerates the active coating. Two reaction chambers are operated in parallel, one for water/CO_2 splitting and one for reduction.

One of the prototype materials for this kind of reaction is Fe_3O_4. The redox pair in this case is FeO/Fe_3O_4. In practice, the pure oxide cannot be cycled because the temperature needed to thermally reduce Fe_3O_4 is higher than its melting point. However, replacing some of the iron in Fe_3O_4 with other metals, such as zinc, manganese, nickel, or cobalt, can lower the reduction temperature while maintaining the spinel structure of these ferrite materials (*9*–*11*). Integrating the ferrites into a stabilizing matrix, such as yttrium-stabilized zirconia or cerium oxide (ceria), can also slow down a potential sintering and deactivation of the metal oxide (*12*).

The second main redox system is based on the redox pair CeO_2-Ce_2O_3. Ceria has the advantage that the melting point is higher than the temperature required for the thermal reduction step. However, other metals need to be added to ceria to improve its reactivity and oxygen uptake capacity (*13*). For both families of materials, the main challenges are the achievement of high oxygen uptake capacities and hydrogen production rates, as well as reduced cost and increased operational lifetime of the redox materials. The coupling of concentrated solar radiation into the process must also be improved, and approaches being investigated include reactors with rotating absorbers and components, fixed and fluidized bed reactors, and the use of heat transfer fluids (*7*, *14*, *15*).

The general concept of solar fuel generation was first proven by developing and operating individual components. Subsequently, a miniplant (which could produce about 10 kW of thermal energy) was created and tested in DLR's solar furnace in Cologne, Germany. This technology has recently been scaled up to the size of 100 kW of thermal energy. The reactor, together with all necessary peripherals, was installed in an experimental solar tower at the Plataforma Solar de Almería, Spain. The benefit of using a solar tower arrangement is that only part of the mirrors (heliostats) have to be refocused to vary the temperatures of the two reactors that produce H_2 and/or CO, rather than physically moving the reactors. Several hydrogen production cycles and metal oxide reduction cycles could be successfully investigated, with conversion of steam to H_2 of up to 30% (*16*). Continuing developments should enable the solar-driven synthesis of fuels from renewable sources to complement the production of electricity.

References

1. M. Becker, B. Gupta, W. Meinecke, M. Bohn, *Solar Energy Concentrating Systems: Applications and Technologies* (Müller Verlag, Heidelberg, Germany 1995).
2. Solar Millennium (2008), "The parabolic trough power plants Andasol 1 to 3"; http://www.solarmillennium.de/upload/Download/Technologie/eng/Andasol1-3engl.pdf.
3. A. T. Kearney (2010), "Solar Thermal Electricity 2025"; www.atkearney.com/images/global/pdf/STE_2025_Study_Report_June_2010.pdf.
4. Deutsches Zentrum für Luft-und Raumfahrt, Institute of Technical Thermodynamics, "Concentrating Solar Power for the Mediterranean Region"; www.DLR.de/tt/med-csp.
5. Deutsches Zentrum für Luft-und Raumfahrt, Institute of Technical Thermodynamics, "Trans-Mediterranean Interconnection for Concentrating Solar Power"; www.DLR.de/tt/trans-csp.
6. DESERTEC Foundation (2009); "Clean Power from Deserts"; www.desertec.org/fileadmin/downloads/DESERTEC-WhiteBook_en_small.pdf.
7. T. Kodama, N. Gokon, *Chem. Rev.* **107**, 4048 (2007).
8. HYDROSOL project, www.hydrosol-project.org.
9. J. Miller *et al*., *J. Mater. Sci.* **43**, 4714 (2008).
10. S. Lorentzou, A. Zygogianni, K. Tousimi, C. Agrafiotis, A. G. Konstandopoulos, *J. Alloy. Comp.* **483**, 302 (2009).
11. F. Fresno *et al*., *Int. J. Hydrogen Energy* **34**, 2918 (2009).
12. T. Kodama, N. Gokon, T. Yamamoto, *Sol. Energy* **82**, 73 (2008).
13. P. Fornasieri *et al*., *J. Catal.* **151**, 168 (1995).
14. H. Kaneko *et al*., *Energy Fuels* **21**, 2287 (2007).
15. R. B. Diver, J. E. Miller, M. D. Allendorf, N. P. Siegel, R. E. Hogan, *J. Sol. Energy Eng.* **130**, 041001 (2008).
16. M. Roeb *et al*., *Sol. Energy*. Published online 11 May 2010.

10.1126/science.1191137

CLIMATE CHANGE

The Carbon Dioxide Exchange

Understanding how carbon dioxide cycles between land and atmosphere is key to developing better climate models.

Peter B. Reich

One key to accurately predicting future levels of atmospheric carbon dioxide (CO_2) is understanding how land and atmosphere exchange CO_2. Each year, photosynthesizing land plants remove (fix) one in eight molecules of atmospheric CO_2, and respiring land plants and soil organisms return a similar number. This exchange determines whether terrestrial ecosystems are a net carbon sink or source. Two papers in this issue contribute to understanding the land-atmosphere exchange by elegantly analyzing rich data sets on CO_2 fluxes from a global network of monitoring sites. On page 834, Beer *et al*. (*1*) estimate total annual terrestrial gross primary production (GPP) in an approach more solidly based on data than previous simple approximations. On page 838, Mahecha *et al*. (*2*) assess how ecosystem respiration (*R*) is related to temperature over short (week-to-month) and long (annual) time scales, and find a potentially important but difficult-to-interpret relationship.

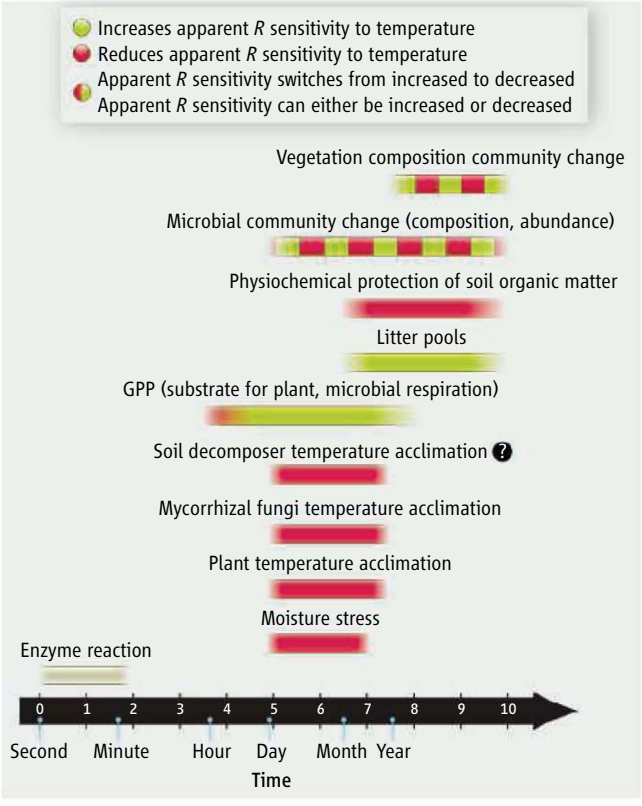
Beer *et al*. focus on quantifying GPP locally and globally. They use general relationships between GPP and several "drivers," such as temperature, rainfall, and biome type, to characterize and estimate GPP at 352 sites. Then, they use five approaches to extrapolate to global estimates; these include three statistical models, estimating GPP indirectly from data on catchment water flux, and modeling GPP from satellite-based estimates of light interception by vegetation. They make an important advance by better quantifying (i) global GPP and the uncertainty surrounding this estimate; (ii) spatial patterns of GPP (how much comes from tropical or boreal forests or from other biomes); and (iii) controls on GPP, such as by rainfall and temperature.

Beer *et al*. note that each of the five approaches includes simplifying assumptions and large uncertainties. They produced estimates of global GPP that vary from ≈105 to ≈130 Pg C $year^{-1}$, with a 95% probability that the value lies between 102 and 135 Pg C $year^{-1}$. This is an advance, yet it shows how far we still are from an accurate estimate of global GPP. The 33 Pg C $year^{-1}$ difference between the low and high values, for instance, is roughly four times the annual CO_2 emissions from fossil-fuel burning.

Mahecha *et al*. address the other half of the land-atmosphere CO_2 flux. Unlike GPP,

University of Minnesota, St. Paul, MN 55108, USA. E-mail: preich@umn.edu

which represents a single process (photosynthesis) involving a single tissue (leaves), *R* represents the aggregate CO_2 flux from the metabolic activities of myriad organisms. The players include plants, their mutualists (mycorrhizal fungi), and decomposers (soil microorganisms). Each has cellular processes that respond almost instantaneously to temperature changes (*3*, *4*). However, the relationship of *R* to temperature over longer periods (weeks, months, and seasons) is influenced by many factors, including the availability of chemical substrates, environmental conditions, changes in microbe abundance and community composition, and physiological mechanisms for adjusting to shifting temperatures (*2*–*13*) (see the figure).



Complex influences. Land plant and microbe respiration of CO_2 into the atmosphere can be increased (yellow) or reduced (red) by a wide range of processes that enhance or limit metabolic processes, operate over varying time scales, and go beyond direct temperature effects on physiology [expanded from (*16*)]. The numbers on the arrow represent time on a logarithmic scale.

Mahecha *et al*. used data from 60 sites to characterize how *R* depends on temperature over time. They used a dividing line of 3 months to distinguish fast (high-frequency) from slow (low-frequency) processes. They show that high-frequency (week-to-month) processes result in a 40% average proportional increase in *R* for every 10°C increase in temperature, or a "Q_{10}" value of 1.4. This value was similar across all sites. In contrast, when assessed conventionally over a year, *R* increased by an average of 130% per 10°C increase, or a Q_{10} of 2.3 (*2*). For context, the short-term (near-instantaneous) response reflecting physiological activity within plants and microbes has a Q_{10} that typically averages between 2 and 3 (*3*, *4*).

Which of Mahecha *et al*.'s estimates better reflects intrinsic responsiveness to temperature—and is thus more relevant to climate modelers trying to predict ecosystem responses to warming? Mahecha *et al*. reasonably argue that the smaller, week-to-month Q_{10} of 1.4 is most relevant, and that the annual Q_{10} overestimates the role of temperature as a driver of ecosystem *R*. In part, that is because the annual estimate is confounded by environmental and seasonal variations that can increase plant and soil respiration independent of, and in addition to, direct temperature effects (*8*–*10*). For example, strong GPP during temperate zone summers provides abundant carbon substrate for both plant and soil microbial respiration, resulting in higher "apparent" sensitivity to temperature than can be attributed to direct temperature effects on respiration kinetics. They report, moreover, that the week-to-month scale sensitivity is stable across sites varying in mean temperature, whereas annual sensitivity varies markedly from cold to warm ecosystems, reflecting differences in the degree of confounding by environmental drivers.

Why is the "week-to-month" Q_{10} lower than the Q_{10} at the instantaneous and annual time scales? Mahecha *et al*. argue that it reflects a direct, "intrinsic" ecosystem functional response to temperature. This explanation is probably true in part, but it is likely that the low week-to-month Q_{10} of 1.4 also reflects a complex response to an aggregation of factors. For instance, plants (*6*, *7*, *11*, *13*, *14*), their fungal mutualists (*15*), and perhaps soil microbes (*12*) exhibit extreme temperature sensitivity that can alter realized *R*. As temperatures warm, plants quickly (e.g., in 2 days) dampen their temperature response by "down-shifting" their base respiration, and then "rev up" again in response to cooling. This acclimation results in a lower Q_{10} over a month than over an hour (*6*, *11*, *13*, *14*). Further, variation in the types, abundance, and food supply of soil microbes can also result in a low Q_{10} at the week-to-month scale.

Regardless of the difficulty of interpreting the processes underlying these numbers, the findings are important. Beer *et al*.'s value for GPP is our best and most broad-based estimate, despite its uncertainty. Mahecha *et al*.'s results are important because they suggest that, at week-to-month scales, *R*'s relationship to temperature converges at a Q_{10} of 1.4 across many varied ecosystems. Their work also reduces fears that respiration fluxes may increase strongly with temperature, accelerating climate change (*4*–*13*). They also add to studies indicating that simple assumptions about respiration-temperature relations can lead to problematic models (*4*–*13*). It is not yet clear, however, whether and how their findings can be used in climate models.

What is also not yet clear is how GPP or *R* will respond to rising CO_2 and to changing temperatures or rainfall. Such forecasting will require understanding and mathematically describing how biological processes will respond to novel environmental conditions outside of the current observational universe—a challenging task indeed. Given the urgent need to quantify and predict future land-atmosphere fluxes, however, we need rapid advances in such understanding in the decade ahead.

References

1. C. Beer *et al*., *Science* **329**, 834 (2010); published online 5 July 2010 (10.1126/science.1184984).
2. M. Mahecha *et al*., *Science* **329**, 838 (2010); published online 5 July 2010 (10.1126/science.1189587).
3. N. Fierer, B. J. Colman, J. P. Schimel, R. B. Jackson, *Global Biogeochem. Cycles* **20**, GB3026 (2006).
4. M. G. Tjoelker, J. Oleksyn, P. B. Reich, *Glob. Change Biol.* **7**, 223 (2001).
5. E. A. Davidson, I. A. Janssens, *Nature* **440**, 165 (2006).
6. P. V. Bostad, P. Reich, T. Lee, *Tree Physiol.* **23**, 969 (2003).
7. K. Wythers, P. B. Reich, M. G. Tjoelker, P. B. Bolstad, *Glob. Change Biol.* **11**, 435 (2005).
8. Y. Luo, S. Wan, D. Hui, L. L. Wallace, *Nature* **413**, 622 (2001).
9. J. Lloyd, J. A. Taylor, *Funct. Ecol.* **8**, 315 (1994).
10. L. Gu, P. J. Hanson, W. Mac Post, Q. Liu, *Global Biogeochem. Cycles* **22**, GB4009 (2008).
11. M. G. Tjoelker, J. Oleksyn, P. B. Reich, R. Zytkoviak, *Glob. Change Biol.* **14**, 782 (2008).
12. M. A. Bradford *et al*., *Ecol. Lett.* **11**, 1316 (2008).
13. O. Atkin *et al*., *Glob. Change Biol.* **14**, 2709 (2008).
14. O. K. Atkin, M. G. Tjoelker, *Trends Plant Sci.* **8**, 343 (2003).
15. G. M. Malcolm, J. C. López-Gutiérrez, D. M. Eissenstat, R. T. Koide, *Glob. Change Biol.* **14**, 1169 (2008).
16. M. Reichstein, C. Beer, *J. Plant Nutr. Soil Sci.* **171**, 344 (2008).

10.1126/science.1194353

RETROSPECTIVE

Stephen Schneider (1945–2010)

Paul R. Ehrlich

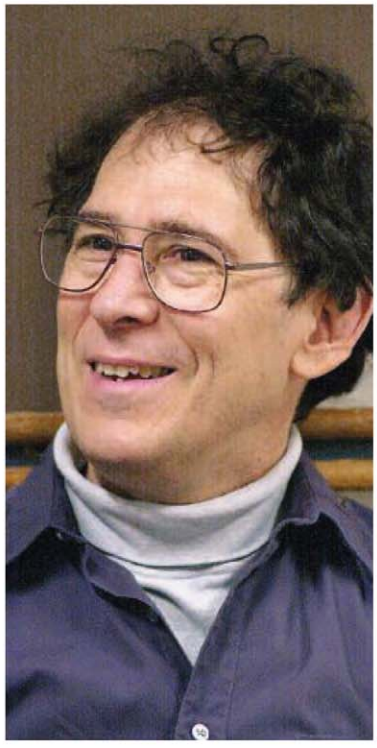
An atmospheric scientist who strove to understand adverse human impacts on climate worked just as hard to educate the general public about them.

Most *Science* readers will know that Steve Schneider was a giant in atmospheric science who made seminal contributions in many areas, ranging from the roles played by cloud feedbacks in the climate system to the impact of aerosol particles in "nuclear winter" scenarios. They will also be aware that he was an indefatigable scientific educator, battling especially to ensure that climate disruption and humans' role in it were explained properly to the public. They likely know that he was well recognized for his contributions to atmospheric science and public policy. He was awarded a MacArthur Foundation "genius" grant in 1992. He was a contributor to all four of the Intergovernmental Panel on Climate Change (IPCC) reports, and he was co-awarded the Nobel Peace Prize in 2007 for his work on climate change.

A less well-known side of Steve is that he was a stickler for getting the science right, regardless of the politics. When we were doing the nuclear winter studies in the early 1980s, he was constantly working to see that all public statements were as accurate as possible. When he and Starley Thompson reexamined the nuclear winter predictions a few years later, and found them to be less dire, Steve did not hesitate to make the revisions public, which led to the currency of the alternative term "nuclear autumn." That's the way he was on all issues. Given new data, he did not hesitate to modify his views.

In the 1970s, we had many discussions of the responsibilities of "public scientists." We agreed that one must first explain the scientific consensus, then say if you agreed with it (and if not, why not), and then give your personal opinion of what policy choices should be made. Being a scientist does not relieve one of the obligations of a citizen to speak out. In my experience, no scientist felt that obligation more strongly, or showed more dedication and courage in meeting it, than Steve Schneider. To the very last, he worked to educate the public and decision makers, ignoring illness and anonymous death threats from persons who opposed the scientific consensus on climate change.

His interest in the effects of climate disruption brought him together with Terry Root, a leader in studying its effects on organisms, especially on the distribution and timing of bird migration. Beginning in the 1990s he began to learn all he could about birds, and under Terry's guidance he quickly became an avid birder. They married and began a long-term collaboration that included influential papers, as well as many bird-watching and environmental exploration expeditions.



Steve also worked with economists and other experts on evaluating the costs and benefits of implementing various solutions to the problems of climate change. He brought attention to efforts that assessed potential impacts of climate change on agriculture, such as drought and soil erosion from flooding, and on public health, such as the spread of tropical disease vectors to higher latitudes.

Steve's nonscientific enthusiasms, aside from Terry, were many, including bird prints, wine tasting, and good food, accompanied by a fine sense of humor and a love of music. Steve delighted in playing folk songs and rock tunes on his 12-string guitar. He said he started playing as an undergraduate at Columbia in the 1960s when, in his words, "guitar-playing was a substitute for a personality." He wasn't shy about singing, despite a less than velvety voice. Steve and Terry hosted many dinners that were followed by spirited guitar-strumming and singing to tunes by Bob Dylan, Simon and Garfunkel, and others. Steve and Stanford environmental economist Larry Goulder collaborated and performed publicly a few original songs as well, including their "Climate Change Blues," and a warped version of the Beatles' "When I'm 64."

In 2001, Steve was diagnosed with mantle cell lymphoma. In his typical fashion, he immediately set out to learn everything about it, ably assisted by Terry. He collaborated with his doctors to design a course of treatment that led to remission. He underwent a bone-marrow transplant, a difficult and painful treatment, but he did more than endure it stoically. Whenever we scrubbed and gowned to visit him in his hospital room, we would find him sitting up in bed with a computer on his lap and Terry handing him papers, working on e-mail or a manuscript, and ready with a quick joke about his condition.

Knowing him well, I have nonetheless been stunned by the outpouring immediately after his death from fellow scientists and former students testifying to Steve's generosity in mentoring others. He was always happy to give time to my wife Anne and me, checking our writing on climate for accuracy and explaining fine points of atmospheric physics. I knew how open he was with students, but I didn't fully realize the scale of his giving. He wrote a book on his medical battle, and then gave much of his time to counsel others with the ailment. His generosity toward others persisted through years of struggle with a debilitating and eventually deadly disease.

When Anne and I try to sort out our impressions of Steve, his brilliant science doesn't come first to mind. It's his rollicking sense of humor, his descriptions of the wine he was serving us, sitting with him and Terry having yak butter tea with the queen of Bhutan, or maybe most of all seeing a tree covered with synchronously flashing fireflies in New Britain when searching for owls with our mutual friend, Tom Lovejoy. Steve was all the usual superlatives—a giant in his field, a wonderful friend, a hero, and more. He was a climate researcher who was also a man for all seasons. His myriad friends will miss him intensely, and so, I'm afraid, will billions of people who never heard of him, whose lives he so determinedly strove to improve.

10.1126/science.1195502

CREDIT: LINDA A. CICERO/STANFORD NEWS SERVICE

Center for Conservation Biology, Department of Biology, Stanford University, Stanford, CA 94305–5020, USA. E-mail: pre@stanford.edu

Call for Papers

Science Translational Medicine

Integrating Medicine and Science

The new journal from the publisher of *Science* stands at the forefront of the unprecedented and vital collaboration between basic scientists and clinical researchers.

- Cardiovascular Disease
- Neuroscience/Neurology/ Psychiatry
- Infectious Diseases
- Cancer
- Health Policy
- Bioengineering
- Chemical Genomics/ Drug Discovery
- Other Interdisciplinary Approaches to Medicine

Submit your research at www.submit2scitranslmed.org



Chief Scientific Adviser
Elias A. Zerhouni, M.D.
Former Director,
National Institutes of Health

Science Translational Medicine
AAAS

ScienceTranslationalMedicine.org



Why Does Academia Prefer Octet For Label-Free Protein Characterization?

"With the affordable, easy-to-use Octet System, protein-protein interactions can be measured right on the benchtop in my own lab at anytime, obviating the need for a large instrumentation grant and core lab, or arranging and scheduling access."

Dr. Jay Groppe, Assoc. Professor
Department of Biomedical Sciences
Texas A&M Health Science Center

Out of the core lab, onto your benchtop
Measure concentration, kinetic and affinity constants and generate SPR-quality data right on your benchtop

Label-free kinetic characterization in a few minutes!
Get experiments completed in minutes rather than days using a Dip and Read™ assay— setup requires only pipeting reagents into a 96- or 384-well microplate

Direct quantitation assays for antibodies and other proteins
Replace HPLC and ELISA with Octet to measure antibody and other protein concentrations in crude samples accurately without secondary reagents

Visit www.fortebio.com or call 888.OCTET-QK today to learn more about the Octet platform.

fortéBIO

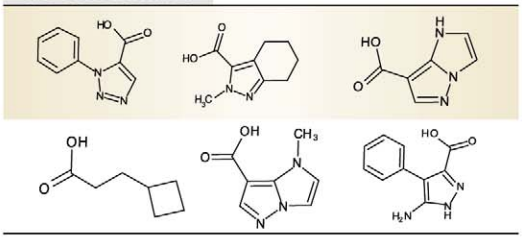
Fast. Accurate. EASY.

URL: http://www.hit2lead.com

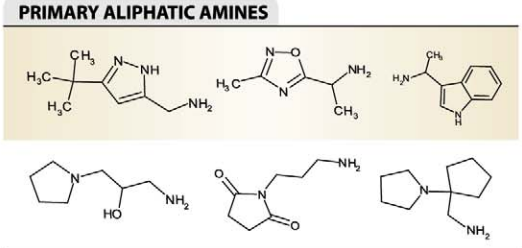
CHEMBRIDGE: THE GOLD STANDARD IN SCREENING COMPOUNDS IS NOW A MAJOR FORCE IN BUILDING BLOCKS

- OVER 12,000 UNIQUE REAGENTS FOR MEDICINAL CHEMISTRY AND LIBRARY SYNTHESIS
- AVAILABLE OVERNIGHT FROM STOCK IN SAN DIEGO VIA E-COMMERCE PORTAL HIT2LEAD.COM

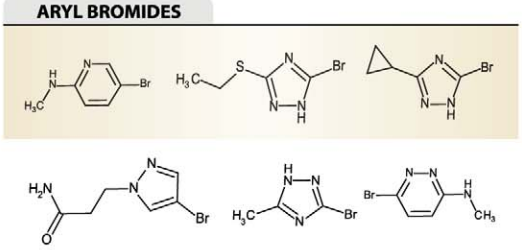
CARBOXYLIC ACIDS



PRIMARY ALIPHATIC AMINES



ARYL BROMIDES



- Discounted online prices
- Over 95% purity by NMR & LCMS
- 24-48 hour delivery for rush orders. One-week delivery worldwide
- Both purchase orders and credit cards are accepted for online order processing

ChemBridge™ Hit2Lead.com™

16981 Via Tazon, Suite G
San Diego, CA 92127
Toll Free: 1+800-964-6143
Tel: +1-858-451-7400, Option#4
Fax: +1-858-451-7401
support@chembridge.com

www.hit2lead.com



THE PREMIER NANOSCIENCE JOURNALS ARE FROM ACS

NANO LETTERS

9.991 IMPACT FACTOR

46,238 TOTAL CITATIONS

Symposium
August 22-24, 2010

Reception
August 25, 2010
5:30 pm-7:30 pm

10th Anniversary Symposium for *Nano Letters*, the Leading Rapid Communications Journal for the Nano-Community

With a 25% increase in 2009 citations over 2008, *Nano Letters* celebrates its 10th Anniversary with a special Symposium and Reception at the ACS Fall National Meeting. "*Nano Letters*: The Next Ten Years" will feature distinguished speakers from all areas of nanoscience, including:

Ali Javey	Harry A. Atwater	Phaedon Avouris	W. E. Moerner
Arthur J Nozik	Itamar Willner	Samuel I Stupp	X. Sunney
Catherine J. Murphy	John A. Rogers	Sharon C. Glotzer	Xie Xiaowei
Chad Mirkin	Mildred S. Dresselhaus	Song Jin	Yi Cui
Eran Rabani	Oleg Prezhdo	Ting Xu	
Gabor A. Somorjai	Peng Chen	Uri Banin	

CO-EDITORS: A. Paul Alivisatos, *University of California, Berkeley,* and Charles M. Lieber, *Harvard University*

Visit **http://pubs.acs.org/nanolett**

ACSNANO

7.493 IMPACT FACTOR

3,313 TOTAL CITATIONS

37% Higher ISI Impact Factor for *ACS Nano* and Still Rising!

Launched mid-year in 2007, *ACS Nano* is already in the top 5 in Impact Factor in Nanoscience & Nanotechnology and in the top 10 in both Multidisciplinary Chemistry and Multidisciplinary Materials Science. *ACS Nano* had an increase in citations of over 300% from 2008, and already has more citations in the first half of 2010 than in all of 2009.

EDITOR-IN-CHIEF: Paul S. Weiss, *University of California, Los Angeles*

Visit **http://pubs.acs.org/acsnano**

THE JOURNAL OF PHYSICAL CHEMISTRY C

4.224 IMPACT FACTOR

25,129 TOTAL CITATIONS

Big Gains for *Journal of Physical Chemistry C*

The Journal of Physical Chemistry C saw an impressive 140% increase in its 2009 citations and a 24% increase in its 2009 Impact Factor compared to the previous year.

EDITOR-IN-CHIEF: George C. Schatz, *Northwestern University*

Visit **http://pubs.acs.org/JPCC**

* As reported in the 2009 Journal Citation Reports from Thomson Reuters®

Visit our free website for the nano research community at **www.ACSNanotation.org.**

ACS Publications
MOST TRUSTED. MOST CITED. MOST READ.



CREDIT: SOLAR MILLENNIUM

INTRODUCTION

Getting Better To Get Bigger

THE END OF THE AGE OF FOSSIL FUELS MAY BE IN SIGHT, BUT WHAT COMES AFTER is still a bit of a blur. There are numerous alternatives to coal, oil, and natural gas from electricity generated by solar farms to biofuels brewed from plants. Scaling up these alternative sources of energy, however, has proved a challenge. This special issue explores the progress that researchers are making in developing better alternatives, and the technical, political, and economic pitfalls associated with scaling them up.

As Kerr (p. 780) notes in a News feature, alternative energies have big shoes to fill. Fossil fuels are widely used in part because they have some unique advantages over other sources of energy. A coal-fired power plant, for instance, can keep running when the Sun isn't shining or the wind dies down, and fossil fuels typically get more energy out of a hectare of land or a liter of raw material than the alternatives. It took about a century to build the energy system that runs on fossil fuels, though, and Kerr reports that it could take just as long to develop alternatives. Still, both Kerr and Cho (p. 786) report that there is potentially more than enough energy available from the Sun, wind, and other renewable sources to replace fossil fuels. Clery (p. 782) reports on one ambitious multinational effort to harness renewable sources to generate electricity in North Africa and then transmit the power across the Mediterranean Sea to Europe. Service (p. 784), however, reports on how high hopes in the United States for one emerging alternative, cellulosic biofuels, have waned because of technical and economic setbacks. Kintisch (p. 788) notes that even a relatively mature alternative technology, wind power, is now encountering public opposition owing to the environmental and aesthetic impacts of wind turbines.

Such grand visions rest in part on vigorous continuing research. Three Perspectives take an in-depth look at how researchers hope to scale up biofuels development successfully. Somerville *et al.* (p. 790) survey the most promising land crops for large-scale development, and Wijffels and Barbosa (p. 796) discuss algae: a source that holds promise because of both its high content of lipids (which more closely resemble petroleum than sugars do) and its low land-area requirements. Richard (p. 793) considers the changes in transport and processing infrastructure that will be necessary to ship biofuels from field to fueling station.

Finally, nuclear power is a perennial player in the carbon-neutral energy discussion. Grimes and Nuttall (p. 799) review a two-stage approach to the expansion of fission-based electricity generation, with the upcoming 20 years focused on shoring up current technology, followed in later years by the design and construction of next-generation plants that reprocess spent fuel for greater efficiency and waste minimization. Together, all of these pieces show that interest in scaling up alternatives remains high and that many attractive new energy sources exist despite the considerable challenges involved in their development.

– DAVID MALAKOFF, JAKE YESTON, JESSE SMITH

Scaling Up Alternative Energy

CONTENTS

News

780 Do We Have the Energy For the Next Transition?

782 Sending African Sunlight to Europe, Special Delivery

784 Is There a Road Ahead For Cellulosic Ethanol?

786 Energy's Tricky Tradeoffs

788 Out of Site
Other Siting Problems

Perspectives

790 Feedstocks for Lignocellulosic Biofuels
C. Somerville et al.

793 Challenges in Scaling Up Biofuels Infrastructure
T. L. Richard

796 An Outlook on Microalgal Biofuels
R. H. Wijffels and M. J. Barbosa

Review

799 Generating the Option of a Two-Stage Nuclear Renaissance
R. W. Grimes and W. J. Nuttall

See also Editorial p. 727, Policy Forum p. 762, Perspective p. 773, and Science *Podcast.*

Science



NEWS

Do We Have the Energy For the Next Transition?

Past energy transitions to inherently attractive fossil fuels took half a century; moving the world to cleaner fuels could be harder and slower

Heated, but how? Fossil fuels have many innate advantages over renewable energy sources.

WIND TURBINES DOT RIDGES, DISTILLERS turn farmers' corn into ethanol by the billions of liters, and solar panels sprout on roofs. The energy revolution that will bring us clean, secure energy is under way, sort of. Never has the world so self-consciously tried to move toward new sources of energy. But the history of past major energy transitions—from wood to coal, and from coal to oil and gas—suggests that it will be a long, tough road to scaling up alternatives to fossil fuels that don't stoke greenhouse warming.

A big problem is that, for the first time, the world is moving to tap new energy sources that are, in many ways, less useful and convenient than the currently dominant sources: fossil fuels. "Up to now, we've always gone to a better fuel," notes economist Robert Kaufmann of Boston University (BU). And oil has proved the best of the better. Compared with wood or even coal or gas, it "is a great fuel," Kaufmann says. Oil is densely packed with energy, easily transported and stored, and efficient at releasing its energy in modern engines.

Renewables are another matter. Fuel sources like corn kernels or wood chips tend to be bulky. Their energy content is diffuse. Planting energy crops and building solar or wind farms is a land-hungry process, and the energy they deliver is often intermittent and hard to store. So far, "you can't run airliners or cars on photovoltaics," Kaufmann says.

"We are confronted with a society built on high-quality energy, dense forms of energy, fossil fuels especially," says Kaufmann's BU colleague, ecological economist Cutler Cleveland. "Could you have the same standard of living with renewables? I don't think we really know. Things might have to change very fundamentally."

Looming large

One of the most daunting aspects of the coming energy transition is its sheer size. It will have to be huge. Since 1800—when wood and animal feed provided more than 95% of U.S. energy—world energy use has increased by a factor of more than 20. Replacing even half of the coal, oil, and gas consumed today would require 6 terawatts of renewable energy, estimates systems analyst Arnulf Grübler of the International Institute for Applied Systems Analysis (IIASA) in Laxenburg, Austria. In contrast, renewables today produce just 0.5 terawatt.

Fossil fuels, however, also had humble beginnings. For tens of thousands of years, wood and other plant products provided humankind's energy needs. Historians do not always agree on exactly which social, technological, and economic forces drove the momentous shift from wood to coal—and then to oil and gas—in the 19th and early 20th centuries. But one factor clearly was the growing scarcity of existing fuels, says environmental historian Brian Black of Pennsylvania State University, Altoona. During the War of 1812, for instance, wood shortages around Philadelphia prompted residents to experiment with burning coal for heat and industry. And when Edwin Drake drilled the first oil well in the United States in 1858, whale oil for lamps was getting harder to come by. U.S. kerosene from oil soon displaced whale oil as an illuminant, and Americans were out of the whaling business.

Scarcity, however, is less of a factor today. The world is not yet running short of fossil fuels, notes energy analyst Richard Nehring of Nehring Associates in Colorado Springs, Colorado. Coal and oil production likely won't "peak" until something like 2030, give or take a decade, he estimates. Natural-gas production could keep pace with rising demand until 2050. Nehring's production peaks are on the early side of published estimates, but they still suggest that broad-based fears of energy shortages will not be driving a shift to renewables for the next decade or two.

The continued abundance of fossil fuels—and their relatively low cost—has also helped highlight some of the other shortcomings of renewables. They include:

Lower density

Solid and liquid fossil fuels are packed with energy. A kilogram of oil, for example, holds three times as much energy as a kilogram of plant biomass, environmental scientist Vaclav Smil of the University of Manitoba in Winnipeg, Canada, estimates in his recent book *Energy Transitions: History, Requirements, Prospects*. The difference swells to almost five times if the comparison is made in terms of energy per unit volume instead of weight.

The gap between fossil fuels and renewables grows even larger when analysts measure "power density," or the amount of energy produced per square meter of Earth's surface. A coal mine or oil field, for instance, yields five to 50 times more power per square meter than a solar facility, 10 to 100 times more than a wind farm, and 100 to 1000 times more than a biomass plant. Even if analysts subtract the energy needed to extract, transport, and process coal, it still yields 50 times more energy than ethanol from corn and 10 times more than ethanol from sugar cane, according to Cleveland. Oil is now 13 times more productive than corn ethanol.

Greater intermittency

Leading renewables are far worse off than fossil fuels and even wood when it comes to another crucial energy quality: its conti-

CREDIT: CORBIS

nuity of supply. A coal-fired power plant—if not down for repairs or maintenance—can be cranked up as needed; not so sun or wind. Coal-fired, gas-fired, or nuclear power plants operate 75% to 90% of the time, Cleveland says. In contrast, wind turbines typically stand idle 65% to 80% of the time. And the sun is guaranteed to be unavailable half the time, not counting the passing cloud. Engineers haven't yet developed energy storage devices suitable for storing solar and wind power, and they would add to the ultimate cost.

Patchiness

There is only one quality—geographic distribution—in which renewables reach parity with fossil fuels. Both are handicapped by their uneven distribution. Oil is famously concentrated in the Middle East, Russia enjoys an abundance of natural gas, and the United States is the Saudi Arabia of coal. But "many of the windiest and sunny regions in the world are virtually uninhabited," Cleveland says, meaning electricity would have to be moved long distances to population centers. The same patchiness holds for other renewables, from geothermal to hydro energy. For biomass, everyone has some arable land for growing energy crops, but much of it is already spoken for. And even if the land were available, energy crop yields would fall short of the need. The ethanol from the whole U.S. corn crop, for instance, could replace just 15% of the country's annual gasoline use, Smil says.

Ray of hope?

The "sobering reality," Smil says, is that there is only one renewable—solar energy—that could by itself meet future energy demands (see p. 786). Wind power could conceivably make a significant contribution, but each of the rest—hydro, biomass, ocean waves, geothermal, ocean currents, and ocean thermal differences—would provide just one-tenth to one-ten-thousandth of today's energy output from fossil fuels.

So the bulk of the burden will fall on solar, but turning the sun's rays into useful energy has a long way to go, Smil notes. Today, photovoltaic electricity accounts for less than 0.1% of the world's electricity. Solar heating, such as solar water heaters, accounts for less than 0.1% of total global energy production.

Such numbers would have to grow rapidly for a long time to make a difference, but renewables' handicaps do not bode well for speeding up the next energy transition. Fossil fuels "were phenomenally attractive," yet it still took 50 to 70 years to bring them into widespread use, says IIASA's Grübler. That's because, no matter how attractive a fuel might be, it takes time to create the infrastructure for extracting and transporting the resource, converting it into a usable form, and conveying it to the end user. It also takes time for inventors to develop end-use technologies—such as steam engines, internal combustion engines, and gas turbines—and for consumers to adopt them and create demand. Renewables "will be slower because they're less attractive," says Grübler. "They don't offer new services; they just cost more."

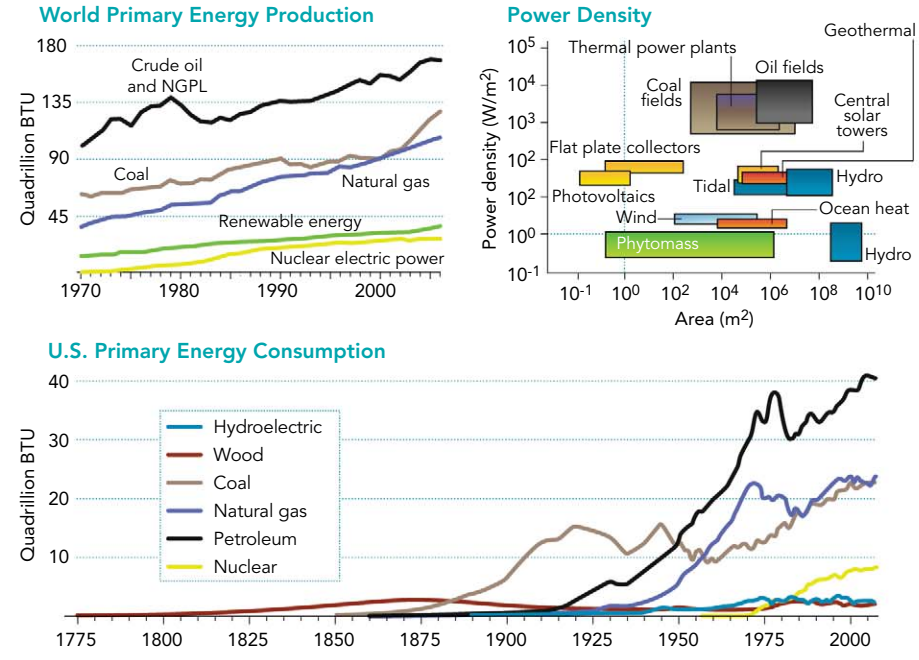
Ambitions to bring down the cost of renewables and accelerate the transition to clean, renewable energy have waxed and waned. In the United States, those hopes hit one acme in 2008, when former Vice President Al Gore challenged the United States "to commit to producing 100% of our electricity from renewable energy and truly clean carbon-free sources within 10 years." Smil calls that the epitome of "The Great Energy Delusion." It's not going to happen that way, he says. No amount of political commitment can erase the technological inertia in the energy production and consumption system or completely counter the quality shortcomings of renewables.

Still, renewable energy does have one clear advantage over fossil fuels: It doesn't produce the greenhouse gas carbon dioxide. Given the dearth of other incentives for scaling up renewables, "we may really need to engineer a transition," says Cleveland, "particularly if we're going to be serious about managing carbon." In practical terms, that re-engineering would mean lawmakers embracing policies that drive up the cost of fossil fuels and heavily subsidize renewables. But public support for such ideas has been lukewarm in the United States—whose citizens are person for person the world's biggest greenhouse gas emitters. Even in the midst of the worst oil spill in U.S. history, for instance, a poll by *The New York Times*/CBS News released 20 June found that although 90% of respondents agreed that "U.S. energy policy either needs fundamental changes or to be completely rebuilt," just 49% supported new taxes on gasoline to fund new and renewable energy sources.

With those kinds of polling results, "the best thing to do is reduce consumption," says BU's Kaufmann, given that "we've got the technology to reduce energy use tremendously." Conservation would buy time for meagerly attractive renewables to make some inroads before fossil fuels begin to bow out.

–RICHARD A. KERR

FOSSIL FUEL SUPREMACY



SOURCE: DOE (TOP LEFT AND BOTTOM); V. SMIL, *ENERGY TRANSITIONS*, PRAEGER (2010)

Top dog, for now. Fossil fuels each took half a century to dominate energy production (*bottom*). Renewables have gained (*top left*), but they are diffuse and therefore less attractive sources (*top right*).





Try to concentrate. Collectors that concentrate sunlight to heat a fluid and boil water are key to Desertec's design.

CREDITS (LEFT TO RIGHT): SOLAR MILLENNIUM; WIKIPEDIA

NEWS

Sending African Sunlight To Europe, Special Delivery

Europe wants clean power. North Africa has lots of sun. Can Desertec move solar electricity across the Mediterranean Sea?

GERHARD KNIES STARTED SERIOUSLY thinking about the problem of energy on 26 April 1986. Working as a particle physicist at the DESY accelerator lab in Hamburg, Germany, he watched in horror as the news broke that nuclear reactor number 4 at Chornobyl in Ukraine had exploded, spreading fallout across Europe. "Why do this to ourselves," he wondered, "when there are other options?"

Like a true physicist, he began asking some basic questions: How much solar energy falls on Earth? Where is it most intense? How many solar collectors would Europe need to meet its energy needs? For Knies, the questions led to only one answer: Build huge solar power farms in the Sahara and transmit the electricity through subsea cables across the Mediterranean Sea to Europe.

Knies's vision has since blossomed into Desertec, one of the world's most ambitious multinational efforts to scale up renewable energy. The goal: to build solar and other renewable power projects across North Africa and the Middle East capable of producing 500 gigawatts (GW) of electricity and so meet 15% of Europe's energy needs by 2050. Planners predict it will cost €400 billion or more to cover tens of thousands of square kilometers of desert with solar collectors and wind turbines, connected by thousands of kilometers of power cables.

The project—which backers compare to the Apollo space program—has yet to generate a single kilowatt. But it has attracted an impressive roster of political and industry supporters in Europe and North Africa. Still, analysts say Desertec faces an array of daunting challenges, from finding ready cash to overcoming thorny political and security issues. "Technology is not the problem," says Max Schön, president of the German branch of the Club of Rome in Hamburg, a think tank that has helped nurture the Desertec concept. "It is getting different cultures and economic structures working together."

Growing momentum

Such worries haven't dampened the hopes of Desertec backers. In June, for instance, European Union (E.U.) Energy Commissioner Günther Oettinger predicted that electricity could start flowing across the Mediterranean in just 5 years. And earlier this year, more than 200 bidders expressed interest in working with the government of Morocco on its first contribution to Desertec: a $9 billion, 10-year plan to build solar power plants producing 2 GW of power. Meanwhile, some heavyweight corporations—including engineering giant Siemens and finance titans Deutsche Bank and Munich Re—are now helping the nonprofit Desertec Foundation develop a business plan by 2012.

Such momentum was a distant dream during the aftermath of Chornobyl, when Knies—now chair of the board of trustees of the Hamburg-based Desertec Foundation—says he couldn't find much enthusiasm for his idea. That changed in the mid-1990s, as climate change became more of an issue. One turning point came when Knies organized a workshop at the Hamburg University of Technology that brought together energy experts to ponder his idea. Among other things, that meeting tackled two of the biggest technical questions facing Desertec: how best to make the electricity and how best to move it. The answers to both, the experts said, involve harnessing some emerging technologies.

Concentration is key

To generate Desertec's power, a number of studies have concluded that the best bet is "concentrating solar power" (CSP) technology, which uses reflectors of various shapes and configurations to heat a fluid such as water, oil, or molten salt. The hot fluid is then used to create steam to drive a turbine and generate electricity.

Experts say CSP has a big advantage over other technologies, particularly photovoltaic solar arrays: Plant operators can store the heat for a few hours by pumping the hot fluid into an insulated container or by transferring its heat to another material such as concrete. That way, once the sun goes down, the heat can be extracted and used to keep the steam turbines producing electricity. In contrast, the only practical way to store large amounts of photovoltaic energy is to use electricity to pump water up to a reservoir and then later release the water through a hydroelectric dam when consumers need power—a relatively expensive and inefficient process.

And CSP has another ace up its sleeve. By using boilers that can also be run on natural gas or biogas, plants can keep producing electricity on the rare cloudy day or if a sandstorm blots out the sun. CSP "looks from every side to be a very effective method," says Hani El Nokraschy, a Germany-based

businessperson who has been involved in Desertec since the late 1990s.

Other power planners have come to similar conclusions. The world's biggest solar plant, the Solar Energy Generating Systems facility in California's Mojave Desert, has been pumping CSP power into the grid since 1984. Another company, Tessera Solar, later this year will start installing CSP systems at two more Californian sites. And in Spain, on the back of generous government incentives, companies are building dozens of new CSP plants.

Go direct

To move the power from Africa to Europe, an influential 2006 study commissioned by Germany's environment ministry suggested that Desertec tap another emerging technology, high-voltage direct-current (HVDC) transmission. HVDC solves a big problem in moving electricity over vast distances: power loss. Typical alternating-current grids can lose up to 45% of their loads when lines are long, El Nokraschy says. DC systems do better but have been limited by a lack of switches that could handle high voltage. In recent years, however, engineers have developed switches that can sustain 800 kilovolts, enabling HVDC lines to move current as far as 4000 kilometers with losses of just 10% to 15%.

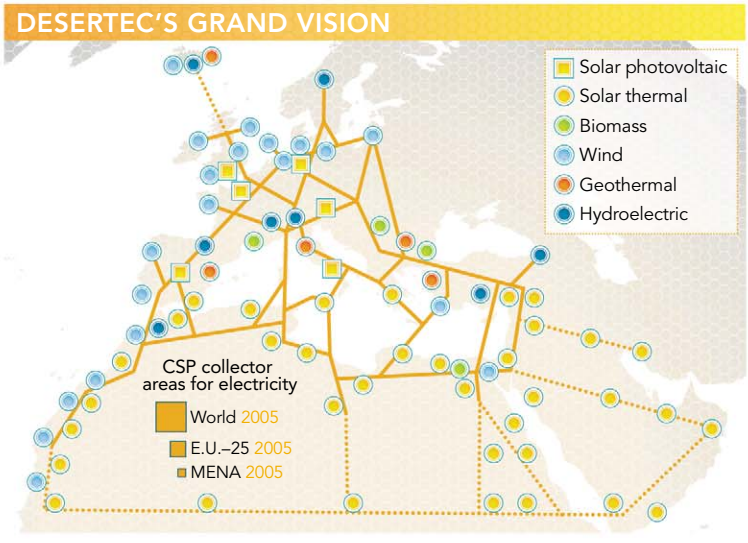
Desertec isn't the only project eyeing HVDC. Nine European countries around the North Sea are planning to build an HVDC grid, in part to smooth the flow of power from plants that generate electricity using intermittent sources such as wind, the sun, and ocean tides. The grid could, for instance, enable power generated overnight by the U.K.'s offshore wind farms to be stored in Norwegian pump storage facilities until the next day. Desertec "can learn from the North Sea grid," says the Club of Rome's Schön.

Progress and worries

The vision of coupling CSP with HVDC has helped Knies attract a diverse network of backers to Desertec's cause, among them the German Physical Society, Greenpeace, and Prince Hassan of Jordan. Today, the project is managed by the Desertec Foundation and an allied business arm, the Desertec Industrial Initiative (DII). In addition to forging partnerships with industry, the foundation and DII are working with governments—including officials from Europe, Morocco, Algeria, Tunisia, Egypt, and Jordan—to build support.

Desertec officials hope Morocco's move to build solar plants is just the start of realizing their ambitious, and expensive, long-term plan. It includes solar farms covering 17,000 square kilometers of desert in North Africa and the Middle East, an area roughly the size of Swaziland. A network of HVDC cables capable of carrying 100 GW would transmit power several thousand kilometers across the Mediterranean and into Europe.

Paying for that infrastructure, however, could be difficult. Planners estimate that the grid alone will cost more than €45 billion, and the entire project could run to €400 billion. Those are big numbers for banks and investors recovering from the biggest financial crisis in decades.



Tied together. Planners dream of linking solar and other renewable energy projects in North Africa to supply 15% of Europe's energy by 2050.

Other worries could also spook potential funders. One is that, despite CSP's promise, its power currently costs considerably more than electricity from traditional sources. As a result, Spain, the United States, and other nations have used an array of incentives to encourage growth, including direct subsidies and rules that require utilities to generate a certain amount of renewable power. Recently, however, even the incentives haven't been enough to overcome the credit crunch. "It's now virtually impossible to get investment" in the United States, says Thomas Mancini, CSP program manager at the U.S. Department of Energy's Sandia National Laboratories in Albuquerque, New Mexico. "This could be a death knell [for the CSP industry] if it goes on too long."

Knies thinks that one key to solving the economic challenge is mass production. If Desertec were to meet all of Europe's energy demand by 2050, for example, it would need to install 12,000 GW of CSP, or roughly 1 GW per day. That sounds like a lot, but making a solar collector is no more complicated than making a car, Knies argues. A carmaker the size of Volkswagen could easily churn out collectors at the required rate. "The industrial capacity to do such a task exists," Knies says.

Other worries facing potential funders include a fragmented European energy grid that could make it difficult to easily move power across national boundaries and the lack of any dependable grid at all in parts of North Africa. The region also lacks harmonized national rules for exporting and importing renewable power. Finally, there are political tensions among North African and Middle Eastern nations, as well as corruption and terrorism, that make large-scale energy cooperation seem a distant prospect. "It's complicated; it's not only about energy and climate, it's also about water, people, and migration," says Schön.

Desertec is beginning to address some of these issues through the Desertec University Network, a group of institutions that aims to train a new generation of North African and Middle Eastern engineers and technicians specializing in renewable energy. Desertec will need trained people, says El Nokraschy: "You can't bring them all from Europe and put them in the desert. You need to take them from the surrounding area."

Ultimately, Knies believes, Desertec could help reduce political tensions. Through cooperation, the countries of the southern Mediterranean could learn to build and run cutting-edge power plants, boosting local employment. They would get plentiful power for their own needs, such as water desalination, and could export power at a profit. At the same time, Europe would get electricity with few carbon emissions and an alternative to potentially problematic power sources like the Chornobyl nuclear plant that originally sparked Knies's efforts. "Where," he asks, "are the losers?" **–DANIEL CLERY**

SOURCE: DESERTEC/SOLAR MILLENNIUM





NEWS

Is There a Road Ahead For Cellulosic Ethanol?

After early optimism, alcohol brewed from farm and forest waste struggles to fulfill its promise as the next great biofuel

JUST A FEW YEARS AGO, THE IDEA OF turning farm and forest wastes into "cellulosic" ethanol, a biofuel to power cars and trucks, seemed a sure winner. Some researchers were predicting that they would soon perfect the new technologies needed to crack the cellulose and lignin molecules that had made grasses, cornstalks, and wood chips so much tougher to brew into ethanol than corn kernels. Both government agencies and private investors were pouring money into the field. In the United States, for instance, the Department of Energy (DOE) in 2007 unveiled plans to spend $385 million to back six commercial-scale reactors, while Congress approved hefty tax credits for biofuel makers. Venture capitalists invested billions in new cellulosic ethanol companies.

That was then. Now, much of the optimism surrounding cellulosic ethanol has faded thanks to the ongoing economic slump, a plentiful supply of ethanol made from corn, and uncertainty among policymakers. Numerous companies have either shelved plans to build commercial-scale cellulosic ethanol plants or walked away altogether. Even the promise of DOE's millions hasn't enticed them back. "In the current financial climate, existing federal policies are simply not enough to encourage the investments that will make these fuels a reality," says Jeremy Martin, a chemist with the Clean Vehicles Program of the Union of Concerned Scientists (UCS) in Washington, D.C.

The upshot: The U.S. government's flagship plan to reduce the nation's dependence on oil by scaling up cellulosic ethanol is in deep trouble, highlighting the complex technical, economic, and political forces buffeting global efforts to create viable alternatives to fossil fuels. And observers say decisions that Congress and federal agencies make this year could shape the nascent U.S. biofuels industry for decades to come. "It's an absolutely critical year for biofuels," says Wally Tyner, an agricultural economist at Purdue University in West Lafayette, Indiana.

A promising start

The plan to build an American biofuels industry on cellulose had been starting to pay off. In 2005, Congress approved new rules mandating a steady ramp-up in biofuels use. By 2022, lawmakers envisioned cars burning up to 36 billion gallons (136 billion liters) of biofuel a year, an amount equivalent to about one-quarter of today's U.S. gasoline use. Much of the early increase was to come from "first-generation" biofuels, primarily ethanol made from corn kernels. That industry has grown steadily, from turning out some 3 billion gallons of corn ethanol in 2005 to 12.1 billion gallons today. Most is blended with gasoline (typically 10% ethanol to 90% gasoline) to help reduce urban smog.

Congress, however, has capped the amount of corn ethanol it wants in gas tanks at 15 billion gallons by 2015. In part, that's because making corn ethanol is energy intensive, so the fuel doesn't do much to offset fossil fuel use or lower greenhouse gas emissions. Beyond that first 15 billion gallons, policymakers envisioned biofuels coming from "advanced" sources, such as ethanol and gasoline-like hydrocarbons made from plant materials high in cellulose.

The ramp-up in cellulosic ethanol production, however, is already well off track. Demonstration facilities are expected to turn out up to 25.5 million gallons this year—far below the 250 million gallons that the U.S. Environmental Protection Agency (EPA) once wanted fuelmakers to produce. In a telling sign of cellulosic ethanol's struggles, over the last year the agency twice scaled back its expectations after it became clear that the industry wouldn't be building commercial-scale plants as quickly as once thought.

What happened to the promise?

Part of the problem in scaling up cellulosic biofuels continues to be technical. To brew ethanol, manufacturers use yeast to ferment simple sugars such as glucose. That task is relatively cheap and easy when starting with a raw material—or "feedstock"—rich in those simple sugars, such as sugar cane in Brazil. In the U.S., brewers using corn as a feedstock face a slightly more complex pro-

CREDITS (LEFT TO RIGHT): CORBIS; PHOTOS.COM

Fueling doubts. Making ethanol from switchgrass (*far left*) can't yet compete with corn.

cess, because they first must use enzymes to break apart the starch in corn kernels into their component glucose molecules. The task becomes even more difficult when using cellulosic feedstocks such as switchgrass, corn stalks, or wood chips. The sugars in these feedstocks are locked in cellulose, hemicellulose, and lignin, biopolymers more complex than starch. Breaking those biopolymers into intermediate compounds that can be converted to ethanol remains a difficult problem. Researchers call it "recalcitrance," and it currently limits brewers to converting just 40% of the energy content available in cellulosic feedstocks to ethanol. Fermentation, by contrast, converts about 90% of the energy in simple sugars to ethanol. That means cellulosic ethanol plants currently need far more raw material than first-generation plants do to make the same amount of ethanol.

Researchers say they are making steady, if slow, progress in increasing the conversion rate. They've engineered novel microbes, for instance, that can break down cellulose into fermentable sugars. "The recalcitrance barrier will fall," predicts Lee Lynd, a metabolic engineer at Dartmouth College.

Hitting the blend wall

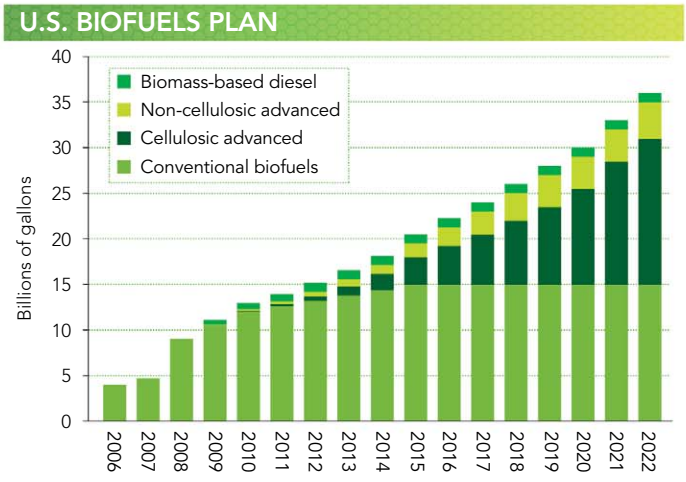
Even if it does, however, that breakthrough may not rejuvenate the field. That's because there is already an oversupply of first-generation ethanol on the market, Tyner says. At the moment, he notes, most ethanol is used to provide the 10% share in blended gasoline. But with the U.S. using a total of about 140 billion gallons of gasoline a year, the demand for ethanol is currently capped at about 14 billion gallons. Biorefineries already make 12.1 billion gallons of corn ethanol annually, he notes, and idled plants are capable of boosting the total to 15 billion gallons. The result is that the industry has reached a "blend wall," he says. "There is no room for cellulosic ethanol."

That could change if the government and carmakers start pushing cars that run on "E85"—a blend of 85% ethanol and 15% petroleum—or if cellulosic ethanol brewers figure out how to make their product cheaper than corn ethanol. (Cellulosic ethanol currently costs about double.) But neither development is likely anytime soon, and that partly explains why investors now shy away from backing cellulosic ethanol. The recent recession didn't help. "You can't get a loan to fund an ethanol plant of any kind right now because of the blend wall," says Bruce Dale, a chemical engineer and ethanol processing expert at Michigan State University, East Lansing.

Policy worries

Investors are also skittish because they aren't sure that government requirements mandating biofuels, and tax credits supporting them, are ironclad. Most of the existing $6 billion a year in ethanol subsidies and tax credits are currently up for renewal by Congress. Lawmakers have already allowed one tax credit for biodiesel to lapse, adding to investors' worries that ethanol subsidies could be next on the chopping block. "Until the government makes it absolutely clear that this is a long-term policy, investors will be reluctant to support the industry," says Sean O'Hanlon, the executive director of the American Biofuels Council in Miami, Florida.

A final challenge facing companies is ensuring long-term supplies of feedstock. Commercial-scale cellulosic ethanol plants, which can cost tens to hundreds of millions of dollars to build, are expected to operate for 3 decades or more. That means making deals with farmers to ensure steady access to agricultural wastes and other feedstocks. But "we don't have the supply chain in place to provide that much cellulosic material," Dale says.



Growing gap. Energy legislation from 2007 mandates an increasing share of cellulosic ethanol (dark green). But the industry is already falling behind.

SOURCE: W. TYNER/PURDUE UNIVERSITY

Driving forward

Despite all these challenges, analysts say Congress, EPA, and others can still make cellulosic ethanol viable. One option is for the government to alter tax incentives for biofuels. The current ethanol tax credit simply pays fuel blenders a flat $0.45 for each gallon of ethanol they use. A smarter option, UCS's Martin says, would be to offer larger credits to fuels—such as cellulosic ethanol—that are cleaner than corn ethanol or that could displace more gasoline.

Purdue's Tyner suggests taking this approach one step further by linking ethanol subsidies to oil prices. Current technology produces cellulosic ethanol at prices equivalent to $120 a barrel, he says, well above oil's recent price of about $77 a barrel. Taxpayers would make up the difference under Tyner's plan. If oil sold for $80 a barrel, cellulosic ethanol makers would get a $40-per-barrel subsidy; if oil rose to $120 a barrel, they'd get nothing. The sliding system would give cellulosic technologies time to become competitive and established, he argues. Another idea, say Dale and others, is simply to require that more—or all—new cars be able to use E85. The change could cost just $100 per car.

Both ideas have at least some support in Congress, but the industry won't know how much until work on a new agriculture bill moves into high gear later this year. Meanwhile, EPA is considering another option: increasing the required amount of ethanol in blended fuels to 12% or even 15%. That would boost demand from the current 12.1 billion gallons to as much as 14.6 billion gallons. Not everyone is in favor. Carmakers say they've optimized their engines to run on current blends, and they ask who would compensate unhappy car owners if the new blends damage engines. EPA is expected to make its decision by November; Tyner believes an increase to 12% would be "the politically and probably technically safe move."

Even such a boost, however, won't do much to attract new investors to build cellulosic ethanol plants, Tyner notes, because companies could meet the extra demand simply by bringing idle corn ethanol plants online. "It's a temporary fix at best," he says. Longer-term solutions to scaling up cellulosic biofuels, it appears, will need to come from the lab—and creative policymakers. **–ROBERT F. SERVICE**

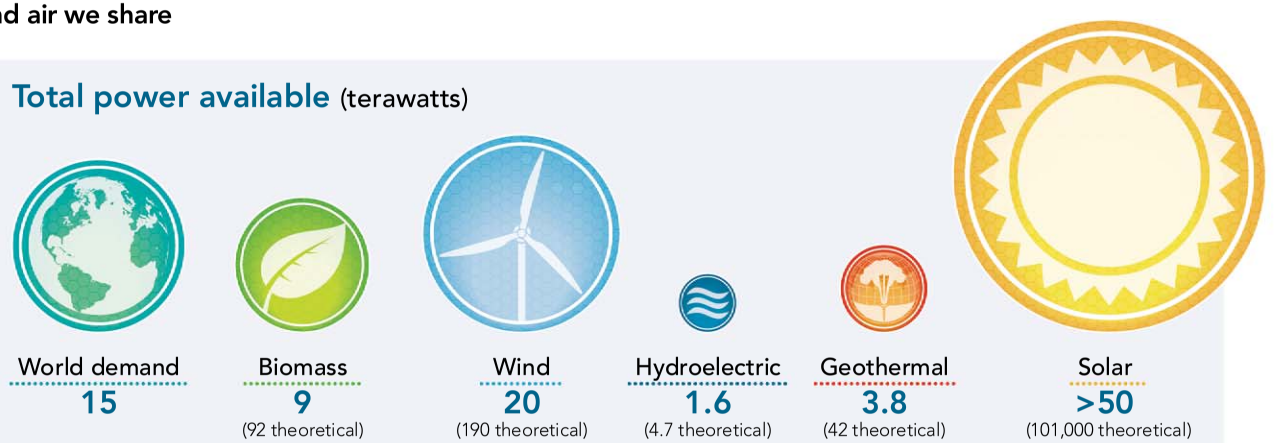
NEWS

Energy's Tricky Tradeoffs

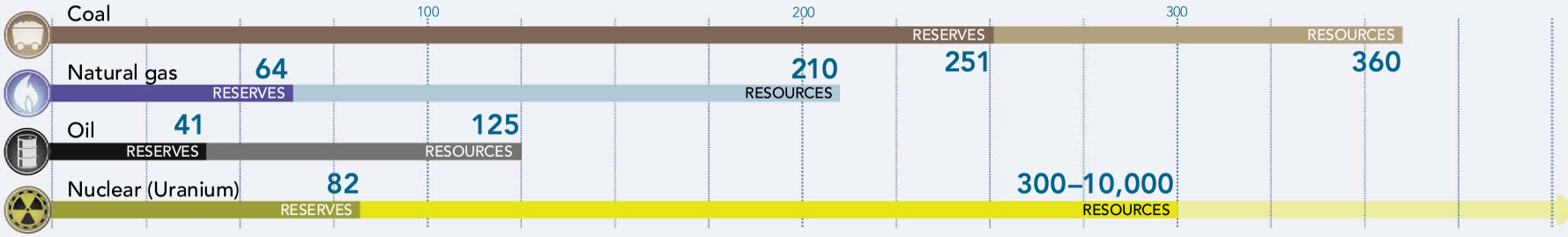
The world's "energy problem" is in fact a slew of technological and sociological challenges involving the use of the land, water, and air we share

I've got sunshine, plenty of sunshine ...
Sooner or later, humanity must move away from fossil fuels, finite resources that produce planet-warming greenhouse gases. At first blush, Earth appears to have power to spare. The total power from sunlight striking the ground is a whopping 101,000 terawatts, and experts estimate that we could capture enough of that to exceed by a wide margin the 15 terawatts of power that the world's population now consumes.

Total power available (terawatts)



How much is left? (years)



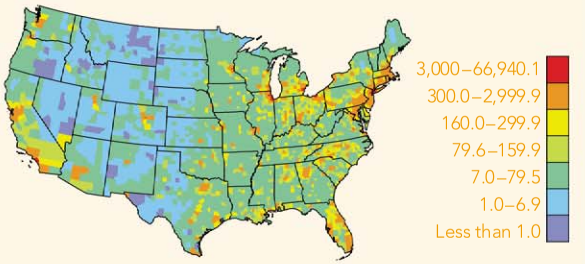
SOURCE: *WORLD ENERGY ASSESSMENT 2000*/UNDP; *WEA 2004*/UNDP; *REPORT OF THE INTL. GEOTHERMAL ASSOCIATION TO THE U.N. COMMISSION ON SUSTAINABLE DEVELOPMENT 2001*; SCLATER *ET AL.*, *JOURNAL OF GEOPHYSICAL RESEARCH* **86** (1981); NASA

GLOBAL

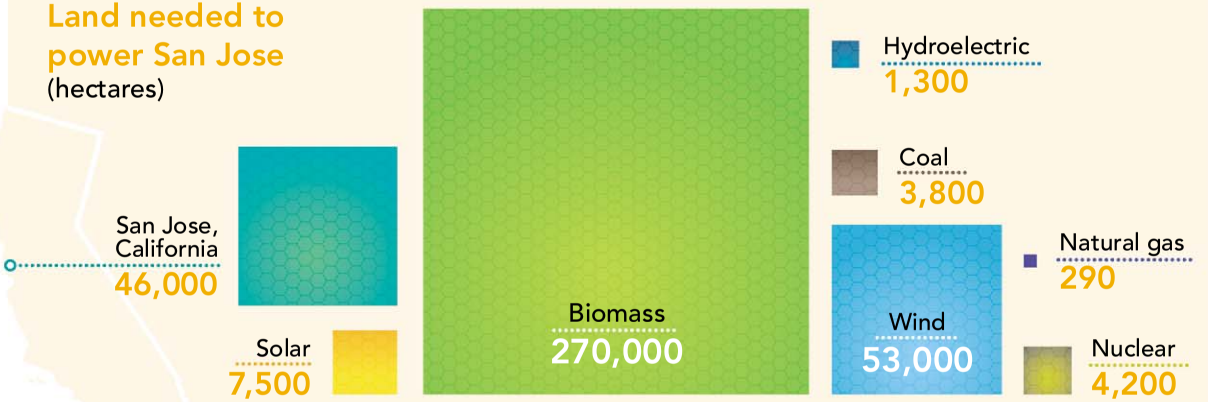
Give me land, lots of land ...
Wind and sunshine deliver energy in a far less dense form than coal, oil, or natural gas. For example, San Jose, California, has just over 1 million residents and consumes an average of 740 megawatts of electrical power. To supply that power, coal mines and coal-fired power plants would have to cover 3,800 hectares of land. In comparison, a wind farm would have to cover 53,000 hectares, an area bigger than the city itself. Unlike a coal mine, however, the wind farm could be used to grow crops at the same time.

Another issue: The sun doesn't necessarily shine the brightest and the wind doesn't blow the fiercest where most people live. And technologies have yet to emerge to store and transport vast amounts of energy generated from sunshine or wind. So delivering that energy where it's needed when it's needed remains a problem.

Population in the U.S. (per square mile)

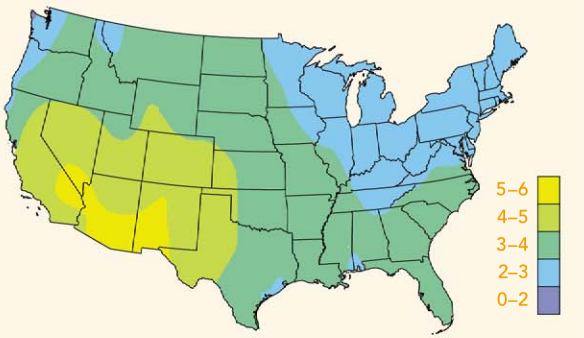


Land needed to power San Jose (hectares)



SOURCE: D. SPITZLEY *ET AL.*, UNIV. OF MICHIGAN CENTER FOR SUSTAINABLE SYSTEMS (2004); *ELECTRICITY FROM RENEWABLE RESOURCES*, NAS (2010); DOE

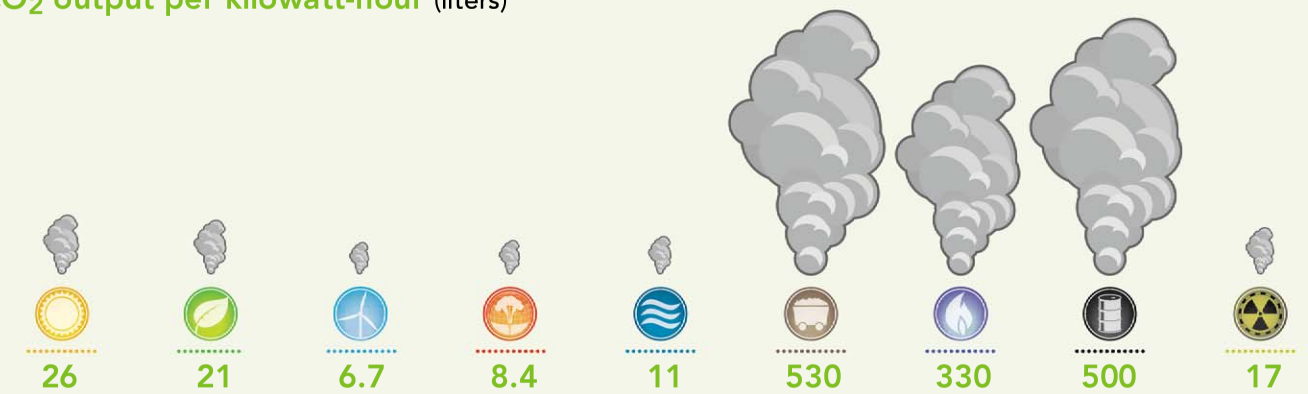
Average daily sunshine (kilowatts per square meter)



SOURCE: U.S. CENSUS BUREAU (TOP); NREL (BOTTOM)

CO_2 output per kilowatt-hour (liters)

SOURCE (TOP): DOE; AWEA; DOE/EPA; *ELECTRICITY FROM RENEWABLE RESOURCES*, NAS (2010); (BOTTOM): DOE; AWEA



A river runs through it.
The energy problem is also a water problem. Work on your computer all day, and you'll use about 1 kilowatt-hour of electricity. If that energy comes from coal, you'll have used 1.8 liters of water. If it comes from solar thermal technologies, you'll use 68% more water. Use power from biomass crops and you'll also use hundreds of liters of water to grow the fuel. Of course, fossil fuels produce heat-trapping carbon dioxide gas. If your kilowatt-hour of energy comes from coal, it produces 0.9 kilograms or 530 liters of pure CO_2—enough to fill 265 large soda bottles.

Water consumption per kilowatt-hour (liters)





No single solution.
To replace fossil fuels, most experts foresee using a mixture of energy sources and technologies. And they say that large gains can be made in improving the efficiency of existing technologies—as much as 60% in industrial processes. Still, reducing overall energy demand may not be easy. In 2007, the city of San Jose instituted a 15-year program that, among other things, seeks to reduce the per capita consumption of electricity and natural gas by 50%. After 2 years, such consumption was down by just 0.5%. **–ADRIAN CHO**



NEWS

Out of Site

Renewables like wind turbines are spreading fast, but can they survive complaints that they mar neighborhoods and threaten wildlife?

Wilting at windmills. Tensions are rising as wind-turbine developers look for land.

WHEN A POWER COMPANY ERECTED three towering white wind turbines on the Maine island of Vinalhaven last year, many residents welcomed the clean electricity the spinning blades would bring. Now, however, the mood has soured for some. "There is this amazing 'wump' as the turbine spins; you can feel the sound," says resident Cheryl Lindgren. "It's very annoying," she adds, and disrupts the "sanctity of the island."

Such complaints are becoming a growing problem for advocates pushing to scale up wind power and other renewable-energy sources. Around the world, an emerging network of groups are marshaling a wide array of arguments—from worries about excessive noise and wrecked views to threats to wildlife, air traffic, and even national security—in bids to block construction of new wind farms. And they are meeting with some success. In the United States, for instance, fierce local opposition has scuttled some major wind projects and delayed others for years.

The siting fights threaten to derail efforts to ultimately use wind turbines to generate up to 20% of U.S. electricity. To reach that goal, U.S. wind-generating capacity would have to increase from about 35 gigawatts today to more than 300 GW. That would require the construction of as many as 100,000 new turbines. Backers argue that they would be cleaner than power plants run on fossil fuels and could reduce per-kilowatt carbon dioxide emissions by 99%. Those benefits, however, haven't quieted critics. "Siting issues will only get worse and worse," predicts Robert Thresher of the National Renewable Energy Laboratory (NREL) in Golden, Colorado. And wind isn't alone: Similar resistance is facing plans to cover vast swaths of desert with solar collectors or scatter energy-producing buoys along coastlines (see sidebar, p. 789). The lesson, analysts say, is that even when new energy technologies are able to overcome substantial technical or economic hurdles—and offer real environmental benefits—they can still face substantial public opposition that backers ignore at their peril. To defuse the threat, government and industry are now taking a hard look at the problems posed by renewable-energy projects such as wind farms and how best to mitigate them.

The birds and the bats

One of the earliest efforts to understand wind power's environmental impacts began 2 decades ago, after thousands of dead birds of prey—including golden eagles—began showing up beneath turbines at one of the nation's first major wind farms on Altamont Pass in California. The kills made headlines and prompted studies aimed at solving the problem. It turned out that the site, a high ridge where many raptors roosted naturally, was unusually prone to bird strikes, says zoologist Dale Strickland of Western EcoSystems Technology in Cheyenne. Engineers reduced the toll by spacing turbines farther apart and removing machines from the most problematic sites.

These days, those lessons are also being applied at other wind farms, and the bird-strike issue has become less of a concern. A newer issue is understanding how the extensive road and fence networks associated with wind farms might act as "barriers to local wildlife," Thresher says. Breezy grasslands could pose particular challenges for turbine planners, he notes, because they host species such as sage grouse, which require extensive open areas.

Scientists are also just beginning to learn about the threat turbines pose to another flying animal: migratory bats. The issue heated up last year, after researchers reported that a single wind farm in West Virginia was killing as many as 4000 bats each year, mostly during fall migrations (*Science*, 24 July 2009, p. 386).

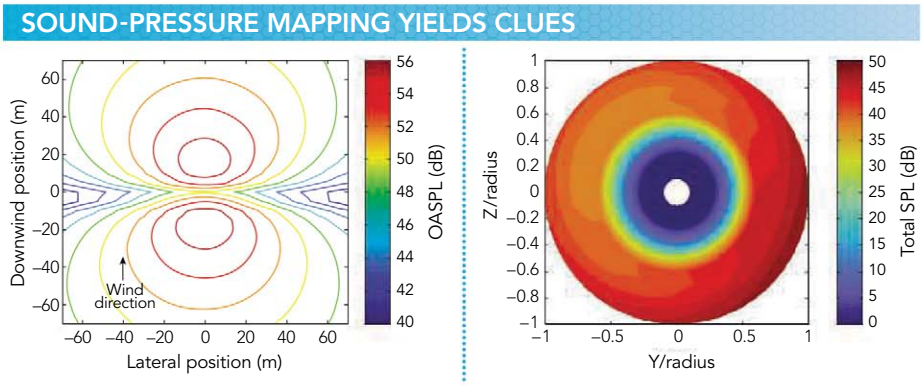
Some scientists hypothesize that the bats are at risk because they navigate along mountain ridges that are also favorable sites for wind farms—but researchers have also documented extensive kills on flat prairies in Alberta, Canada. Infrared video has shown that night-flying bats seem to have a fascination with moving turbine blades, and postmortems suggest that bats may be dying from air-pressure differences created by the blades, along with blunt trauma from collisions.

Scientists are already beginning to try some fixes. One idea is to turn off turbines before and after storms and on evenings with calm winds, times when studies suggest a lot of fatalities occur. Studies have also shown that raising a turbine's "cut in"



Surround sound. Microphone arrays provide data to make maps of turbine noise.

CREDITS (TOP TO BOTTOM): THINKSTOCK; S. OERLEMANS/NLR



Sound advice. Turbines are usually equally noisy front and back (*left*) but especially loud on the lower right of the turbine plane.

speed—the minimum wind speed at which the blades spin—can lower kills dramatically. One unpublished study of 23 turbines in southwestern Pennsylvania, led by wildlife biologist Edward Arnett of Bat Conservation International in Austin, found that "curtailed" turbines killed on average 80% fewer bats than uncurtailed turbines did.

Researchers are also experimenting with using sound to protect bats. Arnett and his colleagues have built so-called bat-aways, which blast ultrasonic sound out of 128 speakers per tower. Researchers say bats tend to avoid the ultrasound, perhaps because it jams their sonar. Last summer, in an unpublished study, the team found that turbines fitted with bat-aways caused only one-fifth to one-half as many bat fatalities as turbines without the devices. Still, Arnett says it's not yet clear the approach "is a viable solution."

Scanning the horizon

Another problem causing static for wind farmers is radar. Turbines that are too close to radar stations show up on controllers' screens as individual flickers, and the spinning blades have electronic signatures very similar to those of small planes. Those signals can confuse military or civilian air traffic controllers, who have objected to a number of planned farms. Overall, radar-related concerns have delayed or scuttled U.S. projects pegged to produce 4200 megawatts' worth of wind power, a 2009 survey by the American Wind Energy Association concluded.

The radar-interference problem will only get worse as the number of wind turbines skyrockets, predicts Gary Seifert of the U.S. Department of Energy's Idaho National Laboratory in Idaho Falls. But he hopes mitigation efforts will bear fruit. Computer programmers, for instance, are hard at work on new techniques to "tune out" the turbines' signatures, perhaps by incorporating supersensitive short-distance radar. Another idea is to make turbine blades "stealthy," or less visible to radar. Danish turbine maker Vestas and a company called QinetiQ are collaborating on stealthy materials that could be used to build or coat turbine parts.

Wumps and thwumps

The toughest challenge facing turbine builders may be mitigating the noise associated with the coming wind storm. People who live near turbines can be subjected to an annoying mix of whooshes, whines, and "thwumps," depending on the model and wind conditions. Wind developers in the United States, the United Kingdom, Canada, and New Zealand have all faced "vehement" local opposition due to noise, says Jim Cummings of the Acoustic Ecology Institute in Santa Fe, New Mexico.

From a simply technical perspective, turbine blades that spin faster make more energy more efficiently—but they also make exponentially more noise. So "there's always a tradeoff between efficiency and noise," says NREL engineer Patrick Moriarty. To get more power out of quieter blades, researchers are developing new tools to measure and mitigate the noise. Traditional noise surveys place single microphones upwind and downwind of turbines, but that provides coarse data, Moriarty says. So he and his colleagues have developed 32-microphone arrays that enable computers to create detailed "sound maps" that pinpoint which blades are producing sound and how it propagates through specific environments—an issue that can be as important as turbine design for nearby residents. The maps also help researchers see if new blade designs—such as serrated edges or holes—reduce noise by disrupting the way air eddies across the turbine.

Other Siting Problems

Geothermal energy, which involves tapping warm or cool temperatures underground, has been deployed on a small scale for decades with few problems. But the technique can cause earthquakes. One project near Basel, Switzerland, was shelved after drilling caused a magnitude-3.4 tremor in 2007.

Experts are also developing ways to retrofit historical buildings with solar panels while preserving their character. British preservation groups have created detailed guidelines for such projects. Meanwhile, the California Energy Commission has recommended against building a proposed solar energy installation in the Mojave Desert because of its potential impact on turtles.

Greening coal faces its own challenges, too. Scientists studying the implications of storing billions of tons of CO_2 from power plants underground say that concerns about causing earthquakes or polluting aquifers so far appear overblown. But such worries have already led to scuttled test projects in Germany, the Netherlands, and in Greenville, Ohio. "Not Under My Backyard" was how one paper put it. **–E.K.**

The easiest way to make turbines less noisy, however, may be simply to run them less. That can be accomplished by raising the cut-in speed, at a cost of cutting power production by a few percent. But some residents complain about noise produced when the turbines are spinning at speeds at which they produce most of their power; companies aren't likely to still turbines when the wind is most valuable.

In the end, technical tweaks may never fly with people who simply don't want to hear—or see—turbines in their backyards. Changing negative attitudes toward wind farms "will mean more than little engineering fixes," predicts Michael Vickerson of a renewable group called RENEW Wisconsin in Madison. One promising finding for wind advocates, Vickerson notes, is that people tend to become more comfortable with nearby wind farms over time: "The older a project is, we find, the more the turbines are accepted." That's a trend many renewable-energy advocates hope proves true.

–ELI KINTISCH

CREDIT: P. MORIARTY/NREL

PERSPECTIVE

Feedstocks for Lignocellulosic Biofuels

Chris Somerville,[1]* Heather Youngs,[1] Caroline Taylor,[1] Sarah C. Davis,[2] Stephen P. Long[2]

In 2008, the world produced approximately 87 gigaliters of liquid biofuels, which is roughly equal to the volume of liquid fuel consumed by Germany that year. Essentially, all of this biofuel was produced from crops developed for food production, raising concerns about the net energy and greenhouse gas effects and potential competition between use of land for production of fuels, food, animal feed, fiber, and ecosystem services. The pending implementation of improved technologies to more effectively convert the nonedible parts of plants (lignocellulose) to liquid fuels opens diverse options to use biofuel feedstocks that reach beyond current crops and the land currently used for food and feed. However, there has been relatively little discussion of what types of plants may be useful as bioenergy crops.

For the purposes of examining this issue in a prospective context, we make the simplifying assumptions that technology will become available for converting to sugars most of the structural polysaccharides that comprise the bodies of plants, that all the sugars can be used for fuel production, and that the process energy required for the conversion of the sugars to fuels will be obtained from combustion of the other components of the biomass, mostly lignin. Thus, in a sugar-to-ethanol bioconversion process using current technology, a metric ton (MT) of switchgrass or poplar, for example, would be expected to yield about 310 liters of ethanol (*1*). Technical improvements may increase the amount to more than 380 liters. Although we refer here to cellulosic ethanol, bioconversion of sugars to butanol, alkanes, terpenes, or other prospective biofuels or other types of conversion technologies (*2*) are expected to result in similar amounts of fuels on an energy basis (*3*).

In terms of global grain or seed production, maize is the largest crop, producing about 820 million MT of grain (*4*) and a similar amount of stems and stripped cobs (stover) that is potentially available for fuel production. Conversion of half the maize stover in the United States to cellulosic ethanol would produce about 51 gigaliters of ethanol (GLE) (Table 1). Thus, the total amount of stover-based ethanol could approximately double the amount of ethanol produced from maize in the United States without expanded land use. However, there is concern that removal of even half the stover would exacerbate loss of soil carbon and erosion and would also require additional inputs of fertilizers to replace lost minerals (*5*). Because of the shortage of labor during harvest season and the costs associated with recovering stover or straw in a separate operation after grain harvest, the development of new farm implements that would allow simultaneous grain harvest and stover baling would probably be necessary to make widespread stover use practical. The low amount of stover, or residues from other crops, produced per hectare may impose relatively large costs for collection and transportation to refineries, reducing economic incentives to use stover (*6*).

Perennial plants that use C_4 photosynthesis, such as sugarcane, energy cane, elephant grass, switchgrass, and Miscanthus, have intrinsically high light, water, and nitrogen use efficiency as compared with that of C_3 species. Additionally, reduced tillage and perennial root systems add carbon to the soil and protect against erosion. The highest annual dry-matter production level for any vegetation is, for such C_4 grasses, 88 MT/ha/year for Napier Grass (*Pennisetum purpureum*) (Fig. 1) in El Salvador and 100 MT/ha/year for natural stands of *Echinochloa polystachya* on the Amazon floodplain (*7*). In the temperate zone, the perennial C_4 grass *Miscanthus x giganteus* (Fig. 1) has attracted considerable interest. It produced in England at 52°N a peak biomass of 30 MT/ha/year and harvestable biomass of 20 MT/ha/year, the highest recorded for a cool temperate climate (*8*). Seasonality leads to an annual cycle of senescence, in which perennial grasses such as Miscanthus mobilize mineral nutrients from the stem and leaves to the roots at the end of the growing season. Thus, harvest of biomass during the winter results in relatively low rates of removal of minerals (*9*). This, coupled with diazotrophic associations, may account for the observation that stands grown at Rothamsted, UK showed no response to added nitrogen during a 14-year period during which all biomass was removed each year (*10*, *11*). In side-by-side trials in central Illinois, unfertilized *M. x giganteus* produced 60% more biomass than a well-fertilized highly productive maize crop, and across the state, winter-harvestable yields averaged 30 MT/ha/year (*9*, *12*). Mechanistic models developed to project yields based on the extensive trials conducted in Europe, when applied to the United States, suggest that many locations east of the Mississippi could support average annual yields of over 30 MT/ha, with a considerable number of areas exceeding 40 MT/ha (Fig. 2) (*13*, *14*). We estimate that if Miscanthus were used as the only feedstock, less than half of the 14.2 Mha currently set aside for the Conservation Reserve Program would be required to deliver the 132 GLE/year mandate of the Energy Independence and Security Act of 2007 [supporting online material (SOM) text]. Similar opportunities may exist in Europe, if the potentially high yielding zones for *M. x giganteus* of Poland, Romania, Belarus, and the Ukraine are included (*15*). Higher yields per hectare are likely for miscanes (sugarcane–Miscanthus hybrids), energy canes, and napier grass in the southernmost U.S. states. A recent study estimated that more than 600 Mha of land worldwide has fallen out of agricultural production, mostly in the last 100 years (*16*). Some of this area appears suitable for production of such perennial grasses or other types of energy crops, but additional research is necessary to categorize the land with respect to potential for various types of energy crops. The lack of proximity to infrastructure of some underutilized land for the production and transportation of fuels may be a major limitation to its utilization in the foreseeable future.

One of the largest current sources of biofuels is Brazilian sugarcane. In 2009, production for fuel on about 4.6 Mha (*4*) resulted in about 27 GLE plus 2 GW of net electricity from combustion of bagasse (*17*). The Brazilian light-duty fleet is mostly composed of flex-fuel vehicles, so this production replaced about 40% of the gasoline used in Brazil (*18*). The Brazilian government recently announced that expansion of the crop would be limited to 63.5 Mha (*19*). This land could be made available, without the clearing of natural ecosystems, by means of a slight increase in the low stocking density on the estimated 237 Mha of cattle ranching (*18*). Assuming that expansion of the amount of the crop used for nonfuel purposes continues at historical rates, approximately 60 Mha could eventually be available for fuel production (SOM text). If changes in fuel production technologies enabled the use of the polysaccharide component of bagasse to produce a liquid fuel, in addition to the fuel produced from sugar we estimate that Brazil could produce up to ~800 GLE (SOM text) or

[1]Energy Biosciences Institute, the University of California Berkeley, Berkeley, CA 94720, USA. [2]Energy Biosciences Institute, the University of Illinois, Urbana, IL 61801, USA.

*To whom correspondence should be addressed. E-mail: crs@berkeley.edu

equivalent amounts of other liquid fuels (*3*). On an energy basis, this would be equivalent to approximately 14% of the current world transportation fuel demand of 4900 Gl in 2006. Many other regions of the world are also well suited to sugarcane production or formerly produced sugarcane on land that has been abandoned. Thus, the total amount of fuel that may be produced from sugarcane worldwide could eventually be a very substantial proportion of global transportation fuels.

Approximately 18% of the terrestrial surface is semi-arid (200 to 800 mm of rainfall and an average growing season temperature >21°C) and prone to drought (*20*). Thus, a potential opportunity for production of biomass for fuels from land that is water-limited is the use of species with high efficiencies of water use and drought resistance, such as various *Agave* species that thrive under arid and semi-arid conditions (Fig. 1). *Agave* spp. use a type of photosynthesis called Crassulacean acid metabolism (CAM) that strongly reduces the amount of water transpired by absorbing CO_2 during the cold desert night and then internally assimilating this into sugars through photosynthesis during the warmer days. By opening their stomata at night, they lose far less water than they would during the day. Thus, *Agave* spp. have a water-use efficiency that may be as much as six times greater than that of C_3 species, such as wheat (*21*). Several *Agave* species have been cultivated on approximately 500,000 ha for production of sisal coarse fibers (*A. sisalana* and *A. fourcroydes*) or alcoholic beverages (*A. tequilana* and *A. salmiana*), so agronomic practices are well established. Somewhat surprisingly, some *Agave* spp. have been reported to exhibit high harvested biomass yields on semi-arid land when harvested on 5- to 6-year cycles. For instance, *A. desertii* grown with 430 mm of rainfall in California yielded 7 dry MT/ha/year, and *A. salmiana* grown with 320 mm of rainfall in Mexico yielded 10 dry MT/ha/year (*22*). *A. sisalana* production fields in Tanzania provided annual harvests of leaves of 58 wet MT/ha/year (*23*). Much of the land that has fallen out of agricultural production worldwide is semi-arid (*16*), and it appears that the amount of land that may be available for cultivation of *Agave* species is vast.

Woody biomass can be harvested sustainably for lumber and paper and may therefore provide biofuel feedstock for some regions. Approximately 89 to 107 Mha of land that were formerly in agriculture globally are now in forests and urban areas (*16*). Although there are large tracts of such forest land that are now mature ecosystems valued for biological diversity, recreation, and carbon sequestration, there are more recently abandoned lands that have lower ecosystem service values and could be used for plantation biomass crops. For example, some areas of the southeastern United States that were formerly managed as pine plantations have not yet succeeded to other uses. The continuing trend to electronic media and paper recycling may reduce the demand for pulp woods and thus presents an opportunity to reallocate woody biomass for energy. Additionally, the U.S. Forest Service confronts a challenge to manage excess wood residues that increase fire risks. The encroachment of the pine bark beetle has led to widespread mortality of trees, which will require their removal to reduce the risk of fueling catastrophic forest fires. Wood resources thus provide regionally specific opportunities for sustainably harvested biomass feedstocks. For perspective, the biomass that is harvested annually in the Northern Hemisphere for wood products has an energy content equivalent to approximately 107% of the liquid fuel consumption in the United States (*24*). Wood is a renewable resource that could contribute to lignocellulosic feedstocks if managed carefully. In order to maximize the amount of woody biomass produced per hectare, the best practice appears to be to coppice harvesting (Fig. 1.), in which the plants are cut near ground level after the end of the growing season every 3 to 5 years, depending on the species and the growing conditions (*25*). The plants rapidly regenerate shoots from the rootstock without any intervention. Thus, this approach minimizes losses of mineral nutrients, soil erosion, and organic carbon emissions and the investment of photosynthate in regrowing the roots. Harvesting in the winter at long intervals also appears to enhance biodiversity in the stands as compared with that of annual crops. Some tree species that appear to be suitable for coppice production have nitrogen-fixing symbionts and mycorhizzal associations that may help to minimize inputs (*25*).

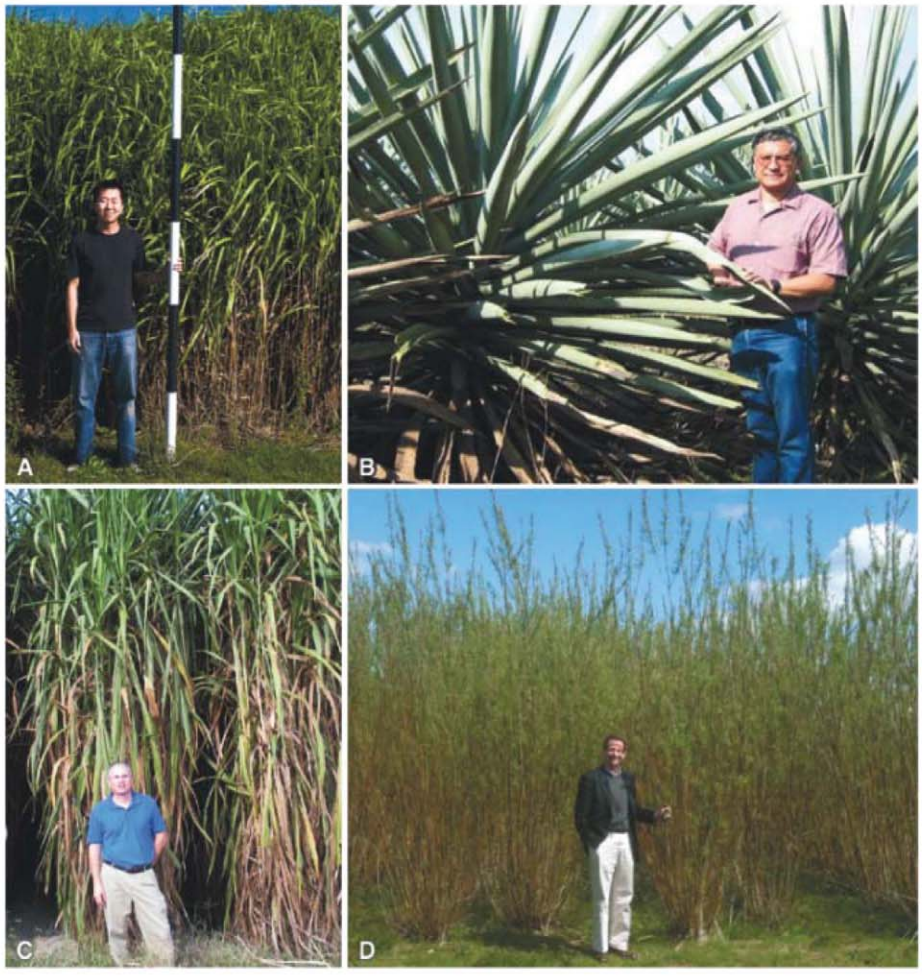


Fig. 1. Examples of some potential bioenergy crops. (**A**) *M. x gigantaeus* in Illinois. (**B**) Modern high production line of 5-year-old *A. tequiliana* in Mexico. Picture is courtesy of Dr. M. C. Alejandro Velázquez Loera, Universidad Autónoma Chapingo, D. F. Mexico. (**C**) One-year-old stand of Napier grass (*Pennisetum purpureum* Schumach.) in Florida. Picture is courtesy of B. Conway, BP. (**D**) Two-year-old willow coppice from 8-year-old roots in England (in third regeneration cycle).

Table 1. Estimated productivity, rainfall, and nitrogen requirements of current or potential bioenergy crops (see SOM for data sources).

Crop	Average productivity (MT ha^{-1} $year^{-1}$)	Ethanol yield (liter ha^{-1})	Seasonal water requirements (cm $year^{-1}$)	Tolerance to drought	Nitrogen requirements (kg ha^{-1} $year^{-1}$)
Corn		3800 (total)	50–80	low	90–120
Grain	7	2900			
Stover	3	900			
Sugarcane	80 (wet)	9950 (total)	150–250	moderate	0–100
Sugar	11	6900			
Bagasse	10	3000			
Miscanthus	15–40	4600–12,400	75–120	low	0–15
Poplar	5–11	1500–3400	70–105	moderate	0–50
Agave spp.	10–34	3000–10,500	30–80	high	0–12

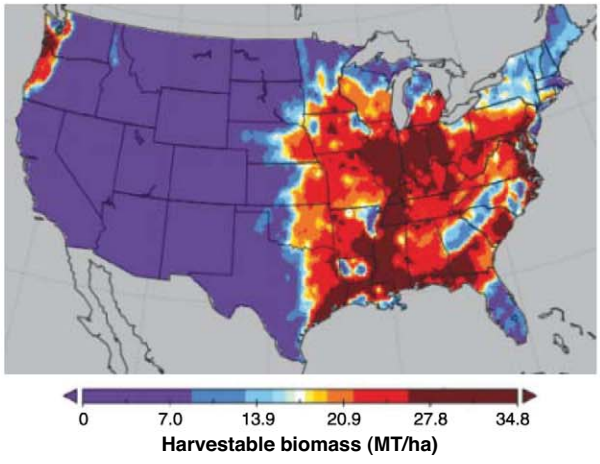


Fig. 2. Projected annual average harvestable yield of *M. x giganteus* in the third year after planting based on weather data for each of the past 30 years, and soil moisture and soil depth gridded across the 48 contiguous states. [Figure courtesy of Fernando Miguez and Germán Bollero using a model parameterized as described previously (*13*)] Projections agreed closely with prior measurements (*12*). After planting, annual average harvestable yields would be expected to increase for the first 3 years and then remain more or less constant for several further years (*10*, *27*). In contrast to maize, projected yields are higher to the south and east of the cornbelt.

The ability to produce lignocellulosic fuels sustainably is of paramount importance. Because the use of groundwater for irrigation is generally not sustainable, we envision that the type of energy crop grown in a given region will be primarily related to water-use efficiency (Table 1). Thus, relatively water-inefficient C_3 species such as poplar will be grown only where rainfall is abundant. Water-efficient C_4 grasses such as sugarcane, switchgrass, and Miscanthus will be grown where rainfall is not in excess, and highly water-efficient CAM plants such as *Agave* spp. will be grown in arid regions. In regard to soil quality, several hundred years of experience with sugarcane production and recent studies of the effects of sugarcane cultivation on soil carbon indicate that the crop can be grown sustainably (*26*). The available evidence also suggests that perennial grasses and trees can be produced sustainably and can improve terrestrial carbon sequestration. Because it is inevitable that some mineral nutrients will be removed when biomass is harvested, it will be essential to recycle mineral nutrients, which are not consumed in the production of biofuels, from biomass-processing facilities back onto the land. Because species diversity supports ecosystem health, and in order to maximize tolerance to both biotic and abiotic stresses, it will be desirable to use genetically diverse, or species diverse, plantations of energy crops. Long-term research concerning the agroecology practices that maximize net biomass productivity, sustainability goals, and environmental benefits in different types of biomass cropping systems is needed to identify the best management practices and varieties and the implications of allocation of land to production of lignocellulosic fuels. Importantly, by focusing on the use of dedicated energy crops—rather than on repurposing food and feed crops—it should be possible to overcome many of the problematic constraints associated with our narrow dependence on a relatively small number of food crops and to develop agroecosystems for fuel production that are compatible with contemporary environmental goals.

References and Notes

1. L. Lynd *et al.*, *Science* **312**, 1746 (2006).
2. Committee on America's Energy Future, *America's Energy Future;* (National Academies Press, Washington, DC, 2009).
3. J. L. Fortman *et al.*, *Trends Biotechnol.* **26**, 375 (2008).
4. FAOSTAT (Food and Agriculture Organization of the United Nations, Rome, 2010); http://faostat.fao.org.
5. R. Lal, *Environ. Int.* **31**, 575 (2005).
6. S. Sokhansanj, A. Turhollow, J. Cushman, J. Cundiff, *Biomass Bioenergy* **23**, 347 (2002).
7. S. P. Long, M. B. Jones, M. J. Roberts, *Primary Productivity of Grass Ecosystems of the Tropics and Sub-tropics* (UNEP/Chapman & Hall, London, 1992).
8. C. V. Beale, S. P. Long, *Plant Cell Environ.* **18**, 641 (1995).
9. F. G. Dohleman, E. A. Heaton, A. D. B. Leakey, S. P. Long, *Plant Cell Environ.* **32**, 1525 (2009).
10. D. G. Christian, A. B. Riche, N. E. Yates, *Ind. Crops Prod.* **28**, 320 (2008).
11. S. C. Davis *et al.*, *Ecosystems* **13**, 144 (2010).
12. E. A. Heaton, F. G. Dohleman, S. P. Long, *Glob. Change Biol.* **14**, 2000 (2008).
13. F. E. Miguez, M. B. Villamil, S. P. Long, G. A. Bollero, *Agric. For. Meteorol.* **148**, 1280 (2008).
14. F. E. Miguez, X. G. Zhu, S. Humphries, G. A. Bollero, S. P. Long, *Glob. Change Biol. Bioenergy* **1**, 282 (2009).
15. J. C. Clifton-Brown, J. Breuer, M. B. Jones, *Glob. Change Biol.* **13**, 2296 (2007).
16. J. E. Campbell, D. B. Lobell, R. C. Genova, C. B. Field, *Environ. Sci. Technol.* **42**, 5791 (2008).
17. The Brazilian Sugarcane Industry Association (UNICA), *Sugarcane Production—Brazil* (2010); http://english.unica.com.br/dadosCotacao/estatistica/.
18. J. Goldemberg, *Biotechnol. Biofuels* **1**, 6 (2008).
19. Decree No 6.961, 17 September 2009, Diário Oficial União de 18.9.10, Brazil.
20. United Nations Environment Programme (UNEP), *Global Environment Outlook: Environment for Development* (UNEP, New York, ed. 4, 2007).
21. A. M. Borland, H. Griffiths, J. Hartwell, J. A. Smith, *J. Exp. Bot.* **60**, 2879 (2009).
22. P. Nobel, *Environmental Biology of Agaves and Cacti* (Cambridge Univ. Press, Cambridge, 1988).
23. J. W. Purseglove, *Tropical Crops— Monocotyledons* (Longman, London, 1972).
24. C. L. Goodale *et al.*, *Ecol. Appl.* **12**, 891 (2002).
25. C. P. Mitchell, *Biomass Bioenergy* **9**, 11 (1995).
26. Centro de Gestão e Estudos Estratégicos (CGEE), *Sugar-cane based bioethanol: Energy for sustainable development—Rio de Janeiro* (Banco Nacional de Desenvolvimento Econômico e Social, Rio de Janeiro, Brazil, 2008).
27. R. Pyter, E. Heaton, F. Dohleman, T. Voigt, S. Long, in *Biofuels: Methods and Protocols,* J. Mielenz, Ed. (Humana Press–Springer Protocols, Clifton, NJ, 2009) pp. 41–52.

28. The preparation of this article was partially supported by a grant from the energy company BP to the University of California, Berkeley.

Supporting Online Material

www.sciencemag.org/cgi/content/full/329/5993/790/DC1
SOM Text
Fig. S1
Tables S1 to S4
References

10.1126/science.1189268

PERSPECTIVE

Challenges in Scaling Up Biofuels Infrastructure

Tom L. Richard

Rapid growth in demand for lignocellulosic bioenergy will require major changes in supply chain infrastructure. Even with densification and preprocessing, transport volumes by mid-century are likely to exceed the combined capacity of current agricultural and energy supply chains, including grain, petroleum, and coal. Efficient supply chains can be achieved through decentralized conversion processes that facilitate local sourcing, satellite preprocessing and densification for long-distance transport, and business models that reward biomass growers both nearby and afar. Integrated systems that are cost-effective and energy-efficient will require new ways of thinking about agriculture, energy infrastructure, and rural economic development. Implementing these integrated systems will require innovation and investment in novel technologies, efficient value chains, and socioeconomic and policy frameworks; all are needed to support an expanded biofuels infrastructure that can meet the challenges of scale.

The next few decades will require massive growth of the bioenergy industry to address societal demands to reduce net carbon emissions. This is particularly true for liquid transportation fuels, where other renewable alternatives to biofuels appear decades away, especially for truck, marine, and aviation fuels. But even for electricity and power, the growth potential of other renewables and nuclear power appears limited by high cost, technology barriers, and/or resource constraints. With estimates of bioenergy potential ranging from just under 10% to more than 60% of world primary energy (*1*–*4*), biomass seems poised to provide a major alternative to fossil fuels. As a point of reference for considering future biomass infrastructure needs, the International Energy Agency (IEA) (*4*) estimates that a 50% reduction in greenhouse gas emissions by 2050 will require a factor of 4 increase in bioenergy production, to 150 EJ/year (1 EJ = 10^{18} J), providing more than 20% of world primary energy.

With both agronomic and societal concerns about further increases in the use of grains and oilseeds for biofuels, almost all of this increased bioenergy will likely come from lignocellulosic feedstocks: dedicated energy crops, crop residues, forests and organic wastes. These materials have considerably lower bulk densities than grains, resulting in significant logistical challenges. The transportation fraction of the energy required to grow and deliver energy crops to a biorefinery is only 3 to 5% for grains and oilseeds, but increases to 7 to 26% for lignocellulosic crops such as switchgrass, miscanthus, and other forages and crop residues (*5*–*7*). These transportation costs represent a diseconomy of scale for lignocellulosic biofuels that contrasts with, and at large scales can overwhelm, the economies of scale associated with advanced conversion technologies.

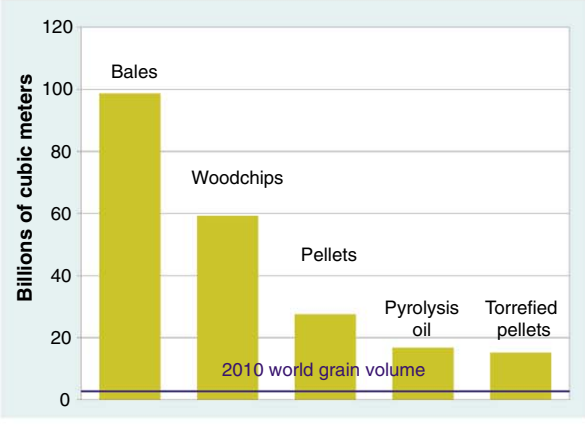


Fig. 1. Global biomass volumes required to achieve a 50% reduction in greenhouse gas emissions by 2050. A wide range of densification options are possible, but even the most effective will still require several times the biomass-handling capacity that the commodity grain system uses today.

To reach the IEA 2050 target of 150 EJ/year, primary energy from biomass would require 15 billion metric tonnes [i.e., megagrams (Mg)] of biomass annually, assuming 60% conversion efficiency (*4*, *7*) and a biomass energy content of 17 MJ/kg dry matter (*8*). A typical dry bulk density of grasses and crop residues is about 70 kg/m^3 when harvested, so without compaction the shipping volume of these 15 billion Mg would require more than 200 billion cubic meters (bcm). At baled grass and woodchip densities of 150 and 225 kg/m^3 (*8*–*10*), this transport volume would be 100 or 60 bcm, respectively (Fig. 1). Using reported energy densities of pellets, pyrolysis oil, and torrefied pellets (*6*), these densified products would require 28, 17, and 15 bcm of transport capacity, respectively.

To gain some perspective on the quantities involved, consider the volumes of related commodities currently being managed. For agricultural commodities, the sum of rice, wheat, soybeans, maize, and other coarse grains and oilseeds will approach 2 billion tons in 2010, with a total volume of 2.75 bcm (*11*). Current global volumes of energy commodities are somewhat larger, with 6.2 bcm of coal and 5.7 bcm of oil transported in 2008 (*12*). Thus, the combination of expected growth in energy demand and the lower density of biomass imply that by 2050, biomass transport volumes will be greater than the current capacity of the entire energy and agricultural commodity infrastructure.

These volumes imply a major growth opportunity for manufacturers of biomass-handling and transport equipment, but also a major stress on the transportation infrastructure, especially in rural regions around the world. If managed poorly, this additional traffic could degrade rural roadways and increase safety concerns. But increased demand for biomass could also provide a strong incentive to improve rural transportation infrastructure, facilitating agricultural and economic development in concert with renewable energy.

The size and efficiency of bioenergy conversion facilities will determine how far these huge volumes of biomass and biofuel will need to travel, and thus transportation's contribution to the energy, economic, and environmental impacts of biomass use. At a community scale, biomass energy can be converted in combined heat and power (CHP) systems producing 1 to 30 MW at efficiencies of 80% or more (*4*). At 80% efficiency, 30 MW of useful energy would require 150 Mg/day of biomass, or roughly five semi-trailer truckloads per day. These decentralized systems have the potential to source feedstock locally with minimum infrastructure costs. In contrast, cellulosic biofuel refineries are expected to achieve economies of scale at 200 to 1000 megaliters (ML) per year (*7*, *13*, *14*). Above this size range, the marginal cost of biomass transport can become greater than the marginal savings of larger biorefinery equipment on a per-unit basis (*13*). At the lower end of this range, feedstock needs would be equivalent to those of a 300-MW power plant, and a single biorefinery would require 50 trucks to deliver the 1600 Mg of biomass consumed each day. At the high end of this range, with 250 trucks per day, one truck would be unloading every 5 min around the clock.

These larger biorefineries and their expected volumes of flow will require a shift to a large-scale

Department of Agricultural and Biological Engineering, Pennsylvania State University, University Park, PA 16802, USA. E-mail: trichard@psu.edu

integrated transportation infrastructure if biomass is going to be a competitive energy resource at the scale of coal and petroleum. For longer distances, rail, ship, and pipeline transport of biomass become increasingly attractive. These represent proven, efficient solutions to transporting large volumes long distances and have been analyzed for a range of biomass types and preprocessing strategies (*6*, *15*–*17*).

Scale issues can also be addressed through synergistic combinations of biomass with other energy resources. Existing coal-fired power plants and petroleum refineries can incorporate properly formatted biomass as an alternative feedstock (*18*–*20*). Local sourcing of that biomass can thus reduce the diseconomies of scale associated with hauling distance while achieving economies of scale in conversion.

Other innovative strategies may help minimize the cost and maximize the value of biomass feedstock supply chains. By moving to a uniform format of particle size and density at or close to the harvest location, diverse biomass feedstocks could be handled by common equipment throughout the commodity chain (*9*). Pretreatment could be performed during transport and storage, as has been investigated for pipeline transport (*21*) and ensiled storage (*22*).

The transportation and logistics at the back end of a biofuel refinery must also be addressed. Ethanol is incompatible with the current fuel pipeline distribution system due to its corrosivity and its azeotrope with water, which can lead to pipe or tank failure and fuel contamination, respectively. That 200 ML/year biofuel plant would require 16 to 20 tanker trucks or railcars per day to move the fuel to market, increasing both traffic and costs (Fig. 2). These fuel distribution challenges are helping drive the interest in "drop-in" fuels that would be compatible with both the existing fuel distribution infrastructure as well as the vehicle fleet. Several such advanced biofuels are nearing commercialization, including butanol, Fischer-Tropsch fuels, and other bio-based gasoline and diesel equivalents. But regardless of the fuel product, massive investments in new pipe, rail, and highway infrastructure are needed to move those fuels from a new biorefinery network dispersed across the landscape. Both feedstock supply and fuel distribution logistics will influence the optimal size required for these biorefineries to achieve economies of scale (*23*).

In recent years several studies have evaluated alternative supply chain configurations to minimize overall feedstock delivery costs from regional to international scales (*6*, *9*, *24*–*30*). Several of these logistics models have identified critical points in the supply chain, where the relationships of distance and density conspire to increase transportation costs. A common feature in optimized high volume long distance biomass supply chains is a preprocessing stage that includes particle size reduction and densification, but can also include pretreatment of the biomass to facilitate both transport and downstream use. Depending on the technology, this preprocessing can be done on-farm or in community-scale satellite processing facilities (*9*).

Densification strategies include baling systems for grasses, crop residues, and forest trimmings as well as higher-density pellets and cubes (*31*–*34*) (see Fig. 1). Densification can be coupled with pretreatment processes that prepare the feedstock for downstream conversion. For biochemical conversion processes, the ammonia fiber expansion pretreatment process can produce a readily pelletized biofuel feedstock that can also be marketed as a highly digestible livestock feed (*35*). For combustion and thermochemical processes, torrefied pellets have a high energy density and become brittle, facilitating efficient combustion or gasification as well as cocombustion with coal at much higher blend rates than are possible for unprocessed biomass (*6*). Another thermochemical pretreatment prospect is pyrolysis, which produces a bio-crude oil. Although capital costs, oil stability, corrosivity, and deoxygenation remain challenges for pyrolysis (*6*), downstream conversion possibilities include gasification and blending with petroleum in conventional refineries. Pyrolysis also produces a biochar coproduct that can be used to improve soil quality, serving as a carrier for returning recovered nutrients to the soil. Interestingly, the economies of scale for most of these densification and preprocessing technologies plateau in the range of 20 to 80 MW thermal equivalent (*6*), similar to that of the decentralized CHP units previously described. Integrating these preprocessing operations with heat and electricity production could provide important synergies for both capital cost and operations.



Fig. 2. Truck transport of feedstock (**top**) and fuel (**bottom**). Brazilian sugar cane factories operate as a plantation system, with monocultures of sugar cane surrounding each refinery. Most sugar cane production is within 100 km of Sao Paulo, Brazil's largest city and industrial base, so the markets for biofuels are relatively close. In the United States, by contrast, midwestern corn ethanol must travel by road and rail more than 1000 km to markets on the east and west coasts.

Economic analysis of both preprocessing and conversion systems highlights the importance of year-round operations, as it is difficult to amortize capital costs for facilities that are only used for a few months of the year (*6*, *13*). However, many biomass feedstocks have optimal harvest periods that may run for only a few weeks. There are likely other seasons during which harvesting should not occur due to weather or various ecosystem constraints. Livestock farmers have been facing a similar problem supplying forages to their 24/7/365 milk- and meat-producing animals for over a thousand years, and have developed effective wet (<70% dry matter) and dry (>80% dry matter) storage systems for grasses and crop residues (Fig. 3). Dry biomass is preferred for pellets, torrefaction, and downstream thermochemical processing, where the presence of water would reduce overall energy efficiency. Wet storage systems couple well with single-pass harvest systems to reduce harvesting and drying operations, can minimize soil contamination and dry matter losses, and can add value to some downstream processes (*10*, *22*). Seasonality constraints

and storage requirements can be minimized by systems with the flexibility to process diverse feedstocks, which should be a consideration throughout the value chain from harvest to fuel conversion (*9*).

The amount of nearby land dedicated to energy crops will also greatly affect the costs of feedstock supply (*26*). Even short supply chains can substantially increase the cost of some biomass resources between the field and the biorefinery gate (*9*, *36*). As the scale of a biomass conversion facility increases, the advantages of maximizing the dedicated acreage near the facility, and thus minimizing feedstock transport distances, clearly increase.

The push-pull between economies of scale for conversion facilities and diseconomies of scale for feedstock supply chains suggests three distinct business models for biomass feedstock supply: independent local suppliers, large contiguous plantations, and regional or global commodity markets.

Independent local feedstock suppliers can work well for smaller biomass energy facilities, including combined heat and power plants that require a few truckloads of biomass each day or week. Such operations would have relatively short haul distances, little need for specialized equipment, and the extra expense required for densification would not be required. Local supply chains are currently common throughout the world, supplying everything from firewood for charcoal to waste oil for biodiesel.

A second model of biomass supply chains is the plantation approach, where a single company controls a large contiguous land area. Plantations have long provided concentrated production of agricultural and forest products for high volume processing and international markets. This strategy is being used today for bioenergy crops in many regions of the world, including sugar cane and soybeans in South America, oil palm in Malaysia, and canola in Ukraine. Most plantation systems have been structured so that the company needing the feedstock directly owns the land—an approach that historically has led to problems with land access, appropriation, and employee rights. However, secure but distributed land ownership patterns in many regions set the stage for alternative financial arrangements, including long-term contracts, profit sharing, and cooperative business financing that allow landowners to recoup their multi-year investments in perennial energy crops, while ensuring a concentrated feedstock supply for a processing facility. Any geographically concentrated feedstock supply system would do well to enhance the genetic diversity of its crops, including diverse varieties and multiple species, and have contingency plans that include backup suppliers to manage the risks of crop failure from weather or disease.

The third business model is the commodity biomass market, which would parallel the trading operations for other agricultural commodities (such as grains and livestock) as well as energy resources (such as petroleum and coal). In a commodity market there are clearly defined specifications for the product, which for biomass should include at a minimum levels of moisture, energy density, particle size, and the allowable content of certain minerals and contaminants. Aggregators can gather large quantities of the commodity, blend as needed to meet specifications, and then sell at market prices to buyers who are guaranteed a uniform feedstock. These aggregators can run the gamut from independent businesses to farmer cooperatives to large corporations. Any size is possible as long as the specification is met. Regardless of the scale of individual actors, a commodity system works most efficiently when transaction and transportation costs are low, so that distances between buyers and sellers have little impact on the price.



Fig. 3. Wet (**top** and **middle**) and dry (**bottom**) biomass storage configurations for lignocellulosic grasses. Because dry storage relies on low water activity to prevent microbial growth, it is most effective in arid regions. Wet storage, or ensilage, under anaerobic conditions encourages a natural acid fermentation that lowers pH and reduces microbial activity. Wet storage can keep dry matter losses below 5% for a full year, even in humid regions (*10*).

Although there is a great deal of interest from the biomass industry in building a commodity market, different feedstock specifications are relevant for combustion, biochemical processes, and thermochemical fuels. Biomass combustion is one bioenergy sector where formal specifications are already being developed to support established commodity supply chains (*37*, *38*). Biomass commodity specifications include explicit, measureable properties of the material as well as implicit value characteristics. The latter include sustainable production practices, which can be either voluntary or regulated and consider different geographical bounds (*39*–*41*). Although there is progress on several sustainability certification initiatives, there remains much uncertainty about where to set the bar, and the risks of unintended consequences are great.

The logistics of harvest, storage, processing, and transport weave a complex web of interactions that will require massive investments in research, development, demonstration and deployment to scale up biomass energy systems to meet societal goals. Although simulation models and commercial demonstrations help chart a course toward promising solutions, these still must be adapted to local feedstocks, infrastructure, and technology, as well as local socioeconomic contexts. Each facility, at every scale, will need to be supported by a cluster of complementary enterprises—a tightly choreographed supply chain that meets both local and global needs. These supply chains must also be value chains, striving to meet economic, environmental, and community goals. That balance requires an innovative, informed, and motivated citizenry—entrepreneurs, farmers, foresters, neighbors, and a host of new workers throughout the feedstock supply chain.

References and Notes

1. G. Berndes, M. Hoogwijk, R. van den Broek, *Biomass Bioenergy* **25**, 1 (2003).
2. E. M. W. Smeets, A. P. C. Faaij, I. M. Lewandowski, W. C. Turkenburg, *Prog. Energy Combust. Sci.* **33**, 56 (2007).
3. J. E. Campbell, D. B. Lobell, R. C. Genova, C. B. Field, *Environ. Sci. Technol.* **42**, 5791 (2008).
4. International Energy Agency, *Energy Technology Perspectives 2008—Scenarios and Strategies to 2050* (International Energy Agency, Paris, 2008), pp. 307–338.
5. A. E. Farrell *et al.*, *Science* **311**, 506 (2006).

6. A. Uslu, A. P. C. Faaij, P. C. A. Bergman, *Energy* **33**, 1206 (2008).
7. M. Laser *et al.*, *Biofuels Bioprod. Bioref.* **3**, 247 (2009).
8. R. C. Brown, *Biorenewable Resources: Engineering New Products from Agriculture* (Blackwell, Boston, 2003).
9. J. R. Hess, C. T. Wright, K. L. Kenney, *Biofuels Bioprod. Bioref.* **1**, 181 (2007).
10. K. J. Shinners, G. C. Boettcher, R. E. Muck, P. J. Weimer, M. D. Casler, *Trans. ASABE* **53**, 359 (2010).
11. World Agricultural Outlook Board, *May 2010 Report* (Office of the Chief Economist, USDA, Washington, DC, 2010).
12. U.S. Energy Information Administration, *International Energy Outlook 2010—Highlights* (DOE/EIA-0484, U.S. Department of Energy, Washington, DC, 2010).
13. A. Aden *et al.*, *Lignocellulosic Biomass to Ethanol Process Design and Economics Utilizing Co-Current Dilute Acid Prehydrolysis and Enzymatic Hydrolysis for Corn Stover* (NREL/TP-510-32438, National Renewable Energy Laboratory, Golden, CO, 2002).
14. S. Phillips, A. Aden, J. Jechura, D. Dayton, T. Eggeman, *Thermochemical Ethanol via Indirect Gasification and Mixed Alcohol Synthesis of Lignocellulosic Biomass* (NREL Technical Report TP-510-41168, National Renewable Energy Laboratory, Golden, CO, 2007).
15. A. Kumar, J. B. Cameron, P. C. Flynn, *Appl. Biochem. Biotechnol.* **113**, 27 (2004).
16. H. Mahmudi, P. C. Flynn, *Appl. Biochem. Biotechnol.* **129**, 88 (2006).
17. E. Searcy, P. C. Flynn, E. Ghafoori, A. Kumar, *Appl. Biochem. Biotechnol.* **137–140**, 639 (2007).
18. A. P. C. Faaij, *Mitig. Adapt. Strategies Glob. Change* **11**, 335 (2006).
19. G. W. Huber, A. Corma, *Angew. Chem. Int. Ed.* **46**, 7184 (2007).
20. G. Berndes, J. Hansson, A. Egeskog, F. Johnsson, *Biomass Bioenergy* **34**, 227 (2010).
21. A. Kumar, J. B. Cameron, P. C. Flynn, *Bioresour. Technol.* **96**, 819 (2005).
22. H. Ren *et al.*, *Biotechnol. Prog.* **22**, 78 (2006).
23. A. Eisentraut, *Sustainable Production of Second-Generation Biofuels: Potential and Perspectives in Major Economies and Developing Countries* (International Energy Agency, Paris, 2010).
24. A. Kumar, J. Cameron, P. C. Flynn, *Biomass Bioenergy* **24**, 445 (2003).
25. L. D. Mapemba, F. M. Epplin, R. L. Huhnke, C. M. Taliaferro, *Biomass Bioenergy* **32**, 1016 (2008).
26. P. P. Ravula, R. D. Grisso, J. S. Cundiff, *Bioresour. Technol.* **99**, 5710 (2008).
27. F. Magelli, K. Boucher, H. T. Bi, S. Melin, A. Bonoli, *Biomass Bioenergy* **33**, 434 (2009).
28. D. Alfonso *et al.*, *Biomass Bioenergy* **33**, 1070 (2009).
29. J. Singh, B. S. Panesar, S. K. Sharma, *Biomass Bioenergy* **34**, 483 (2010).
30. S. Sokhansanj, S. Mani, S. Tagore, A. F. Turhollow, *Biomass Bioenergy* **34**, 75 (2010).
31. M. Gronalt, P. Rauch, *Biomass Bioenergy* **31**, 393 (2007).
32. D. B. Blackwelder, E. Wilkerson, *Supply System Costs of Slash, Forest Thinnings, and Commercial Energy Wood Crops* (Technical Report INL/MIS-09-15228, U.S. DOE Idaho National Lab, Idaho Falls, ID, 2008).
33. S. Sokhansanj, A. F. Turhollow, *Appl. Eng. Agric.* **20**, 495 (2004).
34. L. Eriksson, L. Gustavsson, *Biomass Bioenergy* **34**, 82 (2010).
35. J. E. Carolan, S. V. Joshi, B. E. Dale, *J. Agric. Food Indust. Org.* **5**, 10 (2007).
36. National Academy of Sciences, National Academy of Engineering, National Research Council, *Liquid Transportation Fuels from Coal and Biomass: Technological Status, Costs, and Environmental Impacts* (National Academy of Sciences, Washington, DC, 2009).
37. E. Alakangas, J. Valtanen, J.-E. Levlin, *Biomass Bioenergy* **30**, 908 (2006).
38. M. Kaltschmitt, M. Weber, *Biomass Bioenergy* **30**, 897 (2006).
39. M. Lenox, J. Nash, *Bus. Strategy Environ.* **12**, 343 (2003).
40. I. Lewandowski, A. P. C. Faaij, *Biomass Bioenergy* **30**, 83 (2006).
41. J. van Dam *et al.*, *Biomass Bioenergy* **32**, 749 (2008).

42. I thank C. Taylor, K. Ruamsook, E. Thomchick, and C. Hinrichs for providing helpful comments and sources.

10.1126/science.1189139

PERSPECTIVE

An Outlook on Microalgal Biofuels

René H. Wijffels[1] and Maria J. Barbosa[2]

Microalgae are considered one of the most promising feedstocks for biofuels. The productivity of these photosynthetic microorganisms in converting carbon dioxide into carbon-rich lipids, only a step or two away from biodiesel, greatly exceeds that of agricultural oleaginous crops, without competing for arable land. Worldwide, research and demonstration programs are being carried out to develop the technology needed to expand algal lipid production from a craft to a major industrial process. Although microalgae are not yet produced at large scale for bulk applications, recent advances—particularly in the methods of systems biology, genetic engineering, and biorefining—present opportunities to develop this process in a sustainable and economical way within the next 10 to 15 years.

The concept of using algae to make fuels was already being discussed 50 years ago (*1*), but a concerted effort began with the oil crisis in the 1970s. Large research programs in Japan and the United States focused on developing microalgal energy production systems. From 1978 to 1996, the U.S. Department of Energy's Office of Fuels Development funded a program to develop renewable transportation fuels from algae (*2*). The main focus of the program, known as the Aquatic Species Program (ASP), was the production of biodiesel from high-lipid-content algae grown in ponds, using waste CO_2 from coal-fired power plants. In Japan, the government financed a large research project entitled "Biological CO_2 Fixation and Utilization" from 1990 to 1999 (*3*). These programs yielded some successes—such as promising lipid production strains, open production systems (raceway ponds), and principles for photobioreactor design (the use of fiber optics to bring light inside the systems)—that are still the focus of research today, but none has proven economical on a large scale.

There have been several critical issues that combined have had a large influence on stimulating the resurgence of algal biofuels research. The world has experienced record crude oil prices, increasing energy demand, and environmental concerns that have pushed biofuels research in general to the fore. In the narrower context of

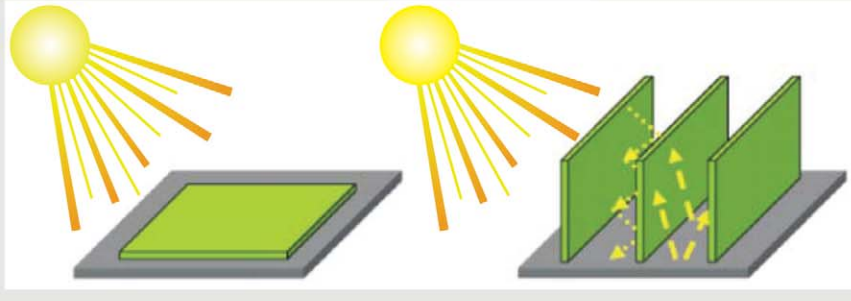


Fig. 1. The principle of light dilution. The light intensity (*I*) striking closely spaced vertical panels is much lower than the intensity striking a horizontal reactor on the same surface.

[1]Wageningen University, Bioprocess Engineering, Post Office Box 8129, 6700 EV Wageningen, Netherlands. [2]Wageningen University and Research Center, Food and Biobased Research, Post Office Box 17, 6700 AA Wageningen, Netherlands. E-mail: rene.wijffels@wur.nl (R.H.W.); maria.barbosa@wur.nl (M.J.B.)

biofuels, the food versus fuel debate and a virtual explosion in biotechnology resulted in a substantial commitment to the development of algal biofuels by the industrial and governmental sectors. The recent investments in microalgae for fuels are well justified by the potential that these microorganisms offer through their higher lipid productivities per ground area than oleaginous agricultural crops, as well as lack of competition for arable land.

Faced with stresses such as nutrient deprivation, algae store chemical energy in the form of oils such as neutral lipids or triglycerides (*4*). The algal oil can be extracted from the organisms and converted into biodiesel by transesterification with short-chain alcohols (*5*) or by hydrogenation of fatty acids into linear hydrocarbons (*6*). Algae also synthesize other fuel products, such as hydrogen (*7*), ethanol (*8*) and long-chain hydrocarbons, that resemble crude oil (*9*), or the algal biomass can be converted to biogas through anaerobic fermentation (*1*).

Despite this potential, the production capacity for microalgae is presently limited in comparison to land-based energy crops. The current worldwide microalgal manufacturing infrastructure (producing the equivalent of ~5000 tons of dry algal biomass) is devoted to extraction of high-value products such as carotenoids and ω-3 fatty acids used for food and feed ingredients. The total market volume is €1.25 billion, implying an average market price for microalgae of €250/kg dry biomass (*10*). As an example for comparison with land-based oleaginous crops, the world production of palm oil is nearly 40 million tons, with a market value of ~0.50 €/kg (*11*).

Production of microalgae for biofuels needs to take place on a much larger scale at much lower costs. If all transport fuels were to be replaced by biodiesel in Europe, there would be an annual need for nearly 0.4 billion m^3 (*12*). If this biodiesel were to be supplied through microalgae, 9.25 million ha (almost the surface area of Portugal) would be needed to supply the European market, assuming a productivity of 40,000 liters per ha per year. This productivity is based on a 3% solar energy conversion to biomass (theoretical maximum is 9%) and a biomass oil content of 50%, under the solar conditions of Portugal. A leap in the development of microalgae technology is therefore required; on a practical level, the scale of production needs to increase at least 3 orders of magnitude, with a concomitant decrease in the cost of production by a factor of 10. In the past few years, there has been a rather polarized debate between researchers in the field over technology readiness and the prospects for productivity enhancement, with some parties pressing for scale-up and commercialization now, while others cautiously stress the need for additional research leading to more careful step-by-step development (*13*).

We believe a multidisciplinary approach will be required to realize the full potential of microalgae as a biofuels feedstock. A comprehensive research portfolio should cover the whole chain of process development in an integrated and iterative way, including fundamental biology, systems biology, metabolic modeling, strain development, bioprocess engineering, scale-up, biorefineries, integrated production chain, and the whole system design, including logistics (*14*). The main objective is to reduce production costs and energy requirements while maximizing lipid productivity and to increase the biomass value by making use of all algal biomass components. For cost and energy reduction and maximization of lipid productivity cell properties, bioreactor design, efficiency in supply, and use of nutrients and resources need to be improved, and to make use of all biomass ingredients, a biorefinery infrastructure needs to be established.

In microbial fermentations, substantial improvements in productivity have been obtained through both technological (reactor design, process control, harvesting, and extraction) and strain improvements. As an example, the present productivity of penicillin synthesis by fungi is 5000 times as high as it was 50 years ago (*15*). Commercial production of microalgae is still based on traditional technologies using a few strains. There are many more species yet to explore; in addition, genetic engineering offers the possibility for strain improvement. High lipid productivity is essential for the commercial production of biodiesel from microalgae. In nonstressed growing algae, lipids are mostly present in the form of phospholipids in the cell membranes. Some microalgae, when exposed to stress conditions (e.g., nutrient deprivation or high light intensities), accumulate lipids in the form of triacylglycerols in so-called oil bodies. This accumulation occurs at the expense of energy used for growth, leading to a decrease in growth rate and a consequent decrease in productivity. Knowledge of the biosynthesis mechanism of triacylglycerols and their accumulation in oil bodies is limited and often based on analogies with higher plants (*4*). If the mechanism were known, it could open the possibility of inducing lipid accumulation in oil bodies without having to apply a stress factor. More broadly, detailed insight into metabolic pathways may lead to strategies to induce lipid accumulation based on process conditions, defined nutrient regimens, and/or the use of metabolic engineering techniques. For this purpose, well-annotated genomes need to be available.

There are still very few algae for which full or near-full genome sequences have been obtained

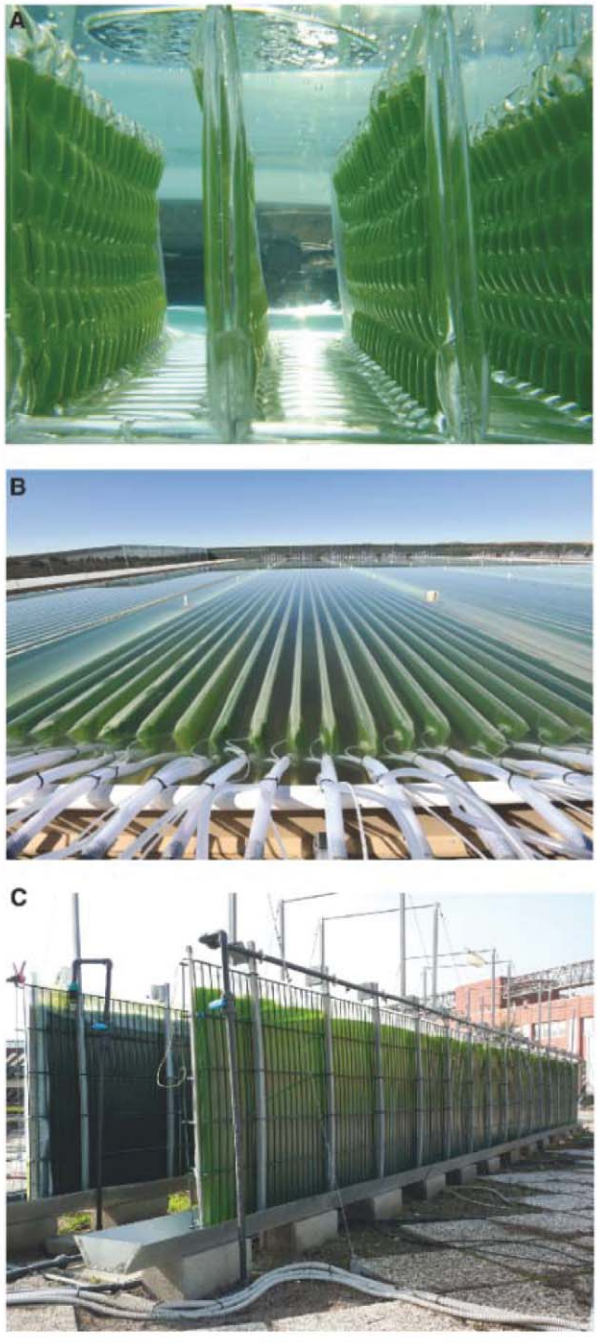


Fig. 2. Development of low-cost photobioreactors. Flat-panel reactors from (**A**) Proviron, Belgium [reproduced with permission from (*29*)], (**B**) Solix Biofuels, USA (reproduced with permission from *Biomass Magazine*), and (**C**) Green Wall Panel reactors from Fotosintetica & Microbiologica S.r.l., Italy.

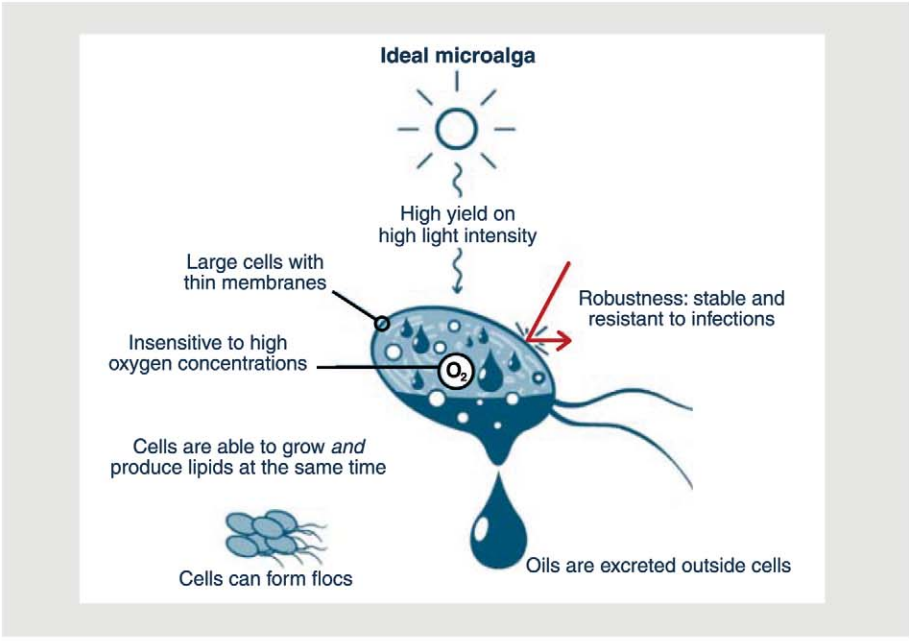


Fig. 3. The ideal photosynthetic cell factory for production of biofuels.

[e.g., *Chlamydomonas reinhardtii* (*16*), *Thalassiosira pseudonana* (*17*), and *Phaeodactylum tricornutum* (*18*)], and transfection systems have barely been developed. Currently, there are about 10 different algal species that can be transformed (*19*). However, sophisticated metabolic engineering, whereby several genes are overexpressed or down-regulated in a single organism, is currently only really possible with *C. reinhardtii*. We expect that the genome of more algal strains will be sequenced in the near future, due to the present high interest in the field, enlargement of the scientific community, and the availability of fast and reliable technologies for genome sequencing.

The main inputs required in addition to the algae themselves are sunlight, water, CO_2, nitrogen, and phosphorus. Large-scale cultivation of microalgae for biofuel production must be based on sunlight as the sole source of light energy. Especially when working in summertime, and/or when working at lower latitudes, sunlight intensities are high and often oversaturate the photosynthetic cycle, limiting growth and leading to a drop in productivity. In recent years, much effort was put into increasing photosynthetic efficiency of microalgae under oversaturating light (the normal condition on a sunny day) by developing new strains with smaller antenna sizes (*20*) and by decreasing the light path of photobioreactors while increasing mixing (turbulence) in high cell density cultures (*21*, *22*). Turbulence requires high energy input and therefore is not suitable for large-scale production of biofuels from microalgae. One strategy to obtain high photosynthetic efficiencies under bright sunlight in systems with lower energy requirements is to reduce the light intensity at the reactor surface. This can be done by stacking the reactor units vertically (Fig. 1): Narrow spacing in the stacks minimizes loss of light to the ground surface (*21*). However, if not combined with a short light path, this setup leads to voluminous reactor systems with low volumetric productivity and low biomass concentration (*23*). To reduce investment costs of these systems, vertical panels can be made from thin plastic films such as polyethylene (Fig. 2). There are examples of thin film systems submerged in large water volumes for good temperature control and a lower associated energy requirement for cooling (*14*). We expect that in the coming years many systems will be developed based on these design principles (Fig. 2). Improvements are to be expected in material lifetime (polyethylene has a lifetime of ~1 year), ease of cleaning, and energy requirements (for example, the energy requirement for cooling can be further reduced by reflecting the near-infrared portion of the light incident on the reactor surface, which otherwise heats the system without contributing to photosynthesis).

Water usage is another important parameter. For the production of 1 liter of biofuel from fuel crops, approximately 10,000 liters of water are needed (*24*). Microalgae need much less water. For photosynthesis alone, ~0.75 liter of water is needed per kg of biomass produced (*25*). Per liter of biofuel, assuming a lipid content of 50%, 1.5 liters of water are required. In practice, water use in production systems is much larger because water is also used for cooling closed systems, and fresh water needs to be added to open ponds to compensate for evaporation. If closed systems are used and cooled with a large saltwater buffer via heat exchangers, freshwater usage can be reduced considerably. Microalgae can also be grown on seawater; even deserts would be suitable if there is access to salt aquifers. Growth could also take place in confined systems on large water surfaces such as lakes or seas, assuming there is adequate protection from the wind.

The production of large quantities of biomass also requires a large amount of CO_2. A total of 1.8 tons of CO_2 is needed to produce 1 ton of algal biomass (*25*). This means that 1.3 billion tons of CO_2 would be required for the production of 0.4 billion m^3 of biodiesel to supply the European transportation market. The European Union produces about 4 billion tons of CO_2, (*26*) so production of microalgae could go some way toward relieving this CO_2 excess. However, the distance across which CO_2 may need to be transported in this context is a matter of concern.

The main nutrients needed for the production of microalgae are nitrogen and phosphorus. The biomass of the algae consists of 7% nitrogen and 1% phosphorus. Consequently, for the European biofuel market ~25 million tons of nitrogen and 4 million tons of phosphorus are needed. This is about twice the amount that is presently produced as fertilizer in Europe (*27*). For sustainable production of biodiesel from microalgae, it will be important to make use of residual nutrient sources (about 8 million tons of nitrogen in Europe) and to recycle nutrients as much as possible.

After production, the biomass needs to be harvested, the lipids extracted, and the remaining cell components recovered. Harvesting of microalgae is currently expensive because of the high energy requirements and capital costs involved. Because most microalgae are small individual cells, centrifugation is often used as a preferred harvesting method. However, as the biomass concentration is generally low (<3 g/L), centrifugation of diluted streams requires a large capacity of the centrifuge, which makes the process energy-demanding and expensive. Flocculation, followed by sedimentation and flotation, before centrifugation or filtration will substantially reduce harvesting costs and energy requirements. Ideally, algae would flocculate spontaneously at a certain stage of the process. After harvesting, the oil needs to be extracted. The cells are first disrupted, and then the oil can be extracted with organic solvents or with more environmentally benign, but more expensive, solvents (e.g., supercritical CO_2). Most microalgae strains are, in general, relatively small and have a thick cell wall. For this reason, very harsh conditions need to be used (e.g., mechanical, chemical, and physical stress) to break the cells for extraction of the products, which may affect the functionality of cell compounds like proteins. Excretion of the oils, in a manner similar to what naturally occurs in the microalgae *Botryococcus braunii*, will lead to a simplified biorefinery and improve the downstream economics. However, it will not provide a complete solution because the remaining

cell components still need to be recovered from the cells. Thin cell membranes, strong enough to prevent shear damage during production, would facilitate cell disruption. Small spherical cells with a thick cell wall, like *Nannochloropsis*, are clearly not ideal fuel sources for this reason.

Currently, some of the desired individual characteristics mentioned above and depicted in Fig. 3 can be found in specific strains but never combined in one ideal strain. In addition, strain characteristics need to be integrated with reactor design principles. For example, if a strain has the capacity to efficiently convert high light intensities into biomass, light dilution will no longer be necessary. If strains are developed that can tolerate high oxygen concentration, the length of tubes in tubular photobioreactors is no longer limited and degassing is no longer required.

Economically feasible production of microalgae for biofuels will only be achieved if combined with production of bulk chemicals, food, and feed ingredients. Despite algae's high suitability for biorefining due to the varied composition of its biomass, the coproduction of multiple products from microalgae remains a challenge. Research is needed to explore mild cell disruption, extraction, and separation technologies that retain the functionality of the different cell components (e.g., proteins, carbohydrates, ω-3 fatty acids, pigments, and vitamins). Biorefining is important not only for cost efficiency but also for the supply of food compounds. The algal biomass that could theoretically supply 0.4 billion m^3 of biodiesel to the European market consists of 40% protein; thus, the total amount of protein produced as a by-product would exceed 0.3 billion tons. This is about 40 times as much as the amount of soy protein (18 million tons of soy beans with ~40% of proteins in 2008) presently imported into Europe (*11*). Therefore, the production of microalgae for fuels would place no pressure on the availability of rich agricultural areas for production of proteins; on the contrary, there is even the possibility of an overproduction of proteins.

In closing, we reiterate our belief that 10 to 15 years is a reasonable projection for the development of a sustainable and economically viable process for the commercial production of biofuels from algal biomass. It is important that further technology development be done in close collaboration with environmental scientists. The production processes should be subjected to life-cycle analysis (*28*) and monitored for their impact on biodiversity.

References and Notes

1. W. J. Oswald, C. G. Golueke, *Adv. Appl. Microbiol.* **2**, 223 (1960).
2. J. Sheehan, T. Dunahay, J. Benemann, P. Roesler, *A Look Back at the U.S. Department of Energy's Aquatic Species Program: Biodiesel from Algae* (Department of Energy, Golden, CO, 1998).
3. N. Usui, M. Ikenouchi, *Energy Convers. Manage.* **38** (suppl. 1), S487 (1997).
4. Q. Hu *et al.*, *Plant J.* **54**, 621 (2008).
5. Y. Chisti, *Biotechnol. Adv.* **25**, 294 (2007).
6. S. Lestari, P. Mäki-Avela, J. Beltramini, G. Q. M. Lu, D. Y. Murzin, *Chem. Sus. Chem.* **2**, 1109 (2009).
7. J. Benemann, *J. Appl. Phycol.* **12**, 291 (2000).
8. M. D. Deng, J. R. Coleman, *Appl. Environ. Microbiol.* **65**, 523 (1999).
9. A. Banerjee, R. Sharma, Y. Chisti, U. C. Banerjee, *Crit. Rev. Biotechnol.* **22**, 245 (2002).
10. O. Pulz, W. Gross, *Appl. Microbiol. Biotechnol.* **65**, 635 (2004).
11. Food and Agriculture Organization of the United Nations, http://faostat.fao.org
12. International Energy Agency (IEA), Oil Market Report, 10 June 2010; http://omrpublic.iea.org
13. L. Reijnders, *Trends Biotechnol.* **26**, 349, author reply 351 (2008).
14. R. H. Wijffels, M. J. Barbosa, M. H. M. Eppink, *Biofuels Bioproducts Biorefining* **4**, 287 (2010).
15. G. J. M. Hersbach, C. P. van der Beek, P. W. M. van Dijck, in *Biotechnology of Industrial Antibiotics*, E. J. van Damme, Ed. (Marcel Decker, New York, 1984), pp. 45–140.
16. S. S. Merchant *et al.*, *Science* **318**, 245 (2007).
17. E. V. Armbrust *et al.*, *Science* **306**, 79 (2004).
18. C. Bowler *et al.*, *Nature* **456**, 239 (2008).
19. T. L. Walker, C. Collet, S. Purton, *J. Phycol.* **41**, 1077 (2005).
20. A. Melis, *Plant Sci.* **177**, 272 (2009).
21. M. Tredici, *Biofuels* **1**, 143 (2010).
22. Q. Hu, A. Richmond, *J. Appl. Phycol.* **8**, 139 (1996).
23. J. W. F. Zijffers *et al.*, *Mar. Biotechnol.*; published online 23 February 2010; 10.1007/s10126-010-9258-2.
24. C. de Fraiture, M. Giordano, Y. Liao, *Water Policy* **10** (suppl. 1), 67 (2008).
25. A. M. J. Kliphuis *et al.*, *Biotechnol. Prog.* **26**, 687 (2010).
26. European Environment Agency, *Greenhouse Gas Emission Trends and Projections in Europe 2008: EEA Report 5* (EEA, Copenhagen, Denmark, 2008).
27. K. van Egmond, T. Bresser, L. Bouwman, *Ambio* **31**, 72 (2002).
28. L. Lardon, A. Hélias, B. Sialve, J. P. Steyer, O. Bernard, *Environ. Sci. Technol.* **43**, 6475 (2009).
29. R. Bosma, M. H. Vermue, J. Tramper, R. H. Wijffels, *Int. Sugar J.* **112**, 74 (2010).

30. The authors acknowledge two large Dutch National Initiatives: the Center of Excellence for Sustainable Water Technology (Wetsus) and Toward Biosolar Cells/AlgaePARC. Through these research programs in collaboration with industry, Wageningen UR has been able to set up a multidisciplinary research program for development of microalgae technology.

10.1126/science.1189003

REVIEW

Generating the Option of a Two-Stage Nuclear Renaissance

Robin W. Grimes[1] and William J. Nuttall[2]

Concerns about climate change, security of supply, and depleting fossil fuel reserves have spurred a revival of interest in nuclear power generation in Europe and North America, while other regions continue or initiate an expansion. We suggest that the first stage of this process will include replacing or extending the life of existing nuclear power plants, with continued incremental improvements in efficiency and reliability. After 2030, a large-scale second period of construction would allow nuclear energy to contribute substantially to the decarbonization of electricity generation. For nuclear energy to be sustainable, new large-scale fuel cycles will be required that may include fuel reprocessing. Here, we explore the opportunities and constraints in both time periods and suggests ways in which measures taken today might, at modest cost, provide more options in the decades to come. Careful long-term planning, along with parallel efforts aimed at containing waste products and avoiding diversion of material into weapons production, can ensure that nuclear power generation remains a carbon-neutral option.

In North America and Europe, the development of nuclear power stalled after the March 1979 Three Mile Island accident in Pennsylvania, and until recently the building of additional nuclear reactors was not likely. Yet today, a nuclear renaissance is underway, and globally 52 reactors are under construction (*1*). How nuclear energy found itself in a state of decline is well documented. Will it continue to move forward and avoid another collapse?

In this article, we assess technological responses and opportunities for nuclear generation technology on two time scales (Fig. 1): first, those of immediate concern and consequence, and second, matters that will dominate in the longer term (beyond about 2030), when nuclear development could once more stall. The immediate future also indicates continued growth of nuclear energy in the Middle East, East Asia, South Asia, and elsewhere.

If the global electricity system is to be largely decarbonized over the first half of this century, then two key challenges must also be surmounted. One will be to develop civil nuclear programs in all parts of the world without risking the proliferation of nuclear weapons technologies (*2*). The other will be to deal with nuclear waste in as safe a manner as possible. Settling on policy options has proved extremely difficult in many

[1]Centre for Nuclear Engineering, Department of Materials, Imperial College London, London HA9 8DT, UK. E-mail: rgrimes@imperial.ac.uk [2]Cambridge Judge Business School, Cambridge CB2 1AG, UK, and Engineering Department, Cambridge University, Cambridge CB2 1PZ, UK. E-mail: wjn21@cam.ac.uk

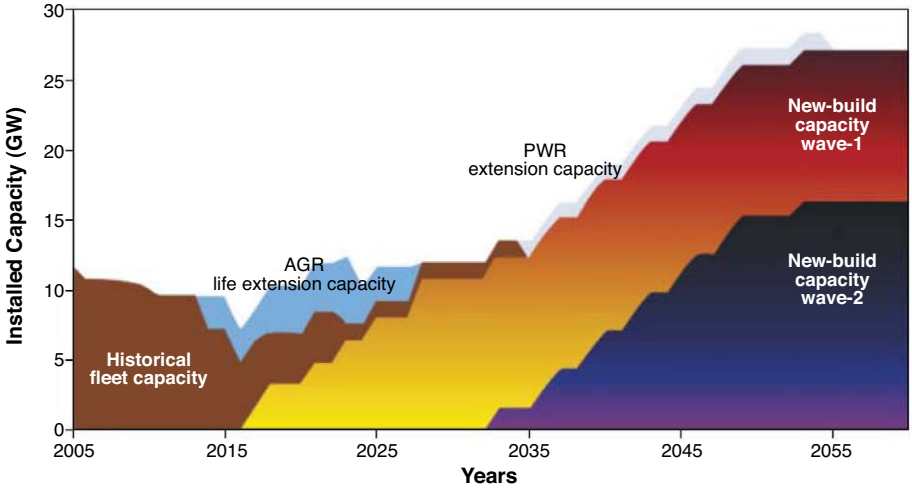


Fig. 1. A possible two-stage nuclear renaissance in the United Kingdom. The first wave is being developed, allowing the United Kingdom to "replace nuclear with nuclear." The second wave would allow nuclear energy to play a major role in electricity decarbonization. [Credit: A. Becker, personal communication]

countries for many decades. Technical proposals are available, including deep geological disposal. The assessment and perception of the risks associated with the transport and storage of radioactive wastes will continue to be reconsidered, given growing concerns about unconstrained fossil fuel wastes being emitted into the atmosphere. Newer reactor designs have the promise of creating less waste or waste that has a shorter lifetime, but some storage issues will still need to be resolved.

The Immediate Time Scale

For many countries with established nuclear programs, the most immediate challenges are nuclear life extension and how best to renew nuclear generation infrastructure. Such steps are no better than neutral in terms of reducing greenhouse gas emissions, but they can preserve diversity of fuel and technology in the electricity mix, thereby helping to preserve a secure energy supply. However, lifetime extensions demand a thorough and precisely justified safety case. This requires prediction of reactor component materials performance under the extreme conditions experienced—still a great challenge to materials science (*3*). Therefore, the length of lifetime extensions is uncertain for all current reactor types.

The electricity industries of most current nuclear energy states are dominated by large centralized power stations that transmit over large-capacity grids to end users metered only infrequently. This transmission system is well suited to what is known as large-scale base-load generation and will be continued by the Generation III (Gen III) nuclear power stations currently planned or under construction (Table 1), which will replace Gen II facilities [definitions of the generation classes of nuclear reactors are given in (*4*)]. Base-load operation means that a power plant is operated at maximum capacity for as long as fueling and maintenance requirements will permit. Nuclear power stations are at their most profitable when operated by this regime (*5*). In the immediate future, only a few countries will need to consider more flexible nuclear technologies optimized to change their output power with changes in demand; such exceptions result from very high reliance on nuclear energy (for example, in France) or because of substantial energy generation from intermittent renewable energies, such as wind (for example, in Germany) (*5*).

Several Gen III nuclear energy technologies are ready for immediate deployment (Table 1). They are each the product of experience gained by a few large companies over many years of operating related reactors. In each case, probabilistic safety assessments (PSAs) have demonstrated even higher safety and reliability of these designs (*6*). PSAs were introduced after the Three Mile Island incident, which did not occur just as the result of one event, but following a sequence of interrelated events (*7*). A PSA can be used to predict the consequence of a series of events to yield, for example, a core fault accident frequency. These important numbers have continued to improve.

Gen II reactors rely on active processes in the event of a fault occurring (for example, a pump will start or a valve will open to mitigate the problem), but active control systems may themselves incur a fault. Some Gen III systems rely on passive processes (such as natural heat convection and gravity) to prevent irrecoverable damage. However, it remains a major challenge to determine the extent to which a specific design truly incorporates passive safety or the length of time that the passive system can operate reliably.

Gen III designs have also benefited considerably from advances as diverse as three-dimensional computer-aided design, concretes with improved microstructural properties, and new powerful lifting equipment. Large complete plant modules are now built away from the site, lifted into place, and fitted into position. Gen II designs often required reactors to be disassembled and then reassembled inside their containment structure.

In addition to their large generating capacity, the reactors in Table 1 are all water-moderated and use a fuel technology in which stacks of uranium oxide pellets (the fissile material) are sealed inside tubes made from zirconium-based alloys (the cladding). Both the pressurized water reactor (PWR) and the boiling water reactor (BWR) designs use light water to moderate down the energy of the neutrons produced during fission so that they can initiate further fission reactions. These designs advance earlier Gen II PWR and BWR light-water

Table 1. A selection of Gen III nuclear power plant types with target electrical generating capacities of at least 1000 MW (*30*). Light water can be pressurized (PWR) or used as boiling water (BWR); the Canadian design uses heavy water (HWR).

	Areva EPR	Westinghouse AP-1000	GE-Hitachi ESBWR	AECL ACR-1000	VVER-1200	Atmea	General Electric ABWR	APR-1400	Mitsubishi APWR
Country of origin	France	USA	USA/Japan	Canada	Russia	Japan	Japan	South Korea	Japan
Maximum capacity (MWe)	1750	1188	1520	1200	1200	1100	1371	1450	1538
Technology	PWR	PWR	BWR	HWR	PWR	PWR	BWR	PWR	PWR
Status March 2009	Under construction (France and Finland)	Under construction (China)	Seeking U.S. NRC license	Final design work	Under construction (Russia)	Concept completed safety review	Constructed	Under construction (South Korea)	Seeking Japanese license

Text Box 1. Specific Global Problems During the Immediate Time Scale

Supply chain for nuclear new build. During the 1990s, the nuclear supply chain (especially for large forged components) had largely wound down to a point where few companies worldwide retained key capabilities. In recent years this trend has started to reverse, but there is still no basis for complacency concerning the nuclear supply chain.

Personnel/expertise. As with the supply chain, the nuclear skills base has also not been replenished, so the nuclear industry suffers from an aging workforce. The problem is particularly acute in areas such as regulatory safety inspectors.

Research facilities. During the past two decades, numerous radiation and reactor test facilities have closed. The absence of such facilities will hamper progress in understanding radiation damage processes in materials and components and the development of alternative fuel cycles for use beyond 2030.

Social factors and waste. The last wave of nuclear power plant construction occurred in a very different geopolitical and social context than today. One consequence is a widespread reluctance to accept the building of new nuclear power stations without a clearly defined policy for nuclear waste management and eventual disposal, not just for future wastes but also for existing ("legacy") wastes.

Plutonium. Legacy plutonium remains problematic in several countries. The use of separated Pu in a LWR via a U/Pu mixed oxide fuel does not rapidly reduce the total inventory of Pu but does convert it from a relatively easily handled oxide powder to a less easily handled (or diverted) radioactive spent fuel assembly. Such considerations are important for international civil nuclear fuel cycles.

reactor (LWR) designs. In the past 4 decades, the proportion of time during which LWRs were available to generate electricity (their availability factor) increased from around 70% to over 90% (*8*).

However, LWRs require the $^{235}U/^{238}U$ isotopic ratio to be enriched by a factor of roughly 5 over that of natural uranium to sustain fission. Although the enrichment process is very energy intensive, more of the uranium atoms undergo fission in enriched fuels, resulting in more energy being extracted per kilogram of fuel (i.e., a high degree of burn-up). Enrichment is not needed in heavy-water designs, because the D atoms capture far fewer neutrons, permitting a chain reaction even when fewer ^{235}U atoms are available for fission. Currently, heavy-water reactor technology is being developed in India as a way to use their domestic thorium reserves (*9*). However, the best-known heavy water reactor is the Gen II Canada deuterium uranium (CANDU) design, which uses natural uranium fuel and can be refueled while remaining online (LWRs have to be shut down when fuel is exchanged). The CANDU design (including the proposed Gen III advanced CANDU) is based on individual but linked pressure tubes, rather than the monolithic pressure vessel of LWR reactors. This feature makes the CANDU design more complex, but it requires no very heavy forgings like those needed to construct a PWR or BWR reactor pressure vessel. This is an important consideration now, because there is some concern about the ability of global supply chains to source sufficient quantities of heavy forgings for PWR and BWR systems. The burn-up reached in CANDU reactors is, however, much lower than in LWRs.

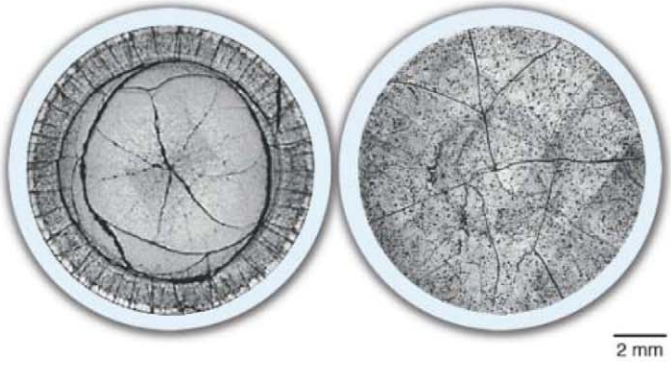


Fig. 2. Polished cross sections of light water reactor fuel pins, showing macroscopic cracks and pores. The material on the left has gone through an experimental high temperature excursion and shows evidence of grain growth (*12*). [Credit: (*12*)]

Burn-up is a crucial economic imperative. Burn-ups in LWRs have been increasing steadily from 20 gigawatt-days per metric ton of uranium (GWd/t) in 1970 to over 50 GWd/t at present (10 GWd/t roughly correspond to 1% of the uranium atoms undergoing fission) (*10*). Further increases in burn-up will require modifications to existing strategies, but to do so more research must be undertaken to satisfy regulators that the fission products are retained safely and securely in the fuel assembly. This will require cladding that maintains its integrity for longer under greater irradiation dose and fuel that can retain the fission products within its crystal lattice for longer. New alloys with better metallographic texture that reduce the (already low) frequency of cladding breach are being developed (*11*), as are fuels with larger grain sizes that may provide longer migration paths for fission products, increasing the times before the fission products can penetrate a breach or chemically attack the cladding (*12*). Nevertheless, the task is one of enormous complexity, given that irradiated fuels contain complex crack patterns, inhomogeneously distributed fission gas bubbles and oxides, and noble metal precipitates (Fig. 2). Advanced modeling techniques can, together with experiment, reveal the chemical processes operating within active fuel and should, in the future, enable more efficient fuel use (*13*).

If uranium prices rise and concerns about future uranium availability increase, then such factors will, in fuel cycles where the fuel is not reprocessed, drive the need for greater efficiency obtained by higher burn-up. Uranium prices are, however, unlikely to be high enough to prompt a resurgence in reprocessing, although key reprocessing competencies should be preserved to keep options open.

Higher burn-up would also reduce the volume of waste, because fewer spent fuel assemblies are generated, or—if reprocessing is used—produce considerably less intermediate-level waste. The total inventory of radiotoxic species is, however, not reduced by the same extent. This is because each kilowatt-hour (kWh) of energy generated requires roughly the same number of fission events, whether that be via low or high burn-up fuel, and gives rise to nearly the same number of fission products.

Beyond 2030

The second phase will be driven mostly by the need to decarbonize electricity supply; however, because developments in nuclear engineering take so long to find their way into nuclear power stations, it is crucial to consider the implications *or* consequences now. In advanced economies, the main challenge will be to decarbonize heating and transport, through either hydrogen fuel or electricity, possibly placing further stress on electricity supply. Furthermore, supply from individual generators—e.g., from wind farms or solar panels—to the electricity system will probably be far more intermittent than it is today. Nuclear power could potentially fill short-term gaps in electricity supply. However, at present, the costs involved in the construction of new nuclear plants do not favor it for an energy gap–filling role, despite the technology's low-carbon credentials (*5*).

The second phase of nuclear technology has the potential to overcome these challenges by moving beyond the electricity generation business. It is well-suited to high-temperature industrial process heat applications (at, for example, 850°C) for the direct thermochemical production of hydrogen as a future vehicle fuel. This latter approach forms part of the Gen IV VHTR (very high temperature reactor) concept (*14*). Competing models for a thermochemical hydrogen economy include hydrogen production via electrolysis or an electricity-only low carbon transport system using battery energy storage. The widespread use of battery cars would help to mitigate volatility in the system caused by the large-scale deployment of intermittent renewable energies and might restore the cost benefits of nuclear energy in the 2030s. Nuclear power could also be widely used for desalination, another efficient way to use surplus power in an electricity system dominated by baseload generation and with fluctuating demand.

In countries that already have a substantial fraction of their power generated via nuclear plant and appropriate grid infrastructure, economic considerations will lead to a demand for power stations with design lifetimes in excess of 70 years, compared with the 40 to 50 years of presently operating plants, and for fuels that can tolerate much higher burn-up. However, these reactors are likely to experience even more extreme temperature and radiation damage conditions than current newly built reactors, especially Gen IV types (*15*, *16*) (which have remaining design work to be done before they can be built even as prototypes). This will dictate a move from designs based largely on permanent, irreplaceable components toward designs allowing almost complete scheduled replacement of parts, some of which may even be recyclable. This approach will alleviate unforeseen materials aging problems and make possible the acceptance of new technology and their associated cost and safety benefits.

Outside established nuclear countries, flexible nuclear technologies will be especially attractive to match supply and demand locally and in real time, reducing the need for grid infrastructures. This may favor small modular nuclear power reactors (*17*). For example, a small ship-borne civil power plant called the Academik Lomonosov is under construction at Sverodvinsk, Russia, which incorporates two KLT-40S reactors (*18*). Another idea that has its origins in naval technology is the fueled-for-life core, that is, a nuclear reactor that never requires refueling. Such a reactor can be delivered as a sealed unit that provides the motive force (probably, but not necessarily, steam from an integrated heat exchanger) to the conventional "island" (the turbine and generator). At the end of its life, which might be as long as 40 years, the reactor is returned to the manufacturer for decommissioning and disposal. Because fuel handling is avoided at the point of electricity generation, the radiation dose to workers would be reduced and monitoring would be much less involved. However, such units will be less efficient than conventional refueled systems, because they would have to work well inside established engineering materials performance parameters to minimize the likelihood of unexpected degradation processes (*3*). These technologies could play an important role in a global roll-out of proliferation-resistant nuclear power technology, because only the country of origin would have access to the spent fuel. The economics of small and fueled-for-life reactors versus large reactors with scheduled replacement will be a constant issue.

Increasingly there will be concern about the long-term sustainability of the nuclear fuel cycle. Nuclear energy will need to move beyond today's conventional "thermal" use of uranium fuel, which is based on a once-through cycle. Alternative technologies may burn thorium, plutonium, and minor actinides or may close the fuel cycle, for example, by reprocessing. Some of these options could sustain power production for more than 1000 years. If it is not possible to make such a transition then, nuclear power development after 2030 could stall once again. Such a scenario would be consistent with a preference expressed by some policy-makers, who take the view that today's Gen III nuclear renaissance is a necessary evil, to be tolerated only until a new, more efficient economy based on renewable energies or fusion can emerge (*19*).

Making the transition requires novel evolutionary fuel designs for high–burn-up Gen III reactors and revolutionary designs for the extreme conditions and higher burn-up anticipated for Gen IV systems. Already, fuels assembled from small (submillimeter) kernels of UO_2 enclosed by concentric shells of pyrolytic graphite and silicon carbide achieve in excess of 19% burn-up of uranium atoms. With their three layers of fuel coating, these are known as TRIstructural ISOtropic, or TRISO, particles (*20*).

The thermal conductivity of fuels must be improved to reduce the temperature gradient across the fuel, thereby keeping the center of the fuel well below its melting point (UO_2 has a poor thermal conductivity). This can be achieved by using either uranium nitride or carbide compounds as fuel or by using a composite. In a composite, a nonfissile second-phase powder, such as MgO or SiC, that has a higher thermal conductivity is mixed with UO_2 powder fuel (*13*).

High-temperature corrosion-resistant fuel cladding materials will be important, for example, silicon carbide fiber—reinforced composite. By providing a high density of damage recombination centers (which can heal radiation damage), nanostructures could well play a role in providing materials with greater radiation tolerance (*21*), especially for areas in the reactor core that receive very high radiation flux. Nanostructure offers other advantages; for example, oxide dispersion steels containing yttrium oxide nanoparticles have superior creep resistance and are being considered as future reactor pressure vessel materials (*22*).

We suggest six possible complementary routes to adopting sustainable nuclear energy.

Option 1: Unconventional Uranium

As mined uranium resources are depleted, prices are expected to rise, but there are abundant resources of unconventional uranium, such as uranium phosphates and uranium in sea water (*23*). At present, extracting such uranium is uneconomic, and only tiny quantities of seawater uranium have been extracted. In such a scenario, it is likely that

Issues Beyond 2030

Fuel availability. A widespread global first wave expansion and its growing demand for uranium resources will by 2060 have made today's once-through uranium fuel cycle increasingly unsustainable. Rising uranium prices will prompt renewed interest in nuclear fuel reprocessing, innovative fuel cycles, or gaining uranium from unconventional sources. It may even become desirable to recycle earlier generations of spent LWR fuel held in long-term storage.

Life extension. This will be needed by 2060 for Gen III reactors built in the immediate time frame.

Design of future plants. Plants must be designed to enable a later three-way choice between life extension, reactor replacement, and full power station decommission and rebuild. The capacity of waste repositories for decommissioning waste in the second half of the century will become a factor.

New degradation mechanisms. They will be discovered for materials that were necessary to facilitate a plant with much longer life than was the hitherto the case.

Regulation and inspection. Both national and international regulators will experience greater demands, in part because of requirements for different reactor types, aging fleet, and repository build and management.

Public acceptance. A major nuclear expansion is very likely to require green-field developments in places with little or no nuclear heritage. This could be a major difficulty regarding public acceptance. It will be necessary for waste repositories to be under construction, not just being planned.

Skills. The young engineers of the 2030s are currently in preschool. We are likely to face a second wave of skills difficulties in the future unless we act now to ensure that science and engineering subjects grow in popularity within the school system.

unconventional uranium will yield a price cap to conventional nuclear fuel. That maximum price is likely, however, to be prohibitively high, and other options may be more attractive.

Option 2: Reprocessing Spent Fuel for Multiple Mixed U-Pu Oxide Fuel Recycle

This potentially long-lived fuel cycle has been developed over many decades in several countries (especially France, United Kingdom, and Russia). It involves the chemical separation of plutonium, in order to fabricate fuel from mixed U-Pu oxide powders (MOX) (*24*). However, because Pu separation is a proliferation-sensitive technology, MOX fuel fabrication is likely to be restricted to the nuclear weapons states, although perhaps with increasing international access to such fuels via appropriate global agreements.

Option 3: Critical Fast Reactors

These reactors are more compact and have much higher energy density than today's nuclear power systems. Consequently the rate at which the neutron density or temperature can change in the event of an accident is faster and therefore a greater engineering challenge. As such, critical fast reactors raise safety and reliability issues beyond those typical of today's nuclear power plants, especially in the event of a loss-of-coolant accident. Also, because of the greater potential for production of fissile material ("breeding"), such technologies raise security concerns. A substantial advantage is that both ^{235}U and ^{238}U isotopes undergo fission in these reactors, thereby using a much greater proportion of the uranium.

Option 4: Thorium Fuel Cycle

Thorium has the potential to become an important nuclear fuel. It is not fissile itself, but in a reactor, thorium-232 can capture neutrons to yield fissile uranium-233. The thorium fuel cycle can then proceed by either (i) fabricating fuel pellets that contain a mix of thorium-232 and a fissile element (such as uranium-233), (ii) placing a blanket of thorium fuel around a reactor core containing fissile material, or (iii) injecting extra neutrons from a particle accelerator (see option 5). Thorium is several times more abundant than uranium, and a thorium fuel cycle can be developed that produces negligible amounts of plutonium and fewer long-lived minor actinides than a uranium cycle. However, fissile uranium-233 is difficult to extract and handle, because it is produced together with other highly radioactive uranium isotopes, and the performance of thorium fuels is not well understood. The proliferation resistance credentials of the thorium fuel cycle deserve greater scrutiny but appear promising.

Option 5: Accelerator-Driven Subcritical Reactors

Despite their complexity, accelerator-driven subcritical reactors (ADSRs) have potentially useful advantages over conventional critical reactor systems. ADSRs can, in principle, produce thorium-fueled nuclear energy, avoiding the need for fissile materials supplied from other sources. In addition, ADSRs show promise for waste treatment. The process of nuclear transmutation using an ADSR has the potential to reduce quantities of long-lived and highly toxic radioactive wastes quite substantially (*25*). Lastly, ADSRs offer improved safety and fuel utilization compared with other sustainable second-phase nuclear options.

Option 6: Nuclear Fusion Energy

Nuclear fusion could provide clean energy with enhanced intrinsic safety and abundant fuel resources. However, the technology has not been demonstrated at industrial scale and reliability. Furthermore, it relies on helium coolants (a co-product of nonrenewable natural gas), although various measures such as cooling with liquid hydrogen have been suggested (*26*, *27*). Fusion is unlikely to move toward commercialization until after 2050. Furthermore, the many commonalities between fusion and fission research—high temperature materials for high radiation environments, fast neutron physics, structural integrity issues—favor a collaborative approach between the fusion and fission communities. Fusion-fission hybrids and fusion-driven fission fuel breeders (*28*, *29*) have been suggested as a route to early commercialization of fusion energy.

Outlook

Nuclear technology is at a crossroads. The community has been tested in recent years as it gears up to renew existing facilities in Europe and North America while continuing or initiating an expansion in other regions. It seems ever more likely that a second larger phase of nuclear development will be required beyond the 2030s to ensure a low-carbon energy future that makes maximal efficient use of nuclear plants and resources. Energy and research policy decisions made now will determine whether we have the capacity to design and develop innovative new systems that contribute to sustainable flexible nuclear energy generation.

Although we are developing other energy generating systems and it is possible that a second larger phase of nuclear development will not be required, it would be unwise at this stage to assume that nuclear energy will not be needed. If we are to generate that option for policy-makers and the energy industries of the 2030s, we must act now.

References and Notes

1. World Nuclear Power Reactors Uranium Requirements, www.world-nuclear.org/info/reactors.html.
2. Cabinet Office, *The Road to 2010: Addressing the Nuclear Question in the Twenty First Century* (publication Cm 7675, Stationery Office, Norwich, UK, 2010).
3. R. W. Grimes, R. J. Konings, L. M. Edwards, *Nat. Mater.* **7**, 683 (2008).
4. Since the U.S. Department of Energy (DOE) launched the Generation IV initiative in 2000, the following has become a commonly used, though somewhat imprecise, terminology: Gen I, prototype power reactors and first designs connected to the grid; Gen II, current operating reactors (from 1970 to 2010); Gen III, designs about to be deployed; Gen IV, new reactor systems that will be available only after ~2030.
5. L. Pouret, N. Buttery, W. J. Nuttall, *Nucl. Future* **5**, 333 (2009).
6. R. R. Fulwood, *Probabilistic Safety Assessment in the Chemical and Nuclear Industries* (Butterworth Heinemann, Woburn, MA, 1999).
7. D. Mosey, *Reactor Accidents* (Nuclear Engineering International Special Publications, Sidcup, UK, ed. 2, 2006), pp. 69–88.
8. International Atomic Energy Agency, "Operating experience with nuclear power stations in member states 2008," International Atomic Energy Agency, STI/PUB/1421 (2009).
9. R. K. Sinha, A. Kakodar, *Nucl. Eng. Des.* **236**, 683 (2006).
10. International Atomic Energy Agency, "Nuclear technology review 2007," International Atomic Energy Agency (2007), pp. 101–103.
11. *Zirconium in the Nuclear Industry: 15th International Symposium* (American Society for Testing and Materials special technical publications, West Conshohocken, PA, 2009), vol. 1505.
12. J. Arborelius *et al.*, *J. Nucl. Mater.* **43**, 967 (2006).
13. "Basic research needs for advanced nuclear energy systems," Report of the Basic Energy Sciences Workshop, Office of Basic Energy Sciences, DOE, 2006.
14. X. Vitart, A. Le Duigou, P. Carles, *Energy Convers. Manage.* **47**, 2740 (2006).
15. T. Abram, S. Ion, *Energy Policy* **36**, 4323 (2008).
16. U.S. DOE Nuclear Energy Research Advisory Committee and the Generation IV International Forum, "*A Technology Roadmap for Generation IV Nuclear Energy Systems*" (2002).
17. DOE Office of Nuclear Energy Factsheet, "Small modular reactors" (2010), available at http://nuclear.energy.gov/pdfFiles/factSheets/2011_SMR_Factsheet.pdf.
18. Y. E. Gorlinskii *et al.*, *At. Energy* **107**, 122 (2009).
19. K. Bickerstaff, I. Lorenzoni, N. F. Pidgeon, W. Poortinga, P. Simmons, *Public Underst. Sci.* **17**, 145 (2008).
20. For more details, see papers in *Proceedings of the 4th International Topical Meeting on High Temperature Reactor Technology* (American Society of Mechanical Engineers, New York, 2009), vol. 1.
21. A. Misra *et al.*, *MRS Symp. Proc.* **1188**, 167 (2009).
22. G. R. Odette, M. J. Alinger, B. D. Wirth, *Annu. Rev. Mater. Res.* **38**, 471 (2008).
23. International Atomic Energy Agency, "Analysis of uranium supply to 2050," International Atomic Energy Agency, STI/PUB/1104 (2001), pp. 64–68.
24. P. D. Wilson, *The Nuclear Fuel Cycle, from Ore to Waste* (Oxford Univ. Press, Oxford, 1996).
25. W. J. Nuttall, J. S. Ireland, J. S. Al-Khalili, W. Gelletly, *Int. J. Crit Infrastruct.* **1**, 380 (2005).
26. W. J. Nuttall, B. A. Glowacki, R. Clarke, *The Engineer* 31 October 2005, p. 16.
27. Z. Cai, R. H. Clarke, B. A. Glowacki, W. J. Nuttall, N. Ward, *Resour. Policy* **35**, 77 (2010).
28. W. Manheimer, *J. Fusion Energ.* **23**, 223 (2004).
29. W. Manheimer, *J. Fusion Energ.* **20**, 131 (2001).
30. World Nuclear Association, www.world-nuclear.org/info/inf08.html.

31. We thank A. Becker and M. Rushton for assistance with the preparation of this paper. A. Becker has considered long-term scenarios for a UK nuclear renaissance (Fig. 1 of this work is inspired by his ideas, and we thank him for permission to use it here). Becker's work is soon to be published in a book from Purdue University Press titled *Energy and Innovation: Structural Change and Policy Implications.* W.N. acknowledges assistance from the ESRC Electricity Policy Research Group.

10.1126/science.1188928

The Kamil Crater in Egypt

Luigi Folco,[1]* Mario Di Martino,[2] Ahmed El Barkooky,[3] Massimo D'Orazio,[4] Ahmed Lethy,[5] Stefano Urbini,[6] Iacopo Nicolosi,[6] Mahfooz Hafez,[5] Carole Cordier,[1] Matthias van Ginneken,[1] Antonio Zeoli,[1] Ali M. Radwan,[5] Sami El Khrepy,[5] Mohamed El Gabry,[5] Mahomoud Gomaa,[5] Aly A. Barakat,[7] Romano Serra,[8] Mohamed El Sharkawi[3]

Impact craters up to a few hundreds of meters in diameter are common structures of solid surfaces of planetary bodies in the solar system. Statistics predict that impacts producing small craters on Earth occur on decadal to secular time scales (*1*, *2*). However, small craters are rare on Earth because they are rapidly eroded, and the few identified so far [15 <300 m in diameter out of 176 craters up to 300 km in diameter (*3*)] have lost most of their primary features.

We report the detection in southern Egypt of a rayed impact crater 45 m in diameter (Fig. 1A) on a Cretaceous sandstone target. The ejecta rays highlight the exceptional freshness of the structure. The crater was identified by V. De Michele during a Google Earth survey and named Kamil Crater after nearby Gebel Kamil. A geophysical expedition undertaken [supporting online material (SOM)] in February 2010 revealed that the crater is bowl shaped and has an upraised rim (~3 m above preimpact surface) (figs. S1 and S2) typical of simple craters (*4*). The true crater floor depth is 16 m and is overlain by ~6-m-thick crater-fill material (fig. S2). Morphometric parameters agree with those predicted by models (*5*) for a transient crater generated by an iron meteorite 1.3 m in diameter (equivalent to 9.1×10^3 kg) impacting at a velocity of 3.5 km s^{-1}, assuming an average meteoroid entry velocity and entry angle of 18 km s^{-1} and 45°, respectively. Centimeter-scale masses of scoriaceous impact melt glass (fig. S3) occur in and close to the crater and indicate local shock pressures >60 GPa (*4*). We identified 5178 iron meteorite specimens totaling ~1.71 tons in the crater and surrounding area during systematic searches (SOM). They consist of <34-kg shrapnel produced by the explosion of the impactor upon hypervelocity collision with the target (Fig. 1B), except one individual fragment of 83 kg (fig. S4). This evidence indicates that the Kamil Crater was generated by an impactor that landed nearly intact without substantial fragmentation in the atmosphere. The meteorite is classified as an ungrouped Ni-rich ataxite [Ni = 19.8 weight % (wt %), Co = 0.75 wt %, Ga = 49.5 μg g^{-1}, Ge = 121 μg g^{-1}, Ir = 0.39 μg g^{-1}; data following (*6*); fig. S5]. Magnetic anomaly data show no evidence of buried meteorites larger than some tens of centimeters (fig. S1).

On the basis of systematic meteorite searches, the estimated total mass of the impactor is of the order of 5×10^3 to 10×10^3 kg, corresponding to a preatmospheric mass of ~20×10^3 to 40×10^3 kg (*2*). According to geophysical models (*2*, *7*), iron masses <3×10^6 kg normally fragment upon impact with Earth's atmosphere, thereby reducing the energy of the impact at Earth's surface. However, the present statistics, which include the recently discovered Whitecourt Crater (*8*) and the Kamil Crater, suggest that ~35% of the iron meteorites in the above mass range are not disrupted in the atmosphere.

References and Notes

1. P. A. Brown, R. E. Spalding, D. O. ReVelle, E. Tagliaferri, S. P. Worden, *Nature* **420**, 294 (2002).
2. P. A. Bland, N. A. Artemieva, *Meteorit. Planet. Sci.* **41**, 607 (2006).
3. Earth Impact Database, www.unb.ca/passc/ImpactDatabase.
4. H. J. Melosh, *Impact Cratering: A Geologic Process*, Oxford Monographs on Geology and Geophysics (Oxford Univ. Press, Oxford, 1989).
5. G. S. Collins, H. J. Melosh, R. A. Marcus, *Meteorit. Planet. Sci.* **40**, 817 (2005).
6. M. D'Orazio, L. Folco, *Geostand. Newsl.* **27**, 215 (2003).
7. P. A. Bland, N. A. Artemieva, *Nature* **424**, 288 (2003).
8. C. D. K. Herd *et al.*, *Geology* **36**, 955 (2008).
9. Work carried out within the "2009 Egyptian-Italian Year of Science and Technology" framework. T. Hussein and F. Porcelli provided diplomatic support; the Egyptian Army, logistical support; G. Negro, field assistance; F. Speranza and P. Rochette, helpful discussion; the European Commission (Marie Curie Actions–RTNs ORIGINS project), Fondazione Cassa di Risparmio di Torino, Banca Monte dei Paschi di Siena S.p.A., and Telespazio S.p.A. (in the European Space Agency–Space Situational Awareness program framework), financial support.

Supporting Online Material

www.sciencemag.org/cgi/content/full/science.1190990/DC1
Materials and Methods
Figs. S1 to S5

15 April 2010; accepted 29 June 2010
Published online 22 July 2010;
10.1126/science.1190990
Include this information when citing this paper.

[1]Museo Nazionale dell'Antartide Università di Siena, Via Laterina 8, 53100 Siena, Italy. [2]Istituto Nazionale di Astrofisica, Osservatorio Astronomico di Torino, 10025 Pino Torinese, Italy. [3]Department of Geology, Faculty of Sciences, Cairo University, Giza, Egypt. [4]Dipartimento di Scienze della Terra, Università di Pisa, Via S. Maria 53, 56126 Pisa, Italy. [5]National Research Institute of Astronomy and Geophysics, Helwan, Egypt. [6]Istituto Nazionale di Geofisica e Vulcanologia, Via di Vigna Murata 605, 00143 Roma, Italy. [7]Egyptian Mineral Resources Authority, 3 Salah Salem Road, Abassiya, Cairo, Egypt. [8]Dipartimento di Fisica, Università di Bologna, Via Irnerio 46, 40126 Bologna, Italy.

*To whom correspondence should be addressed. E-mail: folco@unisi.it

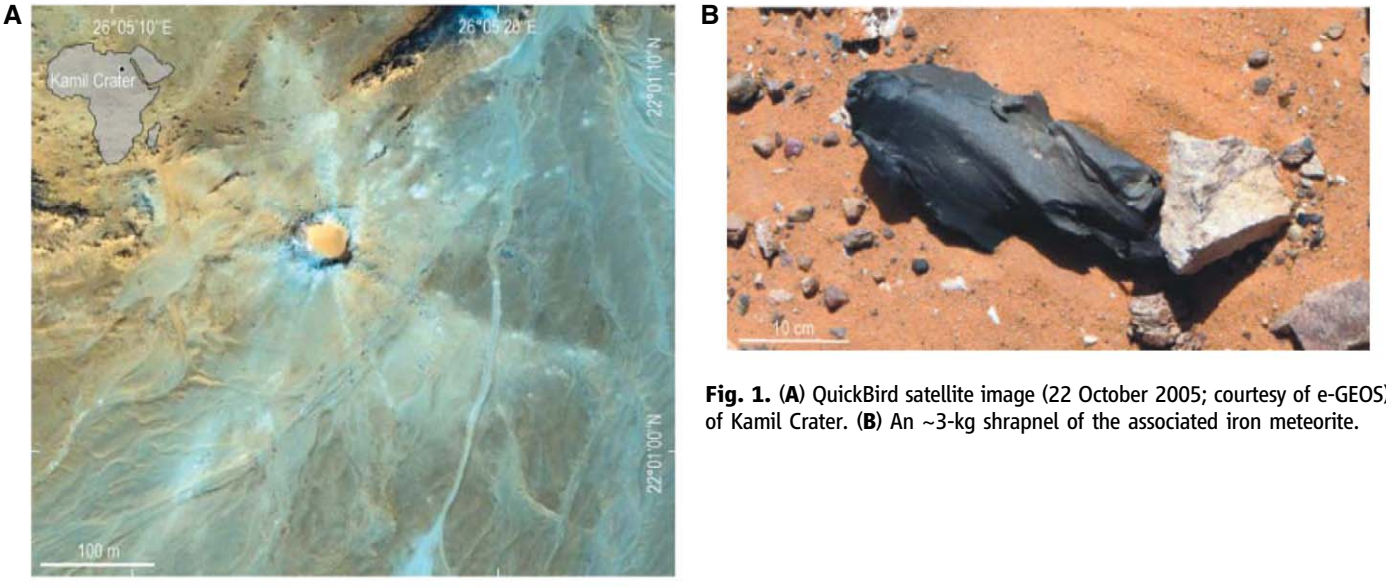


Fig. 1. (**A**) QuickBird satellite image (22 October 2005; courtesy of e-GEOS) of Kamil Crater. (**B**) An ~3-kg shrapnel of the associated iron meteorite.

Peripheral Protein Quality Control Removes Unfolded CFTR from the Plasma Membrane

Tsukasa Okiyoneda,[1] Hervé Barrière,[1] Miklós Bagdány,[1] Wael M. Rabeh,[1] Kai Du,[1] Jörg Höhfeld,[2] Jason C. Young,[3] Gergely L. Lukacs[1]*

Therapeutic efforts to restore biosynthetic processing of the cystic fibrosis transmembrane conductance regulator lacking the F508 residue (ΔF508CFTR) are hampered by ubiquitin-dependent lysosomal degradation of nonnative, rescued ΔF508CFTR from the plasma membrane. Here, functional small interfering RNA screens revealed the contribution of chaperones, cochaperones, and ubiquitin-conjugating and -ligating enzymes to the elimination of unfolded CFTR from the cell surface, as part of a peripheral protein quality-control system. Ubiquitination of nonnative CFTR was required for efficient internalization and lysosomal degradation. This peripheral protein quality-control mechanism probably participates in the preservation of cellular homeostasis by degrading damaged plasma membrane proteins that have escaped from the endoplasmic reticulum quality control or are generated by environmental stresses in situ.

Aberrant polypeptides are generated as a consequence of errors in transcription, translation, and folding, as well as genetic mutations or environmental stress (*1*–*3*). To preserve proteostasis, quality-control (QC) mechanisms have evolved to facilitate folding and elimination of terminally misfolded polypeptides (*3*, *4*). At the endoplasmic reticulum (ER), nonnative membrane proteins are ubiquitinated and retrotranslocated into the cytoplasm to be destroyed by the ubiquitin (Ub) proteasome system (UPS), as part of ER-associated degradation (ERAD). By contrast, nonnative membrane proteins that have escaped the ER or are generated in post-ER compartments are preferentially eliminated by lysosomal degradation (*5*–*7*). The molecular machinery of the peripheral QC responsible for recognition and degradation of nonnative proteins at plasma membrane (PM) remains unknown (*1*, *8*–*10*).

Deletion of the F508 residue (ΔF508), the most prevalent mutation in the cystic fibrosis transmembrane conductance regulator (CFTR), causes a temperature-sensitive folding defect and ERAD of immature, core-glycosylated ΔF508CFTR by

[1]Department of Physiology and Groupe de Recherche Axé sur la Structure des Protéine (GRASP), McGill University, Montreal, Quebec H3G 1Y6, Canada. [2]Cell Biology Institute, University Bonn, D-53121 Bonn, Germany. [3]Department of Biochemistry and Groupe de Recherche Axé sur la Structure des Protéine (GRASP), McGill University, Montreal, Quebec H3G 1Y6, Canada.

*To whom correspondence should be addressed. E-mail: gergely.lukacs@mcgill.ca

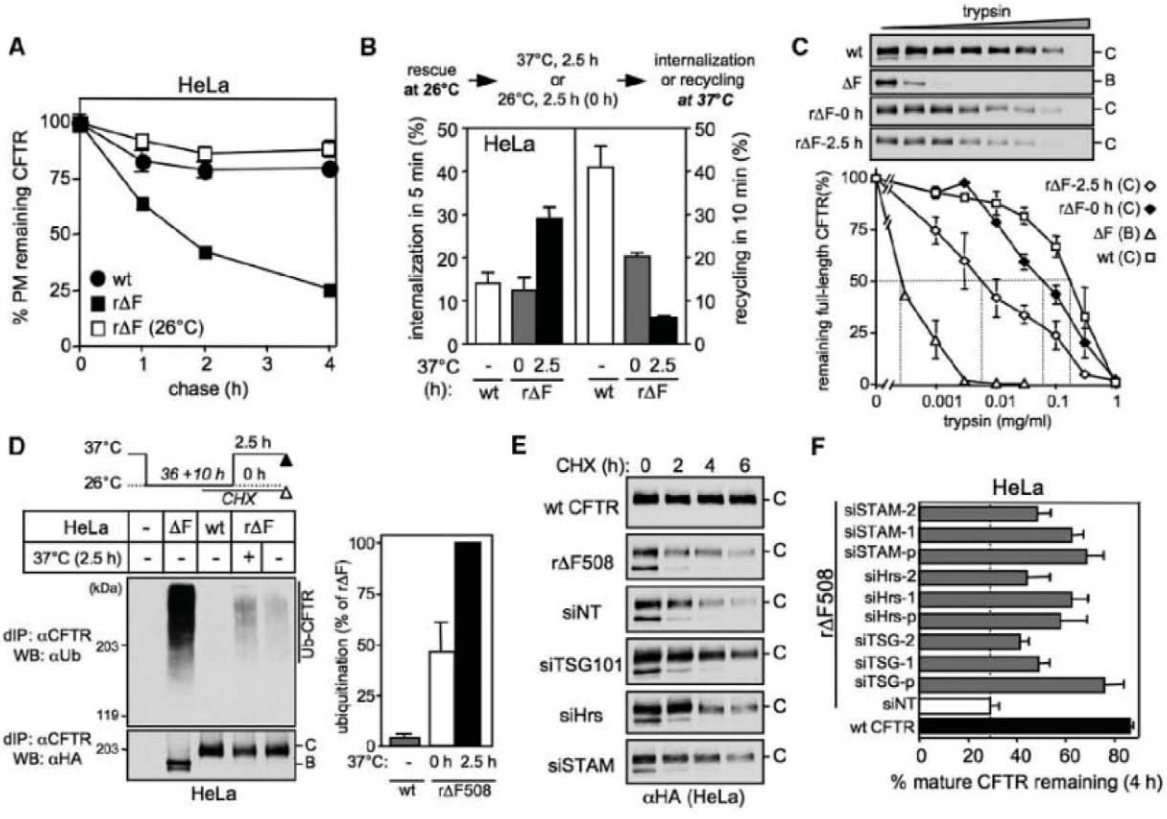


Fig. 1. Conformationally destabilized rΔF508CFTR is ubiquitinated and targeted for ESCRT-dependent degradation. (**A**) CFTR PM stability was determined by enzyme-linked immunosorbent assay (ELISA). ΔF508CFTR was rescued at 26°C for 36 hours, followed by 37°C incubation for 2.5 hours (rΔF) or at 26°C. (**B**) (Left) CFTR internalization and (right) endocytic recycling were measured by ELISA. Unfolding of rΔF508CFTR was accomplished at 37°C (2.5 hours). (**C**) Trypsin susceptibility of CFTR variants in microsomes was measured by quantifying the remaining full-length CFTR with immunoblotting and densitometry. Bands B and C indicate core- and complex-glycosylated CFTR, respectively. (**D**) rΔF508CFTR ubiquitination in post-Golgi compartments was measured by d-IP and normalized for CFTR in precipitates. Nonrescued ΔF508CFTR (ΔF) was used as a positive control. (**E** and **F**) Metabolic stability of rΔF508CFTR was measured by CHX chase at 37°C and immunoblotting with an antibody against HA in ESCRT KD HeLa cells (E). Remaining complex-glycosylated CFTR was quantified by densitometry and expressed as a percentage of the initial amount (F). SMARTpool (p) or single siRNA (1 and 2) were used. siNT; nontargeted siRNA.

the concerted action of chaperones, cochaperones, and E2 Ub-conjugating and E3 Ub-ligating enzymes [carboxyl-terminus heat shock cognate 70 (Hsc70)–interacting protein (CHIP), glycoprotein gp78, and Rma1] (*11*–*14*). Although inhibition of individual E3-ligases failed to restore biosynthetic processing, low temperature (26°C) and small-molecule correctors alone, or in combination with the ablation of E3 ligases, fosters PM accumulation of functional, complex-glycosylated ΔF508CFTR (*15*–*18*). The rescued (r)ΔF508CFTR, however, is metabolically unstable and is rapidly eliminated at 37°C, which hampers therapeutic efforts to restore the PM chloride conductance (*5*, *18*). Mutant CFTR instability was attributed to unfolding and subsequent ubiquitination, internalization, and lysosomal degradation (*5*, *6*).

rΔF508CFTR as a probe of peripheral QC. To identify the rΔF508CFTR ubiquitination mechanism, we generated CFTR-3HA–expressing HeLa and IB3 (bronchial respiratory epithelia) cell lines amenable to small interfering RNA (siRNA) functional screens (*19*). The extracellular hemagglutinin tag (3HA-tag) enabled selective detection of CFTR (*5*). The wild-type (wt) protein was largely complex-glycosylated and localized to PM, whereas ΔF508CFTR was expressed as a core-glycosylated form and retained in the ER at 37°C (fig. S1, A to C). Rescuing the folding defect at 26°C (*15*) partially restored biosynthetic processing and expression of complex-glycosylated ΔF508CFTR at post-Golgi compartments and PM (fig. S1, A to C). Then, rΔF508CFTR was eliminated by accelerated internalization and attenuated recycling at 37°C (Fig. 1, A and B, and fig. S1, D to F) as expected (*5*).

A temperature-sensitive conformational defect of rΔF508CFTR was demonstrated by its protease susceptibility in isolated microsomes from BHK cells (*20*). Newly synthesized core-glycosylated channels were cleared from ER by cycloheximide (CHX) chase (~10 hours) at 26°C to avoid unfolding of complex-glycosylated rΔF508CFTR (fig. S1G). The trypsin susceptibility of rΔF508CFTR was increased 5- to 10-fold after unfolding at 37°C (2.5 hours) before microsome isolation (Fig. 1C). Mature wt CFTR and immature ΔF508CFTR had substantially lower and higher trypsin susceptibility, respectively, than rΔF508CFTR (Fig. 1C), as expected (*21*).

Denaturing immunoprecipitation (d-IP) and anti-Ub immunoblotting revealed a twofold increased ubiquitination of complex-glycosylated rΔF508CFTR after thermal unfolding (Fig. 1D). In the absence of unfolding, rΔF508CFTR PM stability, internalization, endocytic recycling, and ubiquitination level approached the wt phenotype (Fig. 1, A to D). In contrast, temperature dependence of the CD4Tl-Ub chimera PM instability (*22*) (fig. S1H), ubiquitination of cellular proteins, and Ub-ligase activity of CHIP (see below) were negligible (fig. S2, A to C). These observations are in line with the notion that conformational destabilization accounts for augmented rΔF508CFTR ubiquitination and fast PM turnover at 37°C. Indeed, dramatically augmented trypsin susceptibility of ΔF508CFTR paralleled its ~100-fold increased ubiquitination at ER as compared with wt CFTR (Fig. 1, C and D). Thus, CFTR's propensity for ubiquitination is enhanced with its conformational destabilization, not only at ER, but also in post-Golgi compartments, and rΔF508CFTR is a suitable model to investigate the conformation-based QC at PM.

Supporting the function of ubiquitination in CFTR lysosomal degradation, ablation or knockdown (KD) of Hrs, STAM, or TSG101 Ub-binding constituents of the endosomal sorting complex required for transport (ESCRT) using individual or SMARTpool siRNA; (*5*, *6*) metabolically stabilized rΔF508CFTR in HeLa cells (Fig. 1, E and

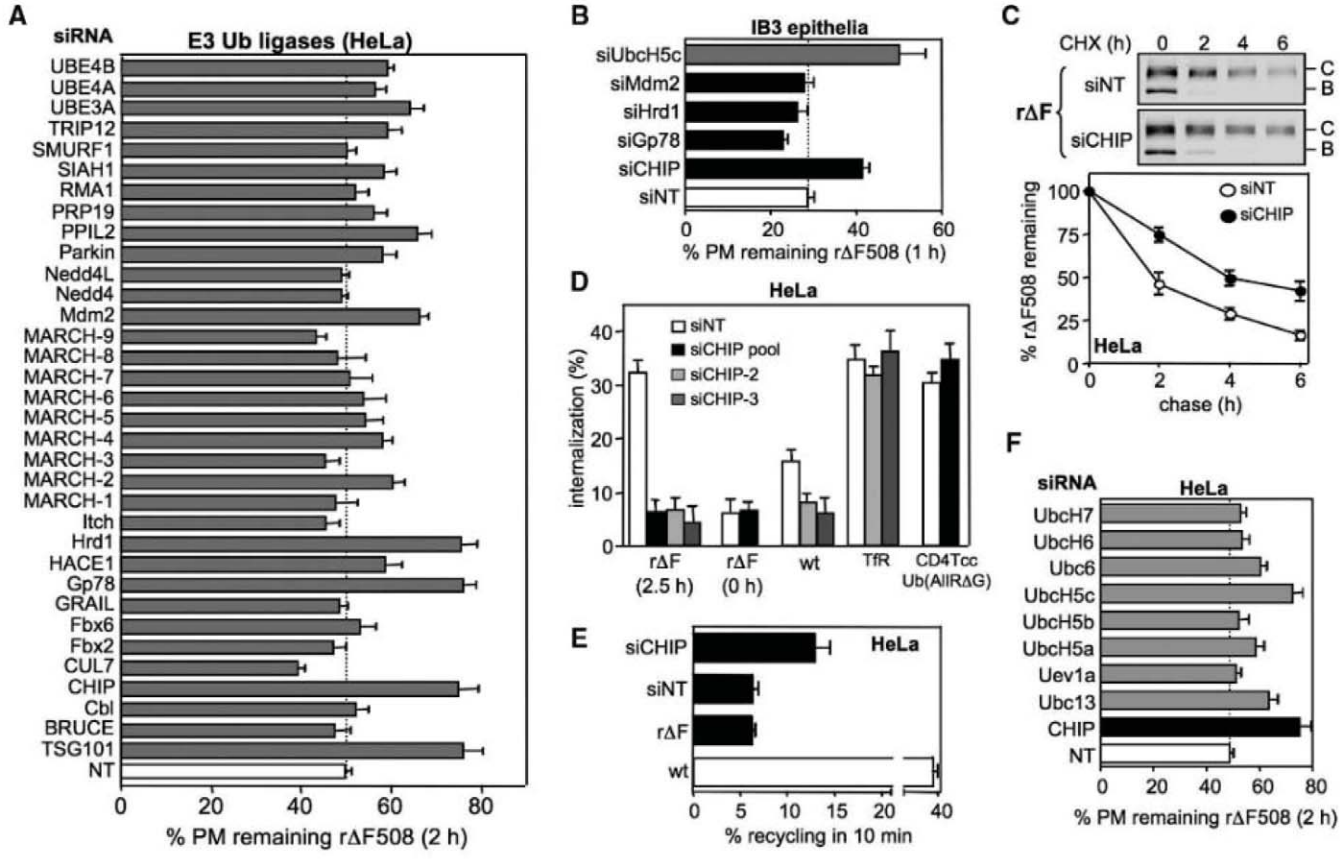


Fig. 2. CHIP mediates rΔF508CFTR elimination from PM. (**A**) Functional siRNA screen to identify Ub ligases responsible for rΔF508CFTR elimination from PM in HeLa cells. Ub ligases were knocked down by 50 nM SMARTpool siRNA, and rΔF508CFTR PM stability was measured at 37°C by ELISA. TSG101 siRNA; positive control. Data are means ± SEM from two or three independent quadruplicate experiments. (**B**) Effect of Ub ligase or UbcH5c KD on rΔF508CFTR PM stability in IB3 cells. (**C**) rΔF508CFTR metabolic stability in post-Golgi compartments was measured by immunoblotting with CHX chase upon CHIP KD by SMARTpool siRNA. Remaining complex-glycosylated CFTR was plotted. (**D**) Internalization of CFTRs (5 min), TfR (5 min), and CD4Tcc-Ub(AllRΔG) (2.5 min) were measured at 37°C in CHIP-KD cells. (**E**) CHIP KD enhanced rΔF508CFTR endocytic recycling. (**F**) rΔF508CFTR PM stability in E2-KD cells was measured as in (**A**).

F and fig. S3, A to C). This could be attributed to impeded lysosomal delivery, monitored by lumenal acidification extent, and rate of endocytic vesicles containing fluorescein isothiocyanate–labeled rΔF508CFTR (fig. S3, D to F). Lysosomal targeting of Lamp1 from PM was not influenced by the ESCRT KD (fig. S3E).

CHIP-dependent ubiquitination removes unfolded CFTR from PM. To identify the ubiquitination machinery of rΔF508CFTR, 33 E3 ligases involved in down-regulation of PM receptors (*8*, *10*, *23*) and CFTR ERAD (*12*, *13*, *24*) were depleted (knocked down) using SMARTpool siRNA, followed by determination of rΔF508CFTR PM stability in HeLa cells. CHIP, gp78, or Hrd1 depletion inhibited the rΔF508CFTR disposal by ~50% (Fig. 2A). Because only the CHIP effect could be confirmed in IB3 cells (Fig. 2B), subsequent experiments focused on CHIP. Individual CHIP siRNA also impeded complex-glycosylated and PM rΔF508CFTR degradation (Fig. 2C and fig. S4, A and B).

Internalization of unfolded rΔF508CFTR was diminished by ~80% upon CHIP KD without affecting transferrin receptor (TfR) and CD4Tcc-Ub (AllRΔG) chimera uptake, signaled by tyrosine- and tetrameric Ub-based endocytic motifs, respectively (Fig. 2D) (*22*). CHIP KD had a marginal effect on slow endocytosis of rΔF508CFTR in the absence of thermal unfolding and wt CFTR (Fig. 2D). CHIP KD also partially restored rΔF508CFTR endocytic recycling (Fig. 2E) and delayed the lysosomal delivery from early endosomes (pH

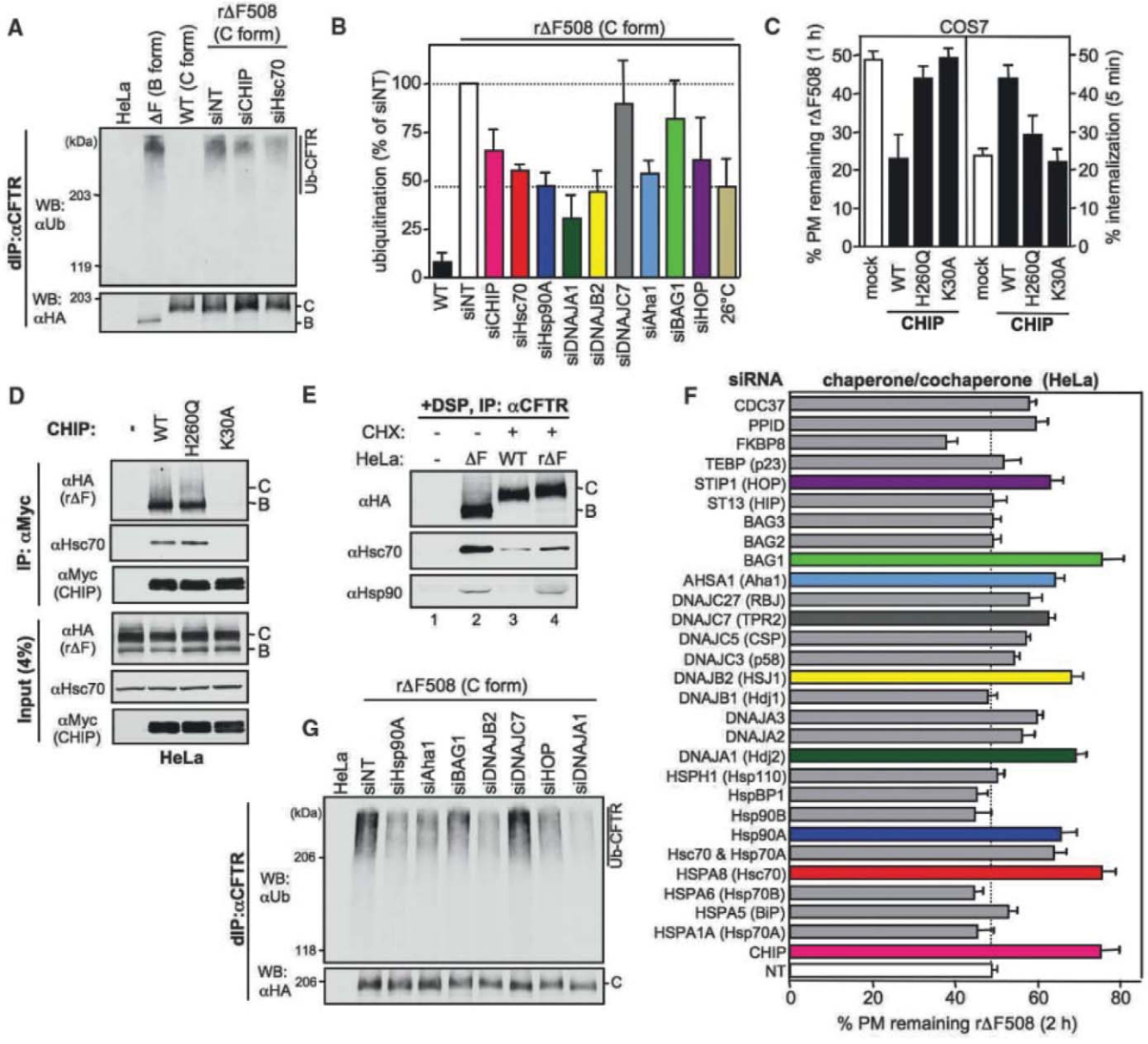


Fig. 3. rΔF508CFTR ubiquitination is regulated by chaperones and cochaperones. (**A**) rΔF508CFTR ubiquitination in post-Golgi compartments was measured in SMARTpool siRNA-transfected HeLa cells as in Fig. 1D. (**B**) Quantification of CFTR ubiquitination in immunoblots (A) and (G). Signal was normalized for CFTR in precipitates and expressed as percentages of rΔF508CFTR ubiquitination in siNT-treated cells after unfolding (37°C, 2.5 hours) as in Fig. 1D. (**C**) (Left) PM stability and (right) internalization of rΔF508CFTR were measured by ELISA in COS7 cells coexpressing myc-CHIP variants. (**D**) CHIP interacts with core- and complex-glycosylated rΔF508CFTR in HeLa cells transfected with myc-CHIP variants. (**E**) Interaction of chaperones with complex-glycosylated rΔF508CFTR was shown by co-IP in HeLa cells after in vivo cross-linking by 0.1 mM dithiobis[succinimidyl propionate] (DSP). Core-glycosylated wt and rΔF508CFTR were minimized by CHX chase (lanes 3 and 4). (**F**) rΔF508CFTR PM stability was evaluated upon KD of chaperone or cochaperone by SMARTpool siRNA as in Fig. 2A. Data are means ± SEM from two or three independent quadruplicate experiments. (**G**) rΔF508CFTR ubiquitination in post-Golgi compartments was measured in SMARTpool siRNA-transfected HeLa cells as in (A).

~6.2) without interfering with Lamp2/CD63 lysosomal targeting and TfR recycling (fig. S4, C to E). In support of the CHIP involvement, ablating UbcH5c, a cognate E2 enzyme of CHIP, impeded the rΔF508CFTR removal from PM in IB3 and HeLa cells (Fig. 2, B and F). CHIP KD also reduced ubiquitination of complex-glycosylated rΔF508CFTR at 37°C to that at 26°C (Fig. 3, A and B), accounting for the attenuated internalization, facilitated recycling, and impeded lysosomal delivery of the unfolded CFTR.

Hsc70 recognizes unfolded CFTR at PM. In support of the CHIP loss-of-function phenotype, overexpression of CHIP wt but not the catalytically inactive CHIP-H260Q [in which His^{260} is replaced by Gln (*25*)] reduced rΔF508CFTR expression and metabolic stability by accelerating endocytosis in cotransfected COS7 cells (Fig. 3C and fig. S4F). Coimmunoprecipitation (co-IP) confirmed CHIP association with the core-glycosylated form (*12*) and revealed that CHIP physically interacted with complex-glycosylated rΔF508CFTR at 37°C (Fig. 3D). Weaker CHIP binding, attributable to a milder structural defect of complex-glycosylated rΔF508CFTR compared with core-glycosylated ΔF508CFTR (Fig. 1C), was stabilized by the CHIP-H260Q mutation, presumably by delaying CFTR dissociation (Fig. 3D). Abolishing Hsc70 and heat shock protein 90 (Hsp90) binding to the CHIP tetratricopeptide repeat (TPR) domain by a K30A mutation (replacement of Lys^{30} with Ala) (*26*) prevented channel down-regulation from PM (Fig. 3C and fig. S4F)

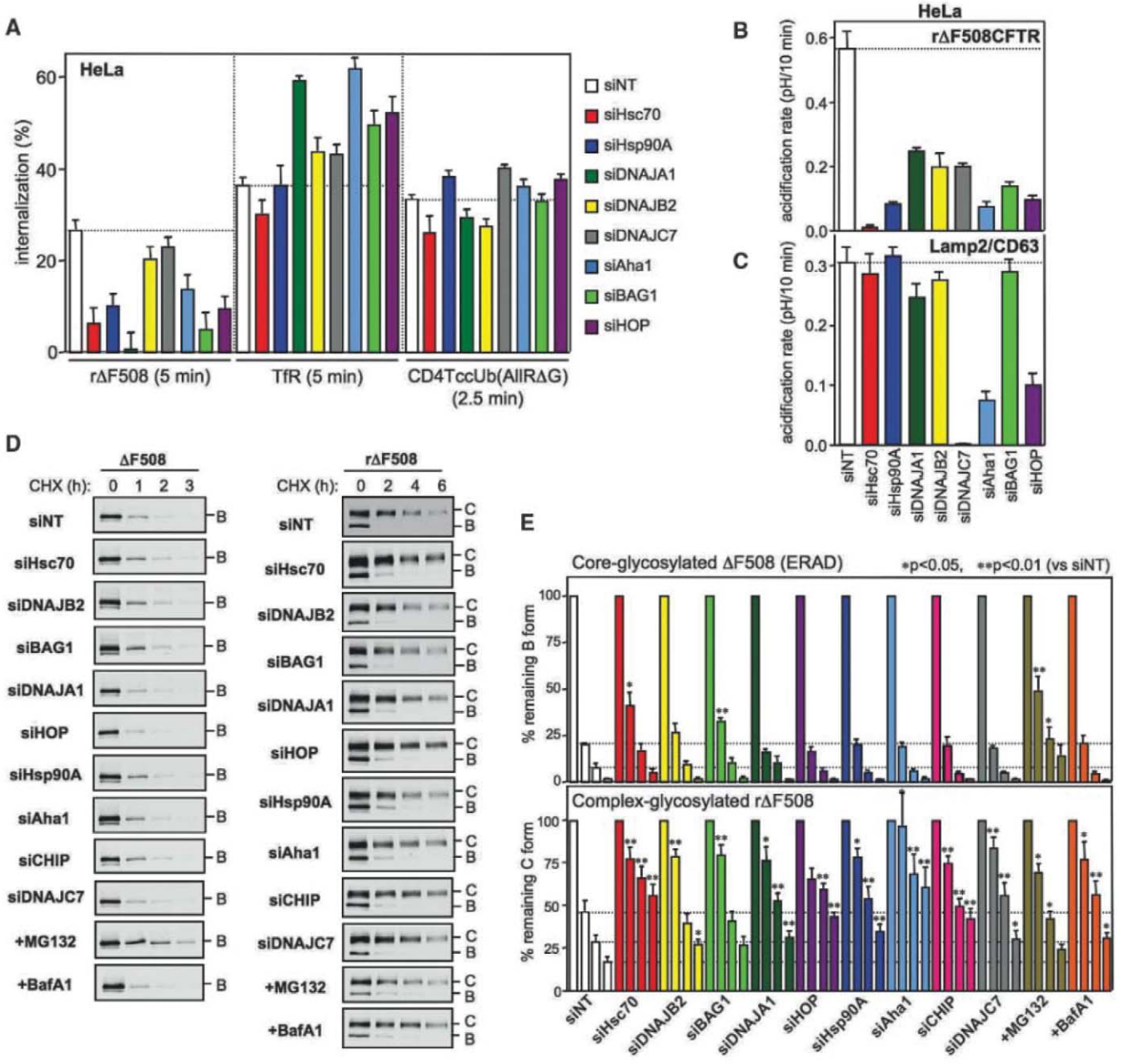


Fig. 4. Internalization and lysosomal targeting of rΔF508CFTR are regulated by distinct sets of chaperones and cochaperones. (**A**) Internalization of unfolded rΔF508CFTR (5 min), TfR (5 min) and CD4Tcc-Ub(AllRΔG) (2.5 min) was determined as in Fig. 2D. (**B** and **C**) Effect of chaperone or cochaperone KD on lysosomal sorting of (B) rΔF508CFTR and (C) Lamp2/CD63 was examined by measuring the acidification rate from early endosomes to lysosomes (see fig. S9). (**D**) Metabolic stability of (left) core-glycosylated ΔF508CFTR and (right) complex-glycosylated rΔF508CFTR in SMARTpool siRNA-transfected HeLa cells was determined by immunoblotting with CHX chase. (**E**) CFTR disappearance was quantified by densitometry and expressed as percentages of initial amount (T-0) in experiments shown in (D). Bar graphs of each sample represent the data (top) at 0- to 3-hour and (bottom) 0- to 6-hour chase. MG132 and bafilomycin A1 (BafA1) were positive controls for ERAD and lysosomal degradation, respectively.

and CHIP-rΔF508CFTR interaction (Fig. 3D). In accord with the Hsc70- and Hsp90-dependent CHIP interaction, association of Hsc70 and, to a lesser extent, Hsp90 with complex-glycosylated rΔF508CFTR, but less with its wt counterpart, was verified by co-IP (Fig. 3E).

Contribution of the molecular chaperones to the rΔF508CFTR peripheral QC was assessed in HeLa cells. Ablation of Hsc70 or Hsp90A (Hsp90α) stabilized rΔF508CFTR at PM (Fig. 3F and fig. S5A) by decreasing its ubiquitination (Fig. 3A, B, and G), internalization, lysosomal delivery, and degradation without interfering with TfR and CD4Tl-ccUb(AllRΔG) endocytosis and Lamp2/CD63 lysosomal sorting (Fig. 4, A to E), which phenocopied of the CHIP KD effect. Up-regulation of Hsp70 and a subset of cochaperones as part of the stress response induced by Hsc70 KD (fig. S6, C and F) was unable to compensate for the Hsc70 loss of function, which may imply functional differences among chaperones and cochaperones (*27*). CHIP-Hsc70 was previously shown to participate in the proteasomal and lysosomal degradation of PM-localized ErbB2 receptor, after the inhibition of Hsp90 by geldanamycin (*28*). It was noteworthy that geldanamycin had a minimal effect on the rΔF508CFTR PM stability (fig. S7), which highlighted the distinct initiating mechanism between rΔF508CFTR and ErbB2 degradation.

The role of CHIP-Hsc70 in the rΔF508CFTR ubiquitination was confirmed in vitro. Complex-glycosylated rΔF508CFTR-His_{10} was isolated by affinity chromatography under native conditions from BHK cells. Catalytic activity of recombinant wt and K30A, but not ΔUbox CHIP, was verified (fig. S8, A to D). Ubiquitination of rΔF508CFTR was reconstituted in the presence of E1, UbcH5c, CHIP, myc-Ub, and adenosine triphosphate (ATP) (Fig. 5A). Omitting any components or using CHIP-ΔUbox compromised the channel ubiquitination (Fig. 5A and fig. S8E). Similar results were obtained by using purified rΔF508CFTR from PM-enriched vesicles (Fig. 5B and fig. S8, F and G). Recombinant Hsc70 profoundly enhanced the CHIP-dependent ubiquitination, whereas CHIP-K30A remained ineffective (Fig. 5B and fig. S8E). Thus, Hsc70 plays an essential role in the recognition of nonnative rΔF508CFTR and CHIP recruitment in post-Golgi compartments. Wt CFTR was largely resistant

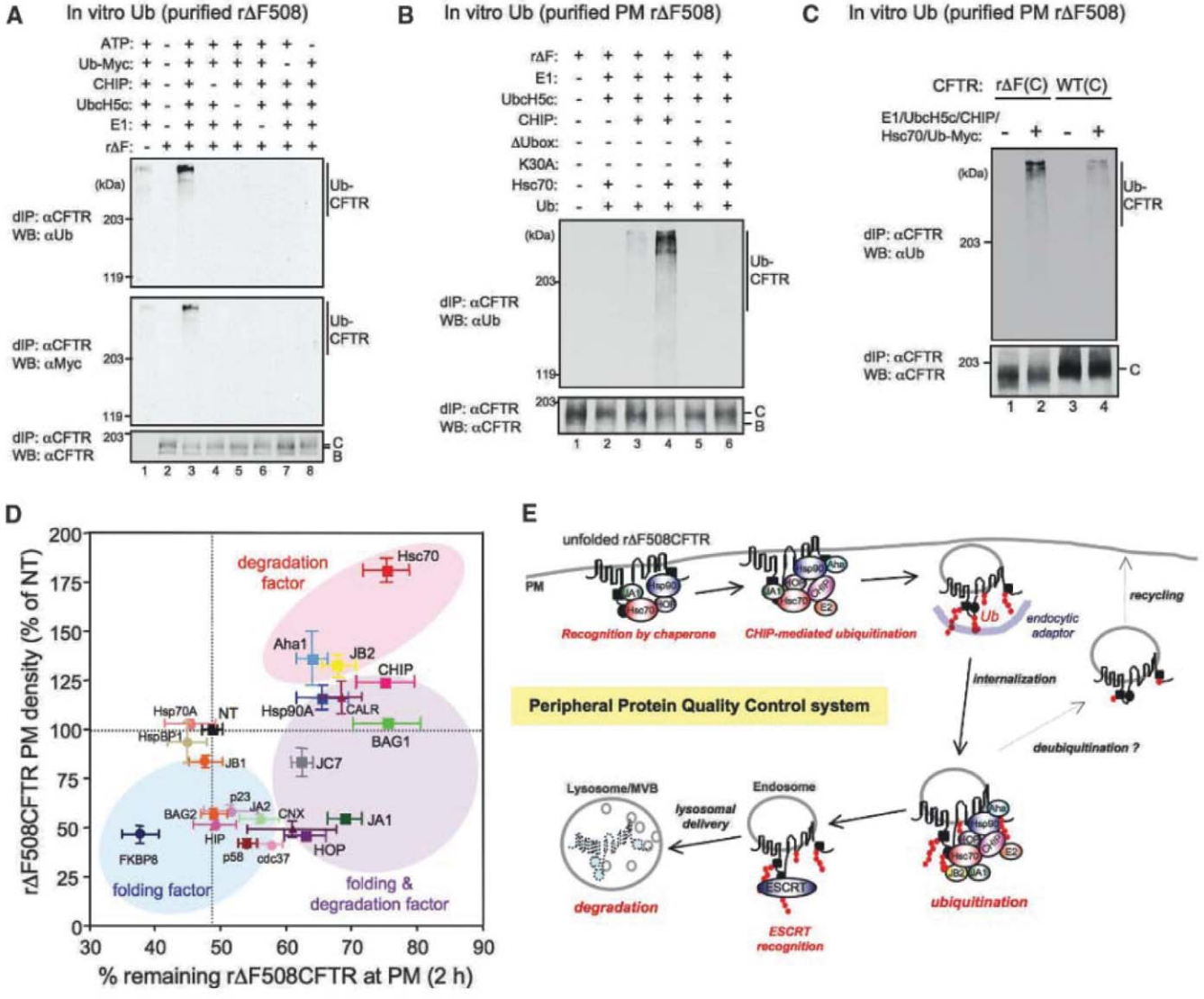


Fig. 5. The peripheral QC machinery ubiquitinates the unfolded CFTR and dictates the PM level. (**A**) Reconstitution of rΔF508CFTR ubiquitination in vitro. Purified complex-glycosylated rΔF508CFTR-His_{10} was incubated with E1, UbcH5c, CHIP, Hsc70, Ub-Myc, and ATP at 30°C for 2 hours. rΔF508CFTR was isolated by d-IP and analyzed by immunoblotting. (**B**) CHIP-dependent ubiquitination of purified rΔF508CFTR from PM-enriched vesicles was stimulated by recombinant Hsc70. (**C**) Wt and rΔF508 CFTR-His_{10} were purified and ubiquitinated as in (B). (**D**) Classification of chaperones/cochaperones based on their effect on rΔF508CFTR PM density (fig. S5E) and stability (Figs. 2A and 3F). Components of the peripheral QC machinery identified are indicated by larger type. (**E**) Working model for the peripheral protein QC of rΔF508CFTR.

to ubiquitination, which confirmed the conformational selectivity of the Hsc70-CHIP-UbcH5 complex in vitro (Fig. 5C) (*12*, *29*).

Cochaperones regulate CFTR peripheral QC. The folding and degradative function of Hsc70-Hsp90 is regulated by cochaperones (*24*, *30*–*32*). Functional screens using SMARTpool and single siRNAs revealed that BAG1, DNAJB2 (HSJ1), DNAJA1 (Hdj2), DNAJC7 (TPR2), HOP (STIP1), and Aha1 (AHSA1) were required for the rΔF508CFTR removal from PM of HeLa cells (Fig. 3F and fig. S5A). Hsc70 and its cochaperones, BAG1, DNAJB2, DNAJA1, and HOP were also effective in IB3 cells, although Hsp90A and Aha1 had marginal impact (fig. S5B).

We verified the contribution of cochaperones to rΔF508CFTR disposal via ubiquitination, internalization, and lysosomal targeting. Ablation of the Hsc70 regulator DNAJA1, the Hsc70-Hsp90 coupling factor HOP, or the Hsp90 cochaperone Aha1 reduced the rΔF508CFTR ubiquitination (Fig. 3, B and G) and internalization without affecting TfR and CD4Tcc-Ub(AllRΔG) uptake (Fig. 4A and table S1). Correlation between the channel ubiquitination and internalization or PM stability suggests that these cochaperones facilitate rΔF508CFTR internalization and disposal by enhancing ubiquitination, presumably through regulation of the CHIP-Hsc70-Hsp90A complexes (fig. S5, C and D).

Lysosomal delivery of rΔF508CFTR from early endosomes was impeded by KD of DNAJA1, DNAJB2, DNAJC7, Aha1, BAG1, or HOP (Fig. 4B and fig. S9). Ablation of DNAJC7, Aha1, or HOP, however, also delayed the Lamp2/CD63 lysosomal targeting (Fig. 4C), which implied their Ub-independent function on cargo lysosomal targeting (table S1). In contrast, DNAJB2 was involved in the lysosomal targeting of rΔF508CFTR by enhancing ubiquitination only at early endosomes (Figs. 3, B and G, and 4, A to C). BAG1 KD selectively inhibited rΔF508CFTR internalization and lysosomal delivery without influencing ubiquitination (Figs. 3, B and G, and 4, A to C), which indicated that it functions after ubiquitination. Because BAG1 is ubiquitinated by CHIP and contains an Ub-like domain (*30*), it may link the chaperone-rΔF508CFTR complex to Ub-binding adaptors of the internalization and lysosomal-sorting machinery.

CFTR PM level is defined by its PM stability and biosynthetic secretion dictated by transcription, translation, and ER-associated folding and degradation rates. Based on the minimal effect of chaperone and cochaperone KD on the core-glycosylated ΔF508CFTR expression (fig. S5F) and ERAD (Fig. 4, D and E, see below), we inferred that CFTR PM density is primarily modulated by folding and/or secretion and PM stability. Thus, at constant secretion, the PM density should be proportional to CFTR peripheral stability. Indeed, ablation of Hsc70, DNAJB2, or Aha1 proportionally increased the rΔF508CFTR PM density and function (Fig. 5D, and figs. S5E and S10), which suggested that these chaperones or cochaperones are primarily involved in peripheral degradation. In contrast, ablation of CHIP or Hsp90A only slightly increased the channel PM density, whereas DNAJA1, BAG1, or HOP KD did not (Fig. 5D and fig. S5E), which suggested that peripheral stabilization was offset by impaired biosynthetic secretion. The observed relation between the PM density and stability also supports the established role of chaperones and cochaperones in CFTR folding [e.g. calnexin (CNX) (*6*, *33*); BAG2 (*30*); p23; FKBP8 (*24*) and stability [calreticulin (CALR) (*34*)].

Discussion. Our results revealed a partial overlap between constituents of the CFTR QC at ER (*4*, *12*, *16*, *35*, *36*) and PM, which suggested that similar principles may govern the recognition of structurally defective channels at different cellular locations. This is in line with the capacity of CHIP-UbcH5c to synthesize Ub-chains with all possible linkages (*37*), conferring a recognition signal for channel degradation by proteasome (*38*) and Ub-binding endocytic and ESCRT adaptors in post-Golgi compartments (*9*). Comparison of ERAD and lysosomal degradation showed that only Hsc70 or BAG1 KD delayed the ΔF508CFTR ERAD, whereas KD of any chaperone or cochaperone identified in our functional screens attenuated rΔF508CFTR degradation (Fig. 4, D and E), which implied that parallel QC pathways, including chaperone-independent systems (*13*, *14*, *39*), have evolved to enhance the fidelity of the ER QC.

Based on our results and proteostatic mechanisms at different subcellular locations (*1*–*4*, *30*), the following model is proposed for the peripheral CFTR QC (Fig. 5E). Recognition of unfolded cytoplasmic regions of CFTR is mediated by Hsc70 in concert with DNAJA1 and possibly by the Hsp90 machinery. Prolonged interaction with the chaperone–cochaperone complex recruits CHIP-UbcH5c and leads to ubiquitination of conformationally damaged CFTR. This ubiquitination is probably influenced by other E3 ligases and deubiquitinating enzyme activities (*40*), culminating in accelerated endocytosis and lysosomal delivery mediated by Ub-binding clathrin adaptors and the ESCRT machinery, respectively. Promiscuous substrate specificity of Hsc70-Hsp90 toward nonnative polypeptides implies that the peripheral QC probably contributes to triage decision of other conformationally defective PM proteins and thereby to pathogenesis of a variety of conformational diseases.

References and Notes

1. T. Anelli, R. Sitia, *EMBO J.* **27**, 315 (2008).
2. D. N. Hebert, M. Molinari, *Physiol. Rev.* **87**, 1377 (2007).
3. E. T. Powers, R. I. Morimoto, A. Dillin, J. W. Kelly, W. E. Balch, *Annu. Rev. Biochem.* **78**, 959 (2009).
4. S. S. Vembar, J. L. Brodsky, *Nat. Rev. Mol. Cell Biol.* **9**, 944 (2008).
5. M. Sharma *et al.*, *J. Cell Biol.* **164**, 923 (2004).
6. R. Glozman *et al.*, *J. Cell Biol.* **184**, 847 (2009).
7. H. Hayashi, Y. Sugiyama, *Mol. Pharmacol.* **75**, 143 (2009).
8. S. Dupré, D. Urban-Grimal, R. Haguenauer-Tsapis, *Biochim. Biophys. Acta* **1695**, 89 (2004).
9. J. H. Hurley, S. D. Emr, *Annu. Rev. Biophys. Biomol. Struct.* **35**, 277 (2006).
10. P. Arvan, X. Zhao, J. Ramos-Castaneda, A. Chang, *Traffic* **3**, 771 (2002).
11. S. Alberti, K. Böhse, V. Arndt, A. Schmitz, J. Höhfeld, *Mol. Biol. Cell* **15**, 4003 (2004).
12. G. C. Meacham, C. Patterson, W. Zhang, J. M. Younger, D. M. Cyr, *Nat. Cell Biol.* **3**, 100 (2001).
13. J. M. Younger *et al.*, *Cell* **126**, 571 (2006).
14. D. Morito *et al.*, *Mol. Biol. Cell* **19**, 1328 (2008).
15. G. M. Denning *et al.*, *Nature* **358**, 761 (1992).
16. J. M. Younger *et al.*, *J. Cell Biol.* **167**, 1075 (2004).
17. D. E. Grove, M. F. Rosser, H. Y. Ren, A. P. Naren, D. M. Cyr, *Mol. Biol. Cell* **20**, 4059 (2009).
18. N. Pedemonte *et al.*, *J. Clin. Invest.* **115**, 2564 (2005).
19. Materials and methods are available as supporting material on *Science* Online.
20. K. Du, M. Sharma, G. L. Lukacs, *Nat. Struct. Mol. Biol.* **12**, 17 (2005).
21. M. Sharma, M. Benharouga, W. Hu, G. L. Lukacs, *J. Biol. Chem.* **276**, 8942 (2001).
22. H. Barriere *et al.*, *Traffic* **7**, 282 (2006).
23. O. Staub, D. Rotin, *Physiol. Rev.* **86**, 669 (2006).
24. X. Wang *et al.*, *Cell* **127**, 803 (2006).
25. Single-letter abbreviations for the amino acid residues used in this article are as follows: A, Ala; H, His; K, Lys; and Q, Gln.
26. C. A. Ballinger *et al.*, *Mol. Cell. Biol.* **19**, 4535 (1999).
27. S. B. Goldfarb *et al.*, *Proc. Natl. Acad. Sci. U.S.A.* **103**, 5817 (2006).
28. W. Xu *et al.*, *Proc. Natl. Acad. Sci. U.S.A.* **99**, 12847 (2002).
29. S. Murata, Y. Minami, M. Minami, T. Chiba, K. Tanaka, *EMBO Rep.* **2**, 1133 (2001).
30. V. Arndt, C. Rogon, J. Höhfeld, *Cell. Mol. Life Sci.* **64**, 2525 (2007).
31. Y. Minami, J. Höhfeld, K. Ohtsuka, F. U. Hartl, *J. Biol. Chem.* **271**, 19617 (1996).
32. S. Tzankov, M. J. Wong, K. Shi, C. Nassif, J. C. Young, *J. Biol. Chem.* **283**, 27100 (2008).
33. T. Okiyoneda *et al.*, *Mol. Biol. Cell* **15**, 563 (2004).
34. K. Harada *et al.*, *J. Biol. Chem.* **281**, 12841 (2006).
35. M. A. Loo *et al.*, *EMBO J.* **17**, 6879 (1998).
36. G. C. Meacham *et al.*, *EMBO J.* **18**, 1492 (1999).
37. M. Zhang *et al.*, *Mol. Cell* **20**, 525 (2005).
38. D. Finley, *Annu. Rev. Biochem.* **78**, 477 (2009).
39. B. K. Sato, D. Schulz, P. H. Do, R. Y. Hampton, *Mol. Cell* **34**, 212 (2009).
40. J. M. Bomberger, R. L. Barnaby, B. A. Stanton, *J. Biol. Chem.* **284**, 18778 (2009).

41. We thank J. Tavares and C. M. Mulvihill for CHIP purification and generating CFTR-His_{10} cells, respectively; H. Stenmark for Hrs antibody; and H. Lewis, C. Lima, and K. Iwai for NBD1-3S, SUMO, Ulp1, and UbcH5 plasmids, respectively. Lamp1, Lamp2, and CD63 antibodies were developed by J. August and J. Hildreth (University of Iowa). T.O. and W.M.R. were supported by a Canadian Cystic Fibrosis Foundation and a Groupe de Recherche Axé sur la Structure des Protéines (GRASP) postdoctoral fellowship, respectively. This work was supported by grants to J.H. from Deutsche Forschungsgemeinschaft, J.C.Y. and G.L.L. from the Canadian Institute of Health Resources, NIH, Cystic Fibrosis Foundation Therapeutics, the Canadian Cystic Fibrosis Foundation, and the Canadian Foundation for Innovation. J.C.Y. and G.L.L. are holders of Canada Research Chairs.

Supporting Online Material

www.sciencemag.org/cgi/content/full/science.1191542/DC1
Materials and Methods
Figs. S1 to S10
Tables S1 to S4
References

27 April 2010; accepted 14 June 2010
Published online 1 July 2010;
10.1126/science.1191542
Include this information when citing this paper.

Structural Basis for Broad and Potent Neutralization of HIV-1 by Antibody VRC01

Tongqing Zhou,[1] Ivelin Georgiev,[1]* Xueling Wu,[1]* Zhi-Yong Yang,[1]* Kaifan Dai,[1] Andrés Finzi,[2] Young Do Kwon,[1] Johannes F. Scheid,[3] Wei Shi,[1] Ling Xu,[1] Yongping Yang,[1] Jiang Zhu,[1] Michel C. Nussenzweig,[3] Joseph Sodroski,[2,4] Lawrence Shapiro,[1,5] Gary J. Nabel,[1] John R. Mascola,[1] Peter D. Kwong[1]†

During HIV-1 infection, antibodies are generated against the region of the viral gp120 envelope glycoprotein that binds CD4, the primary receptor for HIV-1. Among these antibodies, VRC01 achieves broad neutralization of diverse viral strains. We determined the crystal structure of VRC01 in complex with a human immunodeficiency virus HIV-1 gp120 core. VRC01 partially mimics CD4 interaction with gp120. A shift from the CD4-defined orientation, however, focuses VRC01 onto the vulnerable site of initial CD4 attachment, allowing it to overcome the glycan and conformational masking that diminishes the neutralization potency of most CD4-binding-site antibodies. To achieve this recognition, VRC01 contacts gp120 mainly through immunoglobulin V-gene regions substantially altered from their genomic precursors. Partial receptor mimicry and extensive affinity maturation thus facilitate neutralization of HIV-1 by natural human antibodies.

Successful vaccine development often takes advantage of clues from humoral responses elicited by natural infection. For HIV-1, neutralizing antibody responses elicited within the first year or two of infection are generally strain-specific (*1*) and thus provide limited insight into vaccine design (*2*). A few monoclonal antibodies from HIV-1–infected individuals, however, are broadly neutralizing, and an effort has been made to facilitate vaccine design by defining their structures (*3*, *4*).

The well-studied broadly neutralizing antibodies to HIV-1—2G12, 2F5, 4E10, and b12—have unusual characteristics that have posed barriers to eliciting similar antibodies in humans (*5*). Thus, in addition to having broad capacity for neutralization, an appropriate antibody should be present in high enough titers in humans to suggest that it can be elicited in useful concentrations. We and others have screened cohorts of sera from infected individuals to find broadly neutralizing responses that are detectable in a substantial percentage of subjects (*6*–*10*). One serum response that satisfies these criteria has been mapped to the site on the HIV-1 gp120 envelope (Env) glycoprotein that binds to the CD4 receptor (*8*).

Although potentially accessible, the CD4-binding site is protected from humoral recognition through glycan and conformational masking (*11*). The identification of monoclonal antibodies against this site is described in a companion manuscript (*12*). In brief, we created resurfaced, conformationally stabilized probes, with antigenic specificity for the initial site of CD4 attachment to gp120 (*13*). This site, a conformationally invariant subset of the CD4-binding surface, is vulnerable to antibody-mediated neutralization (*13*), and we used probes specific for this site to identify antibodies that neutralize most viruses (*12*). In this work, we analyzed the crystal structure for one of these antibodies, VRC01, in complex with

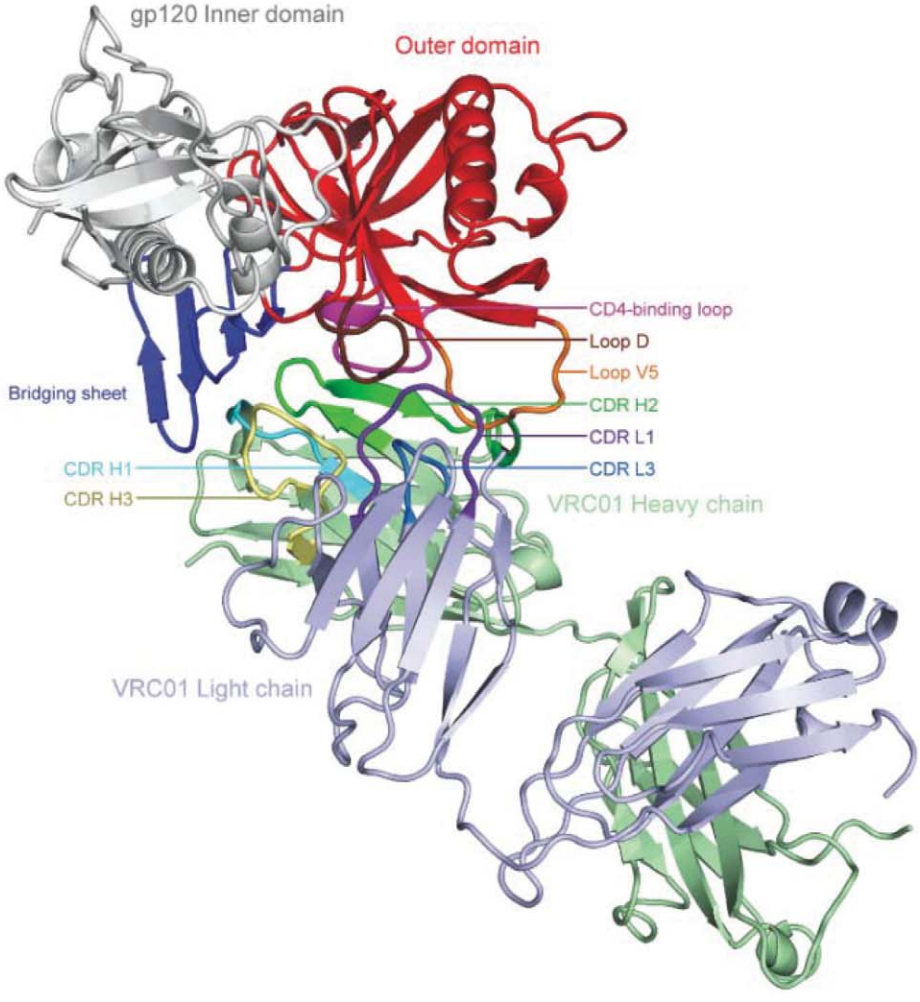


Fig. 1. Structure of antibody VRC01 in complex with HIV-1 gp120. Atomic-level details for broad and potent recognition of HIV-1 by a natural human antibody are depicted with polypeptide chains in ribbon representations. The gp120 inner domain is shown in gray, the bridging sheet in blue, and the outer domain in red, except for the CD4-binding loop (purple), the D loop (brown), and the V5 loop (orange). The light chain of the antigen-binding fragment (Fab) of VRC01 is shown in light blue, with complementarity-determining regions (CDRs) highlighted in dark blue (CDR L1) and marine blue (CDR L3). The heavy chain of Fab VRC01 is shown in light green, with CDRs highlighted in cyan (CDR H1), green (CDR H2), and pale yellow (CDR H3). Both light and heavy chains of VRC01 interact with gp120: The primary interaction surface is provided by the CDR H2, with the CDR L1 and L3 and the CDR H1 and H3 providing additional contacts.

an HIV-1 gp120 core. We deciphered the basis of VRC01 neutralization, identified mechanisms of natural resistance, showed how VRC01 minimizes such resistance, examined potential barriers to elicitation, and defined the role of affinity maturation in gp120 recognition.

Similarities of Env recognition by CD4 and VRC01 antibody. To gain a structural understanding of VRC01 neutralization, we crystallized the antigen-binding fragment (Fab) of VRC01 in complex with an HIV-1 gp120 from the clade A/E recombinant 93TH057 (*14*, *15*). The crystallized gp120 consisted of its inner domain–outer domain core, with truncations in the variable loops V1/V2 and V3 as well as the N- and C-termini, which are regions known to extend away from the main body of the gp120 envelope glycoprotein (*16*). Diffraction to 2.9 Å resolution was obtained from orthorhombic crystals, which contained four copies of the VRC01-gp120 complex per asymmetric unit, and the structure was solved by means of molecular replacement and refined to a crystallographic *R* value of 19.7% (Fig. 1 and table S1) (*17*).

The interaction surface between VRC01 and gp120 encompasses almost 2500 $Å^2$, with 1244 $Å^2$ contributed by VRC01 and 1249 $Å^2$ by gp120 (*18*). On VRC01, both heavy chain (894 $Å^2$) and light chain (351 $Å^2$) contribute to the contact surface (table S2), with the central focus of binding on the heavy chain–second complementarity–determining region (CDR H2). Over half of the interaction surface of VRC01 (644 $Å^2$) involves CDR H2, a mode of binding that is reminiscent of the interaction between gp120 and the CD4 receptor; CD4 is a member of the V-domain class of the immunoglobulin superfamily (*19*), and the CDR2-like region of CD4 is a central focus of gp120 binding (Fig. 2A and table S3) (*20*). For CD4, the CDR2-like region forms antiparallel, intermolecular hydrogen bonds with residues 365_{gp120} to 368_{gp120} of the CD4-binding loop of gp120 (*20*) (Fig. 2B); with VRC01, one hydrogen-bond is observed between the carbonyl oxygen of $Gly54_{VRC01}$ and the backbone nitrogen of $Asp368_{gp120}$. This hydrogen bond occurs at the loop tip, an extra residue relative to CD4 is inserted in the strand, and the rest of the potential hydrogen bonds are of poor geometry or distance (Fig. 2C and table S4). Other similarities and differences with CD4 are found: Of the two dominant CD4 residues ($Phe43_{CD4}$ and $Arg59_{CD4}$) involved in interaction with gp120, VRC01 mimics the arginine interaction but not the phenylalanine one (Fig. 2, B and C). Lastly, substantial correlation was observed between gp120 residues involved in binding VRC01 and CD4 (fig. S1).

Superposition of the gp120 core in its VRC01-bound form with gp120s in other crystalline lattices and bound by other ligands indicates a CD4-bound conformation [Protein Data Bank (PDB) ID number 3JWD] (*16*) to be most closely related in structure, with a Cα-root-mean-square deviation of 1.03 Å (table S5). Such superposition of gp120s from CD4- and VRC01-bound conformations brings the N-terminal domain of CD4 and the heavy chain–variable domain of VRC01 into close alignment (Fig. 2), with 73% of the CD4 N-terminal domain volume overlapping with VRC01 (*21*). This domain overlap is much higher than observed with the heavy chains of other CD4-binding-site antibodies, such as b12, b13, or F105 (table S6). However, when the VRC01 heavy chain is superimposed—on the basis of conserved framework and cysteine residues—on CD4 in the CD4-gp120 complex,

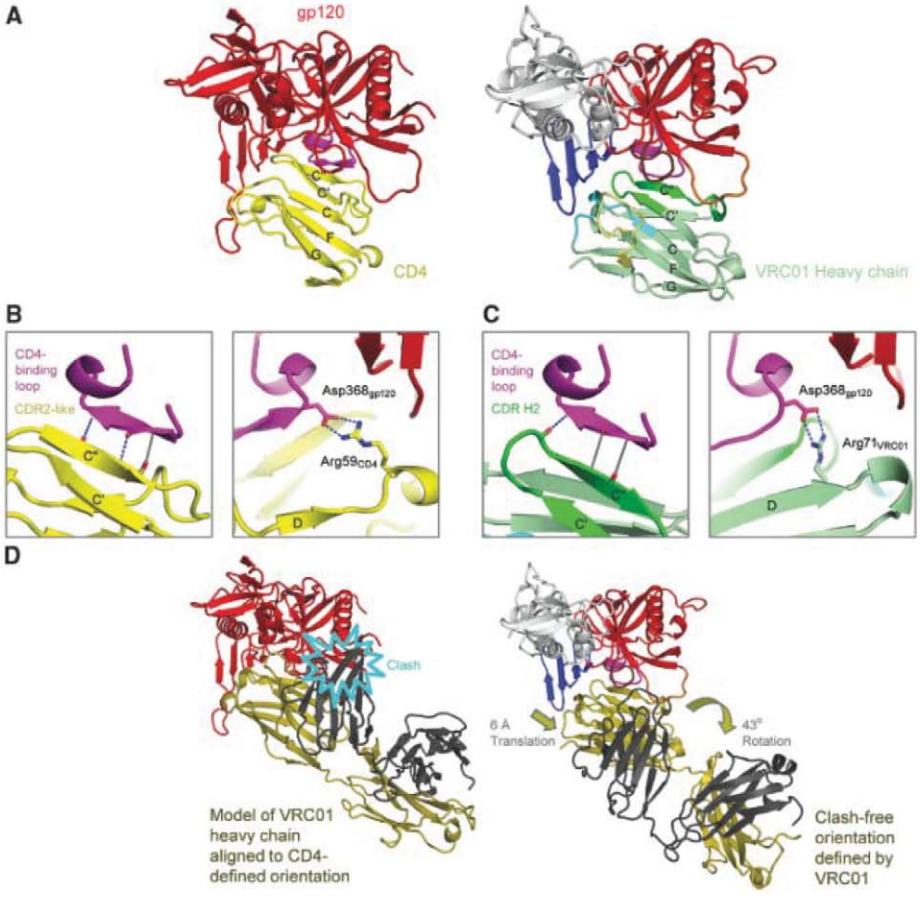


Fig. 2. Structural mimicry of CD4 interaction by antibody VRC01. VRC01 shows how a double-headed antibody can mimic the interactions with HIV-1 gp120 of a single-headed member of the immunoglobulin superfamily, such as CD4. (**A**) Comparison of HIV-1 gp120 binding to CD4 (N-terminal domain) and VRC01 (heavy chain–variable domain). Polypeptide chains are depicted in ribbon representation for (right) the VRC01 complex and (left) the CD4 complex with the lowest gp120 root mean square deviation (table S5). The CD4 complex (3JWD) (*16*) is indicated in yellow for CD4 and red for gp120, except for the CDR-binding loop (purple). The VRC01 complex is colored as in Fig. 1. Immunoglobulin domains are composed of two β sheets, and the top sheet of both ligands is labeled with the standard immunoglobulin-strand topology (strands G, F, C, C′, C″). (**B** and **C**) Interface details for (B) CD4 and (C) VRC01. Close-ups are shown of critical interactions between the CD4-binding loop (purple) and the C″ strand as well as between $Asp368_{gp120}$ and either $Arg59_{CD4}$ or $Arg71_{VRC01}$. Hydrogen bonds with good geometry are depicted by blue dotted lines, and those with poor geometry are depicted in gray. Atoms from which hydrogen bonds extend are depicted in stick representation and colored blue for nitrogen and red for oxygen. In the left panel of (C), the β15-strand of gp120 is depicted to aid comparison with (B), although because of the poor hydrogen-bond geometry, it is only a loop. (**D**) Comparison of VRC01- and CD4-binding orientations. Polypeptides are shown in ribbon representation, with gp120 colored the same as in (A) and VRC01 depicted with heavy chain in dark yellow and light chain in dark gray. When the heavy chain of VRC01 is superimposed onto CD4 in the CD4-gp120 complex, the position assumed by the light chain evinces numerous clashes with gp120 (left). The VRC01-binding orientation (right) avoids clashes by adopting an orientation rotated by 43° and translated by 6 Å.

[1]Vaccine Research Center, National Institute of Allergy and Infectious Diseases, National Institutes of Health (NIH), Bethesda, MD 20892, USA. [2]Department of Cancer Immunology and AIDS, Dana-Farber Cancer Institute, Department of Pathology, Division of AIDS, Harvard Medical School, Boston, MA 02115, USA. [3]Laboratory of Molecular Immunology and Howard Hughes Medical Institute, The Rockefeller University, New York, NY 10065, USA. [4]Department of Immunology and Infectious Diseases, Harvard School of Public Health, Boston, MA 02115, USA. [5]Department of Biochemistry and Molecular Biophysics, Columbia University, New York, NY 10032, USA.

*These authors contributed equally to this work.
†To whom correspondence should be addressed. E-mail: pdkwong@nih.gov

clashes are found between gp120 and the entire top third of the VRC01 variable light chain (Fig. 2D) (*22*). In its complex with gp120, VRC01 rotates 43° relative to the CD4-defined orientation and translates 6 Å away from the bridging sheet, to a clash-free orientation that mimics many of the interactions of CD4 with gp120, although with considerable variation. Analysis of electrostatics shows that the interaction surfaces of VRC01 and CD4 are both quite basic, although the residue types of contacting amino acids are distinct (fig. S2). Thus, although VRC01 mimics CD4 binding to some extent, considerable differences are observed.

Structural basis of VRC01 breadth and potency. When CD4 is placed into an immunoglobulin context by fusing its two N-terminal domains to a dimeric immunoglobulin constant region, it achieves reasonable neutralization. VRC01, however, neutralizes more effectively (Fig. 3A) (*12*). To understand the structural basis for the exceptional breadth and potency of VRC01, we analyzed its interactive surface with gp120. VRC01 focuses its binding onto the conformationally invariant outer domain, which accounts for 87% of the contact surface area of VRC01 (table S7). The 13% of the contacts made with flexible inner domain and bridging sheet are noncontiguous, and we judged these not to be critical for binding. In contrast, CD4 makes 33% of its contacts with the bridging sheet, and many of these interactions are essential (*20*). The reduction in inner domain and bridging sheet interactions by VRC01 is accomplished primarily by a 6 Å translation relative to CD4, away from these regions; critical contacts such as made by $Phe43_{CD4}$ to the nexus of the bridging sheet–outer domain are not found in VRC01, whereas those to the outer domain (such as $Arg59_{CD4}$) are mimicked by VRC01.

To determine the affinity of VRC01 for gp120 in CD4-bound and non–CD4-bound conformations, we used surface-plasmon resonance spectroscopy to measure the affinity of VRC01 and other gp120-reactive antibodies and ligands to two gp120s: a β4-deletion developed by Harrison and colleagues that is restrained from assuming the CD4-bound conformation (*23*) or a disulfide-stabilized gp120 core that is largely fixed in the CD4-bound conformation in the absence of CD4 itself (*13*) (Fig. 3B and fig. S3). VRC01 showed high affinity to both CD4-bound and non–CD4-bound conformations, which is a property shared by the broadly neutralizing b12 antibody (*13*). In contrast, antibodies F105 and 17b as well as soluble CD4 showed strong preference for either one, but not both, of the conformations.

To assess the binding of VRC01 in the context of the functional viral spike, we examined its ability to neutralize variants of HIV-1 with gp120 changes that affect the ability to assume the CD4-bound state. Two of these mutations, $His66Ala_{gp120}$ and $Trp69Leu_{gp120}$, are less sensitive (*24*), whereas a third, $Ser375Trp_{gp120}$, is more sensitive to neutralization by CD4 (*24*, *25*). VRC01 neutralized all three of these variant HIV-1 viruses with similar potency (Fig. 3C), suggesting that VRC01 recognizes both CD4-bound and non–CD4-bound conformations of the viral spike. This diversity in recognition allows VRC01 to avoid the conformational masking that hinders most CD4-binding-site ligands (*26*) and to potently neutralize HIV-1 (*27*).

Precise targeting by VRC01. Prior analysis of effective and ineffective CD4-binding-site antibodies suggested that precise targeting to the vulnerable site of initial CD4 attachment is required to block viral entry (*11*, *28*). This site represents the outer domain contact for CD4 (*13*). Analysis of the VRC01 interaction with gp120 shows that it covers 98% of this site (Fig. 4, A and B, and fig. S4), comprising 1089 $Å^2$ on the gp120 outer domain, which is about 50% larger than the 730 $Å^2$ surface covered by CD4. The VRC01 contact surface outside the target site is largely limited to the conformationally invariant outer domain and avoids regions of conformational flexibility. This concordance of binding is much greater than for ineffective CD4-binding-site antibodies as well as for those that are partially effective, such as antibody b12 (*11*, *13*) (fig. S4).

The outer domain–contact site for CD4 is shielded by glycan (*11*, *20*). Contacts by the VRC01 light chain ($Tyr28_{VRC01}$ and $Ser30_{VRC01}$) are made with the protein-proximal N-acetylglucosamine from the N-linked glycan at residue

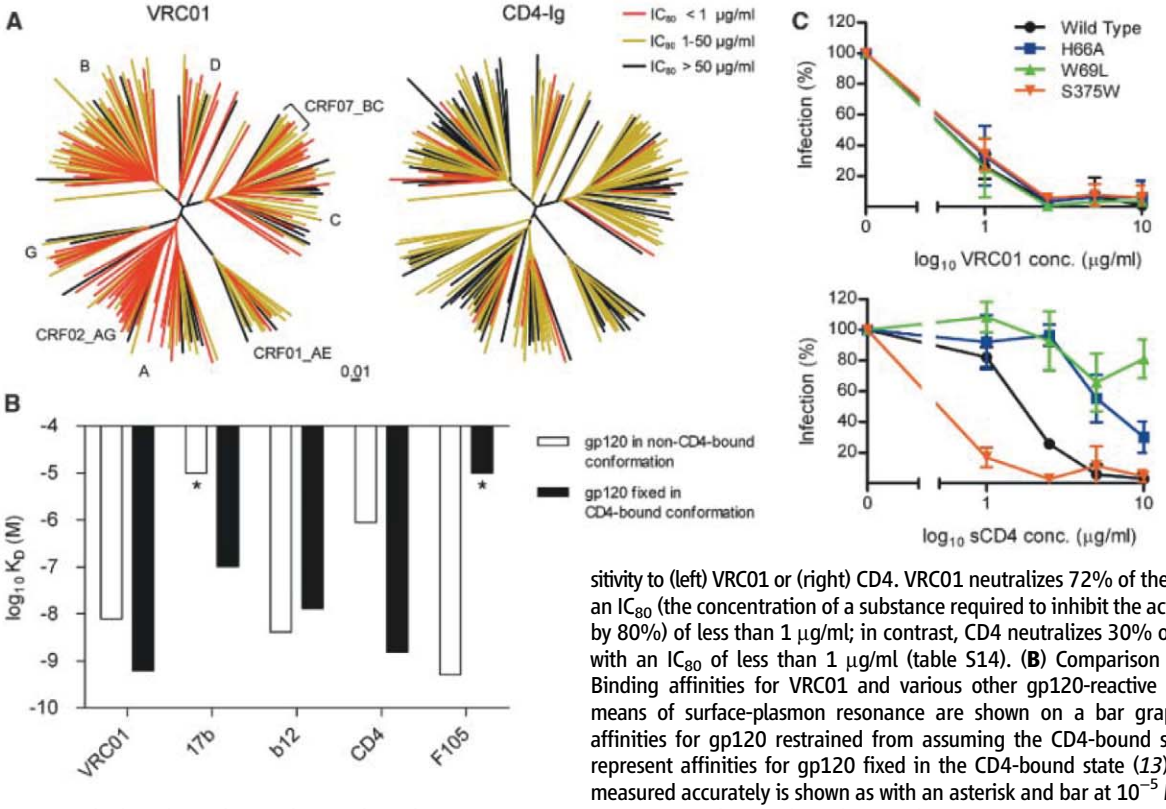


Fig. 3. Structural basis of antibody VRC01 neutralization breadth and potency. VRC01 displays remarkable neutralization breadth and potency, a consequence in part of its ability to bind well to different conformations of HIV-1 gp120. (**A**) Neutralization dendrograms. The genetic diversity of current circulating HIV-1 strains is displayed as a dendrogram, with locations of prominent clades (such as A, B, and C) and recombinants (such as CRF02_AG) labeled. The strains are colored by their neutralization sensitivity to (left) VRC01 or (right) CD4. VRC01 neutralizes 72% of the tested HIV-1 isolates with an IC_{80} (the concentration of a substance required to inhibit the activity of another substance by 80%) of less than 1 μg/ml; in contrast, CD4 neutralizes 30% of the tested HIV-1 isolates with an IC_{80} of less than 1 μg/ml (table S14). (**B**) Comparison of binding affinities (K_d). Binding affinities for VRC01 and various other gp120-reactive ligands as determined by means of surface-plasmon resonance are shown on a bar graph. White bars represent affinities for gp120 restrained from assuming the CD4-bound state (*23*), and black bars represent affinities for gp120 fixed in the CD4-bound state (*13*). Binding too weak to be measured accurately is shown as with an asterisk and bar at 10^{-5} M K_d. (**C**) Neutralization of viruses with altered sampling of the CD4-bound state. Mutant $S375W_{gp120}$ favors the CD4-bound state, whereas mutants $H66A_{gp120}$ and $W69L_{gp120}$ disfavor this state. Neutralization by VRC01 (top) is similar for wild type (WT) and all three mutant viruses, whereas neutralization by CD4 (bottom) correlates with the degree to which gp120 in the mutant viruses favors the CD4-bound state.

276_{gp120} (*29*). Thus instead of being occluded by glycan, VRC01 makes use of a glycan for binding. Other potential glycan interactions may occur with different strains of HIV-1 because the VRC01 recognition surface on the gp120–outer domain extends further than that of the functionally constrained CD4 interaction surface, especially into the loop D and the often-glycosylated V5 region (fig. S5).

Natural resistance to antibody VRC01. In addition to conformational masking and glycan shielding, HIV-1 resists neutralization by antigenic variation. In a companion manuscript, we show that of the 190 circulating HIV-1 isolates tested for sensitivity to VRC01, 173 were neutralized and 17 were resistant (*12*). To understand the basis of this natural resistance to VRC01, we analyzed all 17 resistant isolates by threading their sequences onto the gp120 structure (fig. S5). Variation was observed in the V5 region in resistant isolates, and this variation—along with alterations in gp120 loop D—appeared to be the source of most natural resistance to VRC01 (Fig. 4C and figs. S5 and S6).

Because substantial variation exists in V5, structural differences in this region might be expected to result in greater than 10% resistance. The lower observed frequency of resistance suggests that VRC01 employs a recognition mechanism that allows for binding despite V5 variation. Examination of VRC01 interaction with V5 shows that VRC01 recognition of V5 is considerably different from that of CD4 (fig. S7), with $Arg61_{VRC01}$ in the CDR H2 penetrating into the cavity formed by the V5 and β24 strands of gp120 (fig. S8). The V5 loop fits into the gap between heavy and light chains; thus, by contacting only the more conserved residues at the loop base, VRC01 can tolerate variation in the tip of the V5 loop (Fig. 4D).

Unusual VRC01 features and contribution to recognition. We examined the structure of VRC01 for special features that might be required for its function. A number of unusual features were apparent, including a high degree of affinity maturation, an extra disulfide bond, a site for N-linked glycosylation, a two-amino-acid deletion in the light chain, and an extensively matured binding interface between VRC01 and gp120 (Fig. 5 and fig. S9). We assessed the frequency with which these features were found in HIV-1 Env-reactive antibodies (appendix S1) or in human antibody-antigen complexes (fig. S10 and tables S8 and S9) and measured the effect of genomic reversion of these features on affinity for gp120 and neutralization of virus (Fig. 5, A to D, and table S10).

Higher levels of affinity maturation have been reported for HIV-1–reactive antibodies in general (*30*) and markedly higher levels for broadly neutralizing ones (*31*). These maturation levels could be a by-product of the persistent nature of HIV-1 infection and may not represent a functional requirement. Removal of the N-linked glycosylation or the extra disulfide bond, which connects CDR H1 and H3 regions of the heavy chain, had little effect on binding or neutralization (Fig. 5, A and B, and table S10). Insertion of two amino acids to revert the light chain deletion had moderate effects, which were larger for an Ala-Ala insertion (50-fold decrease in binding affinity) versus a Ser-Tyr insertion (fivefold decrease in affinity), which mimics the genomic sequence (Fig. 5C and table S10). Lastly, reversion of the interface was examined with either single-, four-, seven- or 12-mutant reversions. For the single-mutant reversions of the interface to the genomic antibody sequence, all 12 mutations had minor effects [most with a less than twofold effect on the dissociation constant (K_d), with the largest effect for a Gly54Ser change

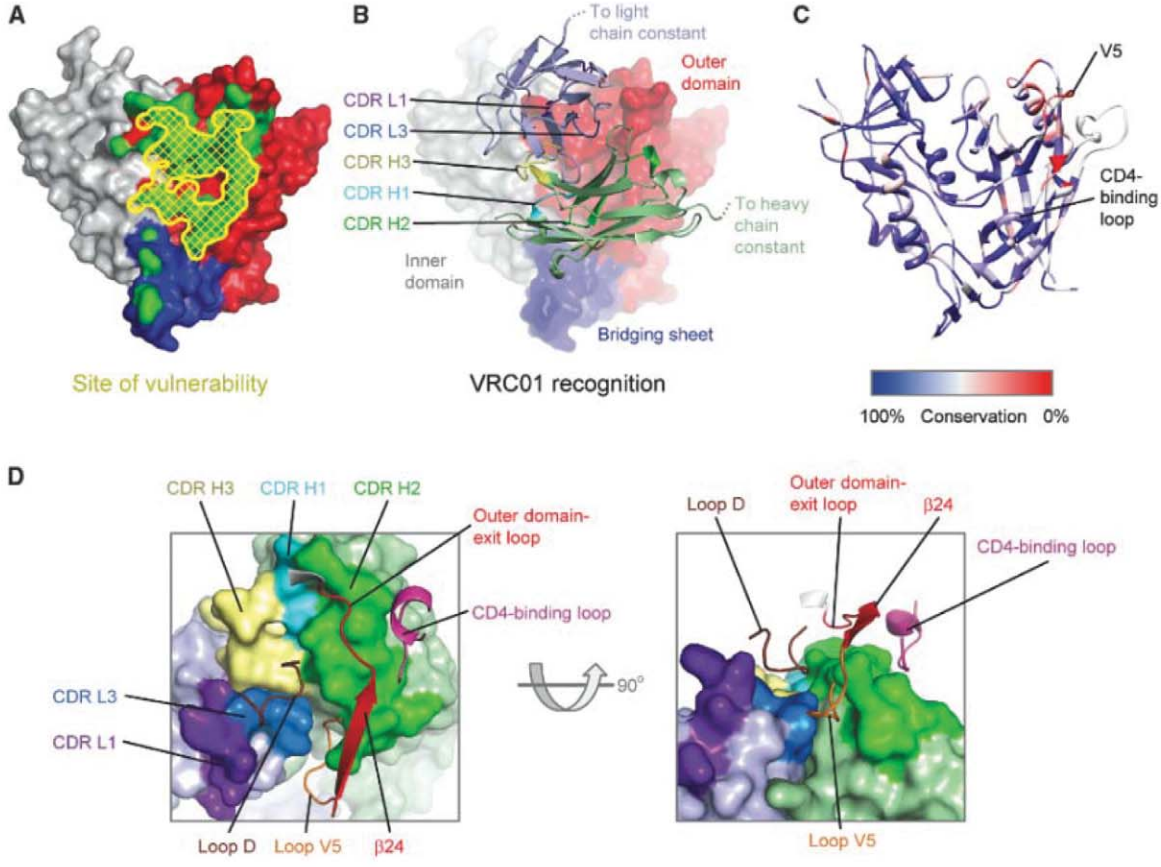


Fig. 4. Natural resistance to antibody VRC01. VRC01 precisely targets the CD4-defined site of vulnerability on HIV-1 gp120. Its binding surface, however, extends outside of the target site, and this allows for natural resistance to VRC01 neutralization. (**A**) Target site of vulnerability. The CD4-defined site of vulnerability is the initial contact surface of the outer domain of gp120 for CD4 and comprises only two thirds of the contact surface of gp120 for CD4 (*13*). The molecular surface of HIV-1 gp120 has been colored according to its underlying domain substructure: red for the conformationally invariant outer domain, gray for the inner domain, and blue for the highly mobile bridging sheet. Regions of the gp120 surface that interact with VRC01 have been colored green, with the CD4-defined site of vulnerability outlined in yellow. The view shown here is rotated 90° about the horizontal from the view in Figs. 1 and 2. (**B**) VRC01 recognition. The molecular surface of gp120 in the VRC01 bound conformation is colored as in (A). The variable domains of VRC01 are shown in ribbon representation, with the heavy and light chains colored as in Fig. 1 and extensions to constant regions indicated. (**C**) Antigenic variation. The polypeptide backbone of gp120 is colored according to sequence conservation: blue if conservation is high and red if conservation is low. (**D**) Molecular surface of VRC01 and select interactive loops of gp120. Variation at the tip of the V5 loop is accommodated by a gap between heavy and light chains of VRC01.

having a K_d of 20.2 nM] (table S10). Larger effects were observed with multiple (four, seven, or 12) changes (Fig. 5D and table S10). Thus, although VRC01 has a number of unusual features, no single alteration to genomic sequence substantially altered binding or neutralization.

Elicitation of VRC01-like antibodies. The probability for elicitation of a particular antibody is a function of each of the three major steps in B cell maturation: (i) recombination to produce nascent antibody heavy and light chains from genomic V_H-D-J and $V_{\kappa/\lambda}$-J precursors, (ii) deletion of auto-reactive antibodies, and (iii) maturation through hypermutation of the variable domains to enhance antigen affinity. For the recombination step, a lack of substantial CDR L3 and H3 contribution to the VRC01-gp120 interface (table S2) indicates that specific $V_{\kappa/\lambda}$-J or V_H(D)J recombination is not required (*32*) (fig. S11). The majority of recognition occurs with elements encoded in single genomic elements or cassettes, suggesting that specific joining events between them are not required. Within the V_H cassette, a number of residues associated with the IGHV1-02*02 precursor of VRC01 interact with gp120; many of these are conserved in related genomic V_Hs, some of which are of similar genetic distance from VRC01 (fig. S12). These results suggest that appropriate genomic precursors for VRC01 are likely to occur at a reasonable frequency in the human antibody repertoire.

Recombination produces nascent B cell–presented antibodies that have reactivities against both self and nonself antigens. Those with autoreactivity are removed through clonal deletion. With many of the broadly neutralizing antibodies to HIV-1, such as 2G12 (glycan reactive) (*33*, *34*), 2F5, and 4E10 (membrane reactive) (*35*, *36*), this appears to be a major barrier to elicitation. Although this remains to be characterized for genomic revertants and maturation intermediates, no autoreactivity has so far been observed with VRC01.

The third step influencing the elicitation of VRC01-like antibodies is affinity maturation, which is a process that involves the hypermutation of variable domains combined with affinity-based selection that occurs during B cell maturation in germinal centers (*37*). In the case of VRC01, 41 residue alterations were observed from the genomic V_H gene and 25 alterations from the V_κ gene (including a deletion of two residues) (fig. S13) (*38*). To investigate the effect of affinity maturation on HIV-1 gp120 recognition, we reverted the V_H and V_κ regions of VRC01, either individually or together, to the sequences of their genomic precursors. We tested the affinity and neutralization of these reverted antibodies (Fig. 6A) and combined these data with the genomic reversion data obtained while querying the unusual molecular features of VRC01 (previous section) (Fig. 6B).

No antibodies containing V_H and V_κ regions, which were fully reverted to their genomic precursors, bound gp120 or neutralized virus (*39*). Binding affinity and neutralization showed significant correlations with the number of affinity-matured residues ($P < 0.0001$). Binding to stabilized gp120 did not correlate well with other types of gp120 or to neutralization (table S11), which is related in part to greater retention of binding to VRC01 variants with genomically reverted V_κ regions. Extrapolation of the correlation to the putative genomic V gene sequences predicted binding affinities of 0.7 ± 0.4 μM K_d for gp120 stabilized in the CD4-bound conformation and substantially weaker affinites for nonstabilized gp120s (Fig. 6B and fig. S14).

No single affinity maturation alteration appeared to affect affinity by more than tenfold, suggesting that affinity maturation occurs in multiple small steps, which collectively enable tight binding

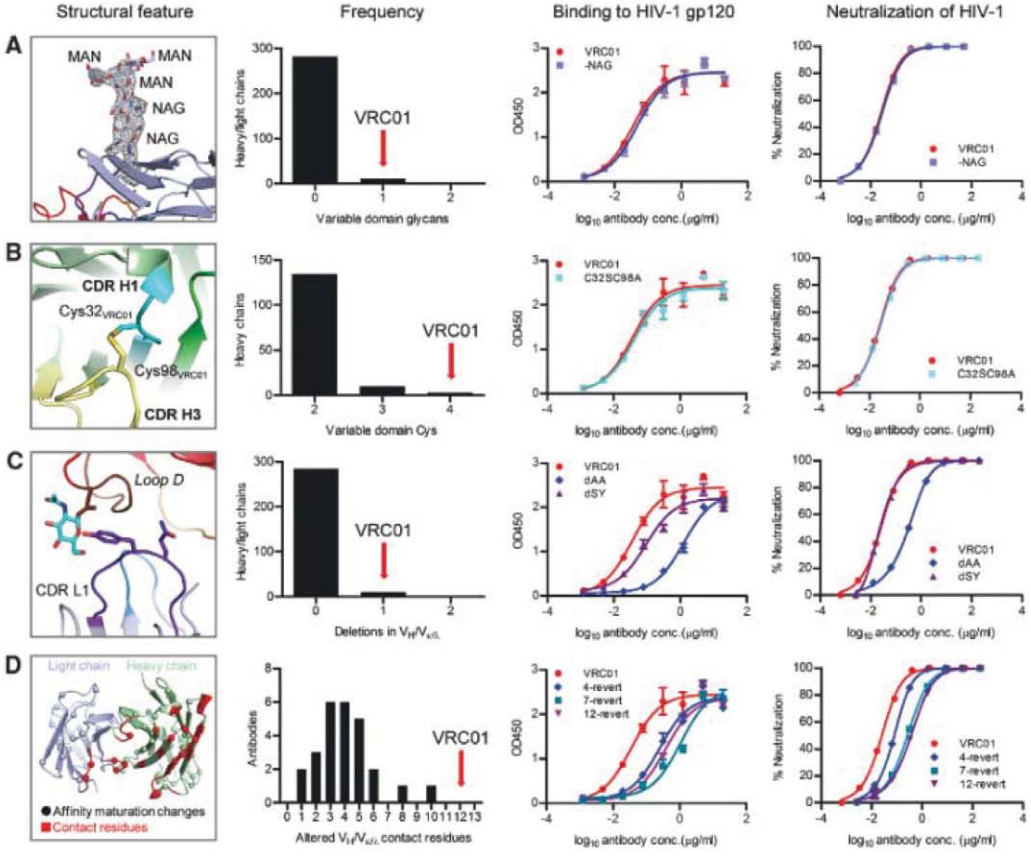


Fig. 5. Unusual VRC01 features. The structure of VRC01 displays a number of unusual features, which if essential for recognition might inhibit the elicitation of VRC01-like antibodies. (**A** to **D**) Unusual features of VRC01 are shown structurally (far left), in terms of frequency as a histogram with other antibodies (second from left), and in the context of affinity and neutralization measurements after mutational alteration (second from right and right). Affinity measurements were made by means of enzyme-linked immunosorbent assay to the gp120 construct used in crystallization (93TH057), and neutralization measurements were made with a clade A HIV-1 strain Q842.d12. Additional binding and neutralization experiments are reported in table S10. (A) N-linked glycosylation. The conserved tri-mannose core is shown with observed electron density, along with frequency and effect of removal on affinity and neutralization. (B) Extra disulfide. Variable heavy domains naturally have two Cys, linked by a disulfide; VRC01 has an extra disulfide linking CDR H1 and H3 regions. This occurs rarely in antibodies, but its removal through mutation to Ser/Ala has little effect on affinity or neutralization. (C) CDR L1 deletion. A two-amino-acid deletion in the CDR L1 prevents potential clashes with loop D of gp120. Such deletions are rarely observed; reversion to the longer loop may have a moderate effect on gp120 affinity. (D) Somatically altered contact surface. (Left) The VRC01 light chain is shown in violet, and the heavy chain is in green. Residues altered by affinity maturation are depicted with "balls," and contacts with HIV-1 gp120 are colored red. Approximately half of the contacts are altered during the maturation process. Analysis of human antibody-protein complexes in PDB shows this degree of contact surface alteration is rare; reversion of each of the contact sites to the genome sequence has little effect (table S10), although in aggregate the effect on affinity is larger.

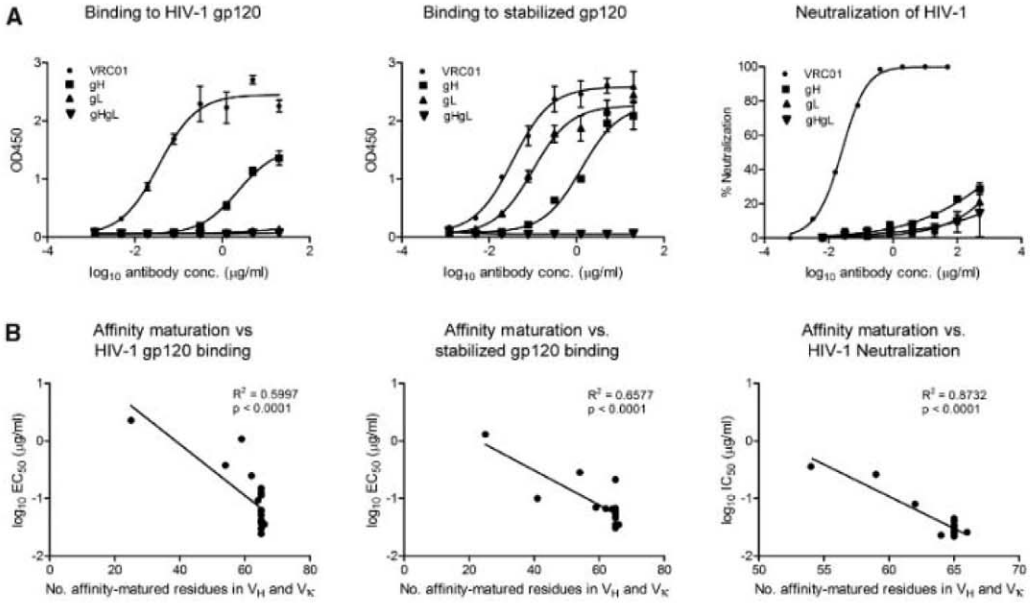


Fig. 6. Somatic maturation and VRC01 affinity. Hypermutation of the variable domain during B cell maturation allows for the evolution of high-affinity antibodies. With VRC01, this enhancement to affinity occurs principally through the alteration of noncontact residues, which appear to reform the genomic contact surface from affinity too low to measure to a tight (nanomolar) interaction. (**A**) Effect of genomic reversions. The V_H- and V_κ-derived regions of VRC01 were reverted to the sequences of their closest genomic precursors, expressed as immunoglobulins, and tested for binding as V_H- and V_κ-revertants (gHgL), as a V_H-only revertant (gH), or as a V_κ-only revertant (gL) to the gp120 construct used in crystallization (93TH057) or to a stabilized HXBc2 core (*13*). These constructs were also tested for neutralization of a clade A HIV-1 strain Q842.d12. Additional neutralization experiments with clade B and C viruses are reported in (*15*). (**B**) Maturation of VRC01 and correlation with binding and neutralization. Affinity and neutralization measurements for the 19 VRC01 mutants created during the structure-function analysis of VRC01 were analyzed in the context of their degree of affinity maturation. Significant correlations were observed, with extrapolation to V_H- and V_κ-genomic precursors suggesting greatly reduced affinity of the initial genomic arrangement for gp120.

to HIV-1 gp120. When the effects of VRC01 affinity maturation reversions are mapped to the structure of the VRC01-gp120 complex, they are broadly distributed throughout the VRC01 variable domains rather than focused on the VRC01-gp120 interface. Noncontact residues therefore appear to influence the interface with gp120 through indirect protein-folding effects. Thus, for VRC01 the process of affinity maturation entails incremental changes of the nascent genomic precursors to obtain high-affinity interaction with the HIV-1 Env surface.

Receptor mimicry and affinity maturation. The possibility that antibodies use conserved sites of receptor recognition to neutralize viruses effectively has been pursued for several decades. The recessed canyon on rhinovirus that recognizes the unpaired terminal immunoglobulin domains of intercellular adhesion molecule–1 highlights the role that a narrow canyon entrance may play in such occlusion of bivalent antibody-combining regions (*40*), although framework recognition can in some instances permit entry (*41*). Partial solutions such as those presented by antibody b12 (neutralization of ~40% of circulating isolates) (*12*, *13*) or by antibody HJ16 (neutralization of ~30% of circulating isolates) (*42*), a recently identified CD4-binding-site antibody, may allow recognition of some HIV-1 isolates.

With VRC01, the potency and breadth of neutralization (over 90%) suggest a more general solution. It remains to be seen how difficult it will be to guide the elicitation of VRC01-like antibodies from genomic rearrangement, through affinity maturation, to broad and potent neutralization of HIV-1. Accumulating evidence suggests that the VRC01-defined mode of recognition is used by other antibodies (*12*). These findings suggest that VRC01 is not an isolated example and probably provides a template for a general mode of recognition. The structure-function insights of VRC01 described here thus provide a foundation for rational vaccine design that is based not only on the particular mode of antibody-antigen interaction but also on defined relationships between genomic antibody precursors, somatic hypermutation, and interface-recognition elements.

References and Notes

1. R. A. Weiss *et al.*, *Nature* **316**, 69 (1985).
2. J. R. Mascola, D. C. Montefiori, *Annu. Rev. Immunol.* **28**, 413 (2010).
3. D. R. Burton, *Nat. Rev. Immunol.* **2**, 706 (2002).
4. D. R. Burton *et al.*, *Nat. Immunol.* **5**, 233 (2004).
5. Antibodies 2F5 and 4E10 require nonspecific membrane interaction (*35*, *36*), antibody 2G12 recognizes carbohydrate and is domain swapped (*33*, *34*), and antibody b12 was originally derived by means of phage display and has heavy-chain-only recognition (*13*).
6. A. K. Dhillon *et al.*, *J. Virol.* **81**, 6548 (2007).
7. Y. Li *et al.*, *J. Virol.* **83**, 1045 (2009).
8. Y. Li *et al.*, *Nat. Med.* **13**, 1032 (2007).
9. J. M. Binley *et al.*, *J. Virol.* **82**, 11651 (2008).
10. D. N. Sather *et al.*, *J. Virol.* **83**, 757 (2009).
11. L. Chen *et al.*, *Science* **326**, 1123 (2009).
12. X. Wu *et al.*, *Science* **329**, 856 (2010).
13. T. Zhou *et al.*, *Nature* **445**, 732 (2007).
14. The Env components of this strain derive from Clade E HIV-1 lineages (*43*).
15. Materials and methods are available as supporting material on *Science* Online.
16. M. Pancera *et al.*, *Proc. Natl. Acad. Sci. U.S.A.* **107**, 1166 (2010).
17. The four independent copies of the VRC01-gp120 complex in the asymmetric unit resembled each other closely for the antibody variable domain–gp120 components, with an Cα-root-mean-square deviation of less than 0.2 Å. Elbow variation, however, between variable and constant domains was apparent, and we found one copy (molecule 1) to be more ordered than the others. In the figures, we display molecule 1; see fig. S15 for a comparison of all of the molecules in the asymmetric unit.
18. Surface areas of interaction reported in this paper were determined with the program PISA, as implemented in CCP4 (*44*). Values were about 20% higher than those reported previously for the gp120-CD4 complex (*20*), which were obtained using the program MS (*45*).
19. P. J. Maddon *et al.*, *Cell* **42**, 93 (1985).
20. P. D. Kwong *et al.*, *Nature* **393**, 648 (1998).
21. The overlap of molecular volumes was calculated by comparing the separate volumes of interacting domains with the combined volume of these domains after gp120 superposition.
22. The relative orientation of the light-chain variable domain and the heavy-chain variable domain of VRC01 is similar to that of other antibodies (fig. S16).
23. S. Rits-Volloch, G. Frey, S. C. Harrison, B. Chen, *EMBO J.* **25**, 5026 (2006).
24. A. Finzi *et al.*, *Mol. Cell* **37**, 656 (2010).
25. S. H. Xiang *et al.*, *J. Virol.* **76**, 9888 (2002).
26. P. D. Kwong *et al.*, *Nature* **420**, 678 (2002).
27. In a companion paper (*12*), we show that VRC01 binding induces 17b and CCR5 binding in the context of monomeric gp120 with an unusual entropy signature characteristic of transiting to the CD4-bound state (*46*); neutralization data, however, show that VRC01 does not induce 17b or CCR5 binding in the context of the viral spike. This difference probably arises from the more constrained gp120 conformation in the trimeric spike. Thus, although VRC01 is able to induce large conformational changes in monomeric HIV-1 gp120 that resemble those induced by CD4, VRC01 interaction with gp120 does not depend on these conformational changes.
28. X. Wu *et al.*, *J. Virol.* **83**, 10892 (2009).
29. Endo H treatment of gp120 for crystallization removed all but the protein-proximal N-acetyl-glucosamine and potential 1,6-fucose from sites of N-linked glycosylation. Examination of the VRC01 interactions with the N-acetyl-glycosamine at residue 276_{gp120} shows that both 1,4 additions and 1,6 additions are tolerated.
30. J. F. Scheid *et al.*, *Nature* **458**, 636 (2009).
31. C. C. Huang *et al.*, *Proc. Natl. Acad. Sci. U.S.A.* **101**, 2706 (2004).
32. Four residues are provided by the CDR H3, $Asp99_{VRC01}$ to $Trp100B_{VRC01}$, with a combined interaction surface of 123 $Å^2$ (tables S3 and S12). These four residues are probably contributed by the D segment (IGHD3-16*02), and none of them appears critical to VRC01 recognition because changes are observed in two of these residues in the closely related

broadly neutralizing antibody VRC03, which was one of two antibodies we isolated along with VRC01 (*12*). Meanwhile, three residues are provided by the CDR L3—Tyr91$_{VRC01}$, Glu96$_{VRC01}$, and Phe97$_{VRC01}$—with a combined interaction surface of 190 Å^2 (tables S3 and S13). These three residues lie at the junction between V and J genes. They make important hydrophobic interactions with loop D of gp120, and two of them are conserved between VRC01 and VRC03. Although it is difficult to know how precisely the CDR L3 needs to be aligned, with only three contact residues variation at the V$_\kappa$-J gene junction should provide sufficient diversity for it to be represented in the repertoire.

33. R. W. Sanders *et al*., *J. Virol.* **76**, 7293 (2002).
34. D. A. Calarese *et al*., *Science* **300**, 2065 (2003).
35. G. Ofek *et al*., *J. Virol.* **78**, 10724 (2004).
36. B. F. Haynes *et al*., *Science* **308**, 1906 (2005).
37. C. Berek, A. Berger, M. Apel, *Cell* **67**, 1121 (1991).
38. Analysis of the HIV-1 Env-reactive antibody repertoire from infected individuals shows increased levels of affinity maturation (*30*). Analysis of a subset of this data (appendix S1) containing 147 heavy and 147 light chains from HIV-1 Env-reactive antibodies reveals an average of 15 alterations (30 maximum) for the heavy chain and an average of 8.6 alterations (22 maximum) for the light chain (fig. S13). In terms of the subset of HIV-1 Env-reactive antibodies that are broadly neutralizing (such as 2G12, 2F5, 4E10, and b12), antibodies b12 and 2G12 have 45 and 51 changes, respectively, relative to nearest genomic precursors in their V$_H$ and J segments of the heavy chain (*31*).
39. Similar significant reductions in affinity have been observed with reversion of other broadly neutralizing antibodies to HIV-1 to putative genomic sequences (*47*–*49*); these observations have led to the suggestion that the dramatically reduced germline affinity for gp120 might hinder the initiation of affinity maturation of these antibodies (*50*). That is, if the affinity for gp120 of the genomic precursor of a broadly neutralizing antibody were below the threshold required for the nascent B cell to mature, then maturation would either not occur or would need to occur in response to a different immunogen. This lack of guided initiation of the maturation process may provide an explanation for the absence of such broadly neutralizing antibodies in the first few years of infection. Conversely, the introduction of modified gp120s with affinity to genomic precursors and affinity maturation intermediates could provide a mechanism by which to elicit antibodies like VRC01.
40. M. G. Rossmann, *J. Biol. Chem.* **264**, 14587 (1989).
41. T. J. Smith, E. S. Chase, T. J. Schmidt, N. H. Olson, T. S. Baker, *Nature* **383**, 350 (1996).
42. D. Corti *et al*., *PLoS ONE* **5**, e8805 (2010).
43. J. P. Anderson *et al*., *J. Virol.* **74**, 10752 (2000).
44. E. J. Dodson, M. Winn, A. Ralph, *Methods Enzymol.* **277**, 620 (1997).
45. M. L. Connolly, *J. Mol. Graph.* **11**, 139 (1993).
46. D. G. Myszka *et al*., *Proc. Natl. Acad. Sci. U.S.A.* **97**, 9026 (2000).
47. X. Xiao, W. Chen, Y. Feng, D. S. Dimitrov, *Viruses* **1**, 802 (2009).
48. X. Xiao *et al*., *Biochem. Biophys. Res. Commun.* **390**, 404 (2009).
49. M. Pancera *et al*., *J. Virol.* **84**, 8098 (2010).
50. D. S. Dimitrov, *MAbs* **2**, 347 (2010).
51. T.Z., I.G., Z.Y., J.S., L.S., G.J.N., J.R.M., and P.D.K. designed the research; T.Z., I.G., X.W., Z.Y., K.D. A.F., W.S., L.X., Y.Y., and J.Z. performed the research; X.W., Y.K., J.F.S., M.C.N., and J.R.M. contributed new reagents or reference data; T.Z., I.G., X.W., J.S., L.S., G.J.N., J.R.M., and P.D.K. analyzed the data; and T.Z., I.G., J.S., L.S., G.J.N., J.R.M., and P.D.K. wrote the paper, on which all authors commented. We thank I. A. Wilson and members of the Structural Biology Section and Structural Bioinformatics Core, Vaccine Research Center, for discussions and comments on the manuscript; the staff of sector 22 for assistance with data collection; and J. Stuckey for assistance with figures. Support for this work was provided by the Intramural Research Program of NIH and by grants from NIH and from the International AIDS Vaccine Initiative's Neutralizing Antibody Consortium. Use of sector 22 (Southeast Region Collaborative Access team) at the Advanced Photon Source was supported by the U.S. Department of Energy, Basic Energy Sciences, Office of Science, under contract W-31-109-Eng-38. Coordinates and structure factors for the VRC01-gp120 complex have been deposited with the PDB under accession code 3NGB.

Supporting Online Material

www.sciencemag.org/cgi/content/full/science.1192819/DC1
Materials and Methods
Figs. S1 to S16
Tables S1 to S14
References
Appendix S1

25 May 2010; accepted 1 July 2010
Published online 8 July 2010;
10.1126/science.1192819
Include this information when citing this paper.

REPORTS

Gamma-Ray Emission Concurrent with the Nova in the Symbiotic Binary V407 Cygni

The Fermi-LAT Collaboration*†

Novae are thermonuclear explosions on a white dwarf surface fueled by mass accreted from a companion star. Current physical models posit that shocked expanding gas from the nova shell can produce x-ray emission, but emission at higher energies has not been widely expected. Here, we report the Fermi Large Area Telescope detection of variable γ-ray emission (0.1 to 10 billion electron volts) from the recently detected optical nova of the symbiotic star V407 Cygni. We propose that the material of the nova shell interacts with the dense ambient medium of the red giant primary and that particles can be accelerated effectively to produce π^0 decay γ-rays from proton-proton interactions. Emission involving inverse Compton scattering of the red giant radiation is also considered and is not ruled out.

V407 Cygni (V407 Cyg) is a binary system consisting of a Mira-type pulsating red giant (RG) with a white dwarf (WD) companion; these properties place it among the class of symbiotic binaries (*1*). Though one of the more active symbiotic systems, V407 Cyg has historically shown an optical spectrum in quiescence dominated by the Mira-like RG (M6 III) and only weak emission lines [see, for example, (*2*)]. Its infrared continuum (consistent with a dusty wind) and maser emission (*3*) are detected at levels similar to other symbiotic Miras [for instance, R Aqr (*4*)]. One outstanding anomaly of V407 Cyg is a strong Li I λ6707 line indicative of an overabundance of Li relative to normal Mira RGs (*5*, *6*). Based on the 745-day pulsation period of the RG (*7*) and the Mira period-luminosity relation (*8*), we adopt the distance D = 2.7 kpc, estimated as the mean derived from photometry in three near-infrared bands, assuming an extinction E_{B-V} = 0.57 (*2*).

A nova outburst from V407 Cyg was detected on 10 March 2010 (*9*); it had a magnitude of ~6.9 in an unfiltered charge-coupled device image obtained at 19:08 UT. Subsequent densely sampled observations show that the outburst was followed by a smooth decay, though the precise epoch of the nova is formally uncertain by up to 3 days, due to the time gap from the pre-outburst image (Fig. 1). Monitoring of the source over the past 2 years indicates pre-outburst magnitude values in the range of 9 to 12 [see the supporting online material (SOM)]. V407 Cyg has been monitored optically for decades and has shown earlier signs of optical brightening on month-long time scales by one to two magnitudes in the B and V bands (around 1936 and 1998) from typical V-band magnitudes of 13 to 16 (*2*, *10*, *11*), but the magnitude of the recent nova was unprecedented.

Here, we report on a high-energy γ-ray source (Fig. 2) positionally coincident with V407 Cyg detected after the nova (*12*) during routine automated processing of all-sky monitoring data from the Fermi Large Area Telescope (LAT) (*13*). A γ-ray light curve (1-day time bins) of this source generated from an analysis of all LAT data reveals that the first significant detection (4.3σ) was, in fact, on 10 March, indicating that the γ-ray activity began on the same day as the reported optical maximum of V407 Cyg (Fig. 1; see also SOM). The observed 10 March flux is up to a factor of 3 larger than the 1-day upper limits (unless otherwise noted, 95% confidence limits are reported throughout) on the pre-outburst days. To further isolate the onset of detectable γ-ray emission, we divided the 10 March data into 6-hour intervals,

*All authors with their affiliations appear at the end of this paper.
†To whom correspondence should be addressed. E-mail: Teddy.Cheung.ctr@nrl.navy.mil (C.C.C.); Adam.Hill@obs.ujf-grenoble.fr (A.B.H.); Pierre.Jean@cesr.fr (P.J.); srazzaque@ssd5.nrl.navy.mil (S.R.); Kent.Wood@nrl.navy.mil (K.S.W.)

and the first indication of a signal was a marginal detection in the 12- to 18-hour bin (2.8σ). This was followed by a highly significant detection (at 5.7σ) in the last 6-hours bin (18 to 24 hours), which had a peak flux that was a factor of ≳3 larger than that of the marginal detection and the limits from earlier in the day (see SOM). The initial detection of the γ-ray source by the Fermi-LAT in the latter 12 hours of 10 March is consistent with the time of the optical nova discovery.

The peak flux in γ-rays (defined in 1-day segments) was observed between 13 to 14 March, 3 to 4 days after the initial γ-ray detection, and with a flux (9×10^{-7} photons cm^{-2} s^{-1}) that was greater than that observed on 10 March by a factor of 2. The data was analyzed up to mid-April, and the last day with a significant detection (>3σ) of the variable γ-ray source was 25 March, amounting to a total lifetime of activity of 2 weeks. Defining an "active" period (*14*) from 10 March 18:00 to 29 March 00:00, we obtained a γ-ray position (Fig. 2) from the cumulative exposure that is 0.040° offset from the optical position of V407 Cyg, which is within the LAT 95% confidence circle (radius = 0.062°). The average spectral energy distribution (SED) of the Fermi-LAT γ-ray source during the defined active period can be described with an exponentially cut-off power-law model (see SOM) with a flux (>100 MeV) of $(4.4 \pm 0.4) \times 10^{-7}$ photons cm^{-2} s^{-1} (and an overall source significance of 18.1σ). A likelihood-ratio test indicates that the addition of the exponential cut-off improves the fit at the 4.9σ level compared with a simpler single–power-law model. We find no evidence for spectral variability over the duration of the active γ-ray period (see SOM). Our analysis of the data from the 2 weeks after the active period (29 March to 12 April) collectively gives a significance of only 1.6σ (and a flux upper limit of 0.8×10^{-7} photons cm^{-2} s^{-1}), indicating that the flux has declined below the level of detectability. Overall, the γ-ray source is brightest at earlier times, consistent with the optical behavior of V407 Cyg. The coincident localization and the observed correlated variability imply that the optical nova is the source of the variable γ-ray flux.

Nuclear γ-ray lines and continuum emission from novae at ≲1-MeV energies have been considered (*15*), but the Fermi-LAT detection of V407 Cyg shows unequivocally that novae can generate high-energy (>100 MeV) γ-rays. The >100-MeV γ-ray luminosity, its spectrum, and its light curve can be understood broadly as consequences of shock acceleration taking place in a nova shell. Such a nova shell is produced by thermonuclear energy release on the WD and initially expands freely into a very dense medium consisting of the RG wind and atmosphere present in the binary system prior to the nova. The radio source detected from V407 Cyg over 22 to 28 March (*16*, *17*) and subsequent imaging, which revealed the emission to be predominantly extended at a few milli–arc seconds resolution (*18*), is consistent with a picture of an extended shell, as was found in the 2006 RS Ophiuchi nova outburst (*19*, *20*).

An initially spherical shell can sweep up mass from the companion RG wind asymmetrically and will reach a deceleration phase during which it expands adiabatically (*21*) with different temporal behavior in different directions from the WD center. Fermi acceleration of protons and electrons takes place in the outgoing nova shock during both the free-expansion and deceleration phases, and we show that the measured γ-ray spectrum can be explained by π^0 decay γ-rays from proton-proton (pp) collisions or inverse Compton (IC) scattering of infrared photons from the RG by electrons. In both of these scenarios, the γ-ray light curve, in conjunction with the delayed rise of the x-ray flux, can be explained qualitatively as a geometrical effect of the nova-shell evolution.

The measured optical peak magnitude of 7 of V407 Cyg (*9*) over 1 day implies an energy release of $\gtrsim 3 \times 10^{42}$ ergs at visible frequencies (after extinction correction). The kinetic energy of the ejecta in the nova shell, $\varepsilon_k \sim 10^{44}$ ergs, can be estimated assuming a nova-shell mass $M_{ej} \sim 10^{-6} M_\odot$ [which is a plausible value for a massive WD > $1.25 M_\odot$ (*22*, *23*), where $M_\odot$ is the mass of the Sun] and the velocity $v_{ej} = 3200 \pm 345$ km s^{-1}, inferred from an Hα atomic emission line-width measurement on 14 March (see SOM). The velocity of the outgoing shock wave is initially $v_{sh} \sim v_{ej}$. The onset of the deceleration phase and subsequent evolution of the shock wave are determined by the density of the RG stellar wind and atmosphere surrounding the nova shell, which depend on two poorly constrained parameters: (i) the WD-RG separation (a) and (ii) the RG mass-loss rate in the wind ($\dot{M}_W$). As we will discuss shortly, the detection of the γ-ray flux within 1 day of the optical detection of the nova, a peak duration of 3 to 4 days, and subsequent decay within 15 days after the optical nova can be modeled as emission from the nova shell in a dense environment and

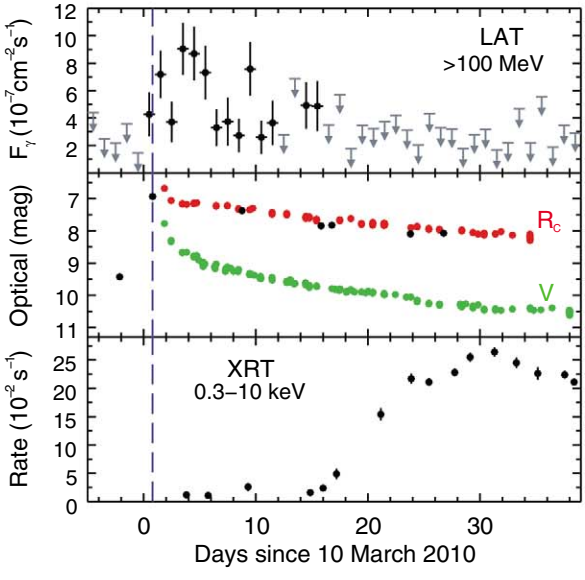


Fig. 1. Light curves of V407 Cyg in γ-rays from the Fermi-LAT (**top**), optical (**middle**), and x-rays from Swift (**bottom**). Vertical bars indicate 1σ statistics errors for all data (the errors are smaller than the points in the optical section). For the γ-ray data, gray arrows indicate 2σ upper limits, and horizontal bars indicate the 1-day binning. In the optical section, unfiltered (black), R_C (red), and V (green) band magnitudes are shown (see SOM). The vertical dashed blue line indicates the epoch of the optical nova detection; the γ-ray peak occurred 3 to 4 days later. $F\gamma$, γ-ray flux; XRT, Swift X-ray Telescope.

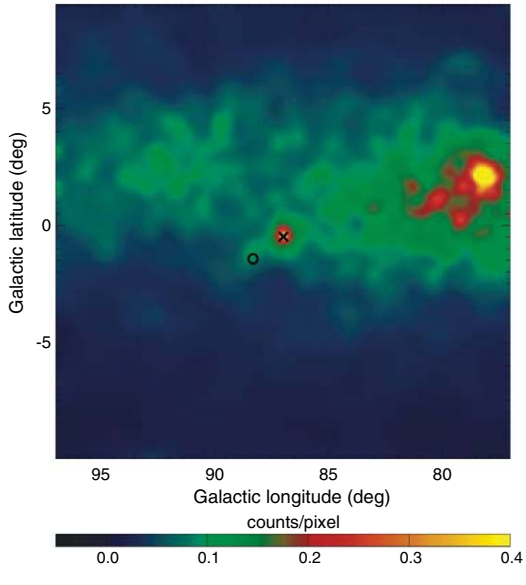


Fig. 2. Fermi-LAT γ-ray counts (200 MeV to 100 GeV) map from 10 March 18:00 to 29 March 00:00 2010 in the region around the position of the γ-ray nova source V407 Cyg (marked by the black cross) at Galactic longitude l = 86.958°, Galactic latitude b = −0.513° (right ascension = 315.551°, declination = +45.737°, J2000.0). The map was adaptively smoothed by imposing a minimum signal-to-noise ratio of 7. The closest known γ-ray source is contained in the first-year LAT catalog (1FGL J2111.3+4607; marked by the black circle) (*29*), ~1.5° away from the star's optical position. The bright source at l = 78.2°, b = +2.1° is LAT PSR J2021+4026. deg, degrees.

mostly from along the WD-RG axis, assuming an inverse-square law wind-density profile from the RG center, with $a \sim 10^{14}$ cm and $\dot{M}_W \sim 3 \times 10^{-7} M_\odot$ year^{-1}. Both of these values are a factor ≈ 2 smaller than those suggested previously for the V407 Cyg system (*2*).

The density of particles in the RG wind is $n(R) = \dot{M}_W [4\pi(R^2 + a^2 - 2aR\cos\theta) v_W \overline{m}]^{-1}$. Here, the RG wind velocity, $v_w \approx 10$ km s^{-1}, is based on optical spectra (see SOM), the mean particle mass is $\overline{m} \approx 10^{-24}$ g, R is the distance from the WD center, and θ is the polar angle relative to the WD center. The energy density in the RG radiation field is, similarly, $u_{IR}(R) = L_{IR}[4\pi(R^2 + a^2 - 2aR\cos\theta)c]^{-1}$, where c is the speed of light. The RG luminosity, $L_{IR} \approx 10^4 L_\odot$ (where $L_\odot$ is the luminosity of the Sun) (*2*, *11*), is consistent with a spectral fit to post-nova infrared measurements with a temperature of ≈ 2500 K (see SOM). Near the WD surface ($R \approx 0.01 R_\odot$, where $R_\odot$ is the radius of the Sun), these densities are $n \sim 10^8$ cm^{-3} and $u_{IR} \sim 0.01$ erg cm^{-3}, and they increase by up to one order of magnitude when the nova shell approaches the RG surface (that is, along θ ≈ 0°) at a radius $r_{RG} \approx 500\ R_\odot$. An equipartition of the energy density in the magnetic field expected to arise from turbulent motions in the wind to the thermal energy density in the RG wind with temperature $T_w \approx 700$ K (*2*) gives a mean magnetic field $B_{sh}(R) = [32\pi n(R) k T_w]^{1/2} \sim 0.03$ G (here, k is the Boltzmann constant) in the shock wave when it is near the WD. Electrons and protons can be accelerated efficiently in this magnetic field (*24*) and interact with the surrounding RG wind particles and radiation.

The time scale for pp interactions for a π^0 model to produce γ-rays in the shock wave is $t_{pp} \approx 1/[4n(R)c\sigma_{pp}] \sim 2.8 \times 10^6$ s when the nova shell is near the WD. Here, $\sigma_{pp} \approx 3 \times 10^{-26}$ cm^2 is the pp cross section. Thus, $t/t_{pp} \sim 3\%$ of the protons can interact to produce π^0 emission on a time scale $t = 1$ day. In an IC scenario, the cooling time scale for electrons with energy $E_e \approx 5$ GeV that upscatter 2500-K photons to ≈ 100 MeV is $t_{IC} = (3/4) m_e^2 c^3 [\sigma_T E_e u_{IR}(R)]^{-1} \sim 3.1 \times 10^5$ s (here, m_e is the mass of the electron, and σ_T is the Thomson electron scattering cross section). Thus, $t/t_{IC} \sim 28\%$ of the electrons produce γ-rays efficiently in a time scale $t = 1$ day. The efficiency for γ-ray production in both the π^0 and IC models increases substantially in the part of the nova shell that expands toward the RG (θ ~ 0°) and reaches the deceleration phase, by accumulating RG wind and atmospheric material of mass equal to M_{ej}, at a distance ~ 7×10^{13} cm in ~2.5 days. The efficiency decreases rapidly in the part of the shell that expands away from the RG (θ ≥ 90°) because of a decreasing density in both the RG wind and radiation.

In our scenario, most of the γ-rays come from the part of the nova shell approaching the RG. This can qualitatively explain the basic features of the γ-ray light curve (Fig. 1): (i) its onset within days of the optical nova and the peak flux reached in 3 days due to an increasing efficiency for pp interactions and an increasing volume of the shock-accelerated particles and (ii) the decline in the flux after ~5 days due to weakening of the shock wave after reaching the deceleration phase. A highly significant 1-day detection (6.5σ) of an increase in γ-ray flux 9 days after the nova discovery (Fig. 1) could be due to the nova shell hitting a part of the RG surface or a nearby remnant of high density with a size scale of $\sim 10^{13} (v_{sh}/1500\ \text{km s}^{-1})(t/1\ \text{day})$ cm.

A representative π^0 decay model fitting the LAT data with a cosmic-ray proton spectrum in the form of an exponentially cut-off power-law $N_p = N_{p,0}(W_p + m_p c^2)^{-s_p} e^{-W_p/E_{cp}}$ (where E_{cp}, W_p, and m_p are the cut-off energy, kinetic energy, and mass of the proton, respectively) is shown in Fig. 3. The γ-ray spectrum is well reproduced with a spectral index $s_p = 2.15^{+0.45}_{-0.28}$, similar to the expected spectrum from the Fermi acceleration mechanism, with $E_{cp} = 32^{+85}_{-8}$ GeV (1σ uncertainties) (see SOM). The total energy in γ-rays above 100 MeV integrated over the active period is $\varepsilon_\gamma \approx 3.6 \times 10^{41}$ erg. The total energy in protons is $\varepsilon_p \approx \epsilon_p^{-1} \langle E_p/E_\gamma \rangle \varepsilon_\gamma$, where ϵ_p is the mean efficiency for pp interactions and $1/\langle E_p/E_\gamma \rangle \approx 0.2$ is the mean fraction of proton energy transfer to γ-rays per interaction in the $E_\gamma \geq 100$ MeV range. The ratio of the total energy in protons that produce γ-rays to the kinetic energy ($\varepsilon_p/\varepsilon_k \sim 9\%$), with $\epsilon_p \sim 0.2$ averaged over the γ-ray source lifetime of 15 days and the whole nova shell, is similar to 1 to 10% estimated in supernova remnants (*25*). The ratio, however, is larger when considering dominant γ-ray emission coming mostly from the part of the shell that expands toward the RG.

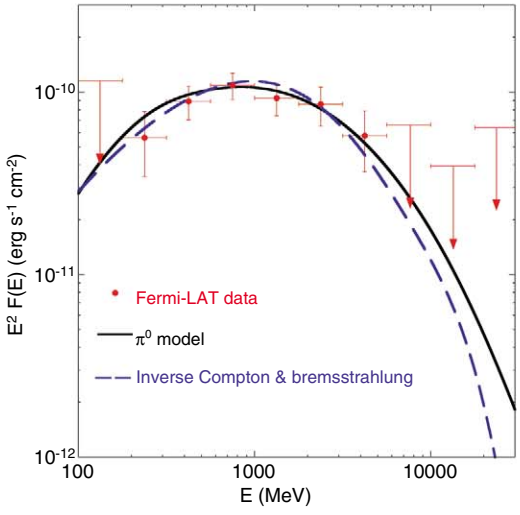


Fig. 3. SED of V407 Cyg in million electron volt/billion electron volt γ-rays measured by the Fermi-LAT instrument over the period from 10 March 18:00 to 29 March 00:00 2010. Vertical bars indicate 1σ statistical errors, red arrows indicate 2σ upper limits, and horizontal bars indicate energy ranges. The best-fit π^0 (black solid line) and leptonic (blue dashed line) models are indicated.

The leptonic model is represented in Fig. 3 as the total of the IC spectrum plus a small contribution from bremsstrahlung emission that arises from the scattering of electrons with protons of density $n(R)$ in the shock wave (see SOM). The exponentially cut-off power-law electron spectrum, $N_e = N_{e,0} W_e^{-s_e} e^{-W_e/E_{ce}}$, where E_{ce} and W_e are the cut-off energy and kinetic energy of electrons (in billion electron volts), respectively, reproduces the γ-ray spectrum with a spectral index $s_e = -1.75^{+2.40}_{-0.59}$ and $E_{ce} = 3.2^{+2.6}_{-0.1}$ GeV (1σ uncertainties) (see SOM). The total number of electrons emitting in the steady state is $N_{e,0} \approx 4 \times 10^{42}$ electrons, with a mean energy of 8.7 GeV, which is larger than E_{ce} because of the steep spectrum. The total energy in electrons over 15 days of γ-ray emission is $\varepsilon_e \approx 4 \times 10^{41}$ ergs, averaged over the nova shell. Thus, the total energy in electrons that produce γ-rays in the IC model is a small fraction of the kinetic energy in the shell ($\varepsilon_e/\varepsilon_k \sim 0.4\%$).

X-ray emission detected from V407 Cyg with the Swift X-ray Telescope as early as 3 days after the onset of the optical nova (Fig. 1) is probably due to shock-heating of ambient gas (*26*, *27*). The x-ray flux starts rising substantially about 2 weeks after the nova, coinciding with when the γ-ray flux declines below the level of detectability. In our geometric scenario, the sharply rising x-ray flux is due to the increasing volume of shocked gas in the nova shell expanding in the direction away from the RG. The x-ray flux peaks about 30 days after the explosion, and its subsequent slow decline is consistent with the longer time scale of the deceleration phase.

The Fermi-LAT detection of V407 Cyg was a surprise and adds novae as a source class to the high-energy γ-ray sky. The particle acceleration mechanism and the γ-ray emission scenarios outlined here require the mass donor to be a RG; that is, a nova in a symbiotic system. Interestingly, several symbiotic stars are known to be recurrent novae (i.e., systems observed to have undergone multiple thermonuclear runaways within the last century), and recurrent novae are often considered candidate progenitors of type Ia supernovae (*28*). V407 Cyg may also belong to this class of binaries, and we have adopted parameters that are consistent with such a classification in modeling the γ-ray emission. In general, these sources can have dramatic influence on the local interstellar medium and Galactic cosmic rays, but few binary systems with a WD are known to have a similar environment; hence, we expect γ-ray novae to be rare.

References and Notes

1. S. J. Kenyon, in *Evolutionary Processes in Interacting Binary Stars*, Y. Kondo *et al*., Eds., International Astronomical Union (IAU) Symposium, vol. 151 (IAU, Kluwer Academic, Dordrecht, Netherlands, 1992), p. 137.
2. U. Munari, R. Margoni, R. Stagni, *Mon. Not. R. Astron. Soc.* **242**, 653 (1990).
3. S. Deguchi, J.-I. Nakashima, T. Miyata, Y. Ita, *Publ. Astron. Soc. Jpn.* **57**, 933 (2005).
4. R. J. Ivison, E. R. Seaquist, P. J. Hall, *Mon. Not. R. Astron. Soc.* **269**, 218 (1994).
5. S. Y. Shugarov, A. A. Tatarnikova, E. A. Kolotilov, V. I. Shenavrin, B. F. Yudin, *Balt. Astron.* **16**, 23 (2007).
6. A. A. Tatarnikova *et al*., *Mon. Not. R. Astron. Soc.* **344**, 1233 (2003).
7. L. Meinunger, *Mitt. Veranderl. Sterne.* **87**, 111 (1966).
8. I. S. Glass, M. W. Feast, *Mon. Not. R. Astron. Soc.* **199**, 245 (1982).
9. K. Nishiyama, F. Kabashima, International Astronomical Union Central Bureau for Astronomical Telegrams, reported by H. Maehara, no. 2199 (2010).
10. C. Hoffmeister, *Veröff. Sternw. Sonneberg.* **1**, 295 (1949).
11. E. A. Kolotilov, V. I. Shenavrin, S. Y. Shugarov, B. F. Yudin, *Astron. Rep.* **47**, 777 (2003).
12. C. C. Cheung *et al*., Fermi-LAT Collaboration, *The Astronomer's Telegram* **2487**, 1 (2010).
13. W. B. Atwood *et al*., *Astrophys. J.* **697**, 1071 (2009).
14. The window was extended by 3 days to include any late low-level emission that would not be detectable on any individual daily bin.
15. M. Hernanz, in *Classical Novae*, M. F. Bode, A. Evans, Eds. (Cambridge Univ. Press, Cambridge, ed. 2, 2008) p. 252.
16. I. Nestoras *et al*., *The Astronomer's Telegram* **2506**, 1 (2010).
17. G. C. Bower, R. Forster, C. C. Cheung, *The Astronomer's Telegram* **2529**, 1 (2010).
18. M. Giroletti *et al*., *The Astronomer's Telegram* **2536**, 1 (2010).
19. T. J. O'Brien *et al*., *Nature* **442**, 279 (2006).
20. M. P. Rupen, A. J. Mioduszewski, J. L. Sokoloski, *Astrophys. J.* **688**, 559 (2008).
21. L. I. Sedov, *Similarity and Dimensional Methods in Mechanics* (Academic Press, New York, 1959).
22. S. Starrfield, W. M. Sparks, J. W. Truran, M. C. Wiescher, *Astrophys. J.* **127** (suppl.), 485 (2000).
23. O. Yaron, D. Prialnik, M. M. Shara, A. Kovetz, *Astrophys. J.* **623**, 398 (2005).
24. V. Tatischeff, M. Hernanz, *Astrophys. J.* **663**, L101 (2007).
25. A. A. Abdo *et al*., *Astrophys. J.* **710**, L92 (2010).
26. J. L. Sokoloski, G. J. M. Luna, K. Mukai, S. J. Kenyon, *Nature* **442**, 276 (2006).
27. J. J. Drake *et al*., *Astrophys. J.* **691**, 418 (2009).
28. W. M. Wood-Vasey, J. L. Sokoloski, *Astrophys. J.* **645**, L53 (2006).
29. A. A. Abdo *et al*., *Astrophys. J.* **188** (suppl.), 405 (2010).

30. The Fermi-LAT Collaboration acknowledges support from a number of agencies and institutes for both the development and operation of the LAT, as well as for scientific data analysis. These organizations include NASA and the U.S. Department of Energy in the United States; CEA/Irfu and IN2P3/CNRS in France; ASI and Istituto Nazionale de Fisica Nucleare in Italy; Ministry of Education, Culture, Sports, Science and Technology (MEXT), High Energy Accelerator Research Organization (KEK), and JAXA in Japan; and the K. A. Wallenberg Foundation, the Swedish Research Council, and the National Space Board in Sweden. We also gratefully acknowledge additional support from INAF in Italy and the Centre National d'Etudes Spatiales in France for science analysis during the operations phase. We acknowledge with thanks the variable star observations from the American Association of Variable Star Observers International Database contributed by observers worldwide and used in this research. J. Conrad is a Royal Swedish Academy of Sciences Research Fellow, funded by a grant from the K. A. Wallenberg Foundation; G.D. and A.B.H. were funded by contract ERC-StG-200911 from the European Community; P.K. was supported by the Astronomical Institute, Academy of Sciences of the Czech Republic (Ondrejov, Czech Republic); and L.T. was partially supported by the International Doctorate on Astroparticle Physics program.

The Fermi-LAT Collaboration

A. A. Abdo,[1,2] M. Ackermann,[3] M. Ajello,[3] W. B. Atwood,[4] L. Baldini,[5] J. Ballet,[6] G. Barbiellini,[7,8] D. Bastieri,[9,10] K. Bechtol,[3] R. Bellazzini,[5] B. Berenji,[3] R. D. Blandford,[3] E. D. Bloom,[3] E. Bonamente,[11,12] A. W. Borgland,[3] A. Bouvier,[3] T. J. Brandt,[13,14] J. Bregeon,[5] A. Brez,[5] M. Brigida,[15,16] P. Bruel,[17] R. Buehler,[3] T. H. Burnett,[18] S. Buson,[9,10] G. A. Caliandro,[19] R. A. Cameron,[3] P. A. Caraveo,[20] S. Carrigan,[10] J. M. Casandjian,[6] C. Cecchi,[11,12] Ö. Çelik,[21,22,23] E. Charles,[3] S. Chaty,[6] A. Chekhtman,[1,24] C. C. Cheung,[1,2]† J. Chiang,[3] S. Ciprini,[12] R. Claus,[3] J. Cohen-Tanugi,[25] J. Conrad,[26,27] S. Corbel,[6,28] R. Corbet,[21,23] M. E. DeCesar,[21,29] P. R. den Hartog,[3] C. D. Dermer,[1] F. de Palma,[15,16] S. W. Digel,[3] D. Donato,[22,29] E. do Couto e Silva,[3] P. S. Drell,[3] R. Dubois,[3] G. Dubus,[30] D. Dumora,[31,32] C. Favuzzi,[15,16] S. J. Fegan,[17] E. C. Ferrara,[21] P. Fortin,[17] M. Frailis,[33,34] L. Fuhrmann,[35] Y. Fukazawa,[36] S. Funk,[3] P. Fusco,[15,16] F. Gargano,[16] D. Gasparrini,[37] N. Gehrels,[21] S. Germani,[11,12] N. Giglietto,[15,16] F. Giordano,[15,16] M. Giroletti,[39] T. Glanzman,[3] G. Godfrey,[3] I. A. Grenier,[6] M.-H. Grondin,[31,32] J. E. Grove,[1] S. Guiriec,[39] D. Hadasch,[40] A. K. Harding,[21] M. Hayashida,[3] E. Hays,[21] S. E. Healey,[3] A. B. Hill,[30]† D. Horan,[17] R. E. Hughes,[14] R. Itoh,[36] P. Jean,[13]† G. Jóhannesson,[3] A. S. Johnson,[3] R. P. Johnson,[4] T. J. Johnson,[21,29] W. N. Johnson,[1] T. Kamae,[3] H. Katagiri,[36] J. Kataoka,[41] M. Kerr,[18] J. Knödlseder,[13] E. Koerding,[6] M. Kuss,[5] J. Lande,[3] L. Latronico,[5] S.-H. Lee,[3] M. Lemoine-Goumard,[31,32] M. Llena Garde,[26,27] F. Longo,[7,8] F. Loparco,[15,16] B. Lott,[31,32] M. N. Lovellette,[1] P. Lubrano,[11,12] A. Makeev,[1,24] M. N. Mazziotta,[16] W. McConville,[21,29] J. E. McEnery,[21,29] J. Mehault,[25] P. F. Michelson,[3] T. Mizuno,[36] A. A. Moiseev,[22,29] C. Monte,[15,16] M. E. Monzani,[3] A. Morselli,[42] I. V. Moskalenko,[3] S. Murgia,[3] T. Nakamori,[41] M. Naumann-Godo,[6] I. Nestoras,[35] P. L. Nolan,[3] J. P. Norris,[43] E. Nuss,[25] M. Ohno,[44] T. Ohsugi,[45] A. Okumura,[44] N. Omodei,[3] E. Orlando,[46] J. F. Ormes,[43] M. Ozaki,[44] D. Paneque,[3] J. H. Panetta,[3] D. Parent,[1,24] V. Pelassa,[25] M. Pepe,[11,12] M. Pesce-Rollins,[5] F. Piron,[25] T. A. Porter,[3] S. Rainò,[15,16] R. Rando,[9,10] P. S. Ray,[1] M. Razzano,[5] S. Razzaque,[1,2]† N. Rea,[19] A. Reimer,[47,3] O. Reimer,[47,3] T. Reposeur,[31,32] J. Ripken,[26,27] S. Ritz,[4] R. W. Romani,[3] M. Roth,[18] H. F.-W. Sadrozinski,[4] A. Sander,[14] P. M. Saz Parkinson,[4] J. D. Scargle,[48] F. K. Schinzel,[35] C. Sgrò,[5] M. S. Shaw,[3] E. J. Siskind,[49] D. A. Smith,[31,32] P. D. Smith,[14] K. V. Sokolovsky,[35,50] G. Spandre,[5] P. Spinelli,[15,16] Ł. Stawarz,[44,51] M. S. Strickman,[1] D. J. Suson,[52] H. Takahashi,[45] T. Takahashi,[44] T. Tanaka,[3] Y. Tanaka,[44] J. B. Thayer,[3] J. G. Thayer,[3] D. J. Thompson,[21] L. Tibaldo,[9,10,6] D. F. Torres,[19,40] G. Tosti,[11,12] A. Tramacere,[3,53,54] Y. Uchiyama,[3] T. L. Usher,[3] J. Vandenbroucke,[3] V. Vasileiou,[22,23] N. Vilchez,[13] V. Vitale,[42,55] A. P. Waite,[3] E. Wallace,[18] P. Wang,[3] B. L. Winer,[14] M. T. Wolff,[1] K. S. Wood,[1]† Z. Yang,[26,27] T. Ylinen,[56,57,27] M. Ziegler,[4] H. Maehara,[58] K. Nishiyama,[59] F. Kabashima,[59] U. Bach,[35] G. C. Bower,[60] A. Falcone,[61] J. R. Forster,[60,62] A. Henden,[63] K. S. Kawabata,[45] P. Koubsky,[64] K. Mukai,[21,23] T. Nelson,[21,23] S. R. Oates,[65] K. Sakimoto,[36] M. Sasada,[36] V. I. Shenavrin,[66] S. N. Shore,[5,67] G. K. Skinner,[22,29] J. Sokoloski,[68] M. Stroh,[59] A. M. Tatarnikov,[66] M. Uemura,[45] G. M. Wahlgren,[69,21] M. Yamanaka[36]

[1]Space Science Division, Naval Research Laboratory, Washington, DC 20375, USA. [2]National Research Council Research Associate, National Academy of Sciences, Washington, DC 20001, USA. [3]W. W. Hansen Experimental Physics Laboratory, Kavli Institute for Particle Astrophysics and Cosmology, Department of Physics and SLAC National Accelerator Laboratory, Stanford University, Stanford, CA 94305, USA. [4]Santa Cruz Institute for Particle Physics, Department of Physics and Department of Astronomy and Astrophysics, University of California at Santa Cruz, Santa Cruz, CA 95064, USA. [5]Istituto Nazionale di Fisica Nucleare, Sezione di Pisa, I-56127 Pisa, Italy. [6]Laboratoire AIM, CEA-IRFU/CNRS/Université Paris Diderot, Service d'Astrophysique, CEA Saclay, 91191 Gif sur Yvette, France. [7]Istituto Nazionale di Fisica Nucleare, Sezione di Trieste, I-34127 Trieste, Italy. [8]Dipartimento di Fisica, Università di Trieste, I-34127 Trieste, Italy. [9]Istituto Nazionale di Fisica Nucleare, Sezione di Padova, I-35131 Padova, Italy. [10]Dipartimento di Fisica "G. Galilei," Università di Padova, I-35131 Padova, Italy. [11]Istituto Nazionale di Fisica Nucleare, Sezione di Perugia, I-06123 Perugia, Italy. [12]Dipartimento di Fisica, Università degli Studi di Perugia, I-06123 Perugia, Italy. [13]Centre d'Étude Spatiale des Rayonnements, CNRS/UPS, BP 44346, F-30128 Toulouse Cedex 4, France. [14]Department of Physics, Center for Cosmology and Astro-Particle Physics, The Ohio State University, Columbus, OH 43210, USA. [15]Dipartimento di Fisica "M. Merlin" dell'Università e del Politecnico di Bari, I-70126 Bari, Italy. [16]Istituto Nazionale di Fisica Nucleare, Sezione di Bari, 70126 Bari, Italy. [17]Laboratoire Leprince-Ringuet, École polytechnique, CNRS/IN2P3, Palaiseau, France. [18]Department of Physics, University of Washington, Seattle, WA 98195–1560, USA. [19]Institut de Ciencies de l'Espai (IEEC-CSIC), Campus UAB, 08193 Barcelona, Spain. [20]Istituto Nazionale di Astrofisica (INAF)–Istituto di Astrofisica Spaziale e Fisica Cosmica, I-20133 Milano, Italy. [21]NASA Goddard Space Flight Center, Greenbelt, MD 20771, USA. [22]Center for Research and Exploration in Space Science and Technology and NASA Goddard Space Flight Center, Greenbelt, MD 20771, USA. [23]Department of Physics and Center for Space Sciences and Technology, University of Maryland Baltimore County, Baltimore, MD 21250, USA. [24]George Mason University, Fairfax, VA 22030, USA. [25]Laboratoire de Physique Théorique et Astroparticules, Université Montpellier 2, CNRS/IN2P3, Montpellier, France. [26]Department of Physics, Stockholm University, AlbaNova, SE-106 91 Stockholm, Sweden. [27]The Oskar Klein Centre for Cosmoparticle Physics, AlbaNova, SE-106 91 Stockholm, Sweden. [28]Institut universitaire de France, 75005 Paris, France. [29]Department of Physics and Department of Astronomy, University of Maryland, College Park, MD 20742, USA. [30]Université Joseph Fourier–Grenoble 1/CNRS, laboratoire d'Astrophysique de Grenoble UMR 5571, BP 53, 38041 Grenoble Cedex 09, France. [31]CNRS/IN2P3, Centre d'Études Nucléaires Bordeaux Gradignan, UMR 5797, Gradignan, 33175, France. [32]Université de Bordeaux, Centre d'Études Nucléaires Bordeaux Gradignan, UMR 5797, Gradignan, 33175, France. [33]Dipartimento di Fisica, Università di Udine and Istituto Nazionale di Fisica Nucleare, Sezione di Trieste, Gruppo Collegato di Udine, I-33100 Udine, Italy. [34]Osservatorio Astronomico di Trieste, Istituto Nazionale di Astrofisica, I-34143 Trieste, Italy. [35]Max-Planck-Institut für Radioastronomie, Auf dem Hügel 69, 53121 Bonn, Germany. [36]Department of Physical Sciences, Hiroshima University, Higashi-Hiroshima, Hiroshima 739-8526, Japan. [37]Agenzia Spaziale Italiana (ASI) Science Data Center, I-00044 Frascati (Roma), Italy. [38]INAF Istituto di Radioastronomia, 40129 Bologna, Italy. [39]Center for Space Plasma and Aeronomic Research, University of Alabama in Huntsville, Huntsville, AL 35899, USA. [40]Institució Catalana de Recerca i Estudis Avançats, Barcelona, Spain. [41]Research Institute for Science and Engineering, Waseda University, 3-4-1, Okubo, Shinjuku, Tokyo, 169-8555 Japan. [42]Istituto Nazionale di Fisica Nucleare, Sezione di Roma "Tor Vergata," I-00133 Roma, Italy. [43]Department of Physics and Astronomy, University of Denver, Denver, CO 80208, USA. [44]Institute of Space and Astronautical Science, Japanese Aerospace Exploration Agency (JAXA), 3-1-1 Yoshinodai, Sagamihara, Kanagawa 229-8510, Japan. [45]Hiroshima Astrophysical Science Center, Hiroshima University, Higashi-Hiroshima, Hiroshima 739-8526, Japan. [46]Max-Planck Institut für extraterrestrische Physik, 85748 Garching, Germany. [47]Institut für Astro- und Teilchenphysik and Institut für Theoretische Physik, Leopold-Franzens-Universität Innsbruck, A-6020 Innsbruck, Austria. [48]Space Sciences Division, NASA Ames Research Center, Moffett Field, CA 94035–1000, USA. [49]NYCB Real-Time Computing, Lattingtown, NY 11560–1025, USA. [50]Astro Space Center of the Lebedev Physical Institute, 117810 Moscow, Russia. [51]Astronomical Observatory, Jagiellonian University, 30-244 Kraków, Poland. [52]Department of Chemistry and Physics, Purdue University Calumet, Hammond, IN 46323–2094, USA. [53]Consorzio Interuniversitario per la Fisica Spaziale, I-10133 Torino, Italy. [54]INTEGRAL Science Data Centre, CH-1290 Versoix, Switzerland. [55]Dipartimento di Fisica, Università di Roma "Tor Vergata," I-00133 Roma, Italy. [56]Department of Physics, Royal Institute of Technology, AlbaNova, SE-106 91 Stockholm, Sweden. [57]School of Pure and Applied Natural Sciences, University of Kalmar, SE-391 82 Kalmar, Sweden. [58]Kwasan and Hida Observatories, Kyoto University, Kyoto 607-8471, Japan. [59]Miyaki-Argenteus Observatory, Miyaki-cho, Saga-ken, Japan. [60]Department of Astronomy, University of California, Berkeley, CA 94720–3411, USA. [61]Department of Astronomy and Astrophysics, Pennsylvania State University, University Park, PA 16802, USA. [62]Hat Creek Observatory, Hat Creek, CA 96040, USA. [63]American

Association of Variable Star Observers, Cambridge, MA 02138, USA. [64]Astronomical Institute, Academy of Sciences of the Czech Republic, Ondrejov, Czech Republic. [65]Mullard Space Science Laboratory, University College London, Holmbury St. Mary, Dorking, Surrey, RH5 6NT, UK. [66]Sternberg Astronomical Institute, Moscow University, Moscow, Russia. [67]Dipartimento di Fisica "Enrico Fermi," Università di Pisa, Pisa I-56127, Italy. [68]Columbia Astrophysics Laboratory, Columbia University, New York, NY 10027, USA. [69]Catholic University of America, Washington, DC 20064, USA.

Supporting Online Material
www.sciencemag.org/cgi/content/full/329/5993/817/DC1
Materials and Methods
SOM Text
Figs. S1 to S6
Tables S1 to S3
References

19 May 2010; accepted 12 July 2010
10.1126/science.1192537

Quantum Oscillations and Hall Anomaly of Surface States in the Topological Insulator Bi_2Te_3

Dong-Xia Qu,[1]* Y. S. Hor,[2] Jun Xiong,[1] R. J. Cava,[2] N. P. Ong[1]*

Topological insulators are insulating materials that display massless, Dirac-like surface states in which the electrons have only one spin degree of freedom on each surface. These states have been imaged by photoemission, but little information on their transport parameters, for example, mobility, is available. We report the observation of Shubnikov–de Haas oscillations arising from the surface states in nonmetallic crystals of Bi_2Te_3. In addition, we uncovered a Hall anomaly in weak fields, which enables the surface current to be seen directly. Both experiments yield a surface mobility (9000 to 10,000 centimeter^2 per volt-second) that is substantially higher than in the bulk. The Fermi velocity of 4×10^5 meters per second obtained from these transport experiments agrees with angle-resolved photoemission experiments.

Recently, the existence of a new class of bulk insulators called topological insulators has been predicted (*1*–*6*). In a topological insulator, the bulk energy gap is traversed by surface states in which the spin of the electron is locked perpendicular to its momentum by strong spin-orbit interaction. On each surface, the electrons have only one spin degree of freedom (fixed helicity). The spin-resolved nature of the surface states has been confirmed in angle-resolved photoemission spectroscopy (ARPES) experiments on BiSb (*7*), Sb (*8*), Bi_2Se_3 (*9*), and Bi_2Te_3 (*10*). The spin locking in BiSb has also been studied by scanning tunneling microscopy (*11*). However, it has been a challenge to resolve the conductance of the surface states from the dominant bulk contribution (*12*, *13*). The lack of transport information, especially the mobility, is a serious hindrance. Moreover, detection of the surface currents is a crucial first step in the investigation of phenomena, such as the Majorana fermion (*5*) and unconventional electrodynamics (*6*), in topological insulators.

We report dual evidence for surface state conduction in Bi_2Te_3 from Shubnikov–de Haas (SdH) oscillations and from the weak-field Hall effect. As in the case of the selenide Bi_2Se_3 (*12*), as-grown crystals of Bi_2Te_3 usually display a metallic resistivity ρ versus temperature T (in Bi_2Te_3, the Fermi energy E_F lies in the valence band VB). By selective cleaving of many crystals from a boule of Bi_2Te_3 grown with a weak compositional gradient (*14*), we have obtained nonmetallic crystals (Fig. 1A). In the nonmetallic samples Q1, Q2, and Q3, ρ rises when T is lowered below 150 K and saturates to values 4 to 5 mohm cm at 4 K or ~50 times larger than the value in the metallic sample N1. The surface state dispersion obtained by ARPES (*10*) is sketched in Fig. 1B, with E_F in our samples indicated. Even in the most resistive sample Q3, the bulk conductance is ~300 times larger than the surface term (see below). Nonetheless, the latter may be resolved by detecting the SdH oscillations in the resistivity and the Hall resistivity ρ_{yx} at low T. Quantum oscillations are well resolved in the raw trace of the Hall conductivity $\sigma_{xy} = \rho_{yx}/(\rho_{xx}^2 + \rho_{yx}^2)$ measured at $T = 0.3$ K (Fig. 1, C and D). In metals, SdH oscillations correspond to successive emptying of Landau levels (LL) as the magnetic field H is increased. The LL index n is related to the extremal cross section S_F of the Fermi surface (FS) by

$$2\pi(n + \gamma) = S_F \frac{\hbar}{eB} \qquad (1)$$

where $\gamma = 0$ or ½, e is the electron charge, h is Planck's constant ($\hbar = h/2\pi$), and B is the magnetic flux density.

For a two-dimensional (2D) FS, the peak positions depend only on the field component $H_\perp = H\cos\theta$ along the axis **c** normal to the cleavage plane (θ is the tilt angle between **H** and **c**). To

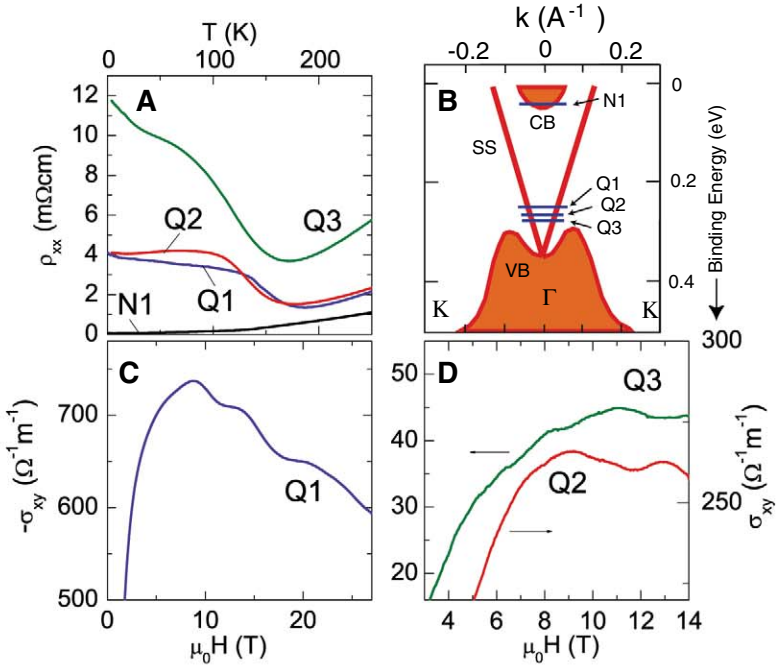


Fig. 1. (**A**) The resistivity profiles ρ versus temperature T of samples Q1, Q2, Q3, and N1. (**B**) Sketch of the surface state dispersion near the Γ point [traced from (*10*)]. The Fermi energies of samples Q1, Q2, Q3, and N1 are indicated by short lines (CB, conduction band). Curves of the Hall conductivity σ_{xy} versus the magnetic field H in sample Q1 (**C**) and in samples Q2 and Q3 (**D**) showing well-resolved SdH oscillations. μ_0 is the permeability.

[1]Department of Physics, Princeton University, Princeton, NJ 08544, USA. [2]Department of Chemistry, Princeton University, Princeton, NJ 08544, USA.

*To whom correspondence should be addressed. E-mail: dqu@princeton.edu (D.-X.Q.); npo@princeton.edu (N.P.O.)

test this hypothesis, we tracked how the SdH extrema shift with θ, in fields up to 30 T [supporting online material (SOM) section S2]. We compare the derivative $d\rho_{xx}/dH$ in nonmetallic Q1 with that in the metallic sample N1 (Fig. 2, A and B, respectively). In sample Q1, the period of the oscillations depends only on $H_\perp$: The magnetic field corresponding to the $n = 3$ minimum varies with θ as 1/cosθ up to 65° (Fig. 1C). For $65° < \theta < 90°$, the oscillations are not resolved. By contrast, the oscillations in N1 survive up to $\theta = 90°$ (Fig. 1B). As $\theta \rightarrow 90°$, S_F in N1 deviates strongly from the 1/cosθ trend, to saturate at a value ~1.5× larger than that at θ = 0. From the comparison, we conclude that the quantum oscillations in the nonmetallic sample arise from a 2D FS (SOM section S2).

To extract more specific information on the surface states, we next analyzed how the SdH amplitudes vary with T in samples Q2 and Q3 (measured with **H**||**c**). As shown in Fig. 3A, the oscillation amplitudes in $d\rho_{xx}/dH$ decrease rapidly as T is raised from 0.3 to 20 K. Although measurements were not carried out at intermediate θ in Q2 and Q3, we verified that the SdH peaks were absent at θ = 90°. In the index plot (Fig. 3B), we confirmed that the (inverse) peak fields $1/B$ fall on a straight line versus the integers n (Eq. 1). For Q2 and Q3, the slopes yield $S_F = 33.3$ and 28.6 T, with Fermi wave vector $k_F = 0.032$ and 0.030 Å^{-1}, respectively (Table 1). In Q1, the shallower slope yields $k_F = 0.036$ Å^{-1}. Extrapolation of the high-field SdH peaks in Q1 is consistent with $0 < \gamma < ½$ (figs. S3 and S4). To find the corresponding E_F, we next determine the Fermi velocity v_F.

The T dependence of the amplitude $\Delta\sigma_{xx}$ of conductivity oscillations is given by $\Delta\sigma_{xx}(T) = \Delta\sigma_{xx}(0)\lambda(T)/\sinh\lambda(T)$. For 2D massless Dirac states, the thermal factor $\lambda(T)$ is given by (*15*, *16*)

$$\lambda(T) = \frac{2\pi^2 k_B T}{\hbar e B} m_{cyc} \qquad (2)$$

where k_B is Boltzmann's constant and $m_{cyc} = E_F/v_F^2$ is the cyclotron mass. In low H, the degree of orbit bending is measured by the Hall mobility μ, given by $\mu = e\tau_{tr}/m_{cyc} = e\ell/\hbar k_F$, where τ_{tr} and ℓ are the transport lifetime and mean free path, respectively. We may find m_{cyc} by fitting the T dependence of the conductivity amplitudes to Eq. 2 (Fig. 3D). Because k_F is known, we calculate $v_F = 3.7$ and 4.2×10^5 m s^{-1} for Q2 and Q3, respectively [from ARPES (*10*), $v_F \sim 4 \times 10^5$ m s^{-1}]. Lastly, this yields $E_F = 94$, 84, and 78 meV above the Dirac point in samples Q1, Q2, and Q3, respectively (Fig. 1B).

The lifetime τ of the surface states can be found by estimating the Dingle factor e^{-D}, where $D = 2\pi^2\Gamma E_F/(\hbar e B v_F^2)$, with $\Gamma = 1/\tau$ the scattering rate. Because $\Delta R/R_0 \sim \frac{\lambda(T)}{\sinh\lambda(T)} e^{-D}$ (where R is resistance), we may find Γ from the slope in the semilog plot of $(\Delta R/R_0)B\sinh\lambda(T)$ versus $1/B$ (Fig. 3, E and F). We find that $v_F\tau = 217$ and 219 nm in Q2 and Q3, respectively (these values are lower bounds for the mean free path $\ell = v_F\tau_{tr}$ because $\tau_{tr} > \tau$ in principle). The metallicity parameter is then $k_F\ell > 69$ and 66 in samples Q2 and Q3, respectively.

The conductance tensor $G_{ij}(B)$ of the 2D Dirac gas may be calculated in the semiclassical Boltzmann approximation (*14*). Defining $G(B) \equiv G_{xx}(B)$, we may express the zero-B con-

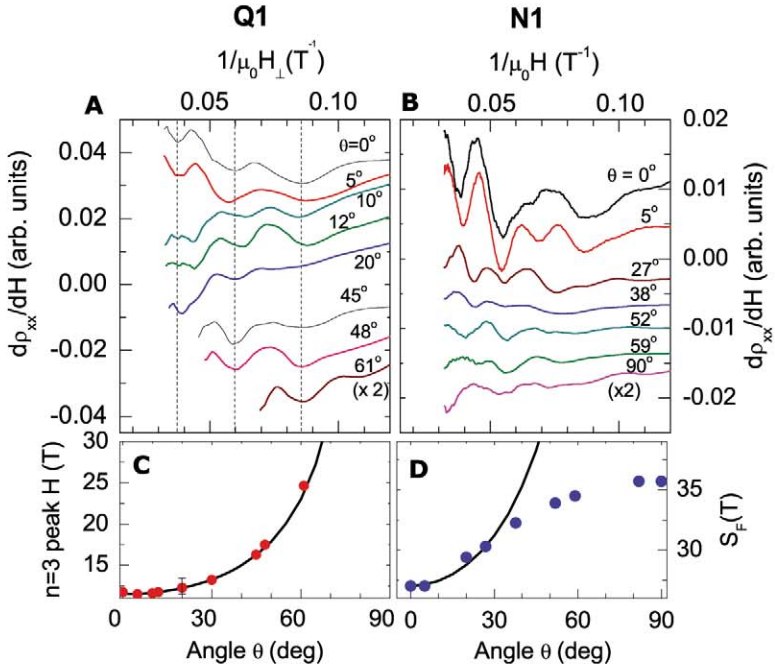


Fig. 2. The resistivity derivative $d\rho_{xx}/dH$ versus $1/H_\perp = 1/(H\cos\theta)$ in (**A**) sample Q1 and (**B**) sample N1 at selected tilt angles θ. In (A), the minima lie on the vertical dashed lines consistent with a 2D FS, whereas in (B), the minima shift systematically with θ. (**C**) The field position of the $n = 3$ LL peak for sample Q1 (red circles) varies with θ as 1/cosθ (black curve), consistent with a 2D FS. (**D**) The period S_F for sample N1 (blue circles) increases by 35% as $\theta \rightarrow 90°$, deviating strongly from 1/cosθ (black curve), consistent with a 3D FS.

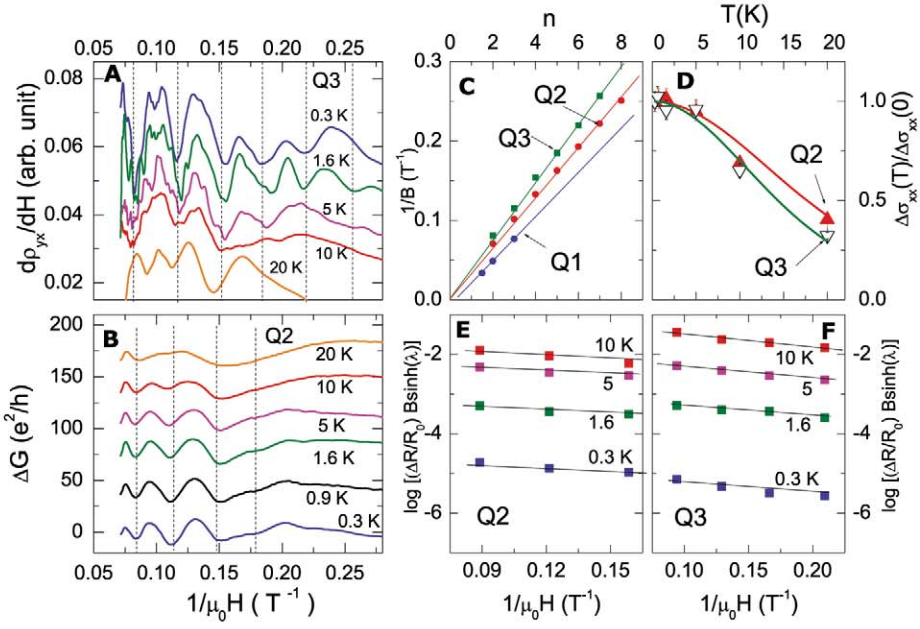


Fig. 3. (**A**) Derivative $d\rho_{yx}/dH$ versus $1/H$ in sample Q3 measured at temperatures T between 0.3 and 20 K. (**B**) ΔG (conductance obtained after subtracting a smooth background based on curves measured above 20 K) for sample Q2 at selected T over the same interval. (**C**) LL index plot $1/B$ versus n for samples Q1, Q2, and Q3. Our results are consistent with $0 < \gamma < ½$ (fig. S3). Values of S_F and k_F derived are reported in Table 1. (**D**) T dependence of the normalized conductivity amplitude $\Delta\sigma_{xx}(T)/\Delta\sigma_{xx}(0)$ at 0.3 K in samples Q2 (with $H = 12$ T) and Q3 (7.8 T). The curves are best fits to $\lambda(T)/\sinh\lambda(T)$ (Eq. 2). Dingle plots of $\log[(\Delta R/R_0)B\sinh\lambda]$ versus $1/H$, used to determine τ and $v_F\tau$ for (**E**) sample Q2 and (**F**) sample Q3.

ductance as $G(0) = (e^2/h)k_F\ell$, whereas the Hall conductance is

$$G_{xy} = \frac{2\pi e^3}{h^2}\frac{B\ell^2}{[1+(\mu B)^2]} \quad (3)$$

(including both spin degrees). With $k_F\ell \sim 70$, we calculate $G(0) \approx 2.4 \times 10^{-3}$ ohm^{-1}, compared with the observed total resistance $R \approx 1.4$ ohm at 0.3 K in sample Q1. Hence, the 2D states account for ~0.3% of the total conductance observed at 0.3 K. Interestingly, the large value of $k_F\ell$ implies a large Hall mobility ($\mu = 10{,}200$ cm^2 V^{-1} s^{-1}). In weak H, the surface Hall current may dominate the low-mobility bulk Hall current.

We next report the detection of this surface Hall current as a distinct anomaly. In Fig. 4A, we plot the observed Hall conductivity σ_{xy} in sample Q3. In addition to the SdH oscillations in high fields (>5 T), we observe a prominent "dispersive" anomaly in weak H corresponding to a high-mobility contribution that is n-type. We express the observed Hall conductivity as the sum

$$\sigma_{xy} = \sigma^{b}_{xy} + \frac{G_{xy}}{t} \quad (4)$$

where $\sigma^{b}_{xy} > 0$ is the bulk, p-type Hall conductivity and $G_{xy} < 0$ the surface Hall conductance given in Eq. 3, with t the crystal thickness. As shown in Fig. 1C and D, the sign of ρ_{yx} in sample Q1, fixed by the bulk carriers, is n-type, whereas Q2 and Q3 are p-type (fig. S4 and SOM section S4). By using Eq. 3 and a Drude-like expression for σ^{b}_{xy}, we have achieved a close fit to the nonmonotonic curve in Fig. 4A (fig. S5).

On subtracting σ^{b}_{xy}, we isolate the surface term G_{xy}, which shows a large dispersive anomaly centered at $H = 0$, with quantum oscillations in the wings (Fig. 4B). The solid curve is the fit to Eq. 3 (the semiclassical expression does not describe the quantum oscillations). By Eq. 3, G_{xy} attains the maximum value $G^{max}_{xy} = (e^2/2h)k_F\ell$ at the peak field $B_p = 1/\mu$ (arrows in Fig. 4B). From the fit, we find $\mu \sim 9000$ cm^2 V^{-1} s^{-1}, $k_F\ell = 94$, $k_F = 0.04$ Å^{-1}, and $\ell = 235$ nm. Given the nonuniformity of the cross-section and the uncertainties in measuring t and the voltage lead spacing L (both ± 10%), these are in good agreement with the numbers inferred from the SdH period and the Dingle analysis (*17*).

The quantitative agreement with 2D states persuades us that the weak-field Hall anomaly originates from Dirac surface states. Because of the large difference in mobilities and the difference in carrier sign, we are able to resolve directly the surface Hall current as the dispersive anomaly superposed on the bulk Hall current. The curve in Fig. 4B is a snapshot of the Dirac surface current from which μ and $k_F\ell$ may be estimated by inspection.

By how much is μ enhanced over the bulk? Unfortunately, in the nonmetallic crystals, it is not straightforward to pin down the hole density p and mobility μ_b of the bulk states. The bulk Hall signal changes sign abruptly as E_F approaches the Dirac point. As shown in fig. S1, samples Q1 and N1 are n-type, whereas Q2 and Q3 are p-type. This suggests competition and compensation between electron and hole bulk bands. A more interesting complication is the unusual magnetoresistance (MR). In samples Q1, Q2, and Q3, the transverse MR measured with **H**||**c** displays a highly unusual linear increase versus H [by contrast, metallic crystals do not show the linear MR (fig. S2)]. As shown in Fig. 4C (for sample Q2), the nonanalytic variation $\frac{\rho(H)}{\rho(0)} - 1 \sim |H|$ extends over 3.5 decades in H (from 30 G to 14 T) at 0.3 K. The expanded view in Fig. 4D shows that, as T is raised to 20 K, the low-H region is rounded. The large linear MR is predominantly caused by coupling of the spin to H. When H is aligned with the current, the longitudinal MR is 50% as large as the transverse MR (fig. S7). This unusual MR, which may arise from a spin-mediated decrease in the bulk carrier density p with H, implies that the bulk states cannot be regarded as conventional impurity bands. However, if we use the bulk value obtained from the fit in Fig. 4B ($\mu_b \sim 860$ cm^2 V^{-1} s^{-1}), we find that the surface mobility is 12 times larger than the bulk value.

By using both the SdH and weak-field Hall anomaly, we have resolved a surface current that is n-type with $k_F \sim 0.035$ Å^{-1} and a velocity $v_F \sim 4 \times 10^5$ m s^{-1}. The observed mobility and $k_F\ell$ are enhanced substantially over the bulk values. These features are consistent with protected surface Dirac states. With the surface current detected, research on topological insulators may now be expanded to include transport experiments.

Table 1. Parameters in samples Q1, Q2, Q3, and N1. S_F and k_F are determined from the SdH period. E_F and v_F are obtained from the T dependence of the amplitude $\Delta\sigma_{xx}(T)/\Delta\sigma_{xx}(0)$. ℓ is found from the Dingle factor e^{-D}. The length (L), width (W), and thickness (t) are in μm. The uncertainty in v_F is ±10%. Dash entries indicate quantities not measured.

units	S_F T	k_F Å^{-1}	E_F meV	$k_F\ell$ –	v_F 10^5 m s^{-1}	$L \times W \times t$ μm^3
Q1	41.7	0.036	94	–	–	650 × 850 × 100
Q2	33.3	0.032	84	69	3.7	1500 × 1200 × 150
Q3	28.6	0.030	78	66	4.2	700 × 1060 × 140
N1	23.3*	0.027	–	–	–	700 × 730 × 40

*measured at θ = 0.

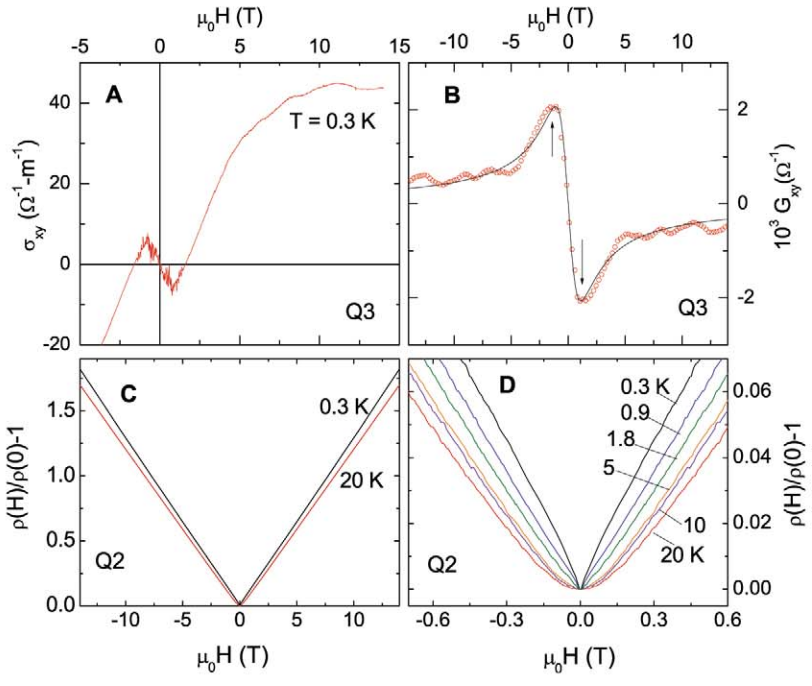


Fig. 4. (**A**) The Hall conductivity σ_{xy} versus H in Q3 measured at 0.3 K, showing quantum oscillations above 5 T and a dispersive anomaly in weak H. (**B**) Surface Hall conductance G_{xy} obtained by subtracting the bulk contribution σ^{b}_{xy} (Eq. 4). The solid curve is the fit to G_{xy} in Eq. 3 (details in SOM section S5). The peak field B_p (arrows) gives 1/μ, whereas the maximum value yields $(e^2/2h)k_F\ell$. (**C**) The linear MR measured with **H**||**c** at 0.3 and 20 K ($\rho \equiv \rho_{xx}$). (**D**) Rounding of the nonanalytic cusp at $H = 0$ in increasing T.

References and Notes

1. L. Fu, C. L. Kane, E. J. Mele, *Phys. Rev. Lett.* **98**, 106803 (2007).
2. L. Fu, C. L. Kane, *Phys. Rev. B* **76**, 045302 (2007).
3. J. E. Moore, L. Balents, *Phys. Rev. B* **75**, 121306 (2007).
4. B. A. Bernevig, T. L. Hughes, S.-C. Zhang, *Science* **314**, 1757 (2006).
5. L. Fu, C. L. Kane, *Phys. Rev. Lett.* **100**, 096407 (2008).
6. X. L. Qi, T. L. Hughes, S. C. Zhang, *Phys. Rev. B* **78**, 195424 (2008).

7. D. Hsieh *et al.*, *Nature* **452**, 970 (2008).
8. D. Hsieh *et al.*, *Science* **323**, 919 (2009).
9. Y. Xia *et al.*, *Nat. Phys.* **5**, 398 (2009).
10. Y. L. Chen *et al.*, *Science* **325**, 178 (2009); published online 11 June 2009 (10.1126/science.1173034).
11. P. Roushan *et al.*, *Nature* **460**, 1106 (2009).
12. J. G. Checkelsky *et al.*, *Phys. Rev. Lett.* **103**, 246601 (2009).
13. A. A. Taskin, Y. Ando, *Phys. Rev. B* **80**, 085303 (2009).
14. Materials and methods are available as supporting material on *Science* Online.
15. K. S. Novoselov *et al.*, *Nature* **438**, 197 (2005).
16. V. P. Gusynin, S. G. Sharapov, *Phys. Rev. B* **71**, 125124 (2005).
17. We may exclude the interpretation of G_{xy} as a bulk term as follows. If we write G_{xy}/t as $n'e\mu^2B/[1 + (\mu B)^2]$ with μ fixed at 10,000 $cm^2\ V^{-1}\ s^{-1}$, we get a bulk density $n' = 1.4 \times 10^{14}\ cm^{-3}$. This tiny 3D FS pocket would have a Fermi cross section S_F' that is far too small, by a factor of 360, to match the SdH period (the wave vector $k'_F = 1.6 \times 10^{-3}\ Å^{-1}$ is 19 times too small).

18. The research is supported by NSF under Materials Research Science and Engineering Centers grant DMR-0819860. We acknowledge valuable comments by J. G. Checkelsky, M. Z. Hasan, A. Yazdani, A. Bernevig, and F. D. M. Haldane. High-field measurements were carried out at the National High Magnetic Field Laboratory, Tallahassee, which is supported by NSF cooperative agreement no. DMR-0084173, by the state of Florida, and by the U.S. Department of Energy.

Supporting Online Material

www.sciencemag.org/cgi/content/full/science.1189792/DC1
Materials and Methods
SOM sections S1 to S6
Figs. S1 to S9

18 March 2010; accepted 12 July 2010
Published online 29 July 2010;
10.1126/science.1189792
Include this information when citing this paper.

In-Plane Resistivity Anisotropy in an Underdoped Iron Arsenide Superconductor

Jiun-Haw Chu,[1,2] James G. Analytis,[1,2] Kristiaan De Greve,[3] Peter L. McMahon,[3] Zahirul Islam,[4] Yoshihisa Yamamoto,[3,5] Ian R. Fisher[1,2]*

High-temperature superconductivity often emerges in the proximity of a symmetry-breaking ground state. For superconducting iron arsenides, in addition to the antiferromagnetic ground state, a small structural distortion breaks the crystal's C_4 rotational symmetry in the underdoped part of the phase diagram. We reveal that the representative iron arsenide $Ba(Fe_{1-x}Co_x)_2As_2$ develops a large electronic anisotropy at this transition via measurements of the in-plane resistivity of detwinned single crystals, with the resistivity along the shorter *b* axis ρ_b being greater than ρ_a. The anisotropy reaches a maximum value of ~2 for compositions in the neighborhood of the beginning of the superconducting dome. For temperatures well above the structural transition, uniaxial stress induces a resistivity anisotropy, indicating a substantial nematic susceptibility.

The iron-arsenide family of compounds appears to present a new paradigm for high-temperature superconductivity. The parent compounds are multiband itinerant antiferromagnets (*1*, *2*) with a Fermi surface consisting of several small pockets resulting from reconstruction due to the broken translational symmetry (*3*, *4*). Suppression of the antiferromagnetic ground state by various means eventually leads to superconductivity, with critical temperatures of up to 55 K (*5*). Notably, the antiferromagnetic transition is always preceded by or coincident with a tetragonal to orthorhombic structural distortion (*6*–*8*). It has been proposed that this structural distortion is driven by an electronic phase transition (*9*–*12*), perhaps due to orbital ordering (*13*–*16*) or fluctuating antiferromagnetism (*9*, *10*). In both proposals, a large in-plane electronic anisotropy is anticipated in the "nematic" state (*17*).

Although electron nematic phases have been intensively studied in quantum Hall systems (*18*) and in $Sr_3Ru_2O_7$ (*19*), there is growing evidence for substantial electronic anisotropy in underdoped cuprates (*20*, *21*) that cannot be explained by the structural orthorhombicity alone. In particular, the recent observation of a large in-plane anisotropy in the Nernst effect in $YBa_2Cu_3O_{7-\delta}$ suggests that the much-debated pseudogap phase is a rotational symmetry-breaking phase (*22*). The crucial experiments in all of these cases probe the in-plane transport anisotropy that arises due to the nematic order (*17*). Here, we report measurements of in-plane resistivity anisotropy of $Ba(Fe_{1-x}Co_x)_2As_2$ over a wide range of doping and temperature, to elucidate the nature of the structural phase transition in the iron pnictides.

One difficulty with probing the in-plane electronic anisotropy of the iron arsenides is that the material naturally forms dense structural twins below the orthorhombic transition at T_S (Fig. 1, A and B) (*23*). Measurements of twinned samples present only an average of the intrinsic anisotropy, from which little detailed information can be extracted. For the present study, we have developed a mechanical cantilever device (shown in Fig. 1 C) that is able to detwin crystals in situ. Crystals were cut such that the orthorhombic *a* and *b* axes were aligned parallel to the direction of applied stress. With only modest pressures

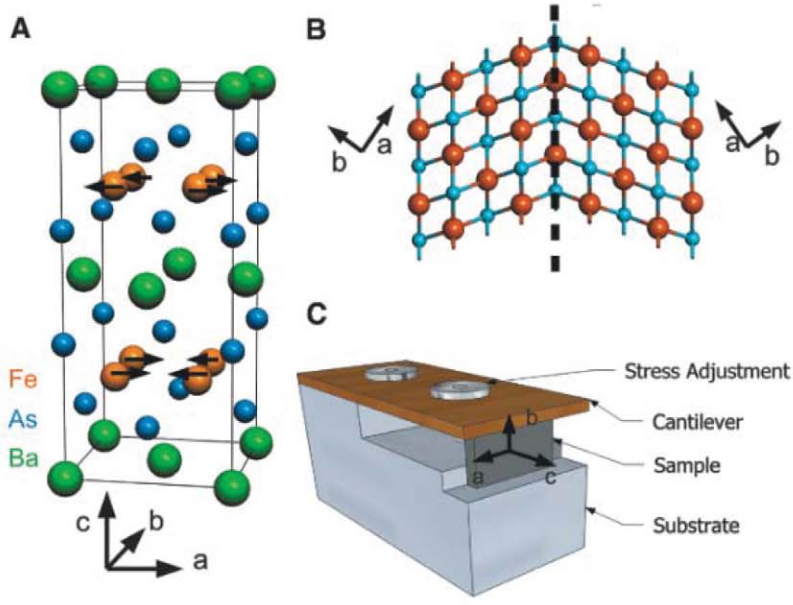


Fig. 1. (**A**) Diagram of the crystal structure of $BaFe_2As_2$ in the antiferromagnetic state. The magnetic moments on the iron sites point in the *a* direction and align antiparallel along the longer *a* axis and parallel along the shorter *b* axis. (**B**) Diagram illustrating a twin boundary between two domains that form on cooling through the structural transition at T_S. Dense twinning in macroscopic crystals obscures any in-plane electronic anisotropy in bulk measurements. (**C**) Diagram of the device used to detwin single crystals in situ. The sample is held sandwiched between a cantilever and a substrate, with a screw in the center of the cantilever to adjust the uniaxial pressure. The (0 0 1) surface of the crystal is exposed, enabling transport measurements.

[1]Department of Applied Physics and Geballe Laboratory for Advanced Materials, Stanford University, Stanford, CA 94305, USA. [2]Stanford Institute of Energy and Materials Science, SLAC National Accelerator Laboratory, 2575 Sand Hill Road, Menlo Park, CA 94025, USA. [3]E. L. Ginzton Laboratory, Stanford University, Stanford, CA 94305, USA. [4]The Advanced Photon Source, Argonne National Laboratory, Argonne, IL 60439, USA. [5]National Institute of Informatics, Hitotsubashi 2-1-2, Chiyoda-ku, Tokyo 101-8403, Japan.

*To whom correspondence should be addressed. E-mail: irfisher@stanford.edu

(~5 MPa, estimated from the deflection of the cantilever), small enough that the critical temperature associated with the Neel order (T_N) is unaffected, the device is able to almost fully detwin underdoped crystals, revealing the previously hidden in-plane electronic anisotropy.

Evidence of the efficacy of this method for detwinning can be obtained from high-resolution x-ray diffraction measurements performed on the 4-ID-D beamline at the Advanced Photon Source (APS). Data shown in Fig. 2A reveal the splitting of the (–2 –2 20) Bragg peak (with respect to the tetragonal lattice) in the orthorhombic state of a crystal with composition $x = 0.025$ held under uniaxial pressure with the cantilever. Comparison of the integrated intensity of the two peaks yields a relative volume fraction of 86% of the twin orientation with the shorter b axis along the applied stress. Direct optical images were also taken to confirm this result. Samples were illuminated by polarized light, and the reflected light was collected through an almost crossed polarizer so as to maximize the contrast caused by the different birefringence of the two twin orientations. Representative images of a $BaFe_2As_2$ sample surface at 5 K are shown for the relaxed cantilever (Fig. 2B) and strained cantilever (Fig. 2C). Stripes associated with the twin domains are clearly visible for the unstrained crystal, but these have completely disappeared for the strained sample.

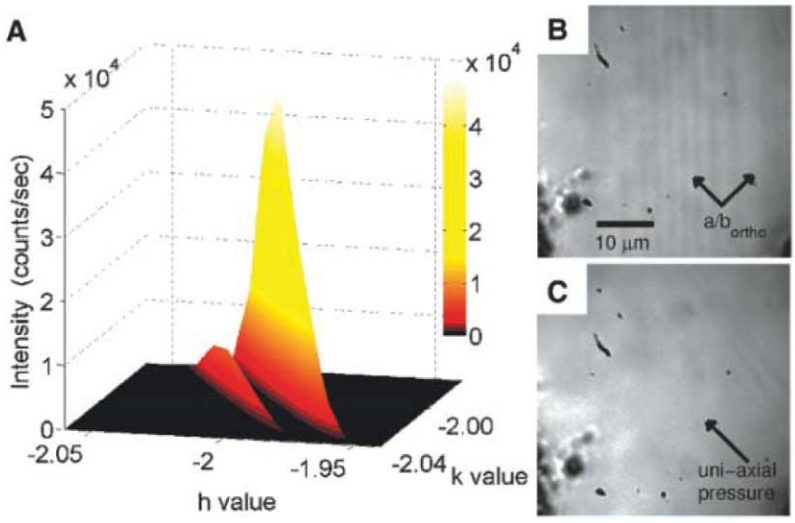


Fig. 2. (**A**) Splitting of the (–2 –2 20) Bragg peak (referenced to the tetragonal lattice) at 40 K for a sample with $x = 0.025$ under uniaxial pressure, as revealed by high-resolution x-ray diffraction. The two-dimensional surface is formed by interpolating between Gaussian fits to a dense mesh of points from h-k scans in reciprocal space. Each peak corresponds to one of the two twin domains. The relative volume fraction of the larger domain, corresponding to the shorter b axis aligned parallel to the applied stress, is approximately 86%. (**B**) Polarized-light image of the surface of an unstressed $BaFe_2As_2$ crystal at 5 K without applying uniaxial pressure. Vertical light and dark stripes reveal the existence of twin domains with a and b axes reversed. (**C**) Polarized-light image on the surface of the same crystal under uniaxial pressure at 5 K. The absence of stripes indicates the applied pressure has detwinned the crystal.

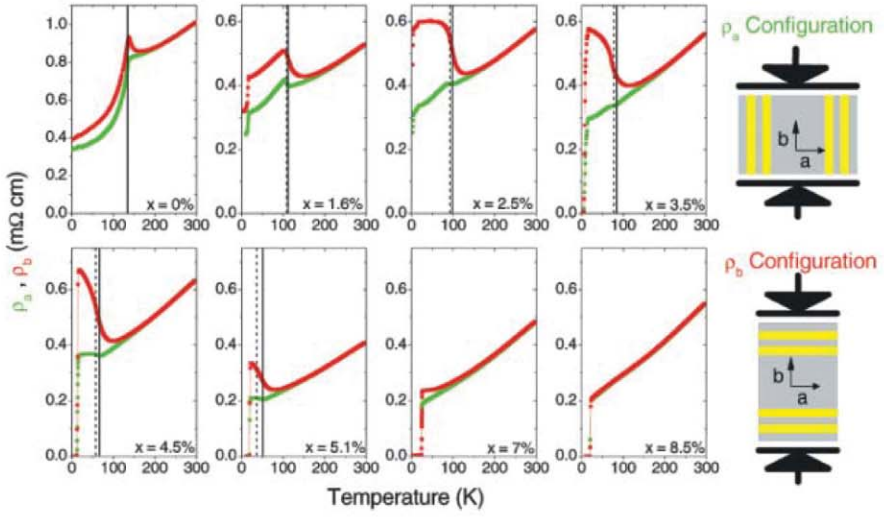


Fig. 3. Temperature dependence of the in-plane resistivity ρ_a (green) and ρ_b (red) of $Ba(Fe_{1-x}Co_x)_2As_2$ for Co concentrations from $x = 0$ to 0.085. Solid and dashed vertical lines mark critical temperatures for the structural and magnetic phase transitions T_S and T_N, respectively, obtained from a combination of scattering, thermodynamic, and transport measurements (*7*). Values of T_N for stressed samples, obtained from the peak in the derivative of the resistivity, are identical to those found for unstressed samples, indicating that the uniaxial pressure serves as a weak symmetry-breaking field to orient twin domains without affecting the bulk magnetic properties. The uniaxial stress does, however, affect the superconducting transitions in some underdoped samples, inducing a partial superconducting transition for $x = 0.016$ and 0.025, which are not observed for unstressed crystals. Diagrams on the right illustrate how measurements of ρ_a and ρ_b were made. Dark arrows indicate the direction in which uniaxial pressure was applied, and smaller arrows indicate the orientation of the a and b crystal axes. In all cases, the same samples and the same contacts (shown in gold for a standard four-point configuration) were used for both orientations.

Resistivity data were collected for detwinned samples as a function of temperature. Eight representative cobalt concentrations were measured, from the undoped parent compound $x = 0$ through to fully overdoped composition ($x = 0.085$). Representative data for each of these compositions are shown in Fig. 3. Measurements were made for currents applied parallel and perpendicular to the applied stress, yielding ρ_b (in red) and ρ_a (in green), respectively.

Inspection of Fig. 3 reveals that $\rho_b > \rho_a$ for all underdoped compositions. This result, anticipated from earlier magnetoresistance measurements (*24*), is somewhat counterintuitive. Given that the a-axis lattice constant is larger than that of the b axis, the smaller orbital overlap along the a axis would ordinarily give rise to a higher resistivity, all else being equal. Equally, the collinear spin arrangement below T_N comprises rows of spins that are arranged ferromagnetically along the b axis and antiferromagnetically along the a axis (Fig. 1A). Scattering from spin fluctuations would ordinarily result in a higher resistivity along the antiferromagnetic a direction. Our observation therefore indicates a more complex situation and provides a strong constraint for theoretical models of the electronic structure in the orthorhombic state. The degree of in-plane anisotropy can be characterized by the ratio ρ_b/ρ_a, which is shown as a color scale in Fig. 4A. The anisotropy varies with temperature and composition but reaches a maximum value close to two for $0.02 \leq x \leq 0.04$ at low temperatures, in the neighborhood of the beginning of the superconducting dome. In contrast, the overdoped composition $x = 0.085$, which remains tetragonal for all temperatures, reveals no in-plane anisotropy.

The temperature dependence of the resistivity (Fig. 3) is especially striking. At high temperatures, the resistivity is isotropic and starts off as almost linear. For currents running in the b direction, the resistivity deviates from this behavior at a temperature well above T_S and increases

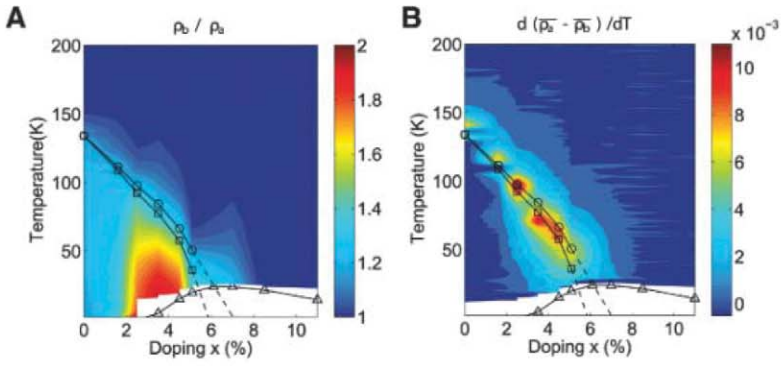


Fig. 4. (**A**) Evolution of the in-plane resistivity anisotropy as a function of temperature and doping, expressed in terms of the resistivity ratio ρ_b/ρ_a. Structural, magnetic and superconducting critical temperatures, determined following (*27*), are shown as circles, squares, and triangles, respectively. Notably, the resistivity ratio deviates from unity at a considerably higher temperature than T_S, indicating that nematic fluctuations extend far above the phase boundary. (**B**) The difference in the temperature derivative of ρ_a and ρ_b: $d(\overline{\rho}_a - \overline{\rho}_b)/dT$, where $\overline{\rho}_a = \rho_a/\rho_a(300K)$ and $\overline{\rho}_b = \rho_b/\rho_b(300K)$, as a function of temperature and doping. The resistivity has been normalized by its room temperature value to avoid uncertainty due to geometric factors. Regions of highest intensity are those regions where ρ_b appears to be insulator-like ($d\rho_b/dT < 0$) while ρ_a remains metallic ($d\rho_a/dT > 0$). This behavior is clearly correlated with the nematic phase between the structural and magnetic transitions.

steeply with decreasing temperature. This insulator-like behavior is cut off near T_N for the lowest doping levels but extends to much lower temperatures for larger cobalt concentrations. In contrast, for currents flowing in the *a* direction, the resistivity behaves similarly to a normal metal, continuing to decrease with decreasing temperature over the entire temperature range, except for a small jump near T_N. The superconducting transition at the lowest temperatures causes both ρ_a and ρ_b to drop to zero. The difference of the temperature derivatives of ρ_b and ρ_a (normalized by the room temperature value), shown in Fig. 4B, reveals a strong correlation with the orthorhombic distortion.

The composition dependence of the anisotropy in the in-plane resistivity (Fig. 4, A and B) is in stark contrast to that of the structural anisotropy that develops below T_S. The orthorhombic distortion, characterized by the ratio of in-plane lattice constants, has a maximum value for $x = 0$ at low temperature of $(a - b)/(a + b) = 0.36\%$ and decreases monotonically with increasing cobalt concentration (*25*), whereas the resistivity anisotropy is a nonmonotonic function of doping, exhibiting a maximum near the beginning of the superconducting dome. These contrasting behaviors suggest that the itinerant electrons do not passively follow the lattice distortion. Rather, it appears that the material suffers an underlying electronic phase transition that profoundly affects the low energy excitations near the Fermi level and in a manner that is much less apparent in the response of the crystal lattice.

Notably, the resistivity anisotropy is evident for temperatures well above T_S. Even though the crystal symmetry is tetragonal in this temperature range, the uniaxial stress applied by the cantilever breaks the fourfold symmetry in the basal plane. The external symmetry-breaking field induces a nonzero order parameter above the critical temperature, smoothing the divergent behavior associated with the critical point observed under ambient conditions (*26*). As the temperature is reduced toward T_S from above, the resistivity anisotropy for the strained samples increases rapidly, indicating that the nematic susceptibility diverges at the critical temperature and providing compelling evidence that the resistivity anisotropy observed above T_S reflects fluctuations associated with the phase transition that occurs at T_S in the zero stress limit (more discussion can be found in the supporting online material). There is no evidence in either thermodynamic or transport properties for a third phase transition above T_S (*27*).

Co-doped $BaFe_2As_2$ was chosen for this initial study because the structural and magnetic transition are clearly separated in temperature and the material can be readily tuned in a controlled and reproducible fashion. However, given the rather generic phase diagram found in this family of compounds (*28*), it is possible that the observed anisotropy is quite general to underdoped iron pnictides. For example, recent scanning tunneling microscopy measurements also reveal a large electronic anisotropy of Co-doped $CaFe_2As_2$ at low temperatures (*29*).

In comparison to other electron nematic systems, such as $Sr_3Ru_2O_7$ (*19*) and the quantum Hall system (*18*), the phase transition of iron pnictides occurs at zero field and at a temperature range between 50 and 150 K, providing an accessible platform for spectroscopy and thermodynamic measurements. Although the pseudo-gap phase in underdoped cuprates exists for similar conditions to these, the iron arsenides have a well-defined phase boundary associated with the nematic phase transition. In this sense, the iron arsenides present a cleaner system in which to investigate the physical origin of nematic order and the consequences for superconductivity.

References and Notes

1. Y. Kamihara, T. Watanabe, M. Hirano, H. Hosono, *J. Am. Chem. Soc.* **130**, 3296 (2008).
2. M. Rotter, M. Tegel, D. Johrendt, *Phys. Rev. B* **78**, 020503 (2008).
3. S. E. Sebastian *et al.*, *J. Phys. Condens. Matter* **20**, 422203 (2008).
4. J. G. Analytis *et al.*, *Phys. Rev. B* **80**, 064507 (2009).
5. Z. Ren *et al.*, *Chin. Phys. Lett.* **25**, 2215 (2008).
6. C. de la Cruz *et al.*, *Nature* **453**, 899 (2008).
7. C. Lester *et al.*, *Phys. Rev. B* **79**, 144523 (2009).
8. D. K. Pratt *et al.*, *Phys. Rev. Lett.* **103**, 087001 (2009).
9. C. Fang, H. Yao, W.-F. Tsai, J. Hu, S. A. Kivelson, *Phys. Rev. B* **77**, 224509 (2008).
10. T. Yildirim, *Phys. Rev. Lett.* **102**, 037003 (2009).
11. C. Xu, M. Muller, S. Sachdev, *Phys. Rev. B* **78**, 020501 (2008).
12. M. Johannes, I. Mazin, *Phys. Rev. B* **79**, 220510 (2009).
13. F. Krüger, S. Kumar, J. Zaanen, J. van den Brink, *Phys. Rev. B* **79**, 054504 (2009).
14. C.-C. Chen, B. Moritz, J. van den Brink, T. P. Devereaux, R. R. P. Singh, *Phys. Rev. B* **80**, 180418 (2009).
15. W. Lv, J. Wu, P. Phillips, *Phys. Rev. B* **80**, 224506 (2009).
16. C.-C. Lee, W.-G. Yin, W. Ku, *Phys. Rev. Lett.* **103**, 267001 (2009).
17. Nematic order refers to a spontaneously broken rotational symmetry without the breaking of translational symmetry. Systems for which the crystal lattice appears to preserve the original rotational symmetry (as found in the quantum Hall effect and $Sr_3Ru_2O_7$) might be dubbed "electron nematic," whereas systems for which the crystal lattice also breaks rotational symmetry [for example, $YBa_2Cu_3O_{7-\delta}$ and $Ba(Fe_{1-x}Co_x)_2As_2$] might be more appropriately named "system nematic." In both cases, a strong electronic anisotropy is observed that is much more pronounced than consideration of the crystal lattice alone would otherwise suggest. We refer to this general phenomenon as "nematic order" in the rest of the text. For a recent review, see (*30*).
18. M. P. Lilly, K. B. Cooper, J. P. Eisenstein, L. N. Pfeiffer, K. W. West, *Phys. Rev. Lett.* **82**, 394 (1999).
19. R. A. Borzi *et al.*, *Science* **315**, 214 (2007).
20. Y. Ando, K. Segawa, S. Komiya, A. N. Lavrov, *Phys. Rev. Lett.* **88**, 137005 (2002).
21. V. Hinkov *et al.*, *Science* **319**, 597 (2008).
22. R. Daou *et al.*, *Nature* **463**, 519 (2010).
23. M. A. Tanatar *et al.*, *Phys. Rev. B* **79**, 180508 (2009).
24. J.-H. Chu *et al.*, *Phys. Rev. B* **81**, 214502 (2010).
25. R. Prozorov *et al.*, *Phys. Rev. B* **80**, 174517 (2009).
26. L. D. Landau, E. M. Lifshitz, *Statistical Physics: Part 1* (Butterworth-Heinemann, Oxford, ed. 3, 1980).
27. J.-H. Chu, J. G. Analytis, C. Kucharczyk, I. R. Fisher, *Phys. Rev. B* **79**, 014506 (2009).
28. For the Fe arsenides and oxy arsenides typified by $BaFe_2As_2$ and LaFeAsO, the structural transition is from tetragonal to orthorhombic symmetry. The closely related Fe chalcogenides, typified by FeTe, also suffer a structural distortion, but in this case from tetragonal to monoclinic (*31*).
29. T. M. Chuang *et al.*, *Science* **327**, 181 (2010).
30. E. Fradkin, S. A. Kivelson, M. J. Lawler, J. P. Eisenstein, A. P. Mackenzie, http://arxiv.org/abs/0910.4166
31. S. Li *et al.*, *Phys. Rev. B* **79**, 054053 (2009).

32. The authors thank C. D. Batista, C.-C. Chen, T. P. Devereaux, S. A. Kivelson, A. P. Mackenzie, R. D. McDonald, S. C. Riggs, D. J. Scalapino, and Z.-X. Shen for helpful discussions. This work is supported by the U.S. Department of Energy (DOE), Office of Basic Energy Sciences, under contract DE-AC02-76SF00515. Use of the APS is supported by the DOE, Office of Science, under contract DE-AC02-06CH11357.

Supporting Online Material

www.sciencemag.org/cgi/content/full/329/5993/824/DC1
Materials and Methods
Figs. S1 to S4
References

5 April 2010; accepted 12 July 2010
10.1126/science.1190482

Small-Scale Mantle Convection Produces Stratigraphic Sequences in Sedimentary Basins

K. D. Petersen,[1]* S. B. Nielsen,[1] O. R. Clausen,[1] R. Stephenson,[2] T. Gerya[3]

Cyclic sedimentary deposits link stratigraphic sequences that are now geographically distant but were once part of the same depositional environment. Some of these sequences occur at periods of 2 to 20 million years, and eustatic sea-level variations or regional tectonic events are likely causes of their formation. Using numerical modeling, we demonstrate that small-scale mantle convection can also cause the development of stratigraphic sequences through recurrent local and regional vertical surface movements. Small-scale convection-driven stratigraphic sequences occur at periods of 2 to 20 million years and correlate only at distances up to a few hundred kilometers. These results suggest that previous sequence stratigraphic analyses may contain erroneous conclusions regarding eustatic sea-level variations.

Stratigraphic sequences are sedimentary units that reflect cyclic changes in deposition rate and depositional environment due to variations in relative sea level (*1*). It is commonly assumed that such variations are due to global (eustatic) sea-level changes that thus provide a general framework for the correlation of stratigraphic sequences globally or regionally (*2*). However, the global universality of sequence stratigraphic events has not been proven unambiguously, and regional variations in relative sea level may be caused by a number of other processes (*3*, *4*). For recurrent cycles occurring at periods of 2 to 20 million years (My) [hereafter defined as intermediate period (IP)], no plausible alternative to eustasy has yet been proposed as the cause of sequence development. Small-scale convection in the sublithospheric mantle may be a possible explanation for the formation of such recurrent stratigraphic sequences, but its role is relatively unknown. Although the specific pattern of large-scale mantle convection is debated (*5*), there seems to be little doubt that convection occurs at two distinct temporal and spatial scales: (i) the creation and subduction of tectonic plates and possibly the movement of plumes originating from the base of the mantle (*5*) and (ii) small-scale convection operating on regional scales (*6*–*11*).

[1]Department of Earth Science, Aarhus University, DK-8000 Aarhus C, Denmark. [2]School of Geosciences, Geology and Petroleum Geology, Meston Building, King's College, University of Aberdeen, Scotland. [3]Department of Geosciences, ETH-Zurich, Zurich, Switzerland.

*To whom correspondence should be addressed. E-mail: kenni@geo.au.dk

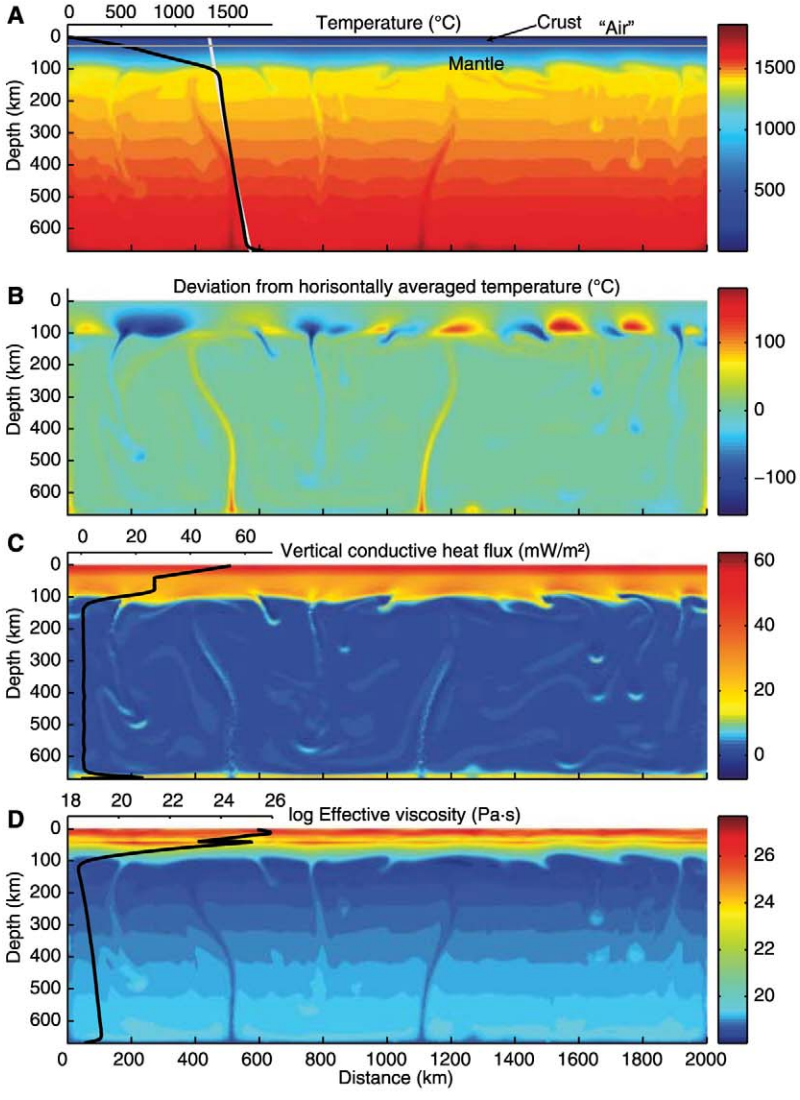


Fig. 1. Snapshot of convecting numerical model of the crust and the upper mantle. (**A**) Temperature. Black curve, horizontally averaged model temperature; gray curve, theoretical isentropic temperature profile for a potential temperature of 1315°C. (**B**) Temperature anomaly (deviation from horizontal average). (**C**) Vertical conductive heat flux and its horizontal average. (**D**) Effective viscosity and its horizontal average. The thermal boundary layer below the lithosphere is dominated by conductive heat flow.

Depending on the amount of crustal heat production (*12*), small-scale convection (*6*) must deliver heat at a rate of about half of a typical continental heat flux of about 60 mW m^{-2} at the base of the lithosphere.

To assess the associated amplitudes and periods of vertical movements of Earth's surface in response to small-scale convection, we used a numerical two-dimensional (2D) thermomechanical model of the upper 660 km of Earth's crust and mantle (Fig. 1) (*13*). The model converges over several hundred My to a near-equilibrium state (fig. S2), characterized by a relatively cold, nondeforming lithosphere of roughly constant thickness overlying an upper mantle with an adiabat of ~0.6°C/km, transporting ~30 mW m^{-2} (Fig. 1C). At the base of the lithosphere and at the bottom of the model, thermal boundary layers with higher temperature gradients are maintained. The convective system receives and delivers heat by conduction.

The model provides a self-consistent representation of the lithosphere and upper mantle, including the asthenosphere, satisfying established knowledge regarding rheology and heat transfer. Small variations within experimentally determined limits for creep parameters in dry olivine (*14*) allowed us to control the mantle heat flux and the resulting lithospheric thickness. When the lowest possible experimentally constrained value of activation volume for dislocation creep is assumed and the pre-exponential factor of diffusion creep is varied within experimental limits (table S1), the thermal state varies from no convection to vigorous convection transporting heat at a rate of more than 50 mW m^{-2}. Diffusion and dislocation creep occur simultaneously, and the latter dominates in the upper part of the upper mantle. We chose the pre-exponential factor for diffusion creep, so that the transition between dislocation and diffusion creep is consistent with the depth at which seismic anisotropy vanishes (*15*) and so that the advected heat flux is ~ 30 mW m^{-2}.

In this model, discrete upwellings form at the basal thermal boundary layer and rise rapidly until they slow down because of viscous drag in the boundary layer at the base of the lithosphere (Fig. 1D). Here they spread out laterally while dissipating heat energy, which ultimately diffuses, with the thermal time constant of the lithosphere (~60 My in the present example), to the surface (Fig. 1B). The arrival of a buoyant upwelling at the base of the lithosphere produces a relatively rapid rise of the surface. Mass conservation means that the arrival of an upwelling requires the displacement of material from the boundary layer. This is accommodated by colder, negatively buoyant downwellings that sink into the asthenosphere. The surface expression of this process is subsidence driven by the slow densification of the cooling lithosphere, followed by rapid surface uplift as material gathered from the basal boundary layer suddenly detaches and sinks.

The time scale and amplitude of convection-induced surface movements depend on the chosen creep parameters [within observational constraints (*14*)] because these affect the scale of convective cells and the lithospheric thickness, and thus its effective elastic thickness. However, as long as the creep parameters result in convection, surface movements occur.

Issues relating to the effects of plate movement, long-term convective stability, and the time and length scale of buoyant loads and resulting vertical surface movements await resolution by 3D high-resolution numerical simulations. For example, the convective pattern may be modified by relative movement between the lithosphere and the asthenosphere, resulting in a 3D convective pattern with Richter rolls parallel to plate movement (*6*, *9*, *10*). Nevertheless, comparisons of 2D and 3D convection models have indicated that the resulting thermal state of the lithosphere remains similar in either case (*16*).

For the present model, vertical surface movements occur with periods spanning two orders of magnitude and with different amplitudes. The long-term component, with periods of up to several hundreds of My and amplitudes of more than 300 m (with no air or sediment filling the evolving depressions), correlates closely with the thermal state of the lithosphere as represented by the surface heat flux (Fig. 2, A and B). These slow changes are caused by transitions between different states of quasi-static long-term organization of convection cells, which last long enough to affect the thermal state of the lithosphere. Although it has been suggested that whole-mantle convection may be required to explain regional stratigraphic events of this time scale (*17*–*19*), the present results show that convection in the upper mantle may also contribute.

Faster surface movements with periods of ~2 to 20 My and amplitudes of ~30 m are related to the erratic movements of individual up- and downwellings and their interactions in the thermal

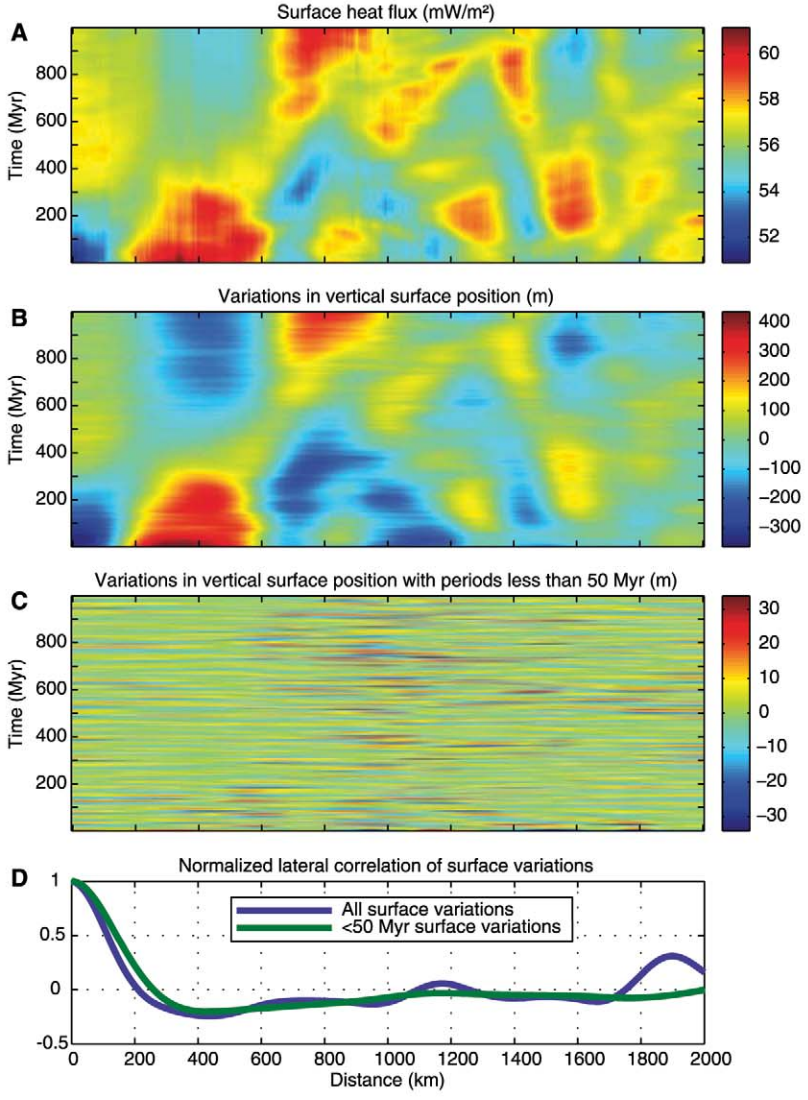


Fig. 2. Temporal evolution of surface heat flux and surface displacements due to small-scale convection. (**A**) Surface heat flux. (**B**) Surface displacement. (**C**) Surface displacements of periods less than 50 My. (**D**) Correlograms of surface displacements (*13*). Long-period surface displacements correlate with the thermal structure of the lithosphere. Short-period displacements are caused by buoyancy variations in the thermal boundary layer at the base of the lithosphere.

boundary layer (Fig. 2C). The buoyancy-induced movements are filtered by the viscoelasticity of the lithosphere (*12*); a stiffer lithosphere (larger effective elastic thickness) controls the response to relatively fast changes in buoyancy distribution in the thermal boundary layer, whereas a weaker lithosphere (smaller effective elastic thickness) controls the response to slower changes (fig. S3). The short-period movements therefore are correlated at larger distances (some 250 km) than are the longer periods (up to 200 km) (Fig. 2D) (fig. S3).

We suggest that these patterns of surface movements may be the overriding control on the formation of IP stratigraphic sequences that are observed ubiquitously in sedimentary basins and on continental margins and platforms (*1*). The surface movements cause changes in relative sea level, controlling patterns of erosion and deposition. Stratigraphic sequences are most easily identified on the margins of sedimentary basins, where sea-level changes have substantial effects on sediment lithofacies distribution and sedimentary architecture and hence facilitate the interpretation of stratigraphic sequences by means of seismic and borehole data (*1*, *20*).

Within a quasi-static convective state, individual up- and downwellings occur at time scales of less than 20 My. The resulting vertical surface movements generally show time-transgressive lateral correlations due to horizontal mass transport in the thermal boundary layer (Fig. 2C). Allowing for diachroniety in the range of 2 to 5 My, as may be the case when correlating via condensed sequences of basin centers using seismic data (*2*), many of the events of Fig. 2C are in fact correlatable at distances up to 800 km (fig. S7).

Sedimentary basins are often formed on continental margins and in intracratonic rifts. With an imposed extension of 60 km, our model produces a rift basin 300 km wide, exhibiting initial fault-controlled subsidence followed by thermal and loading-induced subsidence (Fig. 3) (movie S1) (*21*). However, the thermal decay time is longer than in conventional model predictions, which do not include the feedbacks between advective heat transport and lithospheric thinning (*22*). Furthermore, convection-induced effects, which result in periods of enhanced and decreased subsidence, complicate the post-rift subsidence pattern. They are stimulated by the rifting process and comprise discontinuous axial upwellings and, below the rift flanks, erosion of the base of the lithosphere (*23*). This causes the sedimentary fill to exhibit repeated patterns of transgression and regression, unconformities, and lateral migration of sedimentary facies (Fig. 3, A and D).

A widely held assumption regarding the cause of sea-level changes that control IP stratigraphic cycles is that it is of eustatic origin (*2*, *24*). This widespread view, combined with difficulties in dating rocks and horizons within them, has led to a situation in which sequence boundaries that are well dated in one place are used to date the same sequence boundary where it can be identified and correlated elsewhere (*25*). However, a mechanism driving globally synchronous eustatic variations with this periodicity has not been demonstrated, and, in any case, global synchronicity of such cycles is controversial (*3*, *4*, *17*, *25*).

Besides glacio-eustasy, the only mechanism proposed for generating IP stratigraphic cycles is one of changing tectonic stresses within the crust/lithosphere system, giving rise to vertical motions of the depositional surface from changes in its isostatic (mechanical) equilibrium position (*26*). Sequence boundaries in many sedimentary basins have been inferred to be clearly related to regional tectonic events (*3*, *27*). However, it has never been demonstrated that there should be a systematic oscillation in tectonic stresses in plates with a 2- to 20-My periodicity. On the other hand, there is plentiful evidence to suggest that this occurs at longer and shorter periods, at the scale of 20- to several hundred-My sequences—due to supercontinental cycles and volume changes in oceanic spreading centers—as well as shorter periods of less than 1 My due to glacial eustasy (*17*, *25*, *28*). Models in which changing tectonic stresses (*26*) are invoked to explain IP cycles are thus ad hoc regarding the actual process causing periodic stress changes.

In the model presented here, however, the ubiquitously occurring IP cycles are a natural consequence of the processes that produce and control the evolution of sedimentary basins themselves through the transport of heat out of Earth

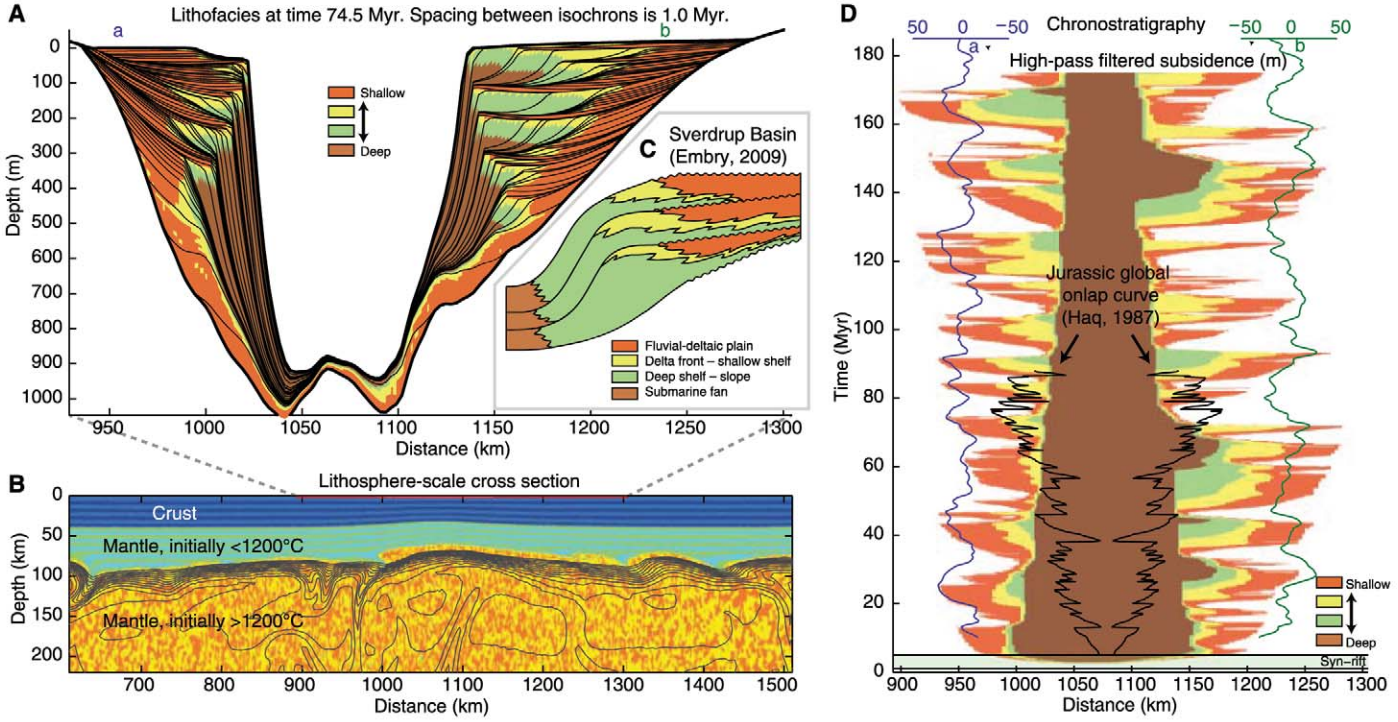


Fig. 3. Rift model with small-scale convection and constant sediment input and eustatic sea level. (**A**) Lithofacies (indicated by paleo water depth). Cyclic deposition is evident from unconformities and lateral migration of lithofacies; subsidence curves for locations a and b appear in (D). (**B**) Lithospheric cross-section showing gently thinned crust and mantle lithosphere and isotherms from 1200° to 1440°C (solid lines). (**C**) Cross section of the Sverdrup Basin, Canada (*29*). (**D**) Chronostratigraphic diagram and short-term vertical basement displacements at locations a and b. The inferred Jurassic global onlap curve (*2*) is shown in black for comparison. Differences in local vertical movements cause the two opposite basin margins to exhibit asymmetric stratigraphic evolution with different onlap patterns. In both cases, the time scale of cyclicity resembles that of the global Jurassic onlap curve.

by small-scale convection. The induced relative sea-level variations are regionally correlatable and are synchronous or nearly synchronous over spatial scales that encompass the dimensions of most shelf-slope systems of sedimentary basins, where sequences are most readily identifiable. This poses a challenge for the use of sequence stratigraphy in regional and global correlation as well as in the construction of global sea-level records. If IP sequences are indeed controlled by sublithospheric convection, they can only be considered locally for dating sedimentary successions. Our study thus provides an explanation for the enigmatic control on IP cycles, between the shorter-period variations caused by Milankovich cycles and those caused by regional in-plane stress changes and other tectonic and nontectonic contributions, including glacio-eustatic sea-level variations.

References and Notes

1. O. Catuneanu *et al.*, *Earth Sci. Rev.* **92**, 1 (2009).
2. B. U. Haq, J. Hardenbol, P. R. Vail, *Science* **235**, 1156 (1987).
3. A. D. Miall, *Geology* **20**, 787 (1992).
4. N. Christie-Blick, G. S. Mountain, K. G. Miller, *Science* **241**, 596 (1988).
5. P. J. Tackley, *Nat. Geosci.* **1**, 157 (2008).
6. F. M. Richter, *J. Geophys. Res.* **78**, 8735 (1973).
7. B. Parsons, D. McKenzie, *J. Geophys. Res.* **83** (B9), 4485 (1978).
8. W. R. Buck, *Nature* **313**, 775 (1985).
9. R. Stephenson, C. Beaumont, in *Mechanisms of Continental Drift and Plate Tectonics*, P. A. Davies, K. Runcorn, Eds. (Academic Press, London, 1980), pp. 111–122.
10. M. D. Ballmer, J. van Hunen, G. Ito, P. J. Tackley, T. A. Bianco, *Geophys. Res. Lett.* **34**, L23310 (2007).
11. S. D. King, J. Ritsema, *Science* **290**, 1137 (2000).
12. G. Ranalli, *Rheology of the Earth* (Chapman & Hall, London, ed. 2, 1995).
13. See supporting data on *Science* Online.
14. S. I. Karato, P. Wu, *Science* **260**, 771 (1993).
15. S. I. Karato, *Geophys. Res. Lett.* **19**, 2255 (1992).
16. J. Huang, S. Zhong, J. Van Hunen, *J. Geophys. Res. B: Solid Earth* **108**, 2405 (2003).
17. R. Moucha *et al.*, *Earth Planet. Sci. Lett.* **271**, 101 (2008).
18. L. L. Sloss, *Geol. Soc. Am. Bull.* **74**, 93 (1963).
19. S. Spasojević, L. Liu, M. Gurnis, R. D. Müller, *Geophys. Res. Lett.* **35**, L08305 (2008).
20. R. M. Mitchum, *Am. Assoc. Pet. Geol. Mem.* **26**, 53 (1977).
21. D. McKenzie, *Earth Planet. Sci. Lett.* **40**, 25 (1978).
22. C. E. Keen, in *Continental Extensional Tectonics* (Blackwell Scientific, London, 1987), p. 67.
23. W. R. Buck, *Earth Planet. Sci. Lett.* **77**, 362 (1986).
24. K. G. Miller *et al.*, *Science* **310**, 1293 (2005).
25. A. D. Miall, *The Geology of Stratigraphic Sequences* (Springer, Berlin, 1997).
26. S. Cloetingh, H. McQueen, K. Lambeck, *Earth Planet. Sci. Lett.* **75**, 157 (1985).
27. S. B. Nielsen, E. Thomsen, D. L. Hansen, O. R. Clausen, *Nature* **435**, 195 (2005).
28. R. D. Müller, M. Sdrolias, C. Gaina, B. Steinberger, C. Heine, *Science* **319**, 1357 (2008).
29. A. Embry, Search and Discovery, www.searchanddiscovery.com/documents/2009/30105embry/ (2009).

30. We thank M. Huuse, E. Thomsen, N. Christie-Blick, and three anonymous reviewers for constructive suggestions and D. L. Egholm for providing computational facilities.

Supporting Online Material

www.sciencemag.org/cgi/content/full/329/5993/827/DC1
Methods
Figs. S1 to S7
Table S1
References
Movie S1

26 March 2010; accepted 2 July 2010
10.1126/science.1190115

Three-Dimensional, Flexible Nanoscale Field-Effect Transistors as Localized Bioprobes

Bozhi Tian,[1]* Tzahi Cohen-Karni,[2]* Quan Qing,[1] Xiaojie Duan,[1] Ping Xie,[1] Charles M. Lieber[1,2]†

Nanoelectronic devices offer substantial potential for interrogating biological systems, although nearly all work has focused on planar device designs. We have overcome this limitation through synthetic integration of a nanoscale field-effect transistor (nanoFET) device at the tip of an acute-angle kinked silicon nanowire, where nanoscale connections are made by the arms of the kinked nanostructure, and remote multilayer interconnects allow three-dimensional (3D) probe presentation. The acute-angle probe geometry was designed and synthesized by controlling cis versus trans crystal conformations between adjacent kinks, and the nanoFET was localized through modulation doping. 3D nanoFET probes exhibited conductance and sensitivity in aqueous solution, independent of large mechanical deflections, and demonstrated high pH sensitivity. Additionally, 3D nanoprobes modified with phospholipid bilayers can enter single cells to allow robust recording of intracellular potentials.

Nanowire and nanotube electrical devices have been exploited for ultrasensitive detection of biological markers (*1*) and high-resolution extracellular recording from cells (*2*–*5*). However, localized and tunable three-dimensional (3D) sensing and recording with the prototypical nanoelectronic device, a nanoscale field-effect transistor (nanoFET) (*6*), have not been demonstrated because almost all examples of these devices are created on planar substrates. Ideally, rather than force the cell to conform to the substrate, a movable nanoFET with the necessary source (S) and drain (D) electrical connections could move into contact with the cell and probe within the cell membrane. However, minimally invasive insertion of a nanoFET into the confined 3D space of single cells, or even 3D cellular networks, is a major challenge because the S and D typically dominate the overall device size and define a planar and rigid structure, regardless of whether the nanoFET is on or suspended above a substrate (*5*, *6*).

Existing probes capable of intracellular sensing and recording include voltage-sensitive optical dyes (*7*, *8*) and single-terminal glass (*9*–*11*) or carbon (*12*–*14*) microelectrodes. Voltage-sensitive dyes can readily be used to interrogate action potentials with high spatial resolution, but they also have limitations in terms of signal-to-noise (S/N) ratio, pharmacological side effects, phototoxicity, and difficulty in differentiating single spikes (*7*, *8*). For electrical probes, the single electrical connection facilitates design and mechanical insertion into cells, but the requirement of direct ionic and/or electrical junctions between probe tips and cytosol also introduce several limitations. First, the tip size of these probes (~0.2 to 5 μm) (*9*–*14*) is a compromise between being small enough to penetrate or rupture the cell membrane with minimum damage (<5 μm) and large enough to yield a junction impedance that is sufficiently low (>0.2 μm) (*9*, *11*) so that small cellular signals can be discerned from thermal noise. Second, direct exposure of intracellular species to extraneous probe surfaces or electrolytes in probe lumen (*9*–*13*), especially for larger glass micropipettes, might induce irreversible changes to cells and, thus, prevent long-term and noninvasive cellular recordings. Finally, these probe techniques are intrinsically passive and are not capable of built-in signal processing and facile integration with other circuitries, especially given the emerging need to enable a cell-machine communication (*15*).

FETs can function in a sub–10-nm-size regime (*16*). NanoFETs could function as mechanically noninvasive probes capable of entering cells through endocytic pathways, as can occur with nanoparticles (*17*). Moreover, when interfacing with cells, the FETs process input/output information without the need for direct exchange with cellular ions; thus, interfacial impedance and biochemical invasiveness to cells can be minimized. In addition, because signals are transduced by change in field/potential at well-isolated surfaces, FETs can detect cellular potential (*2*–*5*), as well as biological macromolecules (*1*), and could be integrated for potential multiplexed intracellular measurements. Unfortunately, and as discussed above, the requirement of two electrical contacts to a FET, the S and D, makes design of 3D probes

[1]Department of Chemistry and Chemical Biology, Harvard University, Cambridge, MA 02138, USA. [2]School of Engineering and Applied Sciences, Harvard University, Cambridge, MA 02138, USA.

*These authors contributed equally to this work.
†To whom correspondence should be addressed. E-mail: cml@cmliris.harvard.edu

and their minimally invasive insertion into a cell or tissue a substantial challenge.

Recently, we demonstrated that variation of reactant pressure during silicon nanowire (SiNW) growth could introduce reproducible 120° kinks (*18*) and that the junction regions could be doped to create p-n diodes and FETs. We used this methodology to create a two-terminal FET probe that could be inserted into single cells. The growth of kinked SiNWs had to be tailored in the following ways: First, we needed to incorporate two or three cis-linked kinked units to yield probe-tip angles of 60° or 0°, respectively (Fig. 1A, top and middle). Because two trans-linked units (Fig. 1A, bottom) would yield an unusable probe tip, the selective synthesis of cis-linked units is central to our probe-geometry design. A representative scanning electron microscopy (SEM) image of an 80-nm diameter, doubly kinked SiNW with an intervening segment length (L) of ~160 nm between kink units (Fig. 1B) shows well-defined cis-linkage and an overall 60° tip angle (Fig. 1A, top). To investigate our ability to synthesize this cis-linkage of kink structural units reproducibly, we analyzed their fraction as a function of L in doubly kinked SiNWs. Notably, the plot of cis/(cis + trans), as L was varied from ~700 to 50 nm (Fig. 1C), shows that the cis conformation becomes dominant as L decreases. We can selectively synthesize cis-linked kinked units in good yield [fig. S1A (*19*)], e.g., ~66% where L ~ 50 nm, and such conformation control is also maintained in the growth of complex probe structures [fig. S1B (*19*)].

The second design consideration made use of selective in situ doping during synthesis to localize and self-label the nanoscale FET element adjacent to the topologically defined probe tip (Fig. 1A, pink segments) and to simultaneously "wire-up" the FET channel with nanowire S/D components (Fig. 1A, blue segments). As in our studies of single-kinked nanowires (*18*), we used heavy n^{++}-type doping for the nanowire S/D arms and reduced the concentration to light n-type doping to introduce a short ~200-nm region immediately following the growth of two sequential kinks and serving as the "pointlike" FET

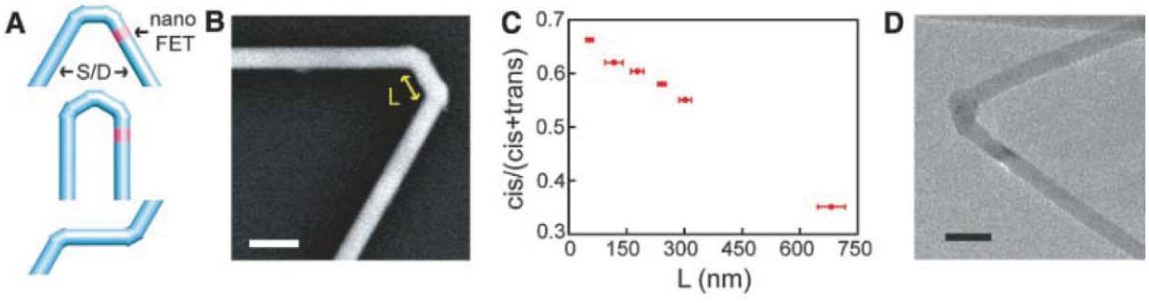


Fig. 1. Synthesis of kinked SiNW probes. (**A**) Schematics of 60° (top) and 0° (middle) multiply kinked nanowires and cis (top) and trans (bottom) configurations in nanowire structures. The blue and pink regions designate the source/drain (S/D) and nanoscale FET channel, respectively. (**B**) SEM image of a doubly kinked nanowire with a cis configuration. L is the length of segment between two adjacent kinks. (**C**) cis/(cis + trans) versus L plot. Error bars indicate ±1 SD from the mean. (**D**) Transmission electron microscopy image of an ultrathin 60° kinked nanowire. Scale bars, 200 nm (B); 50 nm (D).

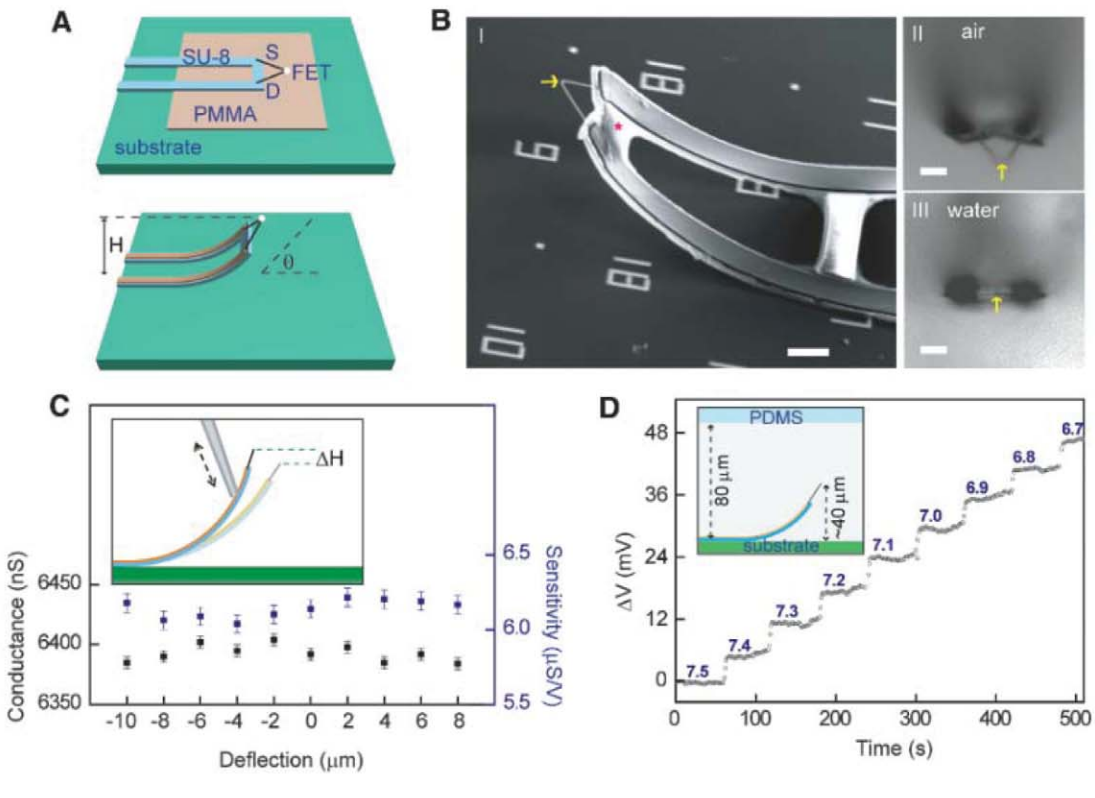


Fig. 2. 3D kinked nanowire probes. (**A**) Schematics of device fabrication. Patterned poly(methyl methacrylate) and SU-8 microribbons [see supporting online material (SOM) materials and methods (*19*)] serve as a sacrificial layer and flexible device support, respectively. The dimensions of the lightly doped n-type silicon segment (white dots) are ~80 by 80 by 200 nm^3. H and θ are the tip height and orientation, respectively, and S and D designate the built-in source and drain connections to the nanoscale FET. (**B**) SEM (I) and bright-field optical microscopy (II, III) images of an as-made device. The yellow arrow and pink star mark the nanoscale FET and SU-8, respectively. II and III are recorded in air and water, respectively. Scale bars, 5 μm. (**C**) Device conductance and sensitivity as a function of deflection of the probe using a micropipette controlled with a micromanipulator. The measurements were carried out in PBS solution. Error bars indicate ±1 SD from the mean. (Inset) Experimental scheme. ΔH, change in tip height. (**D**) Change in potential versus solution pH for a representative 3D nanowire probe. (Inset) Experimental scheme. For clarity, the pointlike FET elements are not labeled in the schematics in (C) and (D).

detector of the overall probe. Scanning gate microscopy (SGM) measurements [fig. S1 (*19*)] showed that nanoscale FETs were integrated at the probe tip during overall synthesis.

We have also examined the size limits of these synthetic bioprobes in terms of the overall nanowire diameter and length L between kinks, and we found that well-defined probe structures are possible for values as small as ~18 and 15 nm, respectively (Fig. 1D and fig. S2) (*19*). These data show that it is possible to create active semiconductor probes with dimensions smaller than microtubules in cells (*20*).

We next designed an unconventional nanoelectronic-device–fabrication approach that would allow these probes to be used as cellular probes. We made remote electrical interconnects to the S/D nanowire arms on ultrathin SU-8 polymer ribbons above a sacrificial layer (Fig. 2A, top). The interfacial stress between materials (*21*) was used to bend the probe upward after a final lift-off process (Fig. 2A, bottom); see fig. S3A for fabrication details (*19*). Our nanoprobes are distinct from previous nanoelectronic devices because (i) the FET channel (Fig. 2A, white dots) and S/D (Fig. 2A, black segments) components are integrated epitaxially at the nanoscale through synthesis (Fig. 1), similar to single-kink structures (*18*), (ii) the nanoscale FET is free-standing, and (iii) the acute-angle kinked-nanowire geometry and extended S/D arms spatially separate the functional nanoscale FET from the bulky interconnects by a distance up to ~30 μm, comparable to the size of single cells, so that the nanoscale interrogation can be realized with minimum interference from macroscopic interconnects.

A representative SEM image of one free-standing device (Fig. 2B, I) demonstrates that the 60° kinked probe is intact after fabrication with the two nanowire arm terminals sandwiched between the SU-8 polymer and the metal contacts. We achieved ≥90% yields with ~30 nanoprobe devices per chip. In addition, the probe height and angle (H and θ, Fig. 2A) were systematically tuned by changing the length and thickness of the free-standing part of the metal interconnects/SU-8 backbone (fig. S3B) (*19*). We also found that the nanoprobe H and θ typically increase when submerged in aqueous solution [H/θ of the device (Fig. 2B, I) are 25 μm/43° and 38 μm/90° in air and water, respectively (Fig. 2B, II and III)]. This change is reversible and suggests that the nanoprobe devices are intrinsically flexible, and moreover, that the specific orientation could be manipulated chemically (*21*). Last, free-standing 3D FET devices have been stored in air for at least 8 months without appreciable changes in nanoprobe orientations and FET sensitivity (<7 and 3%, respectively).

The sensitivity of the 3D nanoscale FET probes was characterized in phosphate-buffered saline (PBS) solution (Fig. 2C and fig. S4A). Measurements of the conductance versus reference potential for the 3D probes yielded sensitivities of 4 to 8 μS/V. Similar sensitivities, 4 to 8 μS/V, were observed for kinked nanowire devices fabricated on planar substrates, thus indicating that there is no degradation in the bent 3D configuration. We note that the sensitivity contribution from the lightly doped nanoFET is >97% of the total device response. Localized detection by the lightly doped region versus the heavily doped S/D nanowire arms is consistent with our SGM measurements on these acute-angle probes (fig. S1) and previous studies of single-kinked nanowires (*18*).

To further highlight the flexibility and robustness of the 3D nanoFET probes, we have characterized the conductance and sensitivity in PBS as a glass micropipette was used to vary the tip height (Fig. 2C, inset). Typical data (Fig. 2C) yield a <20-nS conductance change for a ~±10-μm change in H, which corresponds to <0.31% fluctuation in the total device conductance. Likewise, the device sensitivity remains stable with a maximum change of ~0.15 μS/V or 2.4% variation for this ~±10-μm tip-height change. In addition, repetitive bending does not degrade

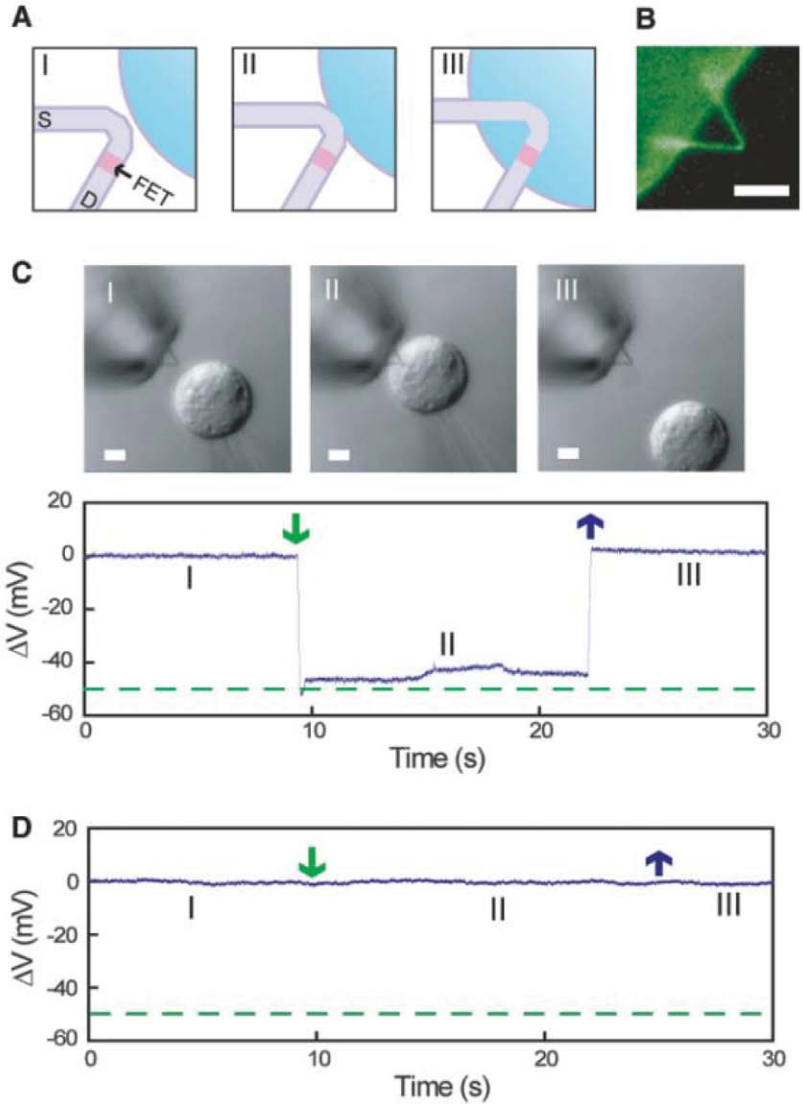


Fig. 3. Surface modification and cellular entry. (**A**) Schematics of nanowire probe entrance into a cell. Dark purple, light purple, pink, and blue colors denote the phospholipid bilayers, heavily doped nanowire segments, active sensor segment, and cytosol, respectively. (**B**) False-color fluorescence image of a lipid-coated nanowire probe. DMPC was doped with 1% nitrobenzoxadiazole dye–labeled lipids and imaged through a 510/21 band-pass filter. (**C**) Differential interference contrast microscopy images (upper panels) and electrical recording (lower panel) of an HL-1 cell and 60° kinked nanowire probe as the cell approaches (I), contacts and internalizes (II), and is retracted from (III) the nanoprobe. A pulled-glass micropipette (inner tip diameter ~ 5 μm) was used to manipulate and voltage clamp the HL-1 cell. The dashed green line corresponds to the micropipette potential. Scale bars, 5 μm. (**D**) Electrical recording with a 60° kinked nanowire probe without phospholipids surface modification. Green and blue arrows in (C) and (D) mark the beginnings of cell penetration and withdrawal, respectively.

the FET performance in these nanowire probes. Finally, the stable FET performance in different bending configurations suggests the capability of reliable sensing and recording in a flexible and tunable 3D manner from single devices, which could be particularly beneficial for interfacing with soft and motile biological systems.

We tested the sensing capabilities of the 3D SiNW probes by recording the response to variations in solution pH within a polydimethylsiloxane (PDMS) microfluidic channel (Fig. 2D, inset). Stepwise potential increases from 7.5 to 6.7 by 0.1 pH units were readily resolved, and the sensitivity of ~58 mV/pH was near the Nernstian limit. High-resolution recording indicates the capability of resolving changes as small as 0.02 pH units [fig. S4B (*19*)] in this physiologically relevant range of pH.

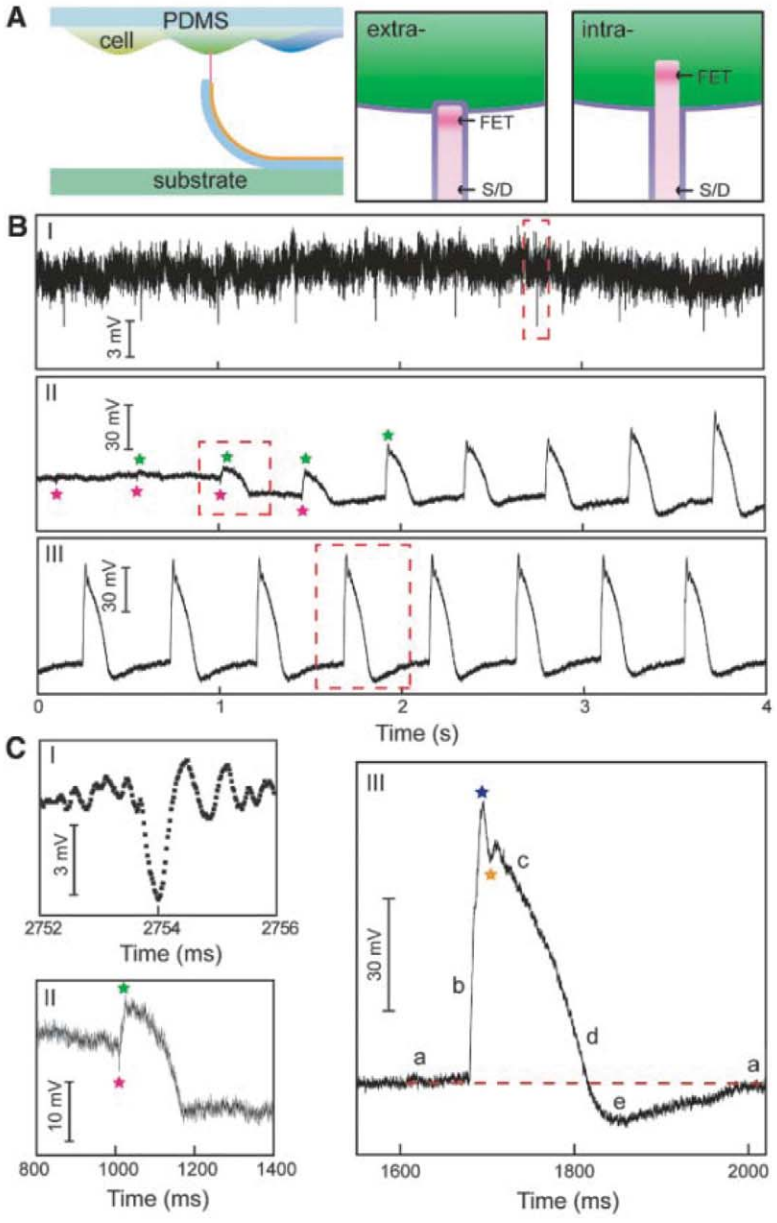


Fig. 4. Electrical recording from beating cardiomyocytes. (**A**) Schematics of cellular recording from the cardiomyocyte monolayer on PDMS (left) and highlight of extracellular (middle) and intracellular (right) nanowire/cell interfaces. The cell membrane and nanowire lipid coatings are marked with purple lines. (**B**) Electrical recording from beating cardiomyocytes: (i) extracellular recording, (ii) transition from extracellular to intracellular recordings during cellular entrance, and (iii) steady-state intracellular recording. Green and pink stars denote the peak positions of intracellular and extracellular signal components, respectively. The red-dashed boxes indicate regions selected for (C). (**C**) Zoom-in signals from the corresponding red-dashed square regions in (B). Blue and orange stars designate features that are possibly associated with inward sodium and outward potassium currents, respectively. The letters a to e denote five characteristic phases of a cardiac intracellular potential, as defined in text. The red-dashed line is the baseline corresponding to intracellular resting state. The cell culture, electronics, and recording details are specified in the SOM materials and methods section (*19*).

To use the 3D nanoFET probes in cells (Fig. 3A), we coated them with phospholipid bilayers, which can form on a variety of nanostructured inorganic materials (*22*–*24*) and also fuse with cell membranes (*24*). Accordingly, we modified the negatively charged SiO_2 surface of the SiNWs by fusion with unilamellar vesicles of phospholipid bilayers [1,2-dimyristoyl-sn-glycero-3-phosphocholine (DMPC)] (*19*, *22*). Fluorescence microscopy images of dye-labeled DMPC modified probes (Fig. 3B) indicate that the lipid bilayers form a continuous shell on our acute-angle nanoprobes, and device measurements show that the lipid surface coating results in <1% changes in both the nanoFET conductance and sensitivity. We then monitored the calibrated potential change of phospholipid-modified nanoFET probe while an isolated HL-1 cell (*25*) was moved into contact and then away from the nanoprobe using a glass micropipette under microscopy visualization (Fig. 3C, top). The micropipette was also used to clamp the intracellular potential at –50 mV (*11*). Notably, measurement of the potential versus time from the nanoFET probe shows a sharp ~52-mV drop within 250 ms after cell-to-tip contact. While the nanoprobe tip is within the cell, the recorded potential maintains a relatively constant value of ~–46 mV and then returns to baseline when the cell was detached from the nanowire probe end. NanoFET probes of similar sensitivity that were not coated with a phospholipid bilayer modification exhibited only baseline fluctuations (<±1 mV), as the HL-1 cell was brought into contact and then retracted (Fig. 3D). These results suggest that the biochemical state of the nanowire probe surfaces (*26*) is critical for assisting access to the intracellular region, possibly through membrane fusion (Fig. 3A) (*24*), and is distinct from larger, more rigid probes commonly used for intracellular electrical recording.

We have also investigated the formation of intracellular interfaces between our 3D nanoFET probes and spontaneously firing electrogenic cells. Embryonic chicken cardiomyocytes were cultured on PDMS substrates (*2*) and then positioned to place individual cells over phospholipid bilayer–modified vertical ($\theta = 90°$) nanoprobes within a cell-perfusion chamber (*2*, *4*), as shown schematically in Fig. 4A. Representative conductance-versus-time data recorded from a 3D nanoFET probe initially in gentle contact with a spontaneously beating cardiomyocyte cell (fig. S5A) (*19*) showed a sequence of distinct features (Fig. 4B). Initially, we observed regularly spaced spikes with a frequency of ~2.3 Hz, consistent with the beating cardiomyocyte (Fig. 4B, I). The peaks have a potential change of ~3 to 5 mV, a S/N ratio ≥ 2, and a submillisecond width (Fig. 4C, I). The peak amplitude, shape, and width are similar to extracellular recordings made with nanowire devices on substrates (*2*); moreover, optical images recorded at

the same time [fig. S5A (*19*)] are consistent with extracellular signals.

After a relatively brief (~40-s) period of extracellular signals, we observed several pronounced changes in recorded signals (Fig. 4, B and C, II and III) without application of external force to the PDMS/cell support. Specifically, the initial extracellular signals gradually disappeared (Fig. 4, B and C, II, pink stars). There was a concomitant decrease in baseline potential, and new peaks emerged that had an opposite sign, similar frequency, much greater amplitude, and longer duration (Fig. 4B, II, green stars). These new peaks, which are coincident with cardiomyocyte cell beating, rapidly reached a steady state (Fig. 4B, III) with an average calibrated peak amplitude of ~80 mV and duration of ~200 ms. The amplitude, sign, and duration are near those reported for whole-cell patch clamp recordings from cardiomyocytes (*27*, *28*); thus, we conclude that these data represent a transition to steady-state intracellular recording (Fig. 4A, right) with the 3D nanowire probe.

Detailed analysis of the latter steady-state peaks (Fig. 4C, III) shows five characteristic phases of a cardiac intracellular potential (*27*, *28*), including (a) resting state, (b) rapid depolarization, (c) plateau, (d) rapid repolarization, and (e) hyperpolarization. In addition, a sharp transient peak (blue star) and the notch (orange star) possibly associated with the inward sodium and outward potassium currents (*28*) can be resolved. Optical images recorded at the same time as these intracellular peaks (fig. S5B) showed the kinked nanowire probe tips in a possible intracellular region of the cell (*19*). When the PDMS/cell substrate was mechanically retracted from the 3D kinked nanowire devices, the intracellular peaks disappeared, but they reappeared when the cell substrate was brought back into gentle contact with the device. This process could be repeated multiple times without degradation in the recorded signal. When vertical 3D nanoprobe devices were bent into a configuration with angle $\theta < \sim 50°$ with respect to the substrate, or when kinked nanowire devices were fabricated on planar substrates, we could record only extracellular signals. These results confirm that electrical recording arises from the highly localized, pointlike nanoFET near the probe tip, which (i) initially records only extracellular potential, (ii) simultaneously records both extracellular and intracellular signals as the nanoFET spans the cell membrane, and (iii) records only intracellular signals when fully inside the cell.

Additional work remains to develop this new synthetic nanoprobe as a routine tool like the patch-clamp micropipette (*10*, *11*), although we believe that there are already clear advantages: Electrical recording with kinked nanowire probes is relatively simple without the need for resistance or capacitance compensation (*9*, *11*); the nanoprobes are chemically less invasive than pipettes, as there is no solution exchange; the small size and biomimetic coating minimizes mechanical invasiveness; and the nanoFETs have high spatial and temporal resolution for recording.

References and Notes

1. D. A. Giljohann, C. A. Mirkin, *Nature* **462**, 461 (2009).
2. T. Cohen-Karni, B. P. Timko, L. E. Weiss, C. M. Lieber, *Proc. Natl. Acad. Sci. U.S.A.* **106**, 7309 (2009).
3. J. F. Eschermann *et al.*, *Appl. Phys. Lett.* **95**, 083703 (2009).
4. Q. Qing *et al.*, *Proc. Natl. Acad. Sci. U.S.A.* **107**, 1882 (2010).
5. I. Heller, W. T. T. Smaal, S. G. Lemay, C. Dekker, *Small* **5**, 2528 (2009).
6. W. Lu, C. M. Lieber, *Nat. Mater.* **6**, 841 (2007).
7. A. Grinvald, R. Hildesheim, *Nat. Rev. Neurosci.* **5**, 874 (2004).
8. M. Scanziani, M. Häusser, *Nature* **461**, 930 (2009).
9. R. D. Purves, *Microelectrode Methods for Intracellular Recording and Ionophoresis* (Academic Press, London, 1981).
10. B. Sakmann, E. Neher, *Annu. Rev. Physiol.* **46**, 455 (1984).
11. A. Molleman, *Patch Clamping: An Introductory Guide to Patch Clamp Electrophysiology* (Wiley, Chichester, UK, 2003).
12. R. M. Wightman, *Science* **311**, 1570 (2006).
13. A. G. Ewing, T. G. Strein, Y. Y. Lau, *Acc. Chem. Res.* **25**, 440 (1992).
14. M. G. Schrlau, N. J. Dun, H. H. Bau, *ACS Nano* **3**, 563 (2009).
15. J. P. Donoghue, *Nat. Neurosci.* **5** (suppl.), 1085 (2002).
16. M. Ieong, B. Doris, J. Kedzierski, K. Rim, M. Yang, *Science* **306**, 2057 (2004).
17. M. Ferrari, *Nat. Rev. Cancer* **5**, 161 (2005).
18. B. Z. Tian, P. Xie, T. J. Kempa, D. C. Bell, C. M. Lieber, *Nat. Nanotechnol.* **4**, 824 (2009).
19. Materials and methods are available as supporting material on *Science* Online.
20. C. Conde, A. Cáceres, *Nat. Rev. Neurosci.* **10**, 319 (2009).
21. T. G. Leong *et al.*, *Proc. Natl. Acad. Sci. U.S.A.* **106**, 703 (2009).
22. N. Misra *et al.*, *Proc. Natl. Acad. Sci. U.S.A.* **106**, 13780 (2009).
23. X. J. Zhou, J. M. Moran-Mirabal, H. G. Craighead, P. L. McEuen, *Nat. Nanotechnol.* **2**, 185 (2007).
24. L. V. Chernomordik, M. M. Kozlov, *Nat. Struct. Mol. Biol.* **15**, 675 (2008).
25. W. C. Claycomb *et al.*, *Proc. Natl. Acad. Sci. U.S.A.* **95**, 2979 (1998).
26. B. D. Almquist, N. A. Melosh, *Proc. Natl. Acad. Sci. U.S.A.* **107**, 5815 (2010).
27. D. M. Bers, *Nature* **415**, 198 (2002).
28. D. P. Zipes, J. Jalife, *Cardiac Electrophysiology: From Cell to Bedside* (Saunders, Philadelphia, ed. 2, 2009).

29. We thank G. Yellen, W. C. Claycomb, B. P. Bean, P. T. Ellinor, G. H. Yu, D. Casanova, B. P. Timko, and T. Dvir for help with experiments and data analysis. C.M.L. acknowledges support from a NIH Director's Pioneer Award (5DP1OD003900), a National Security Science and Engineering Faculty Fellow (NSSEFF) award (N00244-09-1-0078), and the McKnight Foundation Neuroscience award.

Supporting Online Material

www.sciencemag.org/cgi/content/full/329/5993/830/DC1
Materials and Methods
Figs. S1 to S5
References

10 May 2010; accepted 7 July 2010
10.1126/science.1192033

Terrestrial Gross Carbon Dioxide Uptake: Global Distribution and Covariation with Climate

Christian Beer,[1]* Markus Reichstein,[1] Enrico Tomelleri,[1] Philippe Ciais,[2] Martin Jung,[1] Nuno Carvalhais,[1,3] Christian Rödenbeck,[4] M. Altaf Arain,[5] Dennis Baldocchi,[6] Gordon B. Bonan,[7] Alberte Bondeau,[8] Alessandro Cescatti,[9] Gitta Lasslop,[1] Anders Lindroth,[10] Mark Lomas,[11] Sebastiaan Luyssaert,[12] Hank Margolis,[13] Keith W. Oleson,[7] Olivier Roupsard,[14,15] Elmar Veenendaal,[16] Nicolas Viovy,[2] Christopher Williams,[17] F. Ian Woodward,[11] Dario Papale[18]

Terrestrial gross primary production (GPP) is the largest global CO_2 flux driving several ecosystem functions. We provide an observation-based estimate of this flux at 123 ± 8 petagrams of carbon per year (Pg C $year^{-1}$) using eddy covariance flux data and various diagnostic models. Tropical forests and savannahs account for 60%. GPP over 40% of the vegetated land is associated with precipitation. State-of-the-art process-oriented biosphere models used for climate predictions exhibit a large between-model variation of GPP's latitudinal patterns and show higher spatial correlations between GPP and precipitation, suggesting the existence of missing processes or feedback mechanisms which attenuate the vegetation response to climate. Our estimates of spatially distributed GPP and its covariation with climate can help improve coupled climate–carbon cycle process models.

Terrestrial plants fix carbon dioxide (CO_2) as organic compounds through photosynthesis, a carbon (C) flux also known at the ecosystem level as gross primary production (GPP). Terrestrial GPP is the largest global carbon flux, and it drives several ecosystem functions, such as respiration and growth. GPP thus contributes to human welfare because it is the basis for food, fiber, and wood production. In addition, GPP, along with respiration, is one of the major processes controlling land-atmosphere CO_2 exchange, providing the capacity of terrestrial ecosystems to partly offset anthropogenic CO_2 emissions.

Although photosynthesis at the leaf and canopy level are quite well understood, only tentative observation-based estimates of global terrestrial GPP have been possible so far. Plant- and stand-level GPP has previously been calculated as two times biomass production (*1*, *2*), with substantial

variation between biomes and sites (*3*–*5*). In the absence of direct observations, a combined GPP of all terrestrial ecosystems of 120 Pg C year^{-1} was obtained (*6*) by doubling global biomass production estimates (*7*) without an empirical basis of spatially resolved biomass production and its relationship to GPP. A global terrestrial GPP of 100 to 150 Pg C year^{-1} is consistent with the observed variation of ^{18}OCO in the atmosphere (*8*, *9*). However, the ability of ^{18}OCO to constrain GPP depends critically on the isotopic imbalance between GPP and respiration, and large uncertainties remain associated with isotope fractionation processes (*10*). The coupled uptake of carbonyl sulfide and CO_2 by plants (*11*, *12*) could potentially be used to further constrain terrestrial GPP by the combination of atmospheric [COS] measurements with an inversion of the atmospheric transport (*13*) once the ratio of CO_2 versus COS uptake, the additional COS deposition to soils, and the COS efflux from oceans is more precisely quantified.

As an alternative to directly constraining atmospheric data to estimate GPP, local information can be built into a process-oriented biosphere model, which is then applied globally. Knowledge of radiative transfer within vegetation canopies and of leaf photosynthesis has been used to represent GPP within process-oriented biosphere models, which explicitly simulate the behavior of the ecosystem as an interaction of the system components (e.g., leafs, roots, and soil) in a reductionist or mechanistic way. If these models are designed to also simulate a changing state of the biosphere (e.g., leaf area index and carbon pools), predictions of ecosystem dynamics under changing environmental conditions can be attempted (*14*). However, these process-oriented models are complex combinations of scientific hypotheses; hence, their results depend on these embedded hypotheses. A complementary approach is data-oriented or diagnostic modeling where general relationships between existing data sets are first inferred at site-level and then applied globally by using global grids of explanatory variables. Particularly when data-adaptive machine learning approaches are employed (e.g., artificial neural networks), results are much less contingent on theoretical assumptions and can be considered as data benchmarks for process models. However, being essentially a statistical approach, the diagnostic models do lack the capacity of extrapolating to completely different conditions and hinge on the availability of sufficient data. With the advent of a global network of ecosystem-level observations of CO_2 biosphere-atmosphere exchange (*15*) (www.fluxdata.org) and the development of new diagnostic modeling approaches, a data-oriented global estimation of GPP has become feasible. In this study, we estimate terrestrial GPP and its spatial details by diagnostic models and compare spatial correlations with climate variables to results from process-oriented models.

The diagnostic modeling comprises two steps, the parametrization of GPP in relation to explanatory variables at sites and the application of the model by using gridded information about these explanatory variables. For the first step, GPP was estimated by partitioning continuous measurements of net ecosystem exchange (NEE) into GPP and ecosystem respiration at flux tower sites (*16*). Two flux partitioning methods were considered using night-time or day-time NEE (*16*). Such site-level GPP data was then used to calibrate five highly diverse diagnostic models, which relate GPP to meteorology, vegetation type, or remote sensing indices at daily, monthly, or annual time scales (*16*). Two of these approaches are machine learning techniques: a model tree ensemble (MTE) (*17*) and an artificial neural network (ANN) (*18*). The Köppen-Geiger cross Biome (KGB) approach is a look-up table of mean GPP per ecoregion. GPP of whole river catchment areas is estimated by the water use efficiency approach (WUE) (*19*, *20*),

[1]Biogeochemical Model-Data Integration Group, Max Planck Institute for Biogeochemistry, 07745 Jena, Germany. [2]Laboratoire des Sciences du Climat et de L'Environnement, Institut Pierre Simon Laplace, CEA-CNRS-UVSQ, Gif-sur-Yvette, France. [3]Faculdade de Ciências e Tecnologia (FCT), Universidade Nova de Lisboa, Caparica, Portugal. [4]Biogeochemical Systems, Max Planck Institute for Biogeochemistry, 07745 Jena, Germany. [5]McMaster Centre for Climate Change, McMaster University, Hamilton, Ontario, Canada. [6]Department of Environmental Science, Policy and Management and Berkeley Atmospheric Science Center, University of California, Berkeley, CA 94720, USA. [7]National Center for Atmospheric Research, Boulder, CO 80305, USA. [8]Potsdam Institute for Climate Impact Research (PIK), 14473 Potsdam, Germany. [9]Climate Change Unit, Institute for Environment and Sustainability, European Commission, DG Joint Research Centre, Ispra, Italy. [10]Department of Earth and Ecosystem Science, Lund University, Sweden. [11]Department of Animal and Plant Sciences, University of Sheffield, Sheffield S10 2TN, UK. [12]Departement Biologie, Universiteit Antwerpen, Belgium. [13]Centre d'étude de la forêt, Faculté de foresterie, de géographie et de géomatique, Université Laval, Quebec, Canada. [14]Cirad-Persyst, UPR80, Fonctionnement et Pilotage des Ecosystémes de Plantation, Montpellier, France. [15]CATIE (Centro Agronómico Tropical de Investigación y Enseñanza), Turrialba, Costa Rica. [16]Nature Conservation and Plant Ecology Group, Wageningen University, Netherlands. [17]Graduate School of Geography, Clark University, Worcester, MA 01610, USA. [18]Department of Forest Environment and Resources, University of Tuscia, Viterbo, Italy.

*To whom correspondence should be addressed. E-mail: christian.beer@bgc-jena.mpg.de

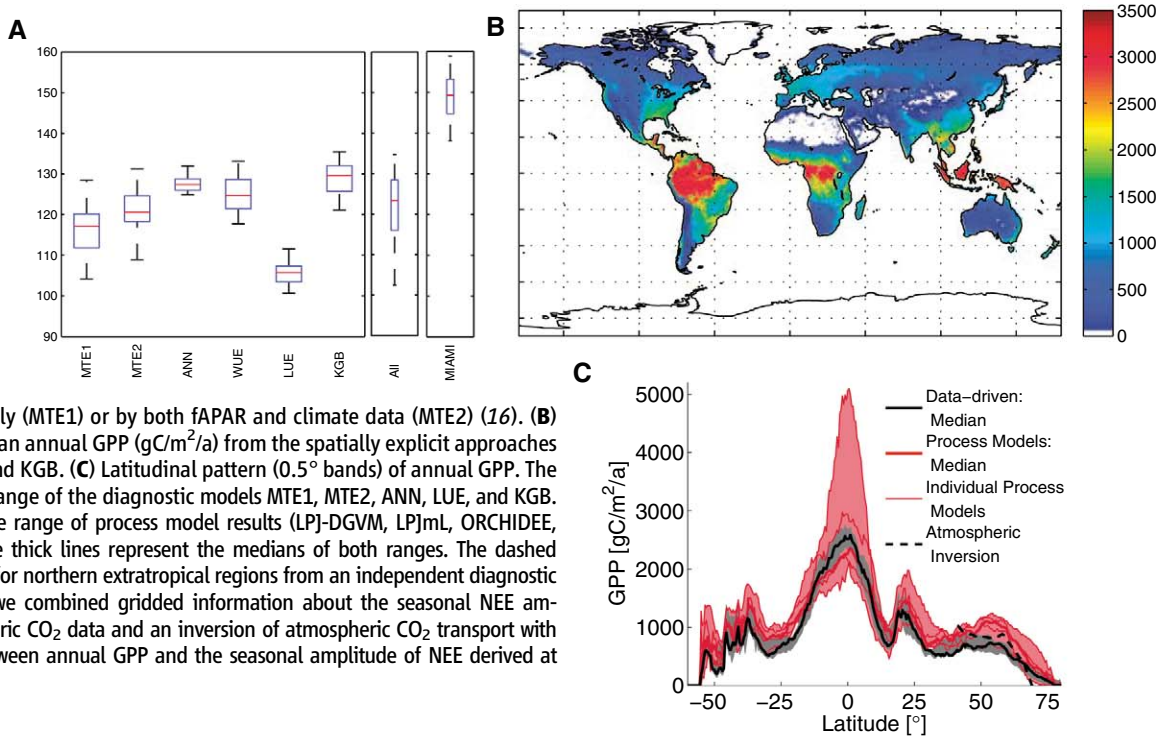


Fig. 1. (**A**) Distributions of global GPP (Pg C year^{-1}) for the five data-driven approaches that are most constrained by data, their combined global GPP distribution, and the GPP distribution by the Miami model. Shown are the median (red horizontal lines), the quartiles (blue boxes), and the 2.5 and 97.5 percentiles (vertical black lines), indicating the 95% confidence interval. MTE is either driven by fAPAR only (MTE1) or by both fAPAR and climate data (MTE2) (*16*). (**B**) Spatial details of the median annual GPP (gC/m^2/a) from the spatially explicit approaches MTE1, MTE2, ANN, LUE, and KGB. (**C**) Latitudinal pattern (0.5° bands) of annual GPP. The gray area represents the range of the diagnostic models MTE1, MTE2, ANN, LUE, and KGB. The red area represents the range of process model results (LPJ-DGVM, LPJmL, ORCHIDEE, CLM-CN, and SDGVM). The thick lines represent the medians of both ranges. The dashed black line shows the result for northern extratropical regions from an independent diagnostic model. In this approach, we combined gridded information about the seasonal NEE amplitude based on atmospheric CO_2 data and an inversion of atmospheric CO_2 transport with empirical relationships between annual GPP and the seasonal amplitude of NEE derived at flux tower sites.

which combines recently derived global WUE fields with the long-term averaged evapotranspiration at the watershed scale. This is an important constraint at the global scale, but the spatial resolution is too coarse to use the WUE approach for estimating the spatial distribution of GPP. The light-use efficiency approach (LUE) (*21*, *22*) was applied by combining in situ Bayesian calibration with an uncertainty propagation per vegetation and climate class. The Miami model (*23*) simply exploits the empirically obtained dependence of photosynthesis on temperature and precipitation. The second step, the mapping of flux tower GPP to the land surface, was performed by applying these diagnostic models to fields of remote sensing (*24*–*26*) and climatic data (*27*–*29*), which are now available with improved accuracy and high spatial resolution. In so doing, we take into account several sources of uncertainty, including uncertainty from model parametrization and from explanatory variables (*16*).

By making use of the new data streams and the ensemble of five diagnostic models, we present an observation-based estimate of an average global terrestrial GPP of 123 Pg C year^{-1} during the period 1998 to 2005 (Fig. 1A). Uncertainties and preprocessing of tower CO_2 flux measurements, tower representativeness, flux partitioning into GPP, uncertainties of climate and remote sensing data sets, and structural uncertainties of the diagnostic models propagate to a global uncertainty with a 95% confidence range from 102 to 135 Pg C year^{-1} or a robust estimate of standard deviation (*30*) of 8 Pg C year^{-1}. Results from the LUE approach were higher when using National Centers for Environmental Prediction (NCEP) radiation. However, we do not show NCEP-driven results because NCEP radiation and precipitation is known to be biased (*31*, *32*). The Miami model overestimates GPP compared to other approaches, particularly in sparsely vegetated areas with strong seasonality, such as savannahs, shrublands, and tundra (*16*) (table S5), because it does not account for the effect of climate-independent changes in vegetation structure (e.g., degradation) and vegetation type on GPP. Indeed, residuals of this model correlate significantly with mean annual fraction of absorbed photosynthetically active radiation (fAPAR) from remote sensing (fig. S14). Hence, being a classic model, it is shown only for comparison, but results from the Miami model were not taken into account in the following analyses.

Tropical forests assimilate 34% of the global terrestrial GPP (Table 1) and have the highest GPP per unit area (table S5). Savannahs account for 26% of the global GPP and are the second most important biome in terms of global GPP. The large area of savannahs (about twice the surface area of tropical forests) explain their high contribution. Moreover, the results highlight the importance of taking into account C4 vegetation in global GPP estimates. Based on the C4 distribution (figs. S6 and S7), more than 20% of terrestrial GPP is conducted by C4 vegetation. Given that there were less than 20 site-years of flux data for C4-dominated ecosystems, our uncertainty is largest for this type of vegetation. Therefore, an expansion of observational networks should focus on tropical C4 ecosystems. Boreal forests show a clear longitudinal gradient in GPP in northern Eurasia where GPP in the boreal zone decreases toward the east, where

Table 1. GPP for biomes of the world as defined by Prentice *et al*. (*6*). Combining the biome extent (fig. S17) with the spatially explicit GPP distributions by the approaches MTE1, MTE2, ANN, LUE, WUE, and KGB led to the respective median GPP per unit area separately for each biome (fig. S4). These medians were then multiplied by the biome area (*6*, *7*) (fig. S4) to estimate GPP in column 2. The estimated GPP total of 122 Pg C year^{-1} does not equal our overall median of 123 Pg C year^{-1} because the biome area defined by fig. S17 and by (*6*) differ slightly. The third column shows GPP as estimated by using NPP numbers from Saugier *et al*. (*7*) under the assumption that NPP/GPP = 0.5 (*6*).

Biome	GPP (Pg C year^{-1})	GPP = 2 × NPP* (Pg C year^{-1})
Tropical forests	40.8	43.8
Temperate forests	9.9	16.2
Boreal forests	8.3	5.2
Tropical savannahs and grasslands	31.3	29.8
Temperate grasslands and shrublands	8.5	14
Deserts	6.4	7
Tundra	1.6	1
Croplands	14.8	8.2
Total	121.7	125.2

*Based on integrated numbers for biomes (*6*, *7*)

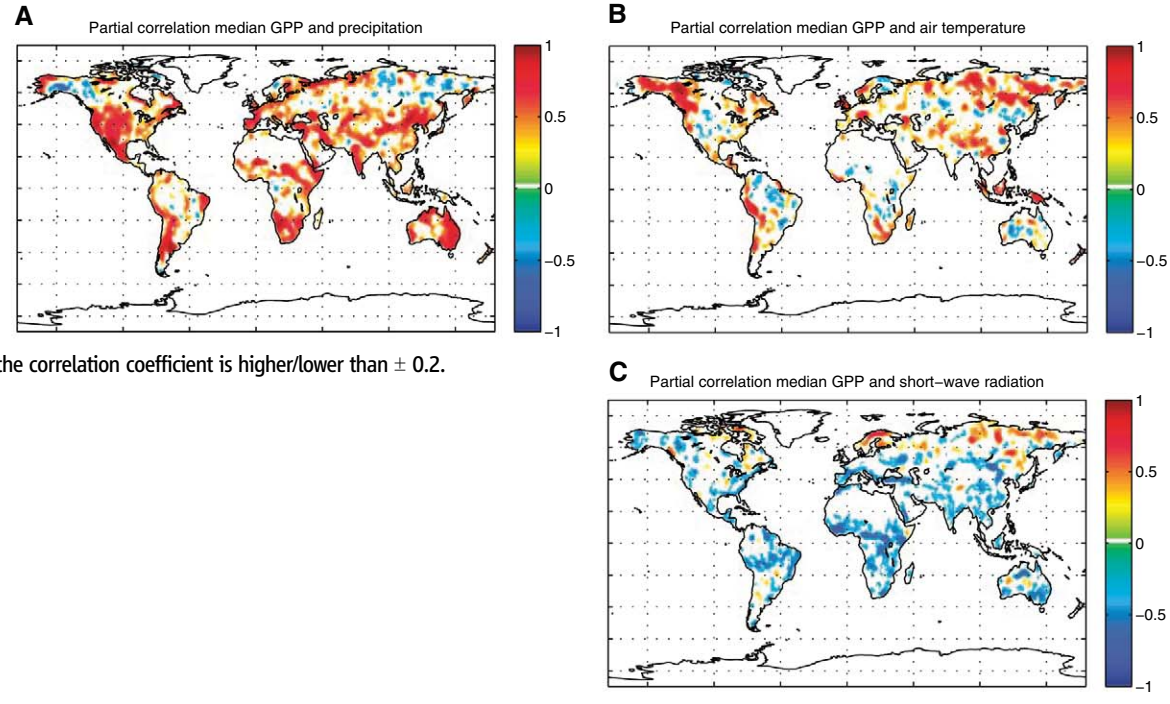


Fig. 2. Partial correlation in the spatial domain between GPP from Fig. 1B and either (**A**) CRU precipitation, (**B**) CRU air temperature, or (**C**) ECMWF ERA-Interim short-wave radiation after applying a moving 4.5° by 4.5° spatial window and subsequent median filtering. Shown are significant correlations ($P < 0.01$) of which the correlation coefficient is higher/lower than ± 0.2.

photosynthesis is subject to an increasingly continental climate (Fig. 1B).

The latitudinal pattern derived by the different diagnostic models falls into a quite narrow range (Fig. 1C). In contrast, there is a larger range among an ensemble of five process-oriented biosphere models (Fig. 1C); in comparison to our data-oriented range, some consistently overestimate GPP, and others underestimate tropical GPP while matching or slightly overestimating GPP in the temperate zone (fig. S26). A standard global parametrization of the process-oriented models has been applied in this study; it was not optimized against flux tower GPP because we aimed at evaluating the process-based GPP fields and their correlations to climatic variables. For comparison, we show results by an additional, completely different approach of scaling GPP from flux tower sites to the regional scale (fig. S16), where a reationship between the seasonal NEE amplitude and annual GPP is derived at flux tower sites and applied to the seasonal NEE amplitude derived through atmospheric inversion [update of (*33*)]. This approach leads to values at the upper end of the range of the diagnostic bottom-up approaches in northern extratropical regions but is still at the lower end of the range estimated by the process-oriented models. The differences between process-oriented and data-oriented estimates could lie in human-induced degradation of GPP by land use (*34*). However, other reasons are possible, including insufficient model parametrization or structural model errors that lead to an overestimation of GPP.

Partial correlation analyses between GPP and climatic variables for 4.5° by 4.5° moving windows show that spatial variation of GPP is associated with precipitation in 50 to 70% of the area of nontundra herbaceous ecosystems (Fig. 2A and Table 2). Also, 50% of the crop production occurs in regions where photosynthesis is colimited by precipitation, stressing the importance of water availability for food security. Interestingly, GPP in the same proportion of temperate forest areas correlates positively with precipitation (Table 2). In contrast, the spatial GPP variability in only 30% of tropical and boreal forests seems to be associated positively with precipitation, but GPP of more than half of the boreal forests correlates positively with air temperature (Table 2). Therefore, the GPP of these biomes seems to be robust against a moderate climate variation in the order of magnitude of the current spatial variability of climate, given the very low probability of a decrease in air temperature in the boreal zone.

We find negative correlations of productivity with incoming short-wave radiation, in particular in savannahs, the Mediterranean, and Central Asian grasslands (Fig. 2C and tables S6 to S8). These negative partial correlations may indicate an additional indirect effect of radiation or temperature on GPP by the water balance. Both climatic variables are usually associated with higher evapotranspiration rates, which will yield more negative water balances with higher temperature or radiation levels with consequent negative effects on primary productivity in these water-limited regions. This interpretation is possible notwithstanding a direct effect of temperature on vegetation by heat stress as well as increased levels of diffuse radiation associated with overall lower levels of radiation (*35*).

After four decades of research on the global magnitude of primary production of terrestrial vegetation (*23*, *36*), we present an observation-based estimate of global terrestrial GPP. Although we arrive at a global GPP of similar magnitude as these earlier estimates, our results add confidence and spatial details. The large range of GPP results by process-oriented biosphere models indicates the need for further constraining CO_2 uptake processes in these models. Furthermore, our spatially explicit GPP results contribute to a quantification of the climatic control of GPP. Complementing theoretical or process-oriented results (*37*, *38*) about climatic limitations of GPP, our observation-based results now constitute empirical evidence for a large effect of water availability on primary production over 40% of the vegetated land (Fig. 3A) and up to 70% in savannahs, shrublands, grasslands, and agricultural areas (Table 2). Our findings imply a high susceptibility of these ecosystems' productivity to projected changes of precipitation over the 21st century (*39*), but a robustness of tropical and boreal forests. Results of current process models show a large range and a tendency to overestimate precipitation-associated GPP (Fig. 3B). Most likely, the association of GPP and climate in process-oriented models can be improved by including negative feedback mechanisms (e.g., adaptation) that might stabilize the systems. Our high spatial resolution GPP estimates, their uncertainty, and their relationship to climate drivers should be useful for evaluating and thus improving coupled climate–carbon cycle process models.

Table 2. Percentage of biome area for which GPP is climatically controlled, indicated by a median partial correlation coefficient higher than 0.2 (or 0.5 in brackets). Several climate grids (CRU, ECMWF ERA-Interim, and GPCP precipitation) were used to perform a partial correlation between the median GPP map (Fig. 1B) and climate variables for 4.5° by 4.5° moving windows (*16*). Then, the fractional area with significant ($P < 0.01$) partial correlation higher than 0.2 (0.5) was calculated.

Biome	P* controlled	T† controlled	R‡ controlled
Tropical forests	29 (12)	39 (26)	4 (1)
Temperate forests	**50** (26)	41 (23)	6 (2)
Boreal forests	20 (5)	**55** (31)	21 (7)
Tropical savannahs and grasslands	**55** (31)	16 (5)	3 (0)
Temperate grasslands and shrublands	**69** (41)	37 (18)	6 (1)
Deserts	**61** (37)	18 (6)	8 (2)
Tundra	24 (13)	37 (27)	32 (12)
Croplands	**51** (25)	28 (13)	5 (1)

*Precipitation †Air temperature ‡Short-wave radiation

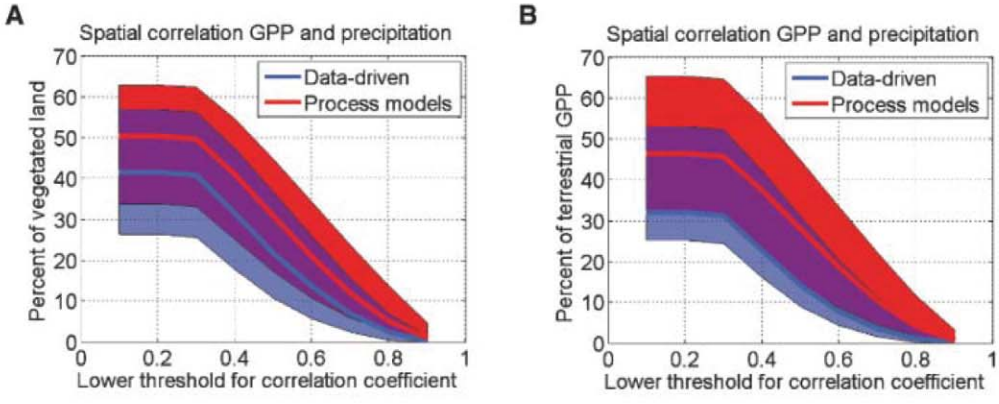


Fig. 3. Percentage of vegetated land surface (**A**) and corresponding GPP (**B**) that is controlled by precipitation, depending on the chosen threshold for the partial correlation coefficients that signal a control of GPP by a climate factor. The blue areas represent the range of data-driven estimates (MTE1, MTE2, ANN, LUE, and KGB) using different climate sources [CRU, ECMWF ERA-Interim, and GPCP (*16*)]. This is compared to the range of process-oriented model results (LPJ-DGVM, LPJmL, ORCHIDEE, CLM-CN, and SDGVM) in red. Purple shows the overlapping area. The thick lines represent the medians of both ranges. For instance, GPP of about 40% of the vegetated land surface is controlled by water availability by defining a water control of GPP as a partial correlation coefficient between GPP and precipitation higher than 0.2.

References and Notes

1. E.-D. Schulze, *Flora* **159**, 177 (1970).
2. H. Poorter, C. Remkes, H. Lambers, *Plant Physiol.* **94**, 621 (1990).
3. E. H. DeLucia, J. E. Drake, R. B. Thomas, M. Gonzalez-Meler, *Glob. Change Biol.* **13**, 1157 (2007).
4. S. Luyssaert *et al.*, *Glob. Change Biol.* **13**, 2509 (2007).
5. C. M. Litton, J. W. Raich, M. G. Ryan, *Glob. Change Biol.* **13**, 2089 (2007).
6. I. C. Prentice *et al.*, *Climate Change 2001: The Scientific Basis. Contribution of Working Group I to the Third Assessment Report of the Intergovernmental Panel on Climate Change*, J. Houghton, *et al.*, Eds. (Cambridge University Press, Cambridge, 2001), pp. 183–237.
7. B. Saugier, J. Roy, H. A. Mooney, *Terrestrial Global Productivity*, J. Roy, B. Saugier, H. A. Mooney, Eds. (Academic Press, San Diego, CA, 2001).
8. G. D. Farquhar *et al.*, *Nature* **363**, 439 (1993).
9. P. Ciais *et al.*, *J. Geophys. Res.* **102** (D5), 5857 (1997).
10. L. Wingate *et al.*, *Proc. Natl. Acad. Sci. U.S.A.* **106**, 22411 (2009).
11. L. Sandoval-Soto *et al.*, *Biogeosciences* **2**, 125 (2005).
12. J. E. Campbell *et al.*, *Science* **322**, 1085 (2008).
13. P. Suntharalingam, A. J. Kettle, S. M. Montzka, D. J. Jacob, *Geophys. Res. Lett.* **35**, L19801 (2008).
14. P. Friedlingstein *et al.*, *J. Clim.* **19**, 3337 (2006).
15. D. Baldocchi, *Aust. J. Bot.* **56**, 1 (2008).
16. Materials and methods are available as supporting material on *Science* Online.
17. M. Jung, M. Reichstein, A. Bondeau, *Biogeosciences* **6**, 2001 (2009).
18. D. Papale, R. Valentini, *Glob. Change Biol.* **9**, 525 (2003).
19. C. Beer, M. Reichstein, P. Ciais, G. D. Farquhar, D. Papale, *Geophys. Res. Lett.* **34**, L05401 (2007).
20. C. Beer *et al.*, *Glob. Biogeochem. Cycles* **23**, GB2018 (2009).
21. J. Monteith, *J. Appl. Ecol.* **9**, 747 (1972).
22. S. W. Running, P. Thornton, R. Nemani, J. Glassy, *Methods in Ecosystem Science*, O. Sala, R. Jackson, H. Mooney, R. Howarth, Eds. (Springer-Verlag, New York, 2000), pp. 44–57.
23. H. Lieth, *Primary Productivity of the Biosphere*, H. Lieth, R. H. Whittaker, Eds. (Springer-Verlag, Berlin, 1975), pp. 237–263.
24. R. Myneni *et al.*, *Remote Sens. Environ.* **83**, 214 (2002).
25. N. Gobron *et al.*, *J. Geophys. Res.-Atmos.* **111** (D13), D13110 (2006).
26. F. Baret *et al.*, *Remote Sens. Environ.* **110**, 275 (2007).
27. M. New, D. Lister, M. Hulme, I. Makin, *Clim. Res.* **21**, 1 (2002).
28. T. D. Mitchell, P. D. Jones, *Int. J. Climatol.* **25**, 693 (2005).
29. A. Simmons, S. Uppala, D. Dee, S. Kobayashi, *ECMWF Newsletter No. 110* (European Centre for Medium-Range Weather Forecasts, Shinfield Park, Reading, UK, 2007).
30. Median absolute deviation times 1.48.
31. B. Fekete, C. Vorosmarty, J. Roads, C. Willmott, *J. Clim.* **17**, 294 (2004).
32. M. Zhao, S. W. Running, R. R. Nemani, *J. Geophys. Res.-Biogeosci.* **111** (G1), G01002 (2006).
33. C. Rödenbeck, S. Houweling, M. Gloor, M. Heimann, *Atmos. Chem. Phys.* **3**, 1919 (2003).
34. A. Bondeau *et al.*, *Glob. Change Biol.* **13**, 679 (2007).
35. L. M. Mercado *et al.*, *Nature* **458**, 1014 (2009).
36. R. H. Whittaker, G. E. Likens, *Primary Productivity of the Biosphere*, H. Lieth, R. H. Whittaker, Eds. (Springer-Verlag, Berlin, 1975), pp. 305–328.
37. R. R. Nemani *et al.*, *Science* **300**, 1560 (2003).
38. D. Gerten *et al.*, *Geophys. Res. Lett.* **32**, L21408 (2005).
39. G. Meehl *et al.*, in *Climate Change 2007: The Physical Science Basis. Contribution of Working Group I to the Fourth Assessment Report of the Intergovernmental Panel on Climate Change*, S. Solomon *et al.*, Eds. (Cambridge University Press, Cambridge and New York, 2007), pp. 747–845.

40. This work used eddy covariance data acquired by the FLUXNET community and in particular by the following networks: AmeriFlux [U.S. Department of Energy, Biological and Environmental Research, Terrestrial Carbon Program (DE-FG02-04ER63917 and DE-FG02-04ER63911)], AfriFlux, AsiaFlux, CarboAfrica, CarboEuropeIP, CarboItaly, CarboMont, ChinaFlux, Fluxnet-Canada (supported by CFCAS, NSERC, BIOCAP, Environment Canada, and NRCan), GreenGrass, KoFlux, LBA, NECC, OzFlux, TCOS-Siberia, and USCCC. We acknowledge the support to the eddy covariance data harmonization provided by CarboEuropeIP, FAO-GTOS-TCO, Integrated Land Ecosystem-Atmosphere Processes Study, Max Planck Institute for Biogeochemistry, National Science Foundation, University of Tuscia, Université Laval and Environment Canada and U.S. Department of Energy and the database development and technical support from Berkeley Water Center, Lawrence Berkeley National Laboratory, Microsoft Research eScience, Oak Ridge National Laboratory, University of California–Berkeley, and University of Virginia. Remotely sensed land cover, fAPAR, and LAI were available through the Joint Research Centre of the European Commission, the National Aeronautics and Space Administration, and the projects GLC2000 and CYCLOPES. Climate data came from the European Centre for Medium-Range Weather Forecasts, the Climate Research Unit of the University of East Anglia, and the GEWEX project GPCP. We thank Mahendra K. Karki at GMAO/NASA for extracting the MOD17 required surface meteorological variables from the GMAO reanalysis dataset and Maosheng Zhao at NTSG of University of Montana for calculating the respective daytime VPD. We further acknowledge support by the European Commission FP7 projects COMBINE and CARBO-Extreme and a grant from the Max-Planck Society establishing the MPRG Biogeochemical Model-Data Integration. C.B., D.P., M.R., P.C., D.B., and S.L. conceived the study. C.B., C.R., D.P., E.T., M.J., M.R., and N.C. contributed diagnostic modeling results. C.B., A.B., G.B.B., M.L., F.I.W., and N.V. contributed process model results. C.B., E.T., and M.R. performed the analysis. C.B. and M.R. wrote the manuscript. All other coauthors contributed with data or substantial input to the manuscript.

Supporting Online Material

www.sciencemag.org/cgi/content/full/science.1184984/DC1
Materials and Methods
SOM Text
Figs. S1 to S34
Tables S1 to S9
References

20 November 2009; accepted 8 June 2010
Published online 5 July 2010;
10.1126/science.1184984
Include this information when citing this paper.

Global Convergence in the Temperature Sensitivity of Respiration at Ecosystem Level

Miguel D. Mahecha,[1,2]* Markus Reichstein,[1] Nuno Carvalhais,[1,3] Gitta Lasslop,[1] Holger Lange,[4] Sonia I. Seneviratne,[2] Rodrigo Vargas,[5] Christof Ammann,[6] M. Altaf Arain,[7] Alessandro Cescatti,[8] Ivan A. Janssens,[9] Mirco Migliavacca,[10] Leonardo Montagnani,[11,12] Andrew D. Richardson[13]

The respiratory release of carbon dioxide (CO_2) from the land surface is a major flux in the global carbon cycle, antipodal to photosynthetic CO_2 uptake. Understanding the sensitivity of respiratory processes to temperature is central for quantifying the climate–carbon cycle feedback. We approximated the sensitivity of terrestrial ecosystem respiration to air temperature (Q_{10}) across 60 FLUXNET sites with the use of a methodology that circumvents confounding effects. Contrary to previous findings, our results suggest that Q_{10} is independent of mean annual temperature, does not differ among biomes, and is confined to values around 1.4 ± 0.1. The strong relation between photosynthesis and respiration, by contrast, is highly variable among sites. The results may partly explain a less pronounced climate–carbon cycle feedback than suggested by current carbon cycle climate models.

Quantifying the intensity of feedback mechanisms between terrestrial ecosystems and climate is a central challenge for understanding the global carbon cycle and a prerequisite for reliable future climate scenarios (*1*, *2*). One crucial determinant of the climate–carbon cycle feedback is the temperature sensitivity of respiratory processes in terrestrial ecosystems (*3*, *4*), which has been subject to much debate (*5*–*10*). On the one hand, empirical studies have found high sensitivities of soil respiration to temperature, with values of Q_{10} (here an indicator of the sensitivity of terrestrial ecosystem respiration to air temperature) well above 2 (*11*, *12*). Dependencies of Q_{10} values on mean temperatures (*12*, *13*) have been attributed to the acclimatization of soil respiration (*5*), among other factors (*13*). On the other hand, global-scale models often make use of globally constant Q_{10} values of 2 or below to generate carbon dynamics consistent with global atmospheric CO_2 growth rates (*3*, *14*, *15*). Nonetheless, several models have directly included empirical dependencies of the parameterization of respiratory processes to environmental dynamics (*16*–*18*). This inclusion is questionable, given that single-site studies have indicated that factors seasonally covarying with temperature can confound the experimental retrieval

[1]Max Planck Institute for Biogeochemistry, 07745 Jena, Germany. [2]Institute for Atmospheric and Climate Science, ETH Zürich, Universitätsstrasse 16, 8092 Zürich, Switzerland. [3]Faculdade de Ciências e Tecnologia, FCT, Universidade Nova de Lisboa, 2829-516 Caparica, Portugal. [4]Norsk Institutt for Skog og Landskap, N-1431 Ås, Norway. [5]Department of Environmental Science, Policy and Management, University of California, Berkeley, CA 94720, USA. [6]Agroscope ART, Federal Research Station, Reckenholzstr. 191, CH-8046 Zürich, Switzerland. [7]McMaster Centre for Climate Change, McMaster University, Hamilton, Ontario L8S 4L8, Canada. [8]European Commission, Joint Research Center, Institute for Environment and Sustainability, I-21027 Ispra, Italy. [9]Department of Biology, University of Antwerpen, Universiteitsplein 1, 2610 Wilrijk, Belgium. [10]Remote Sensing of Environmental Dynamics Laboratory, DISAT, University of Milano-Bicocca, 20126 Milano, Italy. [11]Servizi Forestali, Agenzia per l'Ambiente, Provincia Autonoma di Bolzano, 39100 Bolzano, Italy. [12]Faculty of Sciences and Technologies, Free University of Bozen-Bolzano, Piazza Università 1, 39100 Bolzano, Italy. [13]Harvard University Department of Organismic and Evolutionary Biology, Harvard University Herbaria, 22 Divinity Avenue, Cambridge, MA 02138, USA.

*To whom correspondence should be addressed. E-mail: mmahecha@bgc-jena.mpg.de

of the intrinsic temperature dependence of respiration (*8*, *9*, *19*). Davidson and Janssens (*20*) therefore proposed to distinguish intrinsic temperature sensitivities by quantifying the inherent kinetic properties of substrate decomposition from apparent temperature responses. Moreover, it has been recognized that the direct inference of process sensitivities from emergent ecosystem behavior is not possible (*19*, *21*).

Our aim here was to retrieve the unconfounded (intrinsic) temperature sensitivities of ecosystem respiration across different climates and ecosystems, to resolve the question of whether we have to account for a globally varying and environmentally controlled Q_{10} in global carbon cycle modeling. The study is based on a global collection of eddy covariance CO_2 flux observations—the FLUXNET (*22*, *23*) LaThuile Database—which allows us to investigate greenhouse gas fluxes in response to meteorological variables across ecosystems. To minimize the influence of confounding effects, we apply a model-data fusion approach, scale-dependent parameter estimation (SCAPE) (*24*), that investigates processes on different time scales. The SCAPE concept exploits the idea that measured time series $Y(i)$, $i = 1, ..., N$, result from superimposed modes of characteristic variability X_f, where the index f indicates the attributable frequency class per subsignal (fig. S1). In SCAPE we can distinguish rapid and slow system responses (here, direct responses to temperature versus long-term organic matter dynamics described by the base respiration R_b). SCAPE differentiates the parameter estimation process according to identified time scales. We can therefore report temperature sensitivities ($Q_{10,sc}$) derived from specific (high-frequency) subsignals X_f such that confounding factors that operate on other (generally low-frequency) scales are excluded. Moreover, a nonparametric estimate of the low-frequency R_b time series is directly provided (*24*). In an experiment with artificial data (*24*) (fig. S2), we show that with this methodology the unconfounded $Q_{10,sc}$ of respiration is retrieved within ±0.1 units, even under unfavorable conditions of noise (fig. S3) (*25*).

The examination of the ecosystem respiration data shows that the unconfounded $Q_{10,sc}$ values are generally lower than temperature sensitivities reported by conventional estimates (Fig. 1) with very few exceptions (table S1). Conventional estimates would suggest an average sensitivity to air temperature of $\langle Q_{10} \rangle \approx 2.3$ across sites. The corresponding 95% confidence range is $2.0 \lesssim Q_{10} \lesssim 2.6$, estimated via a block bootstrapping across sites (*24*). This large range of possible Q_{10} values is very likely caused by confounding factors. However, once we derive the sensitivities using SCAPE, the weighted arithmetic mean is $\langle Q_{10,sc} \rangle \approx 1.4$; the 95% confidence range collapses to the narrow interval of $1.3 \lesssim Q_{10,sc} \lesssim 1.5$. The observed systematic difference between apparent and short-term temperature sensitivities corresponds exactly to what was expected by theoretical considerations reported previously (*9*).

The reported range of $Q_{10,sc}$ values is low, given that soil organic matter incubation experiments, which should not be hampered by seasonally confounding effects, typically find sensitivities of $Q_{10} > 2$ (*7*, *26*, *27*). We argue that this discrepancy is due to the controlled laboratory conditions, which partially exclude a number of factors relevant to ecosystem respiration. Measurements at ecosystem level always include multiple processes, such as the mobilization, transport, and transfer (e.g., via depolymerization) of carbon compounds, such that they are metabolizable in the mitochondria. At the end, the rate-limiting step will determine the overall temperature response of a chemical reaction chain, and the overall Q_{10} is lower than for the individual processes (*28*). For instance, it has been shown that the mycorrhizal respiration is largely limited by the carbon supply from the roots but is virtually insensitive to temperature variations (*29*, *30*). Moreover, growth respiration of plants is largely independent of temperature (*31*). Because ecosystem respiration is a mixed response of temperature-sensitive and -insensitive subprocesses, we assume that the comparable low $Q_{10,sc}$ values reported here are plausible estimates.

Despite a narrow range of identified $Q_{10,sc}$ values, the site-to-site variability in the $Q_{10,sc}$ estimates does not fully disappear. These differences may be partially caused by a propagation of noise in the nighttime eddy covariance data into parameter estimates. Also, slightly delayed system responses (*32*) can affect our estimates at ecosystem level. Minor confounding factors operating at comparable time scales, as the effective system responses may also play a role. The latter are not easily distinguishable, given that we are confronted with a signal comprising both soil and plant respiration at ecosystem level. Hence, it is very likely that the intrinsic temperature sensitivities of the involved subprocesses are confined to an even narrower range compared to our approximation at ecosystem level. This is remarkable because it implies a convergence of relative proportions of temperature-sensitive and -insensitive respiration fluxes among ecosystems.

To clarify whether a general environmental control might explain the site-to-site variability in the temperature sensitivities of ecosystem respiration, we investigated the relationship of mean annual temperature to the approximated intrinsic $Q_{10,sc}$ and apparent Q_{10} (Fig. 2). The $Q_{10,sc}$ estimates do not confirm the previously found or hypothesized patterns (Fig. 2B). Our results show a global convergence in the temperature sensitivity of terrestrial ecosystem respiration: An almost universal $Q_{10,sc}$ value across climate zones and ecosystem types (see also Fig. 1) is identified. Using the conventional estimates of Q_{10} instead,

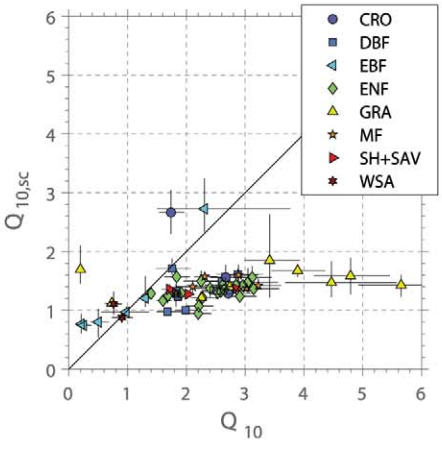


Fig. 1. Estimation of apparent Q_{10} values versus the approximated intrinsic $Q_{10,sc}$ values (SCAPE methodology) across 60 FLUXNET sites using nighttime observations of ecosystem-atmosphere CO_2 fluxes. Error bars show the 95% range of the parameter distributions. These uncertainties are identified via a bootstrapping approach (Q_{10}) or propagated from the SCAPE uncertainties of the time series decomposition [for $Q_{10,sc}$ (*24*)]. The color code indicates the plant functional type at each site: CRO, cropland; SH, shrubs; SAV, savanna; DBF, deciduous broadleaf forest; EBF, evergreen broadleaf forest; ENF, evergreen needleleaf forest; GRA, grassland; MF, mixed forest; WSA, woody savanna.

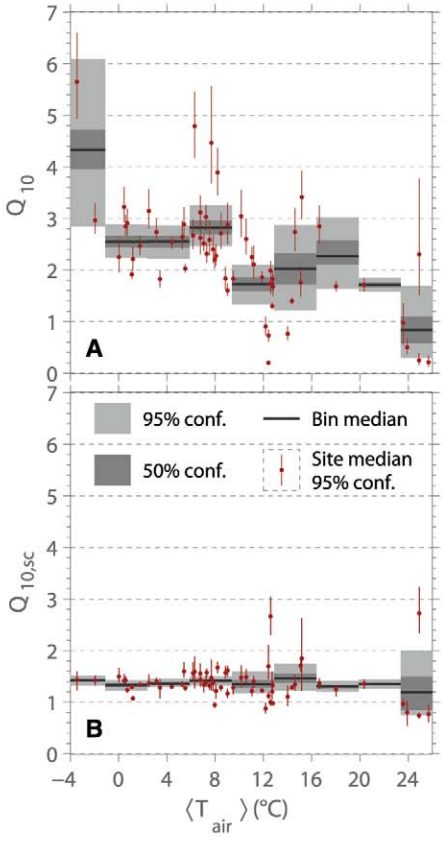


Fig. 2. Apparent Q_{10} and approximated intrinsic $Q_{10,sc}$ values binned over mean annual temperature (bin with 3.5°). Bin medians and their 50% and 95% uncertainty ranges are estimated via block bootstrapping (*24*). Original site-level parameter medians (and 95% confidence ranges) are shown in red. (**A**) The conventionally determined ecosystem-level Q_{10} values suggest an apparent temperature dependence. (**B**) The SCAPE $Q_{10,sc}$ estimates do not show any relationship with the mean annual temperature at the investigated FLUXNET sites.

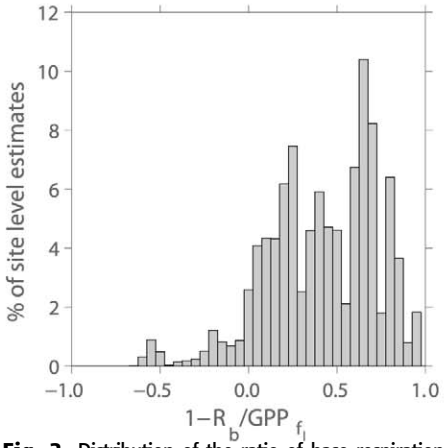


Fig. 3. Distribution of the ratio of base respiration to GPP_{fl}, $1-(R_b/GPP_{fl})$. Base respiration is a low-frequency signal (periods >3 months) and is compared here to *GPP* fluctuations in the same frequency range (f_l) for all sites. The ratio is recomputed 1024 times per site from a randomly chosen combination of subsignal estimates (of GPP_{fl} and R_b), such that the methodological uncertainty is considered (*24*).

we reproduce the effects of an apparent temperature control on the sensitivity (Fig. 2A). This underscores the problem that some unconsidered process, such as substrate supply, can be erratically interpreted as an oversensitivity of ecosystem metabolic processes to temperature.

Our analysis further emphasizes that despite having comparable short-term temperature sensitivities, ecosystems strongly differ in their carbon metabolization on longer time scales (Fig. 3): Low-frequency ecosystem responses are reflected in the temporal dynamics of the base respiration R_b (fig. S5). These time series show a tight relationship with corresponding low-frequency modes in independently estimated time series of gross primary productivity GPP_{fl} (*33*) (fig. S6). If we allow R_b to respond to GPP_{fl} with a time delay of a few days, which is a plausible assumption (*32*), all relationships are close to linear (fig. S7), confirming recent findings (*34*). The ratio $1-(R_b/GPP_{fl})$ hints at how the low-frequency dynamics of carbon uptake is propagated to the metabolization potential of labile soil organic carbon by autotrophic and heterotrophic respiration (*19*). Contrary to the global convergence in the temperature sensitivity, Fig. 3 shows that the low-frequency dynamics within the ecosystem spreads over a wide range. Consequently, future analyses of the climate–carbon cycle feedback have to emphasize the role of long-term dynamics in the terrestrial carbon cycle, rather than focusing on the short-term sensitivities. In particular, the role of intricate nonbiological stabilization processes versus carbon supply rates needs to be further investigated when trying to predict climate change effects on soil carbon dynamics.

The estimated average value for $Q_{10,sc}$ at ecosystem level likely also underlies recent observations of moderate global temperature responses of respiration in the long term (*35*). Also, modeling studies reporting that the global carbon cycle can be well modeled only if it is based on ecosystem-level Q_{10} values below 2 (*36*) are empirically confirmed by our findings. Consequently, carbon process model results will need to be investigated for their capacity to predict similar short-term $Q_{10,sc}$ and the variation of R_b at ecosystem level. However, given the nontrivial ecophysiological interpretation of a multitude of processes summing up to the observed ecosystem respiration, our results do not justify the prescription of $Q_{10} = 1.4$ for all rate constants in soil carbon models. Rather, a deeper understanding of the different factors and processes limiting soil carbon metabolization is needed for overcoming the "dead-soil box modeling paradigm" (*37*). Moreover, continuous time series of soil respiration, measured with automatic chambers, should be analyzed with the presented methodology, using soil temperature as a driving variable. Such studies could allow exclusive insights to the soil system, whereas our analysis at ecosystem level included aboveground respiration. Furthermore, we suggest exploring the SCAPE methodology in other fields of research, where confounding factors at different scales obscure the intrinsic relation between two variables of interest.

Our findings offer substantial evidence for the existence of universal intrinsic temperature sensitivities of terrestrial ecosystem respiration. The empirically inferred results suggest a $Q_{10,sc} \approx 1.4$ at ecosystem level. These results reconcile the empirical evidence with findings that the global carbon cycle can be well modeled only with an ecosystem level sensitivity of $Q_{10} < 2$. Moreover, our results may partly explain recent findings indicating a less pronounced climate–carbon cycle sensitivity (*38*) than assumed by current climate–carbon cycle model parameterizations. Contrary to the global convergence in temperature sensitivities, we find complex patterns in the low-frequency influence of photosynthetic carbon uptake and available assimilates on ecosystem respiration dynamics. Future research should strive for an in-depth understanding of carbon pathways through slow pools in terrestrial ecosystems.

References and Notes

1. C. D. Jones, P. Cox, C. Huntingford, *Tellus B* **55**, 642 (2003).
2. M. Heimann, M. Reichstein, *Nature* **451**, 289 (2008).
3. P. Friedlingstein *et al.*, *J. Clim.* **19**, 3337 (2006).
4. M. U. Kirschbaum, *Glob. Change Biol.* **16**, 2117 (2010).
5. Y. Luo, S. Wan, D. Hui, L. L. Wallace, *Nature* **413**, 622 (2001).
6. W. Knorr, I. C. Prentice, J. I. House, E. A. Holland, *Nature* **433**, 298 (2005).
7. C. Fang, P. Smith, J. B. Moncrieff, J. U. Smith, *Nature* **433**, 57 (2005).
8. M. Reichstein *et al.*, *Glob. Change Biol.* **11**, 1424 (2005).
9. E. A. Davidson, A. Janssens, I. Y. Luo, *Glob. Change Biol.* **12**, 154 (2006).
10. L. Gu, P. J. Hanson, W. Mac Post, Q. Liu, *Global Biogeochem. Cycles* **22**, GB4009 (2008).
11. J. Lloyd, J. A. Taylor, *Funct. Ecol.* **8**, 315 (1994).
12. M. F. U. Kirschbaum, *Soil Biol. Biochem.* **27**, 753 (1995).
13. S. Peng, S. Piao, T. Wang, J. Sun, Z. Shen, *Soil Biol. Biochem.* **41**, 1008 (2009).
14. W. Knorr, M. Heimann, *Tellus B Chem. Phys. Meterol.* **47**, 471 (1995).
15. T. M. Lenton, C. Huntingford, *Glob. Change Biol.* **9**, 1333 (2003).
16. P. E. Thornton *et al.*, *Agric. For. Meteorol.* **113**, 185 (2002).
17. S. Sitch *et al.*, *Glob. Change Biol.* **9**, 161 (2003).
18. G. Krinner *et al.*, *Glob. Biogeochem. Cycles* **19**, GB1015 (2005).
19. D. A. Sampson, I. A. Janssens, J. Curiel Yuste, R. Ceulemans, *Glob. Change Biol.* **13**, 2008 (2007).
20. E. A. Davidson, I. A. Janssens, *Nature* **440**, 165 (2006).
21. M. Reichstein, C. Beer, *J. Plant Nutr. Soil Sci.* **171**, 344 (2008).
22. D. Baldocchi, *Aust. J. Bot.* **56**, 1 (2008).
23. FLUXNET Synthesis data set (www.fluxdata.org).
24. See supporting material on *Science* Online.
25. The whole methodology and results are also reproducible with the Arrhenius model, because this is linearizable in an analog way. However, for the sake of a more intuitive parameter interpretation we chose the Q_{10} model here.
26. T. Kätterer, M. Reichstein, O. Andrén, A. Lomander, *Biol. Fertil. Soils* **27**, 258 (1998).
27. M. Reichstein, J.-A. Subke, A. C. Angeli, J. D. Tenhunen, *Glob. Change Biol.* **11**, 1754 (2005).
28. G. I. Ågren, J. A. M. Wetterstedt, *Soil Biol. Biochem.* **39**, 1794 (2007).
29. A. Heinemeyer, P. Ineson, N. Ostle, A. H. Fitter, *New Phytol.* **171**, 159 (2006).
30. F. Moyano, W. L. Kutsch, C. Rebmann, *Agric. For. Meteorol.* **148**, 135 (2008).
31. J. S. Amthor, *Ann. Bot.* **86**, 1 (2000).
32. Z. Kuzyakov, O. Gavrichovka, *Glob. Change Biol.* 10.1111/j.1365-2486.2010.02179.x (2010).
33. G. Lasslop *et al.*, *Glob. Change Biol.* **16**, 187 (2010).
34. M. Migliavacca *et al.*, *Glob. Change Biol.* 10.1111/j.1365-2486.2010.02243.x (2010).
35. B. Bond-Lamberty, A. Thomson, *Nature* **464**, 579 (2010).
36. J. T. Randerson *et al.*, *Glob. Change Biol.* **15**, 2462 (2009).
37. M. Bahn, I. A. Janssens, M. Reichstein, P. Smith, S. E. Trumbore, *New Phytol.* **186**, 292 (2010).
38. D. C. Frank *et al.*, *Nature* **463**, 527 (2010).

39. This work is the outcome of the La Thuile FLUXNET workshop 2007, which would not have been possible without the support provided by CarboEuropeIP, FAO-GTOS-TCO, the Integrated Land Ecosystem-Atmosphere Processes Study (iLEAPS, a core project of IGBP), Max Planck Institute for Biogeochemistry, NSF, University of Tuscia, and U.S. Department of Energy. Moreover, we acknowledge databasing and technical support from the Berkeley Water Center, Lawrence Berkeley National Laboratory, Microsoft Research eScience, Oak Ridge National Laboratory, University of California–Berkeley, and University of Virginia. The following networks provided flux data: AmeriFlux, AsiaFlux, CarboEuropeIP, ChinaFlux, Fluxnet-Canada, Canadian Carbon Program, LBA, NECC, OzFlux, TCOS-Siberia, and USCCC. AmeriFlux is supported by U.S. Department of Energy, Biological and Environmental Research, Terrestrial Carbon Program grant DE-FG02-04ER63917. This work was also supported by the European Research Council via the ERC-Staring Grant QUASOM, the European Commission project CARBO-Extreme (FP7-ENV-2008-1-226701), and a grant by the Max Planck Society establishing the MPRG Biogeochemical Model-Data Integration. We appreciate the collaboration of the FLUXNET synthesis team as documented at (*23*), and we thank M. Bahn, D. Baldocchi, H.-R. Künsch, D. Papale, P. Rayner, M. Rodeghiero, and S. Zaehle for very valuable comments. M.D.M., M.R., N.C., and G.L. conceived the study and developed the methodology with substantial input from H.L. M.D.M. performed the analysis and co-wrote the paper with M.R. All other authors gave substantial scientific input during the analysis and/or writing phase.

Supporting Online Material

www.sciencemag.org/cgi/content/full/science.1189587/DC1
Materials and Methods
SOM Text
Figs. S1 to S7
Table S1
References

15 March 2010; accepted 15 June 2010
Published online 5 July 2010;
10.1126/science.1189587
Include this information when citing this paper.

Association of Trypanolytic ApoL1 Variants with Kidney Disease in African Americans

Giulio Genovese,[1,2]* David J. Friedman,[1,3]* Michael D. Ross,[4] Laurence Lecordier,[5] Pierrick Uzureau,[5] Barry I. Freedman,[6] Donald W. Bowden,[7,8] Carl D. Langefeld,[8,9] Taras K. Oleksyk,[10] Andrea L. Uscinski Knob,[4] Andrea J. Bernhardy,[1] Pamela J. Hicks,[7,8] George W. Nelson,[11] Benoit Vanhollebeke,[5] Cheryl A. Winkler,[12] Jeffrey B. Kopp,[11] Etienne Pays,[5]† Martin R. Pollak[1,13]†

African Americans have higher rates of kidney disease than European Americans. Here, we show that, in African Americans, focal segmental glomerulosclerosis (FSGS) and hypertension-attributed end-stage kidney disease (H-ESKD) are associated with two independent sequence variants in the *APOL1* gene on chromosome 22 {FSGS odds ratio = 10.5 [95% confidence interval (CI) 6.0 to 18.4]; H-ESKD odds ratio = 7.3 (95% CI 5.6 to 9.5)}. The two *APOL1* variants are common in African chromosomes but absent from European chromosomes, and both reside within haplotypes that harbor signatures of positive selection. ApoL1 (apolipoprotein L-1) is a serum factor that lyses trypanosomes. In vitro assays revealed that only the kidney disease–associated ApoL1 variants lysed *Trypanosoma brucei rhodesiense*. We speculate that evolution of a critical survival factor in Africa may have contributed to the high rates of renal disease in African Americans.

African Americans suffer from kidney failure at high rates compared with individuals without recent African ancestry (*1*–*3*). Genetic variation at a locus in or near the *MYH9* gene on chromosome 22 has been associated with the increased susceptibility to focal segmental glomerulosclerosis (FSGS), HIV-associated nephropathy, and hypertension-attributed end-stage kidney disease (H-ESKD) observed in African Americans (*4*, *5*), but thus far causal mutations in *MYH9* have not been identified (*6*–*8*).

Previous genome-wide analyses have shown a strong signal of natural selection in the region containing the *MYH9* and *APOL1* genes [integrated haplotype score (iHS) data available at http://hgdp.uchicago.edu/] (*9*–*14*). This observation led us to hypothesize that the kidney disease risk alleles might be located in a larger interval than originally thought (*4*, *5*). The longer patterns of linkage disequilibrium (LD) associated with variants undergoing selection suggest that a positively selected risk variant could be in a larger interval containing the APOL genes rather than be confined to *MYH9*. Because the risk allele(s) are likely to be common in people with African ancestry, we reasoned that such alleles would be present in the data from the African individuals whose DNA was sequenced in the 1000 Genomes Project (www.1000genomes.org). We therefore used this newly available sequence data to identify polymorphisms within this expanded risk interval that showed large frequency differences between Africans and Europeans in order to test for association with renal disease.

We performed an initial association analysis comparing 205 African Americans with biopsy-proven FSGS but no family history of FSGS with 180 African-American controls. The strongest genetic associations with FSGS were clustered in a 10-kb region in the last exon of *APOL1*, the gene encoding apolipoprotein L-1 (table S1 and Fig. 1A) (*15*). The strongest signal was obtained for a two-locus allele, termed G1, consisting of the two derived nonsynonymous coding variants rs73885319 [$S^{342}\rightarrow G^{342}$ (S342G) (*15*)] and rs60910145 (I384M) in the last exon of *APOL1*. These two alleles were in perfect LD ($r^2 = 1$). The G1 allele (342G:384M) has a frequency of 52% in FSGS cases and 18% in controls (Table 1, $P = 1.07 \times 10^{-23}$).

When we performed logistic regression to control for G1, we identified a second strong signal (table S1 and Fig. 1B; $P = 4.38 \times 10^{-7}$). This second signal is a 6–base pair (bp) deletion (rs71785313, termed G2) close to G1 in *APOL1*. This deletion removes amino acids N388 and Y389 (*16*). Because of the proximity of rs73885319, rs60910145, and rs71785313, alleles G1 and G2 are mutually exclusive; recombination between them is very unlikely. Allele G2 has a frequency of 23% in FSGS cases and 15% in controls (Table 1).

After performing regressions controlling for both G1 and G2, we observed no other significant associations (table S1 and Fig. 1C). Conversely, controlling for multiple sets of variants in *MYH9* failed to eliminate the *APOL1* signal. The LD patterns in this region show that G1 and G2 are in strong LD with variants in *MYH9* (figs. S1 and S2). In particular, the *MYH9* E-1 haplotype, the best predictor of renal disease in previous studies, is present in most haplotypes containing the G1 or G2 allele. Specifically, E-1 is present in 89% of haplotypes carrying G1 and in 76% of haplotypes carrying G2, explaining the association of *MYH9* E-1 with renal disease.

Haplotype frequencies for FSGS cases and controls are shown in Table 1. No difference in FSGS risk was seen when comparing participants with no risk allele to participants with one risk allele [G1 or G2, $P = 0.81$, odds ratio (OR) = 1.04, confidence interval (CI) 0.63 to 2.13]. Comparing participants with zero or one risk allele to participants with two risk alleles provided an odds ratio for FSGS of 10.5 (CI 6.0 to 18.4). This analysis supports a completely recessive pattern of inheritance.

Next, we tested association of *APOL1* variants and renal disease in a larger cohort of 1030 African-American cases with H-ESKD and 1025 geographically matched African-American controls from the southeastern United States (*7*). In this cohort, we tested 36 variants chosen on the basis of the strongest signals of positive selection in a broader genomic region. We also tested nearby coding variants, including G1, G2, and putative *MYH9* risk single-nucleotide polymorphisms (SNPs). The strongest association was again with rs73885319 (G1 tag SNP; $P = 1.1 \times 10^{-39}$) (table S2). When we controlled for rs73885319 by logistic regression, rs71785313 (G2) again emerged as the strongest association signal ($P = 8.8 \times 10^{-18}$) (table S2). The statistical significance of the combined signal ($P = 10^{-63}$) was 35 orders of magnitude stronger than for *MYH9* SNPs. When we controlled for both G1 and G2, no residual association remained after correction for multiple SNP testing (table S2). Frequencies for these alleles are shown in Table 1.

With this larger population, we were able to examine the mode of inheritance of renal disease caused by G1 and G2 with greater precision. We partitioned cases and controls by genotype. One risk allele was associated with only a small increase in renal disease risk (OR = 1.26, CI 1.01 to 1.56). Two risk alleles versus zero risk alleles yielded an OR of 7.3 (CI 5.6 to 9.5). Two risk alleles compared to one risk allele showed an OR of 5.8 (CI 4.5 to 7.5). Overall, a recessive model best explains these findings and is in agreement with our analysis of the FSGS cohort.

We compared the frequency of G1 and G2 in several HapMap populations by using 1000 Ge-

[1]Division of Nephrology, Department of Medicine, Beth Israel Deaconess Medical Center and Harvard Medical School, Boston, MA 02215, USA. [2]Department of Mathematics, Dartmouth College, Hanover, NH 03755, USA. [3]Center for Vascular Biology Research, Department of Medicine, Beth Israel Deaconess Medical Center and Harvard Medical School, Boston, MA 02215, USA. [4]Renal Division, Department of Medicine, Brigham and Women's Hospital (BWH), Boston, MA 02215, USA. [5]Laboratory of Molecular Parasitology, Institut de Biologie et de Médecine Moléculaires, Université Libre de Bruxelles, B-6041 Gosselies, Belgium. [6]Department of Internal Medicine/Section on Nephrology, Wake Forest University School of Medicine, Winston-Salem, NC 27157, USA. [7]Department of Biochemistry and Center for Diabetes Research, Wake Forest University School of Medicine, Winston-Salem, NC 27157, USA. [8]Center for Human Genomics, Wake Forest University School of Medicine, Winston-Salem, NC 27157, USA. [9]Department of Biostatistical Sciences, Center for Public Health Genomics and Division of Public Health Sciences, Wake Forest University School of Medicine, Winston-Salem, NC 27157, USA. [10]Department of Biology, University of Puerto Rico at Mayaguez, Mayaguez, Puerto Rico 00681. [11]Kidney Disease Section, National Institute of Diabetes, Digestive, and Kidney Disease, National Institutes of Health, Bethesda, MD 20892, USA. [12]Laboratory of Genomic Diversity, SAIC-Frederick, Incorporated, National Cancer Institute–Frederick, Frederick, MD 21702, USA. [13]Broad Institute of Harvard and Massachusetts Institute of Technology, Cambridge, MA 02142, USA.

*These authors contributed equally to this work.
†To whom correspondence should be addressed. E-mail: mpollak@bidmc.harvard.edu (M.R.P.); epays@ulb.ac.be (E.P.)

nomes sequence data. G1 was present in about 40% of Yoruba (from Nigeria in West Africa) chromosomes but not in any chromosomes from European, Japanese, or Chinese individuals. Similarly, G2 was detected in sequence data from three Yoruba participants but not in the other three ancestral groups. This distribution data raised the possibility that these variants were selected for in Africa but not outside of Africa. The high frequency of the disease-associated variants in Yoruba and African Americans suggests that these variants may confer selective advantage in Africa.

Given the strong evidence for selection previously described in this chromosomal region (*9*–*14*), we genotyped G1 and G2 in 180 Yoruba samples from HapMap3 to test these variants for their potential contribution to selection (table S3). The allele frequencies in Yoruba are 38% for G1 and 8% for G2. We focused on statistical tests that detect selection by evaluating differential degrees of LD surrounding a putatively selected allele compared with the LD around the alternate allele at the same locus (*13*, *14*, *17*).

A recent (<10,000 years) selective sweep by a positively selected allele that rises quickly in frequency creates longer patterns of LD around the locus under selection (*18*). To determine whether this is the case for G1 and G2, we computed the extended haplotype homozygosity (EHH) (*17*) for each one of the two risk alleles and the nonrisk allele (Fig. 2A) (fig. S3). We also computed the integrated haplotype score (iHS) (*13*, *14*) and ΔiHH (integrated haplotype homozygosity) (*11*). The iHS statistic is suited to detect selective sweeps where the selected allele has reached intermediate frequency. |iHS| greater than 2 indicates unusual LD at a locus relative to the rest of the genome, a typical signature of natural selection. Because iHS is designed to have a standard normal distribution, its value is significant for the two G1 SNPs (rs73885319 and rs60910145, iHS = –2.45; Fig. 2B). ΔiHH is similar to iHS but tests absolute rather than relative differences in the length of haplotypes (*11*). ΔiHH was high for G1 SNPs (ΔiHH = 0.471 cM, more than 5 SD from the mean) and for rs71785313 (G2) (ΔiHH = 0.275 cM, 2.6 SD from the mean) compared with the genome as a whole, again showing that haplotypes carrying the derived alleles are positively selected (Fig. 2C). Results of multiple tests for selection and population differentiation for the entire region from 34,900 to 35,100 kb [National Center for Biotechnology Information (NCBI) 36] are reported in table S4. These same tests in Europeans showed no deviation from neutrality at *APOL1*.

Taken together, these data are consistent with the hypothesis that G1 rose quickly to high frequency because of positive selection in Africa. There is less power to show an effect for G2 because of its lower frequency in Yoruba (8%) and the more robust effect of G1 within the same interval, but haplotypes containing G2 show higher degrees of homozygosity than haplotypes that contain neither G1 nor G2, again suggesting positive selection for G2 in Africans (Fig. 2A).

Although statistical tests for selection are valuable for identifying haplotypes under selection, only functional tests can convincingly demonstrate the causal variant. Our selection tests indicated that G1 and G2 are on haplotypes that have been strongly selected for in Africa but not

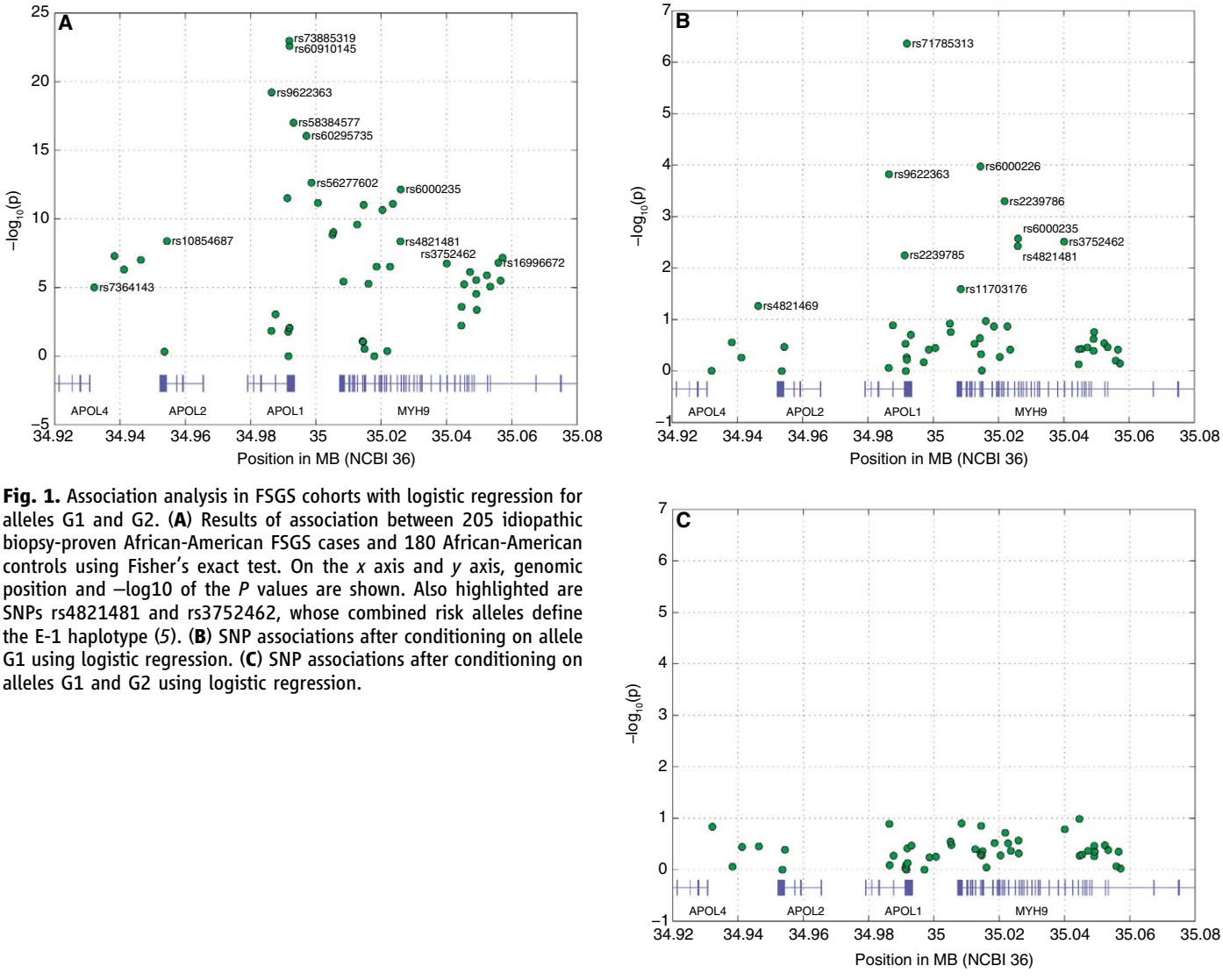


Fig. 1. Association analysis in FSGS cohorts with logistic regression for alleles G1 and G2. (**A**) Results of association between 205 idiopathic biopsy-proven African-American FSGS cases and 180 African-American controls using Fisher's exact test. On the *x* axis and *y* axis, genomic position and −log10 of the *P* values are shown. Also highlighted are SNPs rs4821481 and rs3752462, whose combined risk alleles define the E-1 haplotype (*5*). (**B**) SNP associations after conditioning on allele G1 using logistic regression. (**C**) SNP associations after conditioning on alleles G1 and G2 using logistic regression.

in Europe or Asia. G1 and G2 are plausible candidates for the causal variants because they alter the sequence of the encoded protein.

ApoL1 is the trypanolytic factor of human serum that confers resistance to the *Trypanosoma brucei brucei* (*T. b. brucei*) parasite (*19*, *20*). *T. b. brucei* has evolved into two additional subspecies, *Trypanosoma brucei rhodesiense* and *Trypanosoma brucei gambiense*, which have both acquired the ability to infect humans (*21*, *22*). *T. b. rhodesiense* is predominantly found in Eastern and Southeastern Africa, whereas *T. b. gambiense* is typically found in Western Africa, although some overlap exists (*23*). Because these parasites exist only in sub-Saharan Africa, we hypothesized that the *APOL1* gene may have undergone natural selective pressure to counteract these trypanosoma adaptations. As an initial test of this hypothesis, we performed in vitro assays to compare the trypanolytic potential of the variant, disease-associated forms of ApoL1 proteins with that of the "wild-type" form of ApoL1 protein that is not associated with renal disease.

T. b. rhodesiense can infect humans because of a serum resistance–associated protein (SRA) that interacts with the C-terminal helix of ApoL1 and inhibits its antitrypanosomal activity (*20*, *24*). A recent study showed that mutations and deletions engineered into this helix prevent SRA from binding to ApoL1 (*25*). Intriguingly, one of the G1 sequence variants (I384M) and the 6-bp deletion (G2) are located exactly at the SRA binding site in the ApoL1 C-terminal helix.

We conducted an analysis of the in vitro lytic potential of 75 human plasma samples with different combinations of G1 and G2 genotypes on

Table 1. Number and frequencies of APOL1 genotypes and alleles in FSGS and H-ESKD cases and controls.

	BWH FSGS cases	NIH FSGS cases	Total cases	Controls	H-ESKD cases	Controls
			Genotype			
WT + WT	3	26	29	77	239	409
WT + G1	6	21	27	41	173	250
WT + G2	0	9	9	36	124	155
G1 + G1	25	35	60	9	219	41
G1 + G2	15	38	53	8	203	50
G2 + G2	3	11	14	5	44	18
Total	52	140	192	176	1002	923
			Allele			
G1 Freq.	0.68	0.47	0.52	0.18	0.41	0.21
G2 Freq.	0.19	0.25	0.23	0.15	0.21	0.13

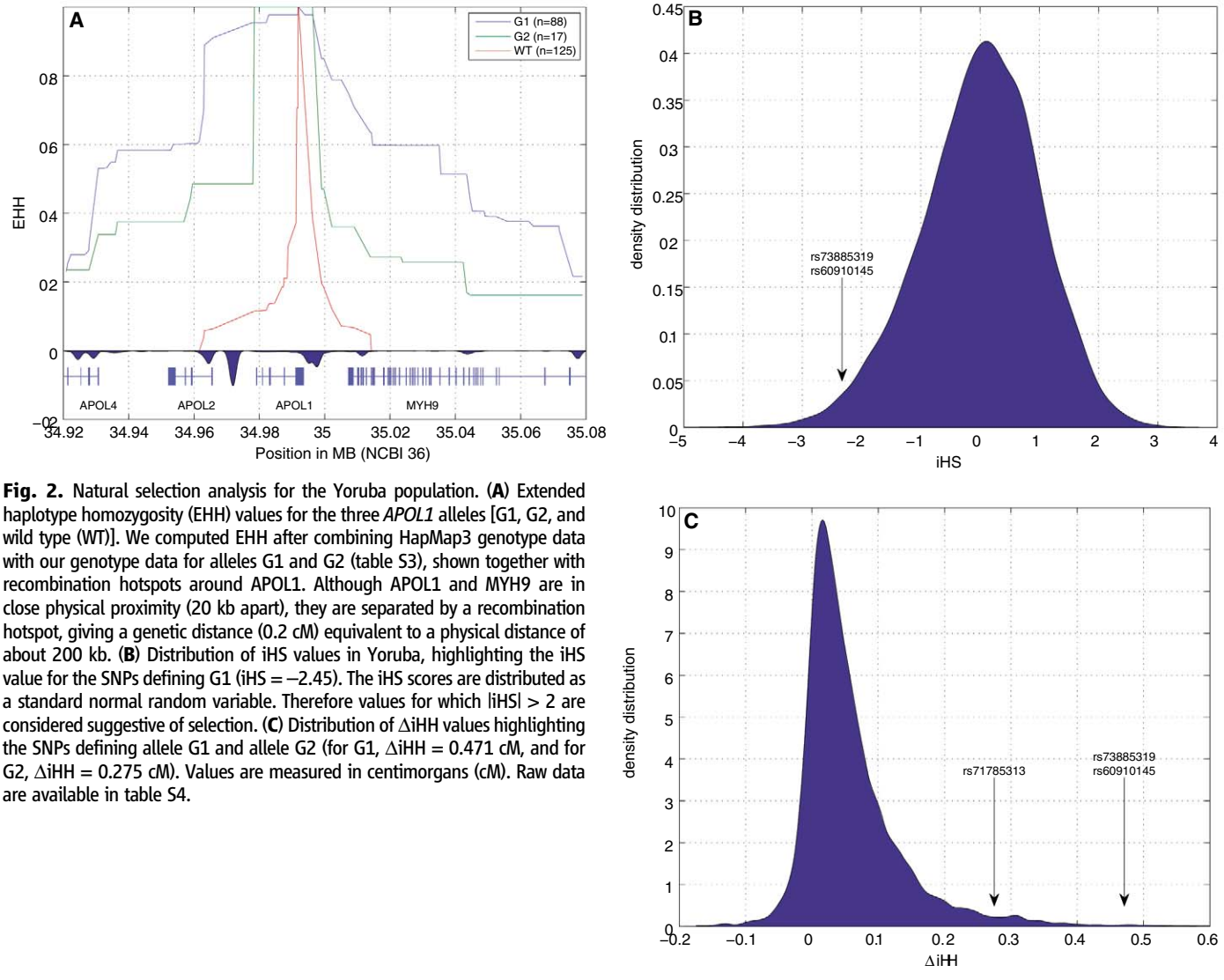


Fig. 2. Natural selection analysis for the Yoruba population. (**A**) Extended haplotype homozygosity (EHH) values for the three *APOL1* alleles [G1, G2, and wild type (WT)]. We computed EHH after combining HapMap3 genotype data with our genotype data for alleles G1 and G2 (table S3), shown together with recombination hotspots around APOL1. Although APOL1 and MYH9 are in close physical proximity (20 kb apart), they are separated by a recombination hotspot, giving a genetic distance (0.2 cM) equivalent to a physical distance of about 200 kb. (**B**) Distribution of iHS values in Yoruba, highlighting the iHS value for the SNPs defining G1 (iHS = −2.45). The iHS scores are distributed as a standard normal random variable. Therefore values for which |iHS| > 2 are considered suggestive of selection. (**C**) Distribution of ΔiHH values highlighting the SNPs defining allele G1 and allele G2 (for G1, ΔiHH = 0.471 cM, and for G2, ΔiHH = 0.275 cM). Values are measured in centimorgans (cM). Raw data are available in table S4.

T. b. brucei, *T. b. rhodesiense*, and *T. b. gambiense*. All 75 plasma samples efficiently lysed *T. b. brucei*, but none of them lysed *T. b. gambiense*. Of the 75 samples, 46 lysed SRA-positive *T. b. rhodesiense* clones, which are typically resistant to lysis by human serum, and all 46 originated from individuals harboring at least one G1 or G2 allele (table S5). As measured by titration using serial dilution, the lytic potency of these plasmas against SRA-positive *T. b. rhodesiense* was higher for G2 than for G1, whereas it was similar for both genotypes against SRA-negative parasites (Fig. 3A). Although lysis of *T. b. rhodesiense* by G2 could be explained by the inability of SRA to bind to this mutant, this conclusion did not hold for G1 ApoL1 variants, which SRA could still efficiently bind (Fig. 3B).

We confirmed these results with recombinant ApoL1 proteins. The S342G/I384M (G1) and delN388/Y389 (G2) (*16*) variants lysed both SRA-negative and SRA-positive *T. b. rhodesiense* parasites (Fig. 3C) but not *T. b. gambiense*. Although G2 was more potent than G1 against SRA-positive *T. b. rhodesiense*, the reverse was true on SRA-negative parasites. Recombinant ApoL1 variants with either S342G alone or I384M alone were less lytic against *T. b. rhodesiense* than when present together, whereas recombinant ApoL1 engineered to have both G1 and G2 mutations was not more active than mutants with G2 alone (Fig. 3C). As shown in Fig. 3, D and E, all measured features of the *T. b. rhodesiense* lytic process (kinetics, transient inhibition by chloroquine, typical swelling of the lysosome) were similar to those observed on *T. b. brucei* with either normal human serum or recombinant ApoL1 (*19*). Therefore, deletion of N388/Y389 was necessary and sufficient to prevent interaction with SRA and to confer on ApoL1 the ability to lyse *T. b. rhodesiense* in vitro, whereas the combination of S342G and I384M was required for maximal ability to lyse *T. b. rhodesiense* despite remaining bound by SRA. None of the variant forms of ApoL1 lysed *T. b. gambiense*.

In summary, we have shown that sequence variation in *APOL1* contributes to the increased risk of renal disease in African Americans. Two lines of evidence support this conclusion: (i) the nonsynonymous variants coded by G1 and the coding region deletion G2 in *APOL1* are the sequence variants showing the strongest association with FSGS and H-ESKD, and (ii) association of renal disease with the *MYH9* sequence variants disappears after controlling for the *APOL1* risk variants. An important question to be addressed in future studies is how sequence variation in ApoL1 mechanistically contributes to the pathogenesis of kidney disease. The recessive model that best fits

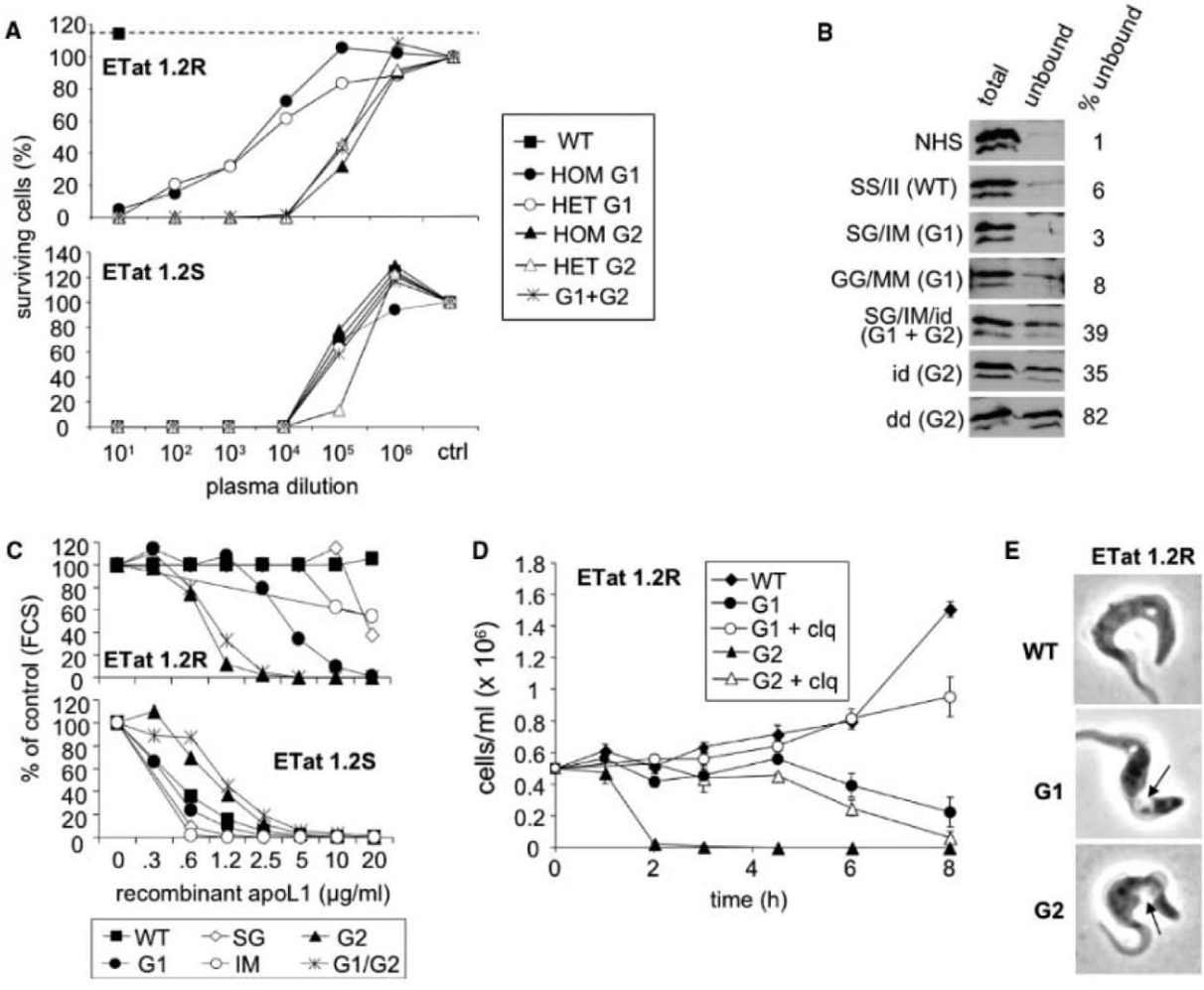


Fig. 3. G1 and G2 alleles of ApoL1 kill *T. b. rhodesiense*. Trypanolytic potential of ApoL1 variants on normal human serum–resistant (SRA+) and normal human serum–sensitive (SRA–) *T. b. rhodesiense* ETat 1.2 clones. ETat 1.2R is resistant to normal human serum, and ETat 1.2S is sensitive to normal human serum. (**A**) Titration of trypanolytic activity in human plasma samples after overnight incubation, expressed as % survival compared with fetal calf serum (FCS) control. hom and het, homozygous and heterozygous mutations, respectively. (**B**) ApoL1 content of various plasma samples before and after affinity chromatography through SRA column (NHS, normal human serum; WT, wild-type ApoL1; S, Ser^{342}; G, Gly^{342}; I, Ile^{384}; M, Met^{384}; i, insertion of N388/Y389; d, deletion of N388/Y389). (**C**) Trypanolytic activity of various recombinant ApoL1 variants after overnight incubation, expressed as % survival compared with fetal calf serum (FCS) control. (**D**) Kinetics of trypanolysis by 20 μg/ml recombinant ApoL1 variants in the presence or absence of 25 μM chloroquine (clq). Error bars indicate SD (n = 3). (**E**) Phenotype of ETat1.2R trypanosomes incubated with various recombinant ApoL1 (20 μg/ml; 1-hour and 30-min and 6-hours incubation, for G1 and G2 respectively; the arrows point to the swelling lysosome).

our genetic data suggests that ApoL1 is performing a critical role in the kidney that is impaired in the setting of the ApoL1 variants, although toxicity of the ApoL1 variants remains a possibility.

We have shown that both ApoL1 variants lyse a deadly subspecies of *Trypanosoma* that is normally completely resistant to ApoL1 lytic activity. The G2 mutation prevents the SRA virulence factor produced by *T. b. rhodesiense* from binding to and inactivating ApoL1. Even 10,000-fold dilutions of plasma containing these mutations (particularly G2) are active against the parasite. This raises the possibility that transfusion of small volumes of plasma, ApoL1-containing HDL particles, or recombinant protein might be effective treatment for trypanosomiasis caused by *T. b. rhodesiense*.

The kidney disease–associated variants are located on haplotypes that show statistical evidence of natural selection. The lytic activity of the variant proteins against *Trypanosoma* provides a plausible—albeit still speculative—biological explanation for natural selection. The results are consistent with a heterozygous advantage model because the protective effect against *T. b. rhodesiense* is dominant whereas the association with renal disease is recessive. Sickle cell disease is a well-established precedent for a model in which mutations conferring heterozygote advantage against a parasitic infection can confer a strong biological disadvantage for homozygotes (*26*). When present in heterozygous form, certain hemoglobin mutations confer protection against malaria but when homozygous cause severe diseases of the red blood cell (for example, sickle cell disease and thalassemia).

It will be interesting to determine the distribution of these mutations throughout sub-Saharan Africa. In present-day Africa, *T. b. rhodesiense* is found in the eastern part of the continent, whereas we noted high frequency of the trypanolytic variants and the signal of positive selection in a West African population. Changes in trypanosome biology and distribution and/or human migration may explain this discrepancy, or resistance to *T. b. rhodesiense* could have favored the spreading of *T. b. gambiense* in West Africa. Alternatively, ApoL1 variants may provide immunity to a broader array of pathogens beyond just *T. b. rhodesiense*, as a recent report linking ApoL1 with anti-Leishmania activity may suggest (*27*). Thus, resistance to *T. b. rhodesiense* may not be the only factor causing these variants to be selected.

The APOL1 risk alleles for renal disease occur in more than 30% of African-American chromosomes. Given their high frequency and their strong effect on disease risk, unraveling the molecular mechanisms by which they contribute to renal injury will be of great importance in understanding and potentially preventing renal disease in individuals of recent African ancestry.

References and Notes

1. C. Byrne, J. Nedelman, R. G. Luke, *Am. J. Kidney Dis.* **23**, 16 (1994).
2. S. G. Satko, B. I. Freedman, S. Moossavi, *Kidney Int. Suppl.* **67**, (s94), S46 (2005).
3. U.S. Renal Data System, National Institutes of Health, National Institute of Diabetes and Digestive and Kidney Diseases, Bethesda, MD, 2009.
4. W. H. Kao *et al.*, *Nat. Genet.* **40**, 1185 (2008).
5. J. B. Kopp *et al.*, *Nat. Genet.* **40**, 1175 (2008).
6. B. I. Freedman *et al.*, *Nephrol. Dial. Transplant.* **24**, 3366 (2009).
7. B. I. Freedman *et al.*, *Kidney Int.* **75**, 736 (2009).
8. G. W. Nelson *et al.*, *Hum. Mol. Genet.* **19**, 1805 (2010).
9. L. B. Barreiro, G. Laval, H. Quach, E. Patin, L. Quintana-Murci, *Nat. Genet.* **40**, 340 (2008).
10. K. A. Frazer *et al.*, *Nature* **449**, 851 (2007).
11. S. R. Grossman *et al.*, *Science* **327**, 883 (2010); published online 7 January 2010 (10.1126/science.1183863).
12. R. Kimura, A. Fujimoto, K. Tokunaga, J. Ohashi, H. Harpending, *PLoS One* **2**, e286 (2007).
13. B. F. Voight, S. Kudaravalli, X. Wen, J. K. Pritchard, *PLoS Biol.* **4**, e72 (2006).
14. T. K. Oleksyk, G. W. Nelson, P. An, J. B. Kopp, C. A. Winkler, *PLoS One* **5**, e11474 (2010).
15. Materials and methods are available as supporting materials on *Science* Online.
16. Single-letter abbreviations for the amino acid residues are as follows: G, Gly; I, Ile; M, Met; N, Asn; S, Ser; and Y, Tyr.
17. P. C. Sabeti *et al.*, *Nature* **419**, 832 (2002).
18. P. C. Sabeti *et al.*, *Science* **312**, 1614 (2006).
19. D. Pérez-Morga *et al.*, *Science* **309**, 469 (2005).
20. L. Vanhamme *et al.*, *Nature* **422**, 83 (2003).
21. W. Gibson, *Trends Parasitol.* **18**, 486 (2002).
22. W. C. Gibson, *Parasitol. Today* **2**, 255 (1986).
23. P. P. Simarro, J. Jannin, P. Cattand, *PLoS Med.* **5**, e55 (2008).
24. H. V. Xong *et al.*, *Cell* **95**, 839 (1998).
25. L. Lecordier *et al.*, *PLoS Pathog.* **5**, e1000685 (2009).
26. T. N. Williams, *Curr. Opin. Microbiol.* **9**, 388 (2006).
27. M. Samanovic *et al.*, *PLoS Pathog.* **5**, e1000276 (2009).

28. We thank members of the Broad Institute Medical and Population Genetics Program for helpful advice and review of the manuscript. We thank the study participants for their participation and J. Robinson for the help provided accessing the 1000 Genomes project data. We thank X. C. Zhou [National Cancer Institute (NCI)] and E. Binns-Roemer (NCI), P. Poelvoorde [Université Libre de Bruxelles (ULB)], P. Tebabi (ULB) and A. Pays (ULB) for excellent technical assistance. We thank the investigators in the BWH and NIH FSGS genetic studies: W. Briggs, R. Dart, S. Korbet, M. Mokrzycki, P. Kimmel, T. Ahuja, J. Berns, E. Simon, M. Smith, H. Trachtman, M. Michel, J. R. Schelling, G. Appel, and A. Katz. The work at the University of Brussels was supported by the "CIBLES" program of the Walloon Region, the Fonds National de la Recherche Scientifique, and the Interuniversity Attraction Poles program of the Belgian Science Policy. This work was also supported by grants from the NIH (R01 DK54931 to M.R.P; K08-DK076868 to D.J.F.; R01 DK066358 and R01 DK053591 to D.W.B.; and R01 HL56266, R01 DK 070941, and R01 DK 084149 to B.I.F.), the National Institute of Diabetes, Digestive, and Kidney Disease Intramural research program (Z01 DK043308 to J.B.K.), the Intramural Research Program of NCI, Center for Cancer Research (Project ZIA BC 010022; C.A.W. and G.W.N.), and the NephCure Foundation (to M.R.P). The content of this publication does not necessarily reflect the views or policies of the Department of Health and Human Services, nor does mention of trade names, commercial products, or organizations imply endorsement by the U.S. Government. The publisher or recipient acknowledges right of the U.S. Government to retain a nonexclusive, royalty-free license in and to any copyright covering the article. This project has been funded in part with federal funds from the NCI, NIH, under contract HHSN261200800001E. All participants gave informed consent for genetic studies, and research was conducted under protocols approved by the appropriate institutional review boards. J.B.K., G.W.N., C.A.W., and the NCI have a patent application pending for chromosome 22 polymorphisms and haplotypes for genetic screening and clinical applications. M.R.P., G.G., the Brigham and Women's Hospital, and Beth Israel Deaconess Medical Center have been added as co-inventors to an amendment to this application naming the specific ApoL1 SNPs described in this manuscript. E.P., L.L., P.U., and ULB have applied for a patent related to the use of plasma from ESKD patients to treat human sleeping sickness by plasma transfer.

Supporting Online Material

www.sciencemag.org/cgi/content/full/science.1193032/DC1
Materials and Methods
Figs. S1 to S3
Tables S1 to S5
References

4 March 2010; accepted 1 July 2010
Published online 15 July 2010;
10.1126/science.1193032
Include this information when citing this paper.

An Allosteric Self-Splicing Ribozyme Triggered by a Bacterial Second Messenger

Elaine R. Lee,[1]* Jenny L. Baker,[2]* Zasha Weinberg,[1,3] Narasimhan Sudarsan,[1,3] Ronald R. Breaker[1,3,4]†

Group I self-splicing ribozymes commonly function as components of selfish mobile genetic elements. We identified an allosteric group I ribozyme, wherein self-splicing is regulated by a distinct riboswitch class that senses the bacterial second messenger c-di-GMP. The tandem RNA sensory system resides in the 5′ untranslated region of the messenger RNA for a putative virulence gene in the pathogenic bacterium *Clostridium difficile*. c-di-GMP binding by the riboswitch induces folding changes at atypical splice site junctions to modulate alternative RNA processing. Our findings indicate that some self-splicing ribozymes are not selfish elements but are harnessed by cells as metabolite sensors and genetic regulators.

Metabolite-sensing riboswitches control gene expression in most bacteria, plants, and fungi (*1*–*3*). Computer-assisted searches (*4*) have recently been used to identify additional riboswitches (*5*), including an RNA motif (Fig. 1A) that associates with genes involved in c-di-GMP (cyclic di-guanosyl-5′-monophosphate) production, degradation, and signaling (fig. S1)

(*6*). The structural characteristics of this motif are distinct from a previously validated c-di-GMP-I riboswitch class (fig. S2) for this second messenger (*7*–*9*) and therefore likely represent a distinct class called c-di-GMP-II.

An 84-nucleotide c-di-GMP-II RNA from *Clostridium difficile* strain 630 (termed 84 Cd) (Fig. 1B) was 5′ ^{32}P-labeled and subjected to in-line probing (*10*, *11*). The pattern of spontaneous RNA cleavage products generated without c-di-GMP (Fig. 1C) is consistent with our secondary structure model. Furthermore, 11 linkages exhibit reduced strand scission in 10 μM c-di-GMP, which indicates that these nucleotides are structurally stabilized on second messenger binding. Probing using a range of c-di-GMP concentrations reveals one-to-one binding with an apparent dissociation constant (K_D) of ~200 pM (Fig. 1D and fig. S3). K_D values for analogs are more than three orders of magnitude poorer (Fig. 1E), revealing molecular discrimination comparable to that exhibited by c-di-GMP-I riboswitches (*7*).

Riboswitch function by other c-di-GMP-II RNAs was validated in vivo using riboswitch–reporter gene fusions (fig. S4, A and B) and in vitro using transcription termination assays (fig. S4, C and D). However, the 84 Cd aptamer lacks normal riboswitch control structures and is located ~600 nucleotides upstream of the putative start codon for its associated open reading frame (ORF) (Fig. 2A). This unusually large gap has all the hallmarks of a group I self-splicing ribozyme (*12*, *13*) (fig. S5); therefore, we speculated that the RNAs may collaborate to function as an allosteric ribozyme wherein splicing is controlled by c-di-GMP.

Allosteric ribozyme function was assessed by using an 864-nucleotide internally ^{32}P-labeled RNA (864 Cd Tandem) carrying the aptamer and ribozyme domains and part of the *C. difficile* CD3246 ORF (Fig. 2B and fig. S5). Incubation of wild-type RNA with guanosine 5′-triphosphate (GTP) yields characteristic group I ribozyme products (Fig. 2C and fig. S6). However, the amount of 5′E-3′E spliced exons increases substantially when both GTP and c-di-GMP are present (Fig. 3, A and B). The dose-response curve for c-di-GMP induction of splicing fits a one-to-one interaction with half-maximal 5′E-3′E production occurring with 30-nM second messenger (fig. S7).

Analysis of in vitro splice products (figs. S8 and S9) reveals an atypical 5′ splice site (ss). Total RNA isolated from cultured *C. difficile* 630 cells produced a dominant reverse transcription polymerase chain reaction product (fig. S10) with a splice junction determined by sequencing that corresponded to that found in our in vitro assays. Furthermore, the extent of splicing increases with culture age. This latter finding is consistent with allosteric activation of splicing by c-di-GMP, whose concentrations should increase with increasing cell density.

Another RNA product (3′E*), determined to be a fragment of the 3′ exon caused by GTP attack far from the 5′ ss (fig. S8), is reduced in the presence of c-di-GMP (Figs. 2C and 3D). Production of both 5′E-3′E and 3′E* RNAs were monitored in subsequent assays. Aptamer mutants M1 and M2 that disrupt c-di-GMP binding no longer respond to the second messenger in splicing reactions (Fig. 2C and fig. S11). In contrast, mutant M3 that carries nucleotide changes to M2 to restore aptamer P3 stem formation recovers c-di-GMP–mediated splicing control (Fig. 2C). Thus, c-di-GMP binding to the aptamer triggers increased production of spliced exons.

We noticed two alternative base-pairing structures, the anti-5′ ss stem (Fig. 2B, blue shading) and the alternative ribozyme P1 stem (green shading), that may explain c-di-GMP splicing control. Anti-5′ ss stem formation disrupts two base pairs of the ribozyme P1 stem, which subsequently favors formation of the alternative ribozyme P1 stem. Because c-di-GMP binding stabilizes aptamer substructures (Fig. 1C), low c-di-GMP concentrations should favor anti-5′ ss stem formation and prevent GTP attack at the 5′ ss. Indeed, a 132-nucleotide construct encompassing the aptamer through nucleotide 130 of the tandem RNA yields an in-line probing pattern consistent with anti-5′ ss stem formation in the absence of second messenger (fig. S12A). Additional mutants were used to validate this c-di-GMP–mediated structural rearrangement (fig. S12, B to D).

[1]Department of Molecular, Cellular, and Developmental Biology, Yale University, Box 208103, New Haven, CT 06520–8103, USA. [2]Department of Chemistry, Yale University, Box 208103, New Haven, CT 06520–8103, USA. [3]Howard Hughes Medical Institute, Yale University, Box 208103, New Haven, CT 06520–8103, USA. [4]Department of Molecular Biophysics and Biochemistry, Yale University, Box 208103, New Haven, CT 06520–8103, USA.

*These authors contributed equally to this work.
†To whom correspondence should be addressed. E-mail: ronald.breaker@yale.edu

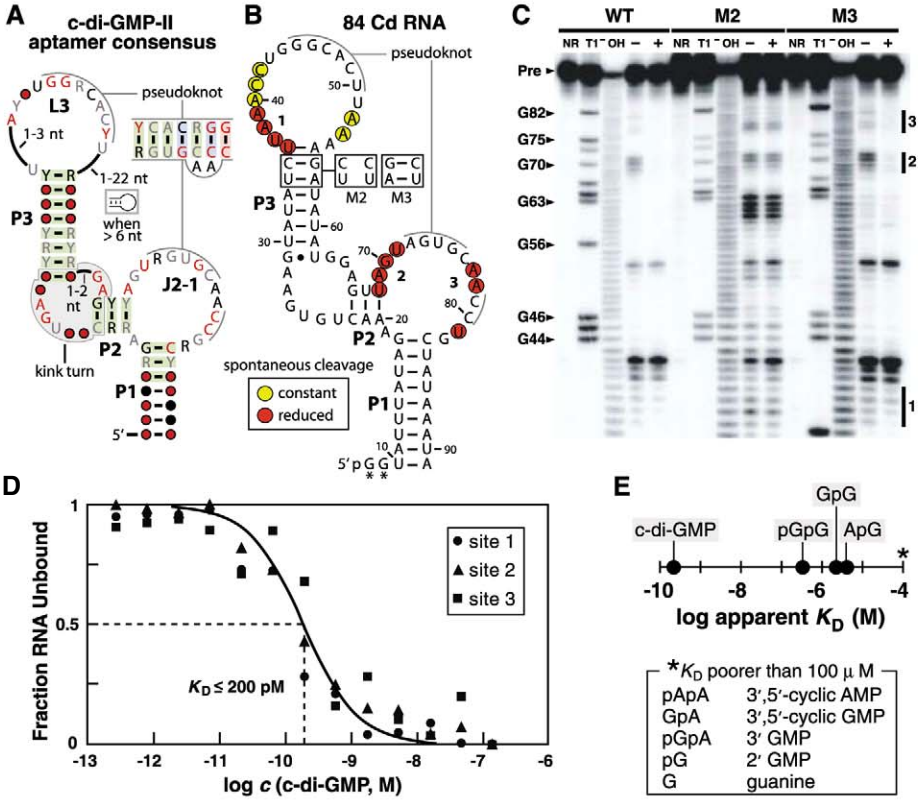


Fig. 1. c-di-GMP-II riboswitches. (**A**) Consensus sequence and secondary structure model for c-di-GMP-II riboswitch aptamers. Nucleotides in red are conserved in >97% of the representatives. Other annotations are described in fig. S2. (**B**) Wild-type (WT) 84 Cd RNA encompassing the motif upstream of a possible virulence gene. Disruptive (M2) and restorative (M3) mutations are depicted, and sites of spontaneous cleavage are derived from C. Asterisks identify nucleotides added to facilitate in vitro transcription. (**C**) Denaturing polyacrylamide gel electrophoresis (PAGE) of WT 84 Cd RNA in-line probing cleavage products. No reaction (NR); partial digestion with ribonuclease (RNase) T1 (T1, cleaves after G residues); alkali (⁻OH, cleaves at all linkages); incubation in the absence (–) or presence (+) of 10 μM c-di-GMP. Selected RNase T1 digestion product bands are identified. (**D**) Plot of the fraction of RNA remaining unbound versus the logarithm of the concentration of c-di-GMP present during in-line probing (fig. S3). (**E**) K_D values for 84 Cd binding to c-di-GMP and various di- and mononucleotide analogs. A, adenosine; G, guanosine.

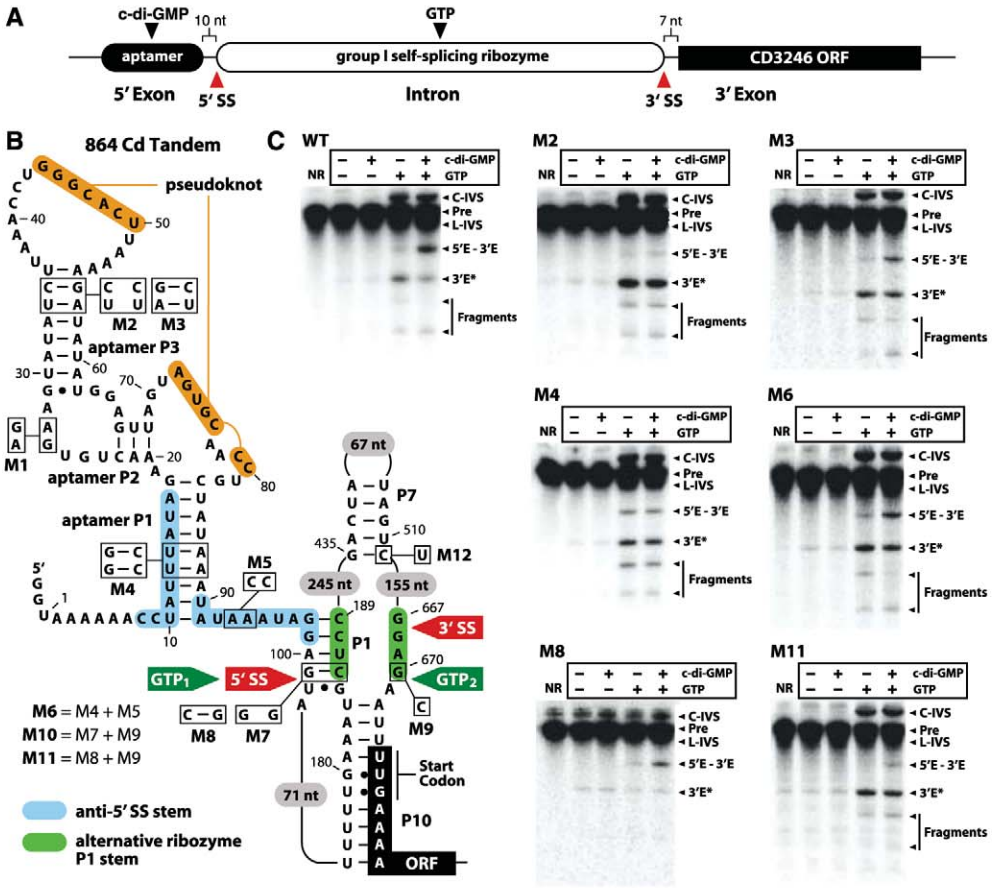


Fig. 2. Architecture, mechanism, and activity of a tandem riboswitch-ribozyme. (**A**) Tandem c-di-GMP-II aptamer and group I ribozyme arrangement. (**B**) Key features of the aptamer-ribozyme system, including validated splice and GTP attack sites (fig. S8). Alternative base-pair interactions guiding allosteric function are shaded blue and green. (**C**) PAGE separation of products generated by self-splicing assays. NR, no reaction; C-IVS and L-IVS, circular and linear intervening sequences, respectively; Pre, 864-nucleotide precursor RNA (fig. S5); 5′E-3′E, spliced exons; 3′E*, 3′ fragment generated by GTP attack at an alternative site; Fragments, additional RNA products presumably created by IVS circularization. Data for some mutants is presented elsewhere (fig. S11).

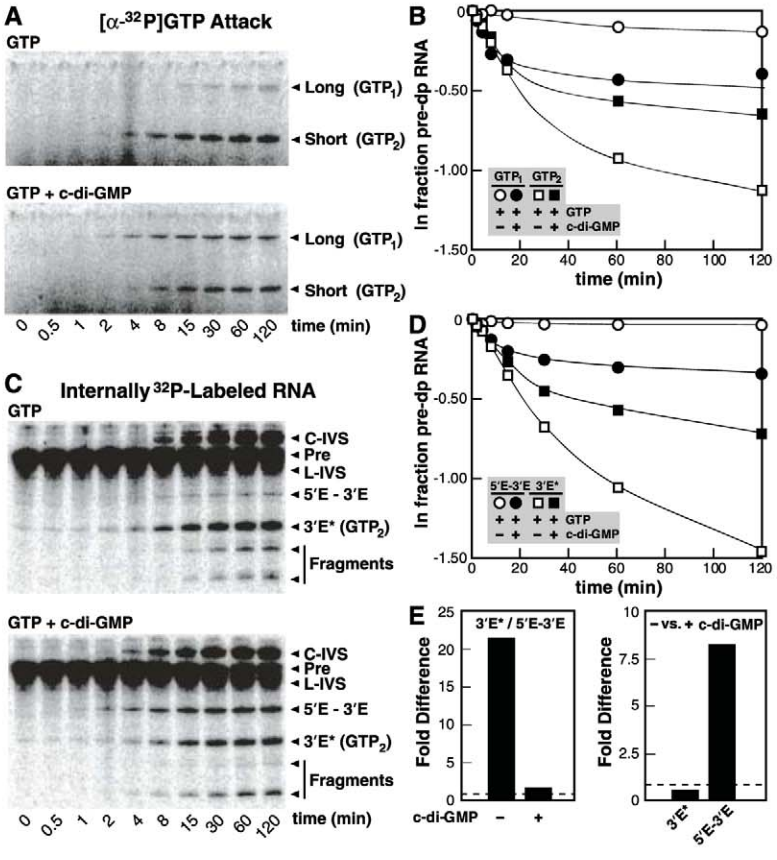


Fig. 3. Rate constant modulation by c-di-GMP. (**A**) Time course of [α-^{32}P]GTP attack at sites GTP_1 or GTP_2 in the absence or presence of c-di-GMP. (**B**) Plot of the natural logarithm of the fraction of unprocessed or differently processed RNA (pre-dp RNA) versus time for the reaction in (A). Values for fraction processed were corrected for ~50% of the precursor remaining after exhaustive incubation. (**C**) Time course of the production of spliced exons (5′E-3′E) or alternative GTP_2 site fragment (3′E*) in the absence or presence of c-di-GMP. Annotations are as described for Fig. 2C. (**D**) Plot of the natural logarithm of the fraction of unprocessed or differently processed RNA versus time for the reaction in (C), corrected as described in (B). (**E**) Changes in splice product yields on introduction of c-di-GMP. (Left) Ratio of the number of 3′E* molecules versus the number of 5′E-3′E spliced exon molecules in the absence or presence of c-di-GMP, respectively. (Right) Ratio of the numbers of 3′E* molecules and the numbers of 5′E-3′E spliced exon molecules in the absence or presence of c-di-GMP, respectively.

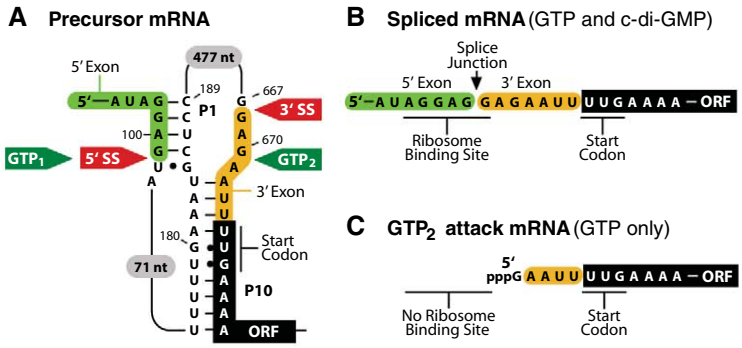


Fig. 4. Proposed mechanism for allosteric ribozyme-mediated gene control. (**A**) Precursor mRNA with the start codon sequestered by the ribozyme P10 stem. (**B**) RNA processed in the presence of GTP and c-di-GMP unmasks the start codon and creates a perfect ribosome binding site. (**C**) RNA processed in the presence of GTP alone lacks a ribosome binding site.

The role of the anti-5′ ss stem was further evaluated by establishing the effects of mutants M4, M5, and M6. Consistent with our model, mutants M4 and M5 disrupt regulation (Fig. 2C and fig. S11), whereas M6 combines these disruptive mutations to yield a construct that restores c-di-GMP binding and regulation. Mutations M7 through M11 were created to assess the importance of the ribozyme P1 stem and the alternative ribozyme P1 stem for allosteric control. Mutations M7 through M10 disrupt specific structures and exhibit expected reductions in particular RNA products. Most notably, normal c-di-GMP regulation is observed for M11, which combines several disruptive mutations to form an RNA that restores alternative base-pairing potential. Finally, M12 lacks any splicing activity due to disruption of the ribozyme's GTP binding site. These findings are consistent with an allosteric ribozyme mechanism wherein c-di-GMP regulates alternative base pairing between distal regions of the precursor mRNA.

Reactions with unlabeled 864 Cd Tandem RNA and [α-^{32}P]GTP (Fig. 3A) were conducted to estimate the observed rate constant (k_{obs}) values for GTP attack (Fig. 3B). A near 13-fold increase in initial rate constant (first 15 min) was observed for GTP attack at the 5′ ss when both GTP and c-di-GMP are present (2.3×10^{-2} min^{-1}). In contrast, there is only a modest reduction in the initial rate constant for GTP attack at the alternative GTP_2 site. This same pattern of ribozyme modulation is observed when internally labeled RNAs are used (Fig. 3C), which results in a 12-fold increase in the initial k_{obs} for spliced product formation in the absence of c-di-GMP.

Similar results are obtained by evaluating the yields of spliced exon and alternative attack products after incubating for 120 min (Fig. 3, C and E). Without c-di-GMP, the ribozyme produces greater than 20-fold more alternative attack product than spliced exons (Fig. 3E, left). Nearly equal amounts are produced when c-di-GMP is present. This change is largely due to an ~8-fold increase in spliced exon production as the ratio of alternative attack product in the absence versus the presence of c-di-GMP drops only modestly (Fig. 3E, right). Thus, c-di-GMP enhances the production of fully spliced exons largely by favoring formation of the ribozyme P1.

The sequences and structures of the precursor mRNA and processed RNAs suggest a mechanism for translation control of the CD3246 ORF (Fig. 4). Although the UUG start codon predicted in annotated *C. difficile* genomes is atypical, this translation start site and initial polypeptide sequence is consistent with similar genes in related organisms. In the precursor RNA, the start codon resides in the right shoulder of the P10 stem (Fig. 4A). This arrangement should restrict ribosome access and preclude translation, which is a common mechanism for translation control by riboswitches (*3*). With sufficient c-di-GMP and GTP, ribozyme action yields a processed mRNA wherein the spliced junction resides in a perfect ribosome binding site (AGGAGG) located an optimal distance upstream of the start codon (Fig. 4B). Thus, allosteric activation of ribozyme self-splicing by c-di-GMP should favor translation. In contrast, ribozyme action in the absence of c-di-GMP favors GTP attack only four nucleotides upstream of the start codon. This product is trimmed of nucleotides that otherwise could serve as a ribosome binding site (Fig. 4C), which should disfavor translation.

Bacteria naturally exploit tandem riboswitch architectures to create more complex gene control elements (*14*–*17*). Our findings add to this complexity by demonstrating how two ligand-responsive RNAs, a self-splicing ribozyme and a riboswitch aptamer, collaborate to function as an allosteric RNA requiring two RNA compounds (GTP and c-di-GMP) to promote splicing. This conjoined riboswitch-ribozyme system validates a prediction made more than 20 years ago (*18*) that some group I ribozymes could be controlled by nucleotide-derived alarmones. Also, this RNA is a natural mimic of an engineered ribozyme that controls splicing and gene expression in response to theophylline binding (*19*).

Some group I ribozymes may independently function as riboswitches that sense GTP because sufficient levels must be present for splicing to occur. If true, then the tandem riboswitch-ribozyme examined in this study may constitute a two-input control system that reads GTP and c-di-GMP concentrations to trigger splicing accordingly. Notably, GTP is the immediate biosynthetic precursor of c-di-GMP, and overproduction of this second messenger causes substantial decreases in GTP concentrations in vivo (*20*).

The harnessing of group I ribozymes by some organisms is suggested by the observation that bacteriophage ribozyme splicing is diminished in a bacterial host when ribosome function is inhibited (*21*). Moreover, the gene associations of some examples are conserved in evolutionarily distant species (*13*), implying useful rather than purely selfish functions. Of at least 10 group I ribozymes present in *C. difficile* 630, 9 are associated with a transposase gene (fig. S12), which facilitates mobility of selfish genetic elements. Only the allosteric ribozyme described in this work lacks a transposase gene, which suggests that this representative is not a selfish RNA but has a location and a function that benefits the host.

References and Notes

1. A. Roth, R. R. Breaker, *Annu. Rev. Biochem.* **78**, 305 (2009).
2. M. D. Dambach, W. C. Winkler, *Curr. Opin. Microbiol.* **12**, 161 (2009).
3. J. E. Barrick, R. R. Breaker, *Genome Biol.* **8**, R239 (2007).
4. H. H. Tseng, Z. Weinberg, J. Gore, R. R. Breaker, W. L. Ruzzo, *J. Bioinform. Comput. Biol.* **7**, 373 (2009).
5. Z. Weinberg *et al.*, *Genome Biol.* **11**, R31 (2010).
6. R. Hengge, *Nat. Rev. Microbiol.* **7**, 263 (2009).
7. N. Sudarsan *et al.*, *Science* **321**, 411 (2008).
8. N. Kulshina, N. J. Baird, A. R. Ferré-D'Amaré, *Nat. Struct. Mol. Biol.* **16**, 1212 (2009).
9. K. D. Smith *et al.*, *Nat. Struct. Mol. Biol.* **16**, 1218 (2009).
10. G. A. Soukup, R. R. Breaker, *RNA* **5**, 1308 (1999).
11. E. E. Regulski, R. R. Breaker, *Methods Mol. Biol.* **419**, 53 (2008).
12. K. Kruger *et al.*, *Cell* **31**, 147 (1982).
13. H. Nielsen, S. D. Johansen, *RNA Biol.* **6**, 375 (2009).
14. M. Mandal *et al.*, *Science* **306**, 275 (2004).
15. R. Welz, R. R. Breaker, *RNA* **13**, 573 (2007).
16. N. Sudarsan *et al.*, *Science* **314**, 300 (2006).
17. E. Poiata, M. M. Meyer, T. D. Ames, R. R. Breaker, *RNA* **15**, 2046 (2009).
18. D. A. Shub, M.-Q. Xu, J. M. Gott, A. Zeeh, L. D. Wilson, *Cold Spring Harb. Symp. Quant. Biol.* **52**, 193 (1987).
19. K. M. Thompson, H. A. Syrett, S. M. Knudsen, A. D. Ellington, *BMC Biotechnol.* **2**, 21 (2002).
20. R. Simm, M. Morr, A. Kader, M. Nimtz, U. Römling, *Mol. Microbiol.* **53**, 1123 (2004).
21. L. Sandegren, B. M. Sjöberg, *J. Bacteriol.* **189**, 980 (2007).

22. We thank J. Davis for assistance with genetic experiments and members of the Breaker laboratory for helpful discussions. We also thank L. Sonenshein for supplying *C. difficile* 630 spores and for training N.S. in *C. difficile* techniques. This work was supported by NIH grant PO1 GM022778 and by the Howard Hughes Medical Institute. Z.W. advises BioRelix. R.R.B. is a cofounder and Scientific Advisory Board member of BioRelix. Yale University has filed a provisional patent application on this riboswitch technology.

Supporting Online Material

www.sciencemag.org/cgi/content/full/329/5993/845/DC1
Materials and Methods
Figs. S1 to S13
Tables S1 and S2
References

9 April 2010; accepted 1 July 2010
10.1126/science.1190713

Activation of β-Catenin in Dendritic Cells Regulates Immunity Versus Tolerance in the Intestine

Santhakumar Manicassamy,[1] Boris Reizis,[2] Rajesh Ravindran,[1] Helder Nakaya,[1] Rosa Maria Salazar-Gonzalez,[1,3] Yi-chong Wang,[1] Bali Pulendran[1,4]*

Dendritic cells (DCs) play a vital role in initiating robust immunity against pathogens as well as maintaining immunological tolerance to self antigens. However, the intracellular signaling networks that program DCs to become tolerogenic remain unknown. We report here that the Wnt–β-catenin signaling in intestinal dendritic cells regulates the balance between inflammatory versus regulatory responses in the gut. β-catenin in intestinal dendritic cells was required for the expression of anti-inflammatory mediators such as retinoic acid–metabolizing enzymes, interleukin-10, and transforming growth factor–β, and the stimulation of regulatory T cell induction while suppressing inflammatory effector T cells. Furthermore, ablation of β-catenin expression in DCs enhanced inflammatory responses and disease in a mouse model of inflammatory bowel disease. Thus, β-catenin signaling programs DCs to a tolerogenic state, limiting the inflammatory response.

A central question in immunology is how the immune system launches robust immunity against invading pathogens while maintaining tolerance to self antigens. This is of particular importance in the intestine because of the trillions of commensal microorganisms and food antigens that confront the intestinal immune system every day. Antigen-presenting cells (APCs) such as dendritic cells (DCs) and macrophages are specialized immune cells that play a vital role in stimulating immune responses (*1*, *2*). Recent evidence suggests that DCs are also critical in suppressing immune responses, through the generation of T regulatory cells (T_{reg} cells) (*2*, *3*). DCs express several pathogen-recognition receptors (PRRs), which are capable of sensing highly conserved structural motifs in pathogens (*4*–*6*) and initiating downstream signaling cascades that are important for controlling the innate and adaptive immune responses (*2*, *7*). Triggering PRRs on DCs can activate DCs and determine the types of cytokines they produce. Such cytokines regulate the differentiation fate of naïve $CD4^+$ T cells into inflammatory cells [T helper 1 (TH1) or TH17] or T_{reg} cells, regulating the balance between immunity and tolerance. In the intestine, emerging evidence indicates that DCs and macrophages play a pivotal role in mediating mucosal tolerance against commensals and dietary antigens while mounting inflammatory responses against harmful pathogens (*8*–*12*). The signaling pathways that program DCs into a tolerogenic or inflammatory state, however, are poorly understood.

To address this, we analyzed gene expression profiles using microarray analysis of purified intestinal lamina propria DCs (LP-DCs) and compared it with those of splenic DCs (spl-DCs) from mice (*13*). Several Wnt-ligands were up-regulated

[1]Emory Vaccine Center, and Yerkes National Primate Research Center, 954 Gatewood Road, Atlanta, GA 30329, USA. [2]Department of Microbiology, Columbia University Medical Center, New York, NY 10032, USA. [3]Molecular Immunology Division, Cincinnati Children's Hospital Medical Center, Cincinnati, OH 45229–3039, USA. [4]Department of Pathology, Emory University, 1364 Clifton Road NE, Atlanta, GA 30322, USA.

*To whom correspondence should be addressed. E-mail: bpulend@emory.edu

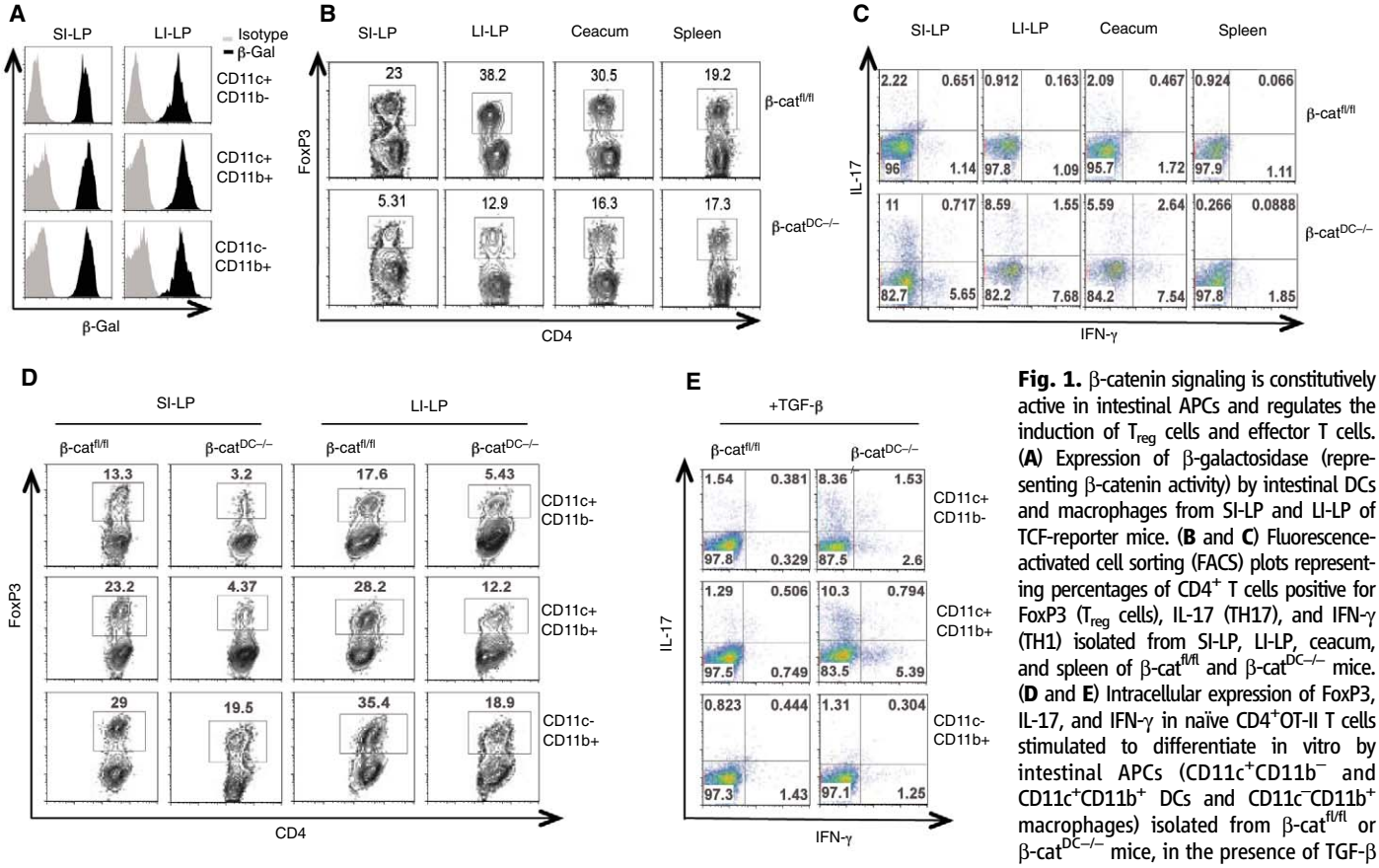


Fig. 1. β-catenin signaling is constitutively active in intestinal APCs and regulates the induction of T_{reg} cells and effector T cells. (**A**) Expression of β-galactosidase (representing β-catenin activity) by intestinal DCs and macrophages from SI-LP and LI-LP of TCF-reporter mice. (**B** and **C**) Fluorescence-activated cell sorting (FACS) plots representing percentages of $CD4^+$ T cells positive for FoxP3 (T_{reg} cells), IL-17 (TH17), and IFN-γ (TH1) isolated from SI-LP, LI-LP, ceacum, and spleen of β-$cat^{fl/fl}$ and β-$cat^{DC-/-}$ mice. (**D** and **E**) Intracellular expression of FoxP3, IL-17, and IFN-γ in naïve $CD4^+$OT-II T cells stimulated to differentiate in vitro by intestinal APCs ($CD11c^+CD11b^-$ and $CD11c^+CD11b^+$ DCs and $CD11c^-CD11b^+$ macrophages) isolated from β-$cat^{fl/fl}$ or β-$cat^{DC-/-}$ mice, in the presence of TGF-β (1 ng/ml). Numbers in FACS plots represent percentage of cells positive for the indicated protein. Data are from one experiment representative of three.

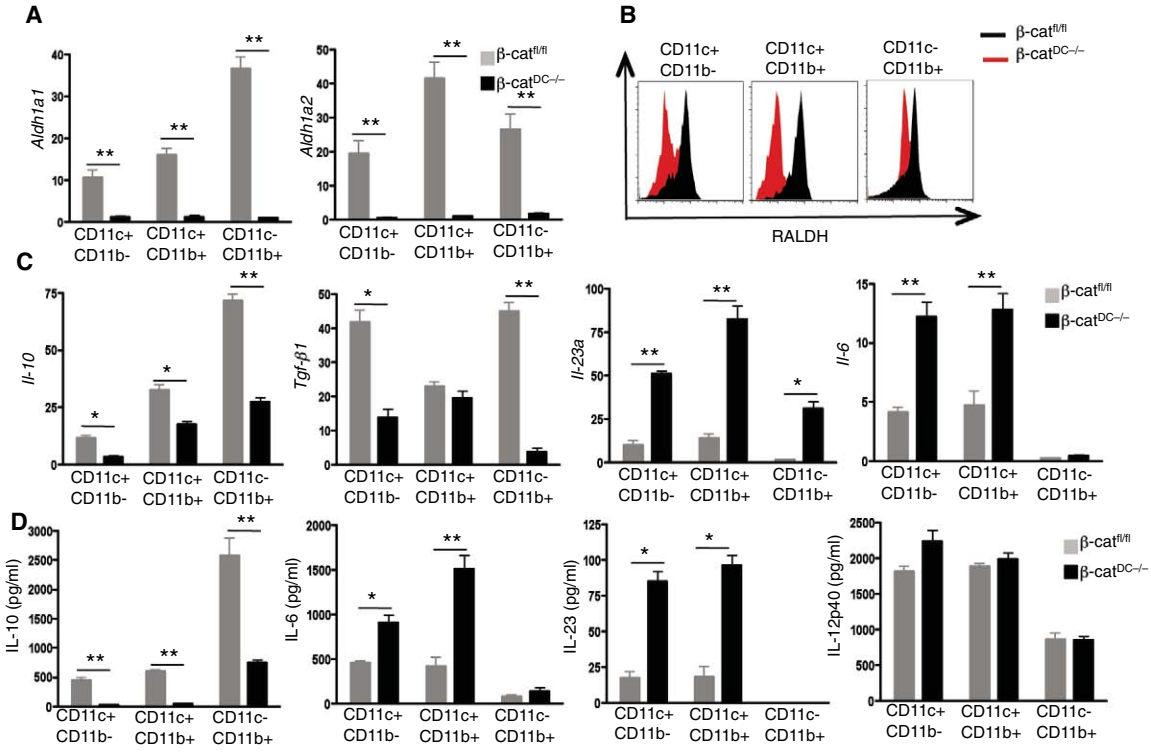


Fig. 2. β-catenin signaling in intestinal DCs promotes the expression of Raldh and suppresses the expression of proinflammatory cytokines. (**A**) Expression of *Aldh1a1* and *Aldh1a2* mRNA in $CD11c^{+}CD11b^{-}$ and $CD11c^{+}CD11b^{+}$ DCs and $CD11c^{-}CD11b^{+}$ macrophages isolated from SI-LP of $\beta\text{-cat}^{fl/fl}$ or $\beta\text{-cat}^{DC-/-}$ mice. (**B**) Expression of Raldh protein by $CD11c^{+}CD11b^{-}$ and $CD11c^{+}CD11b^{+}$ DCs and $CD11c^{-}CD11b^{+}$ macrophages isolated from SI-LP of $\beta\text{-cat}^{fl/fl}$ or $\beta\text{-cat}^{DC-/-}$ mice, as assessed by intracellular staining and flow cytometry. (**C**) Expression of *Il-10*, *Tgf-β1*, *Il-23a*, and *Il-6* mRNAs in $CD11c^{+}CD11b^{-}$ and $CD11c^{+}CD11b^{+}$ DCs and $CD11c^{-}CD11b^{+}$ macrophages isolated from SI-LP of $\beta\text{-cat}^{fl/fl}$ or $\beta\text{-cat}^{DC-/-}$ mice. (**D**) Cytokine concentrations in the supernatants of $CD11c^{+}CD11b^{-}$ and $CD11c^{+}CD11b^{+}$ DCs and $CD11c^{-}CD11b^{+}$ macrophages isolated from SI-LP of $\beta\text{-cat}^{fl/fl}$ or $\beta\text{-cat}^{DC-/-}$ mice after 24 hours. $*P < 0.05$; $**P < 0.005$. Error bars indicate mean ± SEM. Data are representative of three experiments.

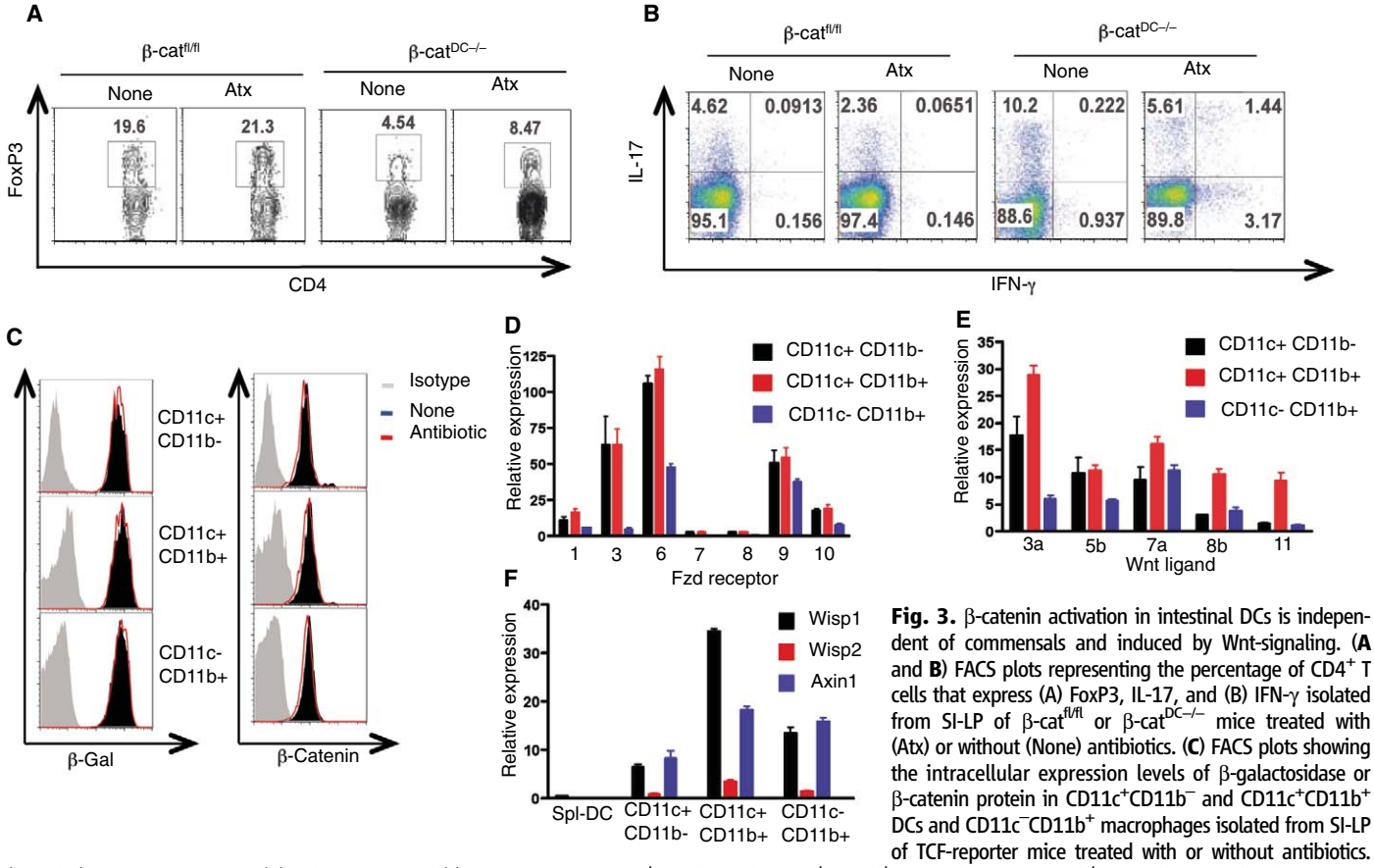


Fig. 3. β-catenin activation in intestinal DCs is independent of commensals and induced by Wnt-signaling. (**A** and **B**) FACS plots representing the percentage of $CD4^{+}$ T cells that express (A) FoxP3, IL-17, and (B) IFN-γ isolated from SI-LP of $\beta\text{-cat}^{fl/fl}$ or $\beta\text{-cat}^{DC-/-}$ mice treated with (Atx) or without (None) antibiotics. (**C**) FACS plots showing the intracellular expression levels of β-galactosidase or β-catenin protein in $CD11c^{+}CD11b^{-}$ and $CD11c^{+}CD11b^{+}$ DCs and $CD11c^{-}CD11b^{+}$ macrophages isolated from SI-LP of TCF-reporter mice treated with or without antibiotics. (**D** and **E**) mRNA expression of (D) Fzd receptors and (E) Wnt ligands in $CD11c^{+}CD11b^{-}$ and $CD11c^{+}CD11b^{+}$ DCs and $CD11c^{-}CD11b^{+}$ macrophages isolated from SI-LP of $\beta\text{-cat}^{fl/fl}$ mice. (**F**) mRNA expression levels of Wnt–β-catenin target genes Wisp1, Wisp2, and Axin1 in $CD11c^{+}CD11b^{-}$ and $CD11c^{+}CD11b^{+}$ DCs and $CD11c^{-}CD11b^{+}$ macrophages isolated from SI-LP of $\beta\text{-cat}^{fl/fl}$ mice. Error bars indicate mean ± SEM. Data are from one experiment representative of three.

in LP-DCs as compared with spl-DCs. Consistent with this, reverse transcriptase polymerase chain reaction (RT-PCR) analysis showed that LP-DCs constitutively expressed several Wnt-ligands as compared with that of spl-DCs in the steady state (fig. S1). β-catenin, a central component in Wnt-signaling, is widely expressed in hematopoietic stem cells, macrophages, DCs, and lymphocytes (*14*). Furthermore, the Wnt–β-catenin pathway has been implicated in the differentiation of DCs from hematopoietic stem cells (*15*, *16*).

Activation of Wnt-Frizzled (fzd) receptor signaling causes translocation of β-catenin from the cytoplasm to the nucleus, where it interacts with T cell factor/lymphoid enhancer factor (TCF/LEF) family members and regulates transcription of several target genes (*14*, *17*). Thus, we assessed whether the β-catenin pathway was active in LP-DCs using the TCF/LEF–lacZ reporter mice (*18*). In contrast to spl-DCs, LP-DCs from TCF-reporter mice showed strong β-galactosidase expression, suggesting that β-catenin signaling pathway is constitutively active in intestinal DCs (fig. S2). Apart from Wnt signaling, disruption of homotypic E-cadherin interactions in DCs results in β-catenin activation and impairs their immune stimulatory capacity (*19*). Whether the constitutive β-catenin signaling in intestinal DCs programs them to induce tolerogenic responses, however, is unknown.

To directly assess the role of β-catenin specifically in DC function, we crossed floxed β-catenin allele mice ($\beta\text{-cat}^{fl/fl}$) (*20*) with transgenic mice (CD11c-cre) expressing the cre enzyme under the control of the CD11c promoter (*21*). This specifically abrogated β-catenin expression in DCs (fig. S3A). Distinct subsets of intestinal DCs and macrophages can be distinguished by the expression patterns of CD11c and CD11b ($CD11c^{+}CD11b^{-}$ and $CD11c^{+}CD11b^{+}$ DCs and $CD11c^{-}CD11b^{+}$ macrophages) (*11*). β-catenin was highly expressed and constitutively active in LP-DC subsets and LP-macrophages in the small and large intestine (Fig. 1A and fig. S3B). In $\beta\text{-cat}^{DC-/-}$ mice, β-catenin expression was abrogated in the $CD11c^{+}CD11b^{-}$ and $CD11c^{+}CD11b^{+}$ DCs but only partially abrogated in $CD11c^{-}CD11b^{+}$ macrophages (fig S3B).

We next determined whether β-catenin signaling in DCs is critical for intestinal homeostasis. We compared the frequencies of T_{reg} cells and TH17/TH1 cells in the intestine of $\beta\text{-cat}^{DC-/-}$ and $\beta\text{-cat}^{fl/fl}$ mice because intestinal DCs and macrophages play an important role in the induction of these subsets (*10*–*12*, *22*). $\beta\text{-cat}^{DC-/-}$ mice had lower frequencies of T_{reg} cells in the small intestine (SI)–LP, the large intestine (LI)–LP, and caecum, but not the spleen, as compared with that of $\beta\text{-cat}^{fl/fl}$ mice (Fig. 1B and fig S4A). To determine whether the reduced frequencies of T_{reg} cells observed in the LP of $\beta\text{-cat}^{DC-/-}$ mice was due to increased frequencies of effector CD4 cells, we examined the frequencies of TH1 and TH17 in the intestine and periphery. We observed higher frequencies of TH17 and TH1 cells in the SI-LP and LI-LP but not in the spleen of $\beta\text{-cat}^{DC-/-}$ mice as compared with that of the $\beta\text{-cat}^{fl/fl}$ mice (Fig. 1C and fig. S4, B and C). Consistent with this, $CD4^{+}$ T cells isolated from SI-LP and LI-LP of $\beta\text{-cat}^{DC-/-}$ mice showed elevated expression of the TH17 cell–associated mRNAs interleukin (IL)–17, IL-21, Rorγt, and the TH1 cell–associated mRNA interferon (IFN)–γ (*23*, *24*) as compared with the $CD4^{+}$ T cells isolated from $\beta\text{-cat}^{fl/fl}$ mice (fig. S5). Thus, β-catenin signaling in intestinal DCs is critical in maintaining the balance between T_{reg} cells and $CD4^{+}$ T effector populations.

Intestinal DCs and macrophages can convert naïve T cells into T_{reg} cells that express the transcription factor Foxp3 and induce effector T cell differentiation (*10*–*12*, *22*, *25*). We thus assessed whether β-catenin signaling in LP-DCs and LP-macrophages is critical for inducing T_{reg}, TH1, and TH17 differentiation of naïve $CD4^{+}$ T cells in vitro using intestinal APCs ($CD11c^{+}CD11b^{-}$ and $CD11c^{+}CD11b^{+}$ DCs and $CD11b^{+}$ macrophages) isolated from $\beta\text{-cat}^{fl/fl}$ or $\beta\text{-cat}^{DC-/-}$ mice. In the absence or presence of TGF-β, a cytokine important for both T_{reg} and TH17 differentiation, LP-DC subsets from $\beta\text{-cat}^{DC-/-}$ were less potent in inducing T_{reg} differentiation as measured with FoxP3 expression, but enhanced TH17 and TH1 cell differentiation as compared with that of DCs from $\beta\text{-cat}^{fl/fl}$ mice (Fig. 1, D and E, and figs. S6 and S7). The ability of LP-DCs to induce T_{reg} cells is chiefly mediated by a specialized subset of $CD103^{+}$ DCs (fig. S8 and S9). Similarly, LP-macrophages of $\beta\text{-cat}^{DC-/-}$ mice were somewhat less potent in inducing T_{reg} cells as compared with the $\beta\text{-cat}^{fl/fl}$ LP-macrophages (Fig. 1D), which is consistent with the partial deletion of β-catenin

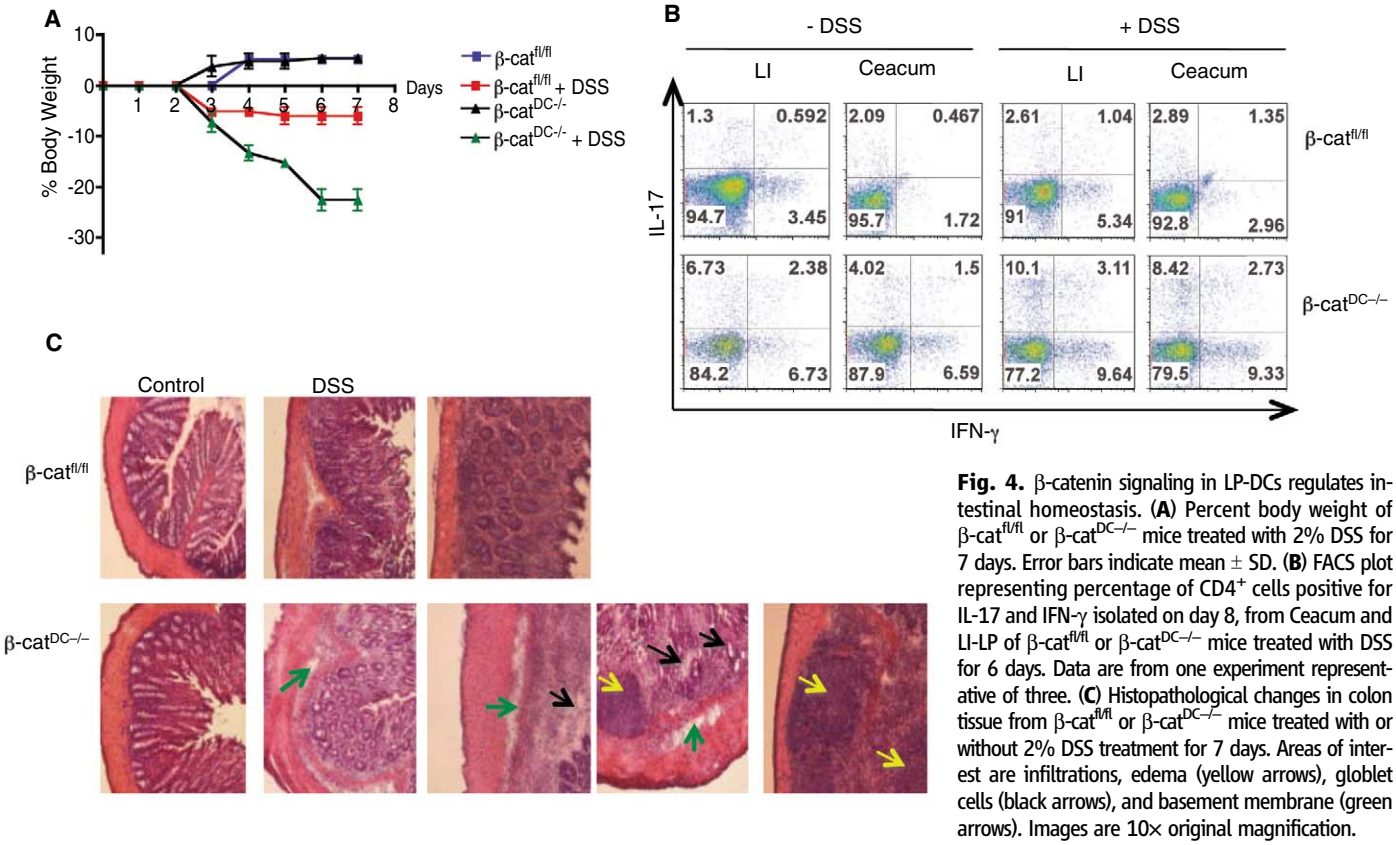


Fig. 4. β-catenin signaling in LP-DCs regulates intestinal homeostasis. (**A**) Percent body weight of $\beta\text{-cat}^{fl/fl}$ or $\beta\text{-cat}^{DC-/-}$ mice treated with 2% DSS for 7 days. Error bars indicate mean ± SD. (**B**) FACS plot representing percentage of $CD4^{+}$ cells positive for IL-17 and IFN-γ isolated on day 8, from Ceacum and LI-LP of $\beta\text{-cat}^{fl/fl}$ or $\beta\text{-cat}^{DC-/-}$ mice treated with DSS for 6 days. Data are from one experiment representative of three. (**C**) Histopathological changes in colon tissue from $\beta\text{-cat}^{fl/fl}$ or $\beta\text{-cat}^{DC-/-}$ mice treated with or without 2% DSS treatment for 7 days. Areas of interest are infiltrations, edema (yellow arrows), globlet cells (black arrows), and basement membrane (green arrows). Images are 10× original magnification.

in macrophages. The absence of β-catenin in DCs did not completely abrogate their ability to induce T_{reg} cells, suggesting that additional pathways are involved in programming DCs to the tolerogenic state. Thus, β-catenin signaling in DCs is required to induce T_{reg} cells and suppress TH1/TH17 responses.

We next explored the molecular mechanisms by which β-catenin signaling in DCs promoted T_{reg} differentiation and suppressed TH1/TH17 cell differentiation. Retinoic acid (RA, a vitamin A metabolite), IL-10, and TGF-β produced by the intestinal APCs and intestinal epithelial cells are critical for the induction of T_{reg} cells (*8*, *10*, *12*, *26*). *Aldh1a1* and *Aldh1a2* encode enzymes that catalyze the conversion of retinal to RA. Furthermore, Toll-like receptor (TLR)–mediated signaling in DCs up-regulates Raldh enzymes and promotes RA production (*27*). Thus, we assessed the expression levels of vitamin A–metabolizing genes by means of RT-PCR and flow cytometry in APC subsets purified from the LP of β-cat$^{fl/fl}$ and β-cat$^{DC-/-}$ mice. We observed that LP-DCs and LP-macrophages of β-cat$^{DC-/-}$ mice expressed much lower amounts of *Aldh1a1* and *Aldh1a2* mRNA in the SI (Fig. 2A) and LI (fig S10A) as compared with those of β-cat$^{fl/fl}$ LP-DCs and LP-macrophages. The relative expression of Raldh protein was similar to that observed with mRNA (Fig. 2B and fig S10B). Because β-cat$^{DC-/-}$ LP-DCs had reduced levels of vitamin A–metabolizing enzymes, we assessed whether addition of exogenous RA can rescue their defect in T_{reg} induction. Addition of exogenous RA to β-cat$^{DC-/-}$ LP-DCs did indeed enhance their capacity to induce T_{reg} cells as well as β-cat$^{fl/fl}$ DCs (fig S11). Thus, β-catenin–mediated signaling promotes T_{reg} induction through the expression of vitamin A–metabolizing enzymes in DCs.

Cytokines such as IL-6 and TGF-β promote the differentiation of TH17 cells, whereas IL-23 is thought to regulate the expansion and survival of TH17 cells (*24*). Thus, we assessed the expression of various pro-inflammatory and anti-inflammatory cytokines in LP-DC subsets isolated from β-cat$^{fl/fl}$ and β-cat$^{DC-/-}$ mice. β-cat$^{DC-/-}$ LP-DCs had higher mRNA levels of the pro-inflammatory cytokines IL-23a and IL-6 and lower mRNA levels of the anti-inflammatory cytokines IL-10 and TGF-β, as compared with that of β-cat$^{fl/fl}$ LP-DCs, from the SI and LI (Fig. 2C and fig S10C). Consistent with these results, β-cat$^{DC-/-}$ LP-DCs produced higher amounts of IL-6 and IL-23 and lower amounts of IL-10 as compared with that of β-cat$^{fl/fl}$ LP-DCs under steady state in both the SI and LI (Fig. 2D and fig. S10D). Thus, β-catenin signaling in LP-DCs is critical for the induction of anti-inflammatory cytokines, which are crucial for the induction of T_{reg} cells and suppression of TH1 and TH17 responses.

Intestinal commensals play an important role in the maintenance of TH17 cells (*25*, *28*, *29*), and commensal DNA limits the induction of T_{reg} cells in the gut (*30*). Moreover, intestinal DCs can directly take up bacteria and are thus constantly exposed to various pathogen-associated molecular patterns. Thus, we determined whether the enhanced frequencies of TH17 and TH1 cells in the β-cat$^{DC-/-}$ mice were dependent on the microbiota by treating the mice with an antibiotic cocktail. In β-cat$^{fl/fl}$ mice, antibiotic treatment resulted in modestly enhanced frequencies of T_{reg} cells in the LI-LP (fig. S12A). In contrast, antibiotic treatment of β-cat$^{DC-/-}$ mice failed to enhance T_{reg} cells in the LI-LP (fig. S12A) but did enhance twofold their frequency in the SI-LP (Fig. 3A). Even with antibiotic treatment, there was a marked reduction in the frequency of T_{reg} cells in β-cat$^{DC-/-}$ mice, relative to β-cat$^{fl/fl}$ mice, demonstrating that commensals were not essential for β-catenin activity (Fig. 3C and fig. S12C) and for the β-catenin–mediated programming of tolerogenic DCs. We also observed a decrease in the frequency of TH17 cells in the LP of β-cat$^{DC-/-}$ and β-cat$^{fl/fl}$ mice after antibiotic treatment (Fig. 3B and fig. S12B). Again, even with antibiotic treatment there was a markedly enhanced frequency of TH17 cells in β-cat$^{DC-/-}$ mice relative to β-cat$^{fl/fl}$ mice (Fig. 3B and fig. S12B), suggesting that commensals are not essential for β-catenin signaling–mediated programming of DCs to induce T_{reg} cells and suppress TH17 responses. Furthermore, in the absence of β-catenin antibiotic treatment resulted in slightly enhanced T_{reg} cells and diminished TH17 responses (Fig. 3, A and B), suggesting that additional β-catenin–independent pathways might be involved in regulating induction of T_{reg} cells and TH17 by DCs.

We next assessed by means of RT-PCR the expression of Wnt ligands and Fzd receptors in intestinal APCs because Wnt-signaling activates β-catenin (*17*). DCs and macrophage subsets from the SI-LP and LI-LP expressed high amounts of various Fzd receptors and Wnt ligands (Fig. 3, D and E, and fig. S12, D and E). To determine whether Fzd-Wnt receptor signaling is active in intestinal DCs and macrophages, we evaluated the expression levels of several Wnt target genes—specifically Wisp1, Wisp2, and Axin1—that are dependent on β-catenin. Compared with spl-DCs, LP-DCs expressed substantially more Wisp1 and Axin1 mRNA (Fig. 3F and fig. S12F). Next, we tested whether activation of the β-catenin pathway is sufficient to promote T_{reg} differentiation in vitro. In order to test this, we used LiCl treatment to activate β-catenin (fig S13A) (*31*). Compared with untreated DCs, LiCl-treated DCs induced greater frequencies of T_{reg} cells (fig S13B). Thus, Wnt-mediated signaling activates β-catenin in intestinal DCs and programs them to induce T_{reg} cells.

Lastly, we determined what impact β-catenin deficiency in DCs might have on the onset of autoimmunity in a mouse model of inflammatory bowel disease (IBD) because β-cat$^{DC-/-}$ LP-DCs more efficiently promote inflammatory TH17 and TH1 effector cells, which are both implicated in IBD (*32*, *33*) and experimental autoimmune encephalomyelitis pathogenesis (*24*). Dextran sulfate sodium (DSS) treatment induced drastic body weight loss, which is a characteristic of severe intestinal inflammation, in β-cat$^{DC-/-}$ mice relative to β-cat$^{fl/fl}$ mice (Fig. 4A). Furthermore, T cells isolated from ceacum and LI-LP of β-cat$^{DC-/-}$ mice treated with DSS had higher frequencies of TH17 and TH1 cells and lower frequencies of T_{reg} cells (Fig. 4B and fig. S14) as compared with that of T cells isolated from the colon of β-cat$^{fl/fl}$ controls. Consistent with this, histological analyses showed increases in inflammatory cell infiltration, edema, epithelial cell hyperplasia, and loss of goblet cells in the colon of β-cat$^{DC-/-}$ mice as compared with β-cat$^{fl/fl}$ mice (Fig. 4C). Thus, deletion of β-catenin in DCs induces a severe inflammatory response to enteric bacteria upon DSS treatment. Collectively, this observation suggests that β-catenin signaling in DCs is critical in the regulation of intestinal homeostasis and tolerance. In addition to β-catenin signaling, recent studies have shown that indoleamine 2,3-dioxygenase (IDO) expressed by gut DCs promotes tolerogenic response (*34*), whereas CD11c$^+$ E-cadherin$^+$ DCs promotes inflammatory response (*35*). However, the role of β-catenin in the regulation of IDO or CD11c$^+$ E-cadherin$^+$ DCs is currently unknown.

In summary, we have demonstrated that a signaling pathway involving β-catenin in DCs regulates the balance between inflammatory versus regulatory responses in the intestine. The present data demonstrate that β-catenin signaling in DCs is critical for maintaining DCs in tolerogenic state, via induction of various anti-inflammatory factors such as RA, IL-10, and TGF-β. Strategies that can activate β-catenin signaling specifically in DCs may be attractive means of controlling autoimmune diseases such as IBD via the induction of T_{reg} cells and concomitant suppression of inflammatory effector T cells.

References and Notes

1. R. M. Steinman, J. Banchereau, *Nature* **449**, 419 (2007).
2. B. Pulendran, *Immunol. Rev.* **199**, 227 (2004).
3. R. M. Steinman, D. Hawiger, M. C. Nussenzweig, *Annu. Rev. Immunol.* **21**, 685 (2003).
4. T. Kawai, S. Akira, *Nat. Immunol.* **11**, 373 (2010).
5. G. Chen, M. H. Shaw, Y. G. Kim, G. Nuñez, *Annu. Rev. Pathol.* **4**, 365 (2009).
6. T. B. Geijtenbeek, S. I. Gringhuis, *Nat. Rev. Immunol.* **9**, 465 (2009).
7. S. Manicassamy, B. Pulendran, *Semin. Immunol.* **21**, 185 (2009).
8. A. Izcue, J. L. Coombes, F. Powrie, *Annu. Rev. Immunol.* **27**, 313 (2009).
9. Y. Belkaid, K. Tarbell, *Annu. Rev. Immunol.* **27**, 551 (2009).
10. C. M. Sun *et al.*, *J. Exp. Med.* **204**, 1775 (2007).
11. T. L. Denning, Y. C. Wang, S. R. Patel, I. R. Williams, B. Pulendran, *Nat. Immunol.* **8**, 1086 (2007).
12. J. L. Coombes *et al.*, *J. Exp. Med.* **204**, 1757 (2007).
13. Materials and methods are available as supporting material on *Science* Online.
14. F. J. Staal, T. C. Luis, M. M. Tiemessen, *Nat. Rev. Immunol.* **8**, 581 (2008).
15. A. Lehtonen *et al.*, *J. Leukoc. Biol.* **82**, 710 (2007).
16. J. Zhou, P. Cheng, J. I. Youn, M. J. Cotter, D. I. Gabrilovich, *Immunity* **30**, 845 (2009).
17. H. Clevers, *Cell* **127**, 469 (2006).

18. S. Maretto *et al.*, *Proc. Natl. Acad. Sci. U.S.A.* **100**, 3299 (2003).
19. A. Jiang *et al.*, *Immunity* **27**, 610 (2007).
20. V. Brault *et al.*, *Development* **128**, 1253 (2001).
21. M. L. Caton, M. R. Smith-Raska, B. Reizis, *J. Exp. Med.* **204**, 1653 (2007).
22. S. Uematsu *et al.*, *Nat. Immunol.* **9**, 769 (2008).
23. I. I. Ivanov *et al.*, *Cell* **126**, 1121 (2006).
24. T. Korn, E. Bettelli, M. Oukka, V. K. Kuchroo, *Annu. Rev. Immunol.* **27**, 485 (2009).
25. K. Atarashi *et al.*, *Nature* **455**, 808 (2008).
26. S. Manicassamy, B. Pulendran, *Semin. Immunol.* **21**, 22 (2009).
27. S. Manicassamy *et al.*, *Nat. Med.* **15**, 401 (2009).
28. I. I. Ivanov *et al.*, *Cell Host Microbe* **4**, 337 (2008).
29. C. Zaph *et al.*, *J. Exp. Med.* **205**, 2191 (2008).
30. J. A. Hall *et al.*, *Immunity* **29**, 637 (2008).
31. P. Clément-Lacroix *et al.*, *Proc. Natl. Acad. Sci. U.S.A.* **102**, 17406 (2005).
32. J. H. Cho, C. T. Weaver, *Gastroenterology* **133**, 1327 (2007).
33. M. Rescigno, U. Lopatin, M. Chieppa, *Curr. Opin. Immunol.* **20**, 669 (2008).
34. G. Matteoli *et al.*, *Gut* **59**, 595 (2010).
35. K. R. Siddiqui, S. Laffont, F. Powrie, *Immunity* **32**, 557 (2010).
36. We thank S.A. Mertens and L. Bronner for assistance with cell sorting and D. Levesque (Emory Vaccine Center) and D. Bonenberger for assistance with maintenance of mice strains at the Emory Vaccine Center vivarium. The work in the laboratory of BP was supported by grants U54AI057157, R37AI48638, R01DK057665, U19AI057266, HHSN266 200700006C, NO1 AI50019, and NO1 AI50025 from the National Institutes of Health and a grant from the Bill & Melinda Gates Foundation. Microarray accession number is GSE2213 (http://www.ncbi.nlm.nih.gov/geo/query/acc.cgi?acc=GSE22136).

Supporting Online Material

www.sciencemag.org/cgi/content/full/329/5993/849/DC1
Materials and Methods
SOM Text
Figs. S1 to S14
Table S1
References

18 February 2010; accepted 11 June 2010
10.1126/science.1188510

Stability of Ecological Communities and the Architecture of Mutualistic and Trophic Networks

Elisa Thébault[1,2]* and Colin Fontaine[1,3]*

Research on the relationship between the architecture of ecological networks and community stability has mainly focused on one type of interaction at a time, making difficult any comparison between different network types. We used a theoretical approach to show that the network architecture favoring stability fundamentally differs between trophic and mutualistic networks. A highly connected and nested architecture promotes community stability in mutualistic networks, whereas the stability of trophic networks is enhanced in compartmented and weakly connected architectures. These theoretical predictions are supported by a meta-analysis on the architecture of a large series of real pollination (mutualistic) and herbivory (trophic) networks. We conclude that strong variations in the stability of architectural patterns constrain ecological networks toward different architectures, depending on the type of interaction.

Robert May (*1*) showed that ecological complexity (defined in terms of the number of interacting species and the frequency of their interactions) constraints the stability of randomly assembled interaction networks. Although May's model included different types of interactions, most theoretical studies since then have focused mainly on trophic interactions. These studies have revealed that many architectural patterns found in real food webs, such as patterns of interaction strength in omnivory loops (*2*, *3*) and allometric degree distributions (*4*), tend to enhance community stability and species coexistence (*5*). During the past decade, studies have also investigated with success the particular architecture of mutualistic interactions (*6*, *7*). For those mutualistic networks, asymmetry in interaction strength (*8*) and nestedness (*9*, *10*) appear to stabilize the community. The variety of approaches used, as well as the focus on a single interaction type at a time, make the differences between trophic and mutualistic networks still unclear and very speculative, especially because food webs are traditionally represented as unipartite networks, whereas mutualistic networks are bipartite (*7*). We made a systematic comparison between trophic and mutualistic bipartite networks, at different levels of complexity, to test whether the type of interaction affects the relationship between network architecture and stability. First, we followed a model approach in which we analyzed the relations between community stability and a wide range of major network architectural patterns in mutualistic and trophic networks. Then we compared the model prediction with observed network architectures in a large collection of real pollination (mutualistic) and herbivory (trophic) networks.

We built a population dynamics model that can simulate the changes in species densities over time in either mutualistic or trophic networks (*11*). We used it to simulate the dynamic of 7.2×10^3 mutualistic and trophic networks, which varied in architecture regarding four main architectural patterns: diversity, connectance, nestedness, and modularity. The values of these indices respectively describe the number of species, the relative number of interactions, the level of sharing of interaction partners among species, and the degree of compartmentalization of the networks. These architectural patterns have been historically described in ecological networks (*7*, *12*), and despite the relationships between them, they can provide complementary information on how interactions are organized in communities (*13*). During the simulations, some species could become extinct before equilibrium was reached, thus altering the initial architecture of the networks. These extinctions led mutualistic networks to become more connected, more nested, and less modular. In contrast, species extinctions led to trophic networks that were less connected, less nested, and more modular (Fig. 1, A to D, F, and G). Because nestedness and modularity values are related to network diversity and connectance, we also calculated the relative nestedness and the relative modularity. These indices measure how nested and modular a network is as compared with the mean expected nestedness and modularity under a given null model. Following the approach developed for the study of nestedness in mutualistic networks, we used a null model that assumes that the probability of interaction between a plant and an animal depends on the observed number of interactions of both species (*7*, *11*). Changes in relative nestedness and relative modularity follow qualitatively the same trend as changes in nestedness and modularity. Mutualistic networks increase in relative nestedness whereas trophic networks increase in relative modularity and decrease in relative nestedness. These results indicate that the alterations in network architecture are linked not only with modifications of diversity and connectance but also with complex arrangements of interactions (Fig. 1, E and H). The dynamic and stability of the networks thus constrain the existing structure of mutualistic and trophic networks toward opposite network patterns.

Because the links between community architecture and stability can depend on the stability metric used (*14*), we measured two distinct indices of stability: persistence (the proportion of persisting species once equilibrium is reached) and resilience (the speed at which the community returns to the equilibrium after a perturbation). We analyzed the results of our simulations by using structural equation modeling (path analysis) to disentangle the direct effects of network diversity and connectance on community stability, as well as their indirect effects mediated through changes in nestedness and modularity. As illustrated in Fig. 2

[1]Division of Biology, Natural Environment Research Council Centre for Population Biology, Imperial College London, Silwood Park Campus, Ascot, Berkshire SL5 7PY, UK. [2]Biometris, Wageningen University, Droevendaalsesteeg 1, 6708 PB Wageningen, Netherlands. [3]Laboratoire de Conservation des Espèces, Restauration et Suivi des Populations, UMR 7204 CNRS-MNHN, Muséum National d'Histoire Naturelle, 61 rue Buffon, 75005 Paris, France.

*Both authors contributed equally to this work.

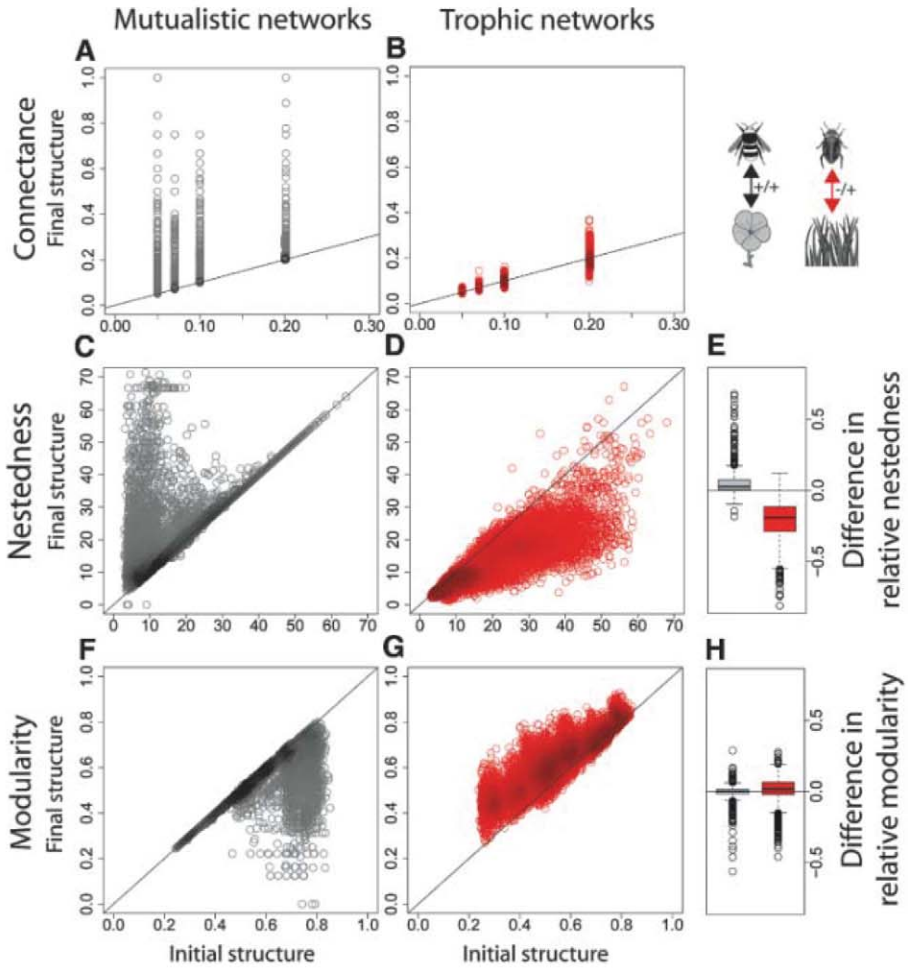


Fig. 1. Final architecture of mutualistic (gray) and trophic (red) networks once equilibrium was reached, against their initial structure, regarding connectance (**A** and **B**), nestedness (**C** and **D**), and modularity (**F** and **G**). (**E**) and (**H**) represent box plots of the difference between final and initial architectures in relative nestedness and relative modularity, respectively, for mutualistic (red) and trophic (gray) networks. The bottom and top limits of each box are the lower and upper quartiles, respectively; the horizontal black band within each box is the median; and error bars equal ±1.5 times the interquartile range.

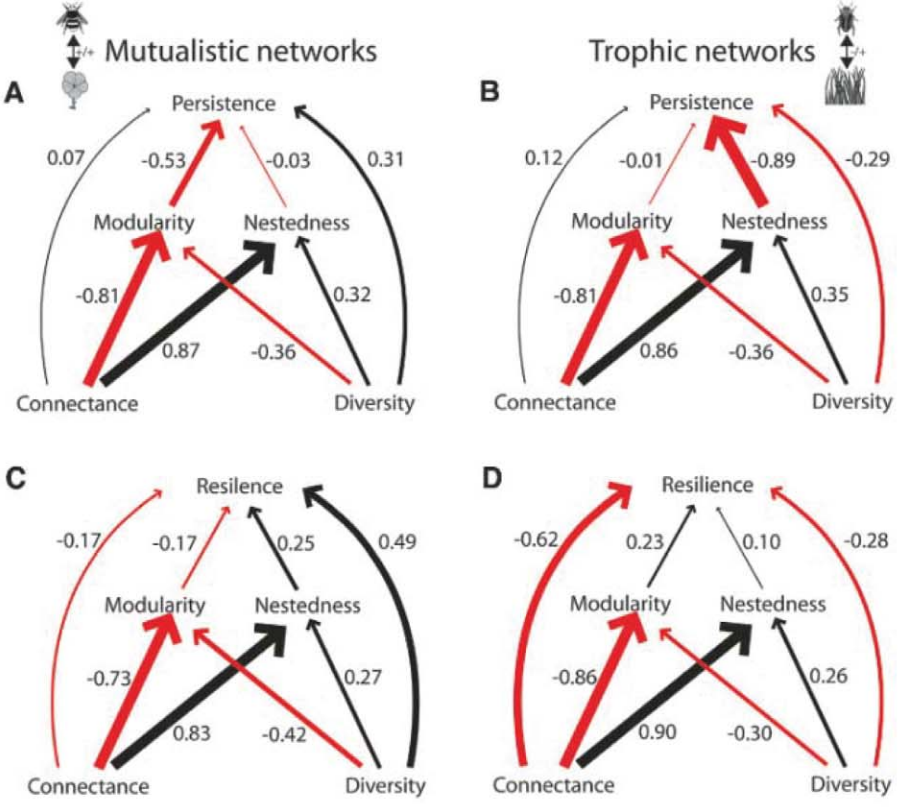


Fig. 2. Summary diagrams of the effects of the different network architectural patterns on the persistence (**A** and **B**) and resilience (**C** and **D**) of mutualistic [(A) and (C)] and trophic [(B) and (D)] networks. The thickness of the arrows is scaled to standardized coefficients from path analysis and illustrates the relative effect strength. Negative effects are represented in red and positive effects in black. The effects of connectance and diversity are split between direct effects and indirect effects through changes in modularity and nestedness. The strength of the indirect effects is calculated by the product of the coefficients along the path. For example, in (A), connectance has a direct effect of strength 0.07, an indirect effect through modularity of strength 0.43 (-0.81×-0.53), and an indirect effect through nestedness of strength -0.026 (0.87×-0.03), which lead to an overall connectance effect of 0.47.

and fig. S1, network architecture has an opposite effect on the stability of mutualistic networks as compared to trophic ones, a result that is consistent along diversity, connectance, nestedness, and modularity gradients and for both the persistence and resilience of the community (*15*). Higher diversity and connectance promote the persistence and resilience of mutualistic networks, but they destabilize trophic networks. For mutualistic networks, modularity decreases the persistence of the network, and nestedness increases its resilience. In contrast, for trophic networks, nestedness decreases the persistence of the network, and modularity enhances its resilience. The results of the structural equation models further reveal that a large part of the effects of connectance and diversity on persistence is mediated through changes in network modularity and nestedness (Fig. 2). On the contrary, connectance and diversity directly affect community resilience, whereas the indirect effects mediated through changes in nestedness and modularity are weaker. These results also show that nestedness and modularity have singular effects on stability, especially on persistence, and despite their strong negative correlation, these two indices thus capture different aspects of network architecture. This highlights the importance of moving beyond traditional measures of topology (such as connectance) and using more integrative indices (such as nestedness and modularity) to improve our understanding of the determinants of community stability.

To test our theoretical predictions, we compiled a large data set of published networks describing either mutualistic or trophic interactions, and we analyzed their architecture (*16*). These networks represent 34 pollination networks and 23 herbivory networks (table S5). Pollination and herbivory network architectures differ in the relationship between diversity and connectance, as well as in their values of nestedness and modularity. Connectance is negatively related to diversity ($F_{1,53}$ = 67.59, P < 0.0001), but it decreases faster with increasing diversity in herbivory networks than in pollination networks ($F_{1,53}$ = 5.01, P = 0.0295; Fig. 3), indicating that highly diverse herbivory webs tend to be less connected than pollination webs of similar diversity. Even after accounting for these differences in connectance, pollination networks are more nested than herbivory networks ($F_{1,51}$ = 25.12, P < 0.0001; Fig. 3, table S2, and fig. S2), whereas the opposite pattern is found for modularity ($F_{1,51}$ = 77.93, P < 0.0001; Fig. 3, table S2, and fig. S2). Two herbivory networks, however, exhibit a very high level of nestedness. Although both involve leaf-chewing insects (grasshoppers), these outliers do not seem to be related to this particular type of feeding (see table S5). We also calculated the relative nestedness of these empirical data sets to test whether the observed values are different from what is expected from a null model. Relative nestedness is significantly higher in pollination networks than in herbivory networks (Welch t test, t = –4.75, df = 25.85, $P = 6 \times 10^{-6}$), thus strengthening our previous results. Although herbivory networks tend to have a higher relative modularity than pollination networks, the difference is not significant (Welch t test, t = 1.47, df = 52.74, P =

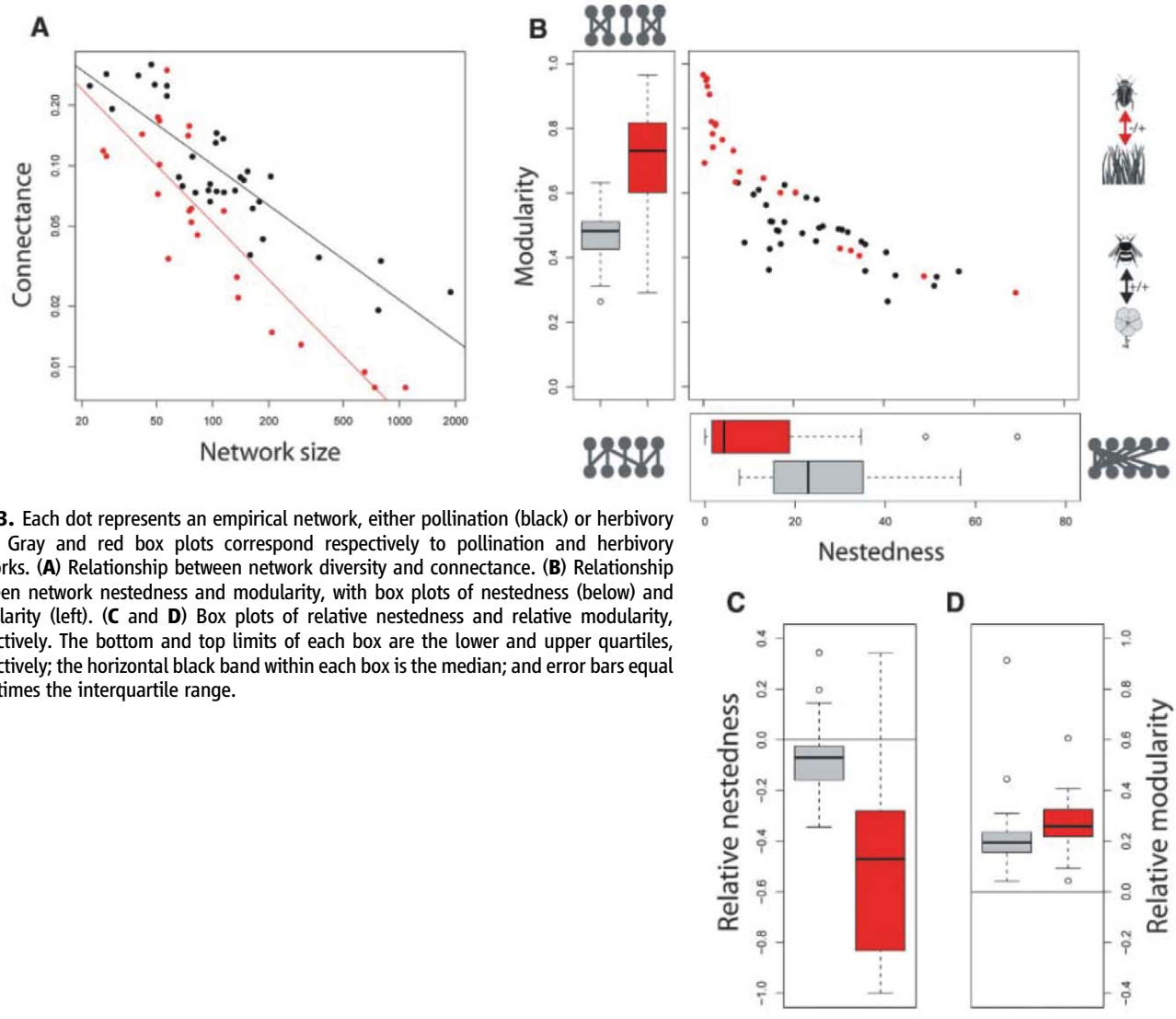


Fig. 3. Each dot represents an empirical network, either pollination (black) or herbivory (red). Gray and red box plots correspond respectively to pollination and herbivory networks. (**A**) Relationship between network diversity and connectance. (**B**) Relationship between network nestedness and modularity, with box plots of nestedness (below) and modularity (left). (**C** and **D**) Box plots of relative nestedness and relative modularity, respectively. The bottom and top limits of each box are the lower and upper quartiles, respectively; the horizontal black band within each box is the median; and error bars equal ±1.5 times the interquartile range.

0.15). This last result indicates that the higher modularity of herbivory networks might be partly linked with their lower connectance. Although recent studies found both nested and modular patterns in a same mutualistic or trophic network (*17*), our results show that nestedness is stronger in mutualistic networks than in trophic ones; in contrast, trophic networks tend to have a higher modularity, in relation with a lower connectance. The network characteristics that are observed in each type of empirical network are thus the ones predicted to promote biodiversity persistence and stability by our model.

This work is a step toward a better understanding of the impact of the type of interaction on the architecture of ecological networks, an issue that has begun to be investigated only recently (*18*–*21*). Previous studies have focused on one type of interaction at a time [but see (*10*)] and usually investigated the effects of one particular architectural pattern (*2*, *3*, *9*, *10*). Here we show that the combination of different architectural patterns is essential to understand the mechanisms behind the stability of communities, and we further predict emerging network architectures that differ strikingly between interaction types. The congruence between these theoretical predictions and the empirical observations in our study strongly suggests that community dynamic and stability constrain mutualistic and trophic networks toward different architectural patterns. The mechanism behind these different architectures might be linked to indirect interactions, maybe even more so than direct interactions. For example, the negative indirect effects of apparent competition should prevail in trophic networks (*22*), restricting the sharing of interacting partners among species and thereby the propagation of negative effects across the network, and thus promoting a low connectance and a high modularity. In contrast, positive indirect effects of apparent facilitation occur in mutualistic networks (*23*) and should favor a highly connected and nested architecture characterized by the sharing of interaction partners in the network (*10*).

Next steps of research will need to tackle two fascinating challenges. First, how these dynamical constraints interact with other determinants of network architecture, such as trait matching, phylogenetic constraints, and coevolutionary dynamics (*24*–*26*). Second, how various interaction networks with different architecture combine themselves to shape the broader network that links all the species within an ecosystem, and how this relates to the functioning and stability of ecosystems.

References and Notes

1. R. M. May, *Nature* **238**, 413 (1972).
2. A. M. Neutel, J. A. P. Heesterbeek, P. C. De Ruiter, *Science* **296**, 1120 (2002).
3. A. M. Neutel *et al*., *Nature* **449**, 599 (2007).
4. S. B. Otto, B. C. Rall, U. Brose, *Nature* **450**, 1226 (2007).
5. J. M. Montoya, S. L. Pimm, R. V. Solé, *Nature* **442**, 259 (2006).
6. J. Bascompte, *Science* **325**, 416 (2009).
7. J. Bascompte, P. Jordano, C. J. Melián, J. M. Olesen, *Proc. Natl. Acad. Sci. U.S.A.* **100**, 9383 (2003).
8. J. Bascompte, P. Jordano, J. M. Olesen, *Science* **312**, 431 (2006).
9. T. Okuyama, J. N. Holland, *Ecol. Lett.* **11**, 208 (2008).
10. U. Bastolla *et al*., *Nature* **458**, 1018 (2009).
11. Details of the model, the procedure to build networks of varying architectures, the stability measures, the path analysis, and the descriptors of network architecture are available in the supporting online material (SOM).
12. A. E. Krause, K. A. Frank, D. M. Mason, R. E. Ulanowicz, W. W. Taylor, *Nature* **426**, 282 (2003).
13. M. A. Fortuna *et al*., *J. Anim. Ecol.* **79**, 811 (2010).
14. A. R. Ives, S. R. Carpenter, *Science* **317**, 58 (2007).
15. A sensitivity analysis of these results is available in the SOM.
16. Details of the statistical analyses of empirical networks are available in the SOM.
17. J. M. Olesen, J. Bascompte, Y. L. Dupont, P. Jordano, *Proc. Natl. Acad. Sci. U.S.A.* **104**, 19891 (2007).
18. P. R. Guimarães Jr. *et al*., *Curr. Biol.* **17**, 1797 (2007).
19. E. Thébault, C. Fontaine, *Oikos* **117**, 555 (2008).
20. F. J. F. Van Veen, C. B. Müller, J. K. Pell, H. C. J. Godfray, *J. Anim. Ecol.* **77**, 191 (2008).
21. C. Fontaine, E. Thébault, I. Dajoz, *Proc. Biol. Sci.* **276**, 3027 (2009).
22. F. J. F. van Veen, R. J. Morris, H. C. J. Godfray, *Annu. Rev. Entomol.* **51**, 187 (2006).
23. J. Ghazoul, *J. Ecol.* **94**, 295 (2006).
24. E. L. Rezende, P. Jordano, J. Bascompte, *Oikos* **116**, 1919 (2007).
25. E. L. Rezende, J. E. Lavabre, P. R. Guimarães, P. Jordano, J. Bascompte, *Nature* **448**, 925 (2007).
26. J. N. Thompson, *The Geographic Mosaic of Coevolution* (Univ. of Chicago Press, Chicago, 2005), vol. II.

27. We thank J. Bascompte, T. Barraclough, C. Devaux, P. de Ruiter, V. Savolainen, and F. van Veen for comments on the manuscript, and F. Ory for the art work. E.T. and C.F. were funded by the UK Natural Environment Research Council.

Supporting Online Material

www.sciencemag.org/cgi/content/full/329/5993/853/DC1
Methods
Figs. S1 to S6
Tables S1 to S5
References

16 February 2010; accepted 15 June 2010
10.1126/science.1188321

Rational Design of Envelope Identifies Broadly Neutralizing Human Monoclonal Antibodies to HIV-1

Xueling Wu,[1]* Zhi-Yong Yang,[1]* Yuxing Li,[1]* Carl-Magnus Hogerkorp,[1]† William R. Schief,[4] Michael S. Seaman,[5] Tongqing Zhou,[1] Stephen D. Schmidt,[1] Lan Wu,[1] Ling Xu,[1] Nancy S. Longo,[1] Krisha McKee,[1] Sijy O'Dell,[1] Mark K. Louder,[1] Diane L. Wycuff,[1] Yu Feng,[1]‡ Martha Nason,[2] Nicole Doria-Rose,[3] Mark Connors,[3] Peter D. Kwong,[1] Mario Roederer,[1] Richard T. Wyatt,[1]‡ Gary J. Nabel,[1]§ John R. Mascola[1]§

Cross-reactive neutralizing antibodies (NAbs) are found in the sera of many HIV-1–infected individuals, but the virologic basis of their neutralization remains poorly understood. We used knowledge of HIV-1 envelope structure to develop antigenically resurfaced glycoproteins specific for the structurally conserved site of initial CD4 receptor binding. These probes were used to identify sera with NAbs to the CD4-binding site (CD4bs) and to isolate individual B cells from such an HIV-1–infected donor. By expressing immunoglobulin genes from individual cells, we identified three monoclonal antibodies, including a pair of somatic variants that neutralized over 90% of circulating HIV-1 isolates. Exceptionally broad HIV-1 neutralization can be achieved with individual antibodies targeted to the functionally conserved CD4bs of glycoprotein 120, an important insight for future HIV-1 vaccine design.

Having crossed from chimpanzees to humans in only the past century, HIV-1 has rapidly evolved a daunting degree of diversity, posing a considerable challenge for vaccine development. The definition of naturally occurring broadly neutralizing antibodies (NAbs) has proven elusive, and the ability to target conserved determinants of the viral envelope (Env) has proven difficult (*1*, *2*). During HIV-1 infection, almost all individuals produce antibodies to Env, but only a small fraction can neutralize the virus (*1*, *2*). Recently, several groups have shown that the sera of 10 to 25% of infected participants contain broadly reactive NAbs (*3*–*6*), including some sera that neutralize the majority of viruses from diverse genetic subtypes (*5*–*7*). NAbs react with the HIV-1 Env spike, which is composed of three heavily glycosylated glycoprotein (gp)120 molecules, each noncovalently associated with a

[1]Vaccine Research Center, National Institute of Allergy and Infectious Diseases, National Institutes of Health, Bethesda, MD 20892, USA. [2]Biostatistics Research Branch, Division of Clinical Research, National Institute of Allergy and Infectious Diseases, National Institutes of Health, Bethesda, MD 20892, USA. [3]Laboratory of Immunoregulation, National Institute of Allergy and Infectious Diseases, National Institutes of Health, Bethesda, MD 20892, USA. [4]Department of Biochemistry, University of Washington, Seattle, WA 98195, USA. [5]Beth Israel Deaconess Medical Center, Harvard Medical School, Boston, MA 02115, USA.

*These authors contributed equally to this work.
†Present address: Department of Molecular Genetics, Novo Nordisk A/S, Novo Nordisk Park, 2760 Måløv, Denmark.
‡Present address: Department of Immunology and Microbial Science, and IAVI Center for Neutralizing Antibody at TSRI, Scripps Research Institute, La Jolla, CA 92037, USA.
§To whom correspondence should be addressed. E-mail: gnabel@nih.gov (G.J.N.); jmascola@nih.gov (J.R.M.)

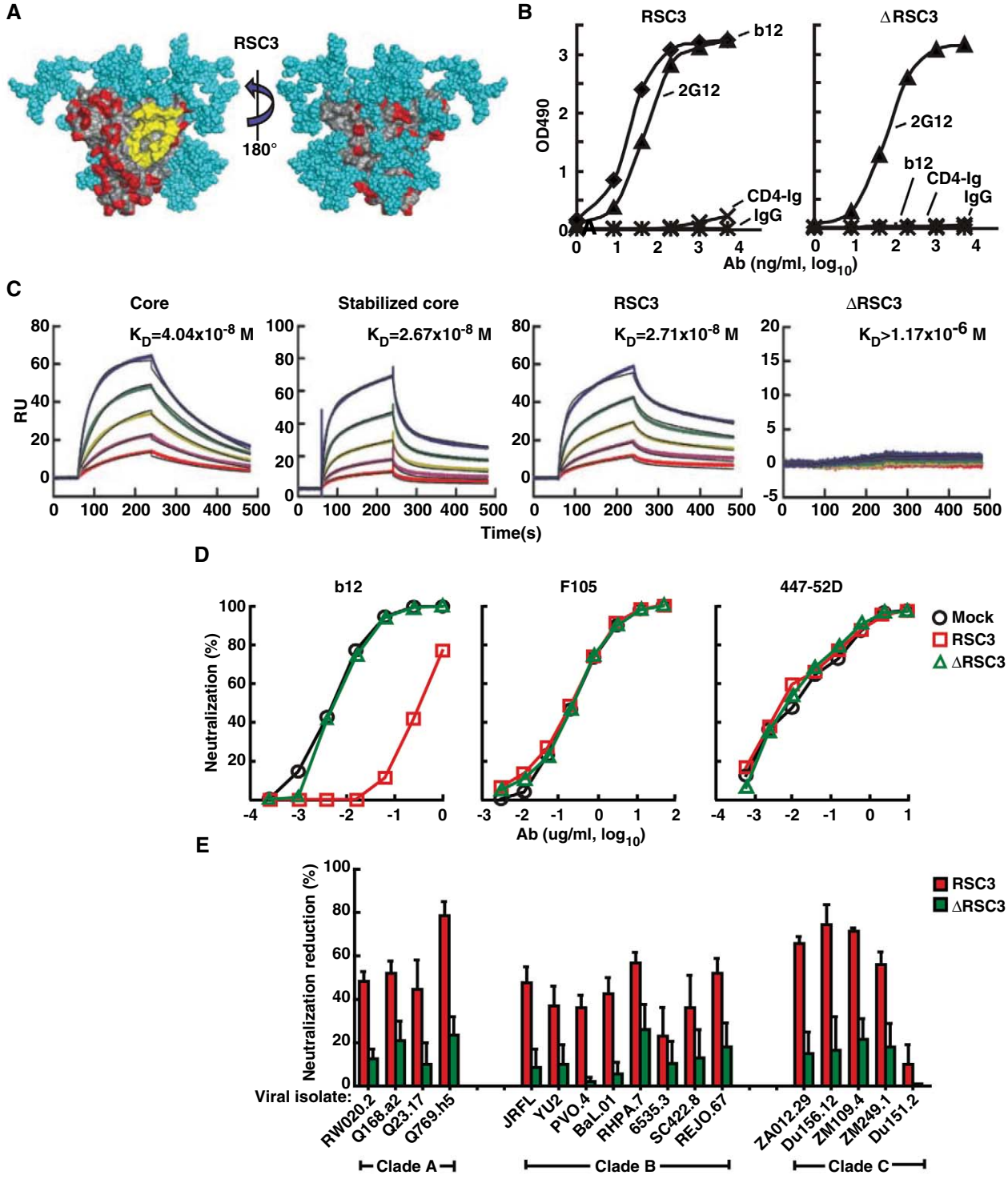


Fig. 1. Design and antigenic profile of RSC3 and analysis of epitope-specific neutralization. (**A**) Surface structure model of the RSC3. The outer domain contact site for CD4 is highlighted in yellow. Regions highlighted in red are antigenically resurfaced areas, shown on both the inner (left) and outer (right) faces of the core protein. Glycans are shown in light blue. (**B**) Antigenicity of the RSC3 protein based on ELISA using the neutralizing CD4bs mAb b12 and CD4-Ig fusion protein. mAb 2G12 was used to confirm the structural integrity of the protein. OD indicates optical density. IgG, irrelevant IgG. (**C**) mAb b12 was immobilized on the sensor chip for SPR kinetic binding analysis with the proteins shown. RU, resonance units. (**D**) RSC3 blockade of HIV-1 viral strain HXB2 neutralization by the broadly neutralizing CD4bs mAb b12 but not mAb F105, which recognizes the CD4bs differently and has limited neutralization breadth. The V3-neutralizing mAb 447-52D is shown as a control. (**E**) Analysis of serum 45 neutralization of a panel of 17 viruses, using RSC3 and ΔRSC3 to block neutralization activity. The percent reduction in the serum 50% inhibitory dilution (ID_{50}) caused by competition with RSC3 or ΔRSC3 is shown on the *y* axis (±SEM of three independent experiments). Viral strains and clades are shown on the *x* axis. Values less than 20% are not considered significant in this assay.

transmembrane gp41 molecule. To initiate viral entry into cells, the gp120 binds to the cell surface receptor CD4 (*8*). We previously reported that selected sera contain NAbs directed against the CD4-binding site (CD4bs) of gp120 (*7*, *9*), and we defined the structure of the CD4bs in complex with the neutralizing monoclonal antibody (mAb) b12 (*10*, *11*). Antibody b12 was isolated from a phage display library in 1992 and can neutralize about 40% of known HIV-1 isolates (*12*–*14*). The more recently isolated CD4bs mAb HJ16 also neutralizes about 40% of viral isolates (*15*). Attempts to isolate more broadly reactive CD4bs-directed NAbs from human B cells have not met with success, in part because the gp120 or gp140 proteins used were reactive with many HIV-1–specific antibodies, including nonneutralizing antibody specificities (*15*, *16*). In this study, we used our knowledge of Env structure, together with computer-assisted protein design, to define recombinant forms of HIV-1 Env that specifically interact with NAb directed to the CD4bs. These Env probes were used to identify and sort individual B cells expressing CD4bs antibodies, enabling the selective isolation of CD4bs-directed mAbs with extensive neutralization breadth.

To generate a molecule that preserved the antigenic structure of the neutralizing surface of the CD4bs but eliminated other antigenic regions of HIV-1, we designed proteins whose exposed surface residues were substituted with simian immunodeficiency virus (SIV) homologs and other non–HIV-1 residues (*17*) (Fig. 1A and fig. S1). These changes were conferred on a core gp120 and a stabilized core gp120, both of which retained the major contact surface for CD4 located on its outer domain (*10*, *11*, *18*). The gp120 core lacked variable regions 1 to 3 and part of the amino and carboxy termini of the full gp120 molecule, and the stabilized core contained cross-links between different subregions of the core protein. Eight resurfaced proteins were designed and expressed, together with CD4bs mutants that served as negative controls by eliminating binding to the neutralizing mAb b12. Three resurfaced core Envs retained strong reactivity with b12 and mAb 2G12 (fig. S2), the latter of which recognizes a surface glycan epitope and served as a positive control for a conformationally intact protein. The resurfaced stabilized core 3 (RSC3) was chosen as the preferred candidate for further studies, because a greater percentage of its surface other than the outer domain CD4bs area was altered compared with the other variants (fig. S2). The conformational integrity and specificity of the RSC3 protein was confirmed by using a

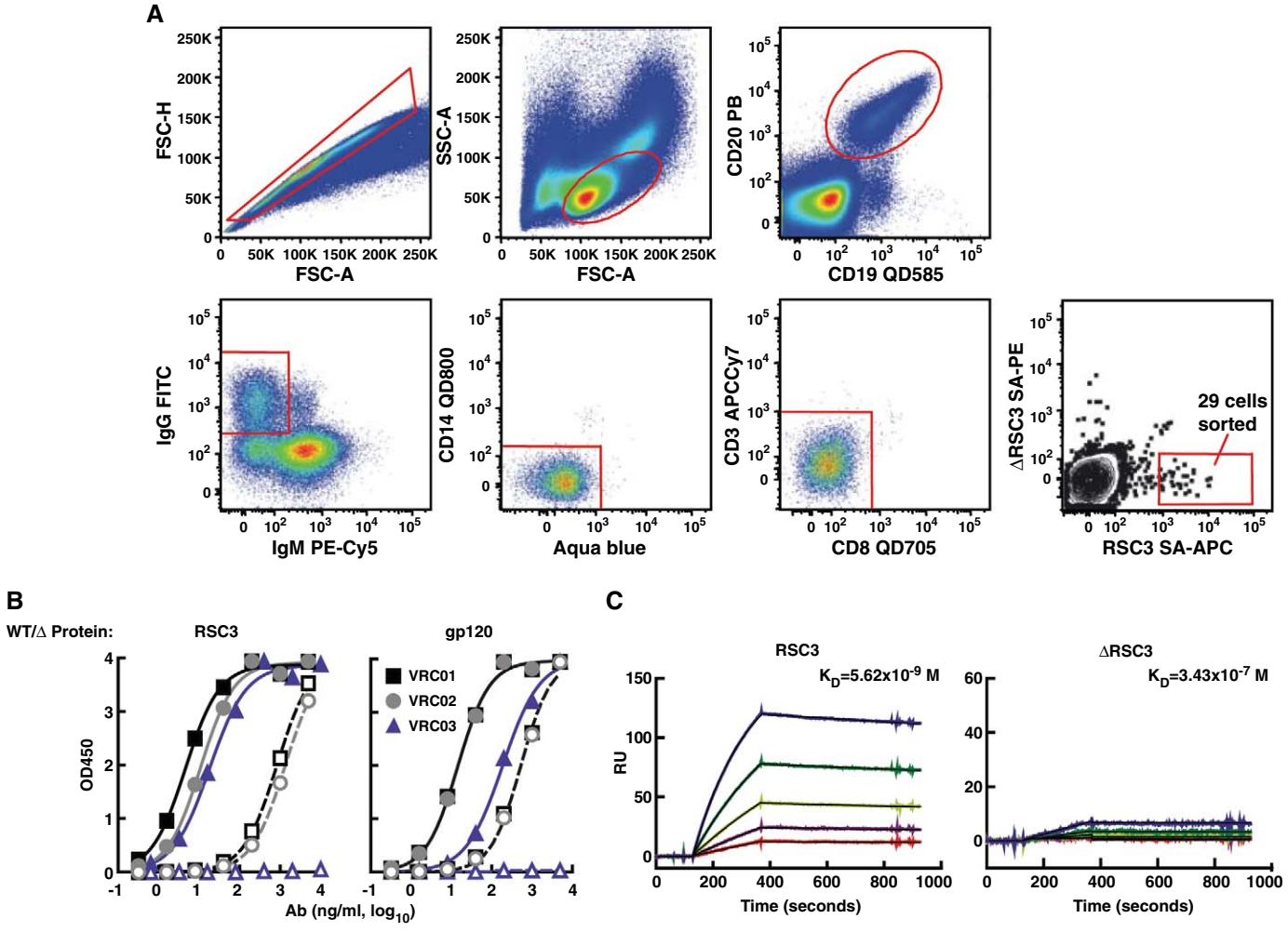


Fig. 2. Isolation of individual CD4bs-directed memory B cells by cell sorting and binding characterization of isolated mAbs. (**A**) Twenty-five million PBMC from donor 45 were incubated with biotin-labeled RSC3 and ΔRSC3 that were complexed with SA-APC and SA-PE, respectively. Memory B cells were selected on the basis of the presented gating strategy. Twenty-nine B cells that reacted with RSC3 and not ΔRSC3 (representing 0.05% of all memory B cells) were sorted into individual wells of a 96-well plate containing lysis buffer. FITC, fluorescein isothiocyanate. FSC-H, forward scatter height; FSC-A, forward scatter area; and SSC, side scatter area. (**B**) ELISA antigen binding profile of three isolated mAbs, VRC01, VRC02, and VRC03. Solid symbols show mAb binding to RSC3 (left) and YU2 gp120 (right). Open symbols indicate binding to ΔRSC3 (left) or to the CD4bs knockout mutant of gp120, D368R (right). WT, wild type. (**C**) SPR binding analysis of VRC01 reacted with RSC3 and ΔRSC3. VRC01 was captured with an antibody against human IgG-Fc that was immobilized on the sensor chip. The SPR and ELISA data shown are from a representative experiment; several additional assays produced similar data.

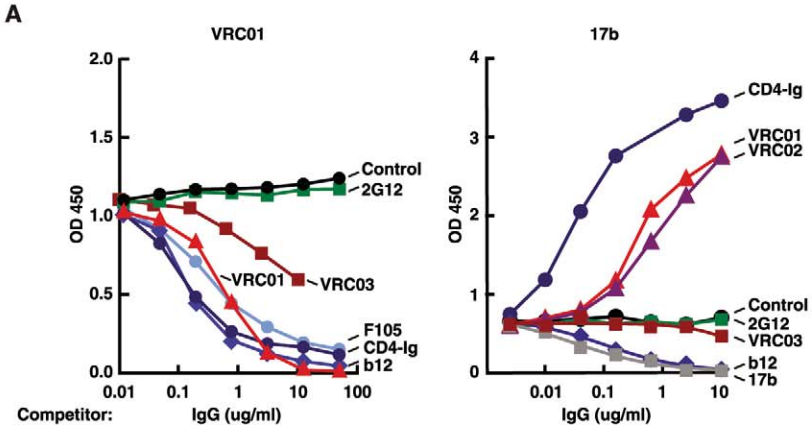
panel of known mAbs (table S1). As expected, RSC3 displayed strong reactivity to mAb b12 and little or no reactivity to a CD4 fusion protein (Fig. 1, B and C) (*19*). RSC3 also reacted with two weakly neutralizing CD4bs mAbs, b13 and m18, but it displayed no reactivity to four CD4bs mAbs that do not neutralize primary HIV-1 isolates, nor with mAbs directed to other regions of the HIV-1 Env, including the coreceptor-binding region of gp120 and the V3 and C5 regions of gp120 (table S1). ΔRSC3, which lacked a single amino acid at position 371 that eliminated b12 binding, served as a negative control. Together, these data confirmed the integrity of the antibody binding surface of this resurfaced protein, and it was used for analyses of sera and to identify B cells from an HIV-1–infected individual whose sera contained broadly reactive NAbs.

We screened a panel of broadly neutralizing sera for the presence of antibodies that could preferentially bind to RSC3 compared with ΔRSC3. CD4bs antibodies were detected in several sera, including serum from donor 45, which was previously reported to contain NAbs directed to the CD4bs of gp120 (fig. S3) (*7*). To determine whether antibodies that bind to RSC3 were responsible for the broad neutralization mediated by serum 45, we performed neutralization studies by using RSC3 to compete cognate antibodies. The utility of this assay was confirmed with the CD4bs mAb b12 and with mAb F105, which binds differently to the CD4bs and does not bind RSC3 (table S1). mAb b12 neutralizes many primary HIV-1 strains, whereas F105 neutralizes mainly laboratory-adapted or other highly sensitive virus strains, such as the HXB2 strain used here. The addition of RSC3 but not ΔRSC3 inhibited b12-mediated neutralization of HXB2. RSC3 had no effect on F105 neutralization, and neither RSC3 nor ΔRSC3 affected neutralization by the anti-V3 mAb 447-52D (Fig. 1D). To interrogate serum 45 neutralization, we performed similar RSC3 competition studies with this serum against a panel of diverse HIV-1 strains (Fig. 1E). This analysis suggested that serum 45 neutralization was principally directed against the CD4bs on functional viral spikes and that the RSC3 faithfully mimicked this structure.

To isolate CD4bs-directed mAbs, we used a recently described method of antigen-specific memory B cell sorting (*16*), together with single-cell polymerase chain reaction (PCR), to amplify immunoglobulin G (IgG) heavy- and light-chain genes from the cDNA of individual B cells (*16*, *20*). RSC3 and ΔRSC3 were expressed with a tagged amino acid sequence that allows biotin labeling. The two proteins could thus be distinguished by fluorescence-activated cell sorting (FACS) analysis after labeling with streptavidin (SA) conjugated to the fluorochromes allophycocyanin (SA-APC) or phycoerythrin (SA-PE), respectively. Peripheral blood mononuclear cells (PBMC) from donor 45 were incubated with RSC3 SA-APC and ΔRSC3 SA-PE, and single antigen-specific memory B cells were sorted into wells of a microtiter plate after selecting for memory B cells ($CD19^+$, $CD20^+$, and IgG^+) that bound to the RSC3 but not the ΔRSC3 probe (Fig. 2A). Out of about 25 million PBMC, 29 single RSC3-specific memory B cells were sorted, and the matching heavy- and light-chain genes were successfully amplified from 12 cells. After cloning into IgG1 expression vectors that reconstituted the heavy- and light-chain constant regions, the full IgG mAbs were expressed. Three antibodies (VRC01, VRC02, and VRC03) bound strongly to RSC3 and weakly or not at all to ΔRSC3 (Fig. 2, B, left, and C, and fig. S4). To confirm the specificity of these antibodies for the CD4bs, we tested enzyme-linked immunosorbent assay (ELISA) binding of each mAb against a wild-type gp120 and the CD4bs-defective Asp^{368}→Arg^{368} (D368R) mutant (Fig. 2B, right). VRC01 and VRC02 bound with ≥100-fold lower relative affinity to the heavy chain variable gene (VH) D368R mutant compared with wild-type gp120, and VRC03 showed no detectable binding to the CD4bs knockout mutant. The ELISA binding profile to an extended panel of mutant Env proteins further confirmed the CD4bs specificity of VRC01, VRC02, and VRC03 (table S1).

Analysis of the heavy- and light-chain nucleotide sequences using JoinSolver software (http://joinsolver.niaid.nih.gov/) and the Immunogenetics Information System (IMGT) database (http://imgt.cines.fr/) revealed that VRC01 and VRC02 were somatic variants of the same IgG1 clone. The heavy-chain CDR3 region of both mAbs was composed of the same 14 amino acids (fig. S5), and both mAbs were highly somatically mutated, with 32% of the heavy chain variable gene (VH) and 17 to 19% of the kappa light chain variable gene (VK) nucleotides divergent from putative germline gene sequences. VRC03 was potentially derived from a different IgG1 clone, but its heavy chain was derived from the same IGHV1-02*02 and IGHJ1*01 alleles as VRC01 and VRC02. VRC03 was also highly somatically mutated, with an unusual seven–amino acid insertion in heavy-chain framework 3 and 30% of VH and 20% of VK nucleotides divergent from putative germline gene sequences. The heavy-chain CDR3 of VRC03 contained 16 amino acids. All three mAbs share common sequence motifs in heavy-chain CDR1, CDR2, and CDR3.

The binding characteristics of the mAbs were further analyzed by surface plasmon resonance (SPR), competition ELISA, and isothermal titration calorimetry (ITC). SPR demonstrated that VRC01 ($K_D = 3.88 \times 10^{-9}$ M) and VRC02 ($K_D = 1.11 \times 10^{-8}$ M) bound gp120 with high affinity whereas VRC03 reacted with about 10-fold lower affinity ($K_D = 7.31 \times 10^{-8}$ M) (fig. S4). To evaluate the epitope reactivity of these mAbs on gp120, we performed competition ELISAs with a panel of well-characterized mAbs. As expected, binding by all three VRC mAbs was competed by CD4bs mAbs b12 and F105 and by CD4-Ig (Fig. 3A left and fig. S6A). Unexpectedly, the binding of mAb 17b to its site in the coreceptor binding region of gp120 was markedly enhanced by the addition of VRC01 or VRC02 (Fig. 3A right). This enhancing effect



B

Antibody	ΔG (kcal/mol)	ΔH (kcal/mol)	ΔT S (kcal/mol)
VRC01	-9.87 +/- 0.18	-48.6 +/- 1.29	38.7 +/- 0.65
VRC03	-8.68 +/- 0.07	-8.47 +/- 0.23	-0.21 +/- 0.12
b12	-11.1 +/- 0.2	-17.0 +/- 1.7	5.9 +/- 1.7
CD4-Ig	-10.7 +/- 0.85	-50.7 +/- 1.38	40.0 +/- 0.81

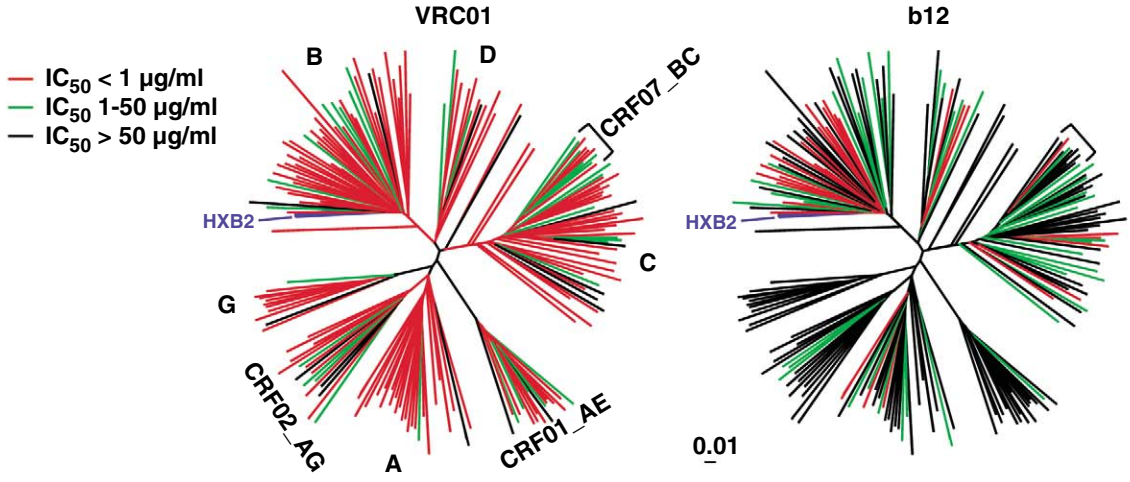
Fig. 3. Antigenic and biophysical characterization of novel CD4bs-directed mAbs. (**A**) Competition ELISA performed with a single concentration of biotin-labeled VRC01 (left) or the co-receptor binding site mAb 17b (right). The mAbs indicated near each line were titrated into the ELISA at increasing concentrations to evaluate the effect on VRC01 and 17b binding, respectively. The results shown are from a representative experiment; two additional assays produced similar data. (**B**) ITC to assess the change in enthalpy (Δ*H*) and entropy (–*T*Δ*S*) upon binding of mAbs to YU2 gp120. Each measured value is shown ±SEM.

was similar, although not as profound, as the known effect of CD4-Ig. In contrast, mAb b12 inhibited mAb 17b binding (Fig. 3A right), as previously shown (*21*). A similar enhancing result was observed for VRC01 in an assay that measures gp120 binding to its CCR5 coreceptor (fig. S6C). Thus, VRC01 and VRC02 act as partial CD4 agonists in their interaction with gp120, whereas VRC03 does not display this effect. Thermodynamic analysis by ITC provided data consistent with the ELISA results and demonstrated a change in enthalpy ($-\Delta H$) associated with the VRC01-gp120 interaction that was similar to the interaction of CD4-Ig and gp120 (Fig. 3B), further demonstrating that VRC01 binding induced conformational changes in gp120. In contrast to the data for gp120 binding, VRC01 did not enhance viral neutralization by mAb 17b (fig. S7). These data suggest that VRC01 and VRC02 partially mimic the interaction of CD4 with gp120. This may explain their broad reactivity, because essentially all HIV-1 isolates must engage CD4 for cell entry.

The potency and breadth of neutralization by VRC01, VRC02, and VRC03, compared with those by b12 and CD4-Ig, were assessed on a comprehensive panel of Env pseudoviruses (Fig. 4 and table S2). These 190 viral strains represented all major circulating HIV-1 genetic subtypes (clades) and included viruses derived from acute and chronic stages of HIV-1 infection (*22*, *23*). VRC01 neutralized 91% of these viruses with a geometric mean value of 0.33 μg/ml (Fig. 4 and table S2). The data for VRC02 were very similar (table S2). Of note, these mAbs were derived from an HIV-1 clade B–infected donor yet displayed neutralization activity against all genetic subtypes of HIV-1. VRC03 was less broad than VRC01 and VRC02, neutralizing 57% of the viruses (table S2) (*24*). In contrast, b12, also derived from a clade B-infected donor, neutralized 41% of viruses tested. Because VRC01 was derived from a donor whose sera was also broadly neutralizing, we assessed the relationship between the neutralization breadth and potency of serum 45 IgG and mAb VRC01. Among 140 viruses tested, there was a significant association ($P = 0.005$; Fisher's exact test) between the number of viruses neutralized by serum 45 IgG and the number neutralized by VRC01 (fig. S8A). Among the 122 viruses neutralized by both serum IgG and VRC01, there was a strong association ($P < 0.0001$; Deming linear regression) between the neutralization potency of the serum IgG and the potency of VRC01 (fig. S8B). Therefore, although VRC01 did not account for all serum 45 IgG neutralization, the VRC01-like antibody specificity largely accounts for the extensive breadth and potency of serum 45. These findings demonstrate that a focused B cell response can target a highly conserved region of the HIV-1 Env in humans (*25*).

Other mAbs are able to neutralize HIV-1, but none has a profile of potency and breadth similar to VRC01 and VRC02 (*1*, *13*, *14*, *26*, *27*). Antibody 4E10 requires relatively high concentrations to neutralize primary strains of HIV-1 (*13*), and it neutralizes only 12% of Env-pseudoviruses at a concentration of less than 1 μg/ml (*14*). The well-characterized CD4bs mAb b12 (*13*, *14*) and the more recently described HJ16 (*15*) are informative with respect to antigen recognition, but each display restricted breadth (~40% of HIV-1 strains). Recently, two broadly neutralizing somatic variant mAbs, PG16 and PG9, were isolated by high-throughput neutralization screening of B cell supernatants (*14*). The PG16 and PG9 neutralized 73% and 79%, respectively, of viruses tested and recognized a glycosylated region of HIV-1 Env that is present on the native viral trimer, but this epitope is not well presented on gp120 or gp140.

VRC01 and VRC02 access the CD4bs region of gp120 in a manner that partially mimics the interaction of CD4 with gp120 (*28*). This observation may explain their impressive breadth of reactivity. The isolation of these mAbs from an HIV-1–infected donor and the demonstration that they neutralize the vast majority of HIV-1 strains by targeting the functionally conserved receptor binding region of Env provides proof of concept that such antibodies can be elicited in humans. The discovery of these mAbs provides new insights into how the human immune system is able to effectively target a vulnerable site on the viral Env.



Titer	VRC01	b12
IC_{50} < 50 μg/ml	91%	41%
IC_{50} < 1 μg/ml	72%	17%
Geometric mean IC_{50} (μg/ml)	0.33	1.79

Fig. 4. Analysis of neutralization by mAbs VRC01 and b12 against a panel of 190 Env pseudoviruses representing all major circulating clades of HIV-1. Dendrograms, made by the neighbor-joining method, show the protein distance of gp160 sequences from 190 HIV-1 primary isolates. The clade B reference strain HXB2 was used to root the tree, and the amino acid distance scale is indicated with a value of 1% distance as shown. The clades of HIV-1 main group, including circulating recombinant forms (CRFs), are indicated. Neutralization potency of VRC01 and b12 is indicated by the color of the branch for each virus. The data under the dendrograms show the percent of viruses neutralized with a 50% inhibitory concentration (IC_{50}) < 50 μg/ml and <1 μg/ml and the geometric mean IC_{50} value for viruses neutralized with an IC_{50} < 50 μg/ml.

References and Notes

1. R. Pantophlet, D. R. Burton, *Annu. Rev. Immunol.* **24**, 739 (2006).
2. D. C. Montefiori, L. Morris, G. Ferrari, J. R. Mascola, *Curr. Opin. HIV AIDS* **2**, 169 (2007).
3. L. Stamatatos, L. Morris, D. R. Burton, J. R. Mascola, *Nat. Med.* **15**, 866 (2009).
4. D. N. Sather *et al*., *J. Virol.* **83**, 757 (2009).
5. M. D. Simek *et al*., *J. Virol.* **83**, 7337 (2009).
6. N. A. Doria-Rose *et al*., *J. Virol.* **84**, 1631 (2010).
7. Y. Li *et al*., *Nat. Med.* **13**, 1032 (2007).
8. R. Wyatt *et al*., *Nature* **393**, 705 (1998).
9. Y. Li *et al*., *J. Virol.* **83**, 1045 (2009).
10. P. D. Kwong *et al*., *Nature* **393**, 648 (1998).
11. T. Zhou *et al*., *Nature* **445**, 732 (2007).
12. D. R. Burton *et al*., *Science* **266**, 1024 (1994).
13. J. M. Binley *et al*., *J. Virol.* **78**, 13232 (2004).
14. L. M. Walker *et al*., *Science* **326**, 285 (2009); published online 3 September 2009 (10.1126/science.1178746).
15. D. Corti *et al*., *PLoS ONE* **5**, e8805 (2010).
16. J. F. Scheid *et al*., *Nature* **458**, 636 (2009).
17. Materials and methods are available as supporting material on *Science* Online.
18. B. Dey *et al*., *J. Virol.* **81**, 5579 (2007).
19. The CD4 binding property of the core proteins would result in their binding to circulating CD4-expressing cells, such as $CD4^+$ T cells in peripheral blood. Because this interaction would confound the selection of B cells expressing CD4bs IgG, we additionally sought to design proteins containing the majority of the CD4bs epitope surface that maintained b12 reactivity but that no longer bound to CD4. Specifically, computer-assisted modeling was used to alter the β20/21 region of gp120 that is required for CD4 binding but is not part of the b12-contact surface (fig. S1).
20. J. Wrammert *et al*., *Nature* **453**, 667 (2008).
21. J. P. Moore, J. Sodroski, *J. Virol.* **70**, 1863 (1996).
22. B. Korber, S. Gnanakaran, *Curr. Opin. HIV AIDS* **4**, 408 (2009).
23. M. S. Seaman *et al*., *J. Virol.* **84**, 1439 (2010).
24. Additional studies using primary PBMC-derived viral isolates and PBMC as target cells confirmed that VRC01, VRC02, and VRC03 were able to neutralize replication-competent uncloned HIV-1 isolates grown in primary T cells (table S3). We also tested the impact of VRC01 on the functional viral spike because VRC01 and VRC02, like CD4, showed the ability to alter the conformation of gp120 and enhanced binding of CD4-induced antibodies like 17b. Unlike CD4, however, VRC01 did not promote the entry of primary HIV-1 isolates into CD4-negative cells, and it did not augment the neutralization potency of mAb 17b (fig. S7).
25. Our successful isolation of CD4bs mAbs with extensive neutralization breadth was likely due to several factors. Recent advances in high-throughput neutralization assays facilitated the identification of HIV-1 antisera containing broad NAbs (*4*–*7*, *29*–*32*). Advances in serum epitope mapping technologies led us to understand that conserved regions of HIV-1 Env may be targeted by such NAbs (*4*, *7*, *9*, *30*, *33*–*37*). The atomic-level structure of gp120 (*10*, *38*) and advances in computational modeling allowed development of the RSC probe pair that was used to identify and sort CD4bs antibody-secreting B cells. Because of the large repertoire of circulating antibodies against gp120, most of them nonneutralizing, the epitope selectivity conferred by the RSC3 protein, together with use of the knock-out mutant, was likely important for the identification of the relatively rare memory B cells secreting NAbs to the CD4bs. Recently, the gp140 form of Env was used to identify HIV-1–specific B cells and study the repertoire of the antibody responses to the Env glycoprotein (*16*). Numerous unique antibodies were derived from each of six HIV-1–infected donors, but no single mAb demonstrated broad and potent neutralization. The ability to identify epitope-specific B cells, and isolate the specific IgG clones, has broad potential application. A similar epitope-specific approach could be used to isolate mAbs to sites of known structure from infectious disease pathogens, including tuberculosis and malaria, and can be applied to the identification of targets of autoimmunity or cancer therapy.
26. S. Zolla-Pazner, *Nat. Rev. Immunol.* **4**, 199 (2004).
27. A. Forsman *et al*., *J. Virol.* **82**, 12069 (2008).
28. Unlike CD4, VRC01 and VRC02 do not appear to require interaction with the conformationally mobile β20/21 region of gp120, because this region was altered in the RSC3 protein.
29. S. G. Deeks *et al*., *J. Virol.* **80**, 6155 (2006).
30. E. S. Gray *et al*., *J. Virol.* **83**, 8925 (2009).
31. D. M. Smith *et al*., *Virology* **355**, 1 (2006).
32. D. D. Richman, T. Wrin, S. J. Little, C. J. Petropoulos, *Proc. Natl. Acad. Sci. U.S.A.* **100**, 4144 (2003).
33. J. M. Binley *et al*., *J. Virol.* **82**, 11651 (2008).
34. E. Yuste *et al*., *J. Virol.* **80**, 3030 (2006).
35. A. K. Dhillon *et al*., *J. Virol.* **81**, 6548 (2007).
36. J. M. Decker *et al*., *J. Exp. Med.* **201**, 1407 (2005).
37. X. Shen *et al*., *J. Virol.* **83**, 3617 (2009).
38. B. Chen *et al*., *Nature* **433**, 834 (2005).

39. This research was supported by the Intramural Research Program of the Vaccine Research Center, the Division of Clinical Research and the Laboratory of Immunoregulation of National Institute of Allergy and Infectious Diseases, NIH. M.S.S. was supported in part by the Bill and Melinda Gates Foundation's Collaboration for AIDS Vaccine Discovery, Comprehensive Antibody-Vaccine Immune Monitoring Consortium, grant number 38619. W.R.S. was supported by the Bill and Melinda Gates Foundation Collaboration for AIDS Vaccine Discovery through a grant to Seattle Biomedical Research Institute and by the International AIDS Vaccine Initiative. Nucleotide sequences of VRC01, VRC02, and VRC03 variable regions are available under GenBank accession numbers GU980702 to GU980707. Patent applications have been filed by the NIH on mAbs VRC01, VRC02, and VRC03 (listed investigators are X.W., Z.Y.Y., Y.L., C.M.H, W.R.S., T.Z., M.C., P.D.K., M.R., R.T.W., G.J.N., and J.R.M.) and on the RSC3 probe (listed investigators are Z.Y.Y., W.R.S., T.Z., P.D.K. and G.J.N.). We thank M. Nussenzweig and J. Scheid (Laboratory of Molecular Immunology, Howard Hughes Medical Institute, Rockefeller University, New York, NY) for sharing expertise and reagents for IgG cloning and expression; B. Haynes (Duke University Medical Center, Durham, NC) for sharing reagents and PCR methods; S. Perfetto, R. Nguyen, and D. Ambrozak for assistance with cell sorting; E. Lybarger for neutralization assays; J. Stuckey and B. Hartman for assistance with figures; A. Tislerics for manuscript preparation; D. Follman for statistical advice; C. Carrico for discussions on resurfacing; Y.-E. A. Ban and L. Kong for glycan modeling; P. Chattopadhyay and J. Yu for fluorescent antibody production and qualification; C. Williamson (University of Capetown, Capetown, South Africa), M. Thomson (Instituto de Salud Carlos III, Madrid, Spain), J. Overbaugh (Fred Hutchinson Cancer Research Center, Seattle, WA), and S. Tovanabutra and E. Sanders-Buell (Henry M. Jackson Foundation and the U.S. Military HIV Research Program, Rockville, MD) for contributing HIV-1 Env plasmids for pseudovirus production.

Supporting Online Material

www.sciencemag.org/cgi/content/full/science.1187659/DC1
Materials and Methods
Figs. S1 to S8
Tables S1 to S3
References

28 January 2010; accepted 4 May 2010
Published online 8 July 2010;
10.1126/science.1187659
Include this information when citing this paper.

NEW PRODUCTS FOCUS: SEQUENCING TECHNOLOGIES



BENCHTOP DNA SEQUENCER

GS Junior Benchtop System provides an integrated sequencing and bioinformatics solution, all in a size that is no bigger than a typical desktop laser printer. This system sequences over 35 million bases of DNA in a single 10-hour instrument run, with average read lengths in the range of 400 base pairs. With the ability to deep sequence gene loci and the sensitivity to identify rare drug-resistant viral variants down to one percent frequency, the technology offers significant advantages over current standards in many areas of medical research. A suite of high-performance data analysis software is included with the system that provides tools for de novo genome and transcriptome assembly and mapping, as well as amplicon variant analysis for the identification of rare variants in targeted sequencing studies.

454 Life Sciences/Roche

For info: 800-262-4911 | www.gsjunior.com

DNA EXTRACTION

The GET AGAROSE DNA kit supplies a method for fast and efficient isolation of DNA fragments from agarose gels. The kit is based on G-Biosciences' GET Spin Columns which have a high binding affinity for DNA. The isolation step involves the release of nucleic acid fragments from gel pieces followed by the capture of the fragments on GET Spin Columns. Washing and elution of the clean nucleic acid fragments can then be performed with a suitable buffer. Features of the kit include rapid isolation of DNA that is ready for downstream applications, including ligation. The kit is suitable for 100 bp to 20,000 bp sized fragments and is compatible with TAE and TBE buffer gels. GET AGAROSE DNA kits are supplied in 50 or 100 prep packages.

G-Biosciences/Genotech

For info: 800-628-7730 | www.GBiosciences.com

BIOFILM DNA/RNA ISOLATION

PowerBiofilm DNA Isolation Kit and PowerBiofilm RNA Isolation Kit are designed to isolate high-quality DNA or RNA from virtually any type of biofilm sample, from dental plaque to microbial mats. Biofilms are a ubiquitous form of microbial life in natural, industrial, and hospital settings with far-reaching impacts from infectious disease to bioremediation. These are the first commercial kits designed to isolate nucleic acids from the wide range of biofilm samples. Each kit includes a brand new bead tube mix which combines both mechanical and chemical cell lysis for optimal penetration of polymeric substances commonly found in biofilms. The kits also contain the patented Inhibitor Removal Technology (IRT) for better sensitivity in polymerase chain reaction (PCR), RT-PCR, or sequencing, and it yields nucleic acids of high quality and purity. With IRT, even biofilms containing heavy amounts of contaminants can be processed to provide inhibitor-free DNA and RNA.

MO BIO Laboratories, Inc.

For info: 800-606-6246 | www.mobio.com

DNA ISOLATION AND PURIFICATION

DNAdvance SP is an extraction kit for the isolation and purification of DNA from saliva samples collected with DNA Genotek's Oragene•DNA Self Collection Kits. The high throughput genomic DNA isolation reagent system enables the purification of high-quality DNA from saliva samples, making it ideal for genotyping applications (SNP, fragment analysis), sequencing, and quantitative polymerase chain reaction. Oragene•DNA is an all-in-one system for the collection, stabilization, transportation, and purification of DNA from saliva that enables easy, reliable, and cost-effective collection of samples from large numbers of individuals while providing high-quality DNA.

DNA Genotek/Beckman Coulter Genomics

For info: 866-813-6354 | www.dnagenotek.com

AMPLICON TAGGING

A new protocol for the Access Array System enables sequencing of amplicon libraries using GS FLX Titanium Series reagents on the 454 GS FLX sequencing system. The Access Array integrated fluidic circuit (IFC) automatically generates emulsion polymerase chain reaction (emPCR)-ready libraries by simultaneously combining 48 samples and 48 primer sets to produce 48 uniquely barcoded samples per chip. Fluidigm's Access Array IFC, when used with a 454 Titanium sequencer, can capture up to 24 kb of sequence data per sample, or 1.15 MB per IFC. The addition of the GS FLX Titanium Series reagents with longer reads expands the amount of sequence that can be captured using the Access Array System. By incorporating adaptor sequences into the primer design, the final PCR product is ready for emPCR as it already contains the necessary capture sequences. The 48.48 Access Array IFC is the first chip that features the ability to recover reaction products automatically.

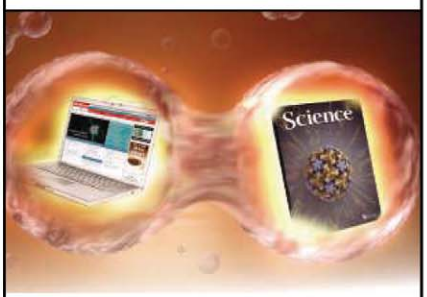
Fluidigm

For info: 866-358-4354 | www.fluidigm.com

Electronically submit your new product description or product literature information! Go to www.sciencemag.org/products/newproducts.dtl for more information.

Newly offered instrumentation, apparatus, and laboratory materials of interest to researchers in all disciplines in academic, industrial, and governmental organizations are featured in this space. Emphasis is given to purpose, chief characteristics, and availability of products and materials. Endorsement by *Science* or AAAS of any products or materials mentioned is not implied. Additional information may be obtained from the manufacturer or supplier.

Multiply The Power of Science



***Science* Careers**
Classified Advertising

For full advertising details, go to ScienceCareers.org and click For Employers, or call one of our representatives.

Tracy Holmes
Worldwide Associate Director
Science Careers
Phone: +44 (0) 1223 326525

UNITED STATES & CANADA

E-mail: advertise@sciencecareers.org
Fax: 202-289-6742

Tina Burks
Midwest/West Coast/
South Central/Canada
Phone: 202-326-6577

Elizabeth Early
East Coast & Industry
Phone: 202-326-6578

Kate Panganiban
Advertising Operations Manager
Phone: 202-326-6582

Online Job Posting Questions
Phone: 202-326-6577

EUROPE & REST OF WORLD

E-mail: ads@science-int.co.uk
Fax: +44 (0) 1223 326532

Alex Palmer
Phone: +44 (0) 1223 326527

Susanne Kharraz Tavakol
Phone: +44 (0) 1223 326529

Dan Pennington
Phone: +44 (0) 1223 326517

Lisa Patterson
Phone: +44 (0) 1223 326528

JAPAN

ASCA Corporation
Jie Chin
Phone: +81-3-6802-4616
Fax: +81-3-6802-4615
E-mail: careerads@sciencemag.jp

To subscribe to *Science*:
In US call 866 434-2227
In the rest of the world call +1 202 326-6417

All ads submitted for publication must comply with applicable US and non-US laws. *Science* reserves the right to refuse any advertisement at its sole discretion for any reason, including without limitation for offensive language or inappropriate content, and all advertising is subject to publisher approval. *Science* encourages our readers to alert us to any ads that they feel may be discriminatory or offensive.

Science Careers
From the journal *Science* AAAS

University of Connecticut Health Center

Chair of the Department of Immunology

The University of Connecticut Health Center's School of Medicine is seeking to recruit a highly qualified individual with an outstanding record of accomplishments in research, education and an excellent record of sustained NIH funding to become Chair of the Department of Immunology. We particularly encourage individuals with a current track record in human or translational immunology. The position is ideal for an energetic and visionary individual who is presently at the Associate or Full Professor level and shows evidence of the leadership skills required to ensure the health and growth of the department and to recognize the importance of interpersonal relationships and team building. The department is the academic home to faculty with nationally and internationally known research programs that focus on the cellular, molecular, and regulatory processes of the immune system. The scope of the department's research is from the most fundamental mechanisms to therapeutic applications. Departmental faculty are educational leaders in the graduate and preclinical medical and dental school curriculum.

The Chair will be responsible for oversight of all research, educational, and administrative activities involving the department. The Chair will work to enhance the funded research portfolio of the department emphasizing basic and translational research; develop and support the education of medical and graduate students and serve as a mentor for trainees at multiple levels; assure the professional development and mentoring of faculty engaged in research, education, and administration; play a major role in active governance at the institutional and departmental levels; be involved in faculty recruiting; and develop a comprehensive budget, which promotes departmental and institutional financial integrity.

The University of Connecticut Health Center is a vibrant organization composed of the School of Medicine, the School of Dental Medicine, the Graduate School of Biomedical Science, the John Dempsey Hospital, and the UCONN Medical Group. The Health Center's campus is situated on 162 acres of wooded hilltop in the beautiful, historic community of Farmington, Connecticut.

Candidates should apply by submitting a curriculum vita via email to the search committee chair, Dr. Paul Dworkin c/o Stephanie Holden, **immuchair@uchc.edu** or via the University of Connecticut Health Center Employment Services website, **https://jobs.uchc.edu**, search code 2011-065.

UCHC is an Equal Opportunity Employer M/F/V/PwD

Westfälische Wilhelms-Universität Münster

The Physics Institute at the Department of Physics of the Westfälische Wilhelms-University Münster invites applications for a tenured

Professorship in Experimental Physics (salary scale W3)

starting in the summer term of 2011.

The successful candidate is expected to have a strong research and teaching record in the field of nanophysics. Close collaboration with other groups of the research focus "nanophysics" in the department is expected. Existing research activities within this focus should be strengthened, complemented, and extended, in particular with respect to coordinated programs. A possible research field of the candidate is the physics of complex nanosystems with novel functionalities. Collaboration with other local research activities (CeNTech, FOKUS, Collaborative Research Center TRR 61) and links to the research focus "nonlinear science" are welcome.
Teaching obligations include all areas of experimental physics. In addition, the successful candidate is expected to participate in the academic administration of the department.
Qualifications include university undergraduate and doctoral degrees, good teaching skills, and a habilitation or equivalent other qualification, which may have been gained outside the University or within a "Juniorprofessur".
The Westfälische Wilhelms-University Münster is an equal opportunity employer and is committed to raising the proportion of women scientists in academic positions. Consequently, we actively encourage applications from suitably qualified women. Women with the qualifications and disciplinary expertise required will be preferentially considered. We also welcome applications from candidates with severe disabilities who, with suitable qualifications, will be preferentially considered.

Applications with a CV, including teaching experience and publication list, copies of degree certificates, and a statement of research interests, should be sent not later than **September 25th, 2010** to the Dean of the Faculty of Physics:

Dekan des Fachbereichs 11 (Physik) - Herrn Prof. Dr. Johannes P. Wessels
Wilhelm-Klemm-Str. 9 - 48149 Münster, Germany

www.uni-muenster.de

DEPUTY DIRECTOR FOR MANAGEMENT

National Cancer Institute
National Institutes of Health





NIH is the center of medical research for the Nation – making essential discoveries that improve health and save lives.

The National Cancer Institute (NCI) coordinates the National Cancer Program and conducts and supports research, training, health information dissemination, and other programs with respect to the causes, diagnosis, prevention, and treatment of cancer, rehabilitation from cancer, and the continuing care of cancer patients and their families. NCI has a staff of approximately 3,500 and an annual budget of approximately $5.0 billion.

Are you an exceptional candidate who can serve as a key member of NCI's leadership team? The Institute is seeking superior candidates for the challenging position of Deputy Director for Management, NCI. This position offers a unique and exciting opportunity to be the principal advisor to the NCI Director and senior staff on all matters that directly affect the business management and administrative operations of NCI. He/She serves as the chief operating officer for NCI, building organizational capability and skillfully presenting ideas and innovative solutions. The Deputy Director for Management coordinates activities and works to ensure that all divisions, labs, offices, and branches within NCI function seamlessly. He/She provides guidance to senior program and scientific staff on human and financial resource utilization, administrative management, contracts and procurement management, information technology and information systems, technology transfer and development, infrastructure, and human capital issues to support and advance the achievement of NCI's mission.

We are looking for applicants with senior level experience who have a commitment to excellence and the energy, enthusiasm, and innovative thinking necessary to lead a dynamic and diverse organization. Applicants must possess senior level experience (GS-14/15 or equivalent) that meets the mandatory Senior Executive Service (SES) Executive Core Qualifications (ECQs) requirements that are detailed at http://www.jobs.nih.gov/vacancies/executive.htm.

The successful candidate for this position will be appointed at a salary of $119,554-179,700, with full Federal benefits, including leave, health and life insurance, retirement, and a savings plan (401K equivalent).

If you are ready for an exciting leadership opportunity, please see the detailed vacancy announcement at http://www.jobs.nih.gov (under Executive Jobs Announcement Number: NCI-10-04SES). Applications are due by August 31, 2010.

DHHS, NIH, and NCI are Equal Opportunity Employers

National Heart Lung and Blood Institute
People Science Health

Human iPS Core Facility Director

An expert is sought in the area of stem cell biology to direct the new human induced pluripotent stem cell (iPS) Core Facility within the Division of Intramural Research (DIR), National Heart, Lung and Blood Institute (NHLBI), NIH in Bethesda, Maryland USA.

The iPS Core Facility is part of a new NHLBI DIR Initiative in Molecular Medicine. We are seeking an experienced scientist (with Ph.D. or equivalent) with an outstanding track record in stem cell biology. A competitive salary commensurate with experience and qualifications is offered. Appointees may be US citizens, resident aliens or non-resident alien with or eligible for a valid employment visa. The review of applications will begin 30 days after the initial posting and the search will remain open until the position is filled.

Please submit a cover letter highlighting key qualifications; current curriculum vitae with complete bibliography; names and addresses of four references; and a one-page summary of the applicant's philosophy of core facility operation as well as current and future research interests in PDF or MS Word format only (no paper applications will be accepted) to:

Robert S. Balaban, Ph.D., Scientific Director, NHLBI
c/o Ariel Herman, IAMB Section Chief, NHLBI
NHLBI_recruit@mail.nih.gov

National Center for Research Resources
NATIONAL INSTITUTES OF HEALTH

The National Center for Research Resources (NCRR), a major research component of the National Institutes of Health (NIH) in the Department of Health and Human Services in Bethesda, MD, seeks applicants for two Health Scientist Administrator (HSA) positions. These positions are located in the Division of Research Infrastructure (DRI), the organization which supports programs that enhance the competitiveness of investigators in underserved states and institutions. Working closely with the biomedical research community, these Health Scientist Administrators will have broad responsibilities in planning, evaluation, and scientific management of the Division's extramural research programs, including the Institutional Development Award (IDeA) program to foster health-related research and improve the competitiveness of investigators in states that receive relatively low levels of NIH funding, and the Research Centers in Minority Institutions (RCMI) program to enhances research capacity and infrastructure at minority-serving colleges and universities that offer doctorates in health sciences. Through grants and cooperative agreements, these programs support a broad range of biomedical and behavioral research, spanning the full spectrum of basic and clinical science, including community-based research addressing health disparities in underserved populations. A Ph.D. degree (or equivalent) and appropriate research experience in health or health-related science fields is required. Salaries commensurate with experience and full benefit packages (retirement savings plans; health, life, and long-term care insurance, etc.) are available.

For qualification requirements, evaluation criteria, and applicant instructions, view the vacancy announcement at http://www.jobs.nih.gov/positions/admin/healthscienceadmin.htm.

To view other job opportunities at NCRR please visit the NCRR website at www.ncrr.nih.gov



Tenure/Tenure-Track Investigator Positions in Systems Immunology and Infectious Disease Modeling

The National Institute of Allergy and Infectious Diseases (NIAID), Division of Intramural Research (DIR), is seeking an outstanding individual for its new Program in Systems Immunology and Infectious Disease Modeling (PSIIM).

Modern technology allows the deep analysis of biological systems at multiple levels. The challenge is not only to collect the large amounts of data new technologies can generate, but also to organize it in a manner that enhances our understanding of how such systems operate. Achieving this goal requires an interdisciplinary effort, and for this reason PSIIM is organized as an integrated team of scientists and support staff structured in groups. These groups will have access to the latest technology for gene expression profiling, next generation sequencing, high content screening of RNAi libraries, imaging, and genomic and proteomic analysis, as well as a substantial computer infrastructure, together with modern conventional laboratory facilities for cell and animal experimentation. They will also have access to BSL-3 facilities for working with infectious agents of high priority for human health and biodefense. Although PSIIM has been established within NIAID and has an immune/infectious disease focus, it is also expected to play a major role in fostering the growth of systems biology efforts throughout NIH. PSIIM staff will interact extensively with investigators in other components of the NIH intramural research program.

Current groups in PSIIM include Immunology, Computational Biology—Modeling and Simulation, Molecular/Cell Biology—High-throughput Screening, Proteomics, and Systems Genomics. PSIIM is now recruiting for a tenure-track or tenure level team leader appointment in the following area:

Transcriptional Networks and Control of Differentiation: The incumbent will be responsible for applying and, as required, developing novel experimental and computational methods for the systems-wide analysis of gene regulatory pathways and networks, with a specific emphasis on the transcription factor circuits that define cell fate and that translate extracellular signaling into cellular responses. As part of this effort, the incumbent will engage in quantitative measurements of transcription factor and gene expression, analysis of protein-DNA interactions, and assessment of the contributions of epigenetic modifications/chromatin remodeling events to regulation of the behavior of such transcriptional networks. PSIIM is especially interested in recruiting an individual with a strong interest in the application of these methods to the integration of information on cell signaling events, developmental state, and gene regulatory circuits into comprehensive models of the control of cellular differentiation, for example, of effector CD4+ T cells or iPS.

This position and its research activities are fully funded by the intramural research program of NIAID. The team leader is expected to build a working group consisting of postdoctoral fellows, students, technicians, and staff scientists. The team leader will work with the program director and other PSIIM faculty to help set the goals for PSIIM and to determine how best to reach these goals as an integrated group. Applicants should be seeking a challenge in which creativity, technical expertise, and a strong desire to achieve in a team setting will be critical for success.

Interested candidates may contact Ronald Germain, M.D., Ph.D., Program Director, PSIIM, DIR, NIAID, at 301-496-1904 or **rgermain@niaid.nih.gov** for additional information about these positions.

Additional information about PSIIM is available online at **www.niaid.nih.gov/LabsAndResources/labs/aboutlabs/psiim/Pages/default.aspx**.

Applicants must have a Ph.D., M.D., or equivalent degree in a relevant field with extensive post-doctoral experience, as well as a strong publication record demonstrating potential for creative research.

To apply, submit your curriculum vitae, bibliography, and a detailed statement of how your expertise can contribute to the success of the PSIIM program to Hanh Ngo at **PSIIM4Search@niaid.nih.gov**. In addition, three letters of reference must be sent directly from the referee to Robert Hohman, Ph.D., Chair, NIAID Search Committee, c/o Hanh Ngo at **PSIIM4Search@niaid.nih.gov** or 10 Center Drive, MSC 1356, Building 10, Room 4A22, Bethesda, MD 20892-1356. Email is preferred. Applications will be reviewed starting on **October 3, 2010**, and will be accepted until the position is filled.

Further information regarding the DIR laboratories is available at **www.niaid.nih.gov/about/organization/dir/**, and information on working at NIAID is available on our Web site at **www.niaid.nih.gov/careers/psgr**.

For more information about the NIAID systems biology program, please visit **www.nih.gov/catalyst/2006/06.09.01/page1.html**

NIAID

National Institute of Allergy and Infectious Diseases

U.S. DEPARTMENT OF HEALTH AND HUMAN SERVICES
National Institutes of Health

National Institute of Allergy and Infectious Diseases

Proud to be Equal Opportunity Employers

Science Careers online @sciencecareers.org

UNIVERSITY OF OREGON

Faculty Positions in Systems Neuroscience
University of Oregon

The **Institute of Neuroscience** (**http://uoneuro.uoregon.edu**) and the **Department of Biology** at the University of Oregon seek to fill up to three tenure-related faculty positions in Fall 2011. Two are at the level of Assistant Professor, and one is open-rank. We are particularly interested in candidates studying neural circuit function, development and plasticity. Researchers working with zebrafish or rodent model systems are especially encouraged to apply, although all model systems will be considered. The interests of our group encompass all levels of analysis – from molecules, genes, and neurons to behavior and cognition – in a wide diversity of model organisms. The successful candidate will complement existing strengths in developmental, systems and cognitive neuroscience, have an outstanding research program, and a commitment to excellence in teaching. Ph.D. required. Interested persons should apply online to the University of Oregon SYSTEMS NEURO SEARCH at **https://academicjobsonline.org/ajo/jobs/345**. Applicants should submit a cover letter, a curriculum vitae including publication list, a statement of research accomplishments and future research plans, a description of teaching experience, and three letters of recommendation. Submission of 1-3 select reprints is encouraged but not required. To be assured of full consideration application materials must be uploaded by October 1, 2010, but the search will remain open until the positions are filled.

Faculty Positions in Zebrafish Cell Biology, Development, or Neuroscience
University of Oregon

The **Institute of Neuroscience (ION)** (**http://uoneuro.uoregon.edu**) and the **Department of Biology** at the University of Oregon seek to fill up to three tenure-related faculty positions in Fall 2011. Two positions are at the Assistant rank, and one is open rank. We are particularly interested in candidates using zebrafish to address fundamental questions in cell biology, development, and neuroscience, but we invite applications from candidates using zebrafish to investigate any fundamental biological processes. Successful candidates will complement the existing strengths of our internationally-recognized zebrafish group, have an outstanding research program, and demonstrate a clear commitment to excellence in teaching. Ph.D. required. Interested persons should apply online to the University of Oregon ZEBRAFISH SEARCH at **https://academicjobsonline.org/ajo/jobs/344**. Applicants should submit a cover letter, a curriculum vitae including publication list, a statement of research accomplishments and future research plans, a description of teaching experience, and three letters of recommendation. Submission of 1-3 select reprints is encouraged but not required. To be assured of full consideration, application materials must be uploaded by **October 1, 2010**, but the search will remain open until the positions are filled.

The University of Oregon is an Equal Opportunity/ Affirmative Action Institution committed to cultural diversity and compliance with the Americans with Disabilities Act. Women and minorities encouraged to apply. We invite applications from qualified candidates who share our commitment to diversity.

THE UNIVERSITY OF HONG KONG
香 港 大 學

Founded in 1911, The University of Hong Kong is committed to the highest international standards of excellence in teaching and research, and has been at the international forefront of academic scholarship for many years. Ranked 24th among the top 200 universities in the world by the UK's *Times Higher Education*, the University has a comprehensive range of study programmes and research disciplines spread across 10 faculties and about 100 sub-divisions of studies and learning. There are over 23,400 undergraduate and postgraduate students coming from 50 countries, and more than 1,200 members of academic and academic-related staff, many of whom are internationally renowned.

Non-Clinical Associate Professor/Assistant Professor in Pharmacy (2 posts)
(Ref.: 20100441)

Applications are invited for appointment as Non-Clinical Associate Professor/Assistant Professor in Pharmacy (2 posts) in the Department of Pharmacology and Pharmacy, from as soon as possible, on a three-year fixed-term basis.

Applicants should possess a B.Pharm. degree and a Ph.D. degree in Pharmaceutical Sciences or Pharmacy, or equivalent qualifications, with teaching experience in the areas of clinical pharmacy, pharmacy practices, pharmaceutics, or industrial/community pharmacy at both undergraduate and postgraduate levels. Those with experience in pharmacy practice and/or pharmacy programme development, assessment and evaluation, work experience in hospital/industrial/community pharmacy, and a good track record of pharmacy research and scholarly activities would have an advantage. They should also have effective verbal and written communication skills, well-developed interpersonal skills, dedication to education, and a commitment to establishing themselves in academic pharmacy. The appointees will contribute to teaching and curriculum development of the Pharmacy programme and establish research programmes in areas complementary to the Department's research interests, to foster excellence in teaching and learning, research and professional engagement in pharmacy. Further information about the Department can be obtained at http://www3.hku.hk/pharma/current/.

Annual salaries will be in the following ranges (subject to review from time to time at the entire discretion of the University):

Associate Professor	:	HK$626,400 – 968,700
Assistant Professor	:	HK$477,360 – 737,700

(approximately US$1 = HK$7.8)

At current rates, salaries tax does not exceed 15% of gross income. The appointments will attract a contract-end gratuity and University contribution to a retirement benefits scheme, totalling up to 15% of basic salary, as well as leave, and medical/dental benefits. Housing benefits will be provided as applicable.

Applicants should submit a completed application form, together with a full C.V. indicating their research orientation. Each applicant should also submit at least three reference letters with specific comments on his/her academic competence. Further particulars and application forms (152/708) can be obtained at http://www.hku.hk/apptunit/; by **fax** (2540 6735 or 2559 2058); **e-mail** (senrappt@hku.hk); **in person** or **by writing** to the Appointments Unit (Senior), Human Resources Section, Registry, Room 10-01, Knowles Building, The University of Hong Kong, Pokfulam Road, Hong Kong. **Closes September 30, 2010**. ***Candidates who are not contacted within 4 months of the closing date may consider their applications unsuccessful.***

The University is an equal opportunity employer and is committed to a No-Smoking Policy

TEXAS STATE UNIVERSITY
SAN MARCOS
The rising STAR of Texas™

FACULTY POSITION
Department of Chemistry and Biochemistry

The Department of Chemistry and Biochemistry at Texas State University-San Marcos seeks to fill a tenure-track position at the assistant or associate professor level with a research emphasis in biochemistry to begin in the Fall of 2011. To be eligible for hire at either rank, candidates must have a Ph.D. in Chemistry, Biochemistry, or related field and postdoctoral research experience. Preference will be given to candidates having research and teaching expertise that compliments existing faculty interests within the department. To be eligible for hire at the Associate Professor rank, candidates must meet all requirements for that rank as established by the department, as well as have an established externally funded research program. The successful candidate will teach undergraduate and graduate courses in the area of chemistry and/or biochemistry.

Texas State University-San Marcos is located in the burgeoning Austin-San Antonio corridor at the edge of the hill country and is Texas's 7th largest campus with more than 30,000 students. The department of chemistry and biochemistry currently has 20 faculty, 30 masters students, and an average of 360 majors who are strongly encouraged to participate in research. For more information please visit **www.txstate.edu/chemistry/**.

Applicants should submit a CV, outline of research interests and plans, a short statement of teaching philosophy including courses you feel most comfortable to teach, plus three letters of reference with contact information to be sent to: **Faculty Search Committee, Department of Chemistry and Biochemistry, Texas State University-San Marcos, 601 University Dr., San Marcos, TX 78666**. In order to assure full evaluation of your package, it must be submitted by **October 15, 2010**.

Texas State University-San Marcos is an Equal Opportunity Employer; women and members of underrepresented minorities and individuals with disabilities are encouraged to apply.

Veterans Health Administration

Research & Development

Improving Veterans' Lives — www.research.va.gov

Director, Rehabilitation Research and Development Service

The Department of Veterans Affairs (VA) Rehabilitation Research & Development (RR&D) Service seeks qualified candidates for the position of Director.

The goal of RR&D is to improve quality of life of Veterans and their families through restoration of physical, psychological, social, and vocational functions. RR&D integrates multiple scientific disciplines to investigate and develop concepts, processes, and products to directly meet the needs of Veterans with chronic disabling diseases and conditions. Emphasized research areas include neurosciences, aging and neurodegenerative diseases, brain and spinal cord injury, musculoskeletal rehabilitation, rehabilitation engineering, prosthetics, psychological health, social reintegration, sensory systems, and regenerative medicine. The RR&D Service portfolio emphasizes basic research to repair injured organs and tissues; translational research to bring basic discoveries to clinical use; prosthetics, orthotics, and assistive device research; and research aimed at restoring physiological function and social integration.

The Director serves as functional leader and directs, plans, and manages ongoing operations of RR&D to generate new scientific knowledge and provide strategic direction for rehabilitation research.

Candidates must be a United States citizen & possess an M.D. or O.D.

Location: Washington, DC; Salary range: 110,000 to 230,000 USD/yr, determined by compensation panel.

For more information, go to:
http://jobview.usajobs.gov/GetJob.aspx?JobID=89528078.

Georgia State University

Three faculty positions in Diagnostics and Therapeutics Research

As part of GSU's Second Century Initiative (2CI) to add 100 faculty members over the next five years in selected areas, the College of Arts and Sciences plans to fill a cluster of three tenure-track faculty positions (rank open) within a year in the areas of chemical probe development (chemical biology), biomarkers, and chemosensors, pending budgetary approval. Emphasis will be on recruiting established investigators with external funding. The planned faculty recruitment is part of an overall effort to establish a Center for Diagnostics and Therapeutics at GSU, and along the strategic directions of Georgia Research Alliance and Georgia Cancer Coalition, two major organizations providing support to biomedical research in Georgia. Each appointment will be made to an academic department in accordance to the individual's degree and area of expertise and will be affiliated with the Center. This Center is housed in the new Petit Science building with 350,000 square feet of space for interdisciplinary research and teaching activities and world-class facilities. The same building also houses the Departments of Biology and Chemistry, the Neuroscience Institute, Center for Biotechnology and Drug Design, an animal facility, a BSL4 lab and several BSL3 labs, Center for Viral Immunology, as well as the Molecular Basis of Disease Program and the Brains and Behavior Program for optimal interactions and collaborations.

Successful candidates must have a Ph.D., M.D. or equivalent degree and demonstrate the ability to establish a vigorous, externally funded research program and to mentor Ph.D. graduate students. Excellence in teaching at both undergraduate and graduate levels is expected. Candidates at senior levels must have strong track records in research and teaching excellence, and in securing external funding. Applicants should submit a CV, detailed research plan(s), a statement of teaching philosophy, and a list of at least three references to: **Dr. Binghe Wang, Diagnostics Faculty Search Committee, Department of Chemistry, Georgia State University, P.O. Box 4098, Atlanta, GA 30302-4098.** Application processing will begin immediately and search will remain open until filled.

Georgia State University is a Research University of the University System of Georgia. Offers of employment will be conditional upon background verification.

URL: http://chemistry.gsu.edu

IAU

DIRECTOR POSITION

IAU Office for Astronomy Development

As a first step in the implementation of the decadal strategic plan "Astronomy for the Developing World – Building from the IYA2009," the International Astronomical Union (**www.iau.org**) has selected the South African Astronomical Observatory (SAAO) in Cape Town as the location for the Office for Astronomy Development (OAD). The OAD will be a joint venture between the IAU and the SAAO to lead and coordinate the development activities of the IAU globally.

We now seek an outstanding individual to fill the role of Director for the OAD to provide the necessary leadership and spearhead the effective implementation of the IAU strategic plan. The success of this important initiative will be critically dependent on the performance of the OAD and its Director, whose drive and commitment will be essential in building up the ambitious programmes envisaged by the IAU.

The successful candidate can be expected to satisfy the following minimum requirements:

- An honours degree or equivalent in astronomy or a closely related field (and a strong affinity with astronomy).
- Proven track record in education and capacity building activities at an international level.
- Demonstrable strategic vision and experience of change management.
- Managerial experience, including people and financial management.
- Demonstrable record of leadership and achievement, as well as a strong international reputation.

Experience in fundraising will be a significant advantage.

The tasks of the Director will include:

- Worldwide management, coordination and evaluation of IAU programmes in the area of development and education and establishment of their annual budgets.
- Liaison with the chairs of relevant IAU programme groups/sector task forces and other relevant stakeholders in planning and implementing the relevant programmes.
- Build up IAU regional astronomy development nodes, liaison with the IAU regional coordinators and nodes in planning and implementing relevant programmes.
- Implementation of new activities, as outlined in the IAU decadal strategic plan.
- Managing the OAD and its staff, including recruitment, establishment and control of the OAD budget, interfacing with the SAAO as host organisation and appropriate regular reporting.
- Proactive coordination and initiation of fund-raising activities for astronomy-driven capacity building activities.

The successful candidate will be expected to have an established network of contacts relevant to the tasks described above.

The Director will report to the Director of the SAAO. The activities of the OAD will be overseen by a Steering Committee comprising nominees of both the IAU and the SAAO.

The SAAO is a facility of the South African National Research Foundation (NRF) and provides a stimulating astronomical environment with a proven record of capacity building located in one of the most beautiful and cosmopolitan cities in the world. The Director will be appointed according to normal conditions of service of NRF employees, with a salary commensurate with their background and experience. This is a contract position for 5 years.

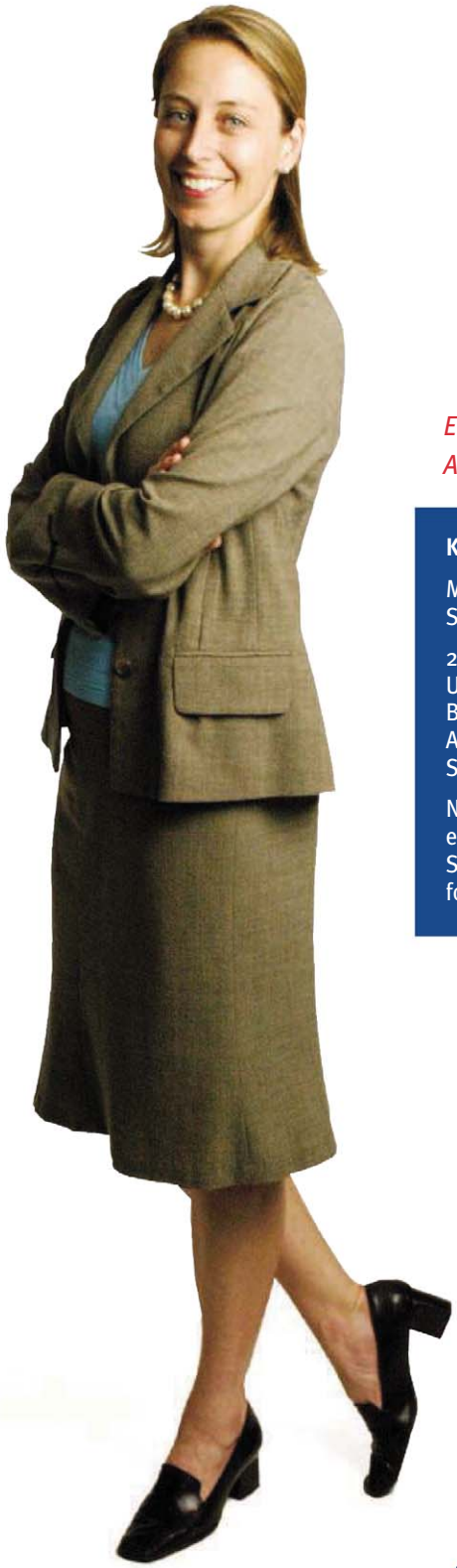
Interested candidates should send a cover letter and full CV, including the contact details of at least 3 references, by email to both the IAU General Secretary, Ian Corbett (**iau@iap.fr**), and SAAO HR Manager, Linda Tobin (**linda@saao.ac.za**). The selection process will begin after 30 September 2010.

For further information please contact the IAU General Secretary, Ian Corbett. Correspondence will be conducted with short-listed candidates only. SAAO is committed to employment equity and redress.

Science Careers online @sciencecareers.org

Science Careers online @sciencecareers.org

PICTURE YOURSELF AS A AAAS SCIENCE & TECHNOLOGY POLICY FELLOW



Make a Difference.
Help give science a greater voice in Washington, DC! Since 1973, AAAS Fellows have applied their skills to federal decision-making processes that affect people in the U.S. and around the world, while learning first-hand about the government and policymaking.

Join the Network.
Year-long fellowships are available in the U.S. Congress and federal agencies. Applicants must hold a PhD or equivalent doctoral-level degree in any behavioral/ social, biological, computational/ mathematical, earth, medical/health, or physical science, or any engineering discipline. Individuals with a master's degree in engineering and three years of post-degree professional experience also may apply. Federal employees are not eligible and U.S. citizenship is required.

Apply.
The application deadline for the 2011-2012 AAAS Fellowships is 5 December 2010. Fellowships are awarded in the spring and begin in September. Stipends range from $74,000 to $97,000.

Note: Additional fellowships are available through approximately 30 scientific society partners. Individuals are encouraged to apply with AAAS as well as with any scientific societies for which they qualify.

Full details at: **fellowships.aaas.org**

Enhancing Public Policy, Advancing Science Careers

Krista Donaldson, PhD

Mechanical Engineering, Stanford University

2004-05 AAAS Fellow at the U.S. Department of State, Bureau of Near Eastern Affairs, Iraq Desk, Economic Section

Now a researcher in engineering design at Stanford University's Center for Design Research

AAAS
ADVANCING SCIENCE, SERVING SOCIETY

BCM

Baylor College of Medicine

The Department of Biochemistry and Molecular Biology invites applications for a tenure-track faculty position at the **ASSISTANT** or **ASSOCIATE PROFESSOR** rank. The Department is deeply committed to interdisciplinary approaches, with strengths in molecular genetics, developmental biology, cell biology, neurobiology, and structural biology. We are seeking outstanding candidates who are pursuing cutting-edge research in any of these fields. We are especially interested in the areas of chemical biology, genome instability, regulatory networks, membrane and organellar biology, and models of human disease.

Our Department offers a collegial, collaborative environment and has a tradition of being very supportive of new faculty. Baylor College of Medicine is located in the heart of the Texas Medical Center in Houston and is affiliated with 11 educational institutions, including the University of Texas Medical School, The UT MD Anderson Cancer Center, and Rice University, to name a few. Academic rank and salary are commensurate with experience and qualifications. Candidates should send a cover letter, curriculum vitae, statement of research interests, and arrange to have three letters of recommendation sent to **Dr. John Wilson** at: **BMBsearch@bcm.edu**. The committee will review applications beginning **October 1, 2010**, and will continue until the position is filled.

Baylor College of Medicine is an Equal Opportunity Affirmative Action and Equal Access Employer.

Molecular and Cellular Biologist

Molecular and Cellular Oncology

The Department of Molecular and Cellular Oncology at The University of Texas MD Anderson Cancer Center is seeking outstanding molecular and cellular oncologists. The department has openings for full-time, tenure-track faculty with demonstrated excellence in molecular and cellular approaches to understanding the molecular mechanisms of cancer development. Although not required, the following expertise is encouraged: proteomic/metabolomic analysis, and signal pathways to elucidate the molecular mechanisms that cause cancer. Incumbents will be responsible for establishing their own independent research and expected to write grants and papers. Applicants must have a doctoral degree, postdoctoral experience and be eligible to apply for federal grants.

Interested applicants should send a letter and curriculum vitae to: **Mien-Chie Hung, PhD, Chair, Department of Molecular and Cellular Oncology, Unit 108 The University of Texas MD Anderson Cancer Center, 1515 Holcombe Blvd., Houston, Texas 77030; Email: nedwards@mdanderson.org**.

THE UNIVERSITY OF TEXAS
MD Anderson Cancer Center

MD Anderson Cancer Center is an equal opportunity employer and does not discriminate on the basis of race, color, national origin, gender, sexual orientation, age, religion, disability or veteran status, except where such distinction is required by law. All positions at MD Anderson are considered security sensitive; drug screening and thorough background checks will be conducted. The University of Texas MD Anderson Cancer Center values diversity in its broadest sense. MD Anderson is a smoke-free environment.

University of Nebraska Lincoln

Assistant Professor
Redox Biology Center and Department of Biochemistry

The Redox Biology Center (RBC) at UNL, supported as a Center of Biomedical Research Excellence by the National Institutes of Health, invites applications for a tenure-leading Assistant Professor position in the Department of Biochemistry in the general area of redox regulation and signaling. Research focus of applicants includes, but is not limited to, the following: (1) Redox-dependent/responsive cellular regulatory processes, (2) Development of sensors and methods for detecting reactive oxygen species (ROS) and ROS-induced cellular response/damage, and (3) Systems biology of redox-related disease.

The Center is an emphasis group for research in redox biology involving investigators at the University of Nebraska – Lincoln and the Eppley Cancer Research Center in Omaha. Areas such as thiol-based redox signaling and gene regulation, redox control of neurodegenerative diseases, cancer and aging, biochemistry of redox-active trace elements, structural biology, proteomics/metabolomics, microbial pathogenesis and redox homeostasis are all current targets of investigation. The Center also operates mass-spectrometry and spectroscopy core research facilities. The position is a state-supported academic year appointment with a generous start-up package and housed in the George W. Beadle Center, which includes state-of-the-art core facilities in proteomics and metabolomics, genomics, crystallography, bioimaging, flow cytometry, bioinformatics, biophysical spectroscopy, and trace element analysis.

It is expected that the investigator will establish a nationally recognized and extramurally funded research program and contribute to the undergraduate and graduate education missions of the Department of Biochemistry. A Ph.D. degree (or equivalent) in a related scientific field and at least 1 year of postdoctoral experience (or equivalent) are required.

To learn more about the Center, please visit **http://www.unl.edu/RedoxBiologyCenter**. To view the complete job details and make an application for the position, go to the web site at **https://employment.unl.edu**. Click on "Search Job Openings", enter requisition number **100335** and make an application according to the instructions. Complete the faculty academic administrative information form and attach a letter of application, curriculum vitae, succinct statement of research interests and arrange to have three letters of reference directly sent to:

RBC Search Committee Chair
Attn: Joyce Ore, Administrative Coordinator
Nebraska Redox Biology Center
University of Nebraska-Lincoln
N146 Beadle Center
Lincoln, NE 68588-0662

Email reference letters will also be accepted at **redox2@unl.edu**. Review of applications will begin on **October 15, 2010** and will continue until a successful candidate has been identified or the recruitment process is closed.

The University of Nebraska has an active National Science Foundation ADVANCE gender equity program, and is committed to a pluralistic campus community through affirmative action, equal opportunity, work-life balance, and dual careers.

Science Careers online @sciencecareers.org

Upcoming Faculty Issue



There's a *Science* to finding the best faculty.

Reach more candidates with our faculty issue focusing on scientists working at smaller research universities. Make sure our readers see your ad.

- 130,000 print subscribers each week including over 65% Ph.D.s
- Special bonus distribution mailing of this issue to 55,000 scientists

Science Careers
From the journal *Science* AAAS

ScienceCareers.org

POSTDOCTORAL RESEARCH ASSOCIATE

Position available to study electrophysiological properties of central neurons in mouse brain slices in models of Huntington's Disease. Focus is on mechanisms regulating intrinsic excitability and synaptic transmission. Candidates will acquire expertise in whole cell recording and in vitro imaging techniques. Position is in the Department of Neuroscience of the Albert Einstein College of Medicine, which provides an outstanding training environment. Applicants should send a letter of interest, CV, and a list of at least three potential references to:

Dr. Donald Faber, Chair,
Department of Neuroscience, KC 903
Albert Einstein College of Medicine
1300 Morris Park Avenue, Bronx, NY 10461
donald.faber@einstein.yu.edu

Albert Einstein College of Medicine is an equal opportunity employer committed to workforce diversity.

EINSTEIN
Albert Einstein College of Medicine
OF YESHIVA UNIVERSITY

UCI
University of California, Irvine

FACULTY POSITION IN PHARMACOLOGY

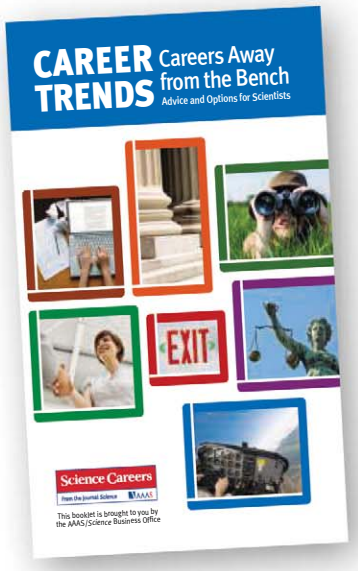
The Department of Pharmacology at the University of California, Irvine (UCI) invites applications for a tenured faculty position at the level of Associate/Full Professor. We seek a scholar with a proven record of research accomplishments. He/she should have specific interest in cellular and molecular mechanisms governing gene expression and their functional links to physiology and metabolism. Special consideration will be given to candidates with expertise and experience in integrating genetic, biochemical and physiological approaches. Other qualifications include an M.D. and/or Ph.D. and a strong drive to pursue a dynamic research program and an interest in and talent for graduate teaching.

Interested applicants must submit cover letter, curriculum vitae, a statement of research, a statement of teaching and contact information for 3-5 references via the University of California Irvine's Academic Personnel RECRUIT System at **http://recruit.ap.uci.edu**.

The University of California, Irvine has an active career partner program and an NSF ADVANCE Program for Gender Equity and is an Equal Opportunity Employer committed to excellence through diversity.

Download your free copy.

ScienceCareers.org/booklets



Science Careers
From the journal *Science* AAAS

Pacific Northwest
NATIONAL LABORATORY
Proudly Operated by Battelle Since 1965

Deputy Director,
Joint Global Change Research Institute
College Park, MD

Pacific Northwest National Laboratory is seeking a **Deputy Director for the Joint Global Change Research Institute**, a collaboration between PNNL and the University of Maryland, in College Park, Md. The Institute houses an interdisciplinary team dedicated to understanding the issues associated with global climate change and their potential resolution. Institute staff bring decades of experience and expertise to bear in science, technology, economics, and policy related to climate change and energy. The Institute is a leading center for research on understanding the role of technology as both a cause of and a solution to anthropogenic climate change.

The successful candidate will have an international reputation in climate change research and demonstrate broad understanding of the interconnected issues associated with global change research. A Ph.D. in Environmental Sciences or Engineering, Economics, Energy Policy or related field and demonstrated experience both managing and participating in multi-disciplinary teams is essential.

To apply, go to http://www.pnl.gov/atmospheric/jobs.stm

For additional information about the Institute, visit http://www.globalchange.umd.edu.

Do you have a passion for cutting-edge science and protecting the public health?

Unleash your passion into a rewarding career as a Physician, Scientist or Consumer Safety Officer at the Center for Biologics Evaluation and Research!

The Center for Biologics Evaluation and Research's mission is to protect and enhance the public health through the regulation of biological products including blood, vaccines, allergenics, tissues, and cellular and gene therapies. Biologics, in contrast to drugs that are chemically synthesized, are derived from living sources (such as human, animals, and microorganisms) and are not easily identified or characterized, and many are manufactured using biotechnology. These products often represent cutting-edge biomedical research and, in time, may offer the most effective means to treat a variety of medical illnesses and conditions that presently have few or no other treatment options. For details on qualifications and salary, please visit our Hiring Opportunities page at **http://www.fda.gov/AboutFDA/CentersOffices/CBER/ucm125465.htm**.

How to Apply: For current vacancies and application procedures, visit: **http://www.fda.gov/AboutFDA/CentersOffices/CBER/ucm103202.htm**. For future vacancies, submit CV/resume and cover letter to our resume bank to: **CBER.Employment@fda.hhs.gov Attn: Job Code: Sci-Gen**

The Center for Biologics Evaluation and Research is part of the Food and Drug Administration, Department of Health and Human Services.

EQUAL OPPORTUNITY EMPLOYER. SMOKE FREE ENVIRONMENT.

America's Veteran: http://www.fedshirevets.gov/

COLUMBIA UNIVERSITY MEDICAL CENTER
Department of Pathology
FACULTY POSITIONS

Columbia University Department of Pathology and Cell Biology seeks highly qualified individuals for faculty positions in surgical pathology, clinical pathology, and research. Appointments can be at the Assistant, Associate, Professor, or Associate Research Scientist level, depending on experience and qualifications. All positions require outstanding academic credentials and a record of scholarly productivity. Clinical positions require board certification and a license in NYS. Research positions require record of publication in leading journals and a statement of research directions. A history of successful research funding is desirable.

To apply online, go to Web site:
https://academicjobs.columbia.edu/applicants/Central?quickfind=53496

Send duplicate of your application to:
Positions, Department of Pathology
Columbia University
630 West 168th Street
New York, NY 10032

Columbia University takes affirmative action toward equal employment opportunity. Women and minorities are encouraged to apply.

POSTDOCTORAL SCIENTIST
Biomimetic Nanopores

Nanopores provide new possibilities for the purification and characterization of macromolecules with profound implications for biology, medicine, pharmacology and biotechnology. The nuclear pore complex is a cellular nanopore which has unique abilities for specifically sorting native macromolecules and their complexes at high speed. In an interdisciplinary project involving biochemists, biophysicists and engineers we have created functionalized artificial nanopores mimicking transport properties of the nuclear pore complex (*Nature* 457 (2009) 1023). We are looking for a postdoctoral scientist who is interested in pursuing the project by applying a whole range of techniques, in particular protein expression and purification, creation of functionalized nanopores, high-resolution light microscopy, innovative flux measurement techniques and the engineering of nanopore-based protein purification machines.

Position available immediately

Interested scientists should send a CV and three references to **Beth Anne Hatton; hattonb@mail.rockefeller.edu, Administrative Assistant to Professors Michael Rout, Brian Chait and Reiner Peters.**

The Rockefeller University
is an Affirmative Action/Equal Opportunity/VEVRAA Employer and solicits applications from women and under-represented minorities.

POSITIONS OPEN

Children's National Medical Center

The Center for Neuroscience Research of the Children's Research Institute (CRI) at Children's National Medical Center has one tenure-track opening at **FULL, ASSOCIATE** or **ASSISTANT PROFESSOR** level. This position is for a highly motivated Ph.D. and/or M.D. neuroscientist with interests in the areas of brain development and/or animal models of neurodevelopmental/autism spectrum disorders. The recruit will join a collegial and highly collaborative multidisciplinary team studying development of the central nervous system, with strengths in mouse genetics, neuroembryology, molecular and cellular manipulation of the developing brain, electrophysiology, confocal microscopy, and time-lapse multiphoton imaging. The Center for Neuroscience Research occupies a total of 12,000 square feet of newly constructed laboratory space, with access to excellent core facilities, including cellular imaging, FACS, and genomics/proteomics cores. This position offers a competitive start-up package, and the successful candidate will have outstanding research credentials, including a substantial record of quality publications. Track record of grant support is preferred, but not required of applicants for the position of Assistant Professor. The position also includes a tenure-track faculty appointment at the George Washington University School of Medicine.

To apply, please send a two-page statement of research interests and goals, curriculum vitae, and two-three letters of recommendation by October 1, 2010 to:

Dr. Vittorio Gallo
Director, Center for Neuroscience Research
Children's Research Institute
Children's National Medical Center
111 Michigan Avenue, NW, 6th floor main
Washington, DC 20010-2970
Telephone: 202-476-4996
E-mail: vgallo@cnmcresearch.org

FACULTY POSITION

The Department of Chemistry at Lawrence University invites applications for a tenure-track Faculty Position beginning fall 2011. Teach courses in the chemistry department primarily in the areas of inorganic chemistry and general chemistry, as well as occasional participation in our college-wide, nationally-recognized freshman studies program. Candidates must be committed to excellence in teaching in a liberal arts environment, and be ready to develop an active research program that will challenge and inspire our undergraduates. A Ph.D. is required. Postdoctoral experience in teaching or research is desirable. The search is open with respect to rank, but we anticipate hiring at the **ASSISTANT PROFESSOR** level. A letter of application, curriculum vitae, statements of teaching philosophy and research plans, undergraduate and graduate transcripts, and three letters of reference should be sent directly to: **Associate Professor David Hall, Chair, Department of Chemistry, Lawrence University, Appleton, WI 54912. Fax: 920-832-6962.** Applicants should address in their letters of application the ways in which they could contribute to Lawrence's institutional mission and goals. Review of applications will begin September 24, 2010. Lawrence University is a private, selective college of liberal arts and sciences with a conservatory of music. About a quarter of its 1400 students major in the natural sciences, and the student-to-faculty ratio is 11:1. Its chemistry department resides in a state-of-the-art science facility that houses a wide array of instrumentation, including a 400 MHz NMR, GC/EPC, HPLC, Raman, FT-IR and UV-Vis spectrometers. *Lawrence University is committed to enhancing the diversity of its faculty, and the diversity of viewpoints and approaches that the faculty represents.*

POSITIONS OPEN

University of Michigan Medical School

ANTHONY AND LILLIAN LU PROFESSORSHIP
Department of Biological Chemistry
University of Michigan Medical School

The Department of Biological Chemistry seeks applications from and nominations of outstanding established investigators for the Anthony and Lillian Lu Endowed Professorship. Areas of emphasis in the Department that we would like to complement with the hiring of a senior investigator are protein folding and processing, structural enzymology, redox signaling, or regulation of gene expression. Qualifications include a Ph.D. and/or M.D., a minimum of eight years of independent research experience, and an existing research program of international stature. In addition to maintaining an active research program, the successful candidate will train doctoral students and postdoctoral fellows and participate in classroom teaching activities of the department.

The Department of Biological Chemistry currently has 45 active faculty members and is in the midst of a phase of expansion. There are many opportunities for interactions both within the Department and across the campus. Further information about the Department of Biological Chemistry can be found at **website: http://www.biochem.med.umich.edu/biochem/.**

Applicants or nominators should submit curriculum vitae and a one or two page summary highlighting previous research accomplishments and plans for future research to: **Ruma Banerjee, Chair, Search Committee, c/o Amanda Howard, Department of Biological Chemistry, 5301 Medical Science Research Building III, 1150 W. Medical Center Dr., University of Michigan Medical School, Ann Arbor, MI 48109-0606.** References will not be contacted without permission of applicants or nominators.

The University is an Affirmative Action/Equal Opportunity Employer.

POSTDOCTORAL POSITIONS are available to study molecular mechanisms of estrogen receptor (ER) action. One project is to study the role of coactivators and corepressors in controlling ER function in breast cancer and a second project is in the area of molecular mechanisms regulating ER-dependent gene expression. Projects utilize molecular cellular biology and high throughput genomics approaches. For details of the laboratory's research, see **website: http://www.bcm.edu/mcb/index.cfm?pmid=7708.**

Required qualifications: Recent Ph.D. with strong background in molecular biology and/or cell biology. Salary commensurate with experience.

To apply, send a letter of application including a short description of research experience and interests, curriculum vitae, and the names and contact information for three references to **Carolyn Smith**, Ph.D. (**e-mail: carolyns@bcm.edu**) and apply online at **website: http://www.medschooljobs.org,** position **#198283.** *Baylor College of Medicine is an Equal Opportunity/Affirmative Action/Equal Action Employer.*

ASSISTANT PROFESSOR of CHEMISTRY

The Department of Chemistry of the University of Chicago invites applications from outstanding individuals for the position Assistant Professor of Chemistry. This search is in the areas broadly defined as inorganic, organic, and physical chemistry. Applicants must apply online to the University of Chicago Academic Career page at **website: http://tinyurl.com/36pmntk.** Applicants must upload a cover letter, curriculum vitae with a list of publications, and a succinct outline of research plans. The cover letter should be addressed to the **Inorganic Search Committee, Organic Search Committee,** or **Physical Search Committee,** depending on the discipline of interest. The successful candidate must have a Ph.D. in Chemistry or related field. In addition, three reference letters will be required. Review of completed applications will begin October 1, 2010. To ensure full consideration, all material should be submitted by that date.

The University of Chicago is an Affirmative Action/Equal Opportunity Employer.

POSITIONS OPEN

Wayne State University School of Medicine

DIABETES GENETICS
at Wayne State University

The Center for Molecular Medicine and Genetics (CMMG) and the Endocrine Division of the Department of Medicine, Wayne State University School of Medicine, announce a joint **FACULTY POSITION.** This position would complement a new faculty position added last year. We welcome motivated physician-scientist and full-time research applicants who hold M.D., M.D.-Ph.D., or Ph.D. degrees. The academic level would be commensurate with prior experience and achievement.

The Diabetes Genetics Program has a broad scope, ranging from population genetics to cellular mechanisms involved in the pathology of diabetes and its complications. Relevant backgrounds include genetics, cell signaling, cell biology, and epidemiology. Candidates should have strong research and communication skills. The Center provides a highly interactive environment with multiple opportunities for multidisciplinary, basic, and translational research.

The appointee will be housed in a recently renovated laboratory supported by nearby core research facilities. An attractive start-up package is available, which includes the proceeds from an endowment to support diabetes research. The Division of Endocrinology serves inpatient and outpatient endocrine/diabetes patients at the Detroit Medical Center hospitals, which are over 1000-bed facilities and provide ample opportunities for both basic and clinical research.

Applications should include a letter of application, curriculum vitae, three to five year research plan, and the names and addresses of at least three references and be electronically sent to **Ms. Suzanne Shaw** at **e-mail: sshaw@wayne.edu.**

WSU is an Equal Opportunity/Affirmative Action Employer.

MULTIPLE FACULTY POSITIONS
Department of Chemistry Emory University

The Department is seeking candidates for two **ASSISTANT PROFESSOR** positions. Applicants should have a proven record of research accomplishments. Successful applicants are expected to establish active independent research programs and have a strong commitment to teaching at both the undergraduate and graduate levels.

The first position is in the area of C–H functionalization. Applicants should have research plans related to C–H functionalization, and experience in relevant areas of chemistry such as organic chemistry, inorganic chemistry, or computational chemistry. Applicants whose research interests complement those of the faculty in our National Science Foundation Phase I Center on C–H functionalization are particularly encouraged to apply. Ph.D. required. Reference job posting **#17791BR.**

The second position is for researchers working at the interface of chemistry and biology, broadly defined. Candidates whose research plans include both experimental and computational approaches are particularly encouraged to apply. Ph.D. required. Reference job posting **#17792BR.**

Please submit a cover letter stating which position you wish to apply for, curriculum vitae, summary of research interests, specific research plans, and a statement of teaching philosophy in a single PDF file by to **e-mail: chemsearch@emory.edu.** Arrange for three letters of recommendation to be sent to the same address. Review of applications will begin September 24, 2010.

Emory University is an Affirmative Action/Equal Opportunity Employer and encourages applications from women and members of minority groups.

MEETINGS

OIST Winter Course "Evolution of Complex Systems"

Date: December 6 – 11, 2010
Location: OIST Seaside House, Onna, Okinawa, Japan
Sponsor: Okinawa Institute of Science and Technology (OIST)

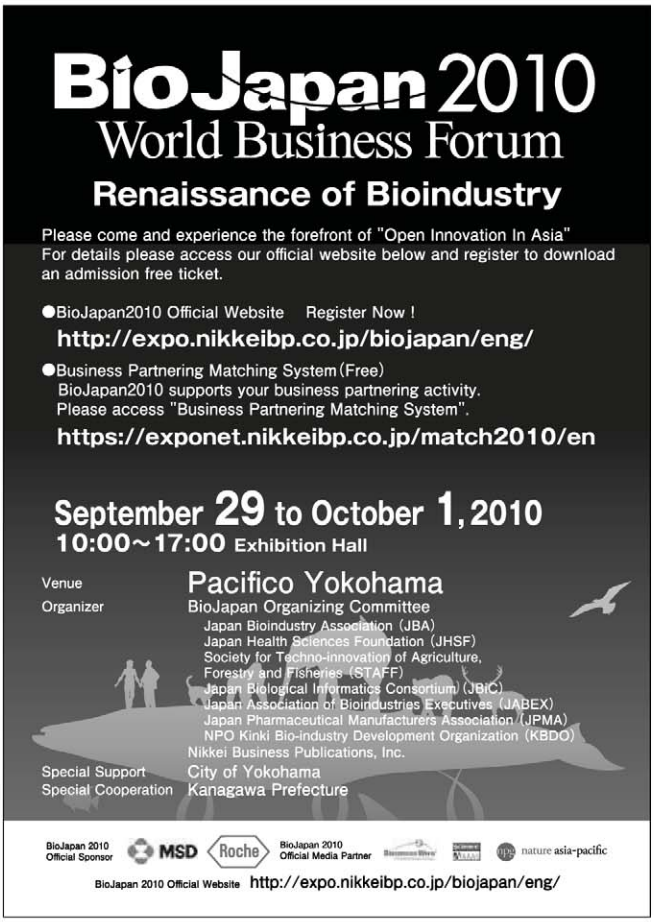
The aim of the OIST Winter Course "Evolution of Complex Systems" (OWECS) is to provide opportunities for young researchers with biological backgrounds to learn the latest advances in the field of evolutionary developmental biology. The OWECS is a combination of lectures and workshop. We invite about 20 graduate students and postgraduate researchers. The sponsor will provide lodging and meals during the course and support travel for those without funding.

Confirmed lecturers: Mike Levine, Robb Krumlauf, Thomas Holstein, Nipam H. Patel, Kiyokazu Agata, Daniel Rokhsar, Nori Satoh, Sydney Brenner

Apply to: http://www.irp.oist.jp/owecs
Deadline of application: September 27, 2010

More information can be obtained from **http://www.irp.oist.jp/owecs** or contact secretariat at **owecs2010@oist.jp**

MEETINGS



Imperial College London

Microbiology Section
Department of Medicine

Non-Clinical Lecturer in Molecular Microbiology

Salary Range: £42,280 - £47,210 p.a.

The Microbiology Section wishes to appoint two Non-Clinical Lecturers to carry out research programmes into infection/immunity relating to bacterial pathogen(s). Applications are invited from suitably qualified individuals with research interests in any aspect of bacterial infection or host immunity; those studying cellular immune mechanisms and Gram-positive bacteria are particularly welcome to apply.

You will be required to attract external research funding, supervise PhD students, post-doctoral fellows and research assistants, and to submit publications to refereed journals. You will also undertake teaching.

You will have a PhD and should be RAE returnable, with a strong research record in an appropriate aspect of prokaryotic biology or immunology.

You will be part of the Centre for Molecular Microbiology and Infection (CMMI), which is located at the South Kensington Campus. The CMMI is an inter-faculty centre of excellence involving the Imperial College London Faculty of Medicine and the Faculty of Life Sciences. Groups in the CMMI study microbial pathogenesis and host immunity, with an emphasis on diseases caused by bacteria (http://www.imperial.ac.uk/cmmi). The Division of Infection was awarded 5* at the last RAE.

Informal enquiries may be made to the Head of Section, Professor David Holden, at d.holden@imperial.ac.uk

Our preferred method of application is online via our website at http://www3.imperial.ac.uk/employment (please select "Job Search" then enter the job title or vacancy reference number into "Keywords"). Please complete and upload an application form as directed **quoting reference number HM2010108**.

Alternatively, if you are unable to apply online, please e-mail: hmrecr@imperial.ac.uk to request an application form.

Closing date: 15 September 2010 (Midnight BST).

Committed to equality and valuing diversity. We are also an Athena Silver SWAN Award winner.

Stonewall TOP 100 EMPLOYERS 2010

POSITIONS OPEN

UC San Diego
SCHOOL OF MEDICINE

FACULTY POSITION
BAC Molecular Geneticist
Assistant or Associate Professor

University of California San Diego (UCSD) Department of Neurosciences (**website: http://neurosciences.ucsd.edu/**).

Position is available for individual with expertise in BAC (Bacterial Artificial Chromosome) mouse models to study neural disease or development in a fully independent research program. UCSD and associated local institutes provide an extremely strong and diverse neuroscience community and environment. Position will be within newly established Translational Neuroscience Institute in the School of Medicine with preference for the Assistant Professor level.

Competitive salary and startup, commensurate with qualifications and based on University of California pay scales. Review of applications will begin 30 September 2010, and will continue until the position is filled.

Application materials should be submitted via UCSD AP On-Line Recruit (**website: https://apol-recruit.ucsd.edu/**), an electronic job application system. See position posting **#10-166** in Recruit.

Please be prepared to provide curriculum vitae, a statement of research interests, and three letters of reference. *UCSD is an Affirmative Action/Equal Opportunity Employer with a strong institutional commitment to excellence through diversity.*

ASSISTANT PROFESSORS of BIOCHEMISTRY
University of Washington, Seattle

The Department of Biochemistry at the University of Washington School of Medicine invites applications for two tenure-track positions at the Assistant Professor level. We seek creative scientists who conduct research on important biological problems using the tools of biochemistry, structural biology or biophysics, cell or molecular or developmental biology, or related fields. Our department is also strongly committed to teaching and service at the undergraduate, graduate, and medical school levels. Applicants should have a Ph.D. or M.D., and should submit curriculum vitae, research prospectus, and reprints or preprints to **e-mail: bcsearch@uw.edu** by October 30, 2010. Three letters of recommendation should be sent separately to the same address, or mailed to: **Alan Weiner, ZymoGenetics Chair, Department of Biochemistry, Box 357350, University of Washington, Seattle, WA 98195-7350.** *The University of Washington is an Affirmative Action/Equal Opportunity Employer.*

FACULTY POSITION

The Saint James School of Medicine, an international medical school (**website: http://www.sjsm.org**), invites applications from candidates with teaching and/or research experience in any of the basic medical sciences for its Caribbean campuses. Senior faculty positions are currently available in anatomy, pathology, and physical diagnosis. Applicants should be M.D., D.O., and/or Ph.D.

Teaching experience in the U.S. system is desirable but not required. Retired persons are encouraged to apply. Attractive salary and benefits. Submit curriculum vitae by **e-mail: info@sjsm.org** or mail to: **Human Resources Development Services Inc., 1480 Renaissance Drive, Suite 300, Park Ridge, IL 60068.**

POSITIONS OPEN

POSTDOCTORAL FELLOW in Human Immunobiology. Immediate opening. Project examines how simultaneous ligation of cell surface receptors on dendritic cells and macrophages with a novel ligand, induces an anti-inflammatory phenotype. We are examining the signaling pathways and soluble mediators produced by these cells postactivation. We are also examining how activation of these innate cells by the anti-inflammatory agent leads to reductions in HIV-1 viral loads. Applicants should have Ph.D., M.D., or D.V.M. degree with experience in human immunobiology. Please send curriculum vitae and names of references to: **Dr. Donald Harn, Department of Infectious Diseases, College of Veterinary Medicine, University of Georgia, Athens, GA. 30602,** or to **e-mail: dharn@uga.edu.** Applications received by August 31, 2010 are assured full consideration. *The University of Georgia is an Equal Opportunity/Affirmative Action employer.*

TWO POSITIONS: MOLECULAR GENETICIST AND CELL BIOLOGIST

The Department of Biology at the University of Richmond invites applications for two tenure-track positions as **ASSISTANT PROFESSORS** of biology. Exceptional candidates at the **ASSOCIATE PROFESSOR** level will also be considered. Candidates should have a doctoral degree and postdoctoral training with a specialization in Molecular Genetics and/or Cell Biology, teaching experience with undergraduates is preferred, but not required, and a record of research productivity is required. The candidate must meet all other required criteria by the time of selection for the position. The successful applicants are expected to commit to highly effective undergraduate teaching including introductory courses in the major, non-major courses, and upper-level electives in Molecular Genetics or Cell Biology and are expected to maintain an active research program that contributes to our biology and our biochemistry and molecular biology majors, attracts extramural funding, and actively engages undergraduate students. We are especially interested in recruiting individuals who have experience working with students from diverse backgrounds.

Applicants should apply online at **website: http://www.urjobs.org** using the Faculty (Instructional/Research) link. Applicants should supply electronically a single letter of application for one or both positions, curriculum vitae, and a single statement describing how their teaching philosophy and research interests will be integrated and maintained for success as a teacher-scholar. Applicants should arrange for three letters of recommendation, including at least one that addresses teaching effectiveness and potential, to be sent electronically to **e-mail: lboland@richmond.edu, Department of Biology, University of Richmond, VA 23173.** The deadline for applications is September 20, 2010.

The University of Richmond is committed to developing a diverse workforce and student body and to being an inclusive community. We strongly encourage applications from candidates who will contribute to these goals. For more information on the department, resources, and teaching responsibilities, see **website: http://biology.richmond.edu/.**

POSTDOCTORAL POSITION
Cardiovascular Research

A Postdoctoral **RESEARCH ASSOCIATE** position is available to study molecular basis of hypertension and vascular diseases. Our research team stands in the forefront of cardiovascular research. This position may have opportunity for advancement and promotion is based on accomplishments of the first two years. Competitive salary and health insurance coverage for family. Ph.D. or/and MD. Prior experience with at least two of the followings is preferred: vascular biology, biochemistry, gene therapy, signal transduction, stem cell biology, protein chemistry, proteomics, or cardiovascular physiology. Send detailed curriculum vitae and three references to: **Dr. Zhongjie Sun, Department of Physiology, University of Oklahoma Health Science Center, USA. E-mail: zhongjie-sun@ouhsc.edu.**

POSITIONS OPEN

UC San Diego
SCHOOL OF MEDICINE

FACULTY POSITION
Bioinformatics Neuroscientist
Assistant or Associate Professor

University of California San Diego (UCSD) Department of Neurosciences (**website: http://neurosciences.ucsd.edu/**). Position available for an individual with expertise in Bioinformatics, including knowledge and skill in performing transcriptomic, proteomic, or lipidomic analysis in models of neural disease or development. Expertise is essential in development and application of analytical bioinformatic methods. The La Jolla neuroscience community is extremely strong and diverse, providing an outstanding opportunity to develop an independent research program. Position will be within newly established Translational Neuroscience Institute in the School of Medicine with a preference for the Assistant Professor level.

Competitive salary and startup, commensurate with qualifications and based on University of California pay scales. Review of applications will begin 30 September 2010, and continue until the position is filled.

Application materials should be submitted via UCSD AP On-Line Recruit (**website: https://apol-recruit.ucsd.edu/**), an electronic job application system. See position posting **#10-165** in Recruit.

Please be prepared to provide curriculum vitae, a statement of research interests, and the names and e-mail addresses of three referees. *UCSD is an Affirmative Action/Equal Opportunity Employer with a strong institutional commitment to excellence through diversity.*

FOUR TENURE-TRACK FACULTY POSITIONS
Texas A&M
Center for Phage Technology

The Departments of Biochemistry and Biophysics, Plant Pathology and Microbiology, and Veterinary Pathobiology invite applications for tenure-track **ASSISTANT** and **ASSOCIATE POSITIONS** in the interdisciplinary Center for Phage Technology (CPT) being established jointly by Texas A&M University and Texas AgriLife Research. The Center is dedicated to basic and applied research in bacteriophage biology and its potential for antibacterial strategies in human and animal medicine, agriculture and industry. Successful candidates are expected to establish research programs consistent with the goals of the CPT and to participate fully in the educational programs of the respective departments. Competitive start-up packages, salaries, and laboratory space will be provided. Please send curriculum vitae, contact information for three individuals who will serve as references, and research précis to: **Center for Phage Technology Interdepartmental Search Committee, 2128 TAMU, College Station, TX 77843-2128. E-mail: cpt@tamu.edu.** Review of applications will commence August 15, 2010 and continue until the positions are filled. Two positions will be filled for academic year 2011-12 and two more the following year.

Equal Opportunity Employer.

MARKETPLACE

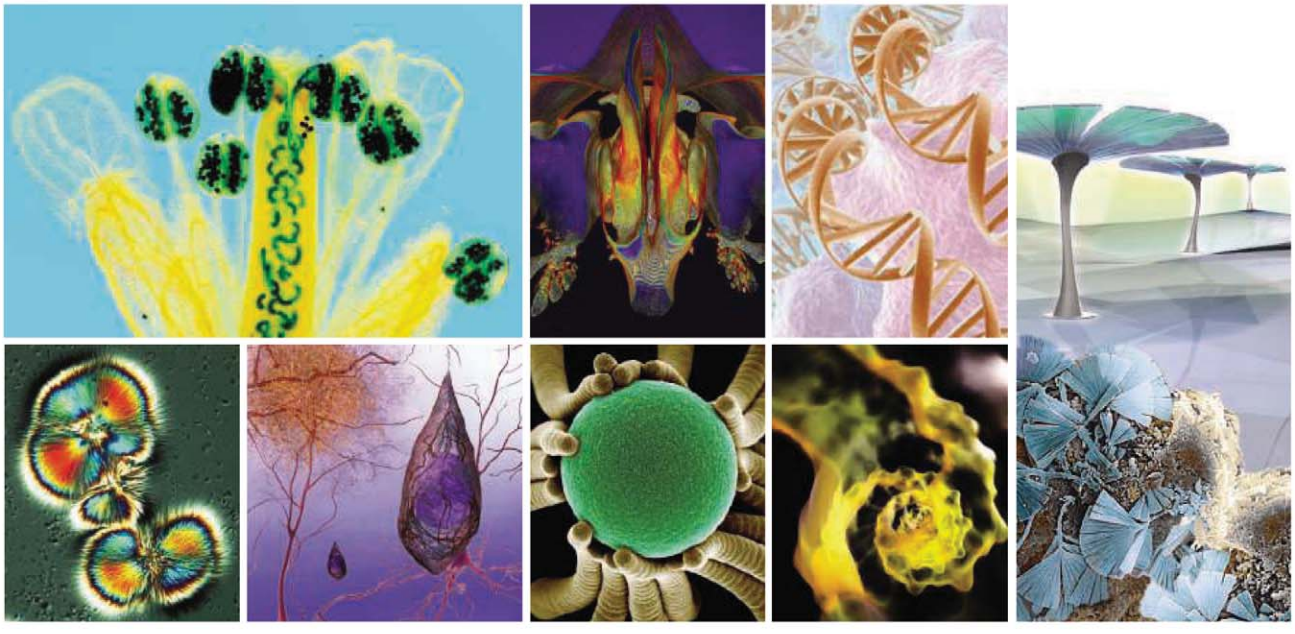
Widely Recognized Original & Guaranteed
KlenTaq1
8¢/u
Truncated Taq DNA Polymerase Withstand 99°C
US Pat #5,436,149
Call: **Ab Peptides**
Fax: 314•968•8988
e-mail: abpeps@msn.com
1•800•383•3362
www.abpeps.com

INTERNATIONAL SCIENCE & ENGINEERING
VISUALIZATION CHALLENGE

COMPETITION DEADLINE APPROACHING

ENTRY DEADLINE: SEPTEMBER 15, 2010

SCIENCE AND ENGINEERING'S MOST POWERFUL STATEMENTS
ARE NOT MADE FROM WORDS ALONE



Visualization in all its forms has the power to illuminate and educate. It explains and makes clear all aspects of the world around us. It feeds insight and provokes curiosity.

The National Science Foundation (NSF) and the journal *Science*, published by the American Association for the Advancement of Science, invite you to participate in this year's Challenge. The competition recognizes scientists, engineers, visualization specialists, and artists who produce innovative work in visual communication.

Winning entries will be published in *Science* and *Science* Online, and will be displayed on the NSF website.

Award Categories

- Photography
- Illustrations
- Informational Posters and Graphics
- Interactive Games
- Non-Interactive Media

Complete Entry Information:
www.nsf.gov/news/scivis



The biggest advance in qPCR since the q.

The new ViiA™ 7 Real-Time PCR System puts high-productivity qPCR at your fingertips.

With a streamlined workflow, one-button protocol feature, and intuitive software, the new ViiA™ 7 Real-Time PCR System is faster to set up, easier to run, and more convenient to automate than any other qPCR platform. And with the new OptiFlex™ optical system, you'll have greater dye flexibility for multiplexing than ever before. The end result is high-accuracy data with minimal distraction, which means you can stay focused on what matters most—your research.

For more information, visit **www.appliedbiosystems.com/viia7**



Optimized for TaqMan® Array Micro Fluidic Cards and reagents.

applied biosystems™
by life technologies™

FOR RESEARCH, FORENSIC OR PATERNITY USE ONLY. NOT INTENDED FOR ANY ANIMAL OR HUMAN THERAPEUTIC OR DIAGNOSTIC USE. The trademarks mentioned herein are the property of Life Technologies Corporation or their respective owners.
TaqMan is a registered trademark of Roche Molecular Systems, Inc. © 2010 Life Technologies Corporation.